Function and Regulation of *Arabidopsis thaliana* Helper NLRs during (Auto-) Immunity

Dissertation

der Mathematisch-Naturwissenschaftlichen Fakultät

der Eberhard Karls Universität Tübingen

zur Erlangung des Grades eines

Doktors der Naturwissenschaften

(Dr. rer. nat.)

vorgelegt von

Svenja Corina Saile

aus Reutlingen

Tübingen

2021

Gedruckt mit Genehmigung der Mathematisch-Naturwissenschaftlichen Fakultät der Eberhard Karls Universität Tübingen.

Tag der mündlichen Qualifikation:	29.03.2022
Dekan:	Prof. Dr. Thilo Stehle
1. Berichterstatter:	Dr. Farid El Kasmi
2. Berichterstatterin:	Prof. Dr. Rosa Lozano-Durán
3. Berichterstatter:	PD Dr. Marcel Wiermer

Danksagung

Zuallererst möchte ich mich bei meinem Doktorvater, Dr. Farid El Kasmi, bedanken, der mich in den letzten Jahren stets gefördert und nie unterfordert hat. Lieber Farid, ich bin Dir unglaublich dankbar für Deine ausgezeichnete Betreuung, Deine Begeisterung für meine Arbeit und Deine kreativen Ideen, die mich immer wieder fasziniert, inspiriert und motiviert haben. Unsere one-to-one Meetings werden mir daher stets als bereichernder Austausch in Erinnerung bleiben. Danke, dass Du mir trotz Deiner Unterstützung ausreichend Raum gelassen hast, um selbst über meine Projekte nachzudenken, Fragestellungen zu entwickeln und Experimente zu planen. Dadurch konnte ich mich zu der Wissenschaftlerin entwickeln, die ich heute bin. Nicht zuletzt danke ich Dir auch dafür, dass Du es mir ermöglicht hast, an vielen verschiedenen Projekten mitzuarbeiten, denn so konnte ich persönlich, wie intellektuell, viel lernen. Ohne Dein entgegengebrachtes Vertrauen hätte ich niemals so viele Dinge ausprobiert und wäre nicht über mich hinausgewachsen. Danke!

Besonders dankbar bin ich auch Prof. Dr. Rosa Lozano-Durán und PD Dr. Marcel Wiermer für das kurzfristige Einspringen als Zweit- bzw. Drittgutachter/in.

Großer Dank gilt auch Prof. Dr. Claudia Oecking, die mir vor allem während Farids krankheitsbedingter Abwesenheit, rund um die Uhr mit Rat und Tat zur Seite stand. Liebe Claudia, ohne Deine Unterstützung, Geduld und weisen Worte, hätte ich einige Aufgaben und Situationen nicht so gut gemeistert bzw. überstanden. Obwohl Du nicht an plant immunity arbeitest, konntest Du mir immer hilfreiche Tipps geben, die mich in die richtige Richtung gelenkt haben. Auch Dein konstruktives Feedback nach meinen Progress Reports schätze ich nach wie vor sehr, da ich mich so von Mal zu Mal verbessern konnte. Zusammenfassend kann ich sagen, dass Du nicht nur eine großartige Wissenschaftlerin mit Vorbildfunktion für mich bist, sondern auch eine hervorragende Mentorin, auf die ich mich zu 100% verlassen kann und dafür bin ich Dir wirklich unendlich dankbar.

Auch möchte ich mich bei meinen TAC Members, Prof. Dr. Klaus Harter und Dr. Andrea Gust, bedanken, die mich während meiner gesamten Doktorarbeit begleitet haben. Liebe Andrea, lieber Klaus, danke für Eure Zeit und den wissenschaftlichen Input, als auch die persönlichen Worte, die Ihr mir regelmäßig mit auf den Weg gegeben habt. Dir, liebe Andrea, bin ich sehr dankbar für Dein Vertrauen und die guten

Ratschläge und Dir, lieber Klaus, für Deine Unterstützung während Farids Abwesenheit und Deine Geduld beim Fertigstellen dieser Arbeit.
Als nächstes möchte ich mich bei allen „langjährigen“ AG El Kasmi lab Members bedanken. Liebe Sruthi, lieber Simon, liebe Christel, liebe Elke, liebe Jutta, danke für die gute Zusammenarbeit und die schönen Momente, die wir zusammen verbracht haben. Besonderer Dank gilt unseren TAs als auch meinen Studenten, die mir immer tatkräftig zur Seite standen. Liebe Christel, liebe Elke, liebe Jutta, lieber Marcel, liebe Sonja, liebe Tamara, liebe Veronika, lieber Frank, Ihr habt die guten Zeiten noch besser und die stressigen Zeiten erträglicher gemacht. Ohne Eure Unterstützung wäre ein Teil meiner Arbeit nicht möglich gewesen.
Großer Dank gilt auch allen AG Oecking lab Members, die mich während der Corona Pandemie in Bay 4 aufgenommen haben. Liebe Lea, liebe Tanja, liebe Atiara, liebe Prabha, liebe Jutta, liebe Andrea, danke für die angenehme Arbeitsatmosphäre, zu der jeder von Euch beigetragen hat. Dir, liebe Lea, bin ich besonders dankbar, dass Du immer ein offenes Ohr für mich hattest und dass wir sowohl im Labor, als auch außerhalb, viel Spaß und eine wunderschöne Zeit zusammen hatten.
Beim gesamten Department für Pflanzenphysiologie, sowie bei allen Gärtnern, möchte ich mich für das gute Miteinander und die Unterstützung bedanken. Auch meinen Kollaborationspartnern danke ich für die gute Zusammenarbeit und das entgegengebrachte Vertrauen. Besonderer Dank gilt Dr. Rory Pruitt für das Korrekturlesen von Teilen dieser Arbeit.
Mein größter Dank gilt meiner Familie und meinen Freunden, die mich auf dem gesamten Weg hier her unterstützt und ertragen haben. Liebe Mama, lieber Papa, ich bin Euch so dankbar, dass Ihr mich mit viel Liebe und Geduld erzogen und mir den respektvollen Umgang mit anderen Menschen gelehrt habt. Danke, dass Ihr immer an mich geglaubt, mich gefördert und mir diese Ausbildung ermöglicht habt. Ohne Eure Rücksicht und Unterstützung wäre diese Arbeit vermutlich noch nicht fertig. Mindestens genauso dankbar bin ich Jenny und Theresa, die immer für mich da waren und mich aufgemuntert haben, wenn es mal nicht so gut lief. Liebe Jenny, liebe Theresa, danke für Eure Unterstützung, Eure Diskussionsbereitschaft rund um die Uhr, die langen Spaziergänge und die wunderschöne Zeit, die wir in den letzten Jahren zusammen verbracht haben. Dank Euch konnte ich in meiner Freizeit vom stressigen Laboralltag abschalten und neue Energie tanken.

Table of contents

I. List of abbreviations

ADP	Adenosine diphosphate
ADPR	Adenosine diphosphate ribose
ADR1	ACTIVATED DISEASE RESISTANCE 1
ADR1-L1	ADR1-LIKE 1
ADR1-L2	ADR1-LIKE 2
ADR1-L3	ADR1-LIKE 3
ATP	Adenosine triphosphate
ATR1	*Arabidopsis thaliana* Recognized 1
BAK1	BRI1-ASSOCIATED RECEPTOR KINASE 1
BiFC	Bimolecular Fluorescence Complementation
BIK1	BOTRYTIS-INDUCED KINASE 1
BKK1	BAK1-LIKE 1
BR	Brassinosteroid
CC	Coiled-coil
CC_R	RPW8-like coiled-coil
CERK1	CHITIN ELICITOR RECEPTOR KINASE 1
CNGC	CYCLIC NUCLEOTIDE-GATED CHANNEL
CNL	CC-type NLR
DAMP	Damage-associated molecular pattern
dATP	Deoxyadenosine triphosphate
EDS1	ENHANCED DISEASE SUSCETIBILITY 1
EFR	EF-TU RECEPTOR
EP	EDS1-PAD4
ER	Endoplasmic reticulum
ETI	Effector-triggered immunity
FLS2	FLAGELLIN SENSITIVE 2
GFP	Green fluorescent protein
GPI	Glycosylphosphatidyl-inositol
GSDMD	Gasdermin D

HeLo	4-helix bundle
HR	Hypersensitive response
LEA14	LATE EMBRYOGENESIS ABUNDANT 14
LORE	LIPOOLIGOSACCHARIDE-SPECIFIC REDUCED ELICITATION
LRR	Leucine-rich repeat
LSD1	LESION SIMULATING DISEASE 1
LysM	Lysin motif
MAPK	MITOGEN-ACTIVATED PROTEIN KINASE
MLKL	MIXED-LINEAGE KINASE DOMAIN-LIKE
NAD	Nicotinamide adenine dinucleotide
NADase	NAD hydrolase
NAM	Nicotinamide
NB	Nucleotide-binding
NDR1	NON-RACE DISEASE RESISTANCE 1
NLR	Nucleotide-binding leucine-rich repeat
NLRC4	NLR Family CARD Domain Containing 4
NLRP3	NOD-, LRR-, and pyrin domain containing protein 3
NRC	NLR REQUIRED FOR CELL DEATH
NRG1	N REQUIREMENT GENE 1
PAD4	PHYTOALEXIN DEFICIENT 4
PAMP	Pathogen-associated molecular pattern
$PBL2^{UMP}$	Uridylated PBS1-LIKE 2
PBL31	PBS1-LIKE 31
PBS1	AvrPphB susceptible 1
PEPR1/2	Perception of the Arabidopsis Danger Signal Peptide 1 or 2
PIP	phosphatidylinositol phosphate
P-loop	Phosphate-binding loop
PM	Plasma membrane
PR1	PATHOGENESIS-RELATED 1
PRR	Pattern-recognition receptor
Pst	*Pseudomonas syringae*
PTI	PAMP-triggered immunity

RAR1	REQUIRED FOR MLA12 RESISTANCE 1
RbohD	Respiratory burst oxidase homolog protein D
RIN4	RPM1 INTERACTING PROTEIN 4
RLCK	Receptor-like cytoplasmic kinase
RLK	Receptor-like kinase
RLP	Receptor-like protein
RNL	CC_R-type NLR
ROQ1	RECOGNITION OF XopQ1
ROS	Reactive oxygen species
RPM1	Resistance to *Pseudomonas syringae* pv*. maculicola* 1
RPP1	Recognition of *Peronospora parasitica* 1
RPP2	Recognition of *Peronospora parasitica* 2
RPP4	Recognition of *Peronospora parasitica* 4
RPS2	RESISTANT TO PSEUDOMONAS SYRINGAE 2
RPS4	RESISTANT TO PSEUDOMONAS SYRINGAE 4
RPS5	RESISTANT TO PSEUDOMONAS SYRINGAE 5
RPW8	RESISTANCE TO POWDERY MILDEW 8
RRS1	RESISTANCE TO RALSTONIA SOLANACEARUM 1
RSK1	RESISTANCE-RELATED KINASE 1
SA	Salicylic acid
sadr	Suppressor of *ADR1-L2*^{D484V}
SAG101	SENESCENCE-ASSOCIATED GENE 101
SERK	SOMATIC-EMBRYOGENESIS RECEPTOR-LIKE KINASE
SGT1	SUPPRESSOR OF G2 ALLELE OF SKP1
SOBIR1	SUPPRESSOR OF BIR1
TIR	Toll-like/Interleukin 1 receptor
Tm-2^2	Tobacco mosaic virus resistance-2^2
TNL	TIR-type NLR
v-cADPR	Variant of cyclic ADPR
WRR4A	WHITE RUST RESISTANCE 4
XopQ	Xanthomonas outer protein Q
ZAR1	HOPZ-ACTIVATED RESISTANCE 1

II. Zusammenfassung

Pflanzen nutzen ein komplexes, rezeptorbasiertes Immunsystem, um sich gegen Angriffe von Krankheitserregern zu wehren. Intrazelluläre NUCLEOTIDE-BINDING LEUCINE-RICH REPEAT (NLR) Proteine erkennen vom Pathogen stammende Effektormoleküle und lösen Abwehrreaktionen aus. Toll/Interleukin-1-Rezeptor-Resistenz (TIR)-Domäne-enthaltende NLRs (TNLs) und Coiled-Coil (CC)-Domäne-enthaltende NLRs (CNLs) stellen die beiden Haupttypen von NLRs dar, die an der Erkennung von Effektoren beteiligt sind und daher als Sensor-NLRs bezeichnet werden. Mehrere CNLs und alle getesteten TNLs benötigen die Anwesenheit einer dritten, evolutionär konservierten Familie von NLRs, der RNL-Klasse, die sich durch eine N-terminale RESISTANCE TO POWDERY MILDEW 8 (RPW8)-ähnliche CC-Domäne (CC_R) auszeichnet. Die RNL-Familie besteht aus zwei Unterfamilien, ACTIVATED DISEASE RESISTANCE 1 (ADR1) und N REQUIREMENT GENE 1 (NRG1). Es ist bekannt, dass Mitglieder beider RNL-Unterfamilien unterhalb von mehreren Sensor-NLRs in *Arabidopsis thaliana* wirken, allerdings sind die spezifischen und redundanten Funktionen von ADR1s und NRG1s weitgehend unbekannt. Wir konnten zeigen, dass ADR1s und NRG1s hauptsächlich als ungleich-redundante Knotenpunkte während der basalen Resistenz und der Sensor-NLR-vermittelten Immunität fungieren, obwohl sie auch eine ausgeprägte Spezifität gegenüber bestimmten Sensor-NLRs aufweisen. Darüber hinaus konnten wir zeigen, dass RNLs Transkriptionsveränderungen vermitteln, die durch TNLs ausgelöst werden. Diese sind den Transkriptionsveränderungen gleich, die durch CNLs induziert werden. Wir schlagen daher vor, dass RNLs ähnlich wie CNLs funktionieren könnten, um Abwehrreaktionen unterhalb von allen TNLs und einigen CNLs zu vermitteln. Unsere Untersuchungen ergaben, dass ADR1s homo- und heterodimerisieren können und dass Mitglieder der ADR1- und NRG1-Unterfamilien für ihre Funktion eine Plasmamembran (PM)-Lokalisierung benötigen. Das entspricht anderen Erkenntnissen, die darauf hinweisen, dass auch RNL-unabhängige CNLs ihre Funktion an der PM ausüben. Bemerkenswerterweise konnten wir auch zeigen, dass RNLs und das RNL-unabhängige CNL Resistance to *Pseudomonas syringae* pv. *maculicola* 1 (RPM1) einen potenziell konservierten Mechanismus für die PM-Lokalisierung nutzen, indem sie direkt an PM-lokalisierte, negativ geladene Phospholipide binden. Die PM-

Lokalisierung von RNLs lässt vermuten, dass sie mit anderen PM-lokalisierten Proteinen interagieren könnten, die für die Pflanzenimmunität wichtig sind. Wir konnten tatsächlich zeigen, dass Mitglieder der ADR1-Unterfamilie mit Rezeptorkinasen interagieren, die für die durch PATTERN RECOGNITION RECEPTOR (PRR) vermittelten Immunreaktionen wichtig sind. Diese Ergebnisse deuten darauf hin, dass ADR1 Proteine an der PRR-vermittelten Immunität beteiligt sein könnten und/oder dass Proteine, die mit der PRR-vermittelten Immunität assoziiert sind, auch für Helfer-NLR-vermittelte Immunantworten erforderlich sein könnten. Wir konnten in der Tat zeigen, dass Mitglieder der ADR1-Familie eine entscheidende Rolle bei der Immunantwort spielen, die durch den PRR RECEPTOR-LIKE PROTEIN 23 (RLP23) vermittelt wird. Darüber hinaus haben wir festgestellt, dass der PRR-Ko-Rezeptor BAK1-LIKE 1 (BKK1) für den Autoimmunphänotyp erforderlich ist, der durch die Expression des autoaktivierten ADR1-LIKE 2 (ADR1-L2^{D484V}) ausgelöst wird. Aus diesen Ergebnissen schließen wir, dass es eine wechselseitige Beziehung zwischen PRR- und NLR-vermittelten Signalwegen gibt, die an dem ADR1-Knotenpunkt zusammenlaufen.

Insgesamt bietet die in dieser Dissertation verfasste Arbeit neue Einblicke in die Funktion und Regulierung von RNLs und eröffnet neue Wege zur Untersuchung der Verbindung zwischen den beiden rezeptorbasierten pflanzlichen Immunitätszweigen - PRR- und NLR-vermittelter Immunität.

III. Summary

Plants use a complex receptor-based immune system to resist pathogen attacks. Intracellular NUCLEOTIDE-BINDING LEUCINE-RICH REPEAT (NLR) proteins recognize pathogen-derived effector molecules to induce defense responses. Toll/interleukin-1 receptor resistance (TIR) domain-containing NLRs (TNLs) and coiled-coil (CC) domain-containing NLRs (CNLs) are the two major types of NLRs involved in effector recognition, and are therefore classified as sensor NLRs. Several CNLs and all tested TNLs require the presence of a third, evolutionary conserved family of NLRs, the RNL class, that is characterized by a N-terminal RESISTANCE TO POWDERY MILDEW 8 (RPW8)-like CC domain (CC_R). The RNL family is formed by two subfamilies, ACTIVATED DISEASE RESISTANCE 1 (ADR1) and N REQUIREMENT GENE 1 (NRG1). While members of both RNL subfamilies are known to act downstream of multiple sensor NLRs in *Arabidopsis thaliana*, the specific and redundant functions of ADR1s and NRG1s are largely unknown. We demonstrated that ADR1s and NRG1s act mainly as unequal redundant nodes during basal resistance and sensor NLR-mediated immunity, albeit they also have distinct specificity towards certain sensor NLRs. Additionally, we showed that RNLs mediate TNL-triggered transcriptional changes that are similar to transcriptional changes induced by CNLs. Therefore, we propose that RNLs function similarly to CNLs to mediate defense responses downstream of all TNLs and some CNLs. Our analyses revealed that ADR1s can homo- and heterodimerize and that members of the ADR1 and NRG1 subfamilies require plasma membrane (PM) localization to function. This is consistent with other findings, indicating that RNL-independent CNLs also function at the PM. Remarkably, we also demonstrated that RNLs and the RNL-independent CNL Resistance to *Pseudomonas syringae* pv*. maculicola* 1 (RPM1) use a potentially conserved mechanism to localize to the PM by directly binding to PM-localized, negatively charged phospholipids. The PM localization of RNLs suggests that they could interact with other PM-localized proteins, important for plant immunity. In fact, we could show that members of the ADR1 subfamily interact with receptor kinases essential for PATTERN RECOGNITION RECEPTOR (PRR)-mediated immune responses. These results suggested that ADR1s might be involved in PRR-mediated

immunity and/or that proteins associated with PRR-mediated immunity could also be required for helper NLR-mediated immune responses. We could indeed demonstrate that ADR1 family members play a critical role in PRR RECEPTOR-LIKE PROTEIN 23 (RLP23)-mediated immunity. Further, we have identified the PRR co-receptor protein BAK1-LIKE 1 (BKK1) as an essential factor for the autoimmune phenotype induced by the expression of the autoactivated ADR1-LIKE 2 (ADR1-L2^{D484V}). Based on these findings we conclude that there is a mutual relationship between PRR- and NLR-mediated signaling that converges on the ADR1 node.

Overall, the work reported in this PhD thesis provides new insights into RNL function and regulation and opens new avenues to study the interconnection of the two receptor-based plant immune branches – PRR- and NLR-mediated immunity.

IV. List of Publications

Accepted manuscripts

2019

Help wanted: helper NLRs and plant immune responses
Jubic, L. M.*, Saile, S. C.*, Furzer, O. J., El Kasmi, F., Dangl, J. L.
*These authors contributed equally to this work.
Current Opinion in Plant Biology. 2019 Aug;50:82-94. doi: 10.1016/j.pbi.2019.03.013.
Review Article

2020

Two unequally redundant "helper" immune receptor families mediate *Arabidopsis thaliana* "sensor" immune receptor functions
Saile, S. C.*, Jacob, P.*, Castel, B., Jubic, L. M., Salas-Gonzáles, I., Bäcker, M., Jones, J. D. G., Dangl, J. L., El Kasmi, F.
*These authors contributed equally to this work.
PLOS Biology. 2020 Sep:18(9): e3000783. doi: 10.1371/journal.pbio.3000783.

2021

The EDS1-PAD4-ADR1 node mediates *Arabidopsis* pattern-triggered immunity
Pruitt, R. N.*, Locci, F.*, Wanke, F., Zhang, L., Saile, S. C., Joe, A., Karelina, D., Hua, C., Fröhlich, K., Wan, W.-L., Hu, M., Rao, S., Stolze, S. C., Harzen, A., Gust, A. A., Harter, K., Joosten, M. H. A. J., Thomma, B. P. H. J., Zhou, J.-M., Dangl, J. L., Weigel, D., Nakagami, H., Oecking, C., El Kasmi, F., Parker, J. E., Nürnberger, T.
*These authors contributed equally to this work.
Nature. 2021.Oct;598:495-499. doi: 10.1038/s41586-021-03829-0

Arabidopsis ADR1 helper NLR immune receptors localize and function at the plasma membrane in a phospholipid dependent manner

Saile, S. C., Ackermann, F. M., Sunil, S., Keicher, J., Bayless, A., Bonardi, V., Wan, L., Doumane, M., Stöbbe, E., Jaillais, Y., Caillaud, M.-C., Dangl, J. L., Nishimura, M. T., Oecking, C., El Kasmi, F.

New Phytologist. 2021 Dec;232:2440-2456. doi: 10.1111/nph.17788

Non-submitted manuscripts

Autoimmunity induced by the Arabidopsis helper NLR ADR1-L2 requires the receptor-like kinase BKK1

Saile, S. C., Bonardi, V., Keicher, J., Wünsch, L. K., Jacob, P., Teixeira P. J. P. L., Dangl, J. L., El Kasmi, F.

V. Personal contributions

Two unequally redundant “helper” immune receptor families mediate Arabidopsis thaliana “sensor” immune receptor functions

Saile and Jacob et al., 2020, PLOS Biology

In this accepted research article, I am listed as equally contributing first author. In collaboration with Pierre Jacob (Dangl lab, UNC, Chapel Hill, USA), Lance Jubic (Dangl lab, UNC, Chapel Hill, USA) and Baptiste Castel (Jones lab, TSL, Norwich, UK), we have systematically compared the *adr1 triple* mutant, the *nrg1 double* mutant and a *helperless* quintuple mutant to characterize RNL function and the genetic interactions between the *ADR1* and *NRG1* subfamilies. Both, the *adr1 triple* mutant (Bonardi *et al.* 2011) and the *nrg1 double* mutant (Castel *et al*. 2019) were published before, whereas the *helperless quintuple* mutant was generated by Baptiste Castel.
I performed bacterial growth curves shown in Figure 1A, 2A, 2C, 3A, S2A, S2B and the conductivity measurements shown in Figure S2F and S2G, with the assistance of Marcel Bäcker. Further, I conducted all cell death assays shown in Figure 2D, 2E, S2C, S2D, S2E. The infection assays with *Alternaria brassicicola* shown in Figure 3D and 3E and the oxidative burst measurements shown in Figure S1 were performed by myself. I carried out statistical analyses for the data presented in Figure 1A, 1B, 2A, 2B, 2C, 3A, 3B, 3C, 3D, S1, S2A, S2B, S2F and S2G. I designed, assembled and edited Figure 1, 2, 3, S1 and S2 as well as Table S1 and Table S2 with contributions from Farid El Kasmi. Moreover, I wrote the material and methods sections for the assays mentioned above and contributed in writing the result sections for “Redundant functions of ADR1 and NRG1 subfamilies in TNL-mediated disease resistance“, „Specific functions of the RNL subfamilies in CNL- and TNL-triggered ETI“, „Unequal redundancy of the RNL families in basal resistance“ and „RNL-independent functions during CNL-triggered ETI“. Further, I was involved in the manuscripts’ revision process.

Saile, S. C., Jacob, P., Jones, J. D. G., Dangl, J. L. and El Kasmi, F. designed research.
Saile, S. C., Jacob, P. and El Kasmi, F. wrote the manuscript.
Saile, S. C., Jacob, P., Castel, B., Jubic, L. M., Salas-Gonzáles, I., Jones, J. D. G., Dangl, J. L. and El Kasmi, F. revised the article.

The EDS1-PAD4-ADR1 node mediates *Arabidopsis* pattern-triggered immunity

Pruitt and Locci et al, 2021, Nature

In this accepted research article, I am listed as co-author. I was involved in generating DNA entry and destination vector constructs (Table 1) and performed co-immunoprecipitation as well as bimolecular fluorescence complementation (BiFC) experiments shown in Extended Data Figure 7B, 7C and 7D.

Pruitt, R. N., Joosten, M. H. A. J, Thomma, B. P. H. J., Dangl, J. L., El Kasmi, F., Parker, J. E. and Nürnberger, T. designed research.
Nürnberger, T. wrote the manuscript.
Pruitt, R. N., Locci, F., Gust, A. A., Joosten, M. H. A. J, Thomma, B. P. H. J., Dangl, J. L., Weigel, D., Parker, J. E. and Nürnberger, T. revised the article.

Table 1: DNA vector constructs used in the manuscript "The EDS1-PAD4-ADR1 node mediates *Arabidopsis* pattern-triggered immunity" (Pruitt and Locci *et al*., 2021).

	Construct	**Name**	**Cloning strategy**
1	*AtADR1 (pDONR221_P3P2)*	Sonja Harter (El Kasmi lab)	*AtADR1*_CDS was amplified with *att*B3 and *att*B2 sites from *AtADR1 pENTR/D-TOPO* (Saile *et al.* 2021) and introduced into *pDONR221_P3P2* vector (Thermo Fisher Scientific) via GATEWAY™ cloning.
2	*AtADR1-L1 (pDONR221_P3P2)*	Sonja Harter (El Kasmi lab)	*AtADR1-L1*_CDS was amplified with *att*B3 and *att*B2 sites from *AtADR1-L1 pDONR221* (Saile *et al.* 2021) and introduced into *pDONR221_P3P2* vector (Thermo Fisher Scientific) via GATEWAY™ cloning.
3	*AtADR1-L2 (pDONR221_P3P2)*	Svenja Saile (El Kasmi lab)	*AtADR1-L2*_CDS was amplified with *att*B3 and *att*B2 sites from *AtADR1-L2 pDONR221* (Saile *et al.* 2021) and introduced into *pDONR221_P1P4* vector

			(Thermo Fisher Scientific) via GATEWAY™ cloning.
4	*AtSOBIR1 (pCR8)*	Weigo Zhang	*AtSOBIR1*_CDS was amplified from Col-0 cDNA.
5	*AtSOBIR1 (pDONR221_P1P4)*	Students of the „Gentechnik Praktikum“ 2018, under supervision of Andrea Gust (Nürnberger lab)	*AtSOBIR1*_CDS was amplified with *att*B1 and *att*B4 sites from construct (4) and introduced into *pDONR221_P1P4* vector (Thermo Fisher Scientific) via GATEWAY™ cloning.
6	*35s::AtADR1-HA (pGWB614)*	Vera Bonardi (Dang lab)	GATEWAY™ LR reaction using *AtADR1 pENTR/D-TOPO* (Saile *et al.* 2021) and *pGWB614* vector (Nakamura *et al.* 2010).
7	*35s::AtADR1-L1-HA (pGWB614)*	Vera Bonardi (Dangl lab)	GATEWAY™ LR reaction using *AtADR1-L1 pDONR221* (Saile *et al.* 2021) and *pGWB614* vector (Nakamura *et al.* 2010).
8	*35s::AtADR1-L2-HA (pGWB614)*	Svenja Saile (El Kasmi lab)	GATEWAY™ LR reaction using *AtADR1-L2 pDONR221* (Saile *et al.* 2021) and *pGWB614* vector (Nakamura *et al.* 2010).
9	*35s::AtSOBIR1-myc-cYFP 35s::AtADR1-HA-nYFP (2in1 BiFC CC)*	Svenja Saile (El Kasmi lab)	GATEWAY™ LR reaction using constructs (5), (1) and *2in1 BiFC CC* vector (Grefen & Blatt 2012; Mehlhorn *et al.* 2018).
10	*35s::AtSOBIR1-myc-cYFP 35s::AtADR1-L1-HA-nYFP (2in1 BiFC CC)*	Svenja Saile (El Kasmi lab)	GATEWAY™ LR reaction using constructs (5), (2) and *2in1 BiFC CC* vector (Grefen & Blatt 2012; Mehlhorn *et al.* 2018).
11	*35s::AtSOBIR1-myc-cYFP 35s::AtADR1-L2-HA-nYFP (2in1 BiFC CC)*	Svenja Saile (El Kasmi lab)	GATEWAY™ LR reaction using constructs (5), (3) and *2in1 BiFC CC* vector (Grefen & Blatt 2012; Mehlhorn *et al.* 2018).

Arabidopsis ADR1 helper NLR immune receptors localize and function at the plasma membrane in a phospholipid dependent manner

Saile et al., 2021, New Phytologist

In this manuscript I am listed as first author. I created RNL entry and destination vector constructs (Table 2) and performed the confocal microscopy analyses shown in Figure 1, 2A, 2C, 2E, 3, S1, S2A, S2B, S2C, S7, S8A, S8C, S8E. Further, I carried out cell death analysis and the corresponding western blots shown in Figure 2A, 4A, 4B, 4D, 4E, 4F, S3, S6A, S9A, S9B, S9C, S9D, S9E. I also performed the degradation experiments and western blots shown in Figure 3B, 3D, 3F, S5, S8B, S8D and S8F. Further, all *in vitro* transcription and translation reactions and PIP strip assays shown in Figure 6 were conducted by myself. I performed subcellular fractionation experiments shown in Figure S2D and S2E. With assistance of Jutta Keicher, I performed co-immunoprecipitation experiments shown in Figure 2C and 2D. With contributions from Farid El Kasmi, I designed, assembled and edited the following Figures: 1, 2, 3, 4, 5, 6, S1, S2, S3, S5, S6, S7, S8, S9 and drew the models shown in Figure 7 and S11. Additionally, I wrote the materials and methods section and revised the text. I was also involved in the manuscripts' revision process.

Saile, S. C., Ackermann, F. M., Nishimura, M. T., El Kasmi F. designed research.
El Kasmi, F. wrote the manuscript with help of Saile, S. C. and Ackermann, F. M.
Saile, S. C., and El Kasmi, F. revised the article with help of Oecking, C.

Table 2: DNA vector constructs used in the manuscript "Arabidopsis ADR1 helper NLR immune receptors localize and function at the plasma membrane in a phospholipid dependent manner" (Saile *et al*. 2021).

	Construct	**Name**	**Cloning strategy**
1	*AtADR1 (pENTR/D-TOPO)*	Vera Bonardi (Dangl lab)	*AtADR1*_CDS with a 5'CACC extension was amplified from Col-0 cDNA and introduced into *pENTR/D-TOPO* vector (Invitrogen) via TOPO® cloning.
2	*AtADR1-L1 (pDONR221_P1P2)*	Vera Bonardi (Dangl lab)	*AtADR1-L1*_CDS was amplified with *att*B1 and *att*B2 sites from Col-0 cDNA and introduced into *pDONR221* vector (Invitrogen) via GATEWAY™ cloning.
3	*AtADR1-L2 (pDONR221_P1P2)*	Vera Bonardi (Dangl lab)	*AtADR1-L2*_CDS was amplified with *att*B1 and *att*B2 sites from Col-0 cDNA and introduced into *pDONR221* vector (Invitrogen) via GATEWAY™ cloning.
4	*AtADR1_CC (1-146 aa) (pDONR207)*	Vera Bonardi (Dangl lab)	*AtADR1_CC* was amplified with *att*B1 and *att*B2 sites from construct (1) and introduced into *pDONR207* vector (Invitrogen) via GATEWAY™ cloning.
5	*AtADR1-L1_CC (1-155 aa) (pDONR207)*	Vera Bonardi (Dangl lab)	*AtADR1-L1_CC* was amplified from construct (2) with *att*B1 and *att*B2 sites and introduced into *pDONR207* vector (Invitrogen) via GATEWAY™ cloning.
6	*AtADR1-L2_CC (1-153 aa) (pDONR207)*	Vera Bonardi (Dangl lab)	*AtADR1-L2_CC* was amplified from construct (3) with *att*B1 and *att*B2 sites and introduced into *pDONR207* vector (Invitrogen) via GATEWAY™ cloning.
7	*AtADR1^{D461V} (pENTR/D-TOPO)*	Svenja Saile (El Kasmi lab)	Site-directed mutagenesis on construct (1).
8	*AtADR1-L1^{D489V} (pDONR221)*	Svenja Saile (El Kasmi lab)	Site-directed mutagenesis on construct (2).
9	*AtADR1-L2^{D484V} (pDONR221)*	Vera Bonardi (Dangl lab)	Site-directed mutagenesis on construct (3).
10	*AtADR1^{212AAA214} (pENTR/D-TOPO)*	Svenja Saile (El Kasmi lab)	Site-directed mutagenesis on construct (1).

11	*AtADR1-L1*^{212AAA214} *(pDONR221)*	Svenja Saile (El Kasmi lab)	Site-directed mutagenesis on construct (2).
12	*AtADR1-L2*^{212AAA214} *(pDONR221)*	Vera Bonardi (El Kasmi lab)	Site-directed mutagenesis on construct (3).
13	*pADR1-L2::AtADR1-L2 (pDONR221)*		Published in (Roberts *et al*. 2013).
14	*pADR1-L1::AtADR1-L1 (pDONR207)*	Svenja Saile (El Kasmi lab)	A 2016 bp *AtADR1-L1* promoter fragment (Wu *et al*. 2020) was amplified from Col-0 genomic DNA with a 5' *att*B1 site and the *AtADR1-L1*_CDS was amplified from construct (2) with a 3' *att*B2 site. *AtADR1-L1* promoter fragment was fused to *AtADR1-L1*_CDS via overlap extension PCR and further introduced into *pDONR207* vector (Invitrogen) via GATEWAY™ cloning.
15	*LI_pADR1 (A-B) (pGEM-T)*	Jutta Keicher (El Kasmi lab)	A 1822 bp *AtADR1* promoter fragment (Wu *et al.* 2020) was amplified with Golden Gate-compatible *Bsa*I overhangs from Col-0 genomic DNA and introduced into the *pGEM®-T* Easy Vector (Promega).
16	*LI_AtADR1 (B-D) (pGEM-T)*	Jutta Keicher (El Kasmi lab)	The *AtADR1*_CDS was amplified with Golden Gate-compatible *Bsa*I overhangs from construct (21) and introduced into the *pGEM®-T Easy* Vector (Promega).
17	*Est::AtADR1-Cit-HA (pMDC7)*	Svenja Saile (El Kasmi lab)	GATEWAY™ LR reaction using construct (1) and a modified *pMDC7* vector (Curtis & Grossniklaus 2003).
18	*Est::AtADR1-L1-Cit-HA (pMDC7)*	Svenja Saile (El Kasmi lab)	GATEWAY™ LR reaction using construct (2) and a modified *pMDC7* vector (Curtis & Grossniklaus 2003).
19	*Est::AtADR1-L2-Cit-HA (pMDC7)*	Svenja Saile (El Kasmi lab)	GATEWAY™ LR reaction using construct (3) and a modified *pMDC7* vector (Curtis & Grossniklaus 2003).

20	*Est::AtADR1-mCherry (pABindmCherry)*	Svenja Saile (El Kasmi lab)	GATEWAY™ LR reaction using construct (1) and the *pABindmCherry* vector (Bleckmann *et al.* 2010).
21	*Est::AtADR1-L1-mCherry (pABindmCherry)*	Svenja Saile (El Kasmi lab)	GATEWAY™ LR reaction using construct (2) and the *pABindmCherry* vector (Bleckmann *et al.* 2010).
22	*Est::AtADR1-L2-mCherry (pABindmCherry)*	Svenja Saile (El Kasmi lab)	GATEWAY™ LR reaction using construct (3) and the *pABindmCherry* vector (Bleckmann *et al.* 2010).
23	*35s::AtADR1-L1-EYFP (pGWB641)*	Svenja Saile (El Kasmi lab)	GATEWAY™ LR reaction using construct (2) and the *pGWB641* vector (Nakamura *et al.* 2010).
24	*35s::AtADR1-L2-EYFP (pGWB641)*	Svenja Saile (El Kasmi lab)	GATEWAY™ LR reaction using construct (3) and the *pGWB641* vector (Nakamura *et al.* 2010).
25	*Est::AtADR1^{D461V}-Cit-HA (pMDC7)*	Svenja Saile (El Kasmi lab)	GATEWAY™ LR reaction using construct (7) and a modified *pMDC7* vector (Curtis & Grossniklaus 2003).
26	*35s::AtADR1^{D461V}-EYFP (pGWB641)*	Svenja Saile (El Kasmi lab)	GATEWAY™ LR reaction using construct (7) and the *pGWB641* vector (Nakamura *et al.* 2010).
27	*Est::AtADR1-L1^{D489V}-Cit-HA (pMDC7)*	Svenja Saile (El Kasmi lab)	GATEWAY™ LR reaction using construct (8) and a modified *pMDC7* vector (Curtis & Grossniklaus 2003).
28	*Est::AtADR1-L2^{D484V}-Cit-HA (pMDC7)*	Svenja Saile (El Kasmi lab)	GATEWAY™ LR reaction using construct (9) and a modified *pMDC7* vector (Curtis & Grossniklaus 2003).
29	*Est::AtADR1^{212AAA214}-mCherry (pABindmCherry)*	Svenja Saile (El Kasmi lab)	GATEWAY™ LR reaction using construct (10) and the *pABindmCherry* vector (Bleckmann *et al.* 2010).
30	*Est::AtADR1-L1^{212AAA214}-mCherry (pABindmCherry)*	Svenja Saile (El Kasmi lab)	GATEWAY™ LR reaction using construct (10) and the *pABindmCherry* vector (Bleckmann *et al.* 2010).

31	*35s::AtADR1-L1^{212AAA214}-EYFP (pGWB641)*	Svenja Saile (El Kasmi lab)	GATEWAY™ LR reaction using construct (11) and the *pGWB641* vector (Nakamura *et al.* 2010).
32	*Est::AtADR1-L2^{212AAA214}-mCherry (pABindmCherry)*	Svenja Saile (El Kasmi lab)	GATEWAY™ LR reaction using construct (12) and the *pABindmCherry* vector (Bleckmann *et al.* 2010).
33	*35s::AtADR1-L2^{212AAA214}-EYFP (pGWB641)*	Svenja Saile (El Kasmi lab)	GATEWAY™ LR reaction using construct (12) and the *pGWB641* vector (Nakamura *et al.* 2010).
34	*Est::AtADR1_CC-Cit-HA (1-146 aa) (pMDC7)*	Svenja Saile (El Kasmi lab)	GATEWAY™ LR reaction using construct (4) and a modified *pMDC7* vector (Curtis & Grossniklaus 2003).
35	*35s::AtADR1_CC-EYFP (1-146 aa) (pGWB641)*	Svenja Saile (El Kasmi lab)	GATEWAY™ LR reaction using construct (4) and the *pGWB641* vector (Nakamura *et al.* 2010).
36	*Est::AtADR1-L1_CC-Cit-HA (1-155 aa) (pMDC7)*	Svenja Saile (El Kasmi lab)	GATEWAY™ LR reaction using construct (5) and a modified *pMDC7* vector (Curtis & Grossniklaus 2003).
37	*35s::AtADR1-L1_CC-EYFP (1-155 aa) (pGWB641)*	Svenja Saile (El Kasmi lab)	GATEWAY™ LR reaction using construct (5) and the *pGWB641* vector (Nakamura *et al.* 2010).
38	*Est::AtADR1-L2_CC-Cit-HA (1-153 aa) (pMDC7)*	Svenja Saile (El Kasmi lab)	GATEWAY™ LR reaction using construct (6) and a modified *pMDC7* vector (Curtis & Grossniklaus 2003).
39	*35s::AtADR1-L2_CC-EYFP (1-153 aa) (pGWB641)*	Svenja Saile (El Kasmi lab)	GATEWAY™ LR reaction using construct (6) and the *pGWB641* vector (Nakamura *et al.* 2010).
40	*pADR1::AtADR1-YFP-tNOS-FASTred (LII_BB10)*	Jutta Keicher (El Kasmi lab)	Golden Gate *Bsa*I cut-ligation using constructs (15), (16), *LI D-E YFP* (Binder *et al.* 2014), *LI E-F nos terminator* (Binder *et al.* 2014) and *LI F-G pFASTred* (Gust, unpublished).
41	*pADR1-L1::AtADR1-L1-EYFP (pGWB640)*	Svenja Saile (El Kasmi lab)	GATEWAY™ LR reaction using construct (14) and the *pGWB640* vector (Nakamura *et al.* 2010).

42	*pADR1-L2::AtADR1-L2-EYFP (pGWB640)*	Svenja Saile (El Kasmi lab)	GATEWAY™ LR reaction using construct (15) and the *pGWB640* vector (Nakamura *et al.* 2010).

Autoimmunity induced by the Arabidopsis helper NLR ADR1-L2 requires the receptor-like kinase BKK1

Saile et al., unpublished

In this manuscript, I am listed as first author. Vera Bonardi initiated and performed together with Farid El Kasmi and Lisa Wünsch the *Suppressor of ADR1-L2^{D484V}* (*SADR)* screen in the Dangl lab (UNC, Capel Hill, USA). Pierre Jacob identified the mutation in the *sadr2* mutant. These results formed the basis of my work presented in this manuscript. All crossed plant lines (F) generated for this study (Table 3) have been created by myself with the technical assistance of Christel Kulibaba-Mattern, Sonja Harter and Jutta Keicher. This includes mainly genetic crossings and technical support with genotyping PCRs. All transgenic plant lines (T, Table 3) were generated by myself, including construct design, cloning, plant transformation and selection. I characterized the mutant phenotypes shown in Figure 1, S1, S2, S3, S4, S5 and S11. Further, I generated most of the DNA constructs used for this study (Table 4) and performed all described experiments: protein-protein-interaction assays shown in Figure 2 and S8, the phosphatase treatment shown in Figure S6, confocal microscopy shown in Figure S7, the subcellular fractionation experiment shown in Figure S9, western blots and RT-PCRs shown in Figure S10. Jutta Keicher isolated RNA and performed cDNA synthesis and RT-PCR of three additional replicates of Figure S10 d. Furthermore, I designed and assembled all figures and wrote the whole manuscript.

Saile, S. C., Bonardi, V. and El Kasmi, F. designed research.
Saile, S.C. wrote the manuscript.
El Kasmi F. revised the article.

Table 3: Plant lines generated for the non-submitted manuscript "Autoimmunity induced by the Arabidopsis helper NLR ADR1-L2 requires the receptor-like kinase BKK1" (Saile *et al.,* unpublished). Note: Not all generated plant lines are present in the current version of the manuscript, but will be the basis of future experiments.

		Plant line	**Generation strategy**
1	F_4	*pADR1-L2::ADR1-L2^{D484V}-HA* (+/+) *adr1-L2-4* (-/-) *bkk1-1* (-/-)	Generated by genetic crossing of *ADR1-L2^{D484V}-HA adr1-L2-4* (Roberts *et al.* 2013) with *bkk1-1* (He *et al.* 2007).
2	F_3	*pADR1-L2::ADR1-L2^{D484V}-HA* (+/+) *adr1-L2-4* (-/-) *sobir1-12* (-/-)	Generated by genetic crossing of *ADR1-L2^{D484V}-HA adr1-L2-4* (Roberts *et al.* 2013) with *sobir1-12* (Gao *et al.* 2009).
3	F_3	*bkk1-1* (-/-) *snc1* (-/-)	Generated by genetic crossing of *bkk1-1* (He *et al.* 2007) with *snc1* (Li *et al.* 2001).
4	F_4	*adr1-1* (-/-) *adr1-L1-1* (-/-) *adr1-L2-4* (-/-) *bkk1-1* (-/-)	Generated by genetic crossing of *adr1 triple* (Bonardi *et al.* 2011) with *bkk1-1* (He *et al.* 2007).
5	F_3	*pADR1-L2::ADR1-L2^{D484V}-HA* (+/-) *adr1-L2-4* (-/-) *bak1-4* (+/-)	Generated by genetic crossing of *ADR1-L2^{D484V}-HA adr1-L2-4* (Roberts *et al.* 2013) with *bak1-4 (Peng et al. 2016).*
6	F_2	*pADR1-L2::ADR1-L2-HA* (+/-) *adr1-L2-4* (+/-) *bkk1-1* (+/-)	Generated by genetic crossing of *ADR1-L2-HA adr1-L2-4* (Roberts *et al.* 2013) with *bkk1-1* (He *et al.* 2007).
7	F_2	*pADR1-L2::ADR1-L2^{D484V}-HA* (+/-) *adr1-L2-4* (+/-) *fls2c* (+/-) *efr-1* (+/-)	Generated by genetic crossing of *ADR1-L2^{D484V}-HA adr1-L2-4* (Roberts *et al.* 2013) with *fls2c efr-1* (Nekrasov *et al.* 2009).
8	T_3	*pADR1-L2::ADR1-L2^{D484V}-HA* (+/+) *pBKK1::BKK1-Myc* (segregating) *adr1-L2-4* (-/-) *bkk1-1* (-/-)	Generated by transforming *pBKK1::BKK1-Myc* (*pGWB16*) into plant line (1).
9	T_3	*pADR1-L2::ADR1-L2^{D484V}-HA* (+/+) *pBKK1::BKK1^{K322E}-Myc* (segregating) *adr1-L2-4* (-/-) *bkk1-1* (-/-)	Generated by transforming *pBKK1::BKK1^{K322E}-Myc* (*pGWB16*) into plant line (1).
10	T_2	*pBKK1::BKK1-Myc* (segregating) *bkk1-1* (-/-)	Generated by transforming *pBKK1::BKK1-Myc* (*pGWB16*) into *bkk1-1* (He *et al.* 2007).

11	T_2	*pBKK1::BKK1^{K322E}-Myc* (segregating) *bkk1-1* (-/-)	Generated by transforming *pBKK1::BKK1^{K322E}-Myc* (*pGWB16*) into *bkk1-1* (He *et al.* 2007).
12	T_2	*pADR1-L2::ADR1-L2^{D484V}-HA* (+/+) *pBKK1::BKK1* (segregating) *adr1-L2-4* (-/-) *bkk1-1* (-/-)	Generated by transforming *pBKK1::BKK1* (*pGWB1*) into plant line (1).
13	T_2	*pADR1-L2::ADR1-L2^{D484V}-HA* (+/+) *pBKK1::BKK1^{K322E}* (segregating) *adr1-L2-4* (-/-) *bkk1-1* (-/-)	Generated by transforming *pBKK1::BKK1^{K322E}* (*pGWB1*) into plant line (1).
14	T_1	*pADR1-L2::ADR1-L2^{D484V}-HA* (+/+) *adr1-L2-4* (-/-) *bkk1*	Generated by transforming *BKK1-KO* (*pDGE347*) into *ADR1-L2^{D484V}-HA adr1-L2-4* (Roberts *et al.* 2013).
15	T_1	*pADR1-L2::ADR1-L2^{D484V}-HA* (+/+) *adr1-L2-4* (-/-) *bak1*	Generated by transforming *BAK1-KO* (*pDGE347*) into *ADR1-L2^{D484V}-HA adr1-L2-4* (Roberts *et al.* 2013).
16	T_1	*pADR1-L2::ADR1-L2^{D484V}-HA* (+/+) *adr1-L2-4* (-/-) *bkk1-1* (-/-) *bak1*	Generated by transforming *BAK1-KO* (*pDGE347*) into plant line (1).
17	T_1	*pADR1-L2::ADR1-L2-EYFP adr1-L2-4*	Generated by transforming *pADR1-L2::ADR1-L2-EYFP* (*pGWB640*) (Saile *et al.* 2021) in *adr1-L2-4* (Bonardi *et al.* 2011).
18	T_1	*pADR1-L2::ADR1-L2^{D484V}-EYFP adr1-L2-4*	Generated by transforming *pADR1-L2::ADR1-L2^{D484V}-EYFP* (*pGWB640*) in *adr1-L2-4* (Bonardi *et al.* 2011).
19	T_1	*pADR1-L2::ADR1-L2-EYFP bkk1-1*	Generated by transforming *pADR1-L2::ADR1-L2-EYFP* (*pGWB640*) (Saile *et al.* 2021) in *bkk1-1 (He et al. 2007).*
20	T_1	*pADR1-L2::ADR1-L2^{D484V}-EYFP bkk1-1*	Generated by transforming *pADR1-L2::ADR1-L2^{D484V}-EYFP* (*pGWB640*) in *bkk1-1 (He et al. 2007).*

Table 4: DNA vector constructs generated for the non-submitted manuscript "Autoimmunity induced by the Arabidopsis helper NLR ADR1-L2 requires the receptor-like kinase BKK1" (Saile *et al.,* unpublished). Note: Not all generated constructs are present in the current version of the manuscript, but will be the basis of future experiments.

	Construct	**Name**	**Cloning strategy**
1	*pBKK1::BKK1 (pUC57)*	Baseclear (Netherlands)	The CDS of *BKK1* (without stop codon) including its native promoter (2065 bp) was synthesized with 5' *attL1* and 3' *attL2* sites into the standard vector *pUC57*.
2	*pBKK1::BKK1^{K322E} (pUC57)*	Baseclear (Netherlands)	The CDS of *BKK1^{K322E}* (without stop codon) including its native promoter (2065 bp) was synthesized with 5' *attL1* and 3' *attL2* sites into the standard vector *pUC57*.
3	*BKK1^{K322E} (pENTR/D-TOPO)*	Svenja Saile (El Kasmi lab)	Site-directed mutagenesis on *BKK1 pENTR/D-TOPO* (Gou *et al.* 2010).
4	*BKK1^{R9K} (pENTR/D-TOPO)*	Svenja Saile (El Kasmi lab)	Site-directed mutagenesis on *BKK1 pENTR/D-TOPO* (Gou *et al.* 2010).
5	*AtADR1-L2 (pDONR221_P1P4)*	Svenja Saile (El Kasmi lab)	*AtADR1-L2*_CDS was amplified with *att*B1 and *att*B4 sites from *AtADR1-L2 pDONR221* (Saile *et al.* 2021) and introduced into pDONR221_P1P4 vector (Thermo Fisher Scientific) via GATEWAY™ cloning.
6	*AtADR1-L2^{D484V} (pDONR221_P1P4)*	Sonja Harter (El Kasmi lab)	Site-directed mutagenesis on construct (5).
7	*BKK1 (pDONR221_P3P2)*	Svenja Saile (El Kasmi lab)	*BKK1*_CDS was amplified with *att*B3 and *att*B2 sites from *BKK1 pENTR/D-TOPO* (Gou *et al.* 2010) and introduced into *pDONR221_P3P2* vector (Thermo Fisher Scientific) via GATEWAY™ cloning.
8	*35s::AtADR1-L2-HA (pGWB614)*		Published in (Pruitt *et al.* 2021).
9	*35s::AtADR1-L2^{D484V}-HA (pGWB614)*	Svenja Saile (El Kasmi lab)	GATEWAY™ LR reaction using *AtADR1-L2^{D484V}* (*pDONR221*) (Saile *et al.* 2021)

			and the *pGWB614* vector (Nakamura *et al.* 2010).
10	*35s::SERK1-Myc (pGWB17)*		Published in (Albert *et al.* 2015)
11	*35s::SERK2-Myc (pGWB17)*		Published in (Albert *et al.* 2015)
12	*35s::SERK3-Myc (pGWB17)*		Published in (Albert *et al.* 2015)
13	*35s::SERK4-Myc (pGWB17)*		Published in (Albert *et al.* 2015)
14	*35s::SERK5-Myc (pGWB17)*		Published in (Albert *et al.* 2015)
15	*35s::BKK1^{K322E}-Myc (pGWB17)*	Svenja Saile (El Kasmi lab)	GATEWAY™ LR reaction using construct (3) and the *pGWB17* vector (Nakamura *et al.* 2010).
16	*35s::BKK1^{R9K}-Myc (pGWB17)*	Svenja Saile (El Kasmi lab)	GATEWAY™ LR reaction using construct (4) and the *pGWB17* vector (Nakamura *et al.* 2010).
17	*35s::BKK1^{K322E}-EYFP (pGWB641)*	Svenja Saile (El Kasmi lab)	GATEWAY™ LR reaction using construct (3) and the *pGWB641* vector (Nakamura *et al.* 2010).
18	*35s::BKK1^{R9K}-EYFP (pGWB641)*	Svenja Saile (El Kasmi lab)	GATEWAY™ LR reaction using construct (4) and the *pGWB641* vector (Nakamura *et al.* 2010).
19	*35s::BKK1-HA-nYFP 35s::ADR1-L2-Myc-cYFP (BiFC 2in1 CC)*	Svenja Saile (El Kasmi lab)	GATEWAY™ LR reaction using constructs (7), (5) and *2in1 BiFC CC* vector (Grefen & Blatt 2012; Mehlhorn *et al.* 2018).
20	*35s::BKK1-HA-nYFP 35s::ADR1-L2^{D484V}-Myc-cYFP (BiFC 2in1 CC)*	Svenja Saile (El Kasmi lab)	GATEWAY™ LR reaction using constructs (7), (6) and *2in1 BiFC CC* vector (Grefen & Blatt 2012; Mehlhorn *et al.* 2018).
21	*35s::ADR1-L2^{D484V}-tRFP (pGWB660)*	Svenja Saile (El Kasmi lab)	GATEWAY™ LR reaction using *ADR1-L2^{D484V} pDONR221* (Saile *et al.* 2021) and

			the *pGWB660* vector (Nakamura *et al.* 2010).
22	*pBKK1::BKK1-Myc (pGWB16)*	Svenja Saile (El Kasmi lab)	GATEWAY™ LR reaction using construct (1) and the *pGWB16* vector (Nakamura *et al.* 2010).
23	*pBKK1::BKK1^{K322E}-Myc (pGWB16)*	Svenja Saile (El Kasmi lab)	GATEWAY™ LR reaction using construct (2) and the *pGWB16* vector (Nakamura *et al.* 2010).
24	*pBKK1::BKK1 (pGWB1)*	Svenja Saile (El Kasmi lab)	GATEWAY™ LR reaction using construct (1) and the *pGWB1* vector (Nakamura *et al.* 2010).
25	*pBKK1::BKK1^{K322E} (pGWB1)*	Svenja Saile (El Kasmi lab)	GATEWAY™ LR reaction using construct (2) and the *pGWB1* vector (Nakamura *et al.* 2010).
26	*pBKK1::BKK1-EYFP (pGWB640)*	Svenja Saile (El Kasmi lab)	GATEWAY™ LR reaction using construct (1) and the *pGWB640* vector (Nakamura *et al.* 2010).
27	*pBKK1::BKK1^{K322E}-EYFP (pGWB640)*	Svenja Saile (El Kasmi lab)	GATEWAY™ LR reaction using construct (2) and the *pGWB640* vector (Nakamura *et al.* 2010).
28	*BAK1-KO (gRNA1+2) (pDGE347)*	Simon Beeh (El Kasmi lab)	*Bsa*I cut-ligation using *BAK1_sgRNA1* (*M1*), *BAK1_sgRNA2* (*M2E*) and *pDGE347* (Ordon *et al.* 2017).
29	*BKK1-KO (gRNA1+2) (pDGE347)*	Svenja Saile (El Kasmi lab)	*Bsa*I cut-ligation using *BKK1_sgRNA1* (*M1*), *BKK1_sgRNA2* (*M2E*) and *pDGE347* (Ordon *et al.* 2017).

1. Introduction

1.1. Plant defense responses

To defend themselves against a wide variety of pathogens, plants have evolved a sophisticated immune system, consisting of both passive and active defense mechanisms. Passive plant defense mechanisms include (i) physical barriers, like the plant cell wall or a waxy cuticle and (ii) chemical barriers, such as secreted enzymatic or toxic components (Osbourn 1996; Isaacson *et al.* 2009; Ramirez *et al.* 2013; Malinovsky *et al.* 2014; Wang *et al.* 2019d). Pathogens that successfully overcome these barriers encounter a complex, receptor-based innate immune system (Figure 1). Activation of this receptor-based immune system initiates a variety of responses that actively combat the invading pathogen, including, amongst others, calcium influxes, the production of reactive oxygen species (ROS) and global transcriptional reprogramming events (Doke 1983; Blume *et al.* 2000; Tao *et al.* 2003; Zipfel *et al.* 2004; Boudsocq *et al*. 2010; Jeworutzki *et al.* 2010; Ranf *et al*. 2011; Nomura *et al*. 2012).

The first layer of the receptor-based immune system is formed by plasma membrane (PM) localized pattern-recognition receptors (PRRs) that perceive highly conserved microbial structures, known as pathogen-associated molecular patterns (PAMPs) or endogenous signals that are released from damaged cells, termed damage-associated molecular patterns (DAMPs) (Gomez-Gomez & Boller 2000; Huffaker *et al.* 2006; Zipfel *et al.* 2006; Miya *et al.* 2007; Galletti *et al.* 2011; Albert *et al.* 2015; Saijo *et al.* 2018). Immune signaling initiated by PAMP or DAMP recognition leads to PAMP-triggered immunity (PTI). Adapted pathogens, however, have evolved effector molecules that are secreted into the apoplast or translocated into plant cells to counteract the induction of PTI and promote virulence (He *et al.* 1993; Gopalan *et al.* 1996; Van den Ackerveken *et al.* 1996; Whisson *et al*. 2007; Gohre *et al.* 2008; Gimenez-Ibanez *et al*. 2009; Macho *et al.* 2014).

To recognize effector molecules, plants have evolved intracellular immune receptors, so called nucleotide-binding leucine-rich repeat (NLR) proteins (El Kasmi 2021). Effector-triggered activation of NLRs results in effector-triggered immunity (ETI) (Jones & Dangl 2006), a robust immune response often associated with a localized cell death

at the infection site, termed hypersensitive response (HR) (Balint-Kurti 2019). Increasing evidence suggests, that several effector-perceiving NLRs (“sensor” NLRs) depend on the presence of members of a certain NLR subfamily, termed “helper” NLRs, to induce (auto-) immunity (Bonardi *et al.* 2011; Dong *et al.* 2016; Wu *et al.* 2017; Castel *et al.* 2018; Wu *et al.* 2019). In solanaceous plant species, members of the helper NLR family NLR REQUIRED FOR CELL DEATH (NRC), were found to form redundant key nodes downstream of multiple, phylogenetically-related sensor NLRs that also exhibit some specificity towards their sensor NLR partners (Wu *et al.* 2017; Wu *et al.* 2018). This suggests that helper NLRs and their corresponding sensor NLRs form a complex and robust genetic network in *Solanaceae* that may help the plant to circumvent suppression by pathogen effectors. Likewise, the *Arabidopsis thaliana* (hereafter Arabidopsis) ACTIVATED DISEASE RESISTANCE 1 (ADR1) and N REQUIREMENT GENE 1 (NRG1) helper NLR families are required for several, genetically-unliked sensor NLRs (Bonardi *et al.* 2011; Dong *et al.* 2016; Castel *et al.* 2019; Wu *et al.* 2019). Whether ADR1s and NRG1s form similar networks with their sensor NLR partners in Arabidopsis, as described for the *Solanaceae*-specific NRC helper NLR family, remains to be determined.

Although the plant receptor-based immune system was historically separated into PTI and ETI, there is increasing evidence suggesting a crosstalk and cooperation between both, extracellular and intracellular, immune receptor systems, since many downstream responses are activated by both PRR- and NLR-mediated signaling (Tsuda & Katagiri 2010; Lu & Tsuda 2021). However, if and how exactly PRR- and NLR-mediated signaling pathways are mechanistically linked is still unclear and under heavy investigation.

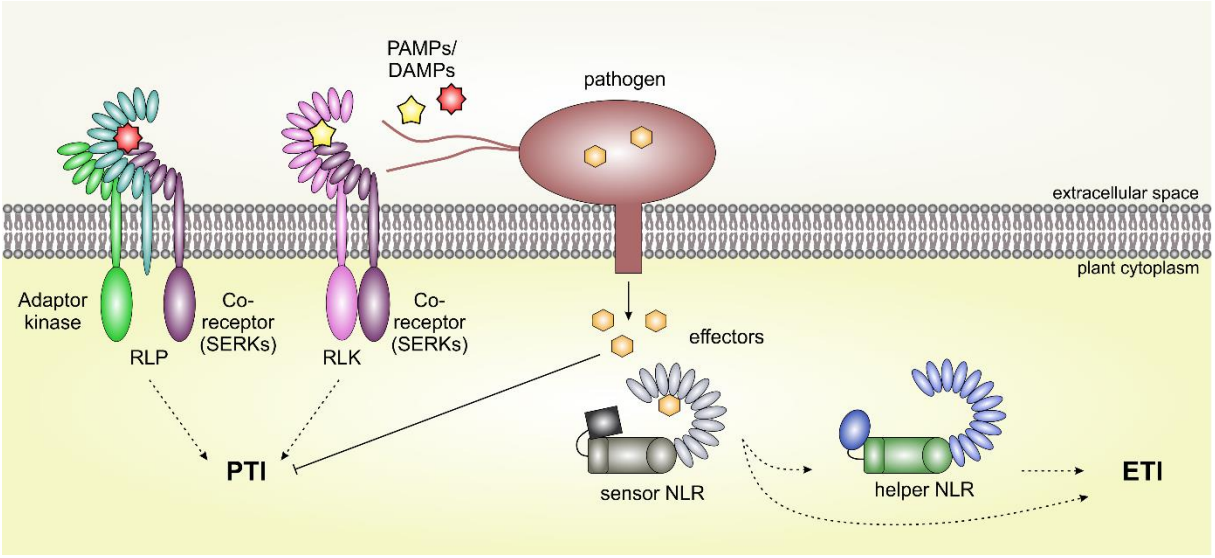

Figure 1: **Core principles of plant receptor-based immunity.** Plants detect pathogens by recognizing conserved pathogen-associated molecular patterns (PAMPs) or damage-associated molecular patterns (DAMPs) that are released from damaged host cells via plasma-membrane localized receptor-like kinases (RLKs) or receptor-like proteins (RLPs). As RLPs lack an intracellular kinase domain, they constitutively associate with an adaptor kinase. Following ligand binding, both RLPs and RLKs interact with a co-receptor, e.g., a RLK of the SOMATIC EMBRYOGENESIS RECEPTOR KINASE (SERK) family, to trigger PAMP-triggered immunity (PTI). Adapted pathogens deliver effector molecules into the plant to suppress PTI. Resistant plants evolved intracellular nucleotide binding leucine-rich repeat (NLR) receptors (sensor NLRs) that perceive effector presence or function and either initiate effector-triggered immunity (ETI) on their own or in cooperation with a certain NLR subfamily, termed helper NLRs. Note: Proteins and molecules are not drawn to scale.

1.2. PRR-mediated immune signaling

1.2.1. Diversity of PRR structural domains

All PRRs described in plants to date are either receptor-like kinases (RLKs) or receptor-like proteins (RLPs) (Couto & Zipfel 2016). RLKs are multi-domain proteins that carry a signal peptide for PM localization at their N-terminus, followed by an extracellular ligand-binding domain, a transmembrane domain and a cytoplasmic kinase domain that controls downstream signaling. RLPs share a similar modular architecture but, on the contrary, lack an intracellular kinase domain (Albert *et al.* 2020; Wang & Chai 2020). PRRs possess a variety of extracellular domains including leucine-rich repeat (LRR) domains, lysin motifs (LysMs) or lectin-like motifs that determine ligand-binding specificity (Albert *et al.* 2020). LRR-containing PRRs typically bind peptides or proteins. Some of the best studied plant LRR-RLKs include Arabidopsis FLAGELLIN SENSITIVE 2 (FLS2) and EF-TU RECEPTOR (EFR) that perceive conserved domains of bacterial flagellin or of the bacterial elongation factor EF-Tu, respectively (Gomez-Gomez & Boller 2000; Kunze *et al.* 2004; Zipfel *et al.*

2006). In contrast, LysM-type RLKs, like the co-receptor CHITIN ELICITOR RECEPTOR KINASE 1 (CERK1), interact with carbohydrate-based ligands, such as fungal chitin or bacterial peptidoglycan and trigger immunity against both fungal and bacterial pathogens (Miya *et al.* 2007; Willmann *et al.* 2011). The lectin-receptor like PRR LIPOOLIGOSACCHARIDE-SPECIFIC REDUCED ELICITATION (LORE), on the other hand, perceives bacterial 3-hydroxy fatty acids (Kutschera *et al.* 2019). Given the various ligand-binding domains, PRRs can recognize diverse PAMPs and DAMPs and initiate PTI to effectively combat most non-adapted pathogens (Jones & Dangl 2006; Albert *et al.* 2020).

1.2.2. Activation and signaling mechanisms of PRRs

Although PRRs differ in their extracellular domains as well as in the presence of a kinase domain, their activation and signaling mechanisms follow similar processes (Figure 2). PRRs recognize and bind their corresponding ligands through their extracellular domains (Albert *et al.* 2010; Sun *et al*. 2013). Upon ligand binding, PRRs rely on the association with a co-receptor to initiate downstream signaling. LRR-RLKs that belong to the SOMATIC-EMBRYOGENESIS RECEPTOR-LIKE KINASE (SERK) family are common co-receptors shared by many LRR-type PRRs (Ma *et al.* 2016). Formation of the PRR/co-receptor core complex leads to a series of auto- and/or trans-phosphorylation events that are required to trigger PTI (Schulze *et al*. 2010; Yan *et al.* 2012; Cao *et al*. 2013; Sun *et al.* 2013). In the case of RLPs, which lack a kinase domain, a constitutively associated adaptor kinase mediates these phosphorylation events (van der Burgh *et al.* 2019). Hence, RLP/adaptor kinase complexes are considered to act equivalently to RLKs (Gust & Felix 2014), albeit they have been found to induce both overlapping and distinct immune outputs (Wan *et al*. 2019b). These findings suggest that RLK- and RLP-mediated signaling likely rely on different downstream components.

To translate ligand binding into downstream responses, PRR/co-receptor complexes phosphorylate other intracellular proteins, such as receptor-like cytoplasmic kinases (RLCKs) (Lu *et al.* 2010a; Lu *et al.* 2010b; Zhang *et al.* 2010). The RLCK BOTRYTIS-INDUCED KINASE 1 (BIK1) interacts with FLS2 and EFR and promotes LRR-RLK-induced PTI (Zhang *et al.* 2010). Interestingly, BIK1 inhibits RLP-dependent PTI

responses (Wan *et al.* 2019b). To date, RLCKs that have a positive role in RLP-mediated PTI are not described.

In terms of LRR-RLK-mediated PTI, it was shown that following ligand binding, the co-receptor SERK3, also known as BRI1-ASSOCIATED RECEPTOR KINASE 1 (BAK1), directly phosphorylates BIK1 and thereby causes the dissociation of BIK1 from FLS2 to activate downstream signaling pathways (Lu *et al.* 2010b; Zhang *et al.* 2010; Lin *et al.* 2014). Upon activation, BIK1 directly phosphorylates the NADPH oxidase Respiratory burst oxidase homolog protein D (RbohD) and thereby promotes ROS production (Li *et al.* 2014), which not only is important for local programmed cell death, but also function as a second messenger inducing the expression of defense genes and stomatal closure, both aiming at restricting pathogen entry and growth (Levine *et al.* 1994; Orozco-Cardenas *et al.* 2001; Mersmann *et al.* 2010). In addition, BIK1 phosphorylates and activates calcium-permeable cyclic nucleotide-gated channels (CNGCs) to trigger calcium (or ion) influx into the cytosol (Tian *et al.* 2019; Wang *et al.* 2019b). Like ROS, calcium functions as a second messenger that stimulates downstream processes, such as defense gene expression (Levy *et al.* 2005; Wang *et al.* 2019b). Furthermore, RLCKs are linked to the activation of mitogen-activated protein kinases (MAPKs) (Feng *et al.* 2012). MAPKs transmit PRR/ligand binding signals via phosphorylation cascades onto downstream targets, such as transcription factors, that induce transcriptional reprogramming events (Djamei *et al*. 2007; Bethke *et al.* 2009; Mao *et al.* 2011; Kang *et al.* 2015). Although, many immune responses induced by RLPs are similar to the ones induced by LRR-RLKs, they can differ in timing and amplitude (Wan *et al.* 2019b). In addition, activation of RLP23 results in the production of the phytoalexin camalexin, which is not observed upon activation of LRR-RLKs (Wan *et al.* 2019b).

Together, ligand binding to a cognate PRR results in a dynamic association/disassociation of PRRs with co-receptors and RLCKs, involving a series of phosphorylation events and thereby inducing downstream immune signaling that triggers multiple defense responses. Although RLK and RLP receptor complexes share a similar architecture, they mediate similar, but also distinct immune outputs. These findings suggest that RLKs and RLPs rely – at least partially - on different downstream signaling components.

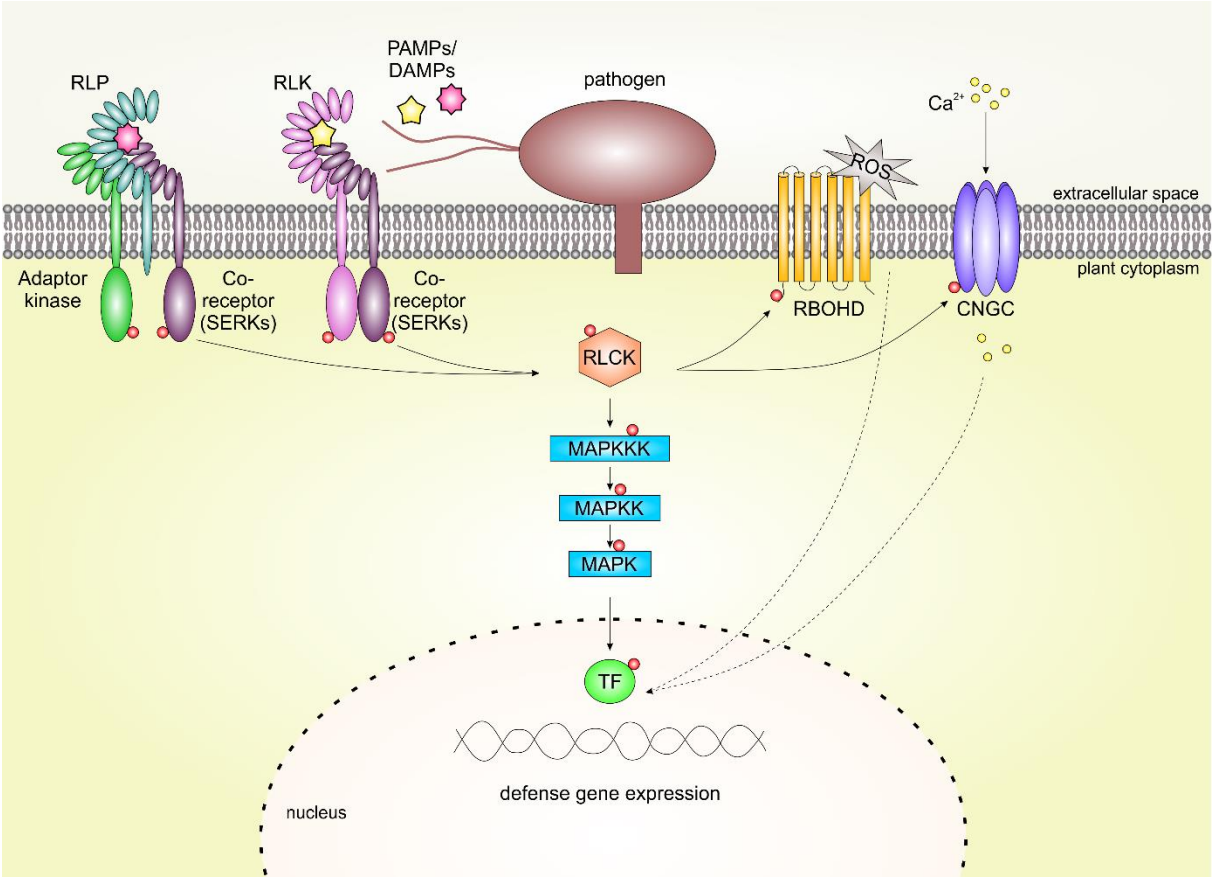

Figure 2: Core principles of PRR-mediated immune signaling. Plasma-membrane localized pattern recognition receptors (PRRs), including receptor-like kinases (RLKs) and receptor-like proteins (RLPs), detect conserved pathogen-associated molecular patterns (PAMPs) or damage-associated molecular patterns (DAMPs). The latter are produced and released by the plant in response to cellular damage during a pathogen attack. Since RLPs lack an intracellular kinase domain, they require a constitutive interaction with an adaptor kinase for the induction of downstream immune signaling. Upon ligand binding, both RLPs and RLKs recruit and interact with a co-receptor, such as a RLK of the SOMATIC EMBRYOGENESIS RECEPTOR KINASE (SERK) family and activate immune signaling by auto- and transphosphorylation (red dots) of their kinase domains. The activated co-receptor phosphorylates and releases downstream receptor-like cytoplasmic kinases (RLCKs). RLCKs phosphorylate and activate (i) the NADPH oxidase RBOHD that is involved in reactive oxygen species (ROS) production, (ii) CYCLIC NUCLEOTIDE GATED CHANNEL (CNGC) proteins that allow calcium (Ca^{2+}) influx, and (iii) MITOGEN ACTIVATED PROTEIN KINASE (MAPK) cascades. Once activated, MAPKs directly phosphorylate and activate transcription factors (TFs) that induce the expression of defense genes. ROS and Ca^{2+} act as second messengers that also contribute to defense gene expression. Note: Proteins and molecules are not drawn to scale.

1.2.3. PRR co-receptors BAK1 and BKK1

BAK1 and BAK1-LIKE 1 (BKK1) belong to the small SERK family that comprises five members in Arabidopsis (Hecht *et al.* 2001). By interacting with various LRR-type RLKs and RLPs (Chinchilla *et al.* 2007; Roux *et al.* 2011; Albert *et al.* 2015; Du *et al.* 2015; Postma *et al.* 2016; Saur *et al*. 2016), SERK proteins are considered to act as shared convergence points connecting multiple RLK-signaling networks involved in plant immunity, growth and development (Li 2010). BKK1 is the closest paralog of BAK1 (He *et al.* 2007), and accordingly, both proteins share common functions in (i)

brassinosteroid (BR) signaling (Li *et al.* 2002; He *et al.* 2007; Gou *et al.* 2012), (ii) FLS2-, EFR- and Perception of the Arabidopsis Danger Signal Peptide 1 or 2 (PEPR1/2)-mediated immune signaling (Roux *et al.* 2011), (iii) HAESA- and HAESE-LIKE 2-mediated floral organ abscission (Meng *et al.* 2016) and (iv) immunity-associated cell death control (He *et al.* 2007). Remarkably, genetic data demonstrated that *BAK1* is the most important SERK in BR- and PTI-signaling, since *bak1* single mutants displayed impaired BR and immune phenotypes that were not observed in a *bkk1* single mutant (He *et al.* 2007; Roux *et al.* 2011; Zhang *et al.* 2013). *BKK1* function was only observed in the absence of *BAK1*, since *bak1 bkk1* double mutants showed an enhanced phenotype compared to each single mutant (He *et al.* 2007; Roux *et al.* 2011). This suggests that most of the interacting LRR-RLKs might favour the co-receptor BAK1 over BKK1.

Given their important function as key regulators in PTI, it is not surprising that BAK1 and BKK1 are targeted by multiple pathogen-derived effectors, including AvrPto, AvrPtoB, HopF2 and HopB1 (Shan *et al.* 2008; Cheng *et al.* 2011; Zhou *et al.* 2014; Li *et al.* 2016). By interfering with SERK/PRR interactions or by causing SERK degradation, these effectors successfully dampen PTI signaling (He *et al.* 2006; Shan *et al.* 2008; Li *et al.* 2016).

BAK1 and BKK1 have been described as redundant negative regulators of cell death, because the simultaneous loss-of-function of both *BAK1* and *BKK1* results in a cell death phenotype reminiscent of NLR-mediated autoimmune phenotypes (He *et al.* 2007; Wu *et al.* 2020). Interestingly, *bak1 bkk1*-induced cell death was recently indeed linked to NLR-mediated signaling, as the genetic loss of the *ADR1* helper NLR subfamily significantly suppressed the *bak1 bkk1* cell death phenotype (Wu *et al.* 2020). These findings highlight the interconnection of PRR- and NLR-mediated signaling pathways.

1.3. NLR-mediated immune signaling

1.3.1. NLR domains

NLRs are modular proteins that are usually composed of a variable N-terminal domain, followed by a central nucleotide-binding (NB) domain and a C-terminal LRR domain (Figure 3) (El Kasmi & Nishimura 2016; El Kasmi 2021). NLRs can be grouped into three classes depending on their N-terminal domains: (i) Toll-like/Interleukin 1 receptor (TIR)-type NLRs (TNLs), (ii) coiled-coil (CC)-type NLRs (CNLs) and (iii) RESISTANCE TO POWDERY MILDEW 8 (RPW8)-like coiled-coil (CC_R)-type NLRs (RNLs) (Shao *et al.* 2016). While most TNLs and CNLs act as effector-specific sensors, RNLs function downstream of many sensor NLRs and help translating effector recognition into immune responses (Peart *et al.* 2005; Bonardi *et al.* 2011; Qi *et al.* 2018; Castel *et al.* 2019; Wu *et al.* 2019). Thus, RNLs are also referred to as helper NLRs (Bonardi *et al.* 2011).

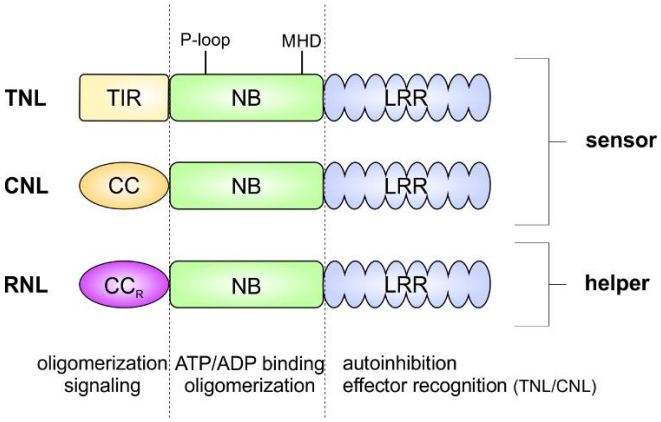

Figure 3: Domain structure of plant NLRs. NLRs display a conserved modular architecture and consist of a variable N-terminal domain, a central nucleotide-binding (NB) domain and a C-terminal leucine-rich repeat (LRR) domain. The Phosphate-binding loop (P-loop) and the methionine-histidine-aspartate (MHD) motif are highly conserved regions that are required for nucleotide binding. NLRs are grouped into three classes depending on their N-terminal domains: Toll-like/Interleukin1 receptor (TIR) NLRs (TNLs), coiled-coil (CC) NLRs (CNLs) and RESISTANCE TO POWDEREY MILDEW 8 (RPW8)-like coiled-coil NLRs (RNLs). Most TNLs and CNLs are involved in effector recognition (sensor NLRs), whereas RNLs act as helpers downstream of sensor NLRs. Note: Domains are not drawn to scale.

1.3.2. Activation mechanisms of NLRs

As NLRs are multi-domain proteins, each domain fulfils specific functions. The central NB domain serves as a molecular switch that is considered to turn full-length NLRs on or off by regulating adenosine triphosphate (ATP) and adenosine diphosphate (ADP) binding, respectively (Tameling *et al.* 2002; Tameling *et al.* 2006; Maekawa *et al.* 2011; Williams *et al.* 2011). There are two highly conserved regions within the NB domain that regulate nucleotide binding. The Phosphate-binding loop (P-loop) is a glycine-rich

loop that contains a highly conserved lysine residue required for binding the β- and γ-phosphates of nucleotides (Tameling *et al.* 2002). Mutations in the P-loop result in reduced nucleotide binding (Tameling *et al.* 2002) and consequently, cause loss-of-function of several NLRs (Peart *et al.* 2005; Mestre & Baulcombe 2006; Roberts *et al.* 2013; Lolle *et al.* 2017). On the contrary, a highly conserved methionine-histidine-aspartate (MHD) motif is coupled with gain-of-function phenotypes. In particular, the exchange of D to valine (V) disrupts ADP binding and thereby renders NLRs constitutively active (Tameling *et al.* 2006; van Ooijen *et al.* 2008; Gao *et al.* 2011; Williams *et al.* 2011; Roberts *et al.* 2013; Wang *et al.* 2019c; Wu *et al.* 2019). To avoid ectopic activation, the NB domain is sterically occluded by the C-terminal LRR domain, promoting a “closed” confirmation and thereby, inhibiting ADP/ATP exchange (Bonardi *et al.* 2012; Hu *et al.* 2013; Bernoux *et al.* 2016; Wang *et al.* 2019c). Deletion of the LRR domain has been shown to render several NLRs autoactive, highlighting its important role as an autoinhibitory domain (Ade *et al.* 2007; Qi *et al.* 2018). Besides its regulatory function, the LRR domain is attributed to effector recognition, which in some, but not all, cases happens through direct binding (Jia *et al.* 2000; Shen *et al.* 2003; Krasileva *et al.* 2010; Ravensdale *et al.* 2012; Ma *et al.* 2020; Martin *et al.* 2020). A direct interaction between a LRR domain and an effector has been demonstrated for example for the rice NLR Pi-Ta and the Arabidopsis NLR *Recognition of Peronospora parasitica* 1 (RPP1) with their corresponding effectors AvrPi-Ta from *Magnaporthe oryzae* and *Arabidopsis thaliana* Recognized 1 (ATR1) from *Hyaloperonospora arabidopsidis*, respectively (Jia *et al.* 2000; Krasileva *et al.* 2010; Ma *et al.* 2020). Interestingly, ATR1 does not only bind to the RPP1 LRR domain but additionally to a C-terminal jelly roll/Ig-like domain that is found in many other TNLs (Ma *et al.* 2020). Remarkably, a number of sensor NLR proteins have genetically incorporated additional domains into their structure to allow direct effector recognition (Deslandes *et al.* 2002; Ortiz *et al.* 2017). These domains normally mimic true effector targets and hence, are termed integrated decoys (Cesari *et al.* 2014a). In most cases, however, NLRs indirectly recognize their cognate effectors by (i) either sensing the action of their corresponding effectors via monitoring the integrity of the effector’s host target (guardee) (Dangl & Jones 2001) or by (ii) guarding decoys that mimic effector host targets (Zipfel & Rathjen 2008). It is proposed that indirect effector recognition

mechanisms have evolved to enable a broad pathogen-recognition spectrum with a limited repertoire of NLRs (Cesari 2018).

Pathogen recognition results in intramolecular conformational changes that cause the activation of the NLR (Wang *et al.* 2019c; Martin *et al.* 2020) and consequently, initiates immune signaling. Interestingly, not all activated NLRs may require ATP binding for their signaling function, as effector-activated RPP1 was found to be bound to ADP (Ma *et al.* 2020).

1.3.3. Oligomerization in NLR signaling

The N-terminal domains of NLRs are considered to be the “signaling domains”, as over-expression of several TIR, CC and CC_R domains is sufficient to trigger cell death (Swiderski *et al.* 2009; Bernoux *et al*. 2011; Collier *et al.* 2011; Maekawa *et al.* 2011; Williams *et al.* 2011; Baudin *et al.* 2017). Self-association or oligomerization of the N-terminal domains is proposed to be required for immune signaling, as mutants that lose their capability to self-associate display an impaired cell death and resistance function (Krasileva *et al.* 2010; Bernoux *et al.* 2016; Casey *et al*. 2016; Cesari *et al*. 2016; El Kasmi *et al*. 2017; Zhang *et al*. 2017; Wang *et al*. 2019a). This is further supported by findings showing that fusion of green fluorescent protein (GFP; or GFP derivatives), which can form weak dimers, to the C-terminal end of N-terminal NLR domains can act to support or stabilize their self-association (Krasileva *et al.* 2010). These data suggest that oligomerization is a central mechanism of NLR signaling.

The long-proposed role of oligomerization in plant NLR signaling was recently confirmed by the structures of three full-length plant NLRs in their activated states (Wang *et al.* 2019a; Wang *et al.* 2019c; Ma *et al.* 2020; Martin *et al.* 2020). In the presence of ATP/deoxyadenosine triphosphate (dATP), the Arabidopsis CNL HOPZ-ACTIVATED RESISTANCE 1 (ZAR1) was shown to form a pentameric complex composed of five protomers, each consisting of ZAR1 and its partner proteins, the pseudokinase RESISTANCE-RELATED KINASE 1 (RSK1) and the uridylated decoy protein PBS1-LIKE 2 ($PBL2^{UMP}$) (Wang *et al.* 2019a). The pentameric complex adapted a wheel-like structure and was termed ZAR1 resistosome (Wang *et al.* 2019a). Interestingly, the very N-terminal α-helix of the ZAR1 CC domain was found to be exposed in the resistosome and all five exposed α1-helices folded into a funnel-shaped

structure that was required for membrane association, cell death and resistance against *Xanthomonas campestris* pv*. campestris* (Wang *et al.* 2019a). Just recently, it was shown that the ZAR1 resistosome forms a cation-selective channel at the PM that is permeable to calcium (Bi *et al.* 2021). Calcium influx into the cytosol is essential for the activation of plant immune responses, not only by NLRs (Steinhorst & Kudla 2013) and thus, regulating ion homeostasis could be a conserved mechanism among NLRs (CNLs) to induce defense responses.

In contrast to the CNL ZAR1, the *Nicotiana benthamiana* (hereafter *N. benthamiana*) TNL RECOGNITION OF XopQ 1 (ROQ1) as well as the Arabidopsis TNL RPP1 were found to form a tetrameric resistosome when bound to their cognate effectors Xanthomonas outer protein Q (XopQ) and ATR1, respectively (Ma *et al.* 2020; Martin *et al.* 2020). Complex assembly brought the TIR domains into close proximity and resulted in either the opening or creation of a nicotinamide adenine dinucleotide (NAD) hydrolase (NADase) active site (Ma *et al.* 2020; Martin *et al.* 2020). TIR domains were demonstrated to have oligomerization-dependent NADase activity that is required for cell death induction (Horsefield *et al.* 2019; Wan *et al.* 2019a). NAD^+ cleavage by plant TIR domains resulted in the generation of nicotinamide (NAM), adenosine diphosphate ribose (ADPR) and a variant of cyclic ADPR (v-cADPR) (Wan *et al.* 2019a). Thus, TNL resistosomes have been proposed to act as effector-inducible holoenzymes for NAD^+ hydrolysis. ADPR and cADPR are known to act as second messengers that activate calcium-permeable channels and promote intracellular calcium fluxes (Wu *et al.* 1997; Fliegert *et al.* 2007; Fliegert *et al.* 2017). Whether and how the generated cleavage products activate (downstream) immune signaling components in plants is, however, still under investigation.

1.3.4. Downstream signaling components of NLR-triggered immunity

Together with biochemical data, the recent release of the first full-length plant NLR structures confirmed that some NLRs, and most likely all, signal via oligomerization. The N-terminal domain seems to determine the mechanism by which immune signaling is further activated. There is another striking difference in how the two types of sensor NLRs, CNLs and TNLs, activate immunity. TNL-mediated ETI requires lipase-like proteins of the ENHANCED DISEASE SUSCETIBILITY 1 (EDS1) family and RNL

helper NLRs (Aarts *et al.* 1998; Bonardi *et al.* 2011; Wagner *et al.* 2013; Qi *et al.* 2018; Castel *et al.* 2019; Wan *et al.* 2019a). In contrast, only some CNLs also require RNLs and many rely on the integrin-like protein NON-RACE DISEASE RESISTANCE 1 (NDR1) for the proper induction of immune responses (Century *et al.* 1995; Century *et al.* 1997; Bonardi *et al.* 2011; Castel *et al.* 2019). Thus, many sensor NLRs cooperate with various key immune regulators to mediate full ETI (Figure 4).

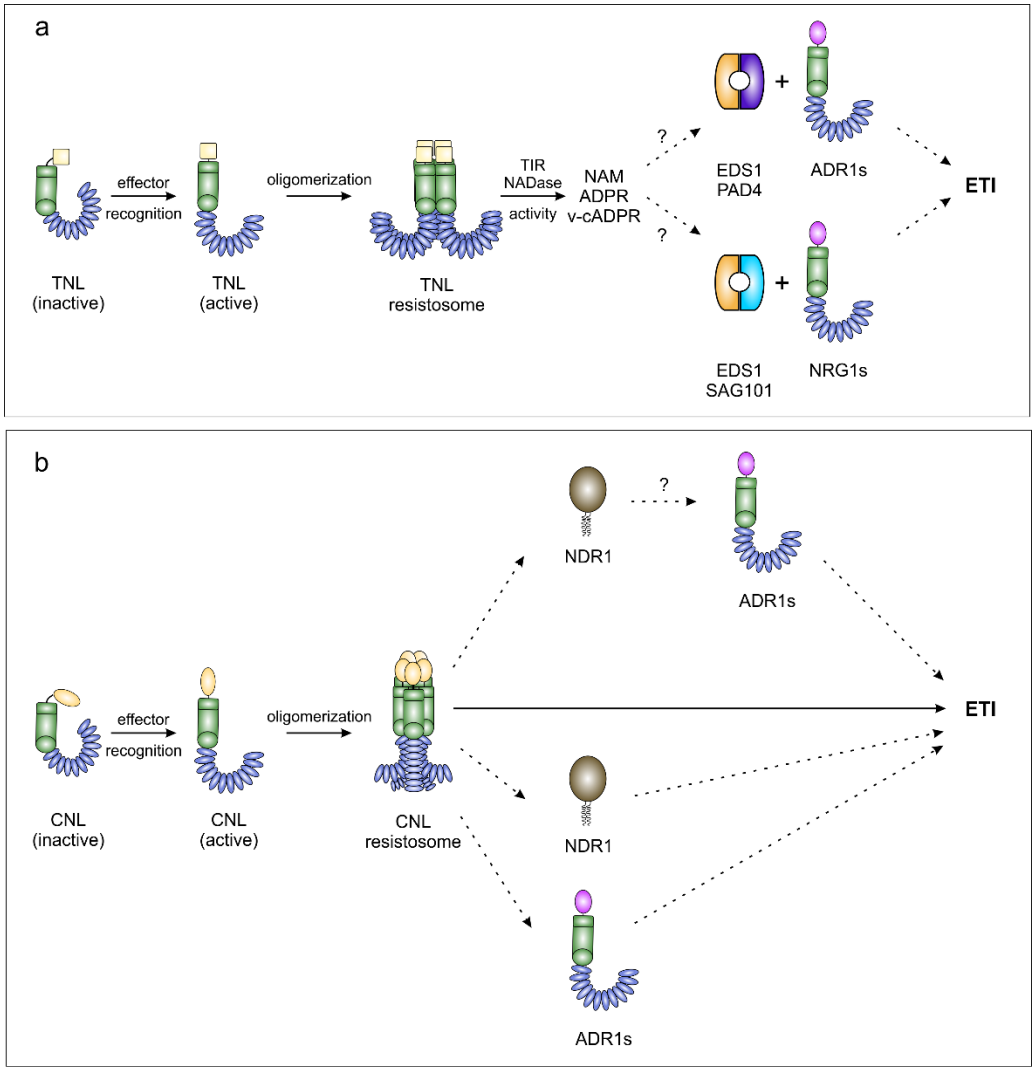

Figure 4: Core principles of NLR-mediated immune signaling. (a) TNL-mediated immune signaling. Pathogen effector recognition by TNLs triggers their self-association and the formation of a tetrameric complex (holoenzyme). This results in the generation or opening of a NADase active site within the TIR domains. NAD^+ hydrolysis leads to the accumulation of the signaling molecules nicotinamide (NAM), adenosine diphosphate ribose (ADPR) and a variant of cyclic ADPR (v-cADPR). The generated cleavage products might activate EDS1-PAD4 or EDS1-SAG101 that signal together with the ADR1 or NRG1 helper NLR subfamily, respectively, to induce ETI. **(b)** CNL-mediated immune signaling. Pathogen effector recognition by CNLs triggers their self-association and – in the case of the Arabidopsis CNL ZAR1 - the formation of a pentameric complex (resistosome). Little is known about the pathways or signaling components downstream of CNLs. ZAR1 (and maybe other CNLs as well) form calcium-permeable channels at the plasma-membrane. Others require NDR1 and/or ADR1s to induce ETI. How exactly NDR1 and ADR1s function downstream of CNLs is, however, still unclear. Note: Domains and proteins are not drawn to scale.

1.3.4.1. Helper NLRs

In order to adapt to evolving pathogens, plants have evolved a complex immune signalling network that contributes to the fine-tuning of defense responses (Smakowska-Luzan *et al.* 2018; Wu *et al.* 2018; Adachi *et al*. 2019b). How this molecular network is constructed in detail is far from being understood. Helper NLRs, however, seem to play a central role as they assist multiple sensor NLRs to translate pathogen recognition into immune responses (Peart *et al.* 2005; Gabriels *et al.* 2007; Bonardi *et al.* 2012; Castel *et al.* 2019; Wu *et al.* 2019). Unlike genetically linked NLR pairs, such as the Arabidopsis RESISTANCE TO PSEUDOMONAS SYRINGAE 4 (RPS4) - RESISTANCE TO RALSTONIA SOLANACEARUM 1 (RRS1) pair or the rice RGA4-RGA5 pair, where one NLR senses the effector and the other executes the defense signaling via physically interacting with each other (Cesari *et al*. 2014b; Huh *et al.* 2017), helper NLRs of the RNL family are capable of transducing signals from multiple, genetically unlinked sensor NLRs (Bonardi *et al.* 2011; Castel *et al.* 2019; Wu *et al.* 2019). Since RNLs have thus far not been shown to physically interact with sensor NLRs, it remains an open question how exactly sensor NLRs transduce effector recognition to helper NLRs.

To date, three small and evolutionary conserved helper NLR groups have been described in plants, all being CC-type NLRs: *ADR1*, *NRG1* and *NRC* (Peart *et al.* 2005; Gabriels *et al.* 2007; Bonardi *et al.* 2011; Collier *et al.* 2011; Wu *et al.* 2017). Members of the *ADR1* and *NRG1* gene families can be found in most angiosperms, whereas the *NRC* family is limited to solanaceous plant species (Collier *et al.* 2011; Wu *et al.* 2017). Based on their N-terminal CC_R domains, the ADR1 and NRG1 proteins form an evolutionary distinct subclade, the RNLs (Collier *et al.* 2011). Since the work reported in this thesis is focused on the ADR1 and NRG1 helper NLRs, the following parts of the introduction are centred exclusively on the *ADR1* and *NRG1* gene families, and not on the *NRC* helper NLRs.

1.3.4.1.1. ADR1s

ADR1 was originally identified in Arabidopsis in an activation-tagging screen for dominant mutants exhibiting an enhanced expression of the defense marker gene *PATHOGENESIS-RELATED 1* (*PR1*) (Grant *et al.* 2003). Overexpression of *ADR1* resulted in severe dwarfism, leaf curling, salicylic acid (SA) accumulation and enhanced resistance against biotrophic pathogens (Grant *et al.* 2003) as well as in enhanced drought tolerance (Chini *et al*. 2004).

In Arabidopsis, the *ADR1* family is comprised of four members, namely *ADR1*, *ADR1-LIKE 1* (*ADR1-L1*), *ADR1-LIKE 2* (*ADR1-L2*) and *ADR1-LIKE 3 (ADR1-L3)* (Grant *et al.* 2003). While *ADR1-L3* encodes for a N-terminally truncated protein, which thus far has no reported function in immunity (Wu *et al.* 2021a), ADR1, ADR1-L1 and ADR1-L2 act redundantly as helper NLRs (Bonardi *et al.* 2011). Accordingly, they support several CNLs and TNLs during ETI, but are also required for autoimmunity induced by autoactivating mutations of several NLRs (Bonardi *et al.* 2011; Dong *et al.* 2016). Additionally, ADR1s are involved in the accumulation of the defense hormone SA during basal resistance (Bonardi *et al.* 2011). As basal resistance is defined as the combination of residual PTI (following effector-induced suppression) and weak ETI (Laflamme *et al.* 2020), it could be possible that ADR1s might also be involved in PRR-induced immune responses, besides their function in NLR-mediated immunity. Interestingly, members of the NRC family, the solanaceous-specific helper NLRs, have been reported to function additionally downstream of several PRRs (Gabriels *et al.* 2007; Wu *et al.* 2016; Leibman-Markus *et al.* 2018; Kourelis *et al.* 2021). Therefore, it appears to be likely that ADR1s might also be involved in PRR-mediated immunity and thus, could form a key signaling node connecting PRR- and NLR-induced signaling cascades.

Although the exchange of ADP for ATP is thought to represent the most likely mode of NLR activation, “helper functions” during ETI were reported to be P-loop independent (at least shown for ADR1-L2) and hence, did not rely on nucleotide binding (Bonardi *et al.* 2011). In contrast, a functional P-loop was required for ADR1-L2’s function in promoting the SA-induced propagation of the unregulated runaway cell death in a mutant defective in *LESION SIMULATING DISEASE 1 (LSD1*) (Roberts *et al.* 2013). How ADR1s regulate the *lsd1*-induced runaway cell death and how exactly they

function downstream of several sensor NLRs is largely unknown and thus, awaits further investigation.

The overexpression of *ADR1s* results in the constitutive activation of immune responses (Grant *et al.* 2003; Nasim *et al.* 2020; Wu *et al.* 2020), similar to the phenotype observed for transgenic plants expressing the autoactivated MHD mutant of *ADR1-L2* (*ADR1-L2*^{D484V}) under the control of its native promoter (Roberts *et al.* 2013). This indicates, that the expression and activity of ADR1s are tightly controlled. Indeed, a tight regulation has been reported for ADR1-L2 on the transcriptional level. The *ADR1-L2* transcript level was found to be directly regulated by nonsense-mediated mRNA decay in a temperature-dependent manner to avoid the inappropriate induction of immune signaling in the absence of pathogens (Nasim *et al.* 2020). Additionally, transcriptional regulation of the autoactivated *ADR1-L2*^{D484V} and ADR1 was found to be partially SA-dependent, with SA inducing the expression of *ADR1-L2*^{D484V} and ADR1 (Grant *et al.* 2003; Roberts *et al.* 2013). Unfortunately, there is no information on how ADR1s are regulated on the protein level, as the chaperone proteins SUPPRESSOR OF G2 ALLELE OF SKP1 (SGT1) and REQUIRED FOR MLA12 RESISTANCE 1 (RAR1) were found to be dispensable for the autoactivity of ADR1 CC_R or ADR1-L2^{D484V}, respectively (Collier *et al.* 2011; Roberts *et al.* 2013). In summary, although ADR1s constitute important players in plant innate immunity, the molecular mechanisms underlying their activity and signaling function remain largely unknown.

1.3.4.1.2. NRG1s

NRG1 was initially identified in *N. benthamiana* in a virus-induced gene silencing screen for mutants that were compromised in TNL N-mediated resistance against the tobacco mosaic virus (Peart *et al.* 2005). While the *N. benthamiana* genome encodes two copies of *NRG* (*NbNRG1* and *NbNRG2*), of which *NbNRG2* is considered to be a pseudogene (Peart *et al.* 2005), the Arabidopsis *NRG1* family is comprised of three paralogs: *AtNRG1.1*, *AtNRG1.2* and the 3'- truncated gene *AtNRG1.3* (Collier *et al.* 2011). Although NbNRG1 is known to function downstream of TNLs for more than a decade (Peart *et al.* 2005; Qi *et al.* 2018), just recently, with the introduction of the CRISPR/Cas9 technology, AtNRG1 proteins have been assigned a clear helper

function in Arabidopsis (auto-) immunity (Castel *et al.* 2019; Lapin *et al.* 2019; Wu *et al.* 2019). AtNRG1.1 and AtNRG1.2 were found to act redundantly downstream of many TNLs (Castel *et al.* 2019; Wu *et al.* 2019). It is worth noting that *NRG1* family members are absent in plant lineages lacking TNLs, confirming an important and evolutionary conserved role of NRG1s in TNL-mediated signaling pathways (Meyers *et al.* 1999; Collier *et al.* 2011). This also applies to the lipase-like protein SENESCENCE-ASSOCIATED GENE 101 (SAG101) (Wagner *et al.* 2013; Gantner *et al.* 2019), which together with EDS1 and NRG1, contributes to TNL-mediated immunity (Gantner *et al.* 2019; Lapin *et al.* 2019; Sun *et al.* 2021). Remarkably, neither AtNRG1.1 nor AtNRG1.2 require a functional P-loop for their helper function in *chilling sensitive 3-2D*-mediated autoimmunity (Wu *et al.* 2019). In contrast, NbNRG1 was shown to depend on a functional P-loop for its function in ROQ1-mediated cell death (Qi *et al.* 2018). The differential requirement of nucleotide binding might be based on differences in TNL-mediated autoimmunity versus pathogen effector recognition induced TNL-mediated cell death. This hypothesis is supported by the observation that AtNRG1.1 requires a functional P-loop for interacting with EDS1-SAG101 in TNL-mediated immunity induced by effector recognition (Sun *et al.* 2021). Despite their important function in TNL-mediated immunity, it is, however, still largely unclear how exactly NRG1.1 and NRG1.2 transduce sensor NLR-mediated effector recognition into downstream immune responses and whether they share their functions equally with their counterpart, the ADR1 subfamily.

Interestingly, the truncated paralog AtNRG1.3 was shown to negatively regulate the function of AtNRG1.1 and AtNRG1.2 in TNL-mediated (auto-)immune signaling when overexpressed, likely by interfering with EDS1-SAG101-NRG1.1/.2 complex formation (Wu *et al.* 2021a). These results suggest that AtNRG1.3 might have an opposite role compared to its full-length paralogs. Likewise, overexpression of *NbNRG2* antagonized the function of NbNRG1 in TNL ROQ1-mediated cell death (Wu *et al.* 2021a). However, it is questionable if these results are of biological relevance, as the antagonistic function of both *AtNRG1.3* and *NbNRG2* was only apparent when the genes were overexpressed.

1.3.4.2. EDS1, PAD4 and SAG101

EDS1, *PHYTOALEXIN DEFICIENT 4* (*PAD4*) and *SAG101* constitute a small family of genes encoding lipase-like proteins that have co-evolved with NLRs, in particular TNLs and RNLs (Gantner *et al.* 2019; Baggs *et al.* 2020). EDS1 family members are characterized by a N-terminal lipase-like domain and a unique C-terminal EDS1-PAD4 (EP) domain (Wagner *et al.* 2013). EDS1 forms exclusive heterodimers with either PAD4 or SAG101 to mediate different immune outputs (Wagner *et al.* 2013). Upon dimerization of EDS1 with PAD4 or EDS1 with SAG101, the interface between the EP domains forms a cavity that is required for TNL-mediated signaling and hence, proposed to be a signaling surface (Bhandari *et al.* 2019). Given their co-occurrence with TNLs, it is not surprising that all tested TNLs were found to signal through EDS1-PAD4 and/or EDS1-SAG101 to trigger (auto-) immunity (Aarts *et al.* 1998; Xu *et al.* 2015; Qi *et al.* 2018; Gantner *et al.* 2019; Lapin *et al.* 2019). Apart from their role in TNL-mediated immunity, the EDS1-PAD4 complex functions additionally in basal immunity (Venugopal *et al.* 2009; Cui *et al*. 2017).

Genetic data demonstrated that EDS1-PAD4 act in concert with the ADR1 helper NLR family, whereas EDS1-SAG101 function together with the NRG1s (Lapin *et al.* 2019; Sun *et al.* 2021). This genetic interaction was recently corroborated by a strict physical interaction of EDS1-PAD4 with ADR1s and EDS1-SAG101 with NRG1s upon effector-driven TNL activation (Sun *et al.* 2021; Wu *et al.* 2021b). Notably, EDS1-PAD4-ADR1s as well as EDS1-SAG101-NRG1s seem to only function together when they come from the same plant genus, as AtEDS1 and AtSAG101 have been demonstrated to be unable to work together with NbNRG1 (Gantner *et al.* 2019; Lapin *et al.* 2019). These results suggest that the EDS1 and RNL families have co-evolved differently in distinct plant lineages to regulate TNL-mediated immunity (Lapin *et al.* 2019).

In summary, the EDS1-PAD4-ADR1s and EDS1-SAG101-NRG1s complexes represent distinct signaling modules that serve as downstream signaling hubs for TNLs. Additionally, EDS1-PAD4-ADR1s are also required for basal immunity against virulent pathogens and thus, might also function during PRR-mediated immunity.

1.3.4.3. NDR1

Like EDS1, NDR1 is a conserved downstream regulator of NLR-mediated signaling (Century *et al.* 1995; Century *et al.* 1997; Aarts *et al.* 1998; Tornero *et al.* 2002). NDR1 is required for immunity mediated by many, but not all CNLs (Century *et al.* 1995; Aarts *et al.* 1998) and shares predicted structural homology with the Arabidopsis integrin-like protein LATE EMBRYOGENESIS ABUNDANT 14 (LEA14) (Knepper *et al.* 2011). In mammalian cells, integrins play crucial roles in signal transduction by perceiving environmental signals that are further transduced inside the cell (Shyy & Chien 2002). Arabidopsis NDR1 localizes to the PM via a C-terminal glycosylphosphatidyl-inositol (GPI) anchor and a N-terminal transmembrane domain (Coppinger *et al.* 2004). GPI anchoring is a common mechanism shared by many eukaryotic organisms to tether proteins to the cell surface (Saha *et al*. 2016). Given its presumably apoplastic localization, NDR1 was proposed to act as a transducer of pathogen-derived signals via directly interacting with pathogenic components (Coppinger *et al.* 2004). The very N-terminal part of NDR1 was predicted to be localized in the cytosol and was shown to interact with the RPM1 INTERACTING PROTEIN 4 (RIN4) in Arabidopsis (Day *et al.* 2006), which is guarded by the CNLs Resistance to *Pseudomonas syringae* pv. *maculicola* 1 (RPM1) and RESISTANT TO PSEUDOMONAS SYRINGAE 2 (RPS2) (Mackey *et al.* 2002; Axtell *et al.* 2003). NDR1/RIN4 interaction is required for RPS2-mediated cell death (Day *et al.* 2006). Likewise, NDR1-like proteins were found to associate with RIN4 at the PM in soybean, and additionally, were shown to bind pathogen-derived effector molecules to inhibit their virulence activities in plants lacking cognate sensor NLRs (Selote *et al*. 2014). Hence, NDR1-like proteins might function in transducing extracellular pathogen-derived signals into the cell and thus represent a critical node for the activation of plant innate immunity. How exactly NDR1 is linked to some CNL-mediated immune responses in Arabidopsis remains, however, elusive.

2. Aims of this work

2.1. Determining the overlapping and unique functions of RNLs

Saile and Jacob et al., 2020, PLOS Biology

NLR proteins are intracellular immune receptors that recognize the presence or activity of pathogen-derived effector molecules and subsequently induce ETI, a robust immune response restricting pathogen proliferation and propagation (El Kasmi 2021). There is emerging evidence that several NLRs require members of a certain NLR subclade, the RNL helper NLRs, to initiate ETI or autoimmunity (Peart *et al.* 2005; Dong *et al.* 2016; Wu *et al.* 2017; Qi *et al.* 2018; Castel *et al.* 2019; Wu *et al.* 2019). The Arabidopsis genome encodes two RNL subfamilies, *ADR1s* and *NRG1s* (Collier *et al.* 2011). Despite their essential roles in plant innate immunity, information on the specific, redundant and synergistic functions of RNLs is still scarce. By characterizing *adr1 triple*, *nrg1 double* and a *helperless quintuple* mutant, this project aims at delineating RNL specificity during both PTI and ETI on a genetic and a transcriptional scale.

2.2. Elucidating the molecular mechanism regulating the subcellular localization of ADR1s

Saile et al., 2021, New Phytologist

Activation of NLRs results in ETI that is often associated with a local cell death response at the infection site. Several NLRs have been demonstrated to require oligomerization and, in some cases, PM localization to induce cell death (Krasileva *et al.* 2010; Gao *et al.* 2011; Qi *et al.* 2012; Cesari *et al.* 2016; El Kasmi *et al.* 2017; Wang *et al.* 2019a; Wang *et al.* 2020). Although ADR1s are critical components involved in plant innate immunity, their subcellular localization as well as the molecular mechanism that regulates their localization has not yet been analysed. Homology modelling proposed that CC_R domains share structural similarities with the 4-helix bundle (HeLo) domain of the mammalian cell death executor protein MIXED-LINEAGE KINASE DOMAIN-LIKE (MLKL) (Bentham *et al.* 2018; Jubic *et al.* 2019) that also requires oligomerization and PM localization for its cell death function (Dondelinger *et*

al. 2014). Interestingly, a stretch of positively charged amino acids on the surface of the MLKL HeLo domain interacts with negatively charged phosphatidylinositol phosphates (PIPs) that promotes MLKL recruitment to the plasma membrane (Dondelinger *et al.* 2014). Based on the predicted structural homology of CC_R domains and the MLKL HeLo domain (Jubic *et al.* 2019), it is likely that cell death induced by activated ADR1s might also rely on oligomerization and PM localization, which might be mediated by the interaction with phospholipids. Thus, this project aims at investigating (i) the subcellular localization of ADR1 family members pre-and post-activation, (ii) how their subcellular localization is regulated and (iii) whether ADR1s oligomerize upon activation.

2.3. Uncovering the mechanistic link between PRR- and NLR-mediated signaling pathways

Pruitt and Locci et al., 2021, Nature

RNLs cooperate with key immune regulators to trigger immunity. NRG1 helper NLRs were shown to act in concert with the lipase-like proteins EDS1 and SAG101 in ETI, whereas ADR1 helper NLRs function together with EDS1 and PAD4 during ETI and basal immunity (Lapin *et al.* 2019; Sun *et al.* 2021). Given their function in basal immunity, it is likely that EDS1-PAD4-ADR1s might also be involved in PRR-mediated immune responses and thus, could act as an integration point for PRR- and NLR-mediated signaling pathways. Remarkably, as ADR1s mainly localize to the PM (Saile *et al.* 2021), they could be directly linked to PRRs or PRR-associated proteins. Therefore, this project addresses genetically and biochemically, whether, how and where PTI signaling components are mechanistically linked with the EDS1-PAD4-ADR1 signaling module.

2.4. Identifying and characterizing ADR1-L2^{D484V} regulators

Saile et al., unpublished

Under unchallenged conditions, NLRs are low abundance proteins that have important functions in surveillance. During pathogen infection, NLRs, including ADR1s, are strongly upregulated in order to respond quickly and robustly to the invading pathogen (Grant *et al.* 2003; Nasim *et al.* 2020). It is, however, still unclear how exactly ADR1s get activated and how they signal downstream to initiate immune responses. The expression of the autoactivated *ADR1-L2^{D484V}* causes autoimmunity that is associated with a reduced plant size in Arabidopsis (Roberts *et al.* 2013). Thus, transgenic plants expressing *ADR1-L2^{D484V}* represent a useful tool for forward genetic screens. To uncover regulators of ADR1-L2^{D484V}, and hence, to learn more about the regulatory mechanisms underlying RNL activity, a forward genetic screen for *suppressors of ADR1-L2^{D484V}* (*sadr*) was performed in the Dangl lab by Vera Bonardi and Farid El Kasmi. From this screen, around 200 suppressor lines were identified, including *sadr2,* which carries a point mutation in the LRR-RLK *BKK1.* This project aims at confirming *BKK1* as a positive regulator of ADR1-L2^{D484V}-mediated autoimmunity and further seeks to reveal whether *BKK1* is a specific or common regulator of NLR-mediated (auto-) immune responses. Moreover, this project tries to address the molecular mechanism underlying the regulation of ADR1-L2^{D484V} by BKK1.

3. Results

3.1. Two unequally redundant "helper" immune receptor families mediate *Arabidopsis thaliana* "sensor" immune receptor functions

Saile, S. C.*, Jacob, P.*, Castel, B., Jubic, L. M., Salas-Gonzáles, I., Bäcker, M., Jones, J. D. G., Dangl, J. L., El Kasmi, F.

*These authors contributed equally to this work.

PLOS Biology. 2020 Sep:18(9): e3000783. doi: 10.1371/journal.pbio.3000783.

RNLs are phylogenetically divided into two subfamilies, the ADR1s, with three functional members, ADR1, ADR1-L1 and ADR1-L2, and the NRG1s, with two functional full-length members, NRG1.1 and NRG1.2. Both, ADR1s and NRG1s were shown to act as helper NLRs in Arabidopsis by transducing sensor NLR-mediated effector recognition into ETI (Bonardi *et al.* 2011; Castel *et al.* 2019; Wu *et al.* 2019). However, since most previous studies were based on the characterization of either Arabidopsis *adr1 triple* or *nrg1 double/triple* mutants, the extent of functional redundancy between RNL subfamilies was not clearly defined. In Saile and Jacob *et al*. (2020), we have systematically analysed and compared immune responses during pathogen infections in *adr1 triple*, *nrg1 double* and a *helperless quintuple* mutant to broaden our understanding of the specific and redundant functions of the ADR1 and NRG1 subfamilies. Our extensive analyses revealed a very interesting observation: For basal resistance against a coronatine-deficient *Pseudomonas syringae* (*Pst*) DC3000 strain and for resistance responses mediated by the TNL pair RPS4-RRS1 and the TNL RECOGNITION OF PERONOSPORA PARASITICA 2 (RPP2), both RNL subfamilies are required in an unequally redundant manner, with a predominant role for the ADR1s. Thus, the ADR1 and NRG1 subfamilies function as unequal redundant nodes during basal- and certain TNL-mediated resistance responses. Apart from their redundant functions, we found that both RNL subfamilies also have specific functions in some CNL- and TNL-mediated ETI responses. We could demonstrate that ADR1s are specifically required for CNL RPS2- and RESISTANT TO PSEUDOMONAS SYRINGAE 5 (RPS5)- and TNL RECOGNITION OF PERONOSPORA PARASITICA 4 (RPP4)-mediated resistance as well as for the timely activation of RPS2-triggerd HR. In contrast, NRG1s are fully and specifically required for RPS4-RRS1-induced HR.

Since both ADR1s and NRG1s are able to induce disease resistance and HR, we propose that the specific requirement of either the ADR1 or NRG1 subfamily depends on the preferential use of the activated sensor NLR. How this is mechanistically achieved is not known and awaits further investigation.

We further could demonstrate that several sensor NLRs, exclusively CNLs, do not rely on the presence of RNLs for their function during ETI. In particular, disease resistance and HR induced by the CNLs RPM1 and ZAR1 and HR triggered by the CNL RPS5 do not require RNLs.

Interestingly, our time-resolved RNA-sequencing analyses demonstrated that RNLs play a prominent role in transcriptional reprogramming during TNL-induced ETI and are also partially required for all tested CNL-triggered transcriptional changes, especially at the onset of ETI. Their function in transcriptional regulation is mostly shared between both RNL subfamilies, although about one third of the genes that were upregulated in an RNL-dependent manner during ETI, were found to be specifically regulated by either the ADR1 or NRG1 subfamily. This, however, can also be largely ascribed to their unequal, redundant functions, as our gene ontology analyses revealed that genes specifically regulated by the ADR1 subfamily were associated with the same functional categories as genes controlled specifically by the NRG1s. This indicates that ADR1s and NRG1s regulate the same categories of genes during ETI. Remarkably, genes that were transcriptionally regulated by the RNLs during TNL-mediated ETI, were also regulated during CNL-mediated ETI, however, mainly in an RNL independent manner (effects were only observed quantitatively). This leads to the suggestion that RNLs act like CNLs in effector-activated and TNL-induced transcriptional reprogramming and that RNLs impact, quantitatively, CNL-mediated ETI responses.

In summary, our detailed analyses of pathogen-induced immune responses in the *adr1 triple*, *nrg1 double* and *helperless quintuple* mutants revealed that both RNL subfamilies (i) are involved in basal resistance, (ii) are fully required for TNL-mediated ETI and (iii) contribute to defense activation during CNL-mediated signaling. We propose that specific functions of the ADR1 and NRG1 subfamilies might be based on molecular properties, such as interaction partners or their subcellular localization.

3.2. Arabidopsis ADR1 helper NLR immune receptors localize and function at the plasma membrane in a phospholipid dependent manner

Saile, S. C., Ackermann, F. M., Sunil, S., Keicher, J., Bayless, A., Bonardi, V., Wan, L., Doumane, M., Stöbbe, E., Jaillais, Y., Caillaud, M.-C., Dangl, J. L., Nishimura, M. T., Oecking, C., El Kasmi, F.

New Phytologist. 2021 Dec;232:2440-2456. doi: 10.1111/nph.17788

Although NLRs are key components of the plant innate receptor-based immune system, their molecular mode of action is poorly understood. Recently, it was shown that activated Arabidopsis CNL ZAR1 oligomerizes and forms calcium-permeable channels at the PM (Wang *et al.* 2019a; Bi *et al.* 2021). As RNLs form a small subclass of CNLs, they might use similar or identical mechanisms to induce immune signaling/cell death. In support of this idea, it has been proposed that CC_R domains share structural similarity with the cell death inducing N-terminal HeLo domain of the mammalian cell death executor protein MLKL (Jubic *et al.* 2019), which requires oligomerization and PM localization for cell death induction (Dondelinger *et al.* 2014). Since many PM-localized NLRs have no predicted transmembrane domain or lipidation motifs, the molecular determinants of PM association of NLRs remain elusive.

In Saile *et al.* (2021) we show that the ADR1s, a RNL subfamily, and the CNL RPM1 localize to the PM by directly interacting with negatively charged, polyacidic phospholipids and that they trigger cell death at the PM. Cell biological and biochemical analyses revealed that ADR1, ADR1-L1 and ADR1-L2 mainly localize to the PM in an activation-independent manner, albeit ADR1 can additionally be found at the endoplasmic reticulum (ER).

The PM is known to be highly electronegative in eukaryotes (Yeung *et al.* 2006; Simon *et al.* 2016) and phosphatidylinositol-4-phosphate (PI4P) is mainly responsible for the electronegativity of the plant PM (Simon *et al.* 2016). Interestingly, by using different genetic systems that specifically cause the depletion of either PI4P or phosphatidylinositol 4,5 bisphosphate $PI(4,5)P_2$ at the PM (Simon *et al.* 2016; Doumane *et al.* 2021), we found that the PM association of the ADR1s and the CNL RPM1 depend on PM PI4P but not PM $PI(4,5)P_2$, indicating that the electronegative

charge of the PM is required for the PM localization of the ADR1s and RPM1. Accordingly, depleting PI4P at the PM resulted in the degradation of RPM1, ADR1-L1 and ADR1-L2 and mis-localization of ADR1 and ADR1s CC_R domains. Mis-localized ADR1 and ADR1s CC_R domains were not functional anymore, as demonstrated by their impaired cell death activity. These data clearly demonstrate that ADR1s execute their cell death activity at the PM. In lipid overlay assays, ADR1s CC_R domains and the RPM1 CC domain directly bound to negatively charged phospholipids characterized by polyacidic head groups, supporting the idea that the PM association of ADR1s and RPM1 is regulated by the direct association with phospholipids. As we identified a basic hydrophobic stretch in the CC_R/CC domains, we propose that positively charged residues in this stretch interact electrostatically with polyacidic phospholipids of the PM and thus, enable ADR1s and RPM1 PM localization, similar to what has been observed for the HeLo domain of mammalian MLKL (Dondelinger *et al.* 2014).

Both MLKL and ZAR1 oligomerize upon activation and are thought to form cation-selective channels at the PM to mediate their cell death function (Chen *et al*. 2014; Xia *et al*. 2016; Huang *et al*. 2017; Wang *et al.* 2019a; Hu *et al*. 2020; Bi *et al.* 2021). To test whether ADR1s use a similar mechanism to induce cell death, we analysed activation-dependent oligomerization of ADR1s by co-immunoprecipitation experiments. We observed that ADR1s form homo- and heterodimers that can be stabilized by mutating the P-loop regions and the QHD motifs. Thus, we propose that ADR1s likely function as dimers/oligomers when inducing cell death, similar as was shown for a member of the other RNL subfamily, NRG1.1 (Qi *et al.* 2018).

Taken together, our data suggest a fundamental role for PI4P or the PM electronegativity in regulating the PM association of ADR1s and the CNL RPM1 and further demonstrate that ADR1s induce cell death at the PM, likely by forming dimers or higher order oligomeric complexes (‘resistosomes’). Thus, ADR1s might use a similar mechanism as MLKL or the CNL ZAR1 to trigger cell death. The exact mechanism/dynamics of how ADR1 oligomers are formed and how they interact with the PM awaits further investigation.

3.3. The EDS1-PAD4-ADR1 node mediates *Arabidopsis* pattern-triggered immunity

Pruitt, R. N.*, Locci, F.*, Wanke, F., Zhang, L., Saile, S. C., Joe, A., Karelina, D., Hua, C., Fröhlich, K., Wan, W.-L., Hu, M., Rao, S., Stolze, S. C., Harzen, A., Gust, A. A., Harter, K., Joosten, M. H. A. J., Thomma, B. P. H. J., Zhou, J.-M., Dangl, J. L., Weigel, D., Nakagami, H., Oecking, C., El Kasmi, F., Parker, J. E., Nürnberger, T.

*These authors contributed equally to this work.

Nature. 2021.Oct;598:495-499. doi: 10.1038/s41586-021-03829-0

Once pathogens overcome mechanical barriers to infection, they encounter two distinct receptor-based immune systems, PTI which is initiated at the cell surface, and ETI which is activated inside the cell (Zhou & Zhang 2020). Although PRR and NLR activation takes place at different subcellular locations, extra- vs. intracellularly, both types of immune receptors induce qualitatively similar immune outputs (Tsuda & Katagiri 2010; Lu & Tsuda 2021). This raises the question, whether immune signaling pathways of both immune systems converge on a common signaling hub. However, whether, where and how the two spatially separated immune branches converge remains unclear.

In Pruitt and Locci *et al.* (2021) we show that PRR- and NLR-mediated immune signaling pathways converge at the PM on the EDS1-PAD4-ADR1 node. Genetic analyses revealed that plants lacking either *EDS1*, *PAD4* or the *ADR1* subfamily, genes which encode well-known signaling components involved in basal immunity and ETI (Bonardi *et al.* 2011; Rietz *et al.* 2011; Cui *et al.* 2017; Lapin *et al.* 2019; Saile *et al*. 2020), are strongly impaired in several RLP23-mediated PTI responses, including callose deposition, ethylene and ROS production. Further genetic analyses demonstrated that EDS1-PAD4 interaction as well as the EP-domain cavity surface that is required for ETI signaling and created by EDS1-PAD4 interaction (Bhandari *et al.* 2019) is essential for RLP23-mediated immunity. This suggests that a signaling-competent EDS1-PAD4 dimer is not only involved in NLR-mediated ETI, but also in RLP-mediated PTI signaling. Remarkably, biochemical and cell biological analyses confirmed the connection of NLR- and RLP-mediated signaling pathways, as we found

that EDS1, PAD4 and ADR1s physically interact with the adaptor kinase SUPPRESSOR of BIR1 (SOBIR1) and the RLCK PBS1-LIKE 31 (PBL31; both required for RLP23-mediated signaling) in a ligand-independent manner at the inner side of the PM. This suggests the formation of a supramolecular, pre-formed complex that could be required for RLP23-mediated signaling.

Taken together, although cell surface and intracellular receptor-mediated immune systems have been considered to operate independently for several decades, we could demonstrate that the EDS1-PAD4-ADR1s module represents a convergent point for signal integration between cell surface and intracellular receptor-based signaling pathways. This might explain why activation of PTI and ETI leads to quantitatively similar immune outputs.

3.4. Autoimmunity induced by the Arabidopsis helper NLR ADR1-L2 requires the receptor-like kinase BKK1

Saile, S. C., Bonardi, V., Keicher, J., Wünsch, L. K., Jacob, P., Teixeira P. J. P. L., Dangl, J. L., El Kasmi, F.

Constitutive activation of immune signaling has tremendous, unfavourable effects for a plant. Thus, homeostasis and signaling of immune receptors, and specifically NLRs, must be precisely controlled to ensure appropriate activation of immune responses (Richard *et al.* 2018). Although significant progress has been made in identifying components regulating sensor NLR homeostasis and signaling, our understanding of how helper NLRs, particularly their activity, are regulated is still very limited. ADR1-L2^{D484V} harbours a gain-of-function mutation in the QHD motif of the helper NLR ADR1-L2. Expression of *ADR1-L2^{D484V}-HA* in the *adr1-L2-4* mutant background leads to an autoimmune phenotype associated with enhanced disease resistance and dwarfism of the plant (Roberts *et al.* 2013). In Saile *et al.* (unpublished) we report that the Arabidopsis LRR-RLK BKK1 is a positive regulator of ADR1-L2^{D484V} autoactivity. We identified BKK1 in a forward genetic screen for suppressors of the *ADR1-L2^{D484V}* (*sadr*) phenotype. By genetic crossing of the *bkk1-1* T-DNA insertion mutant with *ADR1-L2^{D484V} adr1-L2-4*, we could confirm the importance of BKK1 for some ADR1-L2^{D484V}-mediated autoimmune responses, including dwarfism, enhanced disease resistance and (indirectly for) SA accumulation. As the ADR1-L2^{D484V} protein level is not affected in *bkk1-1*, we propose that BKK1 regulates ADR1-L2^{D484V} autoactivity or downstream signaling rather than its homeostasis. Subsequent genetic analyses revealed that BKK1 is likely a specific regulator for the (auto-) activity of ADR1-L2 or the ADR1 subfamily, as phenotypes of other NLR autoimmune mutants were not suppressed by *bkk1-1*. How exactly BKK1 promotes ADR1-L2^{D484V}-induced signaling remains, however, unclear. Biochemical analyses suggest that BKK1 and ADR1-L2 might exist in a pre-formed complex and that BKK1-ADR1-L2 interaction does not require BKK1 kinase activity. In addition, our biochemical analyses revealed that BKK1 does not contribute to the membrane association of ADR1-L2^{D484V}. Furthermore, we observed that PTI responses are activated in NLR autoimmune mutants. However, ADR1-L2^{D484V}-induced potentiation of PTI-outputs are BKK1-independent. In future, it will be

interesting to determine whether BKK1 has a regulatory or structural role in promoting ADR1-L2^{D484V}-induced autoimmunity.

Taken together, autoimmunity induced by the helper NLR ADR1-L2^{D484V} requires the LRR-RLK BKK1, yet the molecular mechanisms underlying this regulation remain obscure.

4. Synopsis

4.1. Arabidopsis RNLs act as redundant nodes in immunity to maintain resilience of the immune system

The plant innate, receptor-based immune system evolved to fight off pathogens (Zhou & Zhang 2020). Plants respond to pathogen attack by using cell surface-localized as well as intracellular immune receptors (Albert *et al.* 2020; El Kasmi 2021). Both immune receptor classes have diversified to form receptor networks (Smakowska-Luzan *et al.* 2018; Adachi *et al.* 2019b), that make the plants' receptor-based immune system more robust against environmental perturbations. PM-localized PRRs that perceive conserved microbial features rely on the physical interaction with a co-receptor for downstream signaling (Ma *et al.* 2016). Likewise, multiple sensor NLRs that perceive pathogen-derived effector molecules depend on the presence of helper NLRs for the activation of immune responses (Wu *et al.* 2017; Castel *et al.* 2019; Jubic *et al.* 2019; Saile *et al.* 2020), though the dependence of sensor NLRs on helper NLRs has thus far only been shown genetically.

Members of the Arabidopsis RNL family act as helper NLRs and are grouped into two subfamilies, the ADR1s and NRG1s (Collier *et al.* 2011). The ADR1 subfamily is comprised of three functional members that act redundantly during ETI downstream of several sensor NLRs, in basal resistance against virulent pathogens and during RLP23-mediated PTI responses (Bonardi *et al.* 2011; Pruitt *et al.* 2021). In contrast, the NRG1 subfamily includes two full-length members that are also functionally redundant towards certain sensor NLRs (Castel *et al.* 2019; Wu *et al.* 2019). Interestingly, functional redundancy is not only present within the RNL subfamilies, but also between both subfamilies (ADR1s and NRG1s) in Arabidopsis (Saile *et al.* 2020). It has been demonstrated that ADR1s and NRG1s share many of their functions, particularly in basal resistance and certain TNL-mediated immune responses, albeit in an unequally redundant manner (Lapin *et al.* 2019; Wu *et al.* 2019; Saile *et al.* 2020). Given their function as downstream signaling hubs, RNLs are likely attractive targets for effector molecules aiming at restricting immune signaling induced by multiple sensing immune receptors. Thus, suppressing RNL function promotes virulence. This actually highlights the importance of functional redundancy among RNLs and might help to explain why RNLs have evolved as redundant nodes downstream of PRRs and

NLRs in Arabidopsis. To date, there are no pathogen effectors described that directly target RNLs, but the RNL-associated protein EDS1 (Bhattacharjee *et al.* 2011).
Like RNLs, the solanaceous-specific NRC helper NLRs exhibit functional redundancy (but also distinct specificity) for their phylogenetically-related CNL sensor NLRs that assemble into a complex immune network to protect the plant against multiple pathogens (Wu *et al.* 2017; Wu *et al.* 2018). As NRCs are required for the signaling function of up to half of the NLRome of solanaceous plants, they represent an ideal target for pathogen effectors. Indeed, it was shown recently that the cell death activities of NRC2 and NRC3 are suppressed by an oomycete and a cyst nematode effector protein, respectively, thereby restricting the function of NRC2/NRC3-dependent sensor NLRs (Derevnina *et al.* 2021). As plants aim to maintain resilience of the immune system in response to evolving pathogens, these findings emphasize again why plants have evolved receptor networks with redundant nodes.

4.2. Localization and signaling partners likely influence the specific functions of RNLs

Apart from their redundant functions during basal resistance and ETI, Arabidopsis ADR1 and NRG1 subfamilies do also play specific roles during some RLP- and sensor NLR-mediated immune responses, and to a lesser extent during RLK-mediated PTI (Saile *et al.* 2020; Pruitt *et al.* 2021; Tian *et al.* 2021). Since ADR1s as well as NRG1s can regulate both disease resistance and HR independently (Lapin *et al.* 2019; Wu *et al.* 2019; Saile *et al.* 2020), it is proposed that their specific functions might rely on the preferential use of either subfamily by the sensing immune receptor. In case sensor NLRs as well as PRRs need to physically interact with RNLs to activate immune signaling, they should be in close proximity and thus, should co-localize to a certain degree. Therefore, the subcellular localization of RNLs could confer some functional specificity. Indeed, ADR1s display a different localization pattern as NRG1s. ADR1s do mainly localize to the PM pre and post activation (Saile *et al.* 2021), whereas NRG1s are found in the cytosol, but also associated with the ER and the PM (Lapin *et al.* 2019; Wu *et al.* 2019; Jacob *et al.* 2021). Interestingly, NRG1.1 was found to increase its PM localization upon autoactivation (Jacob *et al.* 2021), suggesting that NRG1s might function at the PM, though they could be activated at different cellular compartments.

In fact, we could show that members of the ADR1 and NRG1 subfamilies induce cell death at the PM (Jacob *et al.* 2021; Saile *et al.* 2021), supporting the idea that NRG1s might translocate from their initial sites of activation to the PM to function, whereas ADR1s remain at their site of activation. Together, the different subcellular localization patterns of ADR1s and NRG1s might influence their specific functions, likely by controlling their accessibility to protein interaction partners. This idea is supported by our recent findings demonstrating that ADR1 family members associate at the PM with the adaptor kinase SOBIR1 and the RLCK PBL31 that are required for RLP23-mediated signaling (Pruitt *et al.* 2021; Tian *et al.* 2021). As ADR1s play a critical role in several RLP23-mediated immune responses (Pruitt *et al.* 2021; Tian *et al.* 2021), it appears to be likely that a SOBIR1-PBL31-ADR1s complex might be relevant for signaling induced by RLP23. How such a SOBIR1-PBL31-ADR1s complex induces RLP23 signaling will be an interesting topic for future research, but it appears to be very likely that ADR1s regulate together with EDS1-PAD4 dimers RLP23-mediated immunity (Pruitt *et al.* 2021). Further support for this hypothesis comes from genetic data demonstrating that EDS1-PAD4 dimers are required for RLP23-mediated ethylene production and from biochemical data suggesting that SOBIR1, PBL31, ADR1s, EDS1 and PAD4 might be part of the same protein complex (Pruitt *et al.* 2021). Historically, EDS1 and PAD4 were shown to have a nuclear-cytoplasmic localization (Feys *et al.* 2005) and to act in concert with the ADR1 helper NLR subfamily during basal resistance as well as in several ETI responses (Lapin *et al.* 2019; Sun *et al.* 2021). ADR1 family members specifically interact with EDS1-PAD4 upon immune activation (Sun *et al.* 2021), suggesting that they are part of the same signaling complex. How exactly the EDS1-PAD4-ADR1s complex is activated and induces immunity – during both PTI and ETI - has yet to be clarified, but involves SA-dependent and SA-independent pathways (Bonardi *et al.* 2011; Cui *et al.* 2017; Bhandari *et al.* 2019). In contrast, the NRG1 subfamily (that is not involved in RLP23-mediated signaling) cooperates genetically and physically with supposedly nuclear-localized EDS1-SAG101 dimers during TNL-mediated ETI in Arabidoipsis and *N. benthamiana* (Qi *et al.* 2018; Sun *et al.* 2021). In summary, ADR1s and NRG1s differ in their subcellular localizations and are part of distinct signaling complexes that likely mediate their specific functions during certain PTI and ETI responses.

4.3. CNL- and TNL-/RNL-mediated signaling might converge at cellular membranes

4.3.1. RNL-independent CNLs might form cation channels

While all tested TNLs have been found to rely on the presence of RNL helper NLRs (Dong *et al.* 2016; Castel *et al.* 2019; Wu *et al.* 2019; Saile *et al.* 2020) that signal together with either EDS1-PAD4 or EDS1-SAG101 during TNL-mediated ETI (Lapin *et al.* 2019; Sun *et al.* 2021), we could demonstrate and confirm that several CNLs function (at least to a certain degree) independently of RNLs (Bonardi *et al.* 2011; Castel *et al.* 2019; Saile *et al.* 2020). RNL-independent CNLs are thus multifunctional proteins that have both sensor- and executor-activities and have therefore been termed singleton NLRs (Adachi *et al.* 2019b). Given their 'integrated' sensor and executor functions, studying singleton NLRs could provide insights into the signaling mechanism of RNLs.

The CNL ZAR1 is classified as a singleton NLR (Baudin *et al.* 2017; Saile *et al.* 2020) and cryo-electron microscopy combined with biochemical analyses have recently revealed that ZAR1 transforms from an inactive cytosolic monomer (that exist in a pre-formed receptor complex with the pseudokinase RSK1) into a pentameric, PM-associated complex upon effector recognition (Wang *et al.* 2019a; Wang *et al.* 2019c; Hu *et al.* 2020). In detail, indirect effector recognition results in the interaction of the uridylated decoy protein PBL2^{UMP} with the pre-formed ZAR1-RSK1 complex that drives intramolecular conformational changes in ZAR1 leading to the exchange of ADP by ATP/dATP (Wang *et al.* 2019c). ATP/dATP binding ultimately induces the assembly of a high-molecular weight complex, composed of five ZAR1-RSK1-PBL2^{UMP} protomers, termed ZAR1 resistosome (Wang *et al.* 2019a). Within the resistosome, the first alpha (α1) helices of the ZAR1 CC domains are exposed and assemble into a funnel-shaped structure that inserts into the PM (Wang *et al.* 2019a; Hu *et al.* 2020) where it forms a channel that triggers cation influx across the PM, leading to HR (Bi *et al.* 2021). Remarkably, the ZAR1 N-terminal α1 helix is characterized by a specific amino acid sequence, the so-called MADA motif (Adachi *et al.* 2019a). Mutations within this motif have been shown to impair ZAR1-mediated cell death and resistance against *Xanthomonas campestris* pv. *campestris*, albeit they did neither affect ZAR1

oligomerization nor ZAR1 PM localization (Adachi *et al.* 2019a; Wang *et al.* 2019a). It is noteworthy, that the N-terminal MADA motif or a MADA-like motif is conserved in approximately 20% of all CNLs in angiosperms, suggesting that these CNLs could use the same or a similar mechanism to cause ETI (Adachi *et al.* 2019a). Indeed, the MADA motif seems to be functionally conserved across CNLs from distantly related plant species, as chimeric proteins retained the capability to induce HR and disease resistance in transient assays (Adachi *et al.* 2019a). Among the MADA (-like) motif-containing CNLs are the Arabidopsis singleton NLR RPM1 and several members of the solanaceous-specific NRC helper NLR family (Adachi *et al.* 2019a). Similar as for ZAR1, these CNLs do not rely on the presence of downstream signaling components to induce ETI (Wu *et al.* 2017; Saile *et al.* 2020) and thus, they are likely the executors of cell death. In contrast, sensor CNLs that rely on the presence of other NLRs, like NRC-dependent CNLs, lack a canonical MADA (-like) motif, likely because they do not need it as they do not induce ETI on their own (Adachi *et al.* 2019a). Thus, it is an interesting hypothesis that all MADA (-like) motif-containing CNLs might “directly” execute cell death following a similar mechanism as ZAR1. In support with this idea, it has been shown that the MADA-like motif-containing CNL RPM1 self-associates and requires PM localization to function (Gao *et al.* 2011; El Kasmi *et al.* 2017; Saile *et al.* 2021). Remarkably, RPM1-induced HR was abolished by a calcium channel blocker (Grant *et al.* 2000), suggesting that activated RPM1 might directly regulate calcium influx. In addition, the MADA motif-containing helper CNL NRC4 was found to self-associate and to localize in puncta associated with the extrahaustorial membrane and the PM following (auto-) activation, indicating that activated NRC4 might also form membrane-associated resistosomes (Duggan *et al.* 2021). However, it remains to be investigated whether MADA (-like) motif-containing CNLs display a similar structure and accordingly, follow a similar working mechanism as identified for the ZAR1 resistosome.

It is worth noting, that the ZAR1 resistosome shares structural similarities with the inflammasome formed in mammalian cells (Saur *et al*. 2021) that induces pyroptosis, a form of programmed cell death resulting in cell lysis (Vande Walle & Lamkanfi 2016). Like the ZAR1 resistosome, an inflammasome is a multimeric complex that is formed via NLR oligomerization in response to intracellular danger signals (Zheng *et al*. 2020).

In contrast, however, inflammasome-activated pyroptosis is not directly executed by the inflammasome itself but mediated by specific caspases that are recruited and activated by the inflammasome (Chai & Shi 2014). Activated caspases trigger the formation of gasdermin D (GSDMD) pores in the PM, leading to pyroptosis (Liu *et al.* 2016). Unlike the ZAR1 resistosome, GSDMD pores lack ion selectivity (Chen *et al.* 2016) and have a larger pore size (Heilig *et al.* 2018). They have been shown to directly mediate the release of cytokines of the interleukin 1 family into the extracellular space (Evavold *et al.* 2018; Heilig *et al.* 2018; Xia *et al.* 2021). Cytokines act as DAMPs and bind to their corresponding receptors at the cell surface of target cells to activate an intracellular signaling cascade which can result in a localized inflammation reaction (Liu *et al.* 2017; Dinarello 2018). Together, although the plant ZAR1 resistosome is reminiscent to the inflammasome formed in animals, they use distinct mechanisms to induce cell death. This, however, does not rule out the possibility that other plant CNLs (particularly the ones that require the presence of RNL helper NLRs) might use a similar mode of action as inflammasomes or the GSDMD pore.

4.3.2. Several CNLs might have lost their channel activity

It is important to mention again, that the negatively charged residues in the CC domain of ZAR1, that are required for cation influx, are not conserved in all CNLs and remarkably, absent in several helper NLR-dependent CNLs (Adachi *et al.* 2019a). As helper NLRs likely act as immune/cell death executors downstream of several sensor CNLs, it is likely that these sensor CNLs have lost their channel activity throughout their sub-functionalization. However, how exactly these CNLs function to induce robust immune responses, remains yet to be determined, but it is likely that most, if not all, CNLs function (i) via oligomerization and (ii) at membranes. The first hypothesis is based on the observation that mutations in CC domains or in the P-loop region often abolish self-association of the CC or full-length CNLs that in turn, results in impaired cell death and immune signaling (Maekawa *et al.* 2011; Casey *et al.* 2016; El Kasmi *et al.* 2017; Li *et al.* 2020; Wang *et al.* 2020). It remains, however, yet to be investigated whether CNL self-association is required to recruit downstream signaling components (e.g., helper NLRs) or whether it allows CNLs to conduct some defense-activating actions. The second hypothesis (CNLs function at membranes) is supported by the

finding that several CNLs possess a predicted N-terminal lipidation motif, for example a palmitoylation- or a myristoylation site (Qi *et al.* 2012; Qi & Innes 2013; Kawano *et al.* 2014; Wroblewski *et al.* 2018). Both palmitoylation and myristoylation are post-translational modifications that promote protein hydrophobicity and accordingly, can drive membrane association, which, however, does not necessarily mean PM association (Wang *et al.* 2021). For instance, a myristoylated CNL that is studied in our lab localizes to Golgi membranes and the tonoplast and displays an impaired cell death function when mis-localized to the cytosol by mutating the N-terminal lipidation sites (Sunil *et al*., unpublished). Furthermore, CNLs that do not have N-terminal lipidation motifs do also require membrane localization to function, as demonstrated for example for the tomato CNL tobacco mosaic virus resistance-2^2 (Tm-2^2) (Chen *et al.* 2017; Wang *et al.* 2020). Remarkably, the CC domain of Tm-2^2 was shown to trigger cell death only when anchored to the PM, where the full-length Tm-2^2 localizes (Wang *et al.* 2020). In addition, we have recently identified a basic hydrophobic stretch in the CC_R/CC domains of all RNLs and several CNLs that likely mediate interactions with negatively charged phospholipids of the PM (or other membranes) and thus, these interactions could be a conserved mechanism to drive the membrane association of CNLs lacking predicted lipidation motifs (Saile *et al.* 2021). On the basis of these findings, it appears to be likely that most, if not all, CNLs might induce ETI at cellular membranes. Therefore, it might be possible that CNLs which have no channel activity, might form pores similar as observed for GSDMD. Pore formation in the PM might disrupt membrane integrity and thus, could lead to the generation of DAMPs that could be released from the infected cells into the extracellular space by the formed membrane pores. By binding to their corresponding PRRs, DAMPs might then induce a PTI-like response in neighbouring cells. Potential support for this hypothesis comes from recent findings showing that the activation of ETI potentiates PTI responses and induces transcriptional as well as translational upregulation of important PTI components in the analysed leave tissue (Ngou *et al.* 2021). Alternatively and/or additionally, CNL oligomerization could also be required to recruit and activate downstream signaling components, including helper NLRs, similar as shown for mammalian inflammasomes that form a scaffold for the recruitment of specific caspases to initiate immune signaling (Chai & Shi 2014).

In conclusion, it will be interesting to determine whether CNLs (especially the ones that require RNLs) signal downstream by mediating the release of DAMPs and/or by recruiting downstream signaling components. A direct release of DAMPs by CNL pores would very likely require the formation of larger membrane pores than the ones formed by ZAR1. Indeed, it was shown that the CNL RPP7b assembles into a high-molecular weight complex - that is composed of six to seven protomers – to induce autoimmunity (Li *et al.* 2020). Whether such a pore might be large enough to mediate the release of DAMPs needs, however, to be investigated.

4.3.3. (Auto-) activated RNLs form cation channels at the PM

Unlike NRC helper NLRs, RNL helper NLRs lack a MADA (-like) motif at their N-terminal ends (Adachi *et al.* 2019a), but their CC_R domains share structural similarity with the ZAR1 CC domain and also with the N-terminal HeLo domain of the mammalian MLKL protein (Jubic *et al.* 2019; Jacob *et al.* 2021). MLKL proteins can form an octameric cation channel at the PM to trigger necroptosis, a form of programmed cell death (Dondelinger *et al.* 2014; Xia *et al.* 2016; Huang *et al.* 2017). These similarities indicate that RNLs might also have pore-forming ability/channel activity, and further suggest, that RNLs cell death and resistance function is similar to the MADA motif-containing, RNL-independent CNL, ZAR1. The facts that RNLs (i) are a subclass of CNLs (Qian *et al.* 2017), (ii) act like CNLs during TNL-mediated ETI by regulating the same categories of genes (Saile *et al.* 2020), (iii) induce cell death at the PM (Jacob *et al.* 2021; Saile *et al.* 2021) and (iv) self-associate, likely in an activation dependent manner (Qi *et al.* 2018; Saile *et al.* 2021; Wu *et al.* 2021b) support this hypothesis. Indeed, it was recently demonstrated that autoactivated NRG1.1 associates into high-molecular weight complexes, potentially oligomeric resistosomes, that form non-selective, calcium-permeable cation channels at the PM (Jacob *et al.* 2021). This was also demonstrated for the ectopically active wildtype ADR1 (Jacob *et al.* 2021). Although RNL (NRG1.1 and ADR1) channel activity is required for cell death induction (Jacob *et al.* 2021), it remains to be investigated whether sensor NLR-activated ADR1s and NRG1s also induce ETI responses by regulating cellular ion homeostasis. In summary, members of the ADR1 and NRG1 subfamilies form non-selective cation

channels at the PM and thus, might function in a similar way as the CNL ZAR1 (and maybe other RNL-independent CNLs) to induce ETI.

4.3.4. TNLs form holoenzymes for NAD^+ hydrolysis

The working mechanism of CNLs and RNLs contrasts with the mode of action of TNLs. This is actually not surprising given the fact that all tested TNLs rely on the presence of RNL helper NLRs during ETI and also autoimmunity (Dong *et al.* 2016; Castel *et al.* 2019; Wu *et al.* 2019; Saile *et al.* 2020; Schulze *et al.* 2021), suggesting that RNLs act as signal executors downstream of TNLs. How exactly pathogen recognition by TNLs results in the activation of downstream components, including RNLs and the lipase-like proteins EDS1, PAD4 and SAG101, is, however, still under investigation. Thus far it was shown that TIR domains require homo- or hetero-dimerization/-oligomerization to induce immune signaling (Bernoux *et al.* 2011; Williams *et al.* 2014; Ma *et al.* 2020; Martin *et al.* 2020), similar as shown for multiple CNLs. However, unlike the ZAR1 resistosome, the TNLs ROQ1 and RPP1 assemble into a tetrameric complex that has no channel activity (Ma *et al.* 2020; Martin *et al.* 2020). Recently, it was demonstrated that plant TIR domains function upstream of EDS1 and NRG1 as holoenzymes with a NAD^+ hydrolysis function that cleaves NAD^+ into NAM, ADPR and a v-cADPR (Horsefield *et al.* 2019; Wan *et al.* 2019a). Since ADPR and cADPR are known to act as second messengers that activate calcium fluxes (Wu *et al.* 1997; Fliegert *et al.* 2007; Guse 2015), it raises the possibility that the generated enzymatic products might activate downstream signaling components. How exactly these signaling molecules might link TNL activation to the EDS1 family and RNL helper NLRs is, however, still under investigation and thus far completely speculative. One possible idea is that the generated enzymatic products directly bind to a cavity formed in EDS1-PAD4 and EDS1-SAG101 dimers. This cavity is proposed to act as a signaling surface as it is required for TNL-mediated signaling (Bhandari *et al.* 2019; Gantner *et al.* 2019; Lapin *et al.* 2019) and thus, could potentially be the target site for NADase-produced signaling molecules. Since EDS1-PAD4 and EDS1-SAG101 have been shown to specifically interact with the ADR1 or NRG1 helper NLR subfamilies during TNL-mediated ETI, respectively (Sun *et al.* 2021; Wu *et al.* 2021b), binding of the TIR-generated signaling molecules might induce EDS1-PAD4-ADR1s or EDS1-SAG101-

NRG1s complex formation. This, however, raises the question: How do these products actually achieve substrate specificity, as the RNL ROQ1 for example has been shown to rely solely on the presence of the EDS1-SAG101-NRG1 module, whereas the TNL pair RPS4/RRS1 was found to require both, EDS1-PAD4-ADR1s and EDS1-SAG101-NRG1s, signaling modules (Lapin *et al.* 2019). One speculative idea is that TIR domains already select their downstream signaling modules by generating distinct cADPRs. Potential support for this hypothesis comes from a recent finding showing that a bacterial TIR domain produces a new variant of cADPR, called v2-cADPR (Eastman *et al.* 2021), that might have different binding affinities. In future, biochemical experiments might shed light on understanding whether and how TIR domain-generated cleavage products specifically activate downstream signaling components.

Altogether, a combination of structural and biochemical analyses revealed that effector recognition results in the oligomerization of CNLs, TNLs and RNLs into signaling-competent (active) complexes. While TNLs act as NAD^+ cleaving holoenzymes that have to signal through the EDS1 family and RNL helper NLRs to trigger resistance and HR, the RNL-independent CNL ZAR1 as well as members of the RNL subfamilies were shown to form calcium-permeable channels at the PM. Calcium signaling is well-known to play an important role in plant immunity, though it is largely unclear how specifically it regulates immune signaling and cell death during ETI. As RNLs likely act as signal executors downstream of TNLs (and several CNLs), CNL- and TNL-mediated signaling might converge at cellular membranes. Disturbance of cellular ion homeostasis might be a major, but likely not the only mechanism for NLR-triggered immune responses.

4.4. ADR1s as convergence point for PRR- and NLR-mediated signaling

Although PRR- and NLR-mediated signaling pathways are activated at different subcellular compartments, they result largely in common immune outputs, for example calcium influx, ROS production or the transcriptional induction of defense genes (Saile *et al.* 2020; Yuan *et al.* 2021a; Zhao *et al.* 2021). These immune responses differ in their dynamics and amplitudes, and are generally much stronger and sustained during NLR-mediated signaling, which, however, requires the activation of PTI (Ngou *et al.* 2021; Yuan *et al.* 2021b). Based on these findings, it was supposed that PRR- and

NLR-mediated pathways might converge at components upstream of the final immune responses.

Recently, PRRs and PRR co-receptors have been revealed to be genetically required for the robust NLR-triggered immune responses (Ngou *et al.* 2021; Yuan *et al.* 2021a). In this regard, it has been shown that RPS2-, RPS5-, and RPS4/RRS1-mediated resistance responses are severely impaired in PRR/PRR co-receptor mutants, including *fls2 efr cerk1* and *bak1 bkk1 cerk1* triple mutants (Yuan *et al.* 2021a). It is interesting that TNL-mediated cell death required activation of PTI more strongly than the cell death responses mediated by multiple CNLs, including RPM1, RPS2 and RPS5 (Ngou *et al.* 2021). Strikingly, this is very reminiscent of the differential requirement of RNL helper NLRs for CNL- and TNL- mediated immune responses (Saile *et al.* 2020) and thus also suggests, that RNLs might be an integration point for PRR- and NLR (TNL)-mediated signaling pathways. Additional support for this hypothesis comes from the requirement of ADR1s in basal resistance against host-adapted, virulent pathogens (Bonardi *et al.* 2011; Saile *et al.* 2020), their central role during multiple RLP23-mediated immune responses (Pruitt *et al.* 2021; Tian *et al.* 2021), as well as their minor role during RLK-mediated signaling (Pruitt *et al.* 2021; Tian *et al.* 2021). Interestingly, these functions do strongly overlap with the roles of the known ETI key regulators EDS1 and PAD4 (Cui *et al.* 2017; Pruitt *et al.* 2021; Tian *et al.* 2021), indicating that the EDS1-PAD4-ADR1 signaling module might be a convergence node between PRR- and NLR-mediated signaling pathways.

The PM localization of ADR1s (Saile *et al.* 2021) hints to a direct physical link between ADR1s and PRRs/PRR co-receptors. Indeed, ADR1 family members as well as EDS1 and PAD4 were shown to constitutively associate with the adaptor kinase SOBIR1 and the RLCK PBL31 at the inner side of the PM (Pruitt *et al.* 2021; Tian *et al.* 2021). Furthermore, ADR1-L2 was additionally found to associate with the PRR co-receptors BAK1 and BKK1 (Saile *et al*., unpublished; Appendix 7.5). It remains, however, to be determined whether and if so, how these interactions regulate proper PRR- and NLR-mediated signaling. Since it was shown that the activation of TNL-mediated signaling (which fully relies on the presence of RNLs and the EDS1 family) boosts PTI (Saile *et al.* 2020; Ngou *et al.* 2021; Tian *et al.* 2021), one could speculate that the interaction between PRRs/PRR co-receptors, RLCKs and EDS1-PAD4-ADR1s might be essential

for the activation of EDS1, PAD4 or ADR1s. In fact, we have recently identified BKK1 for being required for the autoactivity of ADR1-L2 (Saile *et al*., unpublished; Appendix 7.5), though we still lack a clear mechanistic understanding of how BKK1 regulates ADR1-L2 signaling. Given their constitutive interaction in *N. benthamiana* (Saile *et al*., unpublished; Appendix 7.5), it is possible that BKK1 or a BKK1-target protein (RLCK) might regulate ADR1-L2 activity through post-translational modifications, e.g., phosphorylation, that could result in structural rearrangements, important for the activation of ADR1-L2. In support of a role for phosphorylation in regulating the activity of ADR1-L2 (and maybe other ADR1s as well), phosphorylation of the structurally similar mammalian MLKL as well as of the mammalian helper NLR NLR Family CARD Domain Containing 4 (NLRC4) was found to be critical for their activity by driving self-association or recruitment of downstream components, respectively (Qu *et al.* 2012; Wang *et al*. 2014). Additionally, phosphorylation of mouse NOD-, LRR-, and pyrin domain-containing protein 3 (NLRP3) was demonstrated to be a key priming step for NLRP3 inflammasome activation that results in pyroptotic cell death (Song *et al.* 2017; Weber *et al.* 2020). Interestingly, NLRP3 exists in a membrane-bound oligomeric complex already prior to activation (Andreeva *et al.* 2021), similar as what we have observed for the ADR1s (Saile *et al.* 2021). As ADR1s likely signal through oligomerization (Saile *et al.* 2021; Wu *et al.* 2021b) by forming calcium-permeable cation channels (Jacob *et al.* 2021), it is possible that ADR1s contribute to calcium influx during both PTI and TNL-mediated ETI. This could trigger the transcriptional reprogramming events, resulting in disease resistance.

Another hypothesis that might help to explain how ADR1s as well as EDS1 and PAD4 are activated during PTI and thus, contribute to RLP23-mediated signaling, is that PRRs/PRR co-receptors or associated RLCKs, like PBL31, might phosphorylate TNLs. TNL phosphorylation might result in activation and conformational changes, inducing TIR domain oligomerization and consequently, results in the production of NAD^+ cleavage products that might directly activate EDS1-PAD4-ADR1s complex formation and signaling (Horsefield *et al.* 2019; Wan *et al.* 2019a). Potential support for this hypothesis comes from genetic data demonstrating that mutating the EDS1-PAD4 signaling surface, that is proposed to act as target site for NAD^+ cleavage products, impairs RLP23-mediated ethylene production (Pruitt *et al.* 2021). In conclusion,

identifying additional components (e.g., TNLs) that might interact with PRRs/PRR co-receptors or associated RLCKs, as well as analysing phosphorylation events in associated proteins, including TNLs or ADR1s, and studying the dynamics of the signaling complex(es) might be interesting topics for future research. Furthermore, as PRRs and PRR-co-receptors are required for RNL-mediated ETI responses (Ngou *et al.* 2021; Yuan *et al.* 2021a), it will be interesting to test, whether PRR/PRR-coreceptor-induced phosphorylation of ADR1s during PTI is a critical priming step for the channel formation of ADR1s during ETI. This would be consistent with the activation of the mammalian NLRP3 inflammasome complex that relies on a priming (e.g., phosphorylation) and an activation signal (Weber *et al.* 2020). Addressing these research topics might help to understand the mechanisms underlying signal collaboration between PRR- and NLR-induced immunity and thus, will contribute to extend our knowledge on plant-microbe interactions.

Besides ADR1 helper NLRs, also NRC helper NLRs have been demonstrated to be genetically involved in RLP-mediated signaling (Kourelis *et al.* 2021). Cell death induced by the RLP Cf-4 is mainly mediated by NRC3 in *N. benthamiana*, likely by the formation of calcium-permeable NRC3 resistosomes (Kourelis *et al.* 2021). Thus, both helper NLR classes, although evolutionarily not related, seem to fulfil a conserved core signaling node that links PRR (mainly RLP)-mediated signaling, initiated at the cell surface, to NLR-mediated signaling, induced inside the cell. It is striking that NLRs and RLPs share similar evolutionary patterns compared to RLKs. While RLK encoding genes show a low degree of variation in different Arabidopsis accessions, genes encoding for NLRs and RLPs emerge as polymorphic receptor sensor classes that have undergone a fast evolutionary diversification (Pruitt *et al.* 2021). These findings suggest that RLPs and NLRs share common signaling components and thus, confirm the major role of helper NLRs (RNLs and NRCs) downstream of both PM-localized RLPs and intracellular localized NLRs (Saile *et al.* 2020; Pruitt *et al.* 2021).

5. Conclusion and Outlook

The work described in this PhD thesis has significantly contributed to a better understanding of PRR- and NLR-mediated signal transduction during plant (auto-) immunity. We could demonstrate that PRR- and NLR-mediated signaling cascades converge on RNL helper NLRs (Figure 5). PRRs and multiple sensor NLRs differentially rely on the two subfamilies of RNLs, the ADR1s and NRG1s, to initiate immune responses (Saile *et al.* 2020; Pruitt *et al.* 2021). The PRRs RLP23 and to a lesser extent FLS2, as well as the CNLs RPS2 and RPS5, use specifically the ADR1 subfamily to induce resistance responses (Saile *et al.* 2020; Pruitt *et al.* 2021; Tian *et al.* 2021). In contrast, TNLs, including RPS4/RRS1, RPP2 and WRR4A rely on both RNL subfamilies (Saile *et al.* 2020). ADR1s are known to act in concert with the lipase-like proteins EDS1 and PAD4 during both PTI and TNL-mediated ETI, whereas NRG1s function specifically together with EDS1 and SAG101 during ETI induced by TNLs (Lapin *et al.* 2019; Pruitt *et al.* 2021; Sun *et al.* 2021; Wu *et al.* 2021b). However, the signaling events downstream of PRR and sensor NLR activation that result in the activation of the EDS1-PAD4-ADR1s and EDS1-SAG101-NRG1s nodes are still not fully understood. Recent studies demonstrated that TNLs assemble into tetrameric complexes (Ma *et al.* 2020; Martin *et al.* 2020) that act upstream of EDS1 and RNLs as holoenzymes for NAD^+ hydrolysis (Horsefield *et al.* 2019; Wan *et al.* 2019a). As NADase activity of TIR domains is required for TNL immune functions (Wan *et al.* 2019a), it remains to be investigated whether and how NAD^+ cleavage products are connected with the EDS1-PAD4-ADR1s and EDS1-SAG101-NRG1s signaling modules. Analysing whether the enzymatic products generated by TIR domains directly bind to the cavity of EDS1-PAD4 and EDS1-SAG101 dimers and whether this could drive the interaction with RNLs, remain interesting topics for future research. Another key question in NLR signaling is, how CNLs that partially rely on the presence of RNLs, activate RNLs, or if RNL activation is at all required. As most, if not all, CNLs function via oligomerization, it is possible that CNL oligomers might act as a scaffold to recruit RNLs, similar as observed for NLR inflammasomes formed in mammalian cells (Zheng *et al.* 2020). Testing whether activated CNLs directly interact with RNLs can give some hints to answer this question. Recent progress in the field of CNL signaling has revealed that the RNL-independent CNL ZAR1 assembles into a

pentameric complex that forms a calcium-permeable channel at the PM (Wang *et al.* 2019a; Bi *et al.* 2021). ZAR1 cell death and resistance functions require certain amino acids that are part of a specific motif within its CC domain (Adachi *et al.* 2019a). As this motif is conserved in ~20% of all CNLs, including the RNL-independent CNL RPM1 (Adachi *et al.* 2019a), it raises the question whether all RNL-independent CNLs use the same or a similar mechanism as ZAR1 to induce defense responses. In future, it will be interesting to test whether RNL-independent CNLs oligomerize into high-molecular weight complexes and whether these complexes possess channel activity that is required for triggering immune responses. These findings could help to explain why some CNLs do not depend on RNLs, whereas others do. In fact, like the ZAR1 resistosome, RNLs likely function at the PM through oligomerization by forming calcium-permeable channels (Qi *et al.* 2018; Jacob *et al.* 2021; Saile *et al.* 2021; Wu *et al.* 2021b). Thus, RNLs could act as immune executors downstream of all NLRs that have no channel activity. Whether ADR1s use a similar mechanism during both PTI and ETI to trigger defense responses is an interesting question that also awaits further investigation.

In conclusion, the work described in this PhD thesis together with the outstanding work of our collaborators and other groups has tremendously advanced our understanding of PRR- and NLR-mediated signaling over the last few years. In particular, the presented work in here made great discoveries ranging from RNL regulation, via RNL specificity and RNL function/signaling mechanisms onto how PRR- and NLR-initiated signaling cascades converge. Many questions remain still open, e.g., how exactly RNLs are activated during PTI and ETI, but will be the basis for future research.

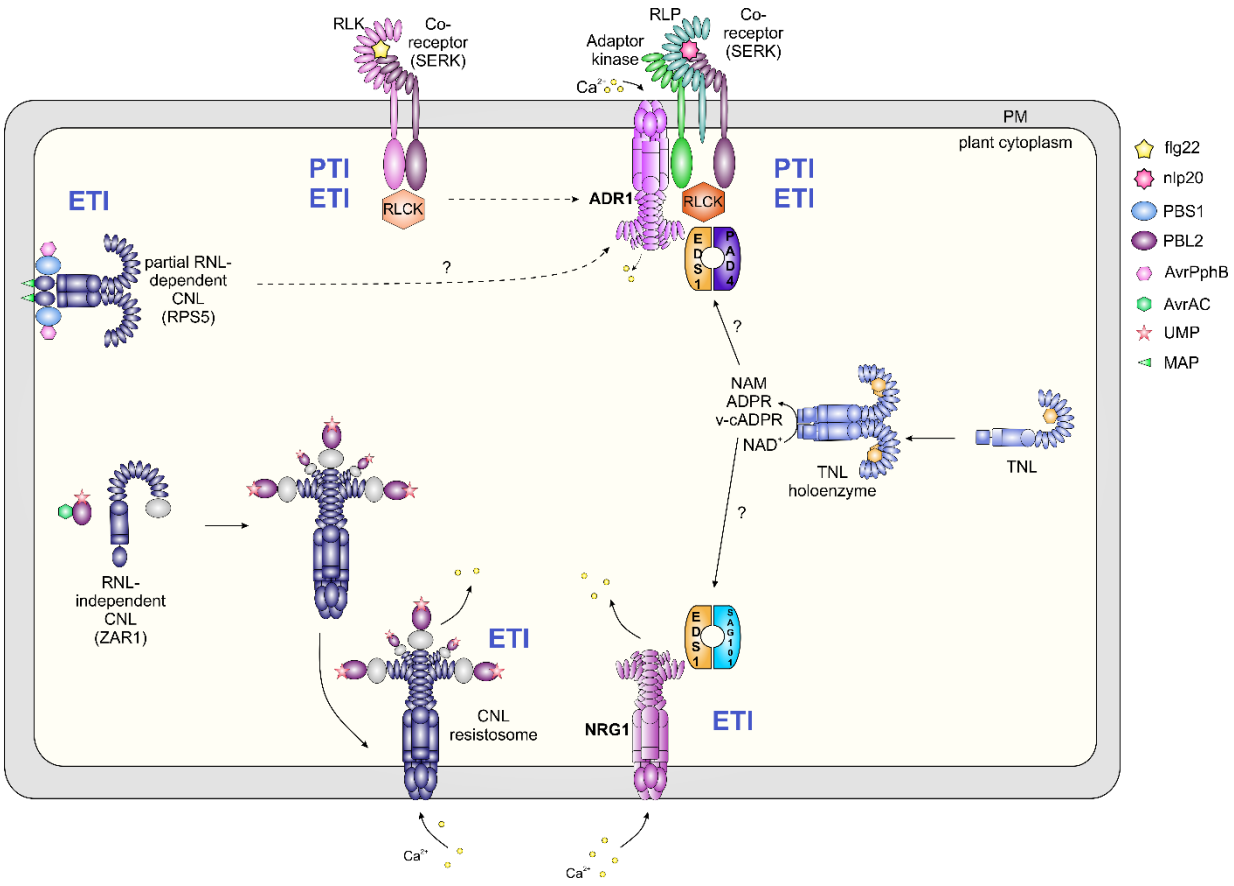

Figure 5: Simplified schematic summary of PRR- and NLR-mediated immunity. Pathogen-derived PRR elicitors, such as flg22 and nlp20, are detected at the cell surface by PM-localized PRRs, including RLKs and RLPs. While RLPs constitutively interact with an adaptor kinase, both LRR-RLKs and RLPs recruit a co-receptor (e.g., a SERK family member) following elicitor perception to activate RLCKs, which in turn activate downstream components, resulting in PTI. RLP23, and to a lesser extent FLS2, require the EDS1-PAD4-ADR1s signaling complex to induce full PTI. *Vice versa*, PRRs and PRR co-receptors are required for full NLR-mediated ETI. EDS1-PAD4-ADR1s interact with the adaptor kinase SOBIR1, the RLCK PBL31 and likely with the co-receptors BAK1 (SERK3) and BKK1 (SERK4) at the inner side of the PM. Activated ADR1s can oligomerize and ectopically active ADR1 forms calcium-permeable channels at the PM. Whether ADR1s use their channel activity for triggering defense responses during both PTI and ETI remains to be analysed. The EDS1-PAD4-ADR1s signaling module is also required for TNL-mediated ETI and thus, is considered to be an integration point of PRR- and NLR-mediated signaling cascades. Following effector recognition, TNLs assemble into a tetrameric complex. Their TIR domains have NADase activity and cleave NAD^+ into NAM, ADPR and v-cADPR. The generated cleavage products are proposed to directly bind to EDS1-PAD4 and EDS1-SAG101 dimers which could induce the recruitment of ADR1s to EDS1-PAD4 and NRG1s to EDS1-SAG101. Autoactivated NRG1.1 forms high-molecular weight complexes at the PM that are permeable to calcium, ultimately resulting in cell death. Whether TNL-mediated activation of NRG1s also leads to the formation of calcium-permeable ion channels, awaits, however, further investigation. The partial RNL-dependent CNL RPS5 (note: RPS2 is not depicted here for simplicity) localizes to the PM via a myristoylation- and palmitoylation site (MAP) and self-associates. Indirect effector recognition likely results in conformational rearrangements of RPS5 leading to ETI. RPS5 relies on the presence of ADR1s for disease resistance against *Pst* DC3000, but can induce cell death on its own. How RPS5 and other ADR1-dependent CNLs are connected to ADR1s and how they execute cell death is still unknown. The RNL-independent CNL ZAR1 exists in a pre-formed complex with the pseudokinase RSK1. Indirect effector recognition results in the interaction of the uridylated decoy protein $PBL2^{UMP}$ with the ZAR1-RSK1 dimer that drives conformational rearrangements, resulting in the formation of a pentameric complex, termed resistosome. The ZAR1 resistosome translocates to the PM where it forms a calcium-permeable channel. Calcium influx results in ZAR1-mediated ETI responses. Whether other RNL-independent CNLs, like RPM1, use a similar working mechanism, remains to be investigated. Note: Proteins, domains and molecules are not drawn to scale.

6. References

1. Aarts N., Metz M., Holub E., Staskawicz B.J., Daniels M.J. & Parker J.E. (1998) Different requirements for EDS1 and NDR1 by disease resistance genes define at least two R gene-mediated signaling pathways in Arabidopsis. Proc Natl Acad Sci U S A 95, 10306-11.

2. Adachi H., Contreras M.P., Harant A., Wu C.H., Derevnina L., Sakai T., Duggan C., Moratto E., Bozkurt T.O., Maqbool A., Win J. & Kamoun S. (2019a) An N-terminal motif in NLR immune receptors is functionally conserved across distantly related plant species. Elife 8.

3. Adachi H., Derevnina L. & Kamoun S. (2019b) NLR singletons, pairs, and networks: evolution, assembly, and regulation of the intracellular immunoreceptor circuitry of plants. Current Opinion in Plant Biology 50, 121-31.

4. Ade J., DeYoung B.J., Golstein C. & Innes R.W. (2007) Indirect activation of a plant nucleotide binding site-leucine-rich repeat protein by a bacterial protease. Proc Natl Acad Sci U S A 104, 2531-6.

5. Albert I., Bohm H., Albert M., Feiler C.E., Imkampe J., Wallmeroth N., Brancato C., Raaymakers T.M., Oome S., Zhang H., Krol E., Grefen C., Gust A.A., Chai J., Hedrich R., Van den Ackerveken G. & Nurnberger T. (2015) An RLP23-SOBIR1-BAK1 complex mediates NLP-triggered immunity. Nat Plants 1, 15140.

6. Albert I., Hua C., Nurnberger T., Pruitt R.N. & Zhang L. (2020) Surface Sensor Systems in Plant Immunity. Plant Physiol 182, 1582-96.

7. Albert M., Jehle A.K., Mueller K., Eisele C., Lipschis M. & Felix G. (2010) Arabidopsis thaliana pattern recognition receptors for bacterial elongation factor Tu and flagellin can be combined to form functional chimeric receptors. J Biol Chem 285, 19035-42.

8. Andreeva L., David L., Rawson S., Shen C., Pasricha T., Pelegrin P. & Wu H. (2021) NLRP3 cages revealed by full-length mouse NLRP3 structure control pathway activation. Cell.

9. Axtell M.J., Chisholm S.T., Dahlbeck D. & Staskawicz B.J. (2003) Genetic and molecular evidence that the Pseudomonas syringae type III effector protein AvrRpt2 is a cysteine protease. Mol Microbiol 49, 1537-46.

10. Baggs E.L., Monroe J.G., Thanki A.S., O'Grady R., Schudoma C., Haerty W. & Krasileva K.V. (2020) Convergent Loss of an EDS1/PAD4 Signaling Pathway in Several Plant Lineages Reveals Coevolved Components of Plant Immunity and Drought Response. Plant Cell 32, 2158-77.

11. Balint-Kurti P. (2019) The plant hypersensitive response: concepts, control and consequences. Mol Plant Pathol 20, 1163-78.

12. Baudin M., Hassan J.A., Schreiber K.J. & Lewis J.D. (2017) Analysis of the ZAR1 Immune Complex Reveals Determinants for Immunity and Molecular Interactions. Plant Physiol 174, 2038-53.

13. Bentham A.R., Zdrzałek R., De la Concepcion J.C. & Banfield M.J. (2018) Uncoiling CNLs: Structure/function approaches to understanding CC domain function in plant NLRs. Plant and Cell Physiology.

14. Bernoux M., Burdett H., Williams S.J., Zhang X., Chen C., Newell K., Lawrence G.J., Kobe B., Ellis J.G., Anderson P.A. & Dodds P.N. (2016) Comparative Analysis of the Flax Immune Receptors L6 and L7 Suggests an Equilibrium-Based Switch Activation Model. Plant Cell 28, 146-59.

15. Bernoux M., Ve T., Williams S., Warren C., Hatters D., Valkov E., Zhang X., Ellis J.G., Kobe B. & Dodds P.N. (2011) Structural and functional analysis of a plant resistance protein TIR domain reveals interfaces for self-association, signaling, and autoregulation. Cell Host Microbe 9, 200-11.

16. Bethke G., Unthan T., Uhrig J.F., Poschl Y., Gust A.A., Scheel D. & Lee J. (2009) Flg22 regulates the release of an ethylene response factor substrate from MAP kinase 6 in Arabidopsis thaliana via ethylene signaling. Proc Natl Acad Sci U S A 106, 8067-72.

17. Bhandari D.D., Lapin D., Kracher B., von Born P., Bautor J., Niefind K. & Parker J.E. (2019) An EDS1 heterodimer signalling surface enforces timely reprogramming of immunity genes in Arabidopsis. Nat Commun 10, 772.

18. Bhattacharjee S., Halane M.K., Kim S.H. & Gassmann W. (2011) Pathogen effectors target Arabidopsis EDS1 and alter its interactions with immune regulators. Science 334, 1405-8.

19. Bi G., Su M., Li N., Liang Y., Dang S., Xu J., Hu M., Wang J., Zou M., Deng Y., Li Q., Huang S., Li J., Chai J., He K., Chen Y.H. & Zhou J.M. (2021) The ZAR1 resistosome is a calcium-permeable channel triggering plant immune signaling. Cell 184, 3528-41 e12.

20. Binder A., Lambert J., Morbitzer R., Popp C., Ott T., Lahaye T. & Parniske M. (2014) A modular plasmid assembly kit for multigene expression, gene silencing and silencing rescue in plants. PLoS One 9, e88218.

21. Bleckmann A., Weidtkamp-Peters S., Seidel C.A. & Simon R. (2010) Stem cell signaling in Arabidopsis requires CRN to localize CLV2 to the plasma membrane. Plant Physiol 152, 166-76.

22. Blume B., Nurnberger T., Nass N. & Scheel D. (2000) Receptor-mediated increase in cytoplasmic free calcium required for activation of pathogen defense in parsley. Plant Cell 12, 1425-40.

23. Bonardi V., Cherkis K., Nishimura M.T. & Dangl J.L. (2012) A new eye on NLR proteins: focused on clarity or diffused by complexity? Curr Opin Immunol 24, 41-50.

24. Bonardi V., Tang S., Stallmann A., Roberts M., Cherkis K. & Dangl J.L. (2011) Expanded functions for a family of plant intracellular immune receptors beyond specific recognition of pathogen effectors. Proc Natl Acad Sci U S A 108, 16463-8.

25. Boudsocq M., Willmann M.R., McCormack M., Lee H., Shan L., He P., Bush J., Cheng S.H. & Sheen J. (2010) Differential innate immune signalling via Ca(2+) sensor protein kinases. Nature 464, 418-22.

26. Cao Y., Aceti D.J., Sabat G., Song J., Makino S., Fox B.G. & Bent A.F. (2013) Mutations in FLS2 Ser-938 dissect signaling activation in FLS2-mediated Arabidopsis immunity. PLoS Pathog 9, e1003313.

27. Casey L.W., Lavrencic P., Bentham A.R., Cesari S., Ericsson D.J., Croll T., Turk D., Anderson P.A., Mark A.E., Dodds P.N., Mobli M., Kobe B. & Williams S.J. (2016) The CC domain structure from the wheat stem rust resistance protein Sr33 challenges paradigms for dimerization in plant NLR proteins. Proc Natl Acad Sci U S A 113, 12856-61.

28. Castel B., Ngou P.M., Cevik V., Redkar A., Kim D.S., Yang Y., Ding P. & Jones J.D.G. (2018) Diverse NLR immune receptors activate defence via the RPW8-NLR NRG1. New Phytol.

29. Castel B., Ngou P.M., Cevik V., Redkar A., Kim D.S., Yang Y., Ding P. & Jones J.D.G. (2019) Diverse NLR immune receptors activate defence via the RPW8-NLR NRG1. New Phytol 222, 966-80.

30. Century K.S., Holub E.B. & Staskawicz B.J. (1995) NDR1, a locus of Arabidopsis thaliana that is required for disease resistance to both a bacterial and a fungal pathogen. Proc Natl Acad Sci U S A 92, 6597-601.

31. Century K.S., Shapiro A.D., Repetti P.P., Dahlbeck D., Holub E. & Staskawicz B.J. (1997) NDR1, a pathogen-induced component required for Arabidopsis disease resistance. Science 278, 1963-5.

32. Cesari S. (2018) Multiple strategies for pathogen perception by plant immune receptors. New Phytol 219, 17-24.

33. Cesari S., Bernoux M., Moncuquet P., Kroj T. & Dodds P.N. (2014a) A novel conserved mechanism for plant NLR protein pairs: the "integrated decoy" hypothesis. Front Plant Sci 5, 606.

34. Cesari S., Kanzaki H., Fujiwara T., Bernoux M., Chalvon V., Kawano Y., Shimamoto K., Dodds P., Terauchi R. & Kroj T. (2014b) The NB-LRR proteins RGA4 and RGA5 interact functionally and physically to confer disease resistance. EMBO J 33, 1941-59.

35. Cesari S., Moore J., Chen C., Webb D., Periyannan S., Mago R., Bernoux M., Lagudah E.S. & Dodds P.N. (2016) Cytosolic activation of cell death and stem rust resistance by cereal MLA-family CC-NLR proteins. Proc Natl Acad Sci U S A 113, 10204-9.

36. Chai J. & Shi Y. (2014) Apoptosome and inflammasome: conserved machineries for caspase activation. National Science Review 1, 101-18.

37. Chen T., Liu D., Niu X., Wang J., Qian L., Han L., Liu N., Zhao J., Hong Y. & Liu Y. (2017) Antiviral Resistance Protein Tm-2(2) Functions on the Plasma Membrane. Plant Physiol 173, 2399-410.

38. Chen X., He W.-t., Hu L., Li J., Fang Y., Wang X., Xu X., Wang Z., Huang K. & Han J. (2016) Pyroptosis is driven by non-selective gasdermin-D pore and its morphology is different from MLKL channel-mediated necroptosis. Cell Research 26, 1007-20.

39. Chen X., Li W., Ren J., Huang D., He W.T., Song Y., Yang C., Li W., Zheng X., Chen P. & Han J. (2014) Translocation of mixed lineage kinase domain-like protein to plasma membrane leads to necrotic cell death. Cell Res 24, 105-21.

40. Cheng W., Munkvold K.R., Gao H., Mathieu J., Schwizer S., Wang S., Yan Y.B., Wang J., Martin G.B. & Chai J. (2011) Structural analysis of Pseudomonas syringae AvrPtoB bound to host BAK1 reveals two similar kinase-interacting domains in a type III Effector. Cell Host Microbe 10, 616-26.

41. Chinchilla D., Zipfel C., Robatzek S., Kemmerling B., Nurnberger T., Jones J.D., Felix G. & Boller T. (2007) A flagellin-induced complex of the receptor FLS2 and BAK1 initiates plant defence. Nature 448, 497-500.

42. Chini A., Grant J.J., Seki M., Shinozaki K. & Loake G.J. (2004) Drought tolerance established by enhanced expression of the CC-NBS-LRR gene, ADR1, requires salicylic acid, EDS1 and ABI1. Plant J 38, 810-22.

43. Collier S.M., Hamel L.P. & Moffett P. (2011) Cell death mediated by the N-terminal domains of a unique and highly conserved class of NB-LRR protein. Mol Plant Microbe Interact 24, 918-31.

44. Coppinger P., Repetti P.P., Day B., Dahlbeck D., Mehlert A. & Staskawicz B.J. (2004) Overexpression of the plasma membrane-localized NDR1 protein results in enhanced bacterial disease resistance in Arabidopsis thaliana. Plant J 40, 225-37.

45. Couto D. & Zipfel C. (2016) Regulation of pattern recognition receptor signalling in plants. Nat Rev Immunol 16, 537-52.

46. Cui H., Gobbato E., Kracher B., Qiu J., Bautor J. & Parker J.E. (2017) A core function of EDS1 with PAD4 is to protect the salicylic acid defense sector in Arabidopsis immunity. New Phytol 213, 1802-17.

47. Curtis M.D. & Grossniklaus U. (2003) A gateway cloning vector set for high-throughput functional analysis of genes in planta. Plant Physiol 133, 462-9.

48. Dangl J.L. & Jones J.D. (2001) Plant pathogens and integrated defence responses to infection. Nature 411, 826-33.

49. Day B., Dahlbeck D. & Staskawicz B.J. (2006) NDR1 interaction with RIN4 mediates the differential activation of multiple disease resistance pathways in Arabidopsis. Plant Cell 18, 2782-91.

50. Derevnina L., Contreras M.P., Adachi H., Upson J., Vergara Cruces A., Xie R., Sklenar J., Menke F.L.H., Mugford S.T., MacLean D., Ma W., Hogenhout S.A., Goverse A., Maqbool A., Wu C.H. & Kamoun S. (2021) Plant pathogens convergently evolved to counteract redundant nodes of an NLR immune receptor network. PLoS Biol 19, e3001136.

51. Deslandes L., Olivier J., Theulieres F., Hirsch J., Feng D.X., Bittner-Eddy P., Beynon J. & Marco Y. (2002) Resistance to Ralstonia solanacearum in Arabidopsis thaliana is conferred by the recessive RRS1-R gene, a member of a novel family of resistance genes. Proc Natl Acad Sci U S A 99, 2404-9.

52. Dinarello C.A. (2018) Overview of the IL-1 family in innate inflammation and acquired immunity. Immunol Rev 281, 8-27.

53. Djamei A., Pitzschke A., Nakagami H., Rajh I. & Hirt H. (2007) Trojan horse strategy in Agrobacterium transformation: abusing MAPK defense signaling. Science 318, 453-6.

54. Doke N. (1983) Generation of superoxide anion by potato tuber protoplasts during hypersensitive response to hyphal wall components of Phytophtora infestans and specific inhibition of the reaction with supressors of hypersensitivity. Physiol. Plant Pathol. 23, 359-67.

55. Dondelinger Y., Declercq W., Montessuit S., Roelandt R., Goncalves A., Bruggeman I., Hulpiau P., Weber K., Sehon C.A., Marquis R.W., Bertin J., Gough P.J., Savvides S., Martinou J.C., Bertrand M.J. & Vandenabeele P. (2014) MLKL compromises plasma membrane integrity by binding to phosphatidylinositol phosphates. Cell Rep 7, 971-81.

56. Dong O.X., Tong M., Bonardi V., El Kasmi F., Woloshen V., Wunsch L.K., Dangl J.L. & Li X. (2016) TNL-mediated immunity in Arabidopsis requires complex regulation of the redundant ADR1 gene family. New Phytol 210, 960-73.

57. Doumane M., Lebecq A., Colin L., Fangain A., Stevens F.D., Bareille J., Hamant O., Belkhadir Y., Munnik T., Jaillais Y. & Caillaud M.C. (2021) Inducible depletion of PI(4,5)P2 by the synthetic iDePP system in Arabidopsis. Nat Plants 7, 587-97.

58. Du J., Verzaux E., Chaparro-Garcia A., Bijsterbosch G., Keizer L.C., Zhou J., Liebrand T.W., Xie C., Govers F., Robatzek S., van der Vossen E.A., Jacobsen

E., Visser R.G., Kamoun S. & Vleeshouwers V.G. (2015) Elicitin recognition confers enhanced resistance to Phytophthora infestans in potato. Nat Plants 1, 15034.

59. Duggan C., Moratto E., Savage Z., Hamilton E., Adachi H., Wu C.H., Leary A.Y., Tumtas Y., Rothery S.M., Maqbool A., Nohut S., Martin T.R., Kamoun S. & Bozkurt T.O. (2021) Dynamic localization of a helper NLR at the plant-pathogen interface underpins pathogen recognition. Proc Natl Acad Sci U S A 118.

60. Eastman S., Smith T., Zaydman M.A., Kim P., Martinez S., Damaraju N., DiAntonio A., Milbrandt J., Clemente T.E., Alfano J.R. & Guo M. (2021) A phytobacterial TIR domain effector manipulates NAD(+) to promote virulence. New Phytol.

61. El Kasmi F. (2021) How activated NLRs induce anti-microbial defenses in plants. Biochemical Society Transactions.

62. El Kasmi F., Chung E.H., Anderson R.G., Li J., Wan L., Eitas T.K., Gao Z. & Dangl J.L. (2017) Signaling from the plasma-membrane localized plant immune receptor RPM1 requires self-association of the full-length protein. Proc Natl Acad Sci U S A 114, E7385-E94.

63. El Kasmi F. & Nishimura M.T. (2016) Structural insights into plant NLR immune receptor function. Proc Natl Acad Sci U S A 113, 12619-21.

64. Evavold C.L., Ruan J., Tan Y., Xia S., Wu H. & Kagan J.C. (2018) The Pore-Forming Protein Gasdermin D Regulates Interleukin-1 Secretion from Living Macrophages. Immunity 48, 35-44 e6.

65. Feng F., Yang F., Rong W., Wu X., Zhang J., Chen S., He C. & Zhou J.M. (2012) A Xanthomonas uridine 5'-monophosphate transferase inhibits plant immune kinases. Nature 485, 114-8.

66. Feys B.J., Wiermer M., Bhat R.A., Moisan L.J., Medina-Escobar N., Neu C., Cabral A. & Parker J.E. (2005) Arabidopsis SENESCENCE-ASSOCIATED GENE101 stabilizes and signals within an ENHANCED DISEASE SUSCEPTIBILITY1 complex in plant innate immunity. Plant Cell 17, 2601-13.

67. Fliegert R., Gasser A. & Guse A.H. (2007) Regulation of calcium signalling by adenine-based second messengers. Biochem Soc Trans 35, 109-14.

68. Fliegert R., Watt J.M., Schobel A., Rozewitz M.D., Moreau C., Kirchberger T., Thomas M.P., Sick W., Araujo A.C., Harneit A., Potter B.V.L. & Guse A.H. (2017) Ligand-induced activation of human TRPM2 requires the terminal ribose of ADPR and involves Arg1433 and Tyr1349. Biochem J 474, 2159-75.

69. Gabriels S.H., Vossen J.H., Ekengren S.K., van Ooijen G., Abd-El-Haliem A.M., van den Berg G.C., Rainey D.Y., Martin G.B., Takken F.L., de Wit P.J. & Joosten M.H. (2007) An NB-LRR protein required for HR signalling mediated by both extra- and intracellular resistance proteins. Plant J 50, 14-28.

70. Galletti R., Ferrari S. & De Lorenzo G. (2011) Arabidopsis MPK3 and MPK6 play different roles in basal and oligogalacturonide- or flagellin-induced resistance against Botrytis cinerea. Plant Physiol 157, 804-14.

71. Gantner J., Ordon J., Kretschmer C., Guerois R. & Stuttmann J. (2019) An EDS1-SAG101 Complex Is Essential for TNL-Mediated Immunity in Nicotiana benthamiana. Plant Cell 31, 2456-74.

72. Gao M., Wang X., Wang D., Xu F., Ding X., Zhang Z., Bi D., Cheng Y.T., Chen S., Li X. & Zhang Y. (2009) Regulation of cell death and innate immunity by two receptor-like kinases in Arabidopsis. Cell Host Microbe 6, 34-44.

73. Gao Z., Chung E.H., Eitas T.K. & Dangl J.L. (2011) Plant intracellular innate immune receptor Resistance to Pseudomonas syringae pv. maculicola 1 (RPM1) is activated at, and functions on, the plasma membrane. Proc Natl Acad Sci U S A 108, 7619-24.

74. Gimenez-Ibanez S., Hann D.R., Ntoukakis V., Petutschnig E., Lipka V. & Rathjen J.P. (2009) AvrPtoB targets the LysM receptor kinase CERK1 to promote bacterial virulence on plants. Curr Biol 19, 423-9.

75. Gohre V., Spallek T., Haweker H., Mersmann S., Mentzel T., Boller T., de Torres M., Mansfield J.W. & Robatzek S. (2008) Plant pattern-recognition receptor FLS2 is directed for degradation by the bacterial ubiquitin ligase AvrPtoB. Curr Biol 18, 1824-32.

76. Gomez-Gomez L. & Boller T. (2000) FLS2: an LRR receptor-like kinase involved in the perception of the bacterial elicitor flagellin in Arabidopsis. Mol Cell 5, 1003-11.

77. Gopalan S., Bauer D.W., Alfano J.R., Loniello A.O., He S.Y. & Collmer A. (1996) Expression of the Pseudomonas syringae avirulence protein AvrB in plant cells alleviates its dependence on the hypersensitive response and pathogenicity (Hrp) secretion system in eliciting genotype-specific hypersensitive cell death. Plant Cell 8, 1095-105.

78. Gou X., He K., Yang H., Yuan T., Lin H., Clouse S.D. & Li J. (2010) Genome-wide cloning and sequence analysis of leucine-rich repeat receptor-like protein kinase genes in Arabidopsis thaliana. BMC Genomics 11, 19.

79. Gou X., Yin H., He K., Du J., Yi J., Xu S., Lin H., Clouse S.D. & Li J. (2012) Genetic evidence for an indispensable role of somatic embryogenesis receptor kinases in brassinosteroid signaling. PLoS Genet 8, e1002452.

80. Grant J.J., Chini A., Basu D. & Loake G.J. (2003) Targeted activation tagging of the Arabidopsis NBS-LRR gene, ADR1, conveys resistance to virulent pathogens. Mol Plant Microbe Interact 16, 669-80.

81. Grant M., Brown I., Adams S., Knight M., Ainslie A. & Mansfield J. (2000) The RPM1 plant disease resistance gene facilitates a rapid and sustained increase

in cytosolic calcium that is necessary for the oxidative burst and hypersensitive cell death. Plant J 23, 441-50.

82. Grefen C. & Blatt M.R. (2012) A 2in1 cloning system enables ratiometric bimolecular fluorescence complementation (rBiFC). Biotechniques 53, 311-14.

83. Guse A.H. (2015) Calcium mobilizing second messengers derived from NAD. Biochim Biophys Acta 1854, 1132-7.

84. Gust A.A. & Felix G. (2014) Receptor like proteins associate with SOBIR1-type of adaptors to form bimolecular receptor kinases. Current Opinion in Plant Biology 21, 104-11.

85. He K., Gou X., Yuan T., Lin H., Asami T., Yoshida S., Russell S.D. & Li J. (2007) BAK1 and BKK1 regulate brassinosteroid-dependent growth and brassinosteroid-independent cell-death pathways. Curr Biol 17, 1109-15.

86. He P., Shan L., Lin N.C., Martin G.B., Kemmerling B., Nurnberger T. & Sheen J. (2006) Specific bacterial suppressors of MAMP signaling upstream of MAPKKK in Arabidopsis innate immunity. Cell 125, 563-75.

87. He S.Y., Huang H.C. & Collmer A. (1993) Pseudomonas syringae pv. syringae harpinPss: a protein that is secreted via the Hrp pathway and elicits the hypersensitive response in plants. Cell 73, 1255-66.

88. Hecht V., Vielle-Calzada J.P., Hartog M.V., Schmidt E.D., Boutilier K., Grossniklaus U. & de Vries S.C. (2001) The Arabidopsis SOMATIC EMBRYOGENESIS RECEPTOR KINASE 1 gene is expressed in developing ovules and embryos and enhances embryogenic competence in culture. Plant Physiol 127, 803-16.

89. Heilig R., Dick M.S., Sborgi L., Meunier E., Hiller S. & Broz P. (2018) The Gasdermin-D pore acts as a conduit for IL-1beta secretion in mice. Eur J Immunol 48, 584-92.

90. Horsefield S., Burdett H., Zhang X., Manik M.K., Shi Y., Chen J., Qi T., Gilley J., Lai J.S., Rank M.X., Casey L.W., Gu W., Ericsson D.J., Foley G., Hughes R.O., Bosanac T., von Itzstein M., Rathjen J.P., Nanson J.D., Boden M., Dry I.B., Williams S.J., Staskawicz B.J., Coleman M.P., Ve T., Dodds P.N. & Kobe B. (2019) NAD(+) cleavage activity by animal and plant TIR domains in cell death pathways. Science 365, 793-9.

91. Hu M., Qi J., Bi G. & Zhou J.M. (2020) Bacterial Effectors Induce Oligomerization of Immune Receptor ZAR1 In Vivo. Mol Plant 13, 793-801.

92. Hu Z., Yan C., Liu P., Huang Z., Ma R., Zhang C., Wang R., Zhang Y., Martinon F., Miao D., Deng H., Wang J., Chang J. & Chai J. (2013) Crystal structure of NLRC4 reveals its autoinhibition mechanism. Science 341, 172-5.

93. Huang D., Zheng X., Wang Z.A., Chen X., He W.T., Zhang Y., Xu J.G., Zhao H., Shi W., Wang X., Zhu Y. & Han J. (2017) The MLKL Channel in Necroptosis Is an Octamer Formed by Tetramers in a Dyadic Process. Mol Cell Biol 37.

94. Huffaker A., Pearce G. & Ryan C.A. (2006) An endogenous peptide signal in Arabidopsis activates components of the innate immune response. Proc Natl Acad Sci U S A 103, 10098-103.

95. Huh S.U., Cevik V., Ding P., Duxbury Z., Ma Y., Tomlinson L., Sarris P.F. & Jones J.D.G. (2017) Protein-protein interactions in the RPS4/RRS1 immune receptor complex. PLoS Pathog 13, e1006376.

96. Isaacson T., Kosma D.K., Matas A.J., Buda G.J., He Y., Yu B., Pravitasari A., Batteas J.D., Stark R.E., Jenks M.A. & Rose J.K. (2009) Cutin deficiency in the tomato fruit cuticle consistently affects resistance to microbial infection and biomechanical properties, but not transpirational water loss. Plant J 60, 363-77.

97. Jacob P., Kim N.H., Wu F., El-Kasmi F., Chi Y., Walton W.G., Furzer O.J., Lietzan A.D., Sunil S., Kempthorn K., Redinbo M.R., Pei Z.M., Wan L. & Dangl J.L. (2021) Plant "helper" immune receptors are Ca(2+)-permeable nonselective cation channels. Science.

98. Jeworutzki E., Roelfsema M.R., Anschutz U., Krol E., Elzenga J.T., Felix G., Boller T., Hedrich R. & Becker D. (2010) Early signaling through the Arabidopsis pattern recognition receptors FLS2 and EFR involves Ca-associated opening of plasma membrane anion channels. Plant J 62, 367-78.

99. Jia Y., McAdams S.A., Bryan G.T., Hershey H.P. & Valent B. (2000) Direct interaction of resistance gene and avirulence gene products confers rice blast resistance. EMBO J 19, 4004-14.

100. Jones J.D. & Dangl J.L. (2006) The plant immune system. Nature 444, 323-9.

101. Jubic L.M., Saile S., Furzer O.J., El Kasmi F. & Dangl J.L. (2019) Help wanted: helper NLRs and plant immune responses. Current Opinion in Plant Biology 50, 82-94.

102. Kang S., Yang F., Li L., Chen H., Chen S. & Zhang J. (2015) The Arabidopsis transcription factor BRASSINOSTEROID INSENSITIVE1-ETHYL METHANESULFONATE-SUPPRESSOR1 is a direct substrate of MITOGEN-ACTIVATED PROTEIN KINASE6 and regulates immunity. Plant Physiol 167, 1076-86.

103. Kawano Y., Fujiwara T., Yao A., Housen Y., Hayashi K. & Shimamoto K. (2014) Palmitoylation-dependent membrane localization of the rice resistance protein pit is critical for the activation of the small GTPase OsRac1. J Biol Chem 289, 19079-88.

104. Knepper C., Savory E.A. & Day B. (2011) Arabidopsis NDR1 is an integrin-like protein with a role in fluid loss and plasma membrane-cell wall adhesion. Plant Physiol 156, 286-300.

105. Kourelis J., Contreras M.P., Harant A., Adachi H., Derevnina L., Wu C.-H. & Kamoun S. (2021) The helper NLR immune protein NRC3 mediates the hypersensitive cell death caused by the cell-surface receptor Cf-4. bioRxiv, 2021.09.28.461843.

106. Krasileva K.V., Dahlbeck D. & Staskawicz B.J. (2010) Activation of an Arabidopsis resistance protein is specified by the in planta association of its leucine-rich repeat domain with the cognate oomycete effector. Plant Cell 22, 2444-58.

107. Kunze G., Zipfel C., Robatzek S., Niehaus K., Boller T. & Felix G. (2004) The N terminus of bacterial elongation factor Tu elicits innate immunity in Arabidopsis plants. Plant Cell 16, 3496-507.

108. Kutschera A., Dawid C., Gisch N., Schmid C., Raasch L., Gerster T., Schaffer M., Smakowska-Luzan E., Belkhadir Y., Vlot A.C., Chandler C.E., Schellenberger R., Schwudke D., Ernst R.K., Dorey S., Huckelhoven R., Hofmann T. & Ranf S. (2019) Bacterial medium-chain 3-hydroxy fatty acid metabolites trigger immunity in Arabidopsis plants. Science 364, 178-81.

109. Laflamme B., Dillon M.M., Martel A., Almeida R.N.D., Desveaux D. & Guttman D.S. (2020) The pan-genome effector-triggered immunity landscape of a host-pathogen interaction. Science 367, 763-8.

110. Lapin D., Kovacova V., Sun X., Dongus J.A., Bhandari D., von Born P., Bautor J., Guarneri N., Rzemieniewski J., Stuttmann J., Beyer A. & Parker J.E. (2019) A Coevolved EDS1-SAG101-NRG1 Module Mediates Cell Death Signaling by TIR-Domain Immune Receptors. Plant Cell 31, 2430-55.

111. Leibman-Markus M., Pizarro L., Schuster S., Lin Z.J.D., Gershony O., Bar M., Coaker G. & Avni A. (2018) The intracellular nucleotide-binding leucine-rich repeat receptor (SlNRC4a) enhances immune signalling elicited by extracellular perception. Plant Cell Environ 41, 2313-27.

112. Levine A., Tenhaken R., Dixon R. & Lamb C. (1994) H2O2 from the oxidative burst orchestrates the plant hypersensitive disease resistance response. Cell 79, 583-93.

113. Levy M., Wang Q., Kaspi R., Parrella M.P. & Abel S. (2005) Arabidopsis IQD1, a novel calmodulin-binding nuclear protein, stimulates glucosinolate accumulation and plant defense. Plant J 43, 79-96.

114. Li J. (2010) Multi-tasking of somatic embryogenesis receptor-like protein kinases. Current Opinion in Plant Biology 13, 509-14.

115. Li J., Wen J., Lease K.A., Doke J.T., Tax F.E. & Walker J.C. (2002) BAK1, an Arabidopsis LRR receptor-like protein kinase, interacts with BRI1 and modulates brassinosteroid signaling. Cell 110, 213-22.

116. Li L., Habring A., Wang K. & Weigel D. (2020) Atypical Resistance Protein RPW8/HR Triggers Oligomerization of the NLR Immune Receptor RPP7 and Autoimmunity. Cell Host Microbe 27, 405-17 e6.

117. Li L., Kim P., Yu L., Cai G., Chen S., Alfano J.R. & Zhou J.M. (2016) Activation-Dependent Destruction of a Co-receptor by a Pseudomonas syringae Effector Dampens Plant Immunity. Cell Host Microbe 20, 504-14.

118. Li L., Li M., Yu L., Zhou Z., Liang X., Liu Z., Cai G., Gao L., Zhang X., Wang Y., Chen S. & Zhou J.M. (2014) The FLS2-associated kinase BIK1 directly phosphorylates the NADPH oxidase RbohD to control plant immunity. Cell Host Microbe 15, 329-38.

119. Li X., Clarke J.D., Zhang Y. & Dong X. (2001) Activation of an EDS1-mediated R-gene pathway in the snc1 mutant leads to constitutive, NPR1-independent pathogen resistance. Mol Plant Microbe Interact 14, 1131-9.

120. Lin W., Li B., Lu D., Chen S., Zhu N., He P. & Shan L. (2014) Tyrosine phosphorylation of protein kinase complex BAK1/BIK1 mediates Arabidopsis innate immunity. Proc Natl Acad Sci U S A 111, 3632-7.

121. Liu T., Zhang L., Joo D. & Sun S.C. (2017) NF-kappaB signaling in inflammation. Signal Transduct Target Ther 2.

122. Liu X., Zhang Z., Ruan J., Pan Y., Magupalli V.G., Wu H. & Lieberman J. (2016) Inflammasome-activated gasdermin D causes pyroptosis by forming membrane pores. Nature 535, 153-8.

123. Lolle S., Greeff C., Petersen K., Roux M., Jensen M.K., Bressendorff S., Rodriguez E., Somark K., Mundy J. & Petersen M. (2017) Matching NLR Immune Receptors to Autoimmunity in camta3 Mutants Using Antimorphic NLR Alleles. Cell Host Microbe 21, 518-29 e4.

124. Lu D., Wu S., Gao X., Zhang Y., Shan L. & He P. (2010a) A receptor-like cytoplasmic kinase, BIK1, associates with a flagellin receptor complex to initiate plant innate immunity. Proc Natl Acad Sci U S A 107, 496-501.

125. Lu D., Wu S., He P. & Shan L. (2010b) Phosphorylation of receptor-like cytoplasmic kinases by bacterial flagellin. Plant Signal Behav 5, 598-600.

126. Lu Y. & Tsuda K. (2021) Intimate Association of PRR- and NLR-Mediated Signaling in Plant Immunity. Mol Plant Microbe Interact 34, 3-14.

127. Ma S., Lapin D., Liu L., Sun Y., Song W., Zhang X., Logemann E., Yu D., Wang J., Jirschitzka J., Han Z., Schulze-Lefert P., Parker J.E. & Chai J. (2020) Direct

pathogen-induced assembly of an NLR immune receptor complex to form a holoenzyme. Science 370.

128. Ma X., Xu G., He P. & Shan L. (2016) SERKing Coreceptors for Receptors. Trends in Plant Science 21, 1017-33.

129. Macho A.P., Schwessinger B., Ntoukakis V., Brutus A., Segonzac C., Roy S., Kadota Y., Oh M.H., Sklenar J., Derbyshire P., Lozano-Duran R., Malinovsky F.G., Monaghan J., Menke F.L., Huber S.C., He S.Y. & Zipfel C. (2014) A bacterial tyrosine phosphatase inhibits plant pattern recognition receptor activation. Science 343, 1509-12.

130. Mackey D., Holt B.F., 3rd, Wiig A. & Dangl J.L. (2002) RIN4 interacts with Pseudomonas syringae type III effector molecules and is required for RPM1-mediated resistance in Arabidopsis. Cell 108, 743-54.

131. Maekawa T., Cheng W., Spiridon L.N., Toller A., Lukasik E., Saijo Y., Liu P., Shen Q.H., Micluta M.A., Somssich I.E., Takken F.L.W., Petrescu A.J., Chai J. & Schulze-Lefert P. (2011) Coiled-coil domain-dependent homodimerization of intracellular barley immune receptors defines a minimal functional module for triggering cell death. Cell Host Microbe 9, 187-99.

132. Malinovsky F.G., Fangel J.U. & Willats W.G. (2014) The role of the cell wall in plant immunity. Front Plant Sci 5, 178.

133. Mao G., Meng X., Liu Y., Zheng Z., Chen Z. & Zhang S. (2011) Phosphorylation of a WRKY transcription factor by two pathogen-responsive MAPKs drives phytoalexin biosynthesis in Arabidopsis. Plant Cell 23, 1639-53.

134. Martin R., Qi T., Zhang H., Liu F., King M., Toth C., Nogales E. & Staskawicz B.J. (2020) Structure of the activated ROQ1 resistosome directly recognizing the pathogen effector XopQ. Science 370.

135. Mehlhorn D.G., Wallmeroth N., Berendzen K.W. & Grefen C. (2018) 2in1 Vectors Improve In Planta BiFC and FRET Analyses. Methods Mol Biol 1691, 139-58.

136. Meng X., Zhou J., Tang J., Li B., de Oliveira M.V.V., Chai J., He P. & Shan L. (2016) Ligand-Induced Receptor-like Kinase Complex Regulates Floral Organ Abscission in Arabidopsis. Cell Rep 14, 1330-8.

137. Mersmann S., Bourdais G., Rietz S. & Robatzek S. (2010) Ethylene signaling regulates accumulation of the FLS2 receptor and is required for the oxidative burst contributing to plant immunity. Plant Physiol 154, 391-400.

138. Mestre P. & Baulcombe D.C. (2006) Elicitor-mediated oligomerization of the tobacco N disease resistance protein. Plant Cell 18, 491-501.

139. Meyers B.C., Dickerman A.W., Michelmore R.W., Sivaramakrishnan S., Sobral B.W. & Young N.D. (1999) Plant disease resistance genes encode members of

an ancient and diverse protein family within the nucleotide-binding superfamily. Plant J 20, 317-32.

140. Miya A., Albert P., Shinya T., Desaki Y., Ichimura K., Shirasu K., Narusaka Y., Kawakami N., Kaku H. & Shibuya N. (2007) CERK1, a LysM receptor kinase, is essential for chitin elicitor signaling in Arabidopsis. Proc Natl Acad Sci U S A 104, 19613-8.

141. Nakamura S., Mano S., Tanaka Y., Ohnishi M., Nakamori C., Araki M., Niwa T., Nishimura M., Kaminaka H., Nakagawa T., Sato Y. & Ishiguro S. (2010) Gateway binary vectors with the bialaphos resistance gene, bar, as a selection marker for plant transformation. Biosci Biotechnol Biochem 74, 1315-9.

142. Nasim Z., Fahim M., Gawarecka K., Susila H., Jin S., Youn G. & Ahn J.H. (2020) Role of AT1G72910, AT1G72940, and ADR1-LIKE 2 in Plant Immunity under Nonsense-Mediated mRNA Decay-Compromised Conditions at Low Temperatures. Int J Mol Sci 21.

143. Nekrasov V., Li J., Batoux M., Roux M., Chu Z.H., Lacombe S., Rougon A., Bittel P., Kiss-Papp M., Chinchilla D., van Esse H.P., Jorda L., Schwessinger B., Nicaise V., Thomma B.P., Molina A., Jones J.D. & Zipfel C. (2009) Control of the pattern-recognition receptor EFR by an ER protein complex in plant immunity. EMBO J 28, 3428-38.

144. Ngou B.P.M., Ahn H.K., Ding P. & Jones J.D.G. (2021) Mutual potentiation of plant immunity by cell-surface and intracellular receptors. Nature 592, 110-5.

145. Nomura H., Komori T., Uemura S., Kanda Y., Shimotani K., Nakai K., Furuichi T., Takebayashi K., Sugimoto T., Sano S., Suwastika I.N., Fukusaki E., Yoshioka H., Nakahira Y. & Shiina T. (2012) Chloroplast-mediated activation of plant immune signalling in Arabidopsis. Nat Commun 3, 926.

146. Ordon J., Gantner J., Kemna J., Schwalgun L., Reschke M., Streubel J., Boch J. & Stuttmann J. (2017) Generation of chromosomal deletions in dicotyledonous plants employing a user-friendly genome editing toolkit. Plant J 89, 155-68.

147. Orozco-Cardenas M., Naravaez-Vasquez J. & Ryan C. (2001) Hydrogen peroxide acts as a second messenger for the induction. Plant Cell 13, 179-91.

148. Ortiz D., de Guillen K., Cesari S., Chalvon V., Gracy J., Padilla A. & Kroj T. (2017) Recognition of the Magnaporthe oryzae Effector AVR-Pia by the Decoy Domain of the Rice NLR Immune Receptor RGA5. Plant Cell 29, 156-68.

149. Osbourn A.E. (1996) Preformed Antimicrobial Compounds and Plant Defense against Fungal Attack. Plant Cell 8, 1821-31.

150. Peart J.R., Mestre P., Lu R., Malcuit I. & Baulcombe D.C. (2005) NRG1, a CC-NB-LRR protein, together with N, a TIR-NB-LRR protein, mediates resistance against tobacco mosaic virus. Curr Biol 15, 968-73.

151. Peng H.C., Mantelin S., Hicks G.R., Takken F.L. & Kaloshian I. (2016) The Conformation of a Plasma Membrane-Localized Somatic Embryogenesis Receptor Kinase Complex Is Altered by a Potato Aphid-Derived Effector. Plant Physiol 171, 2211-22.

152. Postma J., Liebrand T.W., Bi G., Evrard A., Bye R.R., Mbengue M., Kuhn H., Joosten M.H. & Robatzek S. (2016) Avr4 promotes Cf-4 receptor-like protein association with the BAK1/SERK3 receptor-like kinase to initiate receptor endocytosis and plant immunity. New Phytol 210, 627-42.

153. Pruitt R.N., Locci F., Wanke F., Zhang L., Saile S.C., Joe A., Karelina D., Hua C., Frohlich K., Wan W.L., Hu M., Rao S., Stolze S.C., Harzen A., Gust A.A., Harter K., Joosten M., Thomma B., Zhou J.M., Dangl J.L., Weigel D., Nakagami H., Oecking C., Kasmi F.E., Parker J.E. & Nurnberger T. (2021) The EDS1-PAD4-ADR1 node mediates Arabidopsis pattern-triggered immunity. Nature 598, 495-9.

154. Qi D., DeYoung B.J. & Innes R.W. (2012) Structure-function analysis of the coiled-coil and leucine-rich repeat domains of the RPS5 disease resistance protein. Plant Physiol 158, 1819-32.

155. Qi D. & Innes R.W. (2013) Recent Advances in Plant NLR Structure, Function, Localization, and Signaling. Front Immunol 4, 348.

156. Qi T., Seong K., Thomazella D.P.T., Kim J.R., Pham J., Seo E., Cho M.J., Schultink A. & Staskawicz B.J. (2018) NRG1 functions downstream of EDS1 to regulate TIR-NLR-mediated plant immunity in Nicotiana benthamiana. Proc Natl Acad Sci U S A 115, E10979-E87.

157. Qian L.H., Zhou G.C., Sun X.Q., Lei Z., Zhang Y.M., Xue J.Y. & Hang Y.Y. (2017) Distinct Patterns of Gene Gain and Loss: Diverse Evolutionary Modes of NBS-Encoding Genes in Three Solanaceae Crop Species. G3 (Bethesda) 7, 1577-85.

158. Qu Y., Misaghi S., Izrael-Tomasevic A., Newton K., Gilmour L.L., Lamkanfi M., Louie S., Kayagaki N., Liu J., Komuves L., Cupp J.E., Arnott D., Monack D. & Dixit V.M. (2012) Phosphorylation of NLRC4 is critical for inflammasome activation. Nature 490, 539-42.

159. Ramirez V., Lopez A., Mauch-Mani B., Gil M.J. & Vera P. (2013) An extracellular subtilase switch for immune priming in Arabidopsis. PLoS Pathog 9, e1003445.

160. Ranf S., Eschen-Lippold L., Pecher P., Lee J. & Scheel D. (2011) Interplay between calcium signalling and early signalling elements during defence responses to microbe- or damage-associated molecular patterns. Plant J 68, 100-13.

161. Ravensdale M., Bernoux M., Ve T., Kobe B., Thrall P.H., Ellis J.G. & Dodds P.N. (2012) Intramolecular interaction influences binding of the Flax L5 and L6 resistance proteins to their AvrL567 ligands. PLoS Pathog 8, e1003004.

162. Richard M.M.S., Gratias A., Meyers B.C. & Geffroy V. (2018) Molecular mechanisms that limit the costs of NLR-mediated resistance in plants. Mol Plant Pathol 19, 2516-23.

163. Rietz S., Stamm A., Malonek S., Wagner S., Becker D., Medina-Escobar N., Corina Vlot A., Feys B.J., Niefind K. & Parker J.E. (2011) Different roles of Enhanced Disease Susceptibility1 (EDS1) bound to and dissociated from Phytoalexin Deficient4 (PAD4) in Arabidopsis immunity. New Phytol 191, 107-19.

164. Roberts M., Tang S., Stallmann A., Dangl J.L. & Bonardi V. (2013) Genetic requirements for signaling from an autoactive plant NB-LRR intracellular innate immune receptor. PLoS Genet 9, e1003465.

165. Roux M., Schwessinger B., Albrecht C., Chinchilla D., Jones A., Holton N., Malinovsky F.G., Tor M., de Vries S. & Zipfel C. (2011) The Arabidopsis leucine-rich repeat receptor-like kinases BAK1/SERK3 and BKK1/SERK4 are required for innate immunity to hemibiotrophic and biotrophic pathogens. Plant Cell 23, 2440-55.

166. Saha S., Anilkumar A.A. & Mayor S. (2016) GPI-anchored protein organization and dynamics at the cell surface. J Lipid Res 57, 159-75.

167. Saijo Y., Loo E.P. & Yasuda S. (2018) Pattern recognition receptors and signaling in plant-microbe interactions. Plant J 93, 592-613.

168. Saile S.C., Ackermann F.M., Sunil S., Keicher J., Bayless A., Bonardi V., Wan L., Doumane M., Stobbe E., Jaillais Y., Caillaud M.C., Dangl J.L., Nishimura M.T., Oecking C. & El Kasmi F. (2021) Arabidopsis ADR1 helper NLR immune receptors localize and function at the plasma membrane in a phospholipid dependent manner. New Phytol 232, 2440-56.

169. Saile S.C., Jacob P., Castel B., Jubic L.M., Salas-Gonzales I., Backer M., Jones J.D.G., Dangl J.L. & El Kasmi F. (2020) Two unequally redundant "helper" immune receptor families mediate Arabidopsis thaliana intracellular "sensor" immune receptor functions. PLoS Biol 18, e3000783.

170. Saur I.M., Kadota Y., Sklenar J., Holton N.J., Smakowska E., Belkhadir Y., Zipfel C. & Rathjen J.P. (2016) NbCSPR underlies age-dependent immune responses to bacterial cold shock protein in Nicotiana benthamiana. Proc Natl Acad Sci U S A 113, 3389-94.

171. Saur I.M.L., Panstruga R. & Schulze-Lefert P. (2021) NOD-like receptor-mediated plant immunity: from structure to cell death. Nat Rev Immunol 21, 305-18.

172. Schulze B., Mentzel T., Jehle A.K., Mueller K., Beeler S., Boller T., Felix G. & Chinchilla D. (2010) Rapid heteromerization and phosphorylation of ligand-activated plant transmembrane receptors and their associated kinase BAK1. J Biol Chem 285, 9444-51.

173. Schulze S., Yu L., Ehinger A., Kolb D., Saile S.C., Stahl M., Franz-Wachtel M., Li L., Kasmi F.E., Cevik V. & Kemmerling B. (2021) The TIR-NBS-LRR protein CSA1 is required for autoimmune cell death in Arabidopsis pattern recognition co-receptor bak1 and bir3 mutants. bioRxiv, 2021.04.11.438637.

174. Selote D., Shine M.B., Robin G.P. & Kachroo A. (2014) Soybean NDR1-like proteins bind pathogen effectors and regulate resistance signaling. New Phytol 202, 485-98.

175. Shan L., He P., Li J., Heese A., Peck S.C., Nurnberger T., Martin G.B. & Sheen J. (2008) Bacterial effectors target the common signaling partner BAK1 to disrupt multiple MAMP receptor-signaling complexes and impede plant immunity. Cell Host Microbe 4, 17-27.

176. Shao Z.Q., Xue J.Y., Wu P., Zhang Y.M., Wu Y., Hang Y.Y., Wang B. & Chen J.Q. (2016) Large-Scale Analyses of Angiosperm Nucleotide-Binding Site-Leucine-Rich Repeat Genes Reveal Three Anciently Diverged Classes with Distinct Evolutionary Patterns. Plant Physiol 170, 2095-109.

177. Shen Q.H., Zhou F., Bieri S., Haizel T., Shirasu K. & Schulze-Lefert P. (2003) Recognition specificity and RAR1/SGT1 dependence in barley Mla disease resistance genes to the powdery mildew fungus. Plant Cell 15, 732-44.

178. Shyy J.Y. & Chien S. (2002) Role of integrins in endothelial mechanosensing of shear stress. Circ Res 91, 769-75.

179. Simon M.L., Platre M.P., Marques-Bueno M.M., Armengot L., Stanislas T., Bayle V., Caillaud M.C. & Jaillais Y. (2016) A PtdIns(4)P-driven electrostatic field controls cell membrane identity and signalling in plants. Nat Plants 2, 16089.

180. Smakowska-Luzan E., Mott G.A., Parys K., Stegmann M., Howton T.C., Layeghifard M., Neuhold J., Lehner A., Kong J., Grunwald K., Weinberger N., Satbhai S.B., Mayer D., Busch W., Madalinski M., Stolt-Bergner P., Provart N.J., Mukhtar M.S., Zipfel C., Desveaux D., Guttman D.S. & Belkhadir Y. (2018) An extracellular network of Arabidopsis leucine-rich repeat receptor kinases. Nature 553, 342-6.

181. Song N., Liu Z.S., Xue W., Bai Z.F., Wang Q.Y., Dai J., Liu X., Huang Y.J., Cai H., Zhan X.Y., Han Q.Y., Wang H., Chen Y., Li H.Y., Li A.L., Zhang X.M., Zhou T. & Li T. (2017) NLRP3 Phosphorylation Is an Essential Priming Event for Inflammasome Activation. Mol Cell 68, 185-97 e6.

182. Steinhorst L. & Kudla J. (2013) Calcium and reactive oxygen species rule the waves of signaling. Plant Physiol 163, 471-85.

183. Sun X., Lapin D., Feehan J.M., Stolze S.C., Kramer K., Dongus J.A., Rzemieniewski J., Blanvillain-Baufume S., Harzen A., Bautor J., Derbyshire P., Menke F.L.H., Finkemeier I., Nakagami H., Jones J.D.G. & Parker J.E. (2021)

Pathogen effector recognition-dependent association of NRG1 with EDS1 and SAG101 in TNL receptor immunity. Nat Commun 12, 3335.

184. Sun Y., Li L., Macho A.P., Han Z., Hu Z., Zipfel C., Zhou J.M. & Chai J. (2013) Structural basis for flg22-induced activation of the Arabidopsis FLS2-BAK1 immune complex. Science 342, 624-8.

185. Swiderski M.R., Birker D. & Jones J.D. (2009) The TIR domain of TIR-NB-LRR resistance proteins is a signaling domain involved in cell death induction. Mol Plant Microbe Interact 22, 157-65.

186. Tameling W.I., Elzinga S.D., Darmin P.S., Vossen J.H., Takken F.L., Haring M.A. & Cornelissen B.J. (2002) The tomato R gene products I-2 and MI-1 are functional ATP binding proteins with ATPase activity. Plant Cell 14, 2929-39.

187. Tameling W.I., Vossen J.H., Albrecht M., Lengauer T., Berden J.A., Haring M.A., Cornelissen B.J. & Takken F.L. (2006) Mutations in the NB-ARC domain of I-2 that impair ATP hydrolysis cause autoactivation. Plant Physiol 140, 1233-45.

188. Tao Y., Xie Z., Chen W., Glazebrook J., Chang H.S., Han B., Zhu T., Zou G. & Katagiri F. (2003) Quantitative nature of Arabidopsis responses during compatible and incompatible interactions with the bacterial pathogen Pseudomonas syringae. Plant Cell 15, 317-30.

189. Tian H., Wu Z., Chen S., Ao K., Huang W., Yaghmaiean H., Sun T., Xu F., Zhang Y., Wang S., Li X. & Zhang Y. (2021) Activation of TIR signalling boosts pattern-triggered immunity. Nature.

190. Tian W., Hou C., Ren Z., Wang C., Zhao F., Dahlbeck D., Hu S., Zhang L., Niu Q., Li L., Staskawicz B.J. & Luan S. (2019) A calmodulin-gated calcium channel links pathogen patterns to plant immunity. Nature 572, 131-5.

191. Tornero P., Merritt P., Sadanandom A., Shirasu K., Innes R.W. & Dangl J.L. (2002) RAR1 and NDR1 contribute quantitatively to disease resistance in Arabidopsis, and their relative contributions are dependent on the R gene assayed. Plant Cell 14, 1005-15.

192. Tsuda K. & Katagiri F. (2010) Comparing signaling mechanisms engaged in pattern-triggered and effector-triggered immunity. Current Opinion in Plant Biology 13, 459-65.

193. Van den Ackerveken G., Marois E. & Bonas U. (1996) Recognition of the bacterial avirulence protein AvrBs3 occurs inside the host plant cell. Cell 87, 1307-16.

194. van der Burgh A.M., Postma J., Robatzek S. & Joosten M.H.A.J. (2019) Kinase activity of SOBIR1 and BAK1 is required for immune signalling. Molecular Plant Pathology 20, 410-22.

195. van Ooijen G., Mayr G., Kasiem M.M., Albrecht M., Cornelissen B.J. & Takken F.L. (2008) Structure-function analysis of the NB-ARC domain of plant disease resistance proteins. J Exp Bot 59, 1383-97.

196. Vande Walle L. & Lamkanfi M. (2016) Pyroptosis. Curr Biol 26, R568-R72.

197. Venugopal S.C., Jeong R.D., Mandal M.K., Zhu S., Chandra-Shekara A.C., Xia Y., Hersh M., Stromberg A.J., Navarre D., Kachroo A. & Kachroo P. (2009) Enhanced disease susceptibility 1 and salicylic acid act redundantly to regulate resistance gene-mediated signaling. PLoS Genet 5, e1000545.

198. Wagner S., Stuttmann J., Rietz S., Guerois R., Brunstein E., Bautor J., Niefind K. & Parker J.E. (2013) Structural basis for signaling by exclusive EDS1 heteromeric complexes with SAG101 or PAD4 in plant innate immunity. Cell Host Microbe 14, 619-30.

199. Wan L., Essuman K., Anderson R.G., Sasaki Y., Monteiro F., Chung E.H., Osborne Nishimura E., DiAntonio A., Milbrandt J., Dangl J.L. & Nishimura M.T. (2019a) TIR domains of plant immune receptors are NAD(+)-cleaving enzymes that promote cell death. Science 365, 799-803.

200. Wan W.L., Zhang L., Pruitt R., Zaidem M., Brugman R., Ma X., Krol E., Perraki A., Kilian J., Grossmann G., Stahl M., Shan L., Zipfel C., van Kan J.A.L., Hedrich R., Weigel D., Gust A.A. & Nurnberger T. (2019b) Comparing Arabidopsis receptor kinase and receptor protein-mediated immune signaling reveals BIK1-dependent differences. New Phytol 221, 2080-95.

201. Wang B., Dai T., Sun W., Wei Y., Ren J., Zhang L., Zhang M. & Zhou F. (2021) Protein N-myristoylation: functions and mechanisms in control of innate immunity. Cell Mol Immunol 18, 878-88.

202. Wang H., Sun L., Su L., Rizo J., Liu L., Wang L.F., Wang F.S. & Wang X. (2014) Mixed lineage kinase domain-like protein MLKL causes necrotic membrane disruption upon phosphorylation by RIP3. Mol Cell 54, 133-46.

203. Wang J. & Chai J. (2020) Structural Insights into the Plant Immune Receptors PRRs and NLRs1 [OPEN]. Plant Physiology 182, 1566-81.

204. Wang J., Chen T., Han M., Qian L., Li J., Wu M., Han T., Cao J., Nagalakshmi U., Rathjen J.P., Hong Y. & Liu Y. (2020) Plant NLR immune receptor Tm-22 activation requires NB-ARC domain-mediated self-association of CC domain. PLoS Pathog 16, e1008475.

205. Wang J., Hu M., Wang J., Qi J., Han Z., Wang G., Qi Y., Wang H.W., Zhou J.M. & Chai J. (2019a) Reconstitution and structure of a plant NLR resistosome conferring immunity. Science 364.

206. Wang J., Liu X., Zhang A., Ren Y., Wu F., Wang G., Xu Y., Lei C., Zhu S., Pan T., Wang Y., Zhang H., Wang F., Tan Y.Q., Wang Y., Jin X., Luo S., Zhou C., Zhang X., Liu J., Wang S., Meng L., Wang Y., Chen X., Lin Q., Zhang X., Guo

X., Cheng Z., Wang J., Tian Y., Liu S., Jiang L., Wu C., Wang E., Zhou J.M., Wang Y.F., Wang H. & Wan J. (2019b) A cyclic nucleotide-gated channel mediates cytoplasmic calcium elevation and disease resistance in rice. Cell Res 29, 820-31.

207. Wang J., Wang J., Hu M., Wu S., Qi J., Wang G., Han Z., Qi Y., Gao N., Wang H.W., Zhou J.M. & Chai J. (2019c) Ligand-triggered allosteric ADP release primes a plant NLR complex. Science 364.

208. Wang Y., Garrido-Oter R., Wu J., Winkelmuller T.M., Agler M., Colby T., Nobori T., Kemen E. & Tsuda K. (2019d) Site-specific cleavage of bacterial MucD by secreted proteases mediates antibacterial resistance in Arabidopsis. Nat Commun 10, 2853.

209. Weber A.N.R., Bittner Z.A., Shankar S., Liu X., Chang T.H., Jin T. & Tapia-Abellan A. (2020) Recent insights into the regulatory networks of NLRP3 inflammasome activation. J Cell Sci 133.

210. Whisson S.C., Boevink P.C., Moleleki L., Avrova A.O., Morales J.G., Gilroy E.M., Armstrong M.R., Grouffaud S., van West P., Chapman S., Hein I., Toth I.K., Pritchard L. & Birch P.R. (2007) A translocation signal for delivery of oomycete effector proteins into host plant cells. Nature 450, 115-8.

211. Williams S.J., Sohn K.H., Wan L., Bernoux M., Sarris P.F., Segonzac C., Ve T., Ma Y., Saucet S.B., Ericsson D.J., Casey L.W., Lonhienne T., Winzor D.J., Zhang X., Coerdt A., Parker J.E., Dodds P.N., Kobe B. & Jones J.D. (2014) Structural basis for assembly and function of a heterodimeric plant immune receptor. Science 344, 299-303.

212. Williams S.J., Sornaraj P., deCourcy-Ireland E., Menz R.I., Kobe B., Ellis J.G., Dodds P.N. & Anderson P.A. (2011) An autoactive mutant of the M flax rust resistance protein has a preference for binding ATP, whereas wild-type M protein binds ADP. Mol Plant Microbe Interact 24, 897-906.

213. Willmann R., Lajunen H.M., Erbs G., Newman M.A., Kolb D., Tsuda K., Katagiri F., Fliegmann J., Bono J.J., Cullimore J.V., Jehle A.K., Gotz F., Kulik A., Molinaro A., Lipka V., Gust A.A. & Nurnberger T. (2011) Arabidopsis lysin-motif proteins LYM1 LYM3 CERK1 mediate bacterial peptidoglycan sensing and immunity to bacterial infection. Proc Natl Acad Sci U S A 108, 19824-9.

214. Wroblewski T., Spiridon L., Martin E.C., Petrescu A.J., Cavanaugh K., Truco M.J., Xu H., Gozdowski D., Pawlowski K., Michelmore R.W. & Takken F.L.W. (2018) Genome-wide functional analyses of plant coiled-coil NLR-type pathogen receptors reveal essential roles of their N-terminal domain in oligomerization, networking, and immunity. PLoS Biol 16, e2005821.

215. Wu C.H., Abd-El-Haliem A., Bozkurt T.O., Belhaj K., Terauchi R., Vossen J.H. & Kamoun S. (2017) NLR network mediates immunity to diverse plant pathogens. Proc Natl Acad Sci U S A 114, 8113-8.

216. Wu C.H., Belhaj K., Bozkurt T.O., Birk M.S. & Kamoun S. (2016) Helper NLR proteins NRC2a/b and NRC3 but not NRC1 are required for Pto-mediated cell death and resistance in Nicotiana benthamiana. New Phytol 209, 1344-52.

217. Wu C.H., Derevnina L. & Kamoun S. (2018) Receptor networks underpin plant immunity. Science 360, 1300-1.

218. Wu Y., Gao Y., Zhan Y., Kui H., Liu H., Yan L., Kemmerling B., Zhou J.M., He K. & Li J. (2020) Loss of the common immune coreceptor BAK1 leads to NLR-dependent cell death. Proc Natl Acad Sci U S A 117, 27044-53.

219. Wu Y., Kuzma J., Marechal E., Graeff R., Lee H.C., Foster R. & Chua N.H. (1997) Abscisic acid signaling through cyclic ADP-ribose in plants. Science 278, 2126-30.

220. Wu Z., Li M., Dong O.X., Xia S., Liang W., Bao Y., Wasteneys G. & Li X. (2019) Differential regulation of TNL-mediated immune signaling by redundant helper CNLs. New Phytol 222, 938-53.

221. Wu Z., Tian L., Liu X., Huang W., Zhang Y. & Li X. (2021a) The N-terminally truncated helper NLR NRG1C antagonizes immunity mediated by its full-length neighbors NRG1A and NRG1B. The Plant Cell.

222. Wu Z., Tian L., Liu X., Zhang Y. & Li X. (2021b) TIR signal promotes interactions between lipase-like proteins and ADR1-L1 receptor and ADR1-L1 oligomerization. Plant Physiology.

223. Xia B., Fang S., Chen X., Hu H., Chen P., Wang H. & Gao Z. (2016) MLKL forms cation channels. Cell Res 26, 517-28.

224. Xia S., Zhang Z., Magupalli V.G., Pablo J.L., Dong Y., Vora S.M., Wang L., Fu T.M., Jacobson M.P., Greka A., Lieberman J., Ruan J. & Wu H. (2021) Gasdermin D pore structure reveals preferential release of mature interleukin-1. Nature 593, 607-11.

225. Xu F., Zhu C., Cevik V., Johnson K., Liu Y., Sohn K., Jones J.D., Holub E.B. & Li X. (2015) Autoimmunity conferred by chs3-2D relies on CSA1, its adjacent TNL-encoding neighbour. Sci Rep 5, 8792.

226. Yan L., Ma Y., Liu D., Wei X., Sun Y., Chen X., Zhao H., Zhou J., Wang Z., Shui W. & Lou Z. (2012) Structural basis for the impact of phosphorylation on the activation of plant receptor-like kinase BAK1. Cell Res 22, 1304-8.

227. Yeung T., Terebiznik M., Yu L., Silvius J., Abidi W.M., Philips M., Levine T., Kapus A. & Grinstein S. (2006) Receptor activation alters inner surface potential during phagocytosis. Science 313, 347-51.

228. Yuan M., Jiang Z., Bi G., Nomura K., Liu M., Wang Y., Cai B., Zhou J.M., He S.Y. & Xin X.F. (2021a) Pattern-recognition receptors are required for NLR-mediated plant immunity. Nature 592, 105-9.

229. Yuan M., Ngou B.P.M., Ding P. & Xin X.F. (2021b) PTI-ETI crosstalk: an integrative view of plant immunity. Current Opinion in Plant Biology 62, 102030.

230. Zhang J., Li W., Xiang T., Liu Z., Laluk K., Ding X., Zou Y., Gao M., Zhang X., Chen S., Mengiste T., Zhang Y. & Zhou J.M. (2010) Receptor-like cytoplasmic kinases integrate signaling from multiple plant immune receptors and are targeted by a Pseudomonas syringae effector. Cell Host Microbe 7, 290-301.

231. Zhang W., Fraiture M., Kolb D., Loffelhardt B., Desaki Y., Boutrot F.F., Tor M., Zipfel C., Gust A.A. & Brunner F. (2013) Arabidopsis receptor-like protein30 and receptor-like kinase suppressor of BIR1-1/EVERSHED mediate innate immunity to necrotrophic fungi. Plant Cell 25, 4227-41.

232. Zhang X., Bernoux M., Bentham A.R., Newman T.E., Ve T., Casey L.W., Raaymakers T.M., Hu J., Croll T.I., Schreiber K.J., Staskawicz B.J., Anderson P.A., Sohn K.H., Williams S.J., Dodds P.N. & Kobe B. (2017) Multiple functional self-association interfaces in plant TIR domains. Proc Natl Acad Sci U S A 114, E2046-E52.

233. Zhao C., Tang Y., Wang J., Zeng Y., Sun H., Zheng Z., Su R., Schneeberger K., Parker J.E. & Cui H. (2021) A mis-regulated cyclic nucleotide-gated channel mediates cytosolic calcium elevation and activates immunity in Arabidopsis. New Phytol 230, 1078-94.

234. Zheng D., Liwinski T. & Elinav E. (2020) Inflammasome activation and regulation: toward a better understanding of complex mechanisms. Cell Discov 6, 36.

235. Zhou J., Wu S., Chen X., Liu C., Sheen J., Shan L. & He P. (2014) The Pseudomonas syringae effector HopF2 suppresses Arabidopsis immunity by targeting BAK1. Plant J 77, 235-45.

236. Zhou J.M. & Zhang Y. (2020) Plant Immunity: Danger Perception and Signaling. Cell 181, 978-89.

237. Zipfel C., Kunze G., Chinchilla D., Caniard A., Jones J.D., Boller T. & Felix G. (2006) Perception of the bacterial PAMP EF-Tu by the receptor EFR restricts Agrobacterium-mediated transformation. Cell 125, 749-60.

238. Zipfel C. & Rathjen J.P. (2008) Plant immunity: AvrPto targets the frontline. Curr Biol 18, R218-20.

239. Zipfel C., Robatzek S., Navarro L., Oakeley E.J., Jones J.D., Felix G. & Boller T. (2004) Bacterial disease resistance in Arabidopsis through flagellin perception. Nature 428, 764-7.

7. Appendix

7.1. Help wanted: helper NLRs and plant immune responses.

7.2. Two unequally redundant “helper” immune receptor families mediate *Arabidopsis thaliana* “sensor” immune receptor functions.

7.3. The EDS1-PAD4-ADR1 node mediates *Arabidopsis* pattern-triggered immunity.

7.4. Arabidopsis ADR1 helper NLR immune receptors localize and function at the plasma membrane in a phospholipid dependent manner.

7.5. Autoimmunity induced by the Arabidopsis helper NLR ADR1-L2 requires the receptor-like kinase BKK1.

7.1. Jubic and Saile *et al*., 2019

Help wanted: helper NLRs and plant immune responses

Jubic, L. M.*, Saile, S. C.*, Furzer, O. J., El Kasmi, F., Dangl, J. L.

*These authors contributed equally to this work.

Current Opinion in Plant Biology.

2019 Aug;50:82-94.

doi: 10.1016/j.pbi.2019.03.013.

Available online at www.sciencedirect.com

ScienceDirect

Current Opinion in Plant Biology

Help wanted: helper NLRs and plant immune responses

Lance M Jubic[1,3,7], Svenja Saile[2,7], Oliver J Furzer[1], Farid El Kasmi[2] and Jeffery L Dangl[1,3,4,5,6]

Plant nucleotide-binding domain and leucine-rich repeat-containing (NLR) proteins function as intracellular receptors in response to pathogens and activate effector-triggered immune responses (ETI). The activation of some sensor NLRs (sNLR) by their corresponding pathogen effector is well studied. However, the mechanisms by which the recently defined helper NLRs (hNLR) function to transduce sNLR activation into ETI-associated cell death and disease resistance remains poorly understood. We briefly summarize recent examples of sNLR activation and we then focus on hNLR requirements in sNLR-initiated immune responses. We further discuss how shared sequence homology with fungal self-incompatibility proteins and the mammalian mixed lineage kinase domain like pseudokinase (MLKL) proteins informs a plausible model for the structure and function of an ancient clade of plant hNLRs, called RNLs.

Addresses
[1] Department of Biology, University of North Carolina at Chapel Hill, Chapel Hill, USA
[2] ZMBP-Plant Physiology, University of Tübingen, Tübingen, Germany
[3] Howard Hughes Medical Institute, University of North Carolina at Chapel Hill, Chapel Hill, USA
[4] Carolina Center for Genome Sciences, University of North Carolina at Chapel Hill, Chapel Hill, USA
[5] Curriculum in Genetics and Molecular Biology, University of North Carolina at Chapel Hill, Chapel Hill, USA
[6] Department of Microbiology and Immunology, University of North Carolina at Chapel Hill, Chapel Hill, USA

Corresponding authors:
El Kasmi, Farid (farid.el-kasmi@zmbp.uni-tuebingen.de),
Dangl, Jeffery L (dangl@email.unc.edu)
[7] These authors contributed equally to the work.

Current Opinion in Plant Biology 2019, **50**:82–94

This review comes from a themed issue on **Biotic interactions**

Edited by **Rebecca S Bart** and **Ken Shirasu**

https://doi.org/10.1016/j.pbi.2019.03.013

Background

Plants are abundant sources of nutrients and water, and thus attractive hosts to microbial communities. To defend against microbial pathogens, plants have evolved a two-tiered immune system [1]. In the first tier, extracellular pattern recognition receptors (PRRs), typically leucine-rich repeat kinases and lysine motif kinases, recognize conserved microbial-associated molecular pattern (MAMP) ligands, triggering MAMP-triggered immunity (MTI) [1]. In response, pathogens have evolved virulence effectors that delay or suppress MTI [1]. Plants, as a counter measure, have evolved a second tier of defense, initiated by a family of nucleotide-binding leucine-rich repeat (NLR) protein receptors that are activated by recognizing effector presence directly or indirectly [1–4].

In plants, typical NLRs have a variable Nterminal domain: a Toll/interleukin-1 receptor (TIR) domain or a non-TIR domain, which resembles a coiled-coil domain (CC), followed by a central nucleotide binding (NB-ARC) and a C-terminal leucine-rich repeat (LRR) domain [1–4]. NLRs with CC domains are hereafter abbreviated CNLs and NLRs possessing TIR domains are abbreviated TNLs. NLRs are thought to be activated through the exchange of ADP (resting state) for ATP (active state) by the ATPase activity of the NB-ARC domain itself or by NLR-interacting proteins, acting as nucleotide-exchange factors [4,5,6••,7••]. Effector-mediated NLR activation results in a largely re-amplified MTI response termed effector-triggered immunity (ETI) that is typically associated with a hypersensitive cell death response (HR) at the infection site [1–4]. The demarcation between MTI and ETI is increasingly blurred and the action of extracellular receptors can require intracellular receptors [8,9]. For instance, SlNRC4a plays a non-canonical role as a positive regulator of LeEIX2/EIX-mediated MTI defense responses [10]. NLRs that either recognize the effector directly or recognize the effector's action on a host target or decoy of a target are collectively called sensor NLRs (sNLRs) [11]. NLRs have been actively reviewed in this forum [12,13] and we focus on selected new publications.

Sensor NLRs

ID sensor NLR pairs

Some of the functionally defined sNLRs that serve as excellent experimental models are tightly genetically linked to, and form a protein complex with, a co-regulated partner NLR. This functions as a signaling 'executor' module that transduces the effector recognition by the sNLR to initiate an immune response. We consider these pair-specific executors distinct from the helper NLRs later discussed. Some of the sNLR partners in these linked pairs contain an 'integrated domain' (ID) that is likely a decoy of an effector target and binding of an

effector to the ID activates the complex. The two most studied ID pairs are the Arabidopsis TNL RPS4/RRS1 pair and the rice CNL RGA4/RGA5 pair [12,14,15]. In the Arabidopsis RPS4/RRS1 pair, RRS1 carries an integrated WRKY transcription factor domain targeted by two unrelated bacterial effectors AvrRps4 and PopP2 [14,15]. In the rice RGA4/RGA5 pair, RGA5 carries an integrated RATX1 domain targeted by *Magnaporthe oryzae* (Rice blast fungus) effectors Avr-Pia and AVR1-CO39 [12,16]. RPS4 and RGA4 are the executor NLRs of their respective pairs.

Recent progress has been made in the mechanistic understanding of repression and activation of RPS4/RRS1. Deletion of the RRS1 WRKY domain or the WRKY adjacent domain 4 (DOM4) results in an allele that triggers constitutive RPS4-dependent defense activation suggesting that the WRKY domain contributes to maintaining an inactive complex [15]. AvrRps4 interaction with the WRKY domain disrupts WRKY association with a specific domain, leading to activation of the complex [15]. Furthermore, some mutations in RPS4 and RRS1 compromise PopP2 but not AvrRps4 recognition, suggesting that AvrRps4 and PopP2 derepress the complex differently [15].

Sensor partners without IDs

sNLR partners without IDs have been described in both Arabidopsis and rice. Three Arabidopsis TNL sNLRs named SIDEKICK SNC1 1 (SIKIC1), SIKIC2, and SIKIC3 are redundantly required for SNC1-mediated defense [17]. Further, SIKIC2 physically associates with SNC1 [17]. Interestingly, the TNLs are under regulation by distinct E3 ligases, with SNC1 levels regulated by CPR1 while the SIKICs are regulated by MUSE1 and MUSE2 [17]. SOC3 can partner with either of the genetically linked CHS1 or TN2 to monitor the homeostasis of E3 ligase SAUL1. SOC3 appears to be the executor module [18,19].

In addition to RGA4/RGA5, other sNLR partners (without IDs) in rice have been described. The CNL PigmR confers broad-spectrum resistance to *M. oryzae* [20]. The CNL PigmS competitively attenuates PigmR homodimerization by heterodimerizing with PigmR to suppress PigmR-mediated resistance specifically during rice seed development [20].

Orthologous sNLRs

In some cases, sequence divergent sNLRs from distantly related species can be activated by the same effector; these interactions appear to have convergently evolved [21,22]. Few true NLR orthologs have been identified. One example is the discovery of NbZAR1, a likely true ortholog of the *Arabidopsis thaliana* protein ZAR1 (AtZAR1), by a forward genetic screen to identify components required for perception of the bacterial acetyltransferase effector XopJ4 [23•]. In Arabidopsis, ZAR1 serves roles in recognition of multiple bacterial effectors that each have different biochemical activities. In addition to ZAR1, immune activation requires class XII receptor-like cytoplasmic kinases (RLCKs) and additional kinase or pseudokinase targets or decoys [24]. In conjunction with the pseudokinase ZED1, AtZAR1 mediates an ETI response to the acetyltransferase effector HopZ1a [24]. AtZAR1 and the ZRK3 pseudokinase are required for HopF2a-induced disease resistance [25•]. Further, AtZAR1 also functions with the RLCK RKS1 to mount an ETI response to the effector AvrAC. In the recently solved ZAR1 structure, AtRKS1 interacts with AtZAR1 and helps to keep the NLR in a monomeric inactive ADP-bound complex. AvrAC-induced uridylyation of the RCLK PBL2 specifically enables $PBL2^{UMP}$ to bind to RKS1 in the preformed ZAR1–RKS1 complex. This binding induces a conformational change in RKS1, which simultaneously leads to a dislocation of the ZAR1 NB domain and the release of ADP [6••,7••]. This nucleotide-free ZAR1–RSK1–PBL^{UMP} complex, oligomerizes upon ATP binding to form a pentameric complex, a resistosome, that is required for resistance and cell death signaling [6••,7••,26]. PBL2 uridylylation and binding to RKS1 are specifically required for AvrAC triggered immunity [6••,7••,26]. It remains unknown whether NbZAR1 also has evolved as a required resistance component against various type III effectors. However, recognition of XopJ4 by NbZAR1 also requires a class XII RLCK dubbed JIM2 [23•]. Collectively, these data suggest that ZAR1 has evolved to be a flexible platform to monitor RLCK homeostasis and further suggests that RCLKs are a battleground constantly targeted by diverse effectors.

Engineering decoys of sNLRs

With further understanding of the modes of action of specific sNLRs, attention turns to efforts to engineer the decoys that sNLRs guard [27•,28]. The bacterial effector protease AvrPphB cleaves the kinase PBS1, and this activates the Arabidopsis CNL RPS5 [28]. Like BIK1 and PBL2, PBS1 is a member of the RLCK subfamily VII [29]. The precise PBS1 cleavage site is defined, and can be substituted with cleavage sites for other pathogen virulence factor proteases, enabling RPS5 to be activated by these proteases [28]. Further, a modified soybean PBS1 decoy protein containing a cleavage site for the Soybean mosaic virus (SMV) NIa protease triggers cell death in soybean protoplasts when cleaved by this protease. Thus, RPS5 can be coopted to act as a resistance gene against SMV infection. PBS1 decoy engineering appears to be viable in at least one crop, in which endogenous PBS1 and analogous RPS5 proteins exist [27•].

Helper NLRs

In addition to the sensor and executor NLRs noted above, there is emerging evidence that many NLR-mediated

immune responses require the presence and activity of so called 'helper' NLRs (hNLRs) [30••,31••,32–34,35••,36••]. hNLRs seem to serve as downstream signaling hubs for a diverse array of sNLRs [30••,31••,32,33,35••,36••]. We summarize findings demonstrating that hNLRs function downstream of sNLR activation, and we speculate as to how their activity might be regulated. Drawing upon sequence homology of hNLRs to animal cell-death executing proteins and localization, we discuss plausible hNLR roles in ETI, and, specifically, in HR.

RNLs are an ancient and conserved hNLR clade

There are three described hNLR families, all encoding CNLs: the *ACTIVATED DISEASE RESISTANCE 1* (ADR1) family [34], the *N REQUIRED GENE 1* (NRG1) family [37], and *NB-LRR protein required for HR-associated cell death* (NRC) family [38]. In this review, we focus on the ADR1 and the NRG1 hNLRs, which are a unique subclade of CNLs defined by the relatedness of their N-terminal domain to an understudied immune system protein called RPW8; therefore, the ADR1 and NRG1 hNLRs are termed RNLs [33]. RPW8 and its paralogs contribute to powdery mildew resistance and upregulation of MTI responses [39]. We direct readers to Wu *et al.* [32] and Wu *et al.* [36••] for details about the *Solanaceae*-limited CNL NRC family and their functions as hNLRs. It is as yet unclear if and how the RNLs and NRC proteins intersect functionally.

The *ADR1* family and the *NRG1* family are small, ancient, and related RNL families found in all analyzed plant genomes [40]. The *ADR1* and *NRG1* gene families are sister clades in trees built from either their unique N-terminal coiled coil RPW8-like domain (CC_R) (Figure 1) or their CNL-A subclass NB-ARC [33,41,42]. In comparison to the large expansion of TNLs and CNLs, the RNL family expansion has been strikingly limited [33,43,44]. In addition to their limited expansion within genomes, RNLs, like sNLRs, are the targets of regulatory RNAi silencing machinery [13,44,45].

The CC domain most closely related to the CC_R is the CC_{EDVID} subclade (Figure 1), where the EDVID is a conserved amino acid motif in the CC [46]. When the NB-ARC is used as the basis for phylogenic comparison, the CC_{EDVID} CNLs do not cluster with the RNLs suggesting that they do not share a common ancestor. Thus, we hypothesize that the CC_{EDVID} domain and the CC_R domain may be experiencing selection to maintain an amino acid sequence pattern with similar general function at the structural level. Furthermore, there is a lack of evidence that CC_{EDVID} NLRs require CC_R hNLRs to function.

In Arabidopsis, there are four paralogs of ADR1: ADR1, ADR1-L1, ADR1-L2, and a largely N-terminally truncated ADR1-L3 [34]. Arabidopsis contains three NRG1 paralogs, NRG1.1, NRG1.2, and a severely N-terminally truncated NRG1.3. [35••,36••,37,47]. The Arabidopsis genome also encodes a protein with the structure CC_R-NB-ARC-LIM, named DAR5. *Nicotiana benthamiana* possesses a single copy of ADR1 and two NRG members NRG1 and NRG2, where the N-terminally truncated and poorly expressed NRG2 is postulated to be a pseudogene [35••,36••,37,47].

ADR1 and NRG1 families possess both distinct and redundant functions

Redundant functions

ADR1 and NRG1 function as redundant downstream hubs for a diverse array of sNLRs, not unlike the network observed for sNLR activation mediated by members of the NRC protein family in the *Solanaceae* [31••,32] (Figure 2). For instance, the ADR1 family members are redundantly required downstream of both CNL and TNL sNLRs RPS2, RPP2, RPP4, RPS4/RRS1 for full effector-driven ETI, and ADR1s are positive regulators of some NLR auto-immune mutants [33,34,35••,36••,48] (Figure 2). Similarly, the NRG1 family members function redundantly downstream of all tested TNLs [30••,33,35••,36••] (Figure 2).

The broad functional redundancy among the ADR1 and NRG1 families, respectively, was one driver in the creation of a 'helperless' Arabidopsis plant, a *sextuple* hNLR mutant (*adr1 adr1-L1 adr1-L2 nrg1.1 nrg1.2 nrg1.3*) [33,34,35••,36••,48]. Before the creation of the *sextuple* plant, it was not possible to determine if the ADR1 and NRG1 families were functionally redundant, with respect to each other. To date, the helperless plant has only been challenged with two bacterial pathogens, *Psm* ES4326 and *Pst* DC3000 expressing *AvrRps4* or *HopA1*. When challenged with *Psm* ES4326, enhanced disease susceptibility was observed in the *sextuple* compared with that of its parents, *nrg1 triple*, *adr1 triple*, and wild type Col-0, suggesting that ADR1s and NRG1s have a synergistic effect on basal defense. Further, when the mutant genotypes were challenged with DC3000 *AvrRps4* or DC3000 *HopA1*, TNL-mediated defense of the *sextuple* was significantly more compromised compared to *adr1 triple* and *nrg1 triple* as measured by bacterial growth and increased disease symptoms [36••]. The susceptibility of the *sextuple* mutant to the virulent *Psm* ES4326 strain was significantly enhanced in comparison to the immune-compromised *eds1-2* mutant, suggesting that basal defense, and thus also MTI, initiated by extracellular receptors, might depend on RNL activity or presence. This finding further supports the idea of a regulatory interplay between MTI and ETI.

Functions requiring both ADR1 and NRG1 RNLs

The creation of a helperless plant opens the avenues for addressing several lines of inquiry. It is now possible to determine whether the ADR1 and NRG1 families are functionally redundant with respect to multiple NLRs, besides RPS4/RRS1 or RPS6. For instance, it has already been determined through TRV silencing that Rx2-mediated

Figure 1

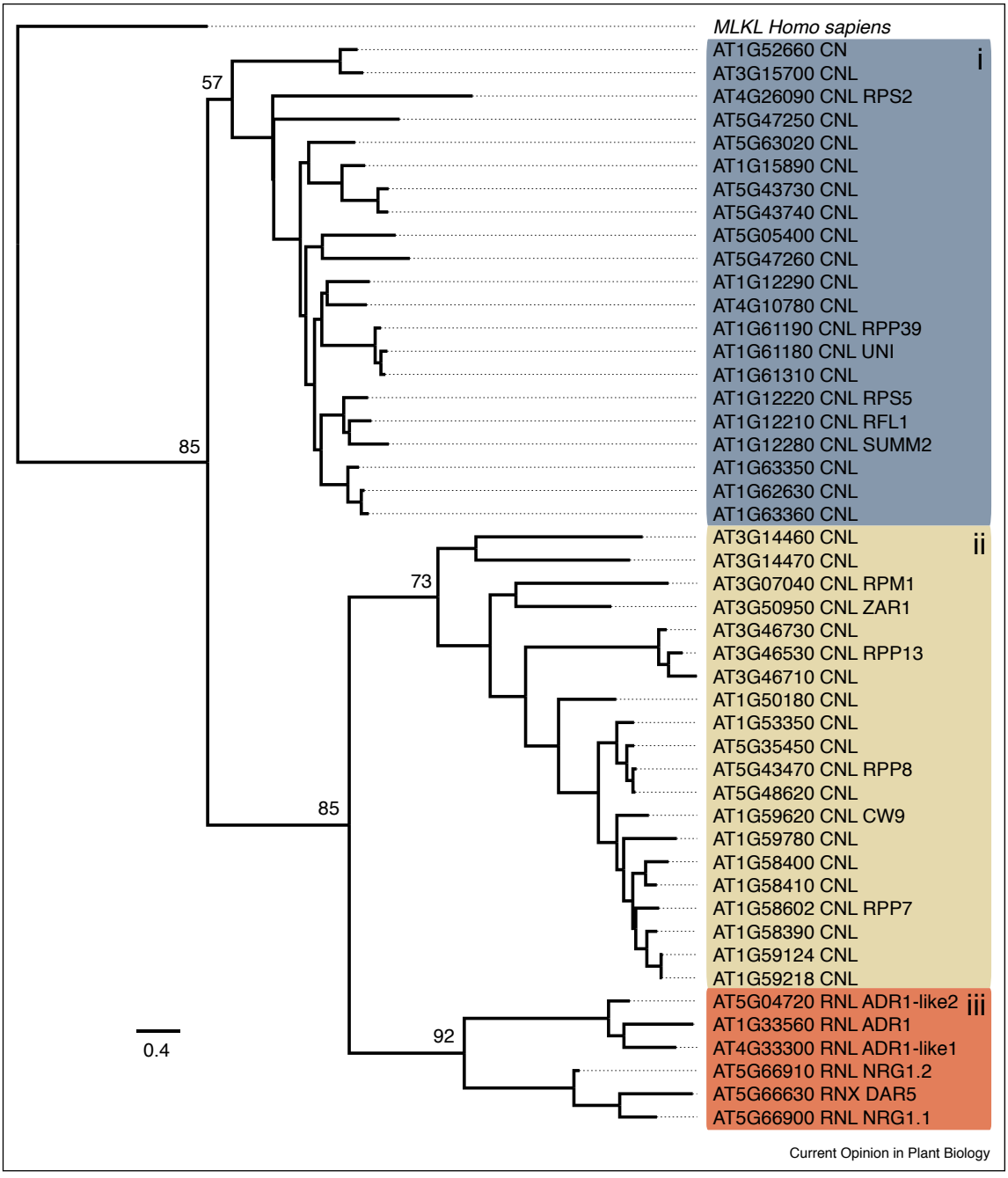

N-terminal end domain maximum-likelihood phylogenetic tree of Arabidopsis coiled-coil and RPW8 domain-containing NLR proteins and Human mixed lineage kinase domain-like pseudokinase protein.
Amino acids 1–180, corresponding to the CC, RPW8, and MLKL N-terminal domain regions, were extracted and aligned iteratively using MUSCLE and CLUSTALW. Several sequences were removed to reduce gaps in the alignment. The Jones, Taylor, Thornton model, with frequencies, three discrete Gamma categories and a 100-bootstrap test of phylogeny, was used to generate the tree. Bootstrap support of major nodes is indicated on the phylogeny. Scale bar indicates amino acid substitutions per site. C = coiled coil, R = RPW8, N = NB, L = LRR, X = other. Clade i) contain no EDVID motifs, clade ii) contain EDVID motifs and clade iii) are the RPW-NLRs and they do not contain EDVID motifs.

Figure 2

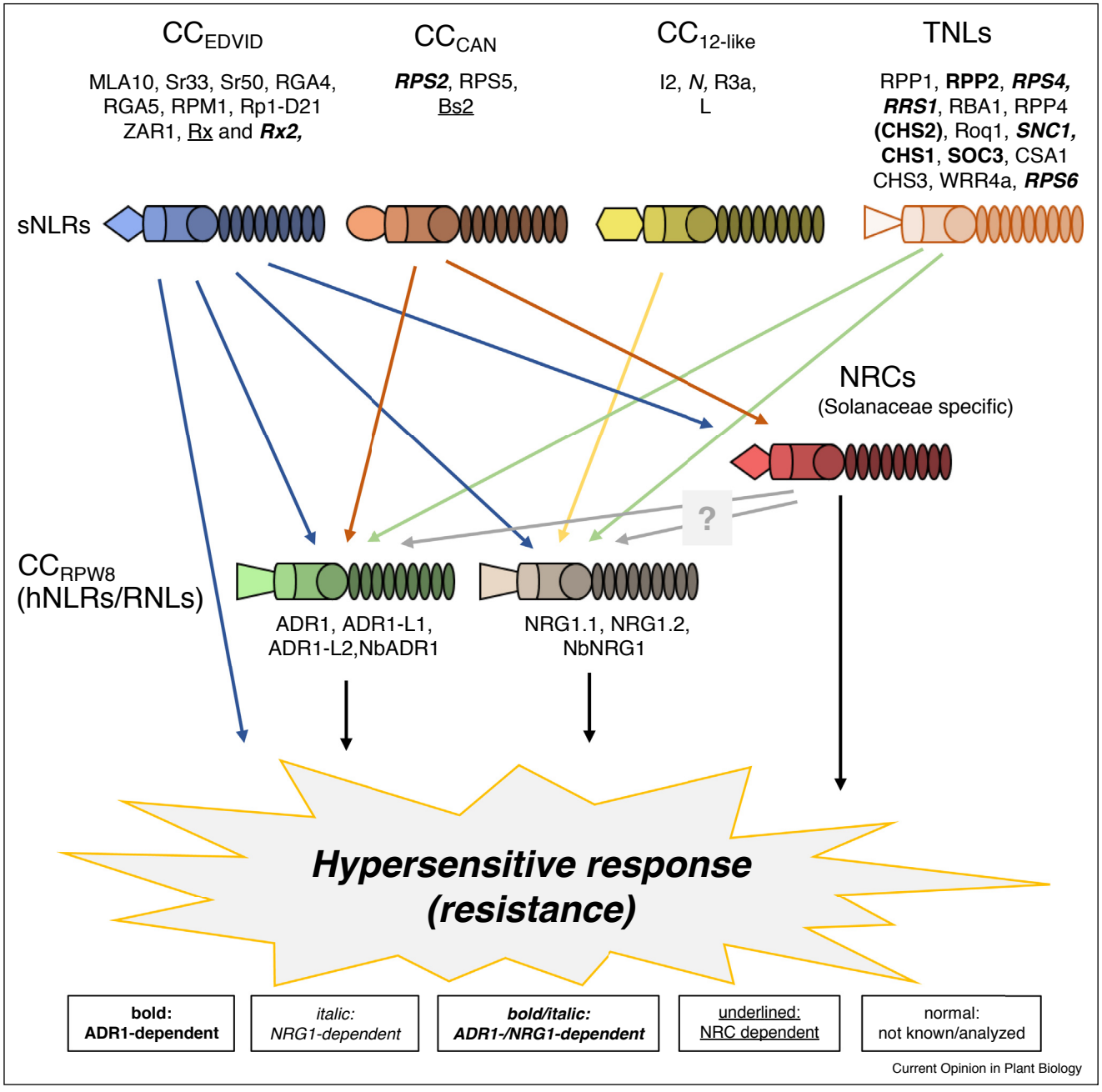

Signaling network of plant sensor and helper NLRs. Figure 4 Signaling network of plant sensor and helper NLRs.
Experimentally proven signaling-dependencies are indicated by colored arrows and listing of NLRs; bold = ADR1-dependent, italic = NRG1-dependent, bold/italic = ADR1-dependent and NRG1-dependent, underlined = NRC-dependent, normal = not known/analyzed. Whether the solanaceous NRCs also require the hNLRs for cell death and resistance signaling is not yet clear, however very likely as Rx2-mediated resistance in *N. benthamiana* was shown to require the hNLRs (Collier *et al.* [33]) and its paralog Rx requires the three NRCs - NRC2,3,4 - for cell death induction (Wu *et al.* [31••]).

resistance requires both ADR1 and NRG1 families for function in *N. benthamiana* [33]. Of special interest, is whether RPM1 mediated HR will be lost in a helperless plant, as RPM1 signaling is not negatively affected either by the loss of the *ADR1* or *NRG1* family individually [34,35••].

Distinct functions

ADR1 family members function upstream of salicylic acid (SA) accumulation and subsequent activation of SA-dependent responses in ETI initiated by multiple sNLRs, including CNLs and TNLs (Figure 2)

[34,36••,49]. ADR1-L*2* may be thus far distinguished from sensor NLRs by the dispensability of its P-loop for helper function in sensor-NLR mediated and executor-NLR mediated immunity [25•,31••,34]. It is unknown if the two other ADR1 paralogs also possess a dispensable P-loop for their helper functions. The necessity of the NRG1 family members' P-loops has also been examined. The *chs3-2D* mutant requires the presence of At*NRG1* family members for the *chs3-2D* auto-immune dwarf phenotype. AtNRG1.1 and AtNRG1.*2* do not require their P-loop activity to contribute to the *chs3-2D* auto-immune dwarf phenotype [36••]. However, NbNRG1 does require its P-loop for HR auto-activity following over-expression in *N. benthamiana* [37].

While ADR1 proteins contribute to both CNL-mediated and TNL-mediated immunity [34], NRG1 proteins are thus far not required for CNL signaling [30••,36••]. By contrast, NRG1 proteins are required for disease resistance initiated by the TNL proteins N, Roq1, RPS4/RRS1, RPP1, SOC3/CHS1, CSA1/CHS3, and WRR4A [30••,35••,36••,37] (Figure 2). Interestingly, NRG1 is required for both TIR-mediated HR response and for a TNL-mediated 'extreme resistance' phenotype that lacks HR [50]. The requirement for NRG1 function by TNLs is supported by evolutionary evidence that NRG1 and TNL genes were simultaneously lost in (most) monocots and the *Lamiales* family [33]. While TNLs seem to have been lost in these lineages, TIR only domains (T), TIR-NB-ARC proteins (TN), or TIR-uncharacterized domain proteins (TX), have been found in some monocots [51]. It remains unknown if these truncated T, TN, TX proteins function in immunity, like the Arabidopsis TIR only RBA1 [52•], and if they do, whether they require hNLRs.

Pore-forming fungi HeLo and HELL domains resemble the RNL CC_R domain

RNLs collectively serve as downstream signaling hubs to a diverse array of sNLRs, yet the precise function of the RNLs in mediating ETI remains unknown. However, shared sequence homology and predicted structural homology with fungal and animal proteins provide valuable insights into their possible mode(s) of action.

Cell death initiated by fungal cells during heterokaryon incompatibility requires an 'NLR-like' protein that activates a downstream cell death executing protein [53,54]. While the fungal 'NLRs' contain a variable N-terminal domain and an NB-ARC or a NACHT domain, they do not contain a LRR domain [53], which is commonly replaced with other repeating superstructures, such as TPR (tetratricopeptide repeats), WD repeats or ANK (ankyrin) repeats [53]. Thus, following precedent in fungal NLR literature [53], we adhere to the NLR designation for these proteins. Fungal proteins acting downstream of fungal NLRs are commonly referred to as effector proteins or as heterokaryon incompatibility proteins, and are composed of an amyloid folding domain and a variable N-terminal domain [53]. To avoid confusion with bacterial effectors, we refer to the fungal proteins as incompatibility proteins.

While both mammalian and plant sNLRs are activated through oligomerization, fungal NLR systems instead operate through amyloid fold templating by the NLR onto the incompatibility protein [53,55,56•,57]. Consider for instance, the NACHT and WD Repeat Domain Containing 2 (NWD2) and Heterokaryon incompatibility protein S (Het-S). In this highly conserved fungal system, the NLR NWD2, upon binding its ligand, activates the downstream Het-S pore-forming protein by converting its prion-forming region into the β-solenoid fold [54,58]. Upon refolding into the β-solenoid fold, Het-S's HeLo domain forms a pore in the membrane leading to cell death (Figure 3) [59,60]. HeLo-like (HELL) domains have been characterized in other filamentous fungi. For instance, the HeLo-like protein (HELLP), possessing an N-terminal HELL domain, behaves analogously to Het-S [61]. Remarkably, the HeLo and HELL domains share sequence homology to both the four helical bundle (4HB) of the N-terminus of the mammalian cell death executor protein MLKL and the plant CC_R domains that define the RNL subclass of hNLRs [61].

The pore-forming protein MLKL shares proposed structural homology with the CC_R domain

Given the sequence homology between the 4HB of MLKL and the CC_R domain [61], we examined how MLKL structure and function might impact the structure and function of RNLs. MLKL is required for the activation of necroptosis [62]. The 4HB domain of MLKL is required for insertion into the plasma membrane following activation and oligomerization which leads to subsequent pore formation (Figure 3) [63–65].

A structural homology search using Phyre*2* revealed that all five Arabidopsis CC_R domains are predicted to fold into a 4HB with strong similarity to MLKL, as noted independently for ADR1 [66]. Further, we could thread with high confidence all AtRNLs onto the MLKL structure (Figure 4). Thus, based on structural homology and the high confidence of secondary structure prediction, we speculate that the CC_R domain of the RNLs adopt a MLKL-like 4HB fold.

We also tested whether canonical CNLs N-terminal domains would potentially fold into similar 4HBs. However, CC domains can vary significantly in terms of residue conservation. Thus, we limited our examination to only canonical CC domains that most closely resemble the CC_R domain sequence. In accordance with the phylogeny of the CC domain of the Arabidopsis CNLs,

Figure 3

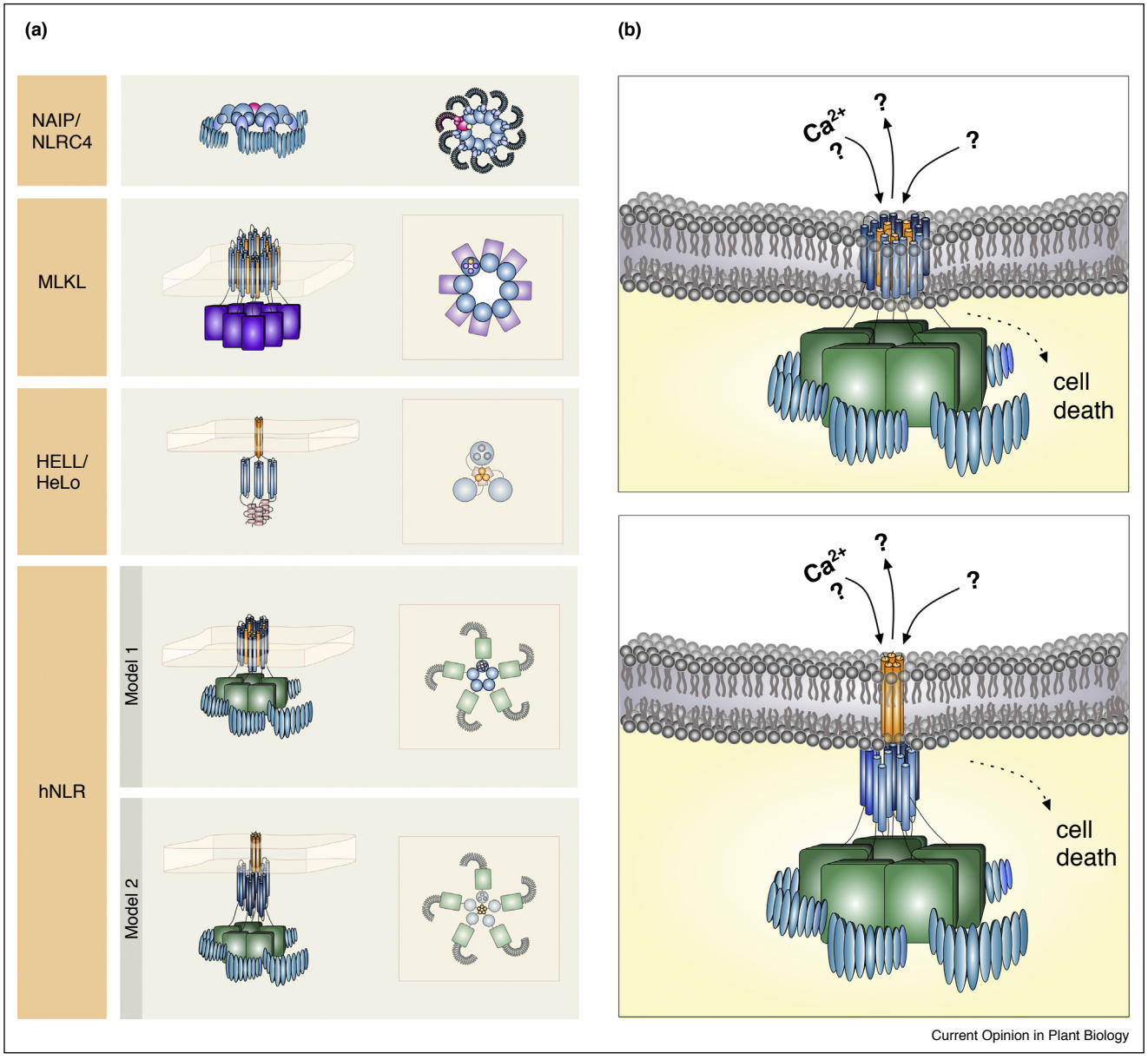

Signalosome and membrane pore formation by regulators of immunogenic cell death in different kingdoms.
A Mammalian innate immune receptors NAIP (pink) and NLRC4 (blue) oligomerize to form a signaling competent inflammasome upon PAMP-detection. The fungal HELL/HeLo-domain containing NLR-like proteins interact upon activation and form a tetrameric complex inserting the first a-helix of their 4HB HELL domain into membranes to initiate hybrid incompatibility. The animal MLKL protein oligomerizes after phosphorylation by RIPK3 forming an amyloid-like structure followed by translocation to the plasma membrane causing cell membrane disruption, which is thought to mediate necroptosis. In plants, the hNLRs might function in a similar way, forming pores with their RPW8 domains in cell membranes after being activated by effector-activated or auto-activated sNLRs. B Two models of RNL mediated pore formation are possible. Model 1: Similar to MLKL pore formation the full 4HB of the RPW8-domain is inserted into membranes allowing membrane deterioration and/or pore formation leading to changes in ion fluxes. Model 2: Only the first alpha-helix of the RPW8-domain is inserted into membranes upon activation and oligomerization of the RNL proteins, similar to HELL/Het-domain containing protein pore formation.

the CC_{EDVID} subclade most resembles the CC_R domain (Figure 1). We built an hmm profile using an alignment of MLKL, HELL and HET domains from [61] as a guide. Performing an hmm-search against the Arabidopsis genome using our hmm as the query, we hit multiple CC_{EDVID} NLRs, such as ZAR1 (Table 1). The hmm-search hit many CC_{EDVID} CNLs, confirming our CC-built phylogenetic tree. Moreover, when Phyre2 is

Figure 4

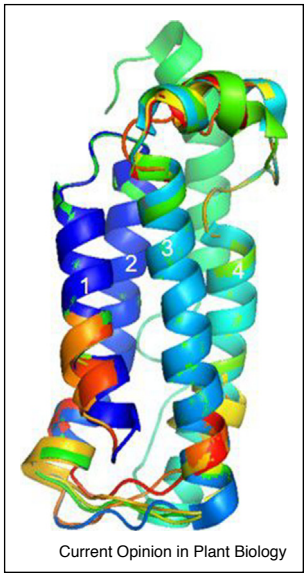

An overlay of the N-terminal MLKL (2msv) and the predicted CC_R domains of ADR1 ADR1-L1, ADR1-L2, NRG1.1, and NRG1.2. The predicted CC_R domain models were produced by threading onto the 2msv structure by Phyre2. All CC_R domains adopt highly similar 4HB structure very similar to the known 4HB MLKL, despite the low shared residue identity (ADR1 20% ID, 97.5% confidence; ADR1-L1 11% ID, 99% confidence; ADR1-L2 14% confidence, 98.6% confidence, NRG1.1 14% ID, 98%; NRG1.2 13% ID, 98.1% ID). Helices predicted to form the 4HB are numbered 1 through 4.

Table 1

Hmm-search results from query of the Arabidopsis genome. We built an hmm profile using an alignment from Ref. [53] as a guide. Performing an hmm-search against the Arabidopsis genome using our hmm as the query, we hit multiple CC_{EDVID} NLRs

NLRs

Atg	Description	Structure	E value
AT5G66900	NRG1.1	RNL	0.034
AT1G58390	unnamed NLR	CC_EDVID-NL	0.039
AT3G50460	HR2	RPW8	0.047
AT1G58807	unnamed NLR	CC_EDVID-NL	0.094
AT1G59124	unnamed NLR	CC_EDVID-NL	0.094
AT5G04720	ADR1-L2	RNL	0.17
AT5G05400	unnamed NLR	CNL	0.024
AT1G58400	unnamed NLR	CC_EDVID-NL	0.33
AT1G58410	unnamed NLR	CC_EDVID-NL	0.45
AT3G50950	ZAR1	CC_EDVID-NL	0.74
AT1G58848	unnamed NLR	CC_EDVID-NL	0.94
AT1G59218	unnamed NLR	CC_EDVID-NL	0.94

Other identified proteins of interest

Atg	Description	E value
AT2G18860	Syntaxin/t-SNARE family protein	0.059
AT2G17780	MCA2; mechanosensitive Ca channel	0.066
AT1G50970	Membrane trafficking VPS53 family protein	0.17
AT1G48240	Putative plant snare 12	0.85

used to predict the folding of the N-terminal regions of ZAR1, MLKL is indicated as one of the top four folding templates. This also fits very well with the recently published cryo-EM structure of full-length AtZAR1 [6••,7••]. The ZAR1 CC domain in the inactive ZAR1 forms a monomeric 4HB structure similar to the published Rx and Sr33 CC structures [57,67,68]. Thus, based on sequence homology, structural folding software predictions and solved structures of plant CC domains it is strongly suggested that CC_R domains and CC_{EDVID} domains may broadly adopt a 4HB fold, supposedly similar to MLKL or other pore-forming and oligomerizing proteins.

In addition to CC_{EDVID} NLRs, our hmm-search hit At2g17780 with high confidence (Table 1). At2g17780 encodes the Arabidopsis protein Mid1-Complementing Activity 2 (MCA2). MCA2 (and likely its paralog MCA1) forms a homotetramer, in which a single N-terminal helix from each subunit is arranged to form a plasma membrane Ca^{2+} channel [69]. Considering the hmmer hit to MCA2 in combination with the structural modeling of the RNLs onto MLKL, we speculate that RNLs, and potentially other CNLs, oligomerize to form pores in plant membranes, similar to the suggested ZAR1 CC domain pore. We present two possible models for activation (Figures 3 and 4). In model one, the RNLs N-termini generally fold into a 4HB like MLKL, and these oligomerize to form a large multimeric tertiary structure in which the entire 4HB of each subunit is embedded into the membrane. In model two, only the first helix of the 4HB of each subunit inserts into the membrane to form a putative cation channel, as suggested for ZAR1 or MCA2. Additionally, HELL and HeLo domains are predicted to have a single helix flip out to cause the pore [59,61]. Mutation of the GxxxG glycine zipper prevents cells death [61]. Interestingly, the GxxxG motif is conserved in the NRG1 proteins [33]. More experimentation, and actual plant RNL structures, are needed to determine the predictive accuracy of the RNL 4HB and the actual mode in which the RNLs trigger HR.

Subcellular localization of RNLs suggests membrane-specific function

The subcellular localization of proteins is important for their function. However, NLR and, in particular, hNLR localization has not been intensively studied. First insights into hNLR localization have recently been provided by Wu *et al.* [36••], who reported a similar steady-state as well as defense-activated localization of AtNRG1.1-mNeonGreen and AtNRG1.2-mNeonGreen transiently expressed from their native promoters in a heterologous system [36••]. Both AtNRG1 proteins localized to the cytosol and partially co-localized with the ER-marker HDEL-mRFP. In addition, AtNRG1.1 also partially co-localized with a PM-marker and was detected at some intracellular ER-associated puncta.

An attractive hypothesis would posit that RNLs would be activated at various subcellular locations and translocate to membranes, reminiscent of the defense-associated functions of RPW8 and MLKL.

In response to powdery mildew infection, RPW8.2 is targeted to the extrahaustorial membrane (EHM) via VAMP722/721-mediated vesicle trafficking [70,71]. Once incorporated into the EHM, RPW8.2 is thought to trigger localized immune responses [70]. In addition to RPW8.2, its paralogs HR1, HR2, and HR3 are also transported to the EHM upon powdery mildew infection to induce post-penetration resistance [72]. Thus, pathogen-induced membrane localization of RPW8.2 and its paralogs contributes to powdery mildew resistance.

The membrane localization of activated MLKL is important for its executor function during necroptosis. Upon necroptosis induction, the N-terminal 4HB of activated MLKL oligomerizes to form a complex consisting of eight protomers which translocate to the PM via phosphatidylinositol phosphate binding. This causes membrane deterioration resulting in necroptotic cell death [73,74••]. However, the exact underlying mechanism by which MLKL causes membrane disruption is still largely unknown. Considering the recent localization data and structural homology between RNLs and MLKL (Figure 4), it is plausible that RNL function is coupled to membrane integrity. However, sophisticated cell biological approaches are required to better understand where RNLs localize pre-activation and post-activation and how they function at membranes.

P-loop function, RNL membrane localization, and helper function

A functional P-loop is important for membrane localization and cell death function of certain NLRs like RPM1, Roq1 or N [30••,75,76]. Interestingly, RNLs (AtADR1-L2, NbNRG1) can require an intact P-loop for their auto-activity and, for ADR1-L2, in the propagation of the unregulated runaway cell death phenotype of the Arabidopsis *lsd1* mutant [30••,37,77]. Considering the possible membrane localization of activated hNLRs, it is possible that P-loop mutant hNLRs lose membrane localization, and, therefore, the ability to induce auto-activity mediated cell death. Equally possible would be that P-loop mutant hNLRs also lack the ability to oligomerize, since a functional P-loop was shown to be important for NLR self-association [30••,75].

In contrast, Arabidopsis RNLs (AtADR1-L2, AtNRG1.1, AtNRG1.2) do not require an intact P-loop for their helper function downstream of either effector-activated or specific auto-active sNLRs [34,36••]. In these cases, the P-loop mutant RNLs might rather act as a scaffold to initiate or support oligomerization with sNLRs or other functional RNLs, leading to their activation and subsequent membrane translocation. This would be consistent with their observed redundancy and could be tested by analyzing complementation of a 'helperless' mutant plant with P-loop mutant hNLR variants. A similar P-loop independent function of the mammalian hNLR NLRC4 was found in pyroptosis, a form of programmed cell death. However, the dispensability of the NLRC4 P-loop for oligomerization of NLRC4 and interaction with the sNLRs NAIP2 and NAIP5 is not yet clear [78,79] (Figure 3).

Interestingly, the helper function of the *N. benthamiana* NbNRG1 in Roq1 (TNL) mediated cell death requires a functional NbNRG1 P-loop [30••]. This suggests that the single NbADR1 cannot compensate for the loss-of-function of NbNRG1 function. It would be very interesting o see if the two different hNLR families would indeed form heteromeric complexes and whether these are biologically functional, and if the Arabidopsis helperless plant can be complemented by the *N. benthamiana* RNLs and vice versa. The generation of a helperless *N. benthamiana* plant is eagerly awaited.

RNLs and CNLs could form membrane-disrupting pores or ion-channels necessary for ETI

Changes in anion and cation fluxes across plant membranes into to the cytosol are a very early response to pathogen attack and a hallmark of MTI and ETI [80,81]. Calcium (Ca^{2+}) is probably the major ion and second messenger involved in mounting a successful immune response in both animals and plants. Although, the activation of specific Ca^{2+} permeable channels and pumps that lead to the early increase in cytosolic Ca^{2+} concentration ($[Ca^{2+}]$cyt) is well characterized for MTI, we still have not unequivocally identified the Ca^{2+} channels or pumps and the mechanisms of their activation in ETI [82]. The timing of the observed second increase in the biphasic $[Ca^{2+}]$cyt burst upon infection of Arabidopsis with different avirulent *Pseudomonas* DC3000 strains correlates with the timing of HR that is specific for the corresponding activated sNLR [83]. It is plausible that effector-recognition by sNLRs leads to the activation of RNLs, resulting in their oligomerization and translocation to cellular membranes, where they might form pores with their CC domains that enable or support ion fluxes, for example of Ca^{2+} ions (Figure 3B). Such a pore-forming function is also suggested for effector-activated AtZAR1 [7••]. Here, the most N-terminal alpha helix is rearranged upon activation and a pentamer of these single helices is formed as the full length protein pentamerizes. Mutations on the inside face of this helix lose activity but retain oligomerization and plasma membrane re-localization, suggesting a specific function for this potential pore forming structure. It is possible that some CNLs, like Arabidopsis RPM1 and ZAR1, might have retained

(or gained) he ability to form pores in membranes, like the plasma membrane, explaining the lack of a documented hNLR requirement [34,35••]. How sNLRs activate hNLRs is still not clear and evidence for physical interaction between effector-activated sNLRs with hNLRs is also eagerly awaited [32,37].

Could TIR activation result in RNL oligomer formation?

All analyzed TNL-mediated immune responses require hNLR function, or more specifically RNL function [30••,34,35••,36••], but no interaction between a TNL and RNL is thus far documented [37]. Nevertheless, a tempting speculation is that all TIR-dependent signaling converges onto RNLs and, given the above discussion, these form membrane pores to drive cell death.

TIR domains in Toll-like receptors (TLR) of animals have a scaffolding function for oligomerization and protein complex formation [84]. Working models suggested that this was the case for plant TNLs as well. However, recent findings reported an ancient NAD^+ (nicotinamide adenine dinucleotide)-consuming enzymatic activity for prokaryotic TIR domains and the TIR-domain of the mammalian SARM1 (sterile alpha and TIR motif containing 1) protein, a TLR adaptor protein that executes pathological axon degeneration [85••,86]. Interestingly, canonical innate immune system TIR domains from Toll-like receptors have lost this activity [85••,86]. Thus, a specific clade of TIR domains cleaves NAD^+ into ADP-ribose (ADPR), cyclic ADRP and nicotinamide and thereby depletes cells of NAD^+. NAD^+ depletion in macrophages and human T lymphocytes can trigger RIPK3 (receptor-interacting serine-threonine kinase 3) and MLKL-dependent necroptosis [87••], suggesting that MLKL or RIPK3 could somehow detect either the NAD^+ depletion or the accumulation of one or more cleavage products.

cADPR and ADPR belong to the adenine-containing second messenger family involved in regulation of cellular Ca^{2+} homeostasis, releasing calcium from intracellular storages like the ER or vacuole in animals and plants [88]. Given the relationship between plant TIR domains and the bacterial or mammalian SARM1 TIR domain [89], it is tempting to speculate that a similar mechanism might be employed by plants, and might include, by analogy, initiation of cell death by RNL-mediated pore formation in cellular membranes. Also, while cADPR can activate defense gene expression in *N. benthamiana*, no clear function of NAD^+ cleavage-products in plant immunity has been demonstrated [90,91]. An alternative hypothesis is informed by the findings of the importance of the TIR domain homodimerization for TNL function [52•,92]. TIR homodimers could recruit RNLs and initiate their oligomerization in an EDS1-dependent manner.

Conclusions

Although the first plant NLR proteins were identified and cloned 25 years ago, we still do not fully understand how their activity is regulated and how their activation is transmitted to a successful immune response. However, it is becoming clearer that most, if not all, NLRs do not function individually, but rather depend on an integrated regular network of sensor NLRs, executer NLRs, and helper NLRs [32,34,35••,36••,48]. Detailed analyses of the two ancient RNL-families, the ADR1s and the NRG1s, will reveal how they cooperate with sNLRs and with each other to transduce-specific immune responses upon effector recognition, and how this activation leads to cell death and disease resistance. The outstanding missing links for the NLR community are structural information for exemplars of various resting state and activated NLR classes and reliable, well controlled cell biology data derived from fluorescence protein-tagged full-length wild type NLRs expressed from their native promoters in appropriate homologous systems.

Conflict of interest statement

Nothing declared.

Acknowledgements

We apologize to those authors whose primary work could not be cited due to space limitations. We are grateful to the El Kasmi and Dangl labs for discussions and to Prof. Sarah Grant for critical comments on the manuscript. Research in the El Kasmi lab is funded by core funding from the University of Tübingen and by the Deutsche Forschungsgemeinschaft [SFB1101 - project D09). O.J.F. is supported by a grant from the Gordon and Betty Moore Foundation to the 2 Blades Foundation (GBMF4725). L. M.J. was supported in part by a grant from the National Institute of General Medical Sciences under award 5T32 GM007092. NLR research in the Dangl lab is supported by grant IOS-1758400 from the United States National Science Foundation and by the HHMI. J.L.D. is an Investigator of the Howard Hughes Medical Institute.

References and recommended reading

Papers of particular interest, published within the period of review, have been highlighted as:

- • of special interest
- •• of outstanding interest

1. Dangl JL, Horvath DM, Staskawicz BJ: **Pivoting the plant immune system from dissection to deployment**. *Science* 2013, **341**:746-751.

2. Jones JD, Dangl JL: **The plant immune system**. *Nature* 2006, **444**:323-329.

3. Jones JD, Vance RE, Dangl JL: **Intracellular innate immune surveillance devices in plants and animals**. *Science* 2016, **354**.

4. Bonardi V, Cherkis K, Nishimura MT, Dangl JL: **A new eye on NLR proteins: focused on clarity or diffused by complexity?** *Curr Opin Immunol* 2012, **24**:41-50.

5. Bernoux M, Burdett H, Williams SJ, Ellis JG, Newell K, Anderson P, Dodds PN, Kobe B, Lawrence G, Zhang X: **Comparative analysis of the flax immune receptors L6 and L7 suggests an equilibrium-based switch activation model**. *Plant Cell* 2016, **28**:146-159.

6. •• Wang J, Wang J, Hu M, Qi J, Wang G, Han Z, Qi Y, Wang H-W, Zhou J-M, Chai J: **Ligand-triggered allosteric ADP release primes a plant NLR complex**. *Science* 2019, **364**:eaav5868.

Wang *et al.* provide the first full length structure of a plant NLR in resting and intermediate pre-activated states. The two uridylyl moieties of $PBL2^{UMP}$ interact with and stabilize the activation segment of RKS1, consequently resulting in a conformational outward rotational change of about 60 degrees only in the ZAR1 NB domain. Thus, uridylylated PBL2 allosterically induces release of ADP from the ZAR1-RKS1-$PBL2^{UMP}$ complex.

7. •• Wang J, Hu M, Wang J, Qi J, Han Z, Wang G, Qi Y, Wang H-W, Zhou J-M, Chai J: **Reconstitution and structure of a plant NLR resistosome conferring immunity**. *Science* 2019, **364**:eaav5870.

Wang *et al.* provide the first full length structure of a plant NLR and the first biochemical explanation of indirect recognition of non-self via a pre-formed NLR heterodimeric complex. An effector-poised ZAR1-RKS1-uridylylated PBL2 intermediate monomer is activated by ATP, causing major structural rearrangements to generate an active pentamer. Pentamerization drives re-localization to the plasma membrane and causes the N-terminal CC domain helix to rearrange, forming a potential pentameric pore.

8. Thomma BP, Nürnberger T, Joosten MH: **Of PAMPs and effectors: the blurred PTI-ETI dichotomy**. *Plant Cell* 2011, **23**:4-15.

9. Leibman-Markus M, Pizarro L, Bar M, Coaker G, Avni A: **NRC proteins-a critical node for pattern and effector mediated signaling**. *Plant Signal Behav* 2018, **13**.

10. Leibman-Markus M, Pizarro L, Schuster S, Lin ZD, Gershony O, Bar M, Coaker G, Avni A: **The intracellular nucleotide binding leucine-rich repeat receptor–SlNRC4a enhances immune signaling elicited by extracellular perception**. *Plant Cell Environ* 2018, **41**:2313-2327.

11. Bonardi V, Tang S, Stallmann A, Roberts M, Cherkis K, Dangl JL: **Expanded functions for a family of plant intracellular immune receptors beyond specific recognition of pathogen effectors**. *Proc Nat Acad Sci U S A* 2011, **108**:16463-16468.

12. Baggs E, Dagdas G, Krasileva K: **NLR diversity, helpers and integrated domains: making sense of the NLR IDentity**. *Curr Opin Plant Biol* 2017, **38**:59-67.

13. Halter T, Navarro L: **Multilayer and interconnected post-transcriptional and co-transcriptional control of plant NLRs**. *Curr Opin Plant Biol* 2015, **26**:127-134.

14. Newman TE, Lee J, Williams SJ, Choi S, Halane MK, Zhou J, Solomon P, Kobe B, Jones JD, Segonzac C: **Autoimmunity and effector recognition in *Arabidopsis thaliana* can be uncoupled by mutations in the RRS 1-R immune receptor**. *New Phytol* 2018, **222**:954-965.

15. Ma Y, Guo H, Hu L, Martinez PP, Moschou PN, Cevik V, Ding P, Duxbury Z, Sarris PF, Jones JD: **Distinct modes of derepression of an Arabidopsis immune receptor complex by two different bacterial effectors**. *Proc Nat Acad Sci U S A* 2018, **115**:10218-10227.

16. Cesari S, Thilliez G, Ribot C, Chalvon V, Michel C, Jauneau A, Rivas S, Alaux L, Kanzaki H, Okuyama Y *et al.*: **The rice resistance protein pair RGA4/RGA5 recognizes the *Magnaporthe oryzae* effectors AVR-Pia and AVR1-CO39 by direct binding**. *Plant Cell* 2013, **25**:1463-1481.

17. Dong OX, Ao K, Xu F, Johnson KC, Wu Y, Li L, Xia S, Liu Y, Huang Y, Rodriguez E: **Individual components of paired typical NLR immune receptors are regulated by distinct E3 ligases**. *Nat Plants* 2018, **4**:699.

18. Tong M, Kotur T, Liang W, Vogelmann K, Kleine T, Leister D, Brieske C, Yang S, Ludke D, Wiermer M *et al.*: **E3 ligase SAUL1 serves as a positive regulator of PAMP-triggered immunity and its homeostasis is monitored by immune receptor SOC3**. *New Phytol* 2017, **215**:1516-1532.

19. Liang W, van Wersch S, Tong M, Li X: **TIR-NB-LRR immune receptor SOC 3 pairs with truncated TIR-NB protein CHS 1 or TN 2 to monitor the homeostasis of E3 ligase SAUL 1**. *New Phytol* 2018, **221**:2054-2066.

20. Deng Y, Zhai K, Xie Z, Yang D, Zhu X, Liu J, Wang X, Qin P, Yang Y, Zhang G: **Epigenetic regulation of antagonistic receptors confers rice blast resistance with yield balance**. *Science* 2017, **355**:962-965.

21. Grant MR, McDowell JM, Sharpe AG, de Torres Zabala M, Lydiate DJ, Dangl JL: **Independent deletions of a pathogen-resistance gene in Brassica and Arabidopsis**. *Proc Nat Acad Sci U S A* 1998, **95**:15843-15848.

22. Carter ME, Helm M, Chapman A, Wan E, Restrepo Sierra AM, Innes R, Bogdanove AJ, Wise RP: **Convergent evolution of effector protease recognition by Arabidopsis and barley**. *Mol Plant-Microbe Interact* 2018 http://dx.doi.org/10.1094/MPMI-07-18-0202-FI.

23. • Schultink A, Qi T, Bally J, Staskawicz B: **Using forward genetics in *Nicotiana benthamiana* to uncover the immune signaling pathway mediating recognition of the *Xanthomonas perforans* effector XopJ4**. *New Phytol* 2018, **221**:1001-1009.

This paper establishes forward genetics in *N. benthamiana*, and it shows that the diverse effector recognition platform of ZAR1 and class XII RLCKs is conserved in distant plant species.

24. Lewis JD, Lee AH-Y, Hassan JA, Wan J, Hurley B, Jhingree JR, Wang PW, Lo T, Youn J-Y, Guttman DS: **The Arabidopsis ZED1 pseudokinase is required for ZAR1-mediated immunity induced by the *Pseudomonas syringae* type III effector HopZ1a**. *Proc Nat Acad Sci U S A* 2013, **110**:18722-18727.

25. • Seto D, Koulena N, Lo T, Menna A, Guttman DS, Desveaux D: **Expanded type III effector recognition by the ZAR1 NLR protein using ZED1-related kinases**. *Nat Plants* 2017, **3** http://dx.doi.org/10.1038/nplants.2017.1027.

This paper further demonstrates that ZAR1 can use multiple ZED1-related kinases to recognize a diverse set of effectors. The authors show that together ZAR1 and ZRK3 mediate HopF2a resistance.

26. Wang G, Roux B, Feng F, Guy E, Li L, Li N, Zhang X, Lautier M, Jardinaud M-F, Chabannes M: **The decoy substrate of a pathogen effector and a pseudokinase specify pathogen-induced modified-self recognition and immunity in plants**. *Cell Host Microbe* 2015, **18**:285-295.

27. • Helm M, Qi M, Sarkar S, Yu H, Whitham SA, Innes RW: **Engineering a decoy substrate in soybean to enable recognition of the Soybean Mosaic Virus NIa protease**. *Mol Plant Microbe Interact* 2019 http://dx.doi.org/10.1094/MPMI-12-18-0324-R.

This preprint furthers NLR engineering in a crop species. The authors show that a PBS1 decoy protein modified to contain a cleavage site for the Soybean mosaic virus (SMV) NIa protease can trigger cell death when cleaved.

28. Kim SH, Qi D, Ashfield T, Helm M, Innes RW: **Using decoys to expand the recognition specificity of a plant disease resistance protein**. *Science* 2016, **351**:684-687.

29. Zhang J, Li W, Xiang T, Liu Z, Laluk K, Ding X, Zou Y, Gao M, Zhang X, Chen S: **Receptor-like cytoplasmic kinases integrate signaling from multiple plant immune receptors and are targeted by a *Pseudomonas syringae* effector**. *Cell Host Microbe* 2010, **7**:290-301.

30. •• Qi T, Seong K, Thomazella DPT, Kim JR, Pham J, Seo E, Cho M-J, Schultink A, Staskawicz BJ: **NRG1 functions downstream of EDS1 to regulate TIR-NLR-mediated plant immunity in *Nicotiana benthamiana***. *Proc Nat Acad Sci U S A* 2018, **114**:E10979-E10987.

The authors show via Co-IP that NbNRG1 self-associates and interacts with NbEDS1 in *N. benthamiana*. Authors also suggest that EDS1 functions upstream of NRG1s based on cell death activity of NbNRG1 in an eds1 mutant *N. benthamiana*.

31. •• Wu CH, Abd-El-Haliem A, Bozkurt TO, Belhaj K, Terauchi R, Vossen JH, Kamoun S: **NLR network mediates immunity to diverse plant pathogens**. *Proc Natl Acad Sci U S A* 2017, **114**:8113-8118.

These authors reveal a complex genetic network of helper NRC proteins that function with the evolutionary-related sNLRs in Solanaceae. The authors propose a model, in which NLR networks increase the robustness of immune signaling to counteract rapidly evolving pathogens.

32. Wu CH, Belhaj K, Bozkurt TO, Birk MS, Kamoun S: **Helper NLR proteins NRC2a/b and NRC3 but not NRC1 are required for Pto-mediated cell death and resistance in *Nicotiana benthamiana***. *New Phytol* 2016, **209**:1344-1352.

33. Collier SM, Hamel LP, Moffett P: **Cell death mediated by the N-terminal domains of a unique and highly conserved class of NB-LRR protein**. *Mol Plant Microbe Interact* 2011, **24**:918-931.

34. Bonardi V, Tang S, Stallmann A, Roberts M, Cherkis K, Dangl JL: **Expanded functions for a family of plant intracellular immune receptors beyond specific recognition of pathogen effectors**. *Proc Natl Acad Sci U S A* 2011, **108**:16463-16468.

35. •• Castel B, Ngou PM, Cevik V, Redkar A, Kim DS, Yang Y, Ding P, Jones JD: **Diverse NLR immune receptors activate defence via the RPW 8-NLR NRG 1**. *New Phytol* 2018, **222**:966-980.
The authors test the ability of a wide array of TNL sensors to mediate resistance in double nrg1 Arabidopsis background and nrg1 *N. benthamiana*. NRG1 is shown to be required for the hypersensitive cell-death response and full oomycete resistance mediated by TNLs, but NRG1 is not required for salicylic acid induction or bacterial resistance.

36. •• Wu Z, Li M, Dong OX, Xia S, Liang W, Bao Y, Wasteneys G, Li X: **Differential regulation of TNL-mediated immune signaling by redundant helper CNL s**. *New Phytol* 2018.
The authors demonstrate that some sensor TNLs differentially use the ADR1 and NRG1 helper families to transduce downstream defense signals. Importantly, the authors also created a plant line devoid of all RNL helper NLRs that can be used to test for synergistic effects of ADR1s and NRG1s in plant immunity.

37. Peart JR, Mestre P, Lu R, Malcuit I, Baulcombe DC: **NRG1, a CC-NB-LRR protein, together with N, a TIR-NB-LRR protein, mediates resistance against tobacco mosaic virus**. *Curr Biol* 2005, **15**:968-973.

38. Gabriëls SH, Vossen JH, Ekengren SK, van Ooijen G, Abd-El-Haliem AM, van den Berg GC, Rainey DY, Martin GB, Takken FL, de Wit PJ *et al.*: **An NB-LRR protein required for HR signalling mediated by both extra- and intracellular resistance proteins**. *Plant J* 2007, **50**:14-28.

39. Li Y, Zhang Y, Wang QX, Wang TT, Cao XL, Zhao ZX, Zhao SL, Xu YJ, Xiao ZY, Li JL: **RESISTANCE TO POWDERY MILDEW 8.1 boosts pattern-triggered immunity against multiple pathogens in Arabidopsis and rice**. *Plant Biotechnol J* 2018, **16**:428-441.

40. Zhong Y, Cheng ZM: **A unique RPW8-encoding class of genes that originated in early land plants and evolved through domain fission, fusion, and duplication**. *Sci Rep* 2016, **6** http://dx.doi.org/10.1038/srep32923.

41. Meyers BC, Kozik A, Griego A, Kuang H, Michelmore RW: **Genome-wide analysis of NBS-LRR-encoding genes in Arabidopsis**. *Plant Cell* 2003, **15**:809-834.

42. Collier SM, Moffett P: **NB-LRRs work a "bait and switch" on pathogens**. *Trends Plant Sci* 2009, **14**:521-529.

43. Shao ZQ, Xue JY, Wu P, Zhang YM, Wu Y, Hang YY, Wang B, Chen JQ: **Large-scale analyses of angiosperm nucleotide-binding site-leucine-rich repeat genes reveal three anciently diverged classes with distinct evolutionary patterns**. *Plant Physiol* 2016, **170**:2095-2109.

44. Zhang Y, Xia R, Kuang H, Meyers BC: **The diversification of plant NBS-LRR defense genes directs the evolution of microRNAs that target them**. *Mol Biol Evol* 2016, **33**:2692-2705.

45. Zhang Q, Ma C, Zhang Y, Gu Z, Li W, Duan X, Wang S, Hao L, Wang Y, Wang S: **A single-nucleotide polymorphism in the promoter of a hairpin RNA contributes to *Alternaria alternata* leaf spot resistance in apple (Malus× domestica)**. *Plant Cell* 2018, **30**:1924-1942.

46. Rairdan GJ, Collier SM, Sacco MA, Baldwin TT, Boettrich T, Moffett P: **The coiled-coil and nucleotide binding domains of the Potato Rx disease resistance protein function in pathogen recognition and signaling**. *Plant Cell* 2008, **20**:739-751.

47. Brendolise C, Martinez-Sanchez M, Morel A, Chen R, Dinis R, Deroles S, Peeters N, Rikkerink EHA, Montefiori M: **NRG1-mediated recognition of HopQ1 reveals a link between PAMP and Effector-triggered Immunity**. *bioRxiv* 2018 http://dx.doi.org/10.1101/293050.

48. Dong OX, Tong M, Bonardi V, El Kasmi F, Woloshen V, Wunsch LK, Dangl JL, Li X: **TNL-mediated immunity in Arabidopsis requires complex regulation of the redundant ADR1 gene family**. *New Phytol* 2016, **210**:960-973.

49. Roberts M, Tang S, Stallmann A, Dangl JL, Bonardi V: **Genetic requirements for signaling from an autoactive plant NB-LRR intracellular innate immune receptor**. *PLoS Genet* 2013, **9** http://dx.doi.org/10.1371/journal.pgen.1003465.

50. Grech-Baran M, Witek K, Szajko K, Witek AI, Morgiewicz K, Wasilewicz-Flis I, Jakuczun H, Marczewski W, Jones JD, Hennig J: **Extreme resistance to potato virus Y in potato carrying the Ry gene is mediated by a TIR-NLR immune receptor**. *bioRxiv* 2018 http://dx.doi.org/10.1101/445031.

51. Meyers BC, Morgante M, Michelmore RW: **TIR-X and TIR-NBS proteins: two new families related to disease resistance TIR-NBS-LRR proteins encoded in Arabidopsis and other plant genomes**. *Plant J* 2002, **32**:77-92.

52. • Nishimura MT, Anderson RG, Cherkis KA, Law TF, Liu QL, Machius M, Nimchuk ZL, Yang L, Chung EH, El Kasmi F *et al.*: **TIR-only protein RBA1 recognizes a pathogen effector to regulate cell death in Arabidopsis**. *Proc Natl Acad Sci U S A* 2017, **114**:E2053-E2062.
The authors isolated the TIR-only protein RBA1 which confers resistance to HopBA1. Both dimerization-interfaces, as in canonical TNLs, are required for RBA1-mediated cell death signaling activity. This paper furthered the understanding about how 'truncated' NLRs function in immunity.

53. Loquet A, Saupe SJ: **Diversity of amyloid motifs in NLR signaling in fungi**. *Biomolecules* 2017, **7** http://dx.doi.org/10.3390/biom7020038.

54. Daskalov A, Habenstein B, Martinez D, Debets AJ, Sabaté R, Loquet A, Saupe SJ: **Signal transduction by a fungal NOD-like receptor based on propagation of a prion amyloid fold**. *PLoS Biol* 2015, **13** http://dx.doi.org/10.1371/journal.pbio.1002059.

55. Le H, Harton J: **Pyrin- and CARD-only proteins as regulators of NLR functions**. *Front Immunol* 2013, **4** http://dx.doi.org/10.3389/fimmu.2013.00275.

56. • Zhang X, Bernoux M, Bentham AR, Newman TE, Ve T, Casey LW, Raaymakers TM, Hu J, Croll TI, Schreiber KJ: **Multiple functional self-association interfaces in plant TIR domains**. *Proc Nat Acad Sci U S A* 2017, **114**:E2046-E2052.
This paper demonstrates that the two interfaces of TIR domains are important for signaling and self-association. The authors show that mutations in either the AE-interface or DE-interface region of the TIR domain disrupt cell-death signaling activity in all tested cases, and self-association in some instances.

57. Casey LW, Lavrencic P, Bentham AR, Cesari S, Ericsson DJ, Croll T, Turk D, Anderson PA, Mark AE, Dodds PN: **The CC domain structure from the wheat stem rust resistance protein Sr33 challenges paradigms for dimerization in plant NLR proteins**. *Proc Nat Acad Sci U S A* 2016, **113**:12856-12861.

58. Daskalov A, Paoletti M, Ness F, Saupe SJ: **Genomic clustering and homology between HET-S and the NWD2 STAND protein in various fungal genomes**. *PloS One* 2012, **7** http://dx.doi.org/10.1371/journal.pone.0034854.

59. Seuring C, Greenwald J, Wasmer C, Wepf R, Saupe SJ, Meier BH, Riek R: **The mechanism of toxicity in HET-S/HET-s prion incompatibility**. *PLoS Biol* 2012, **10** http://dx.doi.org/10.1371/journal.pbio.1001451.

60. Robinson R: **Prion folding sends a death signal in fungus**. *PLoS Biol* 2015, **13** http://dx.doi.org/10.1371/journal.pbio.1002058.

61. Daskalov A, Habenstein B, Sabaté R, Berbon M, Martinez D, Chaignepain S, Coulary-Salin B, Hofmann K, Loquet A, Saupe SJ: **Identification of a novel cell death-inducing domain reveals that fungal amyloid-controlled programmed cell death is related to necroptosis**. *Proc Nat Acad Sci U S A* 2016, **113**:2720-2725.

62. Murphy JM, Czabotar PE, Hildebrand JM, Lucet IS, Zhang J-G, Alvarez-Diaz S, Lewis R, Lalaoui N, Metcalf D, Webb AI: **The pseudokinase MLKL mediates necroptosis via a molecular switch mechanism**. *Immunity* 2013, **39**:443-453.

63. Quarato G, Guy CS, Grace CR, Llambi F, Nourse A, Rodriguez DA, Wakefield R, Frase S, Moldoveanu T, Green DR: **Sequential engagement of distinct MLKL phosphatidylinositol-binding sites executes necroptosis**. *Mol Cell* 2016, **61**:589-601.

64. Su L, Quade B, Wang H, Sun L, Wang X, Rizo J: **A plug release mechanism for membrane permeation by MLKL**. *Structure* 2014, **22**:1489-1500.

65. Hildebrand JM, Tanzer MC, Lucet IS, Young SN, Spall SK, Sharma P, Pierotti C, Garnier J-M, Dobson RC, Webb AI: **Activation of the pseudokinase MLKL unleashes the four-helix bundle domain to induce membrane localization and necroptotic cell death**. *Proc Nat Acad Sci U S A* 2014, **111**:15072-15077.

66. Bentham AR, Zdrzałek R, De la Concepcion JC, Banfield MJ: **Uncoiling CNLs: structure/function approaches to understanding CC domain function in plant NLRs**. *Plant Cell Physiol* 2018, **59**:2398-2408.

67. Cesari S, Moore J, Chen C, Webb D, Periyannan S, Mago R, Bernoux M, Lagudah ES, Dodds PN: **Cytosolic activation of cell death and stem rust resistance by cereal MLA-family CC–NLR proteins**. *Proc Nat Acad Sci U S A* 2016, **113**:10204-10209.

68. Hao W, Collier SM, Moffett P, Chai J: **Structural basis for the interaction between the potato virus X resistance protein (Rx) and its cofactor Ran GTPase-activating protein 2 (RanGAP2)**. *J Biol Chem* 2013, **288**:35868-35876.

69. Shigematsu H, Iida K, Nakano M, Chaudhuri P, Iida H, Nagayama K: **Structural characterization of the mechanosensitive channel candidate MCA2 from *Arabidopsis thaliana***. *PloS One* 2014, **9** http://dx.doi.org/10.1371/journal.pone.0087724.

70. Wang W, Wen Y, Berkey R, Xiao S: **Specific targeting of the Arabidopsis resistance protein RPW8.2 to the interfacial membrane encasing the fungal Haustorium renders broad-spectrum resistance to powdery mildew**. *Plant Cell* 2009, **21**:2898-2913.

71. Kim H, O'Connell R, Maekawa-Yoshikawa M, Uemura T, Neumann U, Schulze-Lefert P: **The powdery mildew resistance protein RPW8.2 is carried on VAMP721/722 vesicles to the extrahaustorial membrane of haustorial complexes**. *Plant J* 2014, **79**:835-847.

72. Berkey R, Zhang Y, Ma X, King H, Zhang Q, Wang W, Xiao S: **Homologues of the RPW8 resistance protein are localized to the extrahaustorial membrane that is likely synthesized de novo**. *Plant Physiol* 2017, **173**:600-613.

73. Dondelinger Y, Declercq W, Montessuit S, Roelandt R, Goncalves A, Bruggeman I, Hulpiau P, Weber K, Sehon CA, Marquis RW *et al.*: **MLKL compromises plasma membrane integrity by binding to phosphatidylinositol phosphates**. *Cell Rep* 2014, **7**:971-981.

74. •• Huang D, Zheng X, Wang ZA, Chen X, He WT, Zhang Y, Xu JG, Zhao H, Shi W, Wang X *et al.*: **The MLKL channel in necroptosis is an octamer formed by tetramers in a dyadic process**. *Mol Cell Biol* 2017, **37**.

The authors demonstrate the MLKL channel is an octamer comprised two previously identified tetramers, and the octamer is the agent of necroptosis. Because of the inability to detect the N or C termini on the outside of the cells, the authors propose MLKLs span the membrane with their termini inside the cell.

75. El Kasmi F, Chung EH, Anderson RG, Li J, Wan L, Eitas TK, Gao Z, Dangl JL: **Signaling from the plasma-membrane localized plant immune receptor RPM1 requires self-association of the full-length protein**. *Proc Natl Acad Sci U S A* 2017, **114**:E7385-E7394.

76. Mestre P, Baulcombe DC: **Elicitor-mediated oligomerization of the tobacco N disease resistance protein**. *Plant Cell* 2006, **18**:491-501.

77. Roberts M, Tang S, Stallmann A, Dangl JL, Bonardi V: **Genetic requirements for signaling from an autoactive plant NB-LRR intracellular innate immune receptor**. *PLoS Genet* 2013, **9**: e1003465.

78. Kofoed EM, Vance RE: **Innate immune recognition of bacterial ligands by NAIPs determines inflammasome specificity**. *Nature* 2011, **477**:592-595.

79. Halff EF, Diebolder CA, Versteeg M, Schouten A, Brondijk TH, Huizinga EG: **Formation and structure of a NAIP5-NLRC4 inflammasome induced by direct interactions with conserved N- and C-terminal regions of flagellin**. *J Biol Chem* 2012, **287**:38460-38472.

80. McDowell JM, Dangl JL: **Signal transduction in the plant immune response**. *Trends Biochem Sci* 2000, **25**:79-82.

81. Cui H, Tsuda K, Parker JE: **Effector-triggered immunity: from pathogen perception to robust defense**. *Annu Rev Plant Biol* 2015, **66**:487-511.

82. Yuan P, Jauregui E, Du L, Tanaka K, Poovaiah BW: **Calcium signatures and signaling events orchestrate plant-microbe interactions**. *Curr Opin Plant Biol* 2017, **38**:173-183.

83. Grant M, Brown I, Adams S, Knight M, Ainslie A, Mansfield J: **The RPM1 plant disease resistance gene facilitates a rapid and sustained increase in cytosolic calcium that is necessary for the oxidative burst and hypersensitive cell death**. *Plant J* 2000, **23**:441-450.

84. Nanson JD, Kobe B, Ve T, Death: **TIR, and RHIM: self-assembling domains involved in innate immunity and cell-death signaling**. *J Leukoc Biol* 2018, **105**:363-375.

85. •• Essuman K, Summers DW, Sasaki Y, Mao X, DiAntonio A, Milbrandt J: **The SARM1 toll/interleukin-1 receptor domain possesses intrinsic NAD(+) cleavage activity that promotes pathological axonal degeneration**. *Neuron* 2017, **93**:1334-1343 e1335.

The authors demonstrate that a diverse set of TIR domains from bacteria and archea have NAD+-consuming enzymatic activity. Multiple bacterial and archaeal TIR domains cleave NAD+ into Nam and ADPR, while a subset of TIR domains generate cADPR. Together, these findings strongly suggest that the primordial function of the TIR domain is to cleave NAD+.

86. Essuman K, Summers DW, Sasaki Y, Mao X, Yim AKY, DiAntonio A, Milbrandt J: **TIR domain proteins are an ancient family of NAD(+)-consuming enzymes**. *Curr Biol* 2018, **28**:421-430 e424.

87. •• Pajuelo D, Gonzalez-Juarbe N, Tak U, Sun J, Orihuela CJ, Niederweis M: **NAD(+) depletion triggers macrophage necroptosis, a cell death pathway exploited by mycobacterium tuberculosis**. *Cell Rep* 2018, **24**:429-440.

The authors show that NAD+ hydrolysis by tuberculosis necrotizing toxin induces necroptosis in mammalian macrophages. However, NAD+ depletion alone is sufficient to activate RIPK3 and MLKL, bypassing the canonical toxin-mediated initiation of the pathway. Importantly, cell death caused by NAD+ depletion is RIPK3- dependent and MLKL-dependent, demonstrating these two proteins to be key mediators of necroptosis.

88. Hunt L, Lerner F, Ziegler M: **NAD–new roles in signalling and gene regulation in plants**. *New Phytol* 2004, **163**:31-44.

89. Zhang Q, Zmasek CM, Cai X, Godzik A: **TIR domain-containing adaptor SARM is a late addition to the ongoing microbe-host dialog**. *Dev Comp Immunol* 2011, **35**:461-468.

90. Durner J, Wendehenne D, Klessig DF: **Defense gene induction in tobacco by nitric oxide, cyclic GMP, and cyclic ADP-ribose**. *Proc Natl Acad Sci U S A* 1998, **95**:10328-10333.

91. Petriacq P, de Bont L, Tcherkez G, Gakiere B: **NAD: not just a pawn on the board of plant-pathogen interactions**. *Plant Signal Behav* 2013, **8**:e22477.

92. Zhang X, Bernoux M, Bentham AR, Newman TE, Ve T, Casey LW, Raaymakers TM, Hu J, Croll TI, Schreiber KJ: **Multiple functional self-association interfaces in plant TIR domains**. *Proc Nat Acad Sci U S A* 2017, **114**:E2046-E2052.

7.2. Saile and Jacob *et al*., 2020

Two unequally redundant "helper" immune receptor families mediate *Arabidopsis thaliana* "sensor" immune receptor functions

Saile, S. C.*, Jacob, P.*, Castel, B., Jubic, L. M., Salas-Gonzáles, I., Bäcker, M., Jones, J. D. G., Dangl, J. L., El Kasmi, F.

*These authors contributed equally to this work.

PLOS Biology.

2020 Sep:18(9): e3000783.

doi: 10.1371/journal.pbio.3000783.

PLOS BIOLOGY

RESEARCH ARTICLE

Two unequally redundant "helper" immune receptor families mediate *Arabidopsis thaliana* intracellular "sensor" immune receptor functions

Svenja C. Saile[1‡], Pierre Jacob[2,3‡], Baptiste Castel[4¤], Lance M. Jubic[2,3,5], Isai Salas-Gonzáles[2,3,6], Marcel Bäcker[1], Jonathan D. G. Jones[4], Jeffery L. Dangl[2,3,5,6,7,8], Farid El Kasmi[1]*

1 Center for Plant Molecular Biology, Eberhard Karls University of Tübingen, Tübingen, Germany, **2** Department of Biology, University of North Carolina at Chapel Hill, Chapel Hill, North Carolina, United States of America, **3** Howard Hughes Medical Institute, University of North Carolina at Chapel Hill, Chapel Hill, North Carolina, United States of America, **4** The Sainsbury Laboratory, Norwich Research Park, Norwich, United Kingdom, **5** Curriculum in Genetics and Molecular Biology, University of North Carolina at Chapel Hill, Chapel Hill, North Carolina, United States of America, **6** Curriculum in Bioinformatics and Computational Biology, University of North Carolina at Chapel Hill, Chapel Hill, North Carolina, United States of America, **7** Carolina Center for Genome Sciences, University of North Carolina at Chapel Hill, Chapel Hill, North Carolina, United States of America, **8** Department of Microbiology and Immunology, University of North Carolina at Chapel Hill, Chapel Hill, North Carolina, United States of America

¤ Current address: Department of Biological Sciences, National University of Singapore, Singapore
‡ These authors contributed equally to this work. JDGJ, JLD, and FEK also contributed equally to this work.
* farid.el-kasmi@zmbp.uni-tuebingen.de

Citation: Saile SC, Jacob P, Castel B, Jubic LM, Salas-Gonzáles I, Bäcker M, et al. (2020) Two unequally redundant "helper" immune receptor families mediate *Arabidopsis thaliana* intracellular "sensor" immune receptor functions. PLoS Biol 18(9): e3000783. https://doi.org/10.1371/journal.pbio.3000783

Academic Editor: Xinnian Dong, Duke University, UNITED STATES

Received: February 27, 2020

Accepted: August 17, 2020

Published: September 14, 2020

Peer Review History: PLOS recognizes the benefits of transparency in the peer review process; therefore, we enable the publication of all of the content of peer review and author responses alongside final, published articles. The editorial history of this article is available here: https://doi.org/10.1371/journal.pbio.3000783

Data Availability Statement: All relevant data are within the paper and its Supporting Information files. All necessary data and scripts to reproduce

Abstract

Plant nucleotide-binding (NB) leucine-rich repeat (LRR) receptor (NLR) proteins function as intracellular immune receptors that perceive the presence of pathogen-derived virulence proteins (effectors) to induce immune responses. The 2 major types of plant NLRs that "sense" pathogen effectors differ in their N-terminal domains: these are Toll/interleukin-1 receptor resistance (TIR) domain-containing NLRs (TNLs) and coiled-coil (CC) domain-containing NLRs (CNLs). In many angiosperms, the RESISTANCE TO POWDERY MILDEW 8 (RPW8)-CC domain containing NLR (RNL) subclass of CNLs is encoded by 2 gene families, *ACTIVATED DISEASE RESISTANCE 1* (*ADR1*) and *N REQUIREMENT GENE 1* (*NRG1*), that act as "helper" NLRs during multiple sensor NLR-mediated immune responses. Despite their important role in sensor NLR-mediated immunity, knowledge of the specific, redundant, and synergistic functions of helper RNLs is limited. We demonstrate that the ADR1 and NRG1 families act in an unequally redundant manner in basal resistance, effector-triggered immunity (ETI) and regulation of defense gene expression. We define RNL redundancy in ETI conferred by some TNLs and in basal resistance against virulent pathogens. We demonstrate that, in *Arabidopsis thaliana*, the 2 RNL families contribute specific functions in ETI initiated by specific CNLs and TNLs. Time-resolved whole genome expression profiling revealed that RNLs and "classical" CNLs trigger similar transcriptome changes, suggesting that RNLs act like other CNLs to mediate ETI downstream of sensor NLR activation. Together, our genetic data confirm that RNLs contribute to basal resistance, are fully

every part of the RNA-Sequencing analysis are deposited in https://github.com/isaisg/helperless.

Funding: JDGJ and BC were supported by a core grant to the Sainsbury lab from the Gatsby foundation, and from a European Research Council grant "ImmunityByPairDesign". PJ, ISG and JLD were supported by the National Science Foundation (Grant IOS-1758400 to J.L.D.) and HHMI. J.L.D. is a Howard Hughes Medical Institute (HHMI) Investigator. L.M.J. was supported in part by a grant from the National Institute of General Medical Sciences under award 5T32 GM007092. SCS, MB and FEK were supported by core funding from the University of Tübingen, through the Deutsche Forschungsgemeinschaft [SFB/CRC1101 - project D09) and the Reinhard Frank Stiftung (Project 'helperless plant'). The funders had no role in study design, data collection and analysis, decision to publish, or preparation of the manuscript.

Competing interests: The authors have declared that no competing interests exist.

Abbreviations: Ac2V, *Albugo candida* race 2; ADR1, *ACTIVATED DISEASE RESISTANCE 1*; BTH, benzothiadiazole; CC, coiled-coil; CDS, coding sequence; cfu, colony-forming units; CNL, CC domain-containing NLR; Col-0, Columbia-0; DI, disease index; dpi, days post infection; DEG, differentially expressed gene; EDS1, *Enhanced Disease Susceptibility 1*; ETI, effector-triggered immunity; FDR, false discovery rate; GO, gene ontology; Hpa, *Hyaloperonospora arabidopsidis*; hpi, hours post infection; HR, hypersensitive response; JA, jasmonic acid; LRR, leucine-rich repeat; lsd1, *lesion simulating disease 1*; NB, nucleotide binding; NLR, NB LRR receptor; NRG1.1, *N REQUIREMENT GENE 1.1*; OD_{600}, optical density at 600 nm; PAD4, *Phytoalexin Deficient 4*; PAMP, pathogen-associated molecular pattern; Pf0-1, *Pseudomonas fluorescens 0–1*; PM, plasma membrane; PRR, PAMP recognition receptor; Psm, *Pseudomonas syringae* pv. *maculicola*; Pst, *Pseudomonas syringae* pv. *tomato*; PTI, pattern-triggered immunity; RK, receptor kinase; RLP, receptor-like protein; RNL, RPW8-CC domain containing NLR; Roq1, RECOGNITION OF XOPQ 1; ROS, reactive oxygen species; RPM1, RESISTANCE TO P. SYRINGAE PV MACULICOLA 1; RPP1, RECOGNITION OF PERONOSPORA PARASITICA 1; RPS2, RESISTANT TO P. SYRINGAE 2; RPS4, RESISTANT TO P. SYRINGAE 4; RPS5, RESISTANT TO P. SYRINGAE 5; RPS6, RESISTANT TO P. SYRINGAE 6; RPW8, RESISTANCE TO POWDERY MILDEW 8; RRS1, RESISTANT TO RALSTONIA SOLANACEARUM 1; SA, salicylic acid; SAG101, *Senescence Associated*

required for TNL signaling, and can also support defense activation during CNL-mediated ETI.

Introduction

Plant defense responses, once initiated, thwart attacking and invading pathogens via multiple mechanisms [1,2]. Microbial pathogens can trigger a first defense response upon detection by plasma membrane (PM)-localized leucine-rich repeat (LRR) receptor kinases (RKs) or receptor-like proteins (RLPs). These receptors perceive conserved pathogen-associated molecular patterns (PAMPs) or danger signals from diverse pathogens and initiate a broad range of immune responses, collectively called pattern-triggered immunity (PTI) [3,4]. PTI effectively inhibits non-host-adapted pathogens and also contributes to resistance to host-adapted pathogens. Plant pathogens deliver virulence effectors into plant cells by a variety of mechanisms to dampen PTI [5]. In turn, plants evolved the ability to recognize effectors or their action on host targets, thereby initiating a second tier of the immune system, effector-triggered immunity (ETI). ETI involves strong activation of defense mechanisms and is often associated with a type of cell death at the site of infection termed the hypersensitive response (HR) [6,7]. In nearly all cases, ETI is mediated by intracellular immune receptors called nucleotide-binding (NB) LRR receptors (NLRs). NLRs are modular proteins, typically exhibiting a C-terminal LRR domain, a central nucleotide-binding (NB) domain, and any of a small variety of N-terminal domains [8,9]. In plants, 2 major types of NLRs have been described which differ in their N-terminal domains. The Toll/interleukin-1 receptor resistance (TIR) domain-containing NLRs (TNLs) and the coiled-coil (CC) domain-containing NLRs (CNLs) can directly or indirectly sense the presence of pathogen effectors [9]. Thus, they are usually designated "sensor" NLRs. Further, there is a unique subclade of CNLs that exhibit an atypical CC-R N-terminal domain sequence-related to the resistance protein RESISTANCE TO POWDERY MILDEW 8 (RPW8), therefore also termed RNLs. RNLs are required for the function of many sensor NLRs and are thus also referred to as helper NLRs [10–15]. CNL and TNL activation by effectors may involve NLR oligomerization—the formation of a so-called resistosome—that is required for NLR function in immunity, as was shown for the *Arabidopsis thaliana* CNL HOPZ-ACTIVATED RESISTANCE 1 (ZAR1) [16–19].

RNLs form an evolutionarily conserved clade of NLRs present in most land plants that share a unique NB domain in addition to the RPW8-like CC-R domain [20,21]. *A. thaliana* has 2 subfamilies of RNLs, ADR1s and NRG1s. The ADR1 family includes ACTIVATED DISEASE RESISTANCE 1 (ADR1) and paralogs ADR1-LIKE 1 (ADR1-L1), ADR1-L2, and ADR1-L3, while the NRG1 family includes N REQUIREMENT GENE 1.1 (NRG1.1) and paralogs NRG1.2 and NRG1.3 [14,22,23]. We will refer to the *NRG1* genes according to The Arabidopsis Information Resource (TAIR; https://www.arabidopsis.org/index.jsp) nomenclature as *NRG1.1*, *NRG1.2*, and *NRG1.3* hereafter. These correspond to *NRG1A*, *NRG1B*, and *NRG1C* as used, e.g., in work by Wu and colleagues [24]. *ADR1-L3* and *NRG1.3* could encode N-terminally truncated proteins but have no documented function in immunity, as recently demonstrated for *NRG1.3* [11].

The study of RNLs unveils complex genetic interactions. *ADR1-L1* and *ADR1-L2* were first studied for their crucial role in the run-away-cell death phenotype initiated by the application of the salicylic acid (SA) analogue benzothiadiazole (BTH) to the *lesion simulating disease 1* (*lsd1*) mutant background [14]. Both the *adr1-L1* and the *adr1-L2* mutation suppressed the *lsd1* runaway-cell-death. Further, the double heterozygous *ADR1-L1*/*adr1-L1 ADR1-L2*/

Gene 101; SAR, systemic acquired resistance; T3SS, type III secretion system; T-DNA, transfer DNA; TAIR, The Arabidopsis Information Resource; TIR, Toll/interleukin-1 receptor resistance; TNL, TIR domain-containing NLR; WRR4, WHITE RUST RESISTANCE 4; ZAR1, HOPZ-ACTIVATED RESISTANCE1.

adr1-L2 mutant also suppressed the *lsd1* runaway-cell-death phenotype. Thus *ADR1-L1* and *ADR1-L2* constitute a rare case of non-allelic non-complementation. This suggested that both genes contribute quantitatively to the cell death phenotype [25]. *ADR1* was not involved in this phenotype but was found to be redundantly involved, with *ADR1-L1* and *ADR1-L2*, in SA accumulation and ETI activation downstream of some sensor NLRs—including examples of both CNLs and TNLs [14,26]—and was also found to elevate disease resistance when overexpressed [23].

NRG1 was first discovered in *Nicotiana benthamiana* via its requirement for ETI induced by the sensor TNL protein N [22]. In *A. thaliana* Columbia-0 (Col-0) plants, 2 tightly linked functional copies of *NRG1* exist, *NRG1.1* and *NRG1.2*. The application of CRISPR-Cas9 technology allowed the generation of *A. thaliana nrg1.1 nrg1.2* double [13,27] and *nrg1.1 nrg1.2 nrg1.3* triple mutants [11]. Recently, a "*helperless*" mutant lacking all RNLs was constructed by combining the *nrg1* double or triple CRISPR-Cas9 alleles with a preexisting *adr1 adr1-L1 adr1-L2* triple mutant (hereafter *adr1 triple*), [11,14,27]. Using the combinatorial *nrg1* mutants, as well as a *N. benthamiana nrg1* mutant, it was determined that NRG1s are broadly required for TNL function (N, Roq1, RPS4/RRS1, RPP1, among others [10–13]).

The immune phenotype of the *helperless* plant was only examined for its effect on 2 sensor TNLs, RPS4/RRS1 and RPS6, as well as in basal defense against *Pseudomonas syringae* pv. *maculicola* (*Psm*) ES4326 [11,13,27]. While *nrg1.1 nrg1.2* did not show significant disease susceptibility, it did enhance the susceptibility phenotype of the *adr1 triple* mutant. Thus, it is likely that an unequal genetic redundancy between *ADR1s* and *NRG1s* has masked the true function of NRG1s and the importance of their helper function during ETI.

We systematically compared the *adr1 triple* mutant, the *nrg1.1 nrg1.2* double mutant, and a newly generated *helperless* mutant to characterize RNL function and the genetic interactions between the *ADR1* and the *NRG1* families. We demonstrate that the 2 RNL subfamilies function redundantly (with some specificity) in disease resistance to biotrophic and hemibiotrophic virulent and avirulent pathogens, ETI-induced gene expression, and HR. We describe an important role for the ADR1s in ETI and basal resistance. Further, we note a partial subfunctionalization or specialization of the 2 RNL families, specifically during sensor NLR-triggered ETI and in resistance against the necrotrophic fungal pathogen *Alternaria brassicicola*. Infection assays with a coronatine-deficient *Pseudomonas syringae* pv. *tomato* (*Pst*) DC3000 cor- show that both RNL families are involved to different extents in regulating SA-related pathways targeted by the jasmonic acid (JA) analogue coronatine.

Finally, time-resolved whole-genome expression profiling revealed that RNL-regulated genes are also CNL regulated and vice versa. Overall, we propose that ADR1s and NRG1s are required downstream of all sensor TNLs to activate ETI and that both RNL families are required to support the activation of—in the case of some CNLs—an orthodox CNL-initiated ETI.

Results

Redundant functions of ADR1 and NRG1 subfamilies in TNL-mediated disease resistance

Although it has been reported that the ADR1s and NRG1s function downstream of some TNLs [11–14,27], we lack a detailed comparison of the different requirements for the ADR1s and NRG1s during TNL-mediated ETI. To describe the specific and redundant immune functions of *ADR1* and *NRG1* subfamilies, we generated a *helperless* mutant by CRISPR-Cas9-mediated knock-out of the 2 full-length *NRG1* genes (*NRG1.1* and *NRG1.2*) in the *adr1 triple* transfer-DNA (T-DNA) line [14]. The *adr1 triple*, *nrg1.1 nrg1.2* double [13] and the

"*helperless*" pentuple mutants were infected with the bacterial pathogen *Pst* DC3000 expressing the effector AvrRps4. AvrRps4-induced ETI requires the cooperative function of the TNLs RPS4 and RRS1 [28]. Three days post infection (dpi), the *nrg1.1 nrg1.2* double mutant displayed wild-type–like resistance (Fig 1A). In contrast however, RPS4/RRS1-mediated resistance was significantly compromised in the *adr1 triple* and *helperless* mutant (Fig 1A). Interestingly, the *helperless* mutant was much more susceptible to *Pst* DC3000 *AvrRps4* infection than either the *adr1 triple* or the *rrs1a rrs1b* control plants (Fig 1A). Our results are consistent with published observations (S1 Table; [11,27]) and indicate that *ADR1s* and *NRG1s* function in an unequally redundant manner in RPS4/RRS1-triggered resistance. This type of genetic interaction occurs when 2 related genes or gene families are engaged in the process of sub-functionalization after gene duplication [29]. In this situation, one of the copies has lost most of the ancestral function, and its loss of function can be fully compensated by the other gene/gene subfamily. However, it can still contribute to the ancestral function, and double mutants have an enhanced phenotype compared to either single mutant. This observation raised the concern that the definition of functions of *NRG1s* in defense may have been effectively hidden by the *ADR1s*. The "residual" resistance of *rrs1a rrs1b* against *Pst* DC3000 A*vrRps4* compared to the *helperless* mutant suggests that additional weak recognition events might be impaired in the *helperless* mutant. This is similar to the phenotype of the *enhanced disease susceptibility 1* (*eds1*) mutant in response to *Pst* DC3000 *AvrRps4* infections. Here, *eds1-12* is also more susceptible than an *rrs1a rrs1b* double mutant [13,30], thus indicating that the *helperless* mutant phenocopies an *eds1* mutant during ETI mediated by RPS4/RRS1.

To further test whether the unequal redundancy between *ADR1s* and *NRG1s* extends beyond RPS4/RRS1-mediated resistance, *adr1 triple*, *nrg1.1 nrg1.2* double, and *helperless* mutants were challenged with the oomycete *Hyaloperonospora arabidopsidis* (*Hpa)* isolate Cala2. Resistance against *Hpa* Cala2 is mediated by the sensor TNL RPP2 in Col-0 [31]. While *nrg1.1 nrg1.2* was as resistant as wild type at 6 dpi, both the *adr1 triple* and *helperless* mutants exhibited increased susceptibility, with the *helperless* mutant being much more susceptible than *adr1 triple* (Fig 1B). The RPP2-dependent immune response in the *helperless* mutant to *Hpa* Cala2 infection was as severely affected as in *eds1-12* and the sensor NLR mutant *rpp2a* (Fig 1B). Together, these data provide another example of unequal redundancy of the 2 RNL families during a TNL-mediated immune response.

Infection of the 3 combinatorial RNL mutants with another obligate biotrophic oomycete pathogen, *Albugo candida* race 2V (Ac2V), which is recognized by the TNL WHITE RUST RESISTANCE 4A (WRR4A) and an unknown recessive disease resistance gene in Col-0 [13,32,33], demonstrated that *NRG1* and *ADR1* families can be fully redundant (Fig 1C). Col-0 and both the *adr1 triple* and *nrg1.1 nrg1.2* mutants were resistant to Ac2V, whereas the *helperless* plant was as sensitive as *eds1-12*. This indicates that *ADR1s* and *NRG1s* are redundantly required for WRR4A-mediated resistance.

Our combined results suggest that the 2 RNL families can act in a fully or unequally redundant manner in TNL-triggered immunity, likely depending on the sensor TNL activated during the infection.

Specific functions of the RNL subfamilies in CNL- and TNL-triggered ETI

Recent studies suggested that *ADR1s* and *NRG1s* have specific, nonredundant functions in sensor NLR-mediated immunity [11,13,27]. The *NRG1* family was suggested to function specifically in HR/cell-death induction after the activation of RPS4/RRS1 or during transient overexpression of auto-active full-length TNLs and TIR domains in *N. benthamiana* [13,27]. Additionally, *A. thaliana NRG1.1* and *NRG1.2* are required for some but not all TNL-mediated

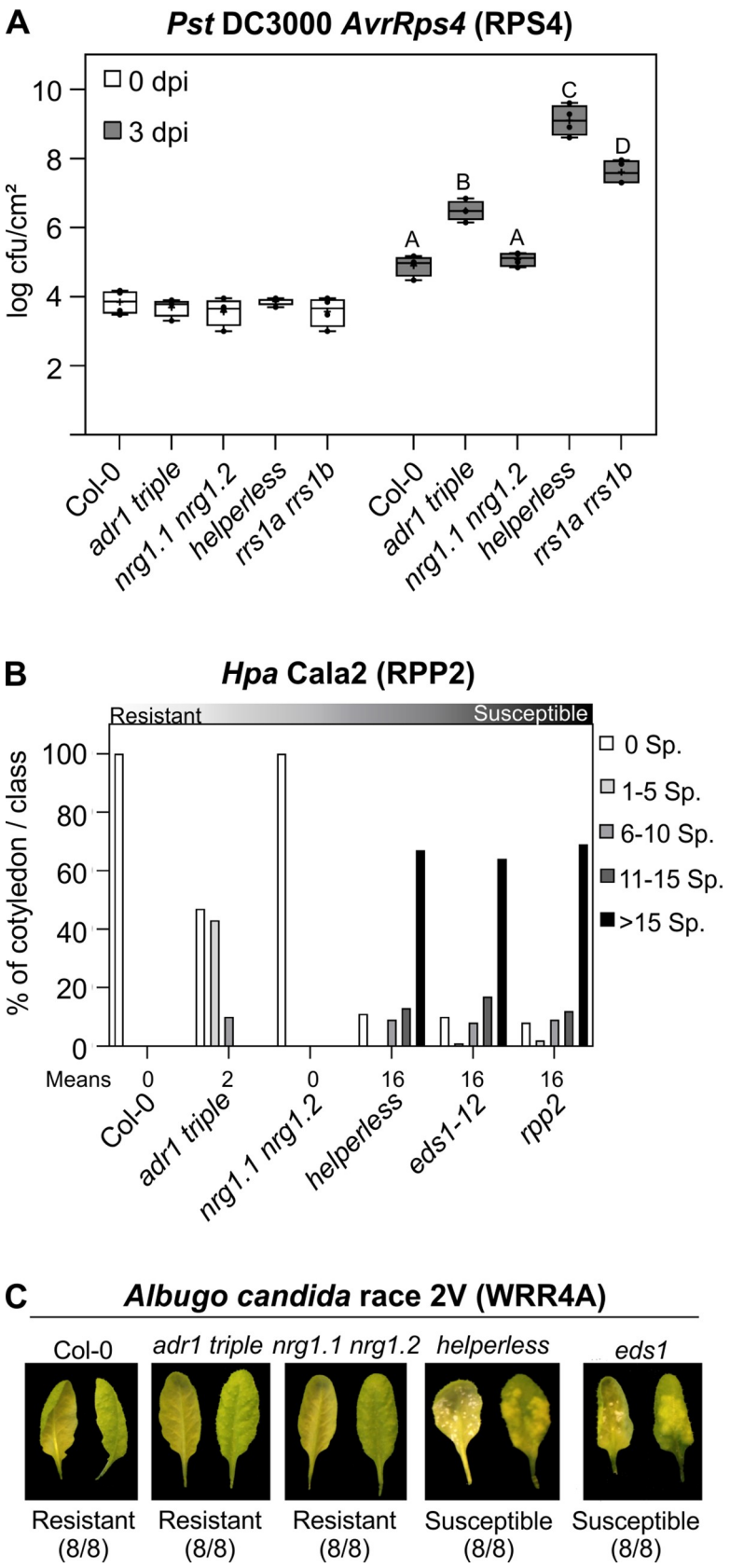
A
Pst DC3000 AvrRps4 (RPS4)
0 dpi
3 dpi
log cfu/cm²
10
8
6
4
2
A
B
A
C
D
Col-0
adr1 triple
nrg1.1 nrg1.2
helperless
rrs1a rrs1b
Col-0
adr1 triple
nrg1.1 nrg1.2
helperless
rrs1a rrs1b
B
Hpa Cala2 (RPP2)
Resistant
Susceptible
% of cotyledon / class
100
80
60
40
20
0
0 Sp.
1-5 Sp.
6-10 Sp.
11-15 Sp.
>15 Sp.
Means
0
2
0
16
16
16
Col-0
adr1 triple
nrg1.1 nrg1.2
helperless
eds1-12
rpp2
C
Albugo candida race 2V (WRR4A)
Col-0
adr1 triple
nrg1.1 nrg1.2
helperless
eds1
Resistant (8/8)
Resistant (8/8)
Resistant (8/8)
Susceptible (8/8)
Susceptible (8/8)

Fig 1. Redundant functions of ADR1 and NRG1 subfamilies in TNL-mediated resistance. (A) Six-week-old plants were hand-infiltrated with *Pst* DC3000 *AvrRps4* (OD_{600} = 0.001), and bacterial growth was assessed at 0 and 3 dpi. Box limit represents upper and lower quartile; maximum and minimum values are displayed in whiskers. The middle line shows the median, the cross the mean cfu/cm^2. Dots represent 4 technical replicates (leaf discs) in one experiment (biological replicate). Experiment was done 3 times with similar results. Letters indicate statistically significant differences following ANOVA with Tukey's test ($\alpha = 0.05$). (B) Ten-day-old seedlings were inoculated with *Hpa* Cala2. Sporangiophores per cotyledon were counted at 5 dpi. Cotyledons were classified as supporting no sporulation (0 Sp./cotyledon), light sporulation (1–5 and 6–10), medium sporulation (11–15), or heavy sporulation (>15). Two independent experiments were performed with an average of 100 cotyledons counted per genotype. Means of Sp./cotyledon for each genotype are noted below. Standard deviations of means for each genotype are as follows: Col-0 ± 0, *adr1 triple* ± 0.25, *nrg1.1 nrg1.2* ± 0, *helperless* ± 0.68, *eds1-12* ± 0.68 and *rpp2a* ± 0.65. Calculations for statistically significant differences following ANOVA with Tukey's test ($\alpha = 0.05$) are provided in S1 Data. (C) Three- to five-week-old plants were spray inoculated with Ac2V. Plants were phenotyped at 12 dpi. Abaxial and adaxial photographs of the same leaf are shown. Numbers indicate the number of individual plants showing a similar phenotype from the number of plants tested. NLRs activated in infection experiments shown in A–C are indicated in parenthesis. Underlying numerical data are provided in S1 Data. Ac2V, *Albugo candida* race 2V; cfu, colony-forming units; Col-0, Columbia-0; dpi, days post infection; *Hpa*, *Hyaloperonospora arabidopsidis*; NLR, nucleotide-binding leucine-rich repeat receptor; OD_{600}, optical density at 600 nm; Pst, *Pseudomonas syringae* pv. *tomato*; Sp., Sporangiophores; TNL, Toll/interleukin-1 receptor resistance domain-containing NLR.

https://doi.org/10.1371/journal.pbio.3000783.g001

autoimmune phenotypes [11–13,34]. The *ADR1s* are required for full ETI mediated by effector-triggered RPS2 and RPP4 [11,13]. We investigated the possibility that unequal genetic redundancy may have hidden some functions of *NRG1s* and *ADR1s* by including the *helperless* plant in all of our *Pst*, *Pseudomonas fluorescens 0–1* (*Pf0-1*; "Effector To Host Analyzer" strain derived from *P. fluorescens* [35]), and *Hpa* infection assays (Fig 2). We confirmed the specific requirement of the *ADR1* family in both RPS2- and RPP4-mediated resistance, as there was no significant increase in susceptibility in the *helperless* mutant compared to the *adr1 triple* in our *Pst* DC3000 *AvrRpt2* and *Hpa* Emwa1 infection assays (Fig 2A and 2B). We observed a slight, but consistent, increase of susceptibility in the *rps2* mutant compared to the *adr1 triple* and *helperless* mutants, suggesting a residual RNL-independent function of RPS2. We did not observe a significant defect in RPS2- and RPP4-mediated resistance in *nrg1.1 nrg1.2* (Fig 2A and 2B). Similarly, we found that resistance to *Pst* DC3000 *AvrPphB* (which activates the CNL RESISTANT TO P. SYRINGAE 5 [RPS5] [36]) was not affected in *nrg1.1 nrg1.2*, while both *adr1 triple* and *helperless* mutants showed an enhanced susceptibility (Fig 2C). The sensitivity phenotype was similar in *adr1 triple* and *helperless* mutants, suggesting that the ADR1 family is specifically required to mediate the defense response to *Pst* DC3000 *AvrPphB*. We next examined the effect of the different RNL mutants on the HR induction upon effector-mediated RPS4 and RPS2 activation. RPS4 activation led to an NRG1-dependent HR (Fig 2D), whereas only the ADR1s were required for HR after RPS2 activation (Fig 2E). There was no visible HR in the *adr1 triple* or *helperless* mutants at 10 hours post infection (hpi) (Fig 2E; [14]). A delayed RPS2-mediated HR was, however, visible at 24 hpi regardless of the genotype, showing that ADR1s are required for the timely activation of RPS2-triggered HR and RPS2-mediated disease resistance (Fig 2A and 2E). Our results suggest that the ADR1s support ETI mediated by the CNLs RPS2 and RPS5, but are required for the full ETI triggered by the TNL RPP4. NRG1s are the RNLs mediating HR triggered by the activation of RPS4/RRS1 and do not have any obvious function during RPS2-mediated HR and disease resistance.

Unequal redundancy of the RNL families in basal resistance

Next, we analyzed whether the 2 RNL families have specific or redundant functions during basal resistance or PTI. Basal resistance is defined as the resistance that is activated by PTI minus the consequences of effector-mediated suppression of PTI, but including any residual weak ETI [2]. ADR1s are required for both basal resistance against virulent pathogens and SA

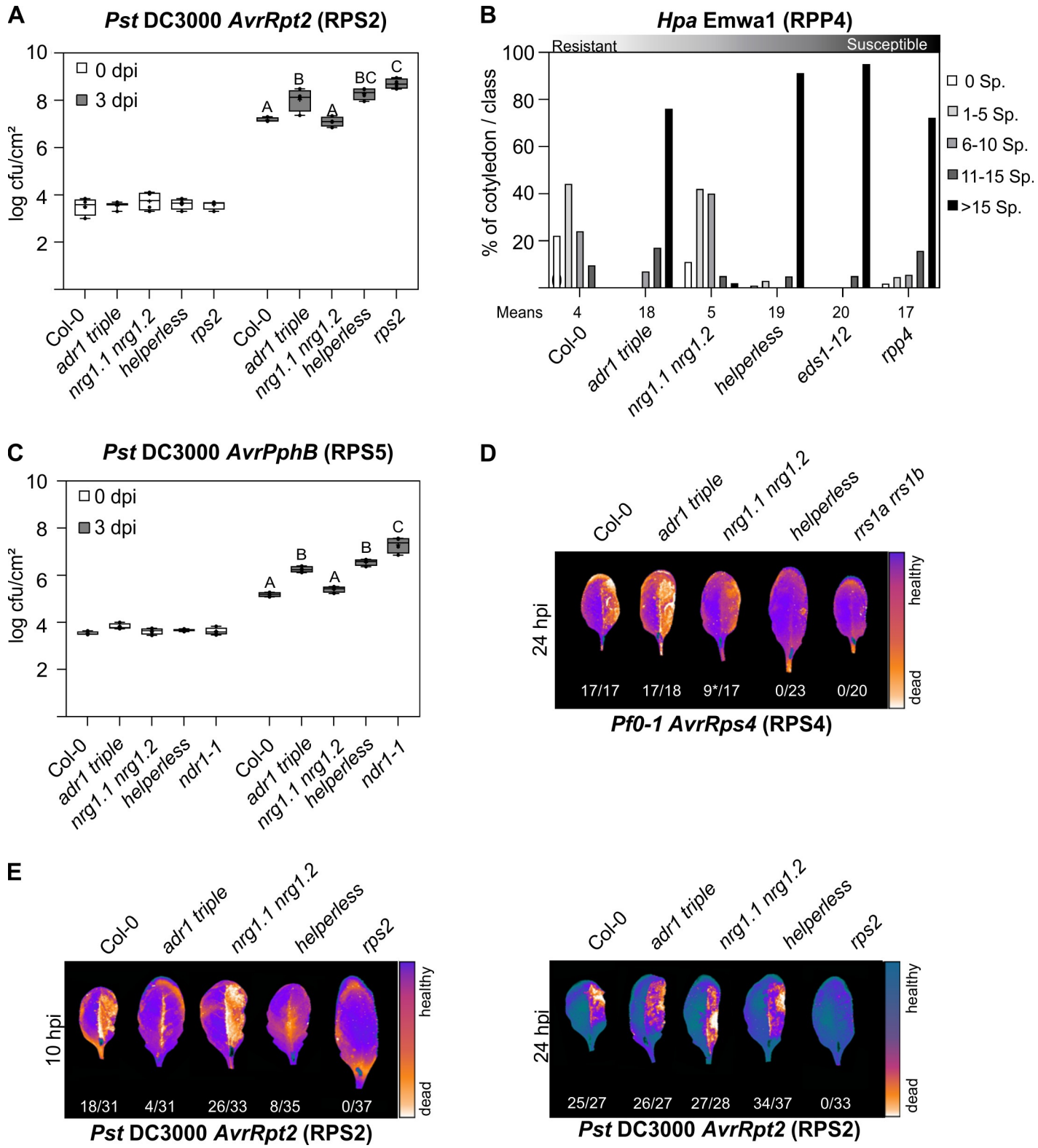

Fig 2. Specific functions of ADR1 and NRG1 subfamilies during ETI. (A, C) Six-week old plants were hand-infiltrated with (A) *Pst* DC3000 *AvrRpt2* (OD_{600} = 0.001) or (C) *Pst* DC30000 *AvrPphB* (OD_{600} = 0.001), and bacterial growth was assessed at 0 and 3 dpi. Box limit represents upper and lower quartile; maximum and minimum values are displayed in whiskers. The middle line shows the median, the cross the mean cfu/cm^2. Dots represent 4 technical replicates (leaf discs) in one experiment (biological replicate). Experiment was done 3 times with similar results. Letters indicate statistically significant differences following ANOVA with Tukey's

test (α = 0.05). (B) Ten-day-old seedlings were inoculated with *Hpa* Emwa1. Sporangiophores per cotyledon were counted at 5 dpi. Cotyledons were classified as supporting no sporulation (0 Sp./cotyledon), light sporulation (1–5 and 6–10), medium sporulation (11–15), or heavy sporulation (>15). Two independent experiments were performed with an average of 100 cotyledons counted per genotype. Two independent experiments were performed with an average of 100 cotyledons counted per genotype. Means of sporangiophores/cotyledon for each genotype are noted below. Standard deviations of means for each genotype are as follows: Col-0 ± 0.77, *adr1 triple* ± 0.36, *nrg1.1 nrg1.2* ± 0.39, *helperless* ± 0.36, *eds1-12* ± 0.13, and *rpp4* ± 0.5. Calculations for statistically significant differences following ANOVA with Tukey's test (α = 0.05) are provided in S1 Data. (D, E) The right leaf half of 6-week-old plants was hand-infiltrated with (D) *Pf0-1 AvrRps4* (OD_{600} = 0.2) or (E) *Pst* DC3000 *AvrRpt2* (OD_{600} = 0.1). The Typhoon laser scanner was used to detect autofluorescence of dead leaf tissue at indicated time points. Representative leaves shown in a false color scale (black to blue: healthy leaf tissue, orange to white: dead leaf tissue). Numbers indicate the amount of leaves showing HR out of the total number of leaves analyzed. Asterisk in D indicates weak HR. NLRs activated in infection experiments shown in A–E are indicated in parentheses. Underlying numerical data are provided in S1 Data. cfu, colony-forming units; Col-0, Columbia-0; dpi, days post infection; ETI, effector-triggered immunity; *Hpa*, *Hyaloperonospora arabidopsidis*; hpi, hours post infection; HR, hypersensitive response; NLR, nucleotide-binding leucine-rich repeat receptor; OD_{600}, optical densitiy at 600 nm; *Pf0-1*, *Pseudomonas fluorescens 0–1*; *Pst*, *Pseudomonas syringae* pv. *tomato*; Sp., Sporangiophores.

https://doi.org/10.1371/journal.pbio.3000783.g002

accumulation during PTI [11,14]. Recently, Wu and colleagues showed an increased susceptibility to *Psm* ES4326 infections due to the loss of *NRG1s* in the *adr1 triple* mutant context, but not in the wild-type context [11]. This suggests that NRG1s might have a function in basal resistance. To further investigate this hypothesis, we infected *adr1 triple*, *nrg1.1 nrg1.2*, and *helperless* mutants with the virulent pathogen *Pst* DC3000 carrying an empty cloning vector (hereafter, EV). We did not observe any significant effect on *Pst* DC3000 EV growth in the *nrg1.1 nrg1.2* mutant, whereas the *adr1 triple* and the *helperless* plants were more susceptible than Col-0, comparable to *eds1-12* (Fig 3A). This result suggests a specific function for the *ADR1*s in basal resistance against *Pst* DC3000 in Col-0, in line with the proposition of collective weak ETI triggered by the recognition of some effectors [7].

Considering the involvement of *NRG1s* in basal defense against *Psm* ES4326 [11], we reasoned that the impact of *nrg1.1 nrg1.2* might be epistatic to some virulence factor of *Pst* DC3000. We took advantage of the coronatine-deficient mutant, *Pst* DC3000 cor-, to further determine the function of *NRG1s* in basal immunity [37]. Coronatine antagonizes SA signaling, which is an important feature of immune signaling by *ADR1s* [14,38,39]. We observed enhanced bacterial growth in the *adr1 triple* and further enhanced growth in the *helperless* mutant, while no difference between *nrg1.1 nrg1.2* and Col-0 was detected. This observation indicates that the *NRG1*s play a role in basal resistance against *Pst* DC3000 that is visible only in an *adr1 triple* mutant background and when the virulence function of coronatine is removed (Fig 3B).

To test whether RNLs are also involved in PTI, we infected the *adr1 triple*, *nrg1.1 nrg1.2*, and *helperless* mutants with the type III secretion system (T3SS)-deficient mutant *Pst* DC3000 Δ*hrcC*. This mutant is impaired in delivering type-III effectors into the host plant, and therefore its growth is severely restricted by the strong activation of PTI responses that are not suppressed by effector functions [40]. None of the infected RNL mutants showed an enhanced bacterial growth of *Pst* DC3000 Δ*hrcC* compared to Col-0 (Fig 3C), suggesting that RNLs do not play a critical role during PTI triggered by this disarmed pathogen. This is further supported by our analysis of the flagellin-22 peptide (flg-22) induced reactive oxygen species (ROS) burst, which is one of the best-characterized PTI responses [41]. We did not observe any statistically significant differences in any RNL mutant compared to Col-0 (S1 Fig), suggesting that RNL function is not essential for this PTI response.

In summary, Fig 3A to 3C demonstrates that *ADR1s* and *NRG1s* do not play a critical role during PTI, but are unequally redundant for basal resistance against virulent *Pseudomonas*. The contribution of the *NRG1s* is only visible in the absence of the prevalent *ADR1s* and in defense mediated against *Pst* DC3000 cor-. Retention of *Pst* DC3000 growth restriction in *nrg1.1 nrg1.2* mutants may be due to the antagonistic effect of coronatine on SA signaling.

SA-dependent defense responses are well known to be required for resistance against biotrophic pathogens, whereas necrotrophic pathogens are better resisted by JA-dependent

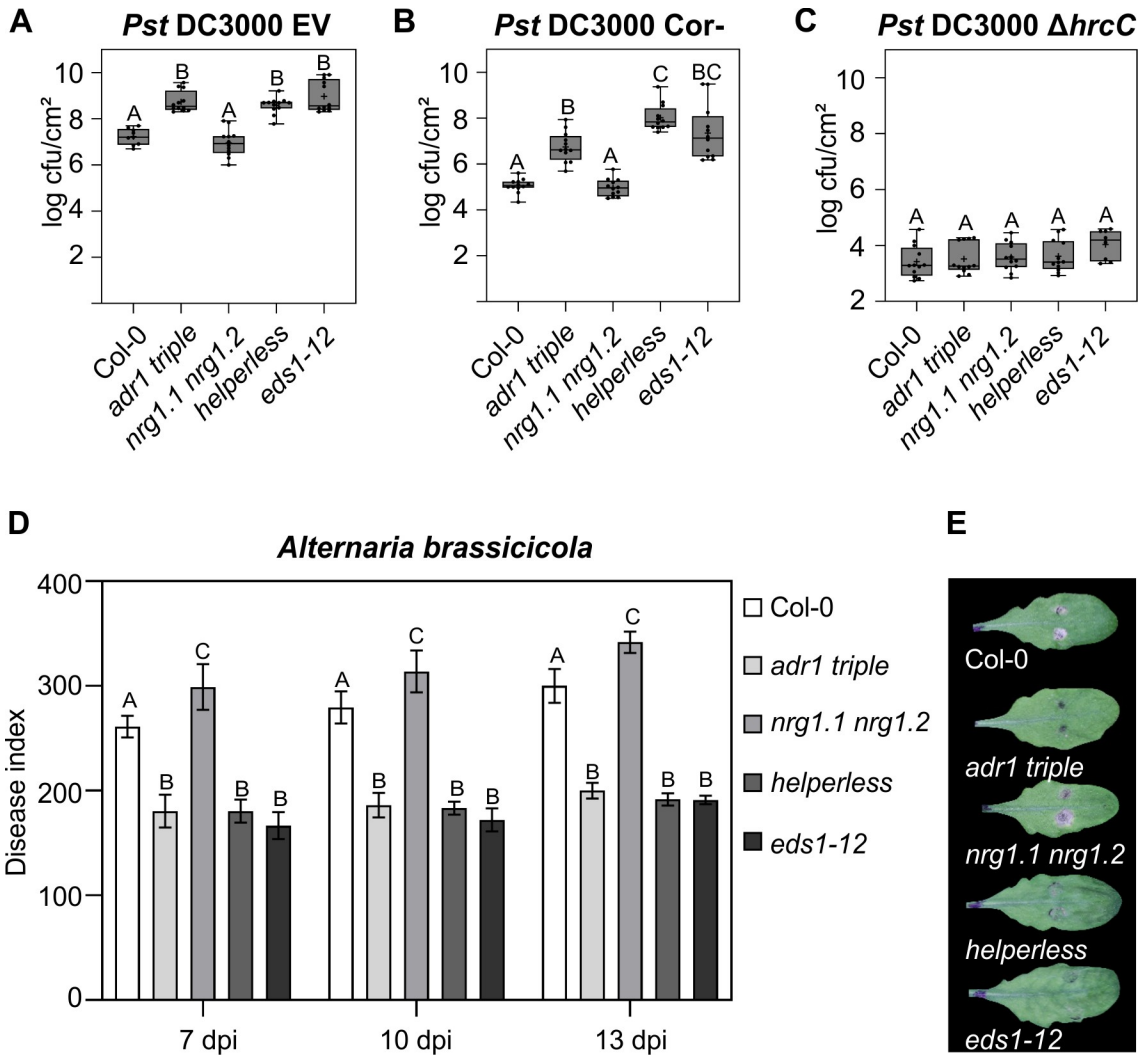

Fig 3. Unequally redundant and specific functions of RNLs during basal resistance and resistance against a necrotrophic pathogen. (A, B, C) Six-week-old plants were hand-infiltrated with (A) *Pst* DC3000 EV (OD_{600} = 0.001), (B) *Pst* DC3000 cor- (OD_{600} = 0.002), or (C) Pst DC3000 Δ*hrcC* (OD_{600} = 0.002), and bacterial growth was assessed at 3 dpi. Dots represent 12 data points (3 biological replicates and 4 technical replicates). Box limit represents upper and lower quartile; maximum and minimum values are displayed in whiskers. The middle line shows the median, the cross the mean cfu/cm^2. Letters indicate statistically significant differences following ANOVA with Tukey's test (α = 0.05). (D) 5.5-week-old plants were inoculated with 1×10^6 spores/mL *A. brassicicola*, and disease symptoms were monitored at 7, 10, and 13 dpi. DIs are shown as mean ± SEM of at least 35 replicates of 2 independent experiments. Letters indicate statistically significant differences at one time point following ANOVA with Tukey's test (α = 0.05). (E) Pictures of representative leaves inoculated with two 5 μL droplets of *A. brassicicola* spores were taken 13 dpi. Underlying numerical data are provided in S1 Data. cfu, colony-forming units; DI, disease index; dpi, days post infection; EV, empty vector; *hrcC*, *HR and pathogenicity gene C*; OD_{600}, optical density at 600 nm; *Pst*, *Pseudomonas syringae* pv. *tomato*.

https://doi.org/10.1371/journal.pbio.3000783.g003

immune responses [42]. The prevalent function of the ADR1s in the regulation of the SA-signaling pathway [13,14] and the antagonistic relationship of the SA and JA pathways [43] prompted us to analyze the resistance of the RNL mutants to the necrotrophic pathogen *Alternaria brassicicola*. Both the *adr1 triple* and *helperless* mutants restricted fungal growth better than wild-type Col-0, phenocopying *eds1-12* (Fig 3D and 3E). The *nrg1.1 nrg1.2* plants were slightly, but consistently, more susceptible to *A. brassicicola* than Col-0. The enhanced resistance in *adr1 triple* and *eds1-12* is most likely due to a loss of the antagonistic function of SA signaling on the JA-dependent immune response in these mutants.

These data confirm a major role of the ADR1s and EDS1 in the positive regulation of SA signaling and accumulation and further support the idea that the ADR1s and EDS1 (and PHYTOALEXIN DEFICIENT 4 [PAD4]) function together or in parallel in plant immunity.

RNL-independent functions during CNL-triggered ETI

We and others showed a requirement of both RNL families in TNL-mediated ETI and that *ADR1*s function in RPS2- and RPS5-mediated ETI (Fig 2) [11–14,27,34]. However, assessment of the 2 RNL families for other CNL-mediated ETI responses is limited. RESISTANCE TO P. SYRINGAE PV MACULICOLA 1 (RPM1)-mediated ETI is independent of *ADR1*s, and a very weak effect on the timing of RPM1-mediated HR was observed in *nrg1.1 nrg1.2* [13,14]. In addition, RPS5-mediated HR was not compromised in *nrg1.1 nrg1.2* [13]. In order to determine the requirement of RNLs in CNL-mediated ETI, we analyzed bacterial growth restriction in RNL mutants upon infection with *Pst* DC3000 expressing AvrRpm1 or HopZ1a (S2 Fig). Bacterial growth restriction upon *Pst* DC3000 *AvrRpm1* or *HopZ1a* infiltration was comparable to Col-0 in all RNL mutants analyzed (S2A and S2B Fig). This demonstrates that RNL presence is not required for RPM1- or ZAR1-mediated bacterial growth restriction.

We further tested whether effector-activated RPM1, ZAR1, and RPS5 require RNLs for HR induction. We analyzed visual HR symptoms in all 3 Arabidopsis RNL mutants at 6 hpi (for RPM1), 22 hpi (for RPS5), and 24 hpi (for ZAR1) with *Pst* DC3000 expressing the respective effectors (S2C–S2E Fig). Additionally, we performed ion leakage assays on all RNL mutants for both *Pf0-AvrRpm1* and *Pst* DC3000 *AvrRpm1* infections (S2G and S2H Fig). Similar to our growth restriction data, we did not observe any effect on HR timing or strength in the RNL mutants, confirming previously published results [13,14].

Our data demonstrate that RPM1- and ZAR1-mediated ETI responses (HR induction and bacterial growth restriction) and RPS5-mediated HR do not require RNLs. It would be interesting to further determine whether this holds true for other CNLs or whether our results are specific for CNLs known (RPM1 and RPS5 [44,45]; ZAR1 [24]) to act at the PM.

RNL requirement in transcriptional reprogramming during PTI

We further investigated the function of RNLs in transcriptional reprogramming during *Pf0-1*-induced PTI and ETI, using time-resolved transcriptomics. We subjected Col-0, *adr1 triple*, *nrg1.1 nrg1.2*, and *helperless* mutants to infections with *Pf0*-EV (RNL-[in]dependent PTI), *Pf0-AvrRps4* (fully RNL-dependent ETI + PTI), *Pf0-AvrRpt2* (partial RNL-dependent ETI + PTI), or *Pf0-AvrRpm*1 (RNL-independent ETI + PTI). Four leaf discs from 4 different plants at time 0 (before treatment), 0.5 hpi (PTI induction), 4 hpi (early ETI), and 8 hpi (late ETI) were used for RNA extraction, and mRNAs were sequenced as single-end, 50-bp reads, yielding approximately 5 million reads per sample. Two independent samples were gathered within each experiment, and the experiment was performed 3 times.

A large number of genes were found differentially expressed during at least one treatment and time point with a false discovery rate (FDR)-adjusted $p < 0.05$ and a fold change > 2 (Fig 4A). Principal component analysis showed the main factors affecting gene expression were (1) treatment time, (2) treatment type, and (3) plant genotype (Fig 4B). At 0.5 hpi, every treatment triggered changes in expression of mostly the same genes compared to time 0 (Fig 4A and 4B), consistent with the fact that type III effectors are generally not delivered at this stage [46]. The differences between genotypes were not clearly distinguishable at 0.5 hpi. The majority of gene expression changes in the RNL mutants resembled that of Col-0 during *Pf0*-EV infection at all 3 time points analyzed (Fig 4A, 4B and 4C). We conclude that the contribution of RNLs to overall gene expression regulation during PTI was very limited.

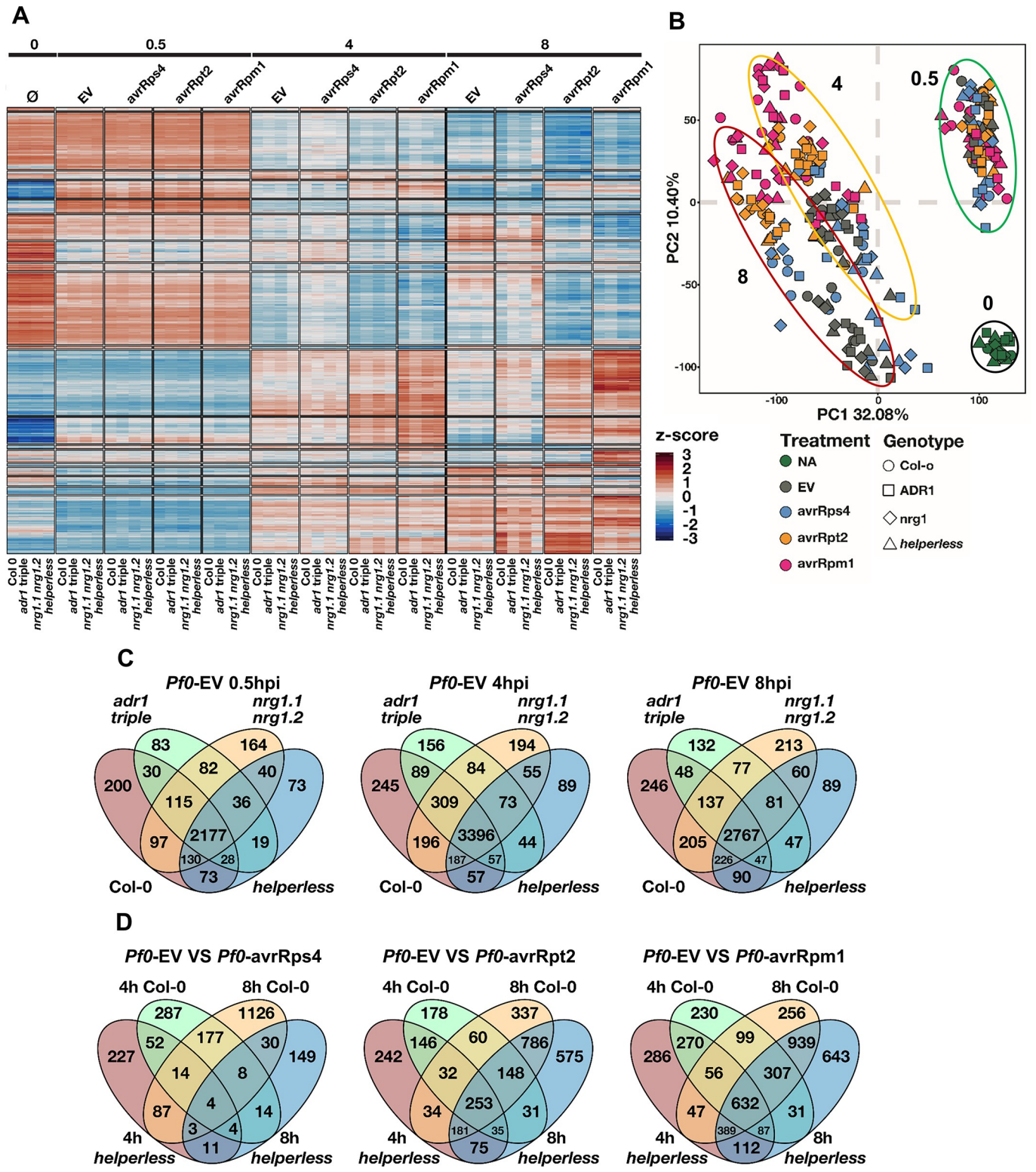

Fig 4. Analysis of RNL-dependent and -independent transcriptional changes. Six-week-old Col-0, *adr1 adr1-L1 adr1-L2* (*adr1 triple*), *nrg1.1 nrg1.2*, or *adr1 adr1-L1 adr1-L2 nrg1.1 nrg1.2* (*helperless*) plants were hand-infiltrated with *Pf0* carrying an EV or expressing AvrRps4, AvrRpm1, or AvrRpt2 (OD_{600} = 0.2). Samples were collected before treatment and 0.5 hpi, 4 hpi, and 8 hpi. (A) Heatmap showing the normalized expression (z-score) of all the genes differentially regulated in at least one condition (FDR-adjusted $p < 0.05$, fold change > 2). Transcriptional response corresponding to PTI and all ETIs involve mostly the same genes. The impact of RNLs is clearly visible during RPS4 ETI. (B) Principal component analysis showing the effect of pathogen treatment on gene

expression in the different genotypes at time 0 (black circle), 0.5 hpi (green circle), 4 hpi (orange circle), and 8 hpi (red circle). The effects of ETI on gene expression are visible at 4 and 8 hpi but not at 0.5 hpi. Most of the variability observed is explained by time, then by treatment type, and lastly by genotype. (C) Venn diagrams comparing PTI-triggered gene up-regulation in Col-0, *adr1 triple*, *nrg1.1 nrg1.2*, and *helperless* mutants at 0.5 hpi, 4 hpi, and 8 hpi with *Pf0*-EV. PTI is largely RNL independent. (D) Venn diagrams comparing ETI-specific gene up-regulation in Col-0 and the *helperless* plants at 4 hpi and 8 hpi with *Pf0-AvrRps4*, *Pf0-AvrRpt2*, or *Pf0-AvrRpm1*. Notably, the vast majority of RPS4-induced gene expression is abolished in the *helperless* mutant at 4 and 8 hpi, whereas RPS2 or RPM1-induced ETIs are largely RNL independent. Underlying numerical data are provided in S1 Data. Col-0, Columbia-0; ETI, effector-triggered immunity; EV, empty vector; FDR,; hpi, hours post infection; NA, no application/treatment; OD_{600}, optical density at 600 nm; PC1, principal component 1; PC2, principal component 2; *Pf0*, *Pseudomonas fluorescens 0*; PTI, pattern-triggered immunity.

https://doi.org/10.1371/journal.pbio.3000783.g004

It was previously reported that SA accumulation during PTI is largely ADR1s dependent and that ADR1-L2 functions in SA-dependent and SA-independent feedback regulatory loops [14,47]. We therefore looked at the behavior of genes induced during *Pf0-1* EV infections (PTI-induced genes) during ETI (S3 Fig). We observed a very small quantitative effect of the *adr1 triple* and the *helperless* mutation on gene expression at 8 hpi with *Pf0-1* EV. We observed that PTI-induced genes were over-induced during *Pf0-1* AvrRps4 infections in an RNL-dependent manner and during *Pf0-1* AvrRpt2 and *Pf0-1* AvrRpm1 infections in an RNL-independent manner (S3 Fig). The NRG1s partially contributed to the induction of SA-related genes during RPS4/RRS1-mediated ETI (S4 Fig), as seen by the severely affected induction of gene expression at 8 hpi in the *helperless* mutant compared to *adr1 triple* (S5B Fig). Considering that ADR1s and NRG1s are involved in basal resistance against virulent pathogens and SA signaling, it would be interesting to observe the impact of RNLs on *Pf0-1* EV-induced (PTI-related) transcriptome regulation at later time points.

Together, our data demonstrate that *Pf0-1* EV-induced (PTI-induced) transcriptional reprogramming—at least up to 8 hpi—is to a great extent RNL independent. However, these PTI-induced genes are over-induced in an RNL-dependent manner during TNL-mediated ETI and in an RNL-independent manner in CNL-mediated ETI.

RNL requirements in transcriptional reprogramming during ETI

We wanted to analyze whether the different requirements of the 2 RNL families in ETI mediated by the CNLs RPS2 and RPM1 and the TNL pair RPS4/RRS1 is also reflected in the transcriptional reprogramming. The effect of NLR activation on gene expression started to be visible at 4 hpi and was even more pronounced at 8 hpi (Fig 4B).

To better understand the impact of RNLs on ETI-specific gene regulation, we compared genes induced by the bacterial delivery of effectors to genes induced by the control *Pf0*-EV. The *helperless* mutant was incapable of mounting normal ETI after *Pst* DC3000 *AvrRps4* infiltration (Fig 1 and Fig 2). This is consistent with the result that, upon infiltration of *Pf0-1 AvrRps4*, 86.8% and 96.9% of the genes induced in Col-0 at 4 and 8 hpi, respectively, were not induced in the *helperless* mutant (Fig 4D, Table 1). Response to *Pf0-AvrRpt2* was also affected at 4 hpi in the *helperless* mutant with 47.2% of the genes induced in Col-0 requiring RNLs. However, the impact of the *helperless* mutant was strongly reduced at 8 hpi with *Pf0-AvrRpt2*, whereas only 25.3% of the control ETI response was affected. A similar tendency was observed with *Pf0-AvrRpm1* infections; 39% and 16.8% of the response was lost in the *helperless* mutant at 4 hpi and 8 hpi, respectively (Fig 4D, Table 1). Many genes were found to be differentially expressed specifically in the *helperless* mutant (Fig 4D).

In summary, RNLs contribute weakly to overall transcriptional reprogramming during PTI, but are fully required for TNL-triggered transcriptional reprogramming and partially required for CNL-mediated transcriptional reprogramming. This partial requirement was more pronounced at the early stage of CNL-mediated ETI. Further, RNLs function in the induction of SA-related gene expression during PTI and ETI responses, with a predominant role of the ADR1s.

Table 1. Fractions of ADR1s and/or NRG1s synergistic, redundant, and specific gene up-regulation during ETI.

	RPS4		RPS2		RPM1	
	4 hpi	8 hpi	4 hpi	8 hpi	4 hpi	8 hpi
RNL dependent	**86.8%** (486/560)	**96.9%** (1,404/1,449)	**47.2%** (417/883)	**25.3%** (463/1,831)	**39.0%** (667/1,712)	**16.8%** (458/2,725)
→*Shared regulation*	**67.1%** (326/486)	**60.0%** (842/1,404)	**59.5%** (248/417)	**63.3%** (293/463)	**67.0%** (447/667)	**65.3%** (229/458)
➢ Synergistic	63.6% (309/486)	36.5% (512/1,404)	46.0% (192/417)	35.4% (164/463)	52.3% (349/667)	44.3% (203/458)
➢ Redundant	3.5% (17/486)	23.5% (330/1,404)	13.4% (56/417)	27.9% (129/463)	14.7% (98/667)	21.0% (96/458)
→ *Specific regulation*	**32.9%** (160/486)	**40.0%** (562/1,404)	**40.5%** (169/417)	**36.7%** (170/463)	**33.0%** (220/667)	**34.7%** (159/458)
➢ ADR1s specific	74.4% (119/160)	72.4% (407/562)	78.1% (132/169)	60.6% (103/170)	62.3% (137/220)	49.7% (79/159)
➢ NRG1s specific	25.6% (41/160)	27.6% (155/562)	21.9% (37/169)	39.4% (67/170)	37.7% (83/220)	50.3% (80/159)

Fractions are defined according to the gene sets and functional categories defined in the text. The "RNL-dependent" fraction is the fraction of "ETI-regulated" genes that require RNLs, whereas the others are fractions of the "RNL-dependent" category. "Shared" is the addition of synergistic and redundant fractions, and "Specific" is the addition of "ADR1s-specific" and "NRG1s-specific" fractions. Fractions of main interest are in bold.

Abbreviations: ADR1, ACTIVATED DISEASE RESISTANCE 1; ETI, effector-triggered immunity; hpi, hours post infection; NRG1, N REQUIEREMNET GENE 1; RNL, RPW8 CC-domain NLR; RPM, RESISTANCE TO P. SYRINGAE PV MACULICOLA 1; RPS2, RESISTANT TO P. SYRINGAE 2; RPS5, RESISTANT TO P. SYRINGAE 5

https://doi.org/10.1371/journal.pbio.3000783.t001

Sub-functionalization of ADR1s and NRG1s

We then sought to identify possible synergistic, redundant, and/or specific effects of the 2 RNL families on gene expression regulation during ETI. "ETI-regulated" gene sets were obtained by comparing *Pf0*-EV–induced genes to *Pf0*-effector–induced genes in Col-0 at 4 and 8 hpi. We first classified the genes into "RNL independent" and "RNL dependent" categories based on their behavior in the *helperless* mutant (S1 Table). We further divided those RNL-dependent genes into 4 functional categories: "ADR1 + NRG1 dependent" are the genes that are not differentially expressed in the absence of either ADR1s or NRG1s; "ADR1/NRG1 redundant" are "RNL dependent" genes that are still differentially expressed in either mutant (*adr1 triple* or *nrg1.1 nrg1.2*) compared to Col-0; and "ADR1 specific" genes are "RNL dependent" genes not expressed in *adr1 triple* mutants and still expressed in *nrg1.1 nrg1.2*. Inversely, "NRG1 specific" genes are "RNL dependent" genes not expressed in *nrg1.1 nrg1.2* and still expressed in *adr1 triple* (S1 Table).

We applied this categorization to differentially expressed genes (DEGs) during RPS4/RRS1-, RPS2-, and RPM1-mediated ETI. The lists of genes belonging to these categories can be found in S1 Dataset. We observed that gene up-regulation induced by RPS4/RRS1-mediated ETI is almost fully RNL dependent at 4 hpi (86.8%, Table 1) and at 8 hpi (96.9%, Table 1). During RPS4/RRS1-mediated ETI, 63.6% (309) of the "RNL dependent" genes required the combined action of both ADR1s and NRG1s at 4 hpi (Table 1). This fraction decreased to 36.5% (512) at 8 hpi (Table 1). However, the fraction of redundantly regulated genes increased from 3.5% (17) at 4 hpi to 23.5% (330) at 8 hpi. This shows that, at the onset of RPS4/RRS1-triggered ETI, both ADR1s and NRG1s are required, but at later stages one subfamily can partially substitute for the loss of the other. In total, 60% of the genes induced by RPS4/RRS1-triggered ETI were redundantly or synergistically regulated by ADR1s and NRG1s at 8 hpi, showing that helper function in gene regulation is mostly shared by both subfamilies.

A smaller fraction (32.9% and 40% at 4 and 8 hpi, respectively) of the "RNL dependent" gene regulation was found to be specific to either subfamily. This could be attributed largely to the ADR1s with 74.4% and 72.4% of the subfamily-specific gene expression regulation relying on ADR1s at 4 and 8 hpi, respectively (Table 1). A similar tendency was observed during infection with *Pf0*-AvrRpt2 (Table 1) or with *Pf0-1* AvrRpm1 (Table 1), especially at 4 hpi. In conclusion, our results show that, during all ETI responses tested, around 60% of RNL-dependent gene regulation is mediated by both ADR1s and NRG1s and that there is an important ADR1-specific gene regulation that cannot be compensated for by the NRG1s. These results are consistent with the unequal redundancy of ADR1s and NRG1s during basal defense and ETI. Further, our results suggest that RPM1 and RPS2 partially rely on the RNLs during the early steps of the transcriptional reprogramming.

Classification of distinct NRG and ADR functions

To learn more about the nature of the RNL function, we looked at gene ontology (GO) terms associated with the "ADR1 + NRG1 dependent," "ADR1/NRG1 redundant," and "ADR1 or NRG1 specific" gene category during RPS4/RRS1-, RPS2-, and RPM1-mediated ETI responses at 4 and 8 hpi (S4 Fig, S2 Dataset). GO terms associated with Col-0 "ETI-regulated" genes were globally related to 4 categories: first, a large category grouping SA, systemic acquired resistance (SAR), JA, ROS metabolism, and defense; second, an HR category; third, a lipoprotein metabolism category; and finally, a category associated with ROS response, autophagy, and protein catabolic processes. In early ETI (at 4 hpi) the majority of up-regulated genes were involved in the category associated with SA/JA- and SAR-related pathways, ROS metabolism, and defense (S4 Fig). Later in ETI (at 8 hpi), up-regulated genes were also associated with the HR category; the lipoprotein metabolism category; and the category associated with ROS response, autophagy, and protein degradation. Our GO term analysis indicates that there was no GO term specifically associated with a particular sensor NLR-mediated ETI response. In other words, cellular processes transcriptionally (up-)regulated by the RNLs during RPS4/RRS1-mediated ETI did not differ strongly from the processes (up-)regulated by the 2 CNLs RPS2 (partially RNL dependent) or RPM1 (RNL independent). This observation prompted us to consider the possibility that RNLs—in RPS4/RRS1-mediated ETI—may ultimately regulate the expression of the same genes as RPM1 and RPS2, although the transcriptional regulation may differ quantitatively.

RNLs act like CNLs

To investigate the hypothesis that RNLs and CNLs regulate the same genes, we looked at the normalized expression of ETI-regulated genes in Col-0 and the *helperless* mutant (Fig 5). The genes differentially regulated during ETI triggered by AvrRps4, AvrRpt2, or AvrRpm1 were largely overlapping, especially at 8 hpi (Fig 5A and 5C). Moreover, the expression of differentially regulated genes during RPS4-induced ETI, which reflects the action of RNLs, was also differentially regulated during RPS2- and RPM1-mediated ETI even in the absence of RNLs (Fig 5B and 5D, S6 Fig). Inversely, the expression of RPS2- and RPM1-regulated genes was globally sustained during RPS4/RRS1-mediated ETI through the action of RNLs, even though not all RPS2- and RPM1-regulated genes pass the threshold of statistical significance in RPS4/RRS1-mediated ETI (Fig 5B and 5D and S6 Fig). Consistent with this observation, the *RNL* deletion in *helperless* plants had a limited quantitative effect on the overall expression level of the RPS2- and RPM1-regulated genes during *Pf0-AvrRpm1* and *Pf0-AvrRpt2* infections (S6 Fig). Thus, RNLs support some quantitative effect on transcriptional regulation during RPS2-

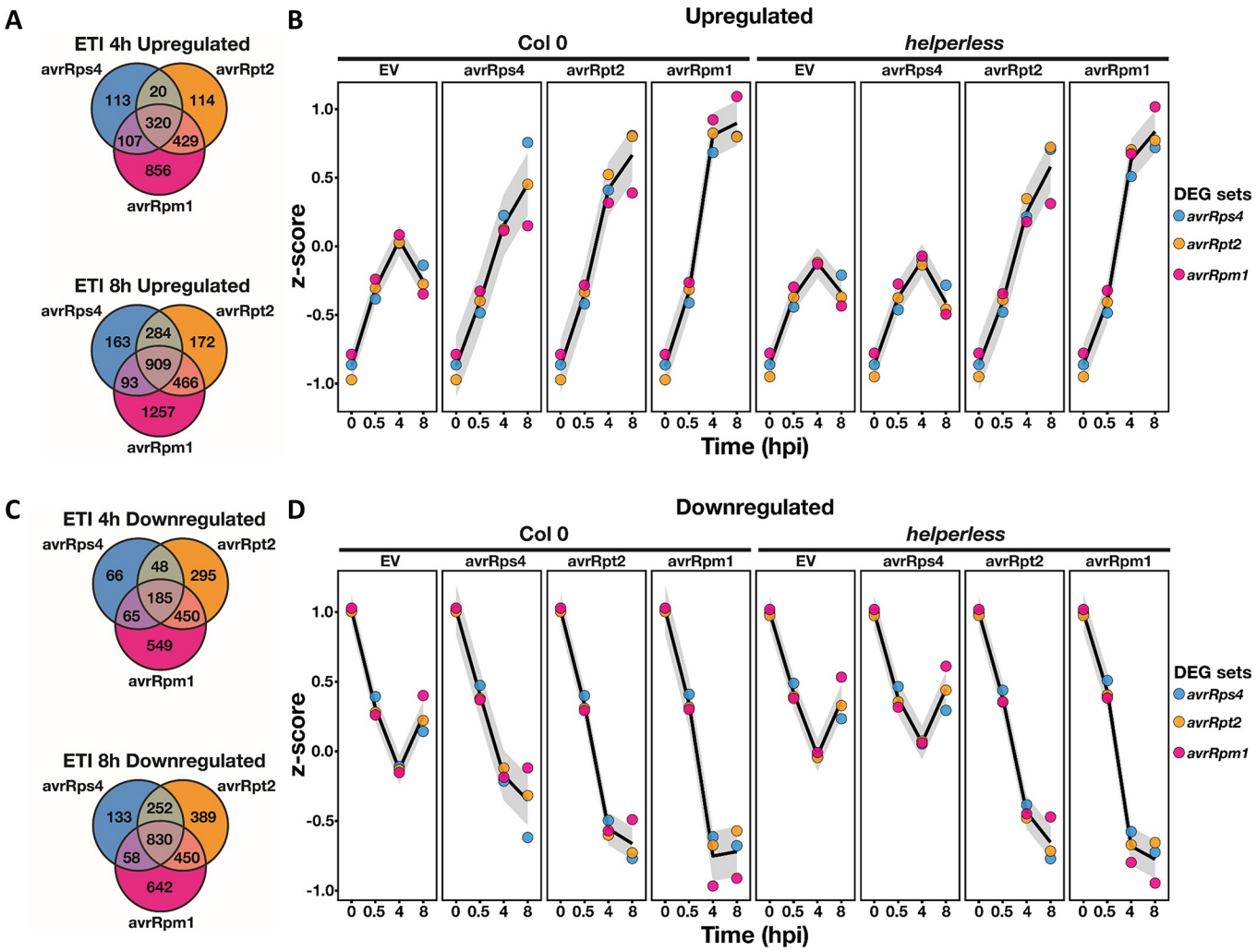

Fig 5. RNLs function as classical CNLs. Comparison of gene up-regulation (A, B) or down-regulation (C, D) across RPS4-, RPS2-, and RPM1-mediated ETIs. (A) and (C) Venn diagrams comparing up-regulated (B) or down-regulated (D) ETI-specific genes showing the extensive overlap between RPS4-, RPS2-, and RPM1-mediated ETIs. RPS4/RRS1 ETI, which reflects the action of RNLs, is very similar to CNL-mediated ETI. The curves in (B) and (D) show the normalized expression of the ETI-regulated gene sets, in Col-0 and *helperless* plants, across all conditions tested in the experiment. Notably, RPS4/RRS1-regulated genes (blue dots), which require RNLs during *Pf0-AvrRps4* infection, are differentially regulated by RPS2 and RPM1 in the absence of RNLs. Similarly, genes differentially regulated by RPM1 and RPS2 are also regulated by RNLs during *Pf0-AvrRps4* infections in Col-0, but the up- or down-regulation is weaker. Underlying numerical data are provided in S1 Data. CNL, coiled-coil domain-containing nucleotide-binding leucine-rich repeat receptor; Col-0, Columbia-0; DEG, differentially expressed gene; ETI, effector-triggered immunity; EV, empty vector; hpi, hours post infection; *Pf0*, *Pseudomonas fluorescens 0*; RNL, RPW8 CC domain containing NLR.

https://doi.org/10.1371/journal.pbio.3000783.g005

and RPM1-mediated ETI, but this effect is—at least in the case of RPM1—not required for an efficient immune response (S2A and S2C Fig).

These results demonstrate that effector-activated, TNL-induced, and RNL-mediated gene expression is very similar to that of an orthodox CNL-activated ETI, and that RNLs contribute quantitatively to CNL-mediated ETIs.

The apparent specificity of some genes for ADR1s may reflect the higher capacity of ADR1s to regulate gene expression. There was no strong enrichment of ADR1 or NRG1 family-dependent genes in any GO terms related to the ETI-mediated transcriptional reprograming. The "ADR1-specific" genes were in general not associated with a specific GO term distinct from the NRG1 family-regulated genes (S4 Fig). For example, we observed that genes related to SA

responses and SAR/SA pathways were strongly *ADR1* family-dependent at 4 hpi in all triggered ETI responses as well as in PTI (S5 Fig). This confirms that ADR1s function similarly or together with EDS1 and PAD4 in the regulation of the SA pathway at early stages of immunity and that this is most obvious in RPS4/RRS1-mediated ETI (S5 Fig, [27]). However, at 8 hpi with *Pf0-AvrRps4*, the up-regulation of the SAR/SA pathway genes in *adr1 triple* was similar to the 8 and 4 hpi samples of Col-0 and *nrg1.1 nrg1.2*, whereas these genes could not be activated in the *helperless* mutant (4 and 8 hpi). This shows that the *NRG1*s could compensate for the loss of the *ADR1*s at this time point (S4 Fig and S5 Fig). Overall, our results suggest that ADR1s and NRG1s redundantly and quantitatively regulate expression of the same genes during ETI and that the apparent specificity of some genes for ADR1s likely results from unequal redundancy. This also suggests that the specific function of the NRG1s in AvrRps4-triggered HR (Fig 2D) is independent of the ultimate transcriptional reprogramming and rather requires a specific function of NRG1s.

Discussion

Recognition of pathogen-derived effectors by intracellular sensor NLRs triggers ETI, in many cases a strong immune response eventually leading to disease resistance and to HR. Many sensor NLRs mediate immune responses that require the presence of helper RNLs (S2 Table) [11–14,27]. Information on whether RNLs act redundantly or are required for specific immune pathways in sensor NLR-mediated ETI is still scarce. We provide a detailed, side-by-side comparison of immune responses in the *adr1 triple*, *nrg1.1 nrg1.2*, and *helperless* mutants to determine the specific, redundant, and synergistic functions of RNLs during immunity. This includes activation of effective disease resistance, HR initiation, and transcriptional reprogramming during PTI and ETI.

The *ADR1* RNL family was shown to be preferentially involved in defense activation and SA accumulation [11,14,26,27]. *A. thaliana* and *N. benthamiana NRG1s*, together with *EDS1* and *SAG101*, are required for TNL-mediated cell death and some TNL-dependent autoimmune phenotypes [11,13,27,48]. Thus, the current working model for RNL function and activity is that ADR1s mediate disease resistance and NRG1s are required for (at least TNL-triggered) cell-death signaling. Here, we observed that the apparent sub-functionalization of *ADR1*s and *NRG1*s is at least partly a case of unequal genetic redundancy. We and others described unequal redundancy in basal defense against *Psm* ES4326 and *Pst* DC3000 cor-, as well as in ETI mediated by RPS4/RRS1, RPP2, and RPS6 (Fig 1A and 1B, Fig 3B, [11]). Indeed, the loss of the 2 *NRG1* genes had no effect, whereas the *adr1 triple* was severely affected in the immune responses noted earlier. The *helperless* mutant was, however, as susceptible, or even more susceptible, than the respective sensor NLR mutant. This shows that the NRG1s can partially substitute for the loss of the ADR1 family function in mediating disease resistance but that the impact of the NRG1s on the overall phenotype is so small that it is only visible in the absence of the ADR1s. Inversely, the ADR1s can fully complement the loss of NRG1 function in resistance mediated by RRS1/RPS4, RPP2, and RPS6 sensor NLRs.

Unequal redundancy of RNLs is also revealed by the level of gene induction during ETI. If ADR1s and NRG1s were specialized to regulate certain genes or genetic pathways, we would expect that genes requiring NRG1s would be associated with a unique function/GO term that is not shared with ADR1s-requiring genes, and vice versa. We did not observe any such association. Genes induced by NRG1s alone or synergistically with ADR1s fall into the same functional categories as those induced by ADR1s (S4 Fig). On the contrary, we observed a quantitative effect of NRG1s and ADR1s on the overall gene expression during ETI (S6 Fig). In particular, ADR1s were shown to be specifically required for SA accumulation [12,14].

However, NRG1s affected the expression of SA metabolism and SA response genes, to a lesser extent, and this effect was only visible in the absence of *ADR1*s and most obvious in late stages of TNL-triggered ETI (S4 Fig, S5B Fig and S6 Fig).

In *A*. *thaliana*, it seems like *ADR1*s predominantly function to regulate/induce most ETI responses. In *N*. *benthamiana*, *NRG1* might play a more significant role, because it is required for cell-death induction downstream of all tested sensor TNLs or TIR domains (S2 Table, [12,13]). The requirements for either or both RNL families in NLR-mediated ETI might be different in other plant species and subjected to co-evolution with likely co-acting components such as EDS1, PAD4, or SAG101 [27,48]. Gantner and colleagues showed that ETI mediated by the *N*. *benthamiana* TNL Roq1 depends on the presence of *N*. *benthamiana EDS1* and *SAG101b* which signal with *NRG1*. In contrast, in *A*. *thaliana*, stable expression of *N*. *benthamiana Roq1* confers resistance to *Pst* DC3000 (naturally expressing the effector HopQ1 that is recognized by Roq1) only in the presence of *A*. *thaliana EDS1* and *PAD4*, which are associated with *ADR1* signaling [12,27,48]. This finding supports the speculation that, in *A*. *thaliana*, the *ADR1*s conserve most of the ancestral RNL function, whereas in *N*. *benthamiana*, *NRG1* seems to play a prominent role. Overall, our data and the current literature suggest that *ADR1s* and *NRG1s* are largely redundant gene families and that the function described in *A*. *thaliana* may vary in other species. It is still unclear whether the observed *N*. *benthamiana NRG1* specialization for TNL-mediated HR/cell death and resistance induction applies in *A*. *thaliana*, given the completely ADR1-dependent TNL RPP4-triggered resistance in *A*. *thaliana* Col-0 plants (Fig 2B, [14]).

During some ETI responses, ADR1s and NRG1s do not act redundantly but rather play specific roles. The induction of HR and defense by the TNL RPP4, the timely induction of HR upon *Pst* DC3000 *AvrRpt2* infection, and the bacterial growth restriction during *Pst* DC3000 *AvrPphB* and *Pst* DC3000 *AvrRpt2* specifically require ADR1s and not NRG1s (Fig 2A, 2B, 2C and 2E). Similarly, NRG1s are specifically required for HR after RPS4/RRS1 activation and for some autoimmune phenotypes (Fig 2D, [11,13,14,26,27]). Considering the fact that both ADR1s and NRG1s can regulate HR and defense independently (e.g., in RPP4- or RPP2-mediated ETI, auto-immune mutants, and sensor NLR or RNL activation-mimic mutants), sensor NLR specificity for either RNL family is likely to be the result of a preferential use of either ADR1s or NRG1s by the sensor NLR. This may include, but does not require, physical association with the relevant sensor NLR, as, e.g., shown for the tobacco sensor NLR N and its RNL helper NRG1 [22]. Specific and convincing interaction of the RNLs with sensor NLRs or with the transcriptional machinery involved in immunity is still lacking. Therefore, it will be of great value to gather detailed insights into RNL subcellular localization(s) before and after activation and to define RNL interactors regulating transcription.

A specific role of the ADR1s in SA signaling and SA accumulation is further supported by our *A*. *brassicicola* infections (Fig 3D and 3E), revealing a negative function of the ADR1s and EDS1 in the JA-dependent resistance against this necrotrophic fungal pathogen. The observed enhanced resistance against *A*. *brassicicola* in *eds1-12* could be explained by the reported function of EDS1 (together with PAD4) in inhibiting the transcriptional regulator MYC2, a basic helix-loop-helix leucine zipper motif containing transcriptional activator and master regulator of JA responses [49]. It is possible that the ADR1s also participate in this regulation. Thus, the ADR1s together with EDS1 and its partner PAD4 might contribute to the regulation of the interplay between SA and JA during plant immunity.

In *A*. *thaliana*, RPS2 and RPS5 ETIs are thus far the only analyzed contexts of CNL-mediated ETIs requiring RNLs for full resistance (this study; [11,13,14]). Although Castel and colleagues suggested a slight contribution of the *A*. *thaliana* NRG1s for RPM1-mediated HR at an early time point (4 hpi with *Pf0*-AvrRpm1; [13]), we were not able to confirm these findings in

our conditions (S2 Fig). Nevertheless, we observed that RNLs do participate in the regulation of gene expression during RPS2- and also RPM1-triggered ETI, in particular during the early stages of ETI (Table 1, Fig 5B and 5D, S6 Fig). However, RNLs were not required for RPM1-mediated defense or HR (S2A, S2C, S2F and S2G Fig). This suggests that RNLs support CNL-mediated ETI responses quantitatively, even though they do not always have a measurable impact on the defense phenotype.

RNL requirement for basal resistance was previously demonstrated for resistance against virulent *Pseudomonas* strains (*Pst* DC3000 and *Psm* ES4326) and the virulent *Hpa* isolate Emco5 [11,14]. We confirmed these results (Fig 3). However, while full basal resistance against *Psm* ES4326 requires the presence of both RNL families, basal resistance against *Pst* DC3000 seemed to only require *ADR1s* in our experimental conditions. This was indicated by the lack of a higher susceptibility of the *helperless* mutant compared to the *adr1 triple* (Fig 3A). We further demonstrated that, when the virulence function of the JA antagonist coronatine was removed (in infections with *Pst* DC3000 cor-), the *helperless* mutant was more susceptible than the *adr1 triple* mutant, resembling the findings for *Psm* infections [11]. This reveals that *NRG1s* function in basal resistance against *Pst* DC3000 like they do in resistance to *Psm* ES4326. However, this function is likely inhibited or antagonized by the effect of coronatine produced by *Pst* DC3000. Surprisingly, the coronatine-producing *Psm* ES4326 does not suppress NRG1s function, perhaps due to some unknown effector(s) contributing redundantly to this virulence function in *Pst* DC3000 [50,51]. We were unable to observe a function of RNLs during PTI (Fig 3C and S1 Fig). Therefore, our results and previously published findings suggest that RNLs are not required for signaling from at least the two RKs FLAGELLIN-SENSITIVE 2 (FLS2) and EF-TU RECEPTOR (EFR) [14]. The *Pseudomonas-A. thaliana* pathosystem that we used in our studies might not be the right tool to analyze RNL function in PTI, since resistance against virulent *Pseudomonas* strains strongly relies on RK function [4]. This idea is further supported by the lack of enhanced susceptibility in any RNL mutant during *Pst* DC3000 *ΔhrcC* infections compared to wild-type Col-0 (Fig 3C).

When we compared the ETI responses triggered by RPS2, RPM1, or RNLs (via RPS4/RRS1), we found that they involved similar genes (Fig 5A and 5C). Moreover, genes regulated by RNLs in RPS4/RRS1-triggered ETI were also regulated in RPS2- and RPM1-triggered ETIs, independently of RNL presence (Fig 5B and 5D, S6 Fig). Conversely, RNLs regulate the expression of RPS2- and RPM1-regulated genes during RPS4/RRS1-induced ETI (Fig 5 and S6 Fig). This shows that RNLs and CNLs regulate the same genes. Therefore, we suggest that RNL function is similar to CNL function in ETI. This hypothesis is further supported by the fact that, contrary to their strict requirement for TNL signaling, RNLs seem to act in parallel with CNLs. Indeed, RNLs are required for basal defense, which is a combination of RK, RLP, and weak NLR signaling, and thus RNL activation might not require or rely solely on sensor NLR activation. Most importantly, RNLs are not strictly required for any CNL function. For example, even though RPS2-triggered HR is delayed in *adr1 triple* and *helperless* mutants, RNLs are not required for RPS2 to ultimately induce HR (Fig 2E). Similarly, although RPS2 and RPM1 ETI-induced transcriptional reprogramming relies on RNLs at 4 hpi, RPS2 or RPM1 presence is sufficient for the regulation of most of the differentially regulated ETI genes at 8 hpi (Table 1, Fig 5C and 5D, S6 Fig). Overall, we propose that RNLs act like orthodox CNLs downstream of TNLs and support and enhance defense activation in parallel with CNLs. We note that RNLs are involved but not required for full defense activation during CNL ETI (Fig 6). Whether RNLs, representing a unique subclade of CNLs, also form oligomeric complexes upon activation, as do other CNLs [17,19,24], remains to be answered.

In summary, *A. thaliana* RNLs have 3 major functions in immunity (Fig 6). RNLs (1) bolster defense activation in the context of basal immunity (Fig 3, [14]), potentially as helpers for

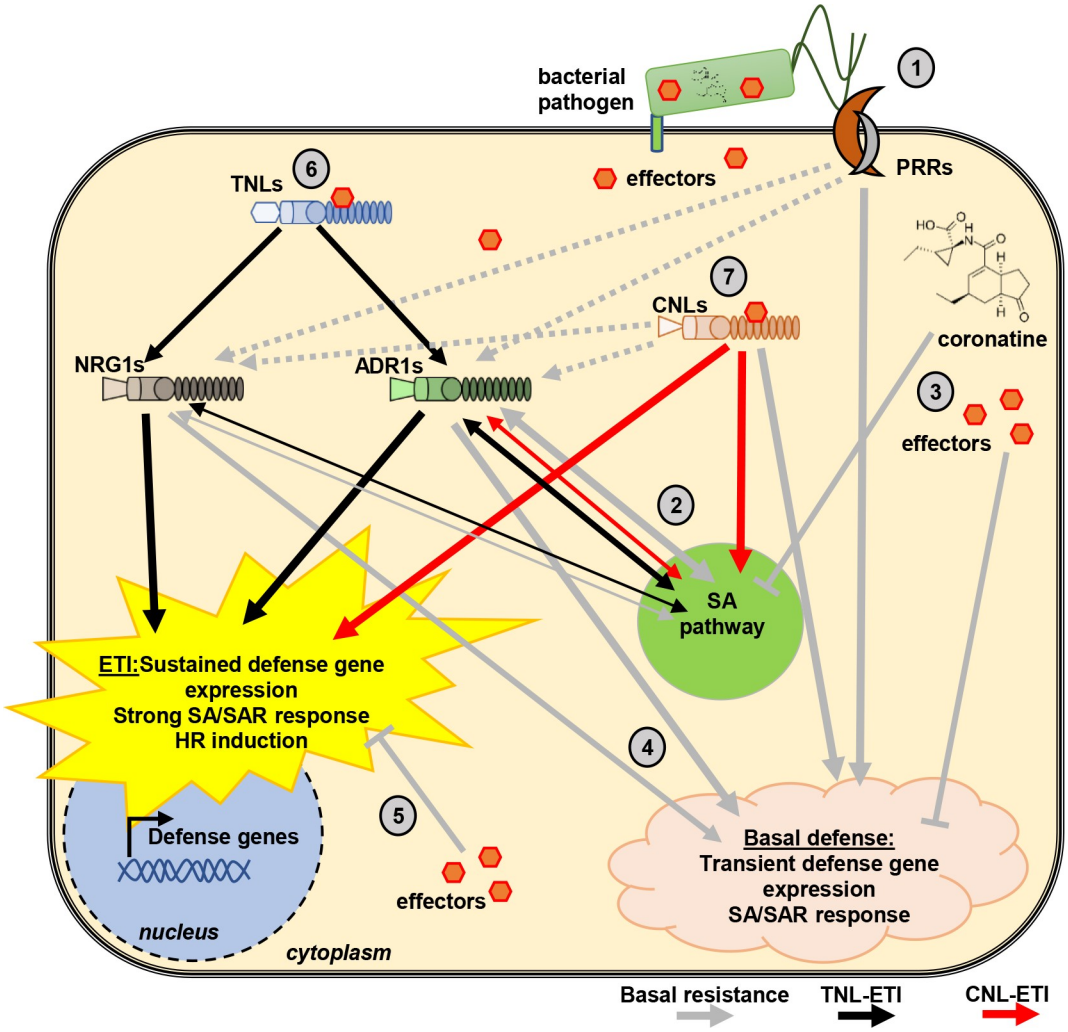

Fig 6. Proposed model of RNL function in immunity. Upon an infection of a plant cell by a pathogen, the first (early) response induced is PTI, irrespective of whether it is an avirulent or virulent pathogen. Thus, basal resistance and ETI happen in cells in which PTI signaling was already initiated and in some or the other way counteracted by effectors and other virulence molecules. Therefore, we propose that RNL function in immunity has to be considered as being part of a complex immune response network depicted in this proposed model. (1) Basal resistance (grey arrows) is initiated by the recognition of PAMPs by cell surface-localized PRRs. (2) PRR-triggered responses lead to the accumulation of SA and induction of SA responses, which requires RNLs [14]. (3) Pathogen-derived (virulence) effectors and the JA analog coronatine counteract PRR- and RNL-induced immunity and SA responses, thereby causing the so called (first) ETS. (4) Many pathogens, especially pathogenic bacteria, have effectors that can be recognized by some sensor TNL or CNLs and only induce a "weak remnant" ETI response [7] during basal resistance. This most likely leads to the activation of RNLs and can explain their requirement for basal resistance (see Fig 3). (5) It is possible that the aforementioned "weak" recognition and sensor NLR activation is also targeted by other effectors, causing the second ETS [62]. (6) RNLs are fully required for TNL-mediated immunity (black arrows) with some structural preferences for either ADR1s or NRG1s. After being activated by TNLs, RNLs act as CNLs to trigger strong and lasting defense activation as well as HR. ADR1s and NRG1s seem partially specialized in defense and HR, respectively, although the sub-functionalization is not strict. For example, ADR1s are specifically required for RPP4 signaling, while NRG1s are specifically required for RPS4-induced HR. (7) In addition, RNLs are involved but not required for CNL-triggered defense gene expression and HR (red arrows), further suggesting that RNLs act not directly downstream but in parallel with CNLs. If the sensor CNL is able to trigger a strong ETI by itself, the RNL involvement does not translate into requirement for proper disease resistance (e.g., RPM1 or ZAR1 ETI). Grey arrows indicate basal resistance (and PTI) signaling; black arrows indicate TNL-mediated ETI, and red arrows indicate CNL-mediated ETI signaling. Structural formula of coronatine was downloaded from Wikipedia (https://en.wikipedia.org/wiki/Coronatine). CNL, coiled-coil domain-containing nucleotide-binding leucine-rich repeat receptor; ETI, effector-triggered immunity; ETS, effector-triggered susceptibility; HR, hypersensitive response; JA, jasmonic acid; NLR, nucleotide-binding leucine-rich repeat receptor; PAMP, pathogen-associated molecular pattern; PRR, PAMP recognition receptor; PTI, pattern-triggered immunity; SA, salicylic acid; SAR, systemic acquired resistance; TNL, TIR domain-containing NLR.

https://doi.org/10.1371/journal.pbio.3000783.g006

weak ETI responses that fail to reach the threshold for HR; (2) mediate immune signaling from all TNLs tested so far, more or less redundantly (RPS6, RPS4/RRS1, RPP2, and RPP4 and TNL-dependent autoimmune phenotypes, Fig 1 and Fig 2, [11,14,26,27]); and (3) promote and contribute to timely defense activation and HR induction during CNL-mediated immunity (Fig 2E, Fig 5 and S6 Fig [14]); we further demonstrate that RNL function in TNL-mediated ETI resembles CNL function during sensor CNL-mediated ETI responses. Even though ADR1s and NRG1s are highly redundant in many aspects of their function in Arabidopsis, the ADR1s are more efficient in triggering defense-associated transcriptional reprograming than the NRG1s. Reciprocally, the NRG1s provide some specific functions, in particular the induction of HR during many TNL-mediated ETI responses.

Materials and methods

Plant material and growth conditions

All *A*. *thaliana* mutant lines are in the Col-0 background. The *adr1 triple* (*adr1-1 adr1-L1-1 adr1-L2-4* [14]), *nrg1.1 nrg1.2* [13], *rrs1a rrs1b* [30], *rpp2a* [52], *eds1-12* [53], *rps2-101C* [54], *rpp4* [55], *rpm1-3* [56], *zar1-3* [57], and *fls2* [58] mutants have been described previously. *zar1-3* seeds were kindly provided by Darrel Desveaux. The *eds1-12* mutant was kindly provided by Johannes Stuttmann and the *fls2* mutant by Georg Felix. *A*. *thaliana* plants were grown at short day conditions (8-hour light/16-hour dark cycle at 21˚C/18˚C and 45% humidity. *A*. *thaliana* sequence data for helper NLRs are available under the following AGI accession numbers: *ADR1/At1g33560*, *ADR1-L1/At4g33300*, *ADR1-L2/At5g04720*, and *NRG1.1/NRG1A/At5g66900*, *NRG1.2/NRG1B/At5g66910*.

Generation of *helperless* mutant using CRISPR/Cas9

A CRISPR/Cas9 construct targeting *NRG1.1* and *NRG1.2*, previously used to generate a Col-0 *nrg1.1 nrg1.2* double mutant [13], was expressed in a Col-0 *adr1-triple* mutant [14]. Briefly, this construct contains a FAST-Red selectable marker, an intron-containing and plant-codon–optimized *Cas9* allele under the control of the *AtRPS5a* promoter and *E9* terminator, and an sgRNA targeting both *NRG1.1* and *NRG1.2* (GTGGAAAGCTGGTCTGAAG[nGG]) under the control of the *AtU6-26* promoter and terminator. In the first generation after transformation, we identified 3 lines (out of 16) with mutations in *NRG1.1* and in *NRG1.2*. By screening the non-transgenic T2 progenies of these lines, we identified a Cas9-free and *nrg1.1 nrg1.2* double mutant line. The mutations are a deletion of guanine 1153 and an insertion of adenine between bases 1161 and 1162 in the coding sequence (CDS) of *NRG1.1* and *NRG1.2*, respectively. These frameshift mutations lead to an early stop at amino acid position 398 and 394 in NRG1.1 and NRG1.2, respectively. This mutant line also contains T-DNA mutant alleles of *adr1*, *adr1-L1*, and *adr1-L2* [14]. We called the *adr1 adr1-L1 adr1-L2 nrg1.1 nrg1.2* pentuple mutant *helperless*.

Bacterial infection assays

Plants for bacterial infiltration assays were grown for 6 weeks under short day conditions (8-hour light/16-hour dark at 21˚C/18˚C and 45% humidity). For bacterial growth curves, *Pst* DC3000 cor-, *Pst* DC3000 Δ*hrcC*, and *Pst* DC3000 expressing either *AvrRps4*, *AvrRpt2*, EV, *AvrRpm1*, *HopZ1a*, or *AvrPphB*—grown on KB plates containing appropriate antibiotics—were re-suspended in 10 mM $MgCl_2$ to a final concentration of 5×10^5 (OD_{600} 0.001) or 1×10^4 colony-forming units (cfu)/mL (OD_{600} 0.002) for the *Pst* DC3000 cor- and *Pst* DC3000 Δ*hrcC* strains. Plants were hand-infiltrated with the bacterial suspension. On the day of

infection (0 dpi), as well as at 3 dpi, leaf discs were taken and ground using a tissue lyser (Mill Retsch MM400, Retsch GmbH, Haan, Germany). Dilution series were plated on KB plates containing appropriate antibiotics, and cfu were counted after 2 days of growth at 28˚C. Statistical analysis from 4 replicates was done by one-way ANOVA Tukey's test using GraphPad Prism 8.0.2. Experiments were repeated at least 3 times with similar results. For the hypersensitive cell-death response (HR), *Pst* DC3000 expressing either *AvrRpt2*, *AvrRpm1*, *HopZ1a*, or *AvrPphB* were re-suspended in 10 mM $MgCl_2$ to 5×10^7 (OD_{600} 0.1). *Pf0-1* (A*vrRps4*) was re-suspended to 1×10^8 (OD_{600} 0.2). Bacterial solutions were hand-infiltrated into the right half of the leaves. Leaves were detached at the indicated time points, and autofluorescence was recorded by scanning the adaxial leaf sides using a Typhoon FLA9500 laser scanner (GE Healthcare, now Cytiva, Chicago, IL). Settings were as follows: Method: Alexa488; PMT: 450V; Laser: 473 nm. Image processing was done using ImageJ. For conductivity measurements, leaves were fully infiltrated with either *Pst* DC3000 expressing *AvrRpm1* (OD_{600} 0.1) or *Pf0-1 AvrRpm1* (OD_{600} 0.2). Leaf discs (5-mm diameter) were excised 1 hpi and incubated in water for 30 minutes. Five leaf discs were transferred together to the wells of a conductivity meter (CM100-2, Reid & Associates, Durban, South Africa) containing 3 mL distilled water, respectively. Conductivity of the solution was measured every hour for 24 hours. Statistical analysis from 5 replicates was done by one-way ANOVA Tukey's test using GraphPad Prism 8.0.2. The experiment was done twice with similar results.

A. candida propagation and infection

For propagation of Ac2V, zoospores were collected from infected *A. thaliana* leaves, suspended in water (approximately 10^5 spores/mL) and incubated on ice for 30 minutes. The spore suspension was then sprayed on plants using a Humbrol spray gun (approximately 700 μL/plant), and plants were incubated at 4˚C in the dark overnight. Infected plants were kept under 10-hour light (20˚C) and 14-hour dark (16˚C) cycles. Phenotypes were monitored 12 days after spraying.

Hpa infections

Hpa isolates Cala2 and Emwa1 were propagated on the susceptible *A. thaliana* ecotypes Ler and Ws, respectively. Infections were conducted as described in [47]. Briefly, conidiospores were re-suspended in distilled water at a concentration of 5×10^4 spores/mL and used to spray-inoculate 10-day-old seedlings. Inoculated plants were covered with a lid to increase humidity, and sporangiophores were counted at 5 dpi.

A. brassicicola infection assay

A. brassicicola MUCL 20297 cultivation and spore production was done as described earlier [59]. The *A. brassicicola* infection assay was conducted as described by [60]: *A. thaliana* plants were grown for 5 to 6 weeks under short day conditions (8-hour light/16-hour dark at 22˚C). *A. brassicicola* spores were diluted with sterile water to a final density of 1×10^6 spores/mL. Two leaves per plant were inoculated with two 5-μl droplets of the spore solution, respectively. Nine plants per genotype were used for each experiment. The experiment was done twice with similar outcomes. Infected plants were kept under 100% humidity. Fungal growth was monitored at 7, 10, and 13 dpi. Disease symptoms were classified into the following categories: 1 (no symptoms), 2 (light brown spots at infection site), 3 (dark brown spots at infection site), 4 (spreading necrosis), 5 (leaf maceration), and 6 (sporulation of the fungus). A disease index (DI) was calculated with the following formula: $DI = \Sigma\, i * n_i$—"i" is the symptom category, and "n_i" is the percentage of leaves in "i." Symptom scores were statistically analyzed with a

two-way ANOVA and Tukey's test using GraphPad Prism 8.0.2. Pictures of representative infected leaves were taken 13 dpi with a Canon EOS 80D Body Camera. *A*. *brassicicola* spores were kindly provided by Birgit Kemmerling.

Oxidative burst measurements

Leaf discs (4-mm diameter) were excised from leaves of 6-week-old plants and incubated in water overnight. Leaf discs ($n = 6$) were placed in a 96-well plate (1 disc/well, Greiner, Kremsmünster, Austria) containing 18 μg/mL luminol L-012 (Wako, Osaka, Japan) and 18 μM horseradish-peroxidase (AppliChem, Darmstadt, Germany). flg22 (Biomatik, Kitchener, Canada) was added to yield indicated concentrations. Luminescence was recorded over time using a TriStar^2 S LB 942 plate reader (Berthold Technologies, Bad Wildbad, Germany). flg22 peptide was kindly provided by Georg Felix. Peptide was dissolved in water and diluted in a solution containing 0.1% BSA and 0.1 M NaCl.

RNA extraction

RNA was purified from plant tissue using the RNeasy 96 Kit (Qiagen, Hilden, Germany). The plant "user-developed protocol" was followed except for the addition of a 96% ethanol wash step after the second RPE wash to ensure removal of residual salts. Purified RNAs were kept at −80˚C.

RNA sequencing

Illumina-based mRNA sequencing libraries were prepared from 1 μg RNA following Finkel and colleagues [61]. Briefly, mRNAs were selected using Sera-mag oligo(dT) magnetic beads (GE Healthcare Life Sciences). RNAs were washed and fragmented at 94˚C for 6 minutes. First-strand cDNA synthesis was performed using random hexamers and reverse transcriptase (Superscript III reverse transcriptase, Invitrogen, Carlsbad, CA). Second-strand cDNA synthesis was done using DNA Polymerase I and RNAseH. Double-stranded cDNAs were end-repaired using T4 DNA polymerase, T4 polynucleotide kinase, and Klenow polymerase. The DNA fragments were then adenylated using Klenow exo-polymerase to allow the ligation of Illumina adapters (Kapa Dual-indexed adapter kit, Roche, Basel, Switzerland). Unless specified, reagents were purchased from Enzymatics. Library quality control and quantification were performed using the 5200 Fragment Analyser and the NGS fragment kit (Agilent Technologies, Santa Clara, CA). Libraries were sequenced using Illumina HiSeq4000 sequencers to generate 50-bp single-end reads.

RNA sequencing read processing

Initial quality assessment of the Illumina RNA sequencing reads was performed using FastQC version 0.11.7. Trimmomatic version 0.36 was used to identify and discard reads containing the Illumina adaptor sequence. The resulting high-quality reads were then mapped against the TAIR10 Arabidopsis reference genome using HISAT2 version 2.1.0 with default parameters. The featureCounts function from the Subread package was then used to count reads that mapped to each one of the 27,206 nuclear protein-coding genes, and we used these counts to construct a raw count table of expression.

We used the package DESeq2 version 1.22.1 to define DEGs using the raw count table described earlier. For visualization purposes, we applied a variance stabilizing transformation to the raw count gene matrix. We then standardized (z-score) each gene along the samples measured. We utilized the package clusterProfiler to map the list of DEGs to gene ontologies;

we took the top 25 GO categories per set of DEGs to construct the heatmap of GOs. We utilized the function UpSet from the package ComplexHeatmap to construct the any upset plot shown along the manuscript. All necessary data and scripts to reproduce every part of the RNA sequencing analysis are deposited in https://github.com/isaisg/helperless.

Supporting information

S1 Fig. RNLs do not function in flg22-induced ROS burst. Left panels: Oxidative burst in leaves of the indicated genotypes after addition of 1 nM, 10 nM, or 100 nM flg22. Results are means × SD ($n = 6$). Right panels: Total ROS production over 34 minutes after flg22 treatment. Values are means × SD ($n = 6$). Letters indicate statistically significant differences following ANOVA with Tukey's test ($\alpha = 0.05$). Experiment was done 3 times. Underlying numerical data are provided in S1 Data.
(TIF)

S2 Fig. RNLs are not required for RPM1, ZAR1, and RPS5 (CNL)-mediated ETI responses. (A, B) Six-week-old plants were hand-infiltrated with *Pst* DC3000 (A), *AvrRpm1* (OD_{600} = 0.001), or (B) *HopZ1a* (OD_{600} = 0.001), and bacterial growth was assessed at 0 and 3 dpi. Box limit represents upper and lower quartile; maximum and minimum values are displayed in whiskers. The middle line shows the median, the cross the mean cfu/cm^2. Dots represent 4 technical replicates (leaf discs) in one experiment (biological replicate). Experiment was done 3 times with similar results. Letters indicate statistically significant differences following ANOVA with Tukey's test ($\alpha = 0.05$). (C–E) The right leaf half of 6-week-old plants was hand-infiltrated with (C) *Pst* DC3000 *AvrRpm1* (OD_{600} = 0.1), (D) *Pst* DC3000 *HopZ1a* (OD_{600} = 0.1) or (E) *Pst* DC3000 *AvrPphB* (OD_{600} = 0.1). A Typhoon laser scanner was used to detect autofluorescence of dead leaf tissue at indicated time points. Representative leaves shown in a false color scale (black to blue: healthy leaf tissue, orange to white: dead). NLRs activated in infection experiments shown in A–E are indicated in parenthesis. (F, G) Leaves of 6-week-old *A. thaliana* plants were fully hand-infiltrated with either (F) *Pst* DC3000 expressing *AvrRpm1* (OD_{600} = 0.1) or (G) *Pf0-1* expressing *AvrRpm1* (OD_{600} = 0.2). Twenty-five leaf discs were collected and rinsed in deionized water, and conductivity of 5 leaf discs immersed in 3 mL deionized water was measured at 4, 8, 12, and 16 hpi. Values are means of conductivity [μS/cm^2] ($n = 5$). Letters indicate statistically significant differences following ANOVA with Tukey's test ($\alpha = 0.05$). Experiment was done twice with similar results. Underlying numerical data are provided in S1 Data.
(TIF)

S3 Fig. RNLs and CNLs enhance the expression of PTI-regulated genes during ETI. Expression profile of PTI-regulated genes at 0.5 hpi, 4 hpi, and 8 hpi with *Pf0-1* EV, *Pf0-1 AvrRps4*, *Pf0-1 AvrRpt2*, or *Pf0-1 AvrRpm1*. PTI genes, which are induced by *Pf0-1* EV infections, are over-induced during RPS4 ETI in an RNL-dependent manner. Underlying numerical data are provided in S1 Data.
(TIF)

S4 Fig. GO terms associated to the RNL function. GO categorization of ETI-up-regulated genes. "Col-0 ETI" refers to the "ETI-regulated" gene set of Col-0. Activation of RPS4/RRS1, RPS2, and RPM1 induce genes involved in the same processes. There is no category associated to "ADR1 specific" that is distinct from the ones regulated redundantly or synergistically by NRG1s and ADR1s. For details see S2 Dataset. Underlying numerical data are provided in S1 Data.
(TIF)

S5 Fig. Effect of loss of RNLs on transcriptional reprogramming of SA-related genes during *A. thaliana* immunity. Comparison of SA-related gene expression in *Pf0-1* EV (A), *Pf0-1 AvrRps4* (B), *Pf0-1 AvrRpt2* (C), and *Pf0-1 AvrRpm1* (D) infiltrations at 0.5 hpi, 4 hpi, and 8 hpi. Genes are clustered according to their expression changes throughout the different samples and time points. Highest (red) and lowest (blue) log2 fold change is shown in heatmap. Visualization and clustering done with CLC Main workbench 20 (QIAGEN Aarhus A/S; www.qiagenbioinformatics.com). Underlying numerical data are provided in S1 Data.
(TIF)

S6 Fig. The effect of *RNL* mutants on ETI-regulated gene expression is quantitative. Normalized expression level of RPS4/RNLs up- (A) or down- (B) regulated genes at 4 and 8 hpi in Col-0 (circles), *adr1 triple* mutant (squares), *nrg1.1 nrg1.2* (diamonds), and *helperless* (triangles) mutants, during *Pf0-1* EV, *Pf0-1* AvrRps4, *Pf0-1* AvrRpt2, or *Pf0-1* AvrRpm1 infection. Colors indicate a statistical difference (post hoc ANOVA, adjusted $p < 0.05$). Notably, RNL loss-of-function mutants affect gene expression quantitatively. This effect is most striking at 8 hpi during RPS4-mediated ETI but is also visible during RPS2- and RPM1-mediated ETI. Underlying numerical data are provided in S1 Data.
(TIF)

S1 Table. Expected expression profiles of ETI-induced genes according to their RNL requirement.
(DOCX)

S2 Table. Overview of helper RNL requirements in (auto)immunity.
(DOCX)

S1 Dataset. Up- and down-regulated helper NLR-dependent genes.
(XLSX)

S2 Dataset. GO terms associated to Col-0 ETI-induced genes and RNL-dependent ETI-induced genes during Pf0-1 AvrRpt2, AvrRps4, or AvrRpm1 infection.
(XLSX)

S1 Data. Summary of all numerical data presented in Fig 1, Fig 2, Fig 3, Fig 4, Fig 5 and S1 Fig, S2 Fig, S3 Fig, S5 Fig and S6 Fig.
(XLSB)

S1 RNAseq Data. Full gene expression data of all tested genotypes, time points and treatments.
(XLSB)

Acknowledgments

We thank Christel Kulibaba-Mattern and Sarina Schulze for technical support. We would also like to thank Dr. Marc Nishimura for valuable discussions and critical reading of the manuscript and all El Kasmi, Dangl, and Jones lab members for helpful comments and discussions.

Author Contributions

Conceptualization: Svenja C. Saile, Pierre Jacob, Jonathan D. G. Jones, Jeffery L. Dangl, Farid El Kasmi.

Data curation: Svenja C. Saile, Pierre Jacob, Baptiste Castel, Lance M. Jubic, Isai Salas-Gonzáles.

Formal analysis: Svenja C. Saile, Pierre Jacob, Baptiste Castel, Lance M. Jubic, Isai Salas-Gonzáles, Marcel Bäcker, Farid El Kasmi.

Funding acquisition: Jonathan D. G. Jones, Jeffery L. Dangl, Farid El Kasmi.

Investigation: Svenja C. Saile, Pierre Jacob, Baptiste Castel, Lance M. Jubic.

Methodology: Svenja C. Saile, Pierre Jacob, Baptiste Castel, Lance M. Jubic, Isai Salas-Gonzáles, Marcel Bäcker.

Project administration: Jonathan D. G. Jones, Jeffery L. Dangl, Farid El Kasmi.

Resources: Jonathan D. G. Jones, Jeffery L. Dangl, Farid El Kasmi.

Supervision: Jonathan D. G. Jones, Jeffery L. Dangl, Farid El Kasmi.

Validation: Svenja C. Saile, Pierre Jacob, Baptiste Castel, Isai Salas-Gonzáles, Jonathan D. G. Jones, Jeffery L. Dangl, Farid El Kasmi.

Visualization: Svenja C. Saile, Pierre Jacob, Baptiste Castel, Isai Salas-Gonzáles.

Writing – original draft: Svenja C. Saile, Pierre Jacob, Farid El Kasmi.

Writing – review & editing: Svenja C. Saile, Pierre Jacob, Baptiste Castel, Lance M. Jubic, Isai Salas-Gonzáles, Jonathan D. G. Jones, Jeffery L. Dangl, Farid El Kasmi.

References

1. Dangl JL, Jones JDG. Plant pathogens and integrated defence responses to infection. Nature. 2001; 411: 826–833. https://doi.org/10.1038/35081161 PMID: 11459065
2. Jones JDG, Dangl JL. The plant immune system. Nature. 2006; 444: 323–329. https://doi.org/10.1038/nature05286 PMID: 17108957
3. Wan WL, Fröhlich K, Pruitt RN, Nürnberger T, Zhang L. Plant cell surface immune receptor complex signaling. Curr Opin Plant Biol. 2019; 50: 18–28. https://doi.org/10.1016/j.pbi.2019.02.001 PMID: 30878771
4. Albert I, Hua C, Nurnberger T, Pruitt R, Zhang L. Surface sensor systems in plant immunity. Plant Physiol. 2019; pp.01299.2019. https://doi.org/10.1104/pp.19.01299 PMID: 31822506
5. Boller T, Felix G. A Renaissance of Elicitors: Perception of Microbe-Associated Molecular Patterns and Danger Signals by Pattern-Recognition Receptors. Annu Rev Plant Biol. Annual Reviews; 2009; 60: 379–406. https://doi.org/10.1146/annurev.arplant.57.032905.105346 PMID: 19400727
6. Balint-Kurti P. The plant hypersensitive response: concepts, control and consequences. Mol Plant Pathol. 2019; 20: 1163–1178. https://doi.org/10.1111/mpp.12821 PMID: 31305008
7. Laflamme B, Dillon MM, Martel A, Almeida RND, Desveaux D, Guttman DS. The pan-genome effector-triggered immunity landscape of a host-pathogen interaction. Science. American Association for the Advancement of Science; 2020; 367: 763–768. https://doi.org/10.1126/science.aax4079 PMID: 32054757
8. van Wersch S, Li X. Stronger When Together: Clustering of Plant NLR Disease resistance Genes. Trends Plant Sci. 2019; 24: 688–699. https://doi.org/10.1016/j.tplants.2019.05.005 PMID: 31266697
9. Jones JDG, Vance RE, Dangl JL. Intracellular innate immune surveillance devices in plants and animals. Science. 2016;354. https://doi.org/10.1126/science.aaf6395 PMID: 27934708
10. Jubic LM, Saile S, Furzer OJ, El Kasmi F, Dangl JL. Help wanted: helper NLRs and plant immune responses. Curr Opin Plant Biol. 2019; 50: 82–94. https://doi.org/10.1016/j.pbi.2019.03.013 PMID: 31063902
11. Wu Z, Li M, Dong OX, Xia S, Liang W, Bao Y, et al. Differential regulation of TNL-mediated immune signaling by redundant helper CNLs. New Phytol. 2019; 222: 938–953. https://doi.org/10.1111/nph.15665 PMID: 30585636

12. Qi T, Seong K, Thomazella DPT, Kim JR, Pham J, Seo E, et al. NRG1 functions downstream of EDS1 to regulate TIR-NLR-mediated plant immunity in Nicotiana benthamiana. Proc Natl Acad Sci U S A. 2018; 115: E10979–E10987. https://doi.org/10.1073/pnas.1814856115 PMID: 30373842

13. Castel B, Ngou PM, Cevik V, Redkar A, Kim DS, Yang Y, et al. Diverse NLR immune receptors activate defence via the RPW8-NLR NRG1. New Phytol. 2019; 222: 966–980. https://doi.org/10.1111/nph.15659 PMID: 30582759

14. Bonardi V, Tang S, Stallmann A, Roberts M, Cherkis K, Dangl JL. Expanded functions for a family of plant intracellular immune receptors beyond specific recognition of pathogen effectors. Proc Natl Acad Sci U S A. 2011; 108: 16463–16468. https://doi.org/10.1073/pnas.1113726108 PMID: 21911370

15. Collier SM, Hamel LP, Moffett P. Cell death mediated by the N-terminal domains of a unique and highly conserved class of NB-LRR protein. Mol Plant-Microbe Interact. 2011; 24: 918–931. https://doi.org/10.1094/MPMI-03-11-0050 PMID: 21501087

16. Wang J, Wang J, Hu M, Wu S, Qi J, Wang G, et al. Ligand-triggered allosteric ADP release primes a plant NLR complex. Science. American Association for the Advancement of Science; 2019;364. https://doi.org/10.1126/science.aav5868 PMID: 30948526

17. Li L, Habring A, Wang K, Weigel D. Atypical Resistance Protein RPW8/HR Triggers Oligomerization of the NLR Immune Receptor RPP7 and Autoimmunity. Cell Host Microbe. Cell Press; 2020; 27: 405–417. e6. https://doi.org/10.1016/j.chom.2020.01.012 PMID: 32101702

18. Schreiber KJ, Bentham A, Williams SJ, Kobe B, Staskawicz BJ. Multiple Domain Associations within the Arabidopsis Immune Receptor RPP1 Regulate the Activation of Programmed Cell Death. Dangl JL, editor. PLOS Pathog. 2016; 12: e1005769. https://doi.org/10.1371/journal.ppat.1005769 PMID: 27427964

19. Hu M, Qi J, Bi G, Zhou J-M. Bacterial effectors induce oligomerization of immune receptor ZAR1 in vivo. Mol Plant. Elsevier BV; 2020;0. https://doi.org/10.1016/j.molp.2020.03.004 PMID: 32194243

20. Chini A, Loake GJ. Motifs specific for the ADR1 NBS-LRR protein family in Arabidopsis are conserved among NBS-LRR sequences from both dicotyledonous and monocotyledonous plants. Planta. 2005; 221: 597–601. https://doi.org/10.1007/s00425-005-1499-3 PMID: 15889273

21. Zhong Y, Cheng ZM. A unique RPW8-encoding class of genes that originated in early land plants and evolved through domain fission, fusion, and duplication. Sci Rep. 2016; 6: 1–13. https://doi.org/10.1038/s41598-016-0001-8 PMID: 28442746

22. Peart JR, Mestre P, Lu R, Malcuit I, Baulcombe DC. NRG1, a CC-NB-LRR protein, together with N, a TIR-NB-LRR protein, mediates resistance against tobacco mosaic virus. Curr Biol. 2005; 15: 968–973. https://doi.org/10.1016/j.cub.2005.04.053 PMID: 15916955

23. Grant JJ, Chini A, Basu D, Loake GJ. Targeted activation tagging of the Arabidopsis NBS-LRR gene, ADR1, conveys resistance to virulent pathogens. Mol Plant-Microbe Interact. American Phytopathological Society; 2003; 16: 669–680. https://doi.org/10.1094/MPMI.2003.16.8.669 PMID: 12906111

24. Wang J, Hu M, Wang J, Qi J, Han Z, Wang G, et al. Reconstitution and structure of a plant NLR resistosome conferring immunity. Science. 2019;364. https://doi.org/10.1126/science.aay2204 PMID: 31624212

25. Pérez-Pérez JM, Candela H, Micol JL. Understanding synergy in genetic interactions. Trends Genet. 2009; 25: 368–376. https://doi.org/10.1016/j.tig.2009.06.004 PMID: 19665253

26. Dong OX, Tong M, Bonardi V, El Kasmi F, Woloshen V, Wünsch LK, et al. TNL-mediated immunity in Arabidopsis requires complex regulation of the redundant ADR1 gene family. New Phytol. 2016; 210: 960–973. https://doi.org/10.1111/nph.13821 PMID: 27074399

27. Lapin D, Kovacova V, Sun X, Dongus JA, Bhandari D, von Born P, et al. A Coevolved EDS1-SAG101-NRG1 Module Mediates Cell Death Signaling by TIR-Domain Immune Receptors. Plant Cell. 2019; 31: 2430–2455. https://doi.org/10.1105/tpc.19.00118 PMID: 31311833

28. Williams SJ, Sohn KH, Wan L, Bernoux M, Sarris PF, Segonzac C, et al. Structural basis for assembly and function of a heterodimeric plant immune receptor. Science. 2014; 344: 299–303. https://doi.org/10.1126/science.1247357 PMID: 24744375

29. Briggs GC, Osmont KS, Shindo C, Sibout R, Hardtke CS. Unequal genetic redundancies in Arabidopsis—a neglected phenomenon? Trends Plant Sci. 2006; 11: 492–498. https://doi.org/10.1016/j.tplants.2006.08.005 PMID: 16949326

30. Saucet SB, Ma Y, Sarris PF, Furzer OJ, Sohn KH, Jones JDG. Two linked pairs of Arabidopsis TNL resistance genes independently confer recognition of bacterial effector AvrRps4. Nat Commun. 2015; 6. https://doi.org/10.1038/ncomms7338 PMID: 25744164

31. Sinapidou E, Williams K, Nott L, Bahkt S, Tör M, Crute I, et al. Two TIR:NB:LRR genes are required to specify resistance to Peronospora parasitica isolate Cala2 in Arabidopsis. Plant J. 2004; 38: 898–909. https://doi.org/10.1111/j.1365-313X.2004.02099.x PMID: 15165183

32. Cevik V, Boutrot F, Apel W, Robert-Seilaniantz A, Furzer OJ, Redkar A, et al. Transgressive segregation reveals mechanisms of Arabidopsis immunity to Brassica-infecting races of white rust (Albugo candida). Proc Natl Acad Sci U S A. 2019; 116: 2767–2773. https://doi.org/10.1073/pnas.1812911116 PMID: 30692254

33. Borhan MH, Gunn N, Cooper A, Gulden S, Tör M, Rimmer SR, et al. WRR4 encodes a TIR-NB-LRR protein that confers broad-spectrum white rust resistance in Arabidopsis thaliana to four physiological races of Albugo candida. Mol Plant-Microbe Interact. 2008; 21: 757–768. https://doi.org/10.1094/MPMI-21-6-0757 PMID: 18624640

34. Wan L, Essuman K, Anderson RG, Sasaki Y, Monteiro F, Chung EH, et al. TIR domains of plant immune receptors are NAD+-cleaving enzymes that promote cell death. Science. 2019; 365: 799–803. https://doi.org/10.1126/science.aax1771 PMID: 31439793

35. Thomas WJ, Thireault CA, Kimbrel JA, Chang JH. Recombineering and stable integration of the Pseudomonas syringae pv. syringae 61 hrp/hrc cluster into the genome of the soil bacterium Pseudomonas fluorescens Pf0-1. Plant J. 2009; 60: 919–928. https://doi.org/10.1111/j.1365-313X.2009.03998.x PMID: 19682294

36. Ade J, DeYoung BJ, Golstein C, Innes RW. Indirect activation of a plant nucleotide binding site-leucine-rich repeat protein by a bacterial protease. Proc Natl Acad Sci U S A. National Academy of Sciences; 2007; 104: 2531–2536. https://doi.org/10.1073/pnas.0608779104 PMID: 17277084

37. Ma S-W. Characterization of a DNA Region Required for Production of the Phytotoxin Coronatine by Pseudomonas syringae pv. tomato. Mol Plant-Microbe Interact. 1991; 4: 69. https://doi.org/10.1094/mpmi-4-069

38. Geng X, Cheng J, Gangadharan A, Mackey D. The Coronatine Toxin of Pseudomonas syringae Is a Multifunctional Suppressor of Arabidopsis Defense. Plant Cell. 2012; 24: 4763–4774. https://doi.org/10.1105/tpc.112.105312 PMID: 23204405

39. Zheng X, Spivey NW, Zeng W, Liu P-P, Fu ZQ, Klessig DF, et al. Coronatine Promotes Pseudomonas syringae Virulence in Plants by Activating a Signaling Cascade that Inhibits Salicylic Acid Accumulation. Cell Host Microbe. 2012; 11: 587–596. https://doi.org/10.1016/j.chom.2012.04.014 PMID: 22704619

40. Brooks DM, Hernández-Guzmán G, Kloek AP, Alarcón-Chaidez F, Sreedharan A, Rangaswamy V, et al. Identification and characterization of a well-defined series of coronatine biosynthetic mutants of Pseudomonas syringae pv. tomato DC3000. Mol Plant-Microbe Interact. American Phytopathological Society; 2004; 17: 162–174. https://doi.org/10.1094/MPMI.2004.17.2.162 PMID: 14964530

41. Gómez-Gómez L, Boller T. FLS2: An LRR receptor-like kinase involved in the perception of the bacterial elicitor flagellin in Arabidopsis. Mol Cell. Cell Press; 2000; 5: 1003–1011. https://doi.org/10.1016/S1097-2765(00)80265-8

42. Grant M, Lamb C. Systemic immunity. Current Opinion in Plant Biology. Curr Opin Plant Biol; 2006. pp. 414–420. https://doi.org/10.1016/j.pbi.2006.05.013 PMID: 16753329

43. Thaler JS, Humphrey PT, Whiteman NK. Evolution of jasmonate and salicylate signal crosstalk. Trends in Plant Science. Elsevier; 2012. pp. 260–270. https://doi.org/10.1016/j.tplants.2012.02.010 PMID: 22498450

44. Qi D, de Young BJ, Innes RW. Structure-function analysis of the coiled-coil and leucine-rich repeat domains of the RPS5 disease resistance protein. Plant Physiol. 2012; 158: 1819–1832. https://doi.org/10.1104/pp.112.194035 PMID: 22331412

45. Gao Z, Chung EH, Eitas TK, Dangl JL. Plant intracellular innate immune receptor Resistance to Pseudomonas syringae pv. maculicola 1 (RPM1) is activated at, and functions on, the plasma membrane. Proc Natl Acad Sci U S A. 2011; 108: 7619–7624. https://doi.org/10.1073/pnas.1104410108 PMID: 21490299

46. Park E, Lee H-Y, Woo J, Choi D, Dinesh-Kumar SP. Spatiotemporal Monitoring of Pseudomonas syringae Effectors via Type III Secretion Using Split Fluorescent Protein Fragments. Plant Cell. 2017; 29: 1571–1584. https://doi.org/10.1105/tpc.17.00047 PMID: 28619883

47. Roberts M, Tang S, Stallmann A, Dangl JL, Bonardi V. Genetic Requirements for Signaling from an Autoactive Plant NB-LRR Intracellular Innate Immune Receptor. PLoS Genet. 2013; 9. https://doi.org/10.1371/journal.pgen.1003465 PMID: 23633962

48. Gantner J, Ordon J, Kretschmer C, Guerois R, Stuttmann J. An EDS1-SAG101 Complex Is Essential for TNL-Mediated Immunity in Nicotiana benthamiana. Plant Cell. 2019; 31: 2456–2474. https://doi.org/10.1105/tpc.19.00099 PMID: 31266900

49. Cui H, Qiu J, Zhou Y, Bhandari DD, Zhao C, Bautor J, et al. Antagonism of Transcription Factor MYC2 by EDS1/PAD4 Complexes Bolsters Salicylic Acid Defense in Arabidopsis Effector-Triggered Immunity. Mol Plant. Cell Press; 2018; 11: 1053–1066. https://doi.org/10.1016/j.molp.2018.05.007 PMID: 29842929

50. Bender CL, Alarcón-Chaidez F, Gross DC. Pseudomonas syringae phytotoxins: mode of action, regulation, and biosynthesis by peptide and polyketide synthetases. Microbiol Mol Biol Rev. 1999; 63: 266–92. PMID: 10357851

51. Yang L, Teixeira PJPL, Biswas S, Finkel OM, He Y, Salas-Gonzalez I, et al. Pseudomonas syringae Type III Effector HopBB1 Promotes Host Transcriptional Repressor Degradation to Regulate Phytohormone Responses and Virulence. Cell Host Microbe. 2017; 21: 156–168. https://doi.org/10.1016/j.chom.2017.01.003 PMID: 28132837

52. Sinapidou E, Williams K, Nott L, Bahkt S, Tör M, Crute I, et al. Two TIR:NB:LRR genes are required to specify resistance to *Peronospora parasitica* isolate Cala2 in *Arabidopsis*. Plant J. 2004; 38: 898–909. https://doi.org/10.1111/j.1365-313X.2004.02099.x PMID: 15165183

53. Ordon J, Gantner J, Kemna J, Schwalgun L, Reschke M, Streubel J, et al. Generation of chromosomal deletions in dicotyledonous plants employing a user-friendly genome editing toolkit. Plant J. 2017; 89: 155–168. https://doi.org/10.1111/tpj.13319 PMID: 27579989

54. Venugopal SC, Jeong R-D, Mandal MK, Zhu S, Chandra-Shekara AC, Xia Y, et al. Enhanced Disease Susceptibility 1 and Salicylic Acid Act Redundantly to Regulate Resistance Gene-Mediated Signaling. PLoS Genet. 2009; 5: e1000545. https://doi.org/10.1371/journal.pgen.1000545 PMID: 19578402

55. van der Biezen EA, Freddie CT, Kahn K, ParkerP JE, Jones JDG. Arabidopsis RPP4 is a member of the RPP5 multigene family of TIR-NB-LRR genes and confers downy mildew resistance through multiple signalling components. Plant J. 2002; 29: 439–451. https://doi.org/10.1046/j.0960-7412.2001.01229.x PMID: 11846877

56. Grant MR, Godiard L, Straube E, Ashfield T, Lewald J, Sattler A, et al. Structure of the Arabidopsis RPM1 gene enabling dual specificity disease resistance. Science. 1995; 269: 843–846. https://doi.org/10.1126/science.7638602 PMID: 7638602

57. Lewis JD, Wu R, Guttman DS, Desveaux D. Allele-Specific Virulence Attenuation of the Pseudomonas syringae HopZ1a Type III Effector via the Arabidopsis ZAR1 Resistance Protein. PLoS Genet. 2010; 6: e1000894. https://doi.org/10.1371/journal.pgen.1000894 PMID: 20368970

58. Zipfel C, Robatzek S, Navarro L, Oakeley EJ, Jones JDG, Felix G, et al. Bacterial disease resistance in Arabidopsis through flagellin perception. Nature. 2004; 428: 764–767. https://doi.org/10.1038/nature02485 PMID: 15085136

59. Thomma BPHJ, Nelissen I, Eggermont K, Broekaert WF. Deficiency in phytoalexin production causes enhanced susceptibility of Arabidopsis thaliana to the fungus Alternaria brassicicola. Plant J. Plant J; 1999; 19: 163–171. https://doi.org/10.1046/j.1365-313x.1999.00513.x PMID: 10476063

60. Kemmerling B, Schwedt A, Rodriguez P, Mazzotta S, Frank M, Qamar SA, et al. The BRI1-Associated Kinase 1, BAK1, Has a Brassinolide-Independent Role in Plant Cell-Death Control. Curr Biol. Curr Biol; 2007; 17: 1116–1122. https://doi.org/10.1016/j.cub.2007.05.046 PMID: 17583510

61. Finkel OM, Salas-González I, Castrillo G, Spaepen S, Law TF, Teixeira PJPL, et al. The effects of soil phosphorus content on plant microbiota are driven by the plant phosphate starvation response. PLoS Biol. 2019; 17: e3000534. https://doi.org/10.1371/journal.pbio.3000534 PMID: 31721759

62. Thordal-Christensen H. A holistic view on plant effector-triggered immunity presented as an iceberg model. Cellular and Molecular Life Sciences. Springer; 2020. pp. 1–14. https://doi.org/10.1007/s00018-019-03364-2 PMID: 31712993

Supplementary Figure 1

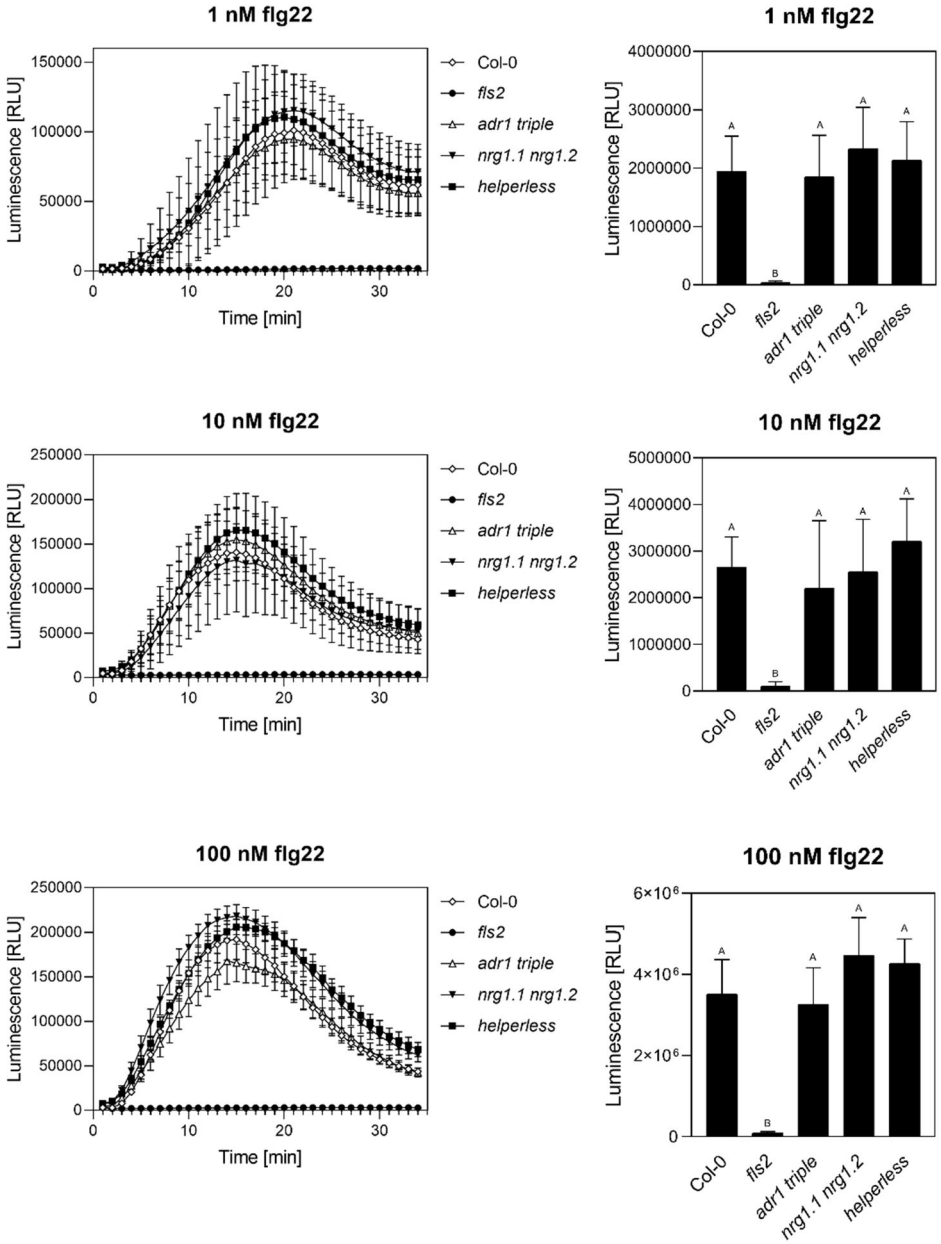

Supplementary Figure 2

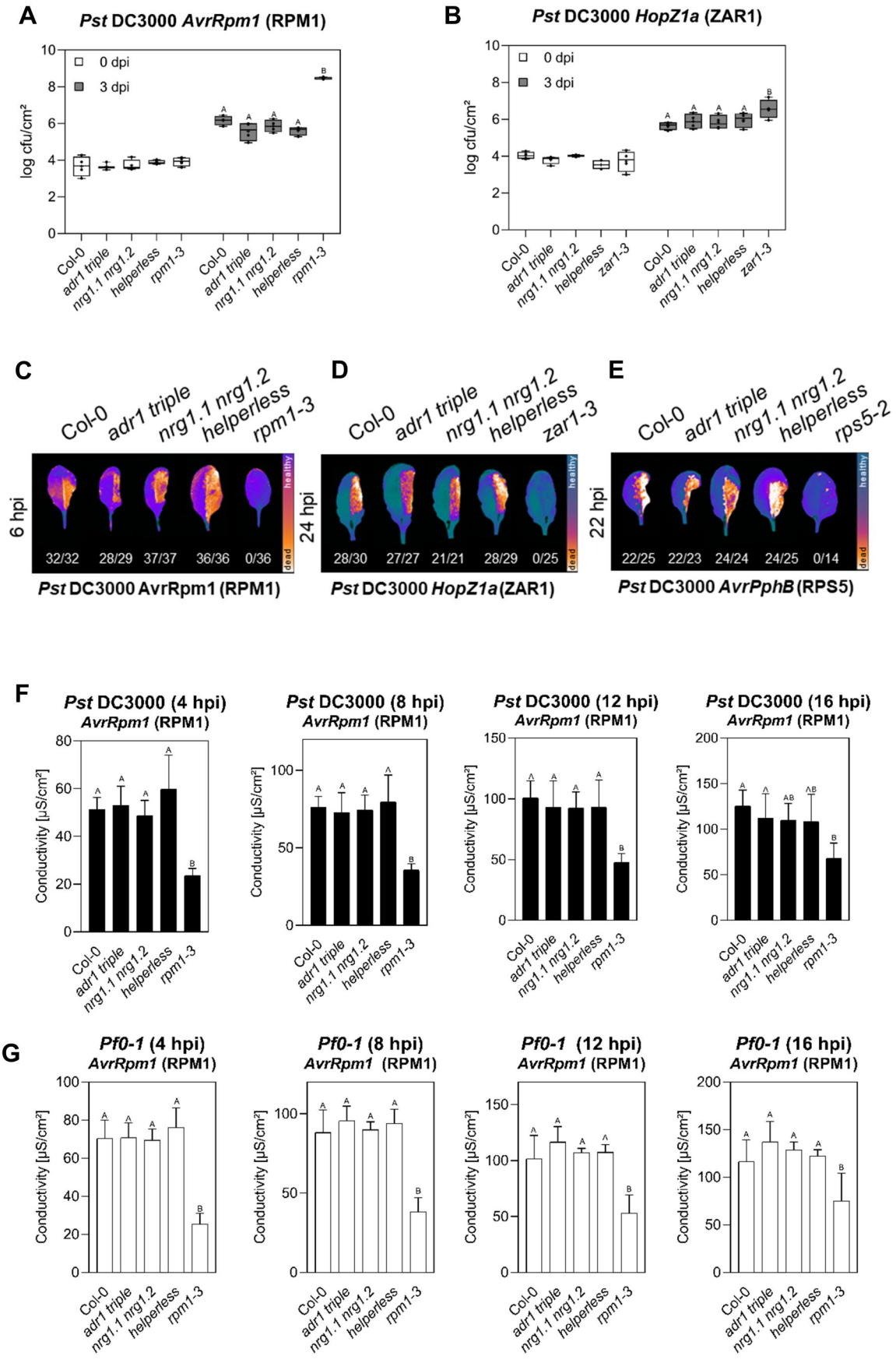

Supplementary Figure 3

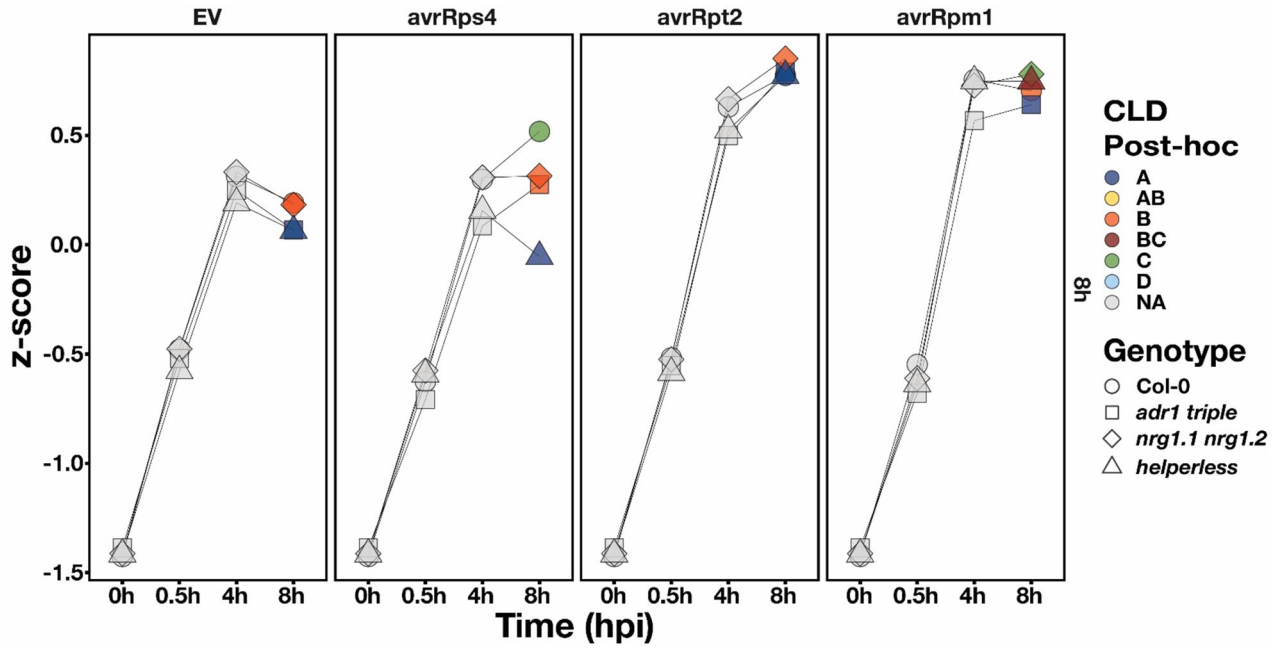

Supplementary Figure 4

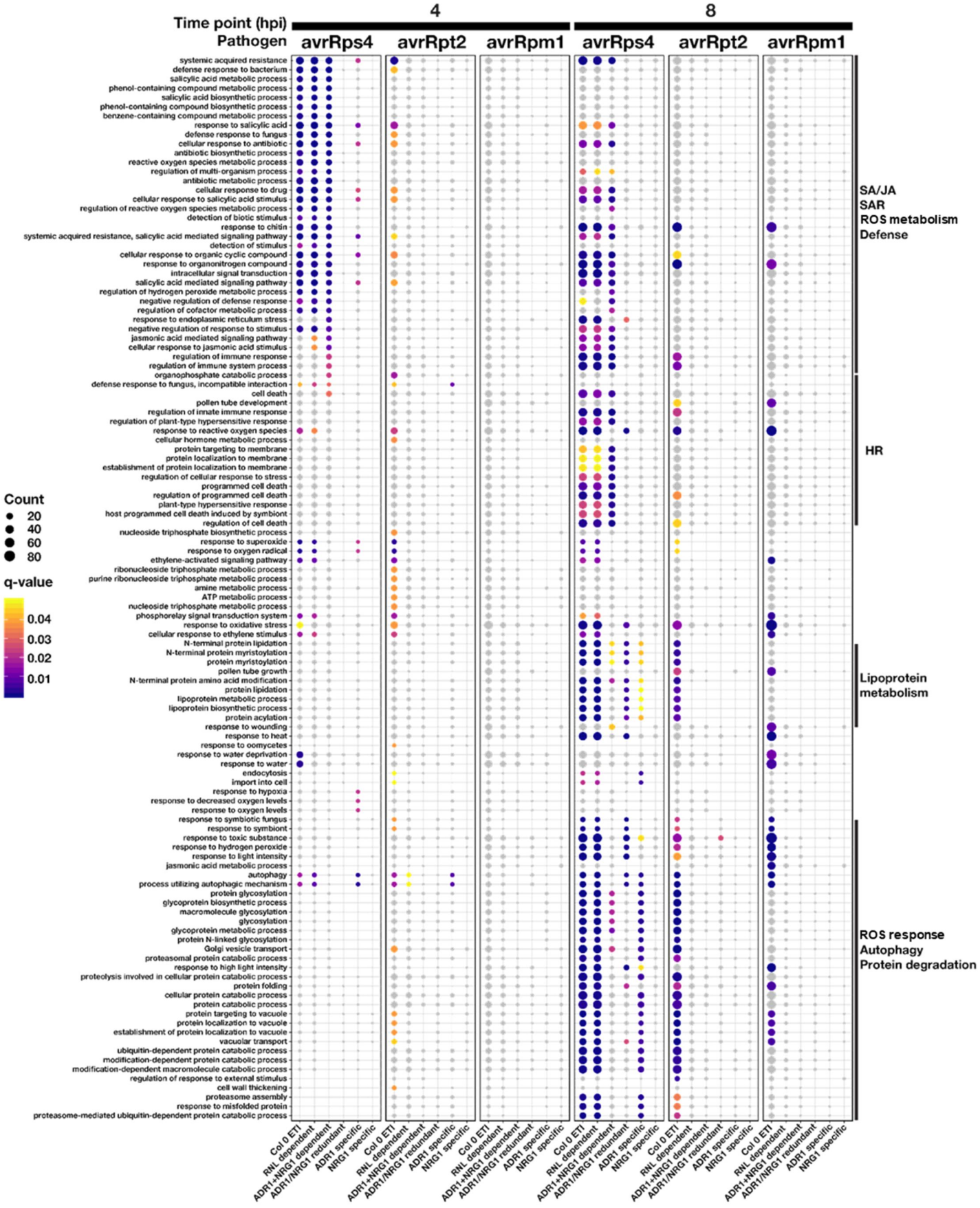

Supplementary Figure 5

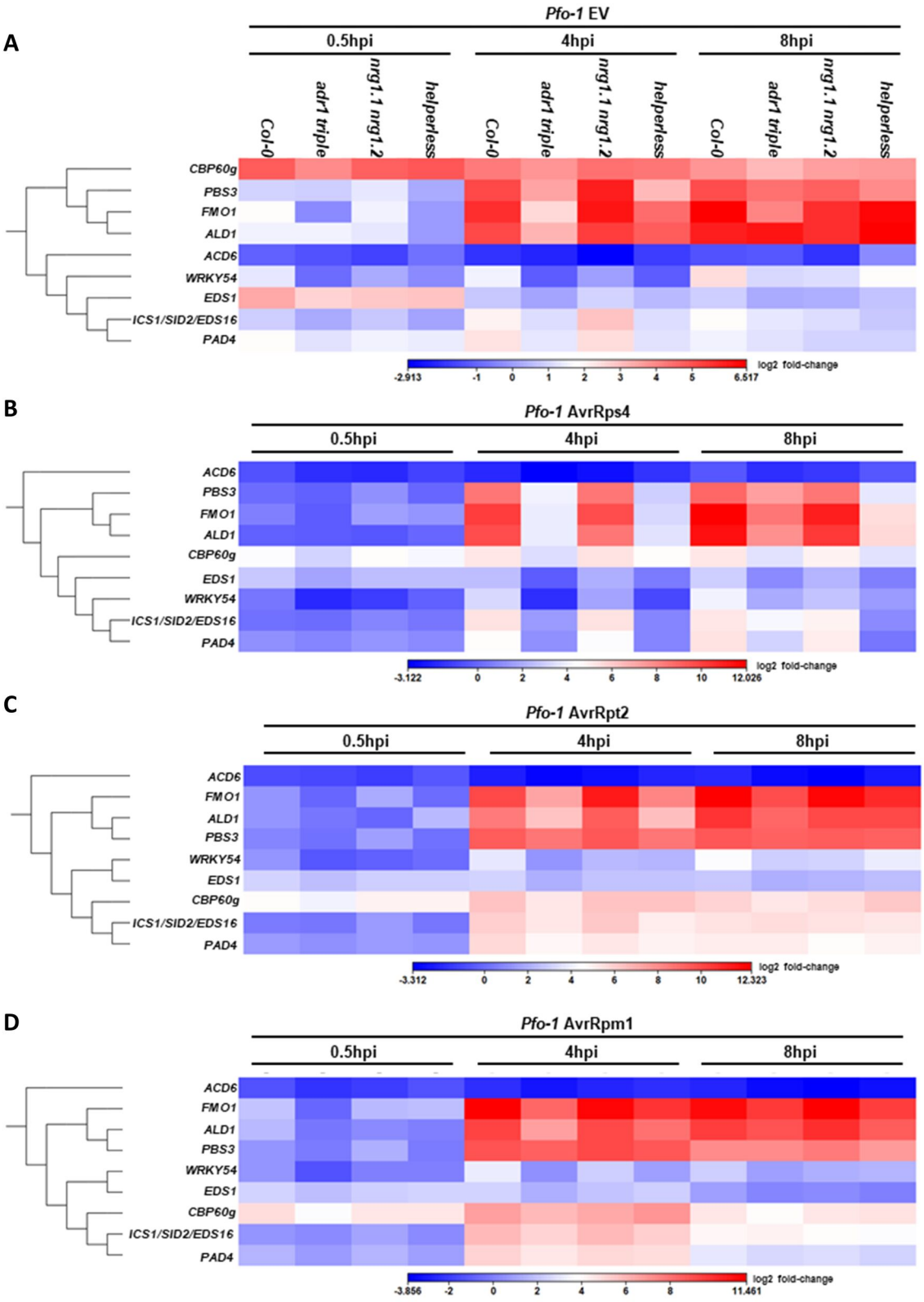

Supplementary Figure 6

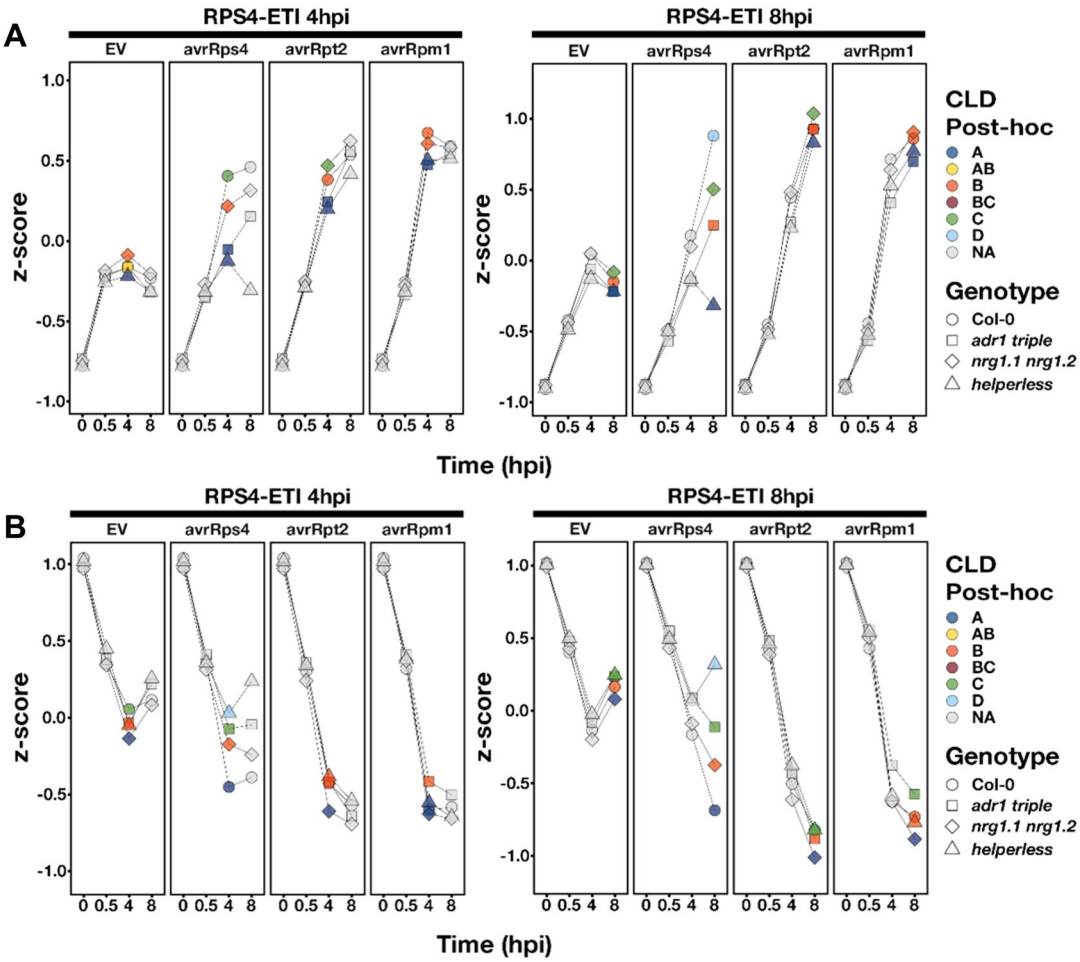

Supplementary Table S1: Expected expression profiles of ETI-induced genes according to their RNL-requirement.

		ETI-induced gene expression			
Category	Genotype	Col-0	*helperless*	*adr1 triple*	*nrg1.1 nrg1.2*
	RNL independent	+	+	+	+
RNL dependent	ADR1/NRG1 dependent	+	-	-	-
	ADR1/NRG1 redundant	+	-	+	+
	NRG1 specific	+	-	+	-
	ADR1 specific	+	-	-	+

'+' and '-' indicate induced and uninduced expression respectively

Supplementary Table S2: Overview of helper RNL requirements in (auto-) immunity:

Response to pathogen infection:

pathogen	effector	Sensor NLR	*adr1 triple*	*nrg1 double*	*helperless*
***Pst* DC3000**	*AvrRpm1*	RPM1 (CNL)	**Bonardi et al. (2011):** RPM1-mediated HR and resistance not compromised **In this study:** RPM1-mediated HR and resistance not compromised	**Castel et al. (2019):** RPM1-mediated HR macroscopically not compromised, but compromised in conductivity measurements at early time points not at late time points (*Pf0-1*) **In this study:** RPM1-mediated HR (*Pst* DC3000 and *Pf0-1*) and resistance (*Pst* DC3000) not compromised	**In this study:** RPM1-mediated HR and resistance not compromised
***Pst* DC3000**	*AvrRpt2*	RPS2 (CNL)	**Bonardi et al. (2011):** RPS2-mediated HR and resistance compromised **Wu et al. (2019):** RPS2-mediated resistance compromised **In this study:** RPS2-mediated HR compromised at early time points (10 hpi), not at late time points (24 hpi). RPS2-mediated resistance compromised	**Wu et al. (2019):** RPS2-mediated resistance not compromised **Castel et al. (2019):** RPS2-mediated HR macroscopically not compromised, but partially reduced in conductivity measurements (Pfo-1). RPS2-mediated resistance not compromised **In this study:** RPS2-mediated HR and resistance not compromised	**In this study:** RPS2-mediated HR compromised at early time points (10 hpi), not at late time points (24 hpi). RPS2-mediated resistance compromised
***Pst* DC3000**	*HopZ1a*	ZAR1 (CNL)	**In this study:** ZAR1-mediated HR and resistance not compromised	**In this study:** ZAR1-mediated HR and resistance not compromised	**In this study:** ZAR1-mediated HR and resistance not compromised
Pf0-1	*AvrPphB*	RPS5 (CNL)	**In this study:** RPS5-mediated HR not compromised, but resistance compromised	**Castel et al. (2019):** RPS5-mediated HR not compromised **In this study:** RPS5-mediated HR and resistance not compromised	**In this study:** RPS5-mediated HR not compromised, but resistance compromised
***Pst* DC3000**	*AvrRps4*	RPS4 (TNL)	**Wu et al. (2019**): RPS4-mediated resistance compromised **Lapin et al. (2019):** RPS4-mediated resistance compromised	**Wu et al. (2019):** RPS4-mediated resistance not compromised **Castel et al. (2019):** RPS4-mediated HR compromised (Pfo-1). RPS4-mediated resistance not	**Wu et al. (2019):** RPS4-mediated resistance severely compromised (stronger than adr1 triple)

			RPS4-mediated HR not compromised. **In this study:** RPS4-mediated resistance compromised RPS4-mediated HR not compromised	compromised (DC3000) **Lapin et al. (2019):** RPS4-mediated resistance not compromised. RPS4-mediated HR compromised **In this study:** RPS4-mediated resistance not compromised. RPS4-mediated HR compromised	**Lapin et al. (2019):** RPS4-mediated resistance severely compromised. RPS4-mediated HR compromised **In this study:** RPS4-mediated resistance severely compromised. RPS4-mediated HR compromised
***Pst* DC3000**	*AvrHopA1*	RPS6 (TNL)	**Wu et al. (2019):** RPS6-mediated resistance compromised	**Wu et al. (2019):** RPS6-mediated resistance not compromised	**Wu et al. (2019):** RPS6-mediated resistance compromised (stronger than in *adr1 triple*)
***Hpa* Emwa1**		RPP4 (TNL)	**Bonardi et al. (2011) and Wu et al.** (2019): RPP4-mediated resistance compromised **In this study:** RPP4-mediated resistance compromised	**Wu et al. (2019)** RPP4-mediated resistance not compromised **Castel et al. (2019):** RPP4-mediated resistance partially requires NRG1 **In this study:** RPP4-mediated resistance not compromised	**In this study:** RPP4-mediated resistance compromised
Hpa Cala2		RPP2 (TNL)	**Bonardi et al. (2011):** RPP2-mediated resistance compromised **In this study:** RPP2-mediated resistance slightly compromised	**Castel et al. (2019):** RPP2-mediated resistance partially requires NRG1 **In this study:** RPP2-mediated resistance not compromised	**In this study:** RPP2-mediated resistance severely compromised
Albugo candida		WRR4A^{Col} (TNL)	**In this study:** WRR4A-mediated resistance not compromised	**Castel et al. (2019):** NRG1s partially required for WRR4A-mediated resistance **In this study:** WRR4A-mediated resistance not compromised	**In this study:** WRR4A-mediated resistance compromised
Albugo candida		WRR4B^{Ws-2} (TNL)		**Castel et al. (2019):** NRG1s required for WRR4B-mediated resistance	
		CSA1 (TNL)		**Castel et al. (2019):** NbNRG1 required for CSA1-induced HR	
		SOC3 (TNL)		**Castel et al. (2019):** NbNRG1 required for SOC3-induced HR	

		CHS1 (TIR-NB)		Castel et al. (2019): NbNRG1 required for CHS1-induced HR	
***Pst* DC3000**	EV		**Bonardi et al. (2011)** Enhanced susceptibility **In this study:** Enhanced susceptibility	**In this study:** Resistance not compromised	**In this study:** Enhanced susceptibility
***Pst* DC3000 cor-**	lacks coronatine		**In this study:** Enhanced susceptibility	**In this study:** Resistance not compromised	**In this study:** Severely enhanced susceptibility
Pst* DC3000 Δ*hrcC			**In this study:** Resistance not compromised	**In this study:** Resistance not compromised	**In this study:** Resistance not compromised
***Hpa* Emco5**			**Bonardi et al. (2011)** Enhanced susceptibility		
***Psm* ES4326**			**Wu et al. (2019):** Enhanced susceptibility	**Wu et al. (2019):** Resistant	**Wu et al. (2019)** Severely enhanced susceptibility

Autoimmunity:

Autoimmune mutant	***adr1 triple***	***nrg1 double***	***helperless***
snc1	**Dong et al. (2016)** ADR1s largely required	**Wu et al. (2019)** NRG1s partially required	**Wu et al. (2019):** *snc1* auto-immunity fully suppressed
chs2-1	**Dong et al. (2016)** ADR1s required: complete suppression		
chs3-1	**Dong et al. (2016)** Weak or partial suppression		
slh1-9	**Dong et al. (2016)** ADR1s partially required		
uni-1D	**Dong et al. (2016)** Weak suppression		
chs3-2D		**Wu et al. (2019)** NRG1s completely required **Castel et al. (2019):** NbNRG1 required for chs3-2D induced HR	
Snc2-1D		**Wu et al. (2019)** NRG1s not required	
***mekk1-5* (SUMM2 (CNL))**		**Wu et al. (2019)** NRG1s not required	
chs1-2		**Wu et al. (2019)** NRG1s not required	
ADR1-L2-D484V		**Wu et al. (2019)** NRG1s not required	
CSA1 (TNL)		**Castel et al. (2019):** NbNRG1 required for CSA1-induced HR	
SOC3 (TNL)		**Castel et al. (2019):** NbNRG1 required for SOC3-induced HR	
CHS1 (TIR-NB)		**Castel et al. (2019):** NbNRG1 required for CHS1-induced HR	

CC MLA10 (CNL)	**Castel et al. (2019):** NbNRG1 not required for MLA7 CC-induced HR
RPM1-D505V (CNL)	**Castel et al. (2019):** NbNRG1 not required for RPM1-autoactivity
RPS5 (CNL)	NbNRG1 not required for cell death activity upon effector-dependent activation

7.3. Pruitt and Locci *et al*., 2021

The EDS1-PAD4-ADR1 node mediates *Arabidopsis* pattern-triggered immunity

Pruitt, R. N.*, Locci, F.*, Wanke, F., Zhang, L., Saile, S. C., Joe, A., Karelina, D., Hua, C., Fröhlich, K., Wan, W.-L., Hu, M., Rao, S., Stolze, S. C., Harzen, A., Gust, A. A., Harter, K., Joosten, M. H. A. J., Thomma, B. P. H. J., Zhou, J.-M., Dangl, J. L., Weigel, D., Nakagami, H., Oecking, C., El Kasmi, F., Parker, J. E., Nürnberger, T.

*These authors contributed equally to this work.

Nature.

2021.Oct;598:495-499.

doi: 10.1038/s41586-021-03829-0.

Article

The EDS1–PAD4–ADR1 node mediates *Arabidopsis* pattern-triggered immunity

https://doi.org/10.1038/s41586-021-03829-0

Received: 11 December 2020

Accepted: 16 July 2021

Published online: 8 September 2021

Check for updates

Rory N. Pruitt[1,13], Federica Locci[2,13], Friederike Wanke[3], Lisha Zhang[1], Svenja C. Saile[3], Anna Joe[1], Darya Karelina[4], Chenlei Hua[1], Katja Fröhlich[1], Wei-Lin Wan[1,11], Meijuan Hu[5], Shaofei Rao[5,12], Sara C. Stolze[6], Anne Harzen[6], Andrea A. Gust[1], Klaus Harter[3], Matthieu H. A. J. Joosten[7], Bart P. H. J. Thomma[7,8], Jian-Min Zhou[5], Jeffery L. Dangl[9], Detlef Weigel[4], Hirofumi Nakagami[6], Claudia Oecking[3], Farid El Kasmi[3], Jane E. Parker[2,8]✉ & Thorsten Nürnberger[1,10]✉

Plants deploy cell-surface and intracellular leucine rich-repeat domain (LRR) immune receptors to detect pathogens[1]. LRR receptor kinases and LRR receptor proteins at the plasma membrane recognize microorganism-derived molecules to elicit pattern-triggered immunity (PTI), whereas nucleotide-binding LRR proteins detect microbial effectors inside cells to confer effector-triggered immunity (ETI). Although PTI and ETI are initiated in different host cell compartments, they rely on the transcriptional activation of similar sets of genes[2], suggesting pathway convergence upstream of nuclear events. Here we report that PTI triggered by the *Arabidopsis* LRR receptor protein RLP23 requires signalling-competent dimers of the lipase-like proteins EDS1 and PAD4, and of ADR1 family helper nucleotide-binding LRRs, which are all components of ETI. The cell-surface LRR receptor kinase SOBIR1 links RLP23 with EDS1, PAD4 and ADR1 proteins, suggesting the formation of supramolecular complexes containing PTI receptors and transducers at the inner side of the plasma membrane. We detected similar evolutionary patterns in LRR receptor protein and nucleotide-binding LRR genes across *Arabidopsis* accessions; overall higher levels of variation in LRR receptor proteins than in LRR receptor kinases are consistent with distinct roles of these two receptor families in plant immunity. We propose that the EDS1–PAD4–ADR1 node is a convergence point for defence signalling cascades, activated by both surface-resident and intracellular LRR receptors, in conferring pathogen immunity.

Arabidopsis thaliana (hereafter *Arabidopsis*) cell-surface LRR receptor kinases (LRR-RKs) and LRR receptor protein (LRR-RP)–SOBIR1 complexes recruit the co-receptor BAK1 and signal through receptor-like cytoplasmic kinases (RLCKs) to elicit PTI[3]. Intracellular coiled-coil (CC)-nucleotide-binding LRR (NLR) or TOLL-INTERLEUKIN 1 RECEPTOR (TIR)-NLR receptors[4] require ADR1-type and NRG1-type helper NLRs (hNLRs) and the lipase-like EDS1 family proteins EDS1, PAD4 and SAG101 to confer ETI[5,6]. While the defence outputs for PTI and ETI are qualitatively similar[2], where and how pathways activated in different cell compartments converge remain unclear. Effective plant defence relies on mutual potentiation of PTI and ETI pathways[7,8], suggesting mechanistic links between these two tiers of the plant immune system.

RLCKs PBL30 and PBL31 mediate PTI

The *Arabidopsis* class VII RLCK (RLCK-VII) BIK1 promotes LRR-RK-mediated PTI but is a negative regulator of LRR-RP-mediated PTI[9]. To identify RLCK-VII members with positive roles in LRR-RP-dependent PTI, we screened an *Arabidopsis* RLCK-VII transfer DNA mutant library[10] for ethylene production elicited by fungal pg13(At)[11], oomycete nlp20 and bacterial eMax (which are recognized by RLP42, RLP23 and RLP1, respectively)[3] (Extended Data Fig. 1a). A *pbl31* mutant was defective in response to these elicitors compared with wild-type plants (Columbia-0 (Col-0)) (Extended Data Fig. 1a). PBL31 belongs to RLCK-VII subfamily 7, together with PBL30 (also known as CST) and PBL32 (ref. [10]). The LRR-RP elicitors nlp20, eMax

[1]Department of Plant Biochemistry, Centre of Plant Molecular Biology (ZMBP), University of Tübingen, Tübingen, Germany. [2]Department of Plant–Microbe Interactions, Max Planck Institute for Plant Breeding Research, Cologne, Germany. [3]Department of Plant Physiology, Centre of Plant Molecular Biology (ZMBP), University of Tübingen, Tübingen, Germany. [4]Department of Molecular Biology, Max Planck Institute for Developmental Biology, Tübingen, Germany. [5]State Key Laboratory of Plant Genomics, Institute of Genetics and Developmental Biology, Innovation Academy for Seed Design, Chinese Academy of Sciences, Beijing, China. [6]Proteomics Group, Max Planck Institute for Plant Breeding Research, Cologne, Germany. [7]Laboratory of Phytopathology, Wageningen University, Wageningen, Netherlands. [8]Cluster of Excellence on Plant Sciences (CEPLAS), Cologne University, Cologne, Germany. [9]Department of Biology, Howard Hughes Medical Institute, University of North Carolina at Chapel Hill, Chapel Hill, NC, USA. [10]Department of Biochemistry, University of Johannesburg, Johannesburg, South Africa. [11]Present address: Department of Biological Sciences, National University of Singapore, Singapore, Singapore. [12]Present address: State Key Laboratory for Managing Biotic and Chemical Threats to the Quality and Safety of Agro-products, Institute of Plant Virology, Ningbo University, Ningbo, China. [13]These authors contributed equally: Rory N. Pruitt, Federica Locci. ✉e-mail: parker@mpipz.mpg.de; nuernberger@uni-tuebingen.de

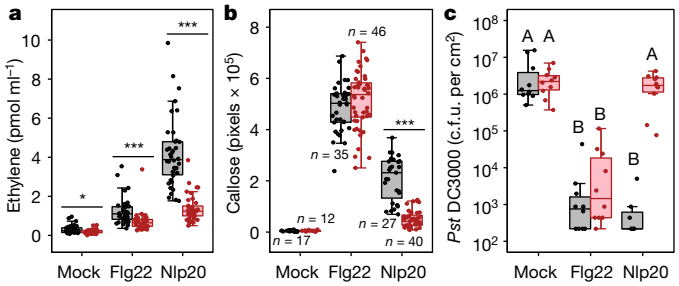

Fig. 1 | RLCK-VII-7 subfamily members are required for LRR-RP-mediated immunity. a, Elicitor-induced ethylene production in Col-0 and the *pbl30 pbl31 pbl32* mutant (grey and pink, respectively, in all panels). $n = 38$ (nlp20) or 36 (mock and flg22) samples, each comprising 3 leaf pieces. Data are from 10 independent experiments. For **a**, **b**, a two-sided Wilcoxon rank-sum test with continuity correction was used to analyse significant differences between Col-0 and the *pbl30 pbl31 pbl32* mutant for the given elicitor treatment (*$P \leq 0.05$, ***$P \leq 0.0001$). **b**, Callose deposition in Col-0 and the *pbl30 pbl31 pbl32* mutant. $n \geq 12$ images from at least 3 leaves; exact n values are provided in the graph. **c**, Elicitor-induced defence against infection is impaired in the *pbl30 pbl31 pbl32* mutant. Leaves were infiltrated with the indicated elicitor and challenged with *Pst* DC3000 after 24 h. Boxes show bacterial colonization 3 d after infection. $n = 10$ (for Col-0) and $n = 7$ (for nlp20) biological replicates, each comprising 2 leaf discs. Data points with different letters indicate significant differences of $P \leq 0.05$ (Kruskal–Wallis test with a post-hoc two-sided Steel–Dwass test). c.f.u., colony forming units. For the box plots, the centre line indicates the median, the bounds of the box show the 25th and the 75th percentiles, and the whiskers indicate 1.5 × IQR (that is, the interquartile range between the 25th and the 75th percentile). Experiments in **b** and **c** were performed at least three times with similar results. Exact *P* values for all experiments are provided in Supplementary Table 5.

and IF1 (which is recognized by RLP32)[12] triggered a reduced ethylene response in a *pbl30* mutant, although in some cases, differences were not statistically significant; responses in the *pbl32* mutant were not impaired to any elicitor (Extended Data Fig. 1). Ethylene production in *pbl30 pbl31* double mutant and *pbl30 pbl31 pbl32* triple mutant lines was reduced more strongly than in any single mutant (Extended Data Fig. 1b). The LRR-RK elicitors flg22 and elf18, which activate the LRR-RKs FLS2 and EFR[3], respectively, also induced lower ethylene responses in *pbl30 pbl31* and *pbl30 pbl31 pbl32* mutants than in the wild type, but to a lesser extent than observed for LRR-RP elicitors (Fig. 1a, Extended Data Fig. 1b). Nlp20-induced ethylene production in *pbl30 pbl31 pbl32* mutants was complemented by overexpression of PBL31, but not by the kinase-inactive variant PBL31^{K201A} (Extended Data Fig. 2a–c).

We tested whether the RLCK-VII-7 subfamily mediates other RLP23-mediated immunity outputs. Nlp20-induced production of reactive oxygen species (ROS) was virtually abolished in *pbl30 pbl31* and *pbl30 pbl31 pbl32* mutants, whereas flg22-induced ROS production was reduced (Extended Data Fig. 3a, b). Nlp20-triggered callose deposition was strongly impaired in *pbl30 pbl31* and *pbl30 pbl31 pbl32* mutants, whereas flg22-triggered callose production was unaltered in these mutants (Fig. 1b, Extended Data Fig. 3c). Nlp20-induced expression of the phytoalexin synthesis genes *PAD3* and *CYP71A13* (ref. [13]) and the systemic acquired resistance marker *FMO1* (ref. [14]) was impaired in *pbl30 pbl31 pbl32* leaves (Extended Data Fig. 3d). Inhibition of seedling growth in the presence of elf18 or flg22 (a response unaffected by LRR-RP ligands[15]) was similar in Col-0 and the *pbl30 pbl31 pbl32* mutant, and both lines displayed similar levels of nlp20-induced and flg22-induced MAPK phosphorylation (Extended Data Fig. 3e, f). These results identify the roles of the RLCK-VII-7 family RLCKs PBL30 and PBL31 in a subset of PTI responses.

We found that nlp20–RLP23-induced resistance to infection by virulent *Pseudomonas syringae* pv. *tomato* (*Pst*) DC3000 was abolished in *pbl30 pbl31* and *pbl30 pbl31 pbl32* mutants, whereas flg22-induced resistance was reduced (Fig. 1c, Extended Data Fig. 3g). ETI conferred by the TIR-NLR receptor pair RRS1–RPS4 or the CC-NLR RPS2 was unaffected in the *pbl30 pbl31 pbl32* mutant (Extended Data Fig. 3h). Hence, PBL30 and PBL31 are dispensable for ETI but are essential positive regulators of LRR-RP-mediated PTI, with less prominent roles in LRR-RK-mediated PTI.

EDS1–PAD4 dimers mediate PTI

EDS1 forms exclusive heterodimers with SAG101 or PAD4 that control different immunity branches in ETI[5,16,17]. *Arabidopsis* EDS1–PAD4 dimers promote not only ETI transcriptional defence but also basal immunity[18,19]. Accordingly, *eds1* and *pad4* mutants are hypersusceptible to pathogens without recognized effectors[5]. To test whether reduced basal immunity is due to impaired PTI signalling, we measured PTI responses in *pad4*, *eds1* and *sag101* mutants (Fig. 2, Extended Data Fig. 4). *Pad4* and *eds1*, but not *sag101*, mutants produced substantially less ethylene than the wild type in response to nlp20, IF1 and pg13(At) (Fig. 2a, Extended Data Fig. 4a). Ethylene production mediated by FLS2 and EFR was not significantly reduced in *pad4* and *eds1* mutants (Fig. 2a, Extended Data Fig. 4a).

An EDS1 variant (EDS1^{LLIF}) that cannot dimerize with PAD4 (ref. [19]) failed to restore LRR-RP-mediated ethylene responses (Fig. 2b, Extended Data Fig. 4a). Likewise, mutation of a cationic residue (EDS1^{R493A}) at a signalling surface in the EDS1–PAD4 dimer that disables ETI[20] also abolished RLP23-mediated ethylene production (Fig. 2b). EDS1 and PAD4 variants (EDS1^{SDH} and PAD4^{S}) with mutations in their putative α/β-hydrolase catalytic residues are functional in ETI and basal immunity[19] and also fully complement nlp20-induced ethylene production in an *eds1 pad4* mutant (Extended Data Fig. 4b). Fungal thaxtomin A, a selective activator of PAD4-dependent immunity[21], enhanced nlp20-induced, but not flg22-induced, ethylene production in Col-0 but not in the *pad4* mutant (Extended Data Fig. 4c). These data indicate predominant involvement of the EDS1–PAD4 dimer in LRR-RP signalling.

The production of ROS and callose was strongly reduced in *pad4* and *eds1* mutants upon nlp20, but not flg22, treatment (Fig. 2c, d). Moreover, nlp20-triggered *PAD3*, *CYP71A13* and *FMO1* transcript accumulation was reduced in the *pad4* mutant compared with wild-type Col-0 (Extended Data Fig. 4d). Inhibition of seedling growth in the presence of flg22 or elf18 was similar in Col-0 and the *pad4* mutant (Extended Data Fig. 4e), as was elicitor-induced MAPK activation (Extended Data Fig. 4f). In induced pathogen resistance assays, nlp20 failed to confer protection to *Pst* DC3000 infection in *pad4* and *eds1* mutants; flg22-induced resistance was also partially impaired in these mutants (Fig. 2e). Both elicitors conferred full protection in the *sag101* mutant (Fig. 2e). We concluded that a signalling-competent EDS1–PAD4 complex is essential for many aspects of NLR-mediated ETI, for LRR-RP-mediated PTI and partly for LRR-RK signalling.

To assess possible regulatory effects of PAD4 on the expression of PTI-associated genes, we measured transcript levels of key receptor, co-receptor and signalling components in *pad4* and Col-0 plants. All transcript levels were similar in both genotypes (Extended Data Fig. 5a), and transcriptomic data suggest similar transcript levels in *eds1* and *adr1* triple genotypes[20,22]. Likewise, accumulation of BAK1, FLS2, MPK3, MPK4 and MPK6 proteins was similar between Col-0 and the *pad4* mutant (Extended Data Fig. 5b). These data, together with intact elicitor-induced MAPK activation in the *eds1 pad4 sag101* mutant (Extended Data Fig. 4f), suggest that machineries involved in early PTI signalling are not severely affected by the lack of EDS1 and PAD4.

ADR1 family hNLRs signal in PTI

Arabidopsis EDS1–SAG101 dimers work with NRG1 family hNLRs in TIR-NLR ETI signalling[16,17]. By contrast, EDS1–PAD4 dimers function

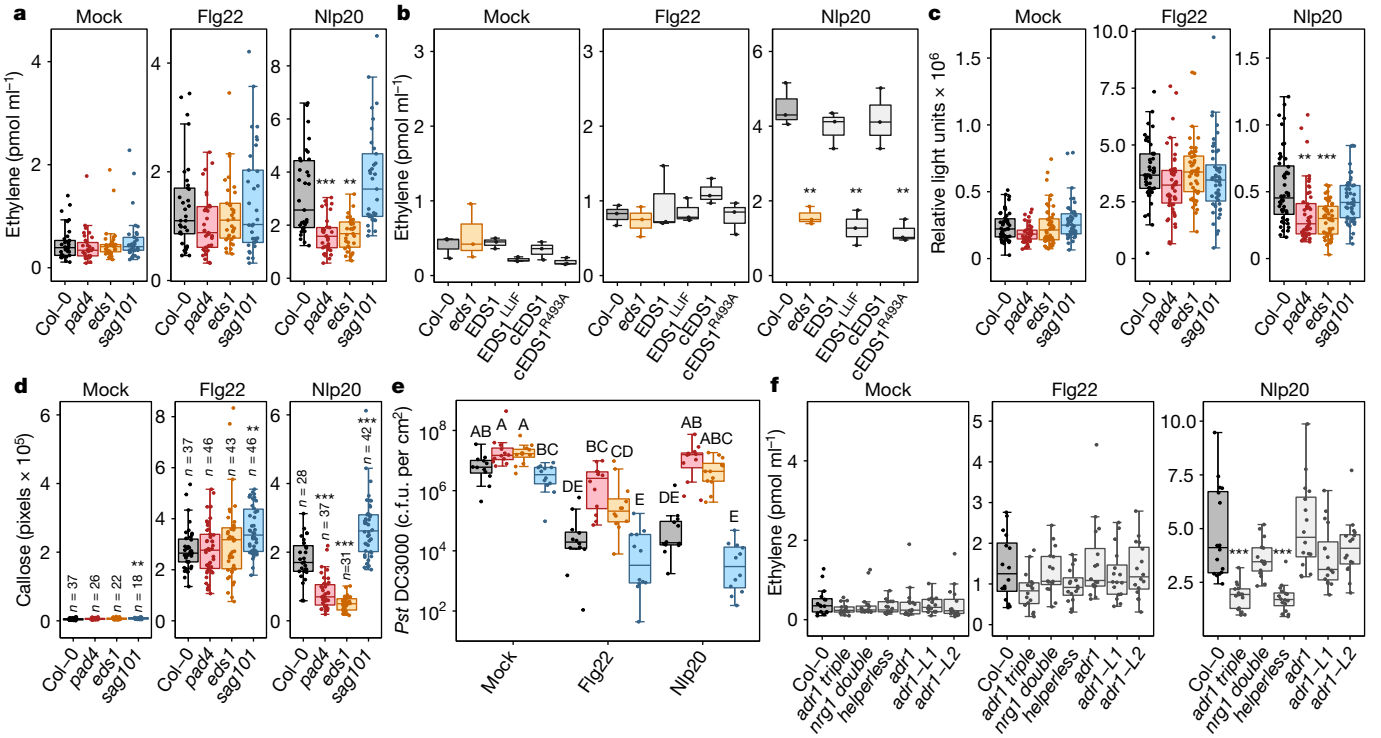

Fig. 2 | PAD4, EDS1 and ADR1 helper NLRs are positive regulators of LRR-RP signalling. a, Elicitor-induced ethylene production in Col-0, *pad4*, *eds1* and *sag101* mutants (grey, pink, orange and blue, respectively, in all panels). $n = 33$, each from 3 leaf pieces. Data are from eight independent experiments. For **a**, **c**, **d** and **f**, statistical differences between Col-0 and the indicated mutants were analysed using a Kruskal–Wallis test with a post-hoc two-sided Steel–Dwass test (**$P \leq 0.01$, ***$P \leq 0.0001$). **b**, Ethylene production depends on the PAD4–EDS1 heterodimer. $n = 3$, each from 3 leaf pieces. Statistical differences between Col-0 and the indicated mutants were analysed by two-sided Welch's pairwise tests (**$P \leq 0.01$). For the complementation constructs cEDS1 and EDS1, see Supplementary Table 3. **c**, Total elicitor-induced ROS production over 30 min. $n = 48$ leaf pieces from 3 independent experiments. **d**, Callose deposition in Col-0, *pad4*, *eds1* and *sag101* mutants. $n \geq 12$ images from at least 3 leaves; exact n values are indicated in the graph. **e**, Elicitor-induced defence against infection is impaired in *pad4* and *eds1* mutants. Leaves were infiltrated with the indicated elicitor and challenged with *Pst* DC3000 after 24 h. Boxes show bacterial colonization 3 d after infection. $n = 12$ biological replicates comprising 2 leaf discs. Data points with different letters indicate significant differences of $P \leq 0.05$ (Kruskal–Wallis test with post-hoc two-sided Steel–Dwass test). **f**, Nlp20-induced ethylene production is dependent on ADR1 helper NLRs. $n = 20$, each from 3 leaf pieces. Data are from four independent experiments. For the box plots, the centre line indicates the median, the bounds of the box show the 25th and the 75th percentiles, and the whiskers indicate 1.5 × IQR. Experiments in **b**, **d** and **e** were performed at least three times with similar results. Exact P values for all experiments are provided in Supplementary Table 5.

with ADR1 family hNLRs to promote TIR-NLR ETI, CC-NLR ETI and basal immunity[16,17]. Consistent with our observations that LRR-RP responses require PAD4 but not SAG101, we found that nlp20 responses were strongly impaired in an *ADR1* family triple mutant (*adr1* triple)[22] but not an *NRG1* family double mutant (*nrg1* double)[22] (Fig. 2f, Extended Data Fig. 6a–c). A '*helperless*' mutant[22] lacking all *ADR1* and two functional full-length *NRG1* genes behaved similarly to the *adr1* triple mutant (Fig. 2f, Extended Data Fig. 6a–c). The *helperless* mutant was not impaired in elicitor-induced MAPK activation (Extended Data Fig. 6d) and was similar to Col-0 in seedling growth inhibition assays with flg22 or elf18 (Extended Data Fig. 6e). However, both nlp20-induced and flg22-induced resistance to *Pst* DC3000 was impaired in the *adr1* triple and *helperless* mutants compared with Col-0 (Extended Data Fig. 6f). Our data highlight a shared requirement of cell-surface-initiated PTI and intracellular ETI signalling for the EDS1–PAD4–ADR1 node.

SOBIR1 connects RLP23 to PAD4–EDS1–ADR1

Because PBL31 kinase, EDS1–PAD4 dimers and ADR1 family hNLRs have roles in LRR-RP-mediated PTI, including early responses such as ROS burst (Fig. 2c, Extended Data Figs. 3a, b, 6b), we tested for possible spatial proximity between RLP23 and the constitutively associated co-receptor SOBIR1 with these components by co-immunoprecipitation assays in *Nicotiana benthamiana* plants. Epitope-tagged RLP23 and SOBIR1 precipitated PBL31 independent of nlp20 elicitation, suggesting a ligand-independent stable interaction between PBL31 and the receptor complex (Extended Data Fig. 7a). PBL31 was not precipitated by the GFP-tagged plasma membrane protein LTI6b (Extended Data Fig. 7a). Similarly, SOBIR1 interacted in a ligand-independent manner with PAD4, EDS1, ADR1 and the ADR1 isoforms ADR1-L1 and ADR1-L2 (Extended Data Fig. 7a, b). Bimolecular fluorescence complementation assays confirmed association between SOBIR1 and ADR1-L1 and ADR1-L2, but not ADR1, at the plasma membrane (Extended Data Fig. 7c, d). Spatial proximity of SOBIR1 with ADR1-L1, but not with PAD4 or EDS1, was corroborated in luciferase complementation assays (Extended Data Fig. 7e, f).

To investigate potential associations at the plasma membrane, we used fluorescently tagged proteins and assessed their spatial proximity by Förster resonance energy transfer by fluorescence lifetime (FLT) imaging (FRET-FLIM). Tested proteins (SOBIR1, ADR1, ADR1-L1, ADR1-L2, EDS1, PAD4, SAG101 and PBL31) localized, at least partly, to the plasma membrane when expressed in *N. benthamiana* (Extended Data Fig. 8a, b). Using SOBIR1–GFP as donor, we observed reduced GFP FLT in the presence of RFP-tagged EDS1, PAD4, PBL31, ADR1 and the ADR1 isoforms ADR1-L1 and ADR1-L2 (Fig. 3a). Because EDS1–PAD4 dimers mediate the RLP23 immune response (Fig. 2b), we co-expressed non-fluorescently labelled EDS1 with PAD4–RFP and vice versa with SOBIR1–GFP (Fig. 3a). Reduction in FLT was observed but was less pronounced than with

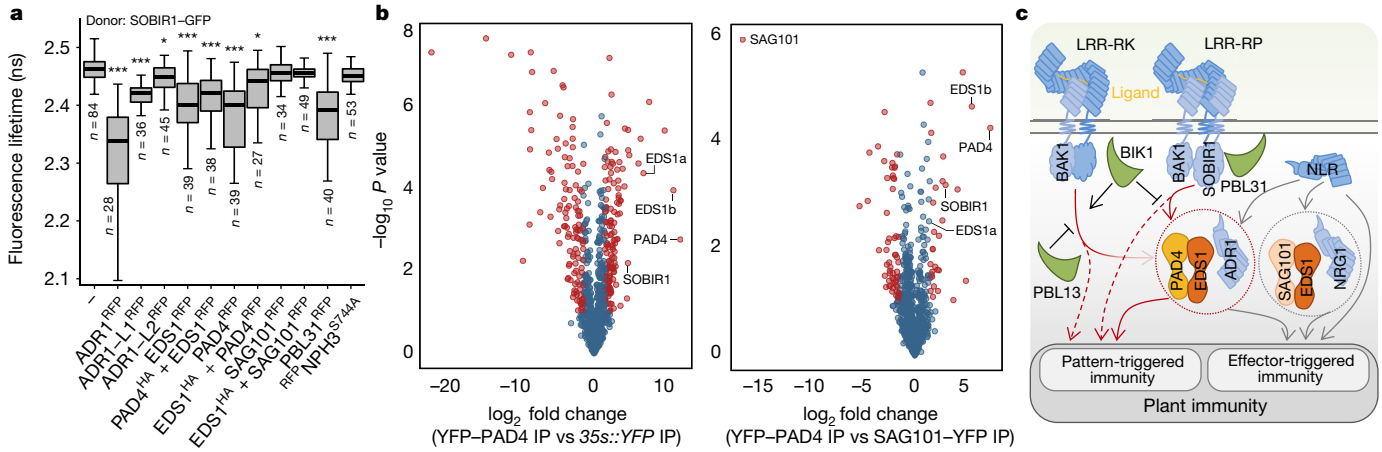

Fig. 3 | SOBIR1 associates with EDS1, PAD4 and ADR1 hNLRs to form a potential signalling node. a, FRET-FLIM reveals spatial proximity of SOBIR1 with PBL31, PAD4, EDS1 and ADR1 hNLRs. Membrane-associated NPH3^{S744A} serves as the control. Statistical differences in FLT between SOBIR1–GFP alone and the indicated FRET pair were analysed using a Kruskal–Wallis test with a post-hoc two-sided Steel–Dwass test (*$P \leq 0.05$, ***$P \leq 0.0001$). Exact P values are provided in Supplementary Table 5. $n \geq 27$ from at least 3 biological replicates. n values are shown below the boxes. The centre line indicates the median, the bounds of the box show the 25th and the 75th percentiles, and the whiskers indicate 1.5 × IQR. ns, nanoseconds. **b**, SOBIR1 specifically co-purifies with YFP–PAD4 in *Arabidopsis* leaves. A *pad4 sag101* mutant complemented with YFP–PAD4 or SAG101–YFP, and wild-type Col-0 expressing *35S::YFP* (YFP), were used for IP assays. Volcano plots show normalized abundances of proteins detected by MS after IP of total protein extracts from 4.5-week-old leaves infiltrated with DMSO for 10 min. Corresponding data for nlp20-treated leaves are provided in Extended Data Fig. 9a. The red dots indicate enriched proteins ($|\log_2(\text{YFP–PAD4/YFP})| \geq 1$ or $|\log_2(\text{YFP–PAD4/SAG101–YFP})| \geq 1$ using a permutation-based false discovery rate of 0.05). The two functional Col-0 EDS1 isoforms (EDS1a and EDS1b) were enriched in YFP–PAD4 samples, and EDS1a was enriched in SAG101–YFP IPs, as found in ETI-triggered tissues[16]. Samples were collected in four independent experiments. **c**, The EDS1–PAD4–ADR1 node mediates both PTI and ETI. Upon ligand perception, LRR-RK and LRR-RP receptors dimerize with BAK1 to activate PTI. The EDS1–PAD4–ADR1 node has a key role in LRR-RP signalling (red arrows) and a less prominent role in LRR-RK signalling (faded arrow). Some PTI outputs do not require EDS1–PAD4–ADR1 (dashed lines). ETI mediated by NLRs is dependent on the EDS1–PAD4–ADR1 and/or SAG101–EDS1–NRG1 nodes or is independent of either signalling node (grey arrows). The RLCK-VII kinases BIK1, PBL31 and PBL13 regulate LRR-RP and LRR-RK signalling.

SOBIR1–GFP and EDS1–RFP or PAD4–RFP alone (Fig. 3a). Reduction in FLT was not observed when SOBIR1–GFP was co-expressed with SAG101–RFP or plasma membrane-associated RFP–NPH3^{S744A} (ref. [23]) (Fig. 3a). While *Arabidopsis* SAG101 localizes primarily to nuclei[5,17], a small pool was detected close to the plasma membrane in these assays (Extended Data Fig. 8a, b). Using PBL31–GFP as donor confirmed its association with SOBIR1, ADR1-L1–RFP and EDS1–RFP, but not with ADR1–RFP, ADR1-L2–RFP, PAD4–RFP, SAG101–RFP or RFP–NPH3^{S744A} (Extended Data Fig. 8c). Co-expression of EDS1–haemagglutinin (HA) also led to reduction in FLT with the FRET pair PBL31–GFP + PAD4–RFP (Extended Data Fig. 8c), suggesting a close proximity of these proteins.

To monitor protein associations in *Arabidopsis*, we performed immunoprecipitations followed by tandem mass spectrometry (IP MS/MS) using *pad4 sag101* mutant lines stably expressing YFP–PAD4 or SAG101–YFP under control of their native promoters, and a wild-type Col-0 line constitutively expressing *p35S::YFP* as control[16]. Whereas RLCKs and ADR1 family members were not detected (Supplementary Tables 1, 2), SOBIR1 was enriched with YFP–PAD4 but not SAG101–YFP or YFP alone in mock-treated and nlp20-treated tissues and at 10 min or 3 h (Fig. 3b, Extended Data Fig. 9a–e). Together, the protein interaction data suggest that plasma membrane-resident LRR-RP–SOBIR1 receptors form a constitutive complex with PBL31 and components of the EDS1–PAD4–ADR1 node for PTI signalling.

LRR-RP and NLR genes are polymorphic

Having established that LRR-RPs and NLR immune receptors share signalling components, we assessed whether they have similar evolutionary patterns. Within species and populations, NLR genes have diversified, with signatures of both rapid and balancing evolution[24]. *Arabidopsis* LRR-RP-type immune receptors recognize widespread microbial surface patterns[3], but the encoding genes, like NLRs, often occur within gene clusters[25]. To gauge LRR-RP gene variation, reads from 80 *Arabidopsis* accessions[26,27] were mapped onto the Col-0 reference genome. Genes were categorized as conserved, displaying complex variation, or exhibiting presence or absence polymorphisms. This within-species analysis revealed a similar proportion of variable genes in NLR and LRR-RP families, whereas LRR-RK genes had low variation, comparable to the genomic background (Extended Data Fig. 10a). LRR-RP genes encoding known receptors were found in all three classes: RLP23, RLP30 and RLP32 are conserved, RLP42 has a complex pattern, and RLP1 has a presence or absence polymorphism (Extended Data Fig. 10b). We conclude that LRR-RP and NLR genes have similar evolutionary dynamics in maintaining sequence diversity, whereas LRR-RK-encoding genes are more constrained.

Discussion

Cell-surface LRR-type receptors share a dependence on the EDS1–PAD4–ADR1 node with cytoplasmic NLRs for activating plant immunity (Fig. 3c). These signalling components are essential for LRR-RP-mediated immunity, whereas LRR-RK-induced defences rely partially on them (Fig. 2, Extended Data Figs. 4, 6). This finding, together with differential involvement of RLCKs in LRR-RP-mediated (PBL31 and BIK1) and LRR-RK-mediated (BIK1 and PBL13) PTI[9,28] (Fig. 1, Extended Data Figs. 1–3), supports the concept of distinct immune pathways being activated through different receptor systems[9] (Fig. 3c). A requirement for EDS1–PAD4–ADR1 in cell-surface and intracellular receptor-mediated immunity might explain similar defences upon activation of ETI or PTI[2].

We show that EDS1, PAD4, ADR1-type hNLRs and RLCK PBL31 reside in close proximity with transmembrane LRR-RP–SOBIR1 complexes in resting and elicited states (Fig. 3a, b, Extended Data Figs. 7–9). Thus, ligand-induced recruitment of the co-receptor BAK1 into

transmembrane complexes with LRR-RP-type receptors might initiate PTI signalling through a preformed SOBIR1-anchored platform at the plasma membrane.

Cell-surface LRR-RPs and cytoplasmic NLRs emerge as two polymorphic immune sensor classes (Extended Data Fig. 10). In contrast to NLRs, the LRR-RP repertoire includes conserved sensors for widespread microbial patterns[3,29], accession-specific polymorphic sensors for common patterns[11] and sequence-divergent sensors for microbial pathovar-specific effectors[29]. LRR-RPs confer partial (for example, RLP23)[3] or full (for example, Cf proteins)[29] resistance to host-adapted microbial pathovars. LRR-RPs thus qualify as sensors that mediate both PTI and ETI, which erodes the strict distinction between the two layers of innate immunity[29,30].

Online content

Any methods, additional references, Nature Research reporting summaries, source data, extended data, supplementary information, acknowledgements, peer review information; details of author contributions and competing interests; and statements of data and code availability are available at https://doi.org/10.1038/s41586-021-03829-0.

1. Jones, J. D. & Dangl, J. L. The plant immune system. *Nature* **444**, 323–329 (2006).
2. Lu, Y. & Tsuda, K. Intimate association of PRR- and NLR-mediated signaling in plant immunity. *Mol. Plant Microbe Interact.* **34**, 3–14 (2021).
3. Wan, W. L., Fröhlich, K., Pruitt, R. N., Nürnberger, T. & Zhang, L. Plant cell surface immune receptor complex signaling. *Curr. Opin. Plant Biol.* **50**, 18–28 (2019).
4. Monteiro, F. & Nishimura, M. T. Structural, functional, and genomic diversity of plant NLR proteins: an evolved resource for rational engineering of plant immunity. *Annu. Rev. Phytopathol.* **56**, 243–267 (2018).
5. Lapin, D., Bhandari, D. D. & Parker, J. E. Origins and immunity networking functions of EDS1 family proteins. *Annu. Rev. Phytopathol.* **58**, 253–276 (2020).
6. Feehan, J. M., Castel, B., Bentham, A. R. & Jones, J. D. Plant NLRs get by with a little help from their friends. *Curr. Opin. Plant Biol.* **56**, 99–108 (2020).
7. Yuan, M. et al. Pattern-recognition receptors are required for NLR-mediated plant immunity. *Nature* **592**, 105–109 (2021).
8. Ngou, B. P. M., Ahn, H. K., Ding, P. & Jones, J. D. G. Mutual potentiation of plant immunity by cell-surface and intracellular receptors. *Nature* **592**, 110–115 (2021).
9. Wan, W. L. et al. Comparing *Arabidopsis* receptor kinase and receptor protein-mediated immune signaling reveals BIK1-dependent differences. *New Phytol.* **221**, 2080–2095 (2019).
10. Rao, S. et al. Roles of receptor-like cytoplasmic kinase VII members in pattern-triggered immune signaling. *Plant Physiol.* **177**, 1679–1690 (2018).
11. Zhang, L. et al. Distinct immune sensors for fungal endopolygalacturonases in closely related Brassicaceae. *Nat. Plants*, https://doi.org/10.1038/s41477-021-00982-2 (2021).
12. Fan, L. et al. Genotyping-by-sequencing-based identification of *Arabidopsis* pattern recognition receptor RLP32 recognizing proteobacterial translation initiation factor IF1. Preprint at https://doi.org/10.1101/2021.03.04.433884 (2021).
13. Böttcher, C. et al. The multifunctional enzyme CYP71B15 (PHYTOALEXIN DEFICIENT3) converts cysteine-indole-3-acetonitrile to camalexin in the indole-3-acetonitrile metabolic network of *Arabidopsis thaliana*. *Plant Cell* **21**, 1830–1845 (2009).
14. Mishina, T. E. & Zeier, J. The *Arabidopsis* flavin-dependent monooxygenase FMO1 is an essential component of biologically induced systemic acquired resistance. *Plant Physiol.* **141**, 1666–1675 (2006).
15. Böhm, H. et al. A conserved peptide pattern from a widespread microbial virulence factor triggers pattern-induced immunity in *Arabidopsis*. *PLoS Pathog.* **10**, e1004491 (2014).
16. Sun, X. et al. Pathogen effector recognition-dependent association of NRG1 with EDS1 and SAG101 in TNL receptor immunity. *Nat. Commun.* **12**, 3335 (2021).
17. Lapin, D. et al. A coevolved EDS1–SAG101–NRG1 module mediates cell death signaling by TIR-domain immune receptors. *Plant Cell* **31**, 2430–2455 (2019).
18. Cui, H. et al. A core function of EDS1 with PAD4 is to protect the salicylic acid defense sector in *Arabidopsis* immunity. *New Phytol.* **213**, 1802–1817 (2017).
19. Wagner, S. et al. Structural basis for signaling by exclusive EDS1 heteromeric complexes with SAG101 or PAD4 in plant innate immunity. *Cell Host Microbe* **14**, 619–630 (2013).
20. Bhandari, D. D. et al. An EDS1 heterodimer signalling surface enforces timely reprogramming of immunity genes in *Arabidopsis*. *Nat. Commun.* **10**, 772 (2019).
21. Joglekar, S. et al. Chemical activation of EDS1/PAD4 signaling leading to pathogen resistance in *Arabidopsis*. *Plant Cell Physiol.* **59**, 1592–1607 (2018).
22. Saile, S. C. et al. Two unequally redundant "helper" immune receptor families mediate *Arabidopsis thaliana* intracellular "sensor" immune receptor functions. *PLoS Biol.* **18**, e3000783 (2020).
23. Reuter, L. et al. Light-triggered and phosphorylation-dependent 14-3-3 association with NONPHOTOTROPIC HYPOCOTYL 3 is required for hypocotyl phototropism. Preprint at https://doi.org/10.1101/2021.04.09.439179 (2021).
24. Koenig, D. et al. Long-term balancing selection drives evolution of immunity genes in *Capsella*. *eLife* **8**, e43606 (2019).
25. Guo, Y. L. et al. Genome-wide comparison of nucleotide-binding site-leucine-rich repeat-encoding genes in *Arabidopsis*. *Plant Physiol.* **157**, 757–769 (2011).
26. 1001 Genomes Consortium. 1,135 Genomes reveal the global pattern of polymorphism in *Arabidopsis thaliana*. *Cell* **166**, 481–491 (2016).
27. Cao, J. et al. Whole-genome sequencing of multiple *Arabidopsis thaliana* populations. *Nat. Genet.* **43**, 956–963 (2011).
28. Lin, Z. J., Liebrand, T. W., Yadeta, K. A. & Coaker, G. PBL13 is a serine/threonine protein kinase that negatively regulates *Arabidopsis* immune responses. *Plant Physiol.* **169**, 2950–2962 (2015).
29. Thomma, B. P., Nürnberger, T. & Joosten, M. H. Of PAMPs and effectors: the blurred PTI–ETI dichotomy. *Plant Cell* **23**, 4–15 (2011).
30. Gust, A. A., Pruitt, R. & Nürnberger, T. Sensing danger: key to activating plant immunity. *Trends Plant Sci.* **22**, 779–791 (2017).

Methods

Plant material

All *Arabidopsis* mutants used in this study were in the *A. thaliana* Col-0 ecotype and are listed in Supplementary Table 3. Complemented transgenic lines and their respective mutant backgrounds are described in Supplementary Table 3. *Arabidopsis* plants were grown in soil in climate chambers under short day conditions (8 h/16 h (light/dark), 150 µmol m^{-2} s^{-1} white fluorescent light, 40–60% humidity, 22 °C). *N. benthamiana* wild-type plants were grown in soil in either a greenhouse or climate chambers under 12 h/12 h light/dark cycle at 60–70% humidity and 24–26 °C.

Elicitors used in this study

Flg22, elf18, nlp20 and pg13(At) peptides were synthesized according to the published sequences[11,15,31,32] by Genscript, prepared as 10 mM stock solutions in DMSO and diluted in ddH_2O before use. Full-length IF1 from *Escherichia coli* was synthesized by Genscript as a biotinylated fusion protein and resuspended in ddH_2O as a 1 mM stock solution[12]. The RLP1 elicitor eMax was originally identified in *Xanthomonas*[33]. We found that eMax is also present in other Proteobacteria including *Lysobacter*. Here we used eMax partially purified from the *Lysobacter* strain Root690 (ref. [34]). *Lysobacter* was grown in SOB medium overnight at 28 °C with shaking at 200 r.p.m. and collected by centrifugation. The pellet was resuspended in 50 mM MES, pH 5.7, and 50 mM NaCl, and cells were lysed by sonication, after which the supernatant was fractionated using a HiTrapQ FF (Cytiva) anion-exchange column. An eMax-containing fraction with high ethylene-inducing activity on *fls2 efr* leaves, but no activity on *rlp1* leaves[33]was used for the RLCK-VII mutant screen as shown in Extended Data Fig. 1a.

Measurement of ethylene production

Leaves of 6-week-old *Arabidopsis* plants were cut into pieces (about 0.5 × 0.5 cm) and floated on H_2O overnight. For Extended Data Fig. 4c, leaves were floated on either water or 100 nM thaxtomin A. Three leaf pieces were incubated in a sealed 6.5-ml glass tube with 0.4 ml of 50 mM MES buffer, pH 5.7, and the indicated elicitor. Ethylene accumulation was measured after 4 h by gas chromatographic analysis (GC-14A; Shimadzu) of 1 ml of the air drawn from the closed tube with a syringe.

Measurement of ROS production

ROS assays were performed as previously described[31,35]. Leaves of 5-week-old *Arabidopsis* plants were cut into pieces of equal size and floated on H_2O overnight. One leaf piece per well was transferred to a 96-well plate containing 20 µM L-012 (Wako Pure Chemical Industries) and 2 µg ml^{-1} peroxidase. Luminescence was measured over 1 h following elicitation or mock treatment using a Mithras LB 940 luminometer (Berthold Technologies). Total relative light unit production was determined by calculating the area under the scatter curve for 30 min post-elicitation.

Measurement of elicitor-induced callose deposition

Leaves of 5-week-old *Arabidopsis* plants were infiltrated with 500 nM elicitor and incubated for 16 h. Leaves were bleached with 95% ethanol and stained with aniline blue as described[36]. Images were collected at a magnification of ×64 on an AxioZoom.V16 microscope equipped with an AxioCam503 colour camera (Zeiss) and a DAPI filter (excitation filter: 390 nM, emission filter: 460 nM) using ZenBlue software. Image colours were inverted and converted to black and white. Black pixels indicating callose were counted with ImageJ.

MAPK activation

Arabidopsis leaves (4.5–6-week old) were infiltrated with water, 1 or 0.5 µM nlp20, or 1 µM flg22. At the indicated time points, leaves were harvested and frozen in liquid nitrogen. MAPK activation was assessed by blotting with a phospho-specific p44-p42 antibody (1:3,000; Cell Signaling) as previously described[37].

Seedling growth inhibition

Sterilized seeds were placed on ½ MS plates (1% sucrose, 0.8% agar). After vernalization, seeds were incubated in a long day chamber (16 h/8 h (light/dark), 150 µmol $m^{-2}s^{-1}$ white fluorescent light, 22 °C). After 5 d, seedlings were transferred to ½ MS with 1% sucrose, 10 mM NaCl, 0.01% BSA and 100 nM elf18 or flg22. After 7 d, seedlings were blotted dry and fresh weight was measured. Nlp20 does not cause seedling growth inhibition and thus was not tested here[15].

Quantitative reverse transcription PCR

Leaves from 6-week-old *Arabidopsis* plants were infiltrated with water (mock) or the indicated elicitors. Total RNA was isolated from leaves harvested at the indicated time point using the NucleoSpin RNA Plus Kit (Macherey-Nagel). cDNA was synthesized from 2 µg of total RNA using the RevertAid First Strand cDNA Synthesis Kit (Thermo Scientific). Quantitative PCRs and measurements were performed with a CFX384 Real-Time PCR detection system or an iQ5 Multi-Colour Real-Time PCR detection system (Bio-Rad) using the SYBR Green Fluorescein Mix (Thermo Scientific) and the primers listed in Supplementary Table 4. Transcript levels of target genes were normalized to the transcript levels of the housekeeping genes *EF1a* or *UBIQUITIN 5*.

Pathogenicity assays

Pst DC3000 inoculations were performed as described[15]. For induced resistance assays, leaves of 4–6-week-old *Arabidopsis* plants were infiltrated with 1 µM nlp20, 1 µM flg22 or mock-treated 24 h before bacterial infection. Leaves were infiltrated with *Pst* DC3000 or *Pst* DC3000 AvrRPS4 at a density of 10^4 cell per ml and bacterial growth was quantified after 3 d.

Cloning of recombinant PBL31

PBL31 and *PBL31*^{K201A} were cloned into pDEST15 and transformed into BL21-AI (Thermo Scientific). Cultures were grown at 37 °C to OD_{600} = 0.3 and then transferred to 17 °C. Expression was induced with 0.2% L-arabinose when the culture reached OD_{600} = 0.6 and incubated overnight. The recombinant proteins were purified by immobilized metal ion affinity chromatography using a HisTrap HP column (Cytiva) and then dialysed against 20 mM Tris, pH 8, and 100 mM NaCl. Proteins were diluted to 0.25 mg ml^{-1} and treated with 200 U ml^{-1} calf intestinal phosphatase (Sigma) or mock-treated for 3 h at 37 °C in the presence of 1× calf intestinal phosphatase buffer (Sigma). Samples were analysed by anti-His protein blot (Abcam).

N. benthamiana and *Arabidopsis* IPs and protein blotting

Leaves of *N. benthamiana* were transiently transformed with the indicated constructs and harvested after 2–3 d. For the elicitor-treated samples, leaves were infiltrated with water or 1 µM nlp20 10 min before harvesting. IPs were performed with 200–250 mg of tissue. Tagged proteins were immunoprecipitated for 1 h at 4 °C using GFP-Trap beads (ChromoTek) as previously described[38,39]. Protein blotting was performed using antibodies to GFP (1:4,000; Torrey Pines Biolabs), HA (1:2,000; Sigma) or Myc (1:5,000; Sigma). For Extended Data Fig. 7b, d, protein blotting was performed using antibodies to GFP (1:1,500; Roche) and HA (1:2,000; Roche).

Immunoblotting was used to check the background levels of FLS2 (1:2,000; Agrisera), BAK1 (1:10,000; Agrisera), MPK3 (1:5,000; Sigma), MPK4 (1:1,000; Sigma) and MPK6 (1:1,000; Sigma) in 5–6-week-old *Arabidopsis*. For split luciferase (Luc) experiments, protein abundance was checked with Luc and CLuc antibodies (1:5,000; Sigma). *Arabidopsis* plants (4.5-week old) containing *p35S::StrepII-3×HA-YFP* (Col-0), *pPAD4::YFP-PAD4* (*pad4-1 sag101-3* background) or *pSAG101::SAG101-YFP* (*pad4-1 sag101-3* background) were

syringe-infiltrated with mock (DMSO) or 0.5 µM nlp20 and harvested after 10 min or 3 h. Protein extraction and IP using anti-GFP agarose beads (Chromotek) were performed as previously described[16]. Protein quality in inputs was checked on immunoblots (Extended Data Fig. 9c) using antibodies to GFP (1:2,500; Roche).

Ratiometric bimolecular fluorescence complementation

The coding sequences of SOBIR1, ADR1, ADR1-L1 and ADR1-L2 were cloned into the 2in1 bimolecular fluorescence complementation CC gateway-compatible destination vector[40,41]. Destination vectors were transiently expressed in *N. benthamiana*, and complementation of YFP was analysed at 24 h after infection with the confocal laser scanning microscope LSM880 (Zeiss) using a ×63 water-immersion objective. Settings were as follows: YFP was excited using a 514-nm laser, collecting emission between 516 and 556 nm; RFP was excited using a 561-nm laser with an emission spectrum of 597–634 nm. Images were processed with ZENblue software (Zeiss) for adjustment of brightness and contrast.

Split Luc assays

Firefly Luc complementation assays were performed as previously described[42]. In brief, the cDNA of indicated genes were amplified and cloned into 35S-pCAMBIA1300-Nluc or 35S-pCAMBIA1300-Cluc. The *A. tumefaciens* strain GV3101 carrying these plasmids was infiltrated into *N. benthamiana* leaves. After 48 h of infiltration, leaf discs were taken and incubated with 1 mM luciferin in a 96-well plate. The Luc activity was measured by the EnSpire Multimode Plate Reader (Perkin Elmer). Protein expression was detected by immunoblot against CLuc and Luc (Sigma) (Extended Data Fig. 7f).

FRET-FLIM

For FRET-FLIM analysis, C-terminal GFP fusions of SOBIR1 (pSol2095)[43] and PBL31 (in PGWB5 (ref. [44])) were used as donor constructs. C-terminal RFP fusions of SOBIR1, PBL31, PAD4, EDS1, SAG101, ADR1, ADR1-L1 and ADR1-L2 (in pB7RWG2 (ref. [45])) were used as acceptors. N-terminally tagged RFP–NPH3^{S744A} (in pB7WGR2 (refs. [23,45])) served as a plasma membrane-associated control; the S744A mutation blocks light-triggered dissociation from the plasma membrane[23]. EDS1–HA and PAD4–HA were expressed from pGWB14 (ref. [44]). These binary vectors and a p19-expressing construct as silencing inhibitor were transformed into the *A. tumefaciens* strain GV3101. For transformation of *N. benthamiana* leaves, *Agrobacterium* cultures were adjusted to an OD_{600} of 0.2 in infiltration medium, and a 1:1:1(:1) mixture was infiltrated into leaves of 3–4-week-old plants. FLIM measurements were performed, according to a modified protocol of ref. [46], 26–48 h after infiltration on a SP8 confocal laser scanning microscope (Leica Microsystems) with Leica Microsystems Application Suite software and a FastFLIM upgrade from PicoQuant consisting of Sepia Multichannel Picosecond Diode Laser, PicoQuant Timeharp 260, TCSPC Module and Picosecond Event Timer (Picoquant). Imaging was done by using a ×63/1.20 water-immersion objective and focusing on the plasma membrane of the abaxial epidermal cells. The presence of the fluorophores was shown by excitation with 488 nm or 561 nm, and 500–550-nm or 600–650-nm detection range for GFP or RFP, respectively. HA-tagged proteins were detected by western blot analysis. Colocalization was demonstrated by reading out signal intensities over the plasma membrane. As laser power and gain were varied, the intensities do not reflect the absolute expression levels towards each other but validate the colocalization at the plasma membrane. The GFP FLT τ [ns] in cells co-expressing different constructs was determined by excitation with a pulsed laser with a 470-nm wavelength and a repetition rate of 40 MHz. The maximal count rate was set to about 10,000 kCnts s^{-1} and photons were collected until 500 photons in the brightest pixel were reached at a resolution of 256 × 256 pixels. Data processing was performed with SymPhoTime software. A region of interest covering the plasma membrane was defined and FLT [ns] was determined by biexponential curve fitting and a correction for the instrument response function.

FRET-FLIM data are derived from at least three independent biological replicates with a total sample size of $n \geq 11$ per FRET pair or donor-only control. All sample numbers and statistical analysis data can be found in Supplementary Table 5. As cell death, which was a problem in several co-expression combinations, correlates with high A[2] values, samples were only included in the analysis when the A[1] [kCnts] to A[2] [kCnts] ratio was above 1; the other measurements were discarded. As data were not equally distributed, a Wilcoxon or Kruskal–Wallis test was performed, followed by a post-hoc test (Steel–Dwass all-pairs comparison).

Preparation of peptides for LC–MS/MS, data acquisition and data analyses

Proteins (from GFP-trap enrichment) were submitted to an on-bead digestion. In brief, dry beads were re-dissolved in 25 µl digestion buffer 1 (50 mM Tris, pH 7.5, 2M urea, 1 mM DTT and 5 ng $µl^{-1}$ trypsin) and incubated for 30 min at 30 °C in a Thermomixer with 400 r.p.m. Next, beads were pelleted and the supernatant was transferred to a fresh tube. Digestion buffer 2 (50 mM Tris, pH 7.5, 2M urea and 5 mM CAA) was added to the beads. After mixing, the beads were pelleted and supernatants were collected. Combined supernatants were incubated overnight at 32 °C in a Thermomixer with 400 r.p.m.; samples were protected from light during incubation. The digestion was stopped by adding 1 µl TFA and desalted with C18 Empore disc membranes according to the StageTip protocol[47]. Dried peptides were re-dissolved in 2% ACN and 0.1% TFA (10 µl) and diluted to 0.2 µg $µl^{-1}$ for analysis. Samples were analysed using an EASY-nLC 1000 (Thermo Fisher) coupled to a Q Exactive mass spectrometer (Thermo Fisher). Peptides were separated on 16-cm frit-less silica emitters (New Objective; with an inner diameter of 75 µm), packed in-house with reversed-phase ReproSil-Pur C18 AQ 1.9 µm resin (Dr. Maisch). Peptides were loaded on the column and eluted for 115 min using a stepwise linear gradient of 5% to 95% solvent B (0–5 min, 0-5% B; 5–65 min, 5-20% B; 65–90 min, 20-35% B; 90–100 min, 35-55% B; 100–105 min, 55-95% B; 105–115 min, 95% B) (solvent A 0% ACN and 0.1% FA; solvent B 80% ACN and 0.1% FA) at a flow rate of 300 nl min^{-1}. Mass spectra were acquired in data-dependent acquisition mode with a TOP15 method. MS spectra were acquired in the Orbitrap analyser with a mass range of 300–1,750 m/z at a resolution of 70,000 FWHM and a target value of 3×10^6 ions. Precursors were selected with an isolation window of 2.0 m/z. HCD fragmentation was performed at a normalized collision energy of 25. MS/MS spectra were acquired with a target value of 10^5 ions at a resolution of 17,500 FWHM, a maximum injection time of 55 ms and a fixed first mass of m/z 100. Peptides with a charge of +1, greater than 6 or with unassigned charge state were excluded from fragmentation for MS2; dynamic exclusion for 30 s prevented repeated selection of precursors. Raw data were processed using MaxQuant software (version 1.6.3.4; http://www.maxquant.org/)[48] with label-free quantification (LFQ) and iBAQ enabled[49]. MS/MS spectra were searched by the Andromeda search engine against a combined database containing the sequences from *A. thaliana* (TAIR10_pep_20101214; https://www.arabidopsis.org/download/index-auto.jsp?dir=%2Fdownload_files%2FProteins%2FTAIR10_protein_lists) and sequences of 248 common contaminant proteins and decoy sequences. Trypsin specificity was required and a maximum of two missed cleavages were allowed. The minimal peptide length was set to seven amino acids. Carbamidomethylation of cysteine residues was set as fixed, and oxidation of methionine and protein N-terminal acetylation were set as variable modifications. Peptide spectrum matches and proteins were retained if they were below a false discovery rate of 1%. Statistical analysis of the MaxLFQ values was carried out using Perseus (version 1.5.8.5; http://www.maxquant.org/). Quantified proteins were filtered for reverse hits and hits 'identified by site', and MaxLFQ values were $\log_2$ transformed. After grouping samples by condition, only those proteins that had three valid

values in one of the conditions were retained for the subsequent analysis. Two-sample *t*-tests were performed using a permutation-based false discovery rate of 5%. Alternatively, quantified proteins were grouped by condition and only those hits that had four valid values in one of the conditions were retained. Missing values were imputed from a normal distribution (1.8 downshift, separately for each column). Volcano plots were generated in Perseus using a false discovery rate of 0.05 and an S0 = 1. The Perseus output was exported and further processed using Excel (Supplementary Tables 1, 2). The MS proteomics data have been deposited to the ProteomeXchange Consortium[50] via the PRIDE[51] partner repository with the dataset identifier PXD026120.

Conservation analysis of LRR-RKs, LRR-RPs and NLRs in *Arabidopsis*

Illumina reads from 80 *Arabidopsis* accessions from the first phase study of the 1001 Genomes project[26,27] were mapped to the reference genome of Col-0 using version 0.7.15-r1140 of the BWA-backtrack algorithm[52] with parameters: $k = 1$ in bwa aln command; $n = 10{,}000$; with the maximal number of mismatches allowed being 1. Paired-end information was discarded. The TAIR10 assembly of the *Arabidopsis* Col-0 genome was used for the reference genome (https://arabidopsis.org). The output mapped files were processed with samtools mpileup version 1.9 (ref. [53]); parameters: *aa*; $d = 10{,}000$; $Q = 0$. A total list of 163 NLR genes was used in the analysis, which was based on 159 NLR genes previously identified[25] and 4 additional, manually curated genes (*AT1G63860*, *AT1G72920*, *AT1G72930* and *AT5G45230*). The coding sequence (CDS) portions of the genes were extracted, defined as the union of all the CDS models of the gene based on the TAIR10 annotation. Fractions of the CDS sequence with non-zero coverage were calculated for each gene–accession combination (hereafter known as 'coverage fractions'). Genes were assigned into conserved, complex and presence/absence categories using a threshold-based approach. To define thresholds, *k* means algorithm was initiated with three centres at 0, 0.5 and 1 and applied to the coverage fractions, resulting in thresholds at 0.37 and 0.81. Coverage fractions were then discretized by applying these thresholds into 'absent', 'intermediate' and 'present' categories, from lowest to highest values. NLR genes were assigned as conserved if there were no accessions with 'absent' coverage and at least 95% of all accessions had high coverage. Genes with more than 5% of accessions having 'intermediate' coverage values were assigned as complex, and genes that were absent in at least one accession not classified as complex, were assigned as presence/absence. This procedure was also applied to LRR-RP-encoding genes[54] and LRR-RK-encoding genes[55]. The conserved category does not necessarily imply functional or structural conservation but is used in the genomic sense to indicate sequence conservation, as measured by the presence of sub-sequences whose identities are within the applied thresholds.

Data analysis

No statistical methods were used to predetermine sample size. The experiments were not randomized. The investigators were not blinded to allocation during experiments and outcome assessment. Data were plotted using R Studio (https://www.r-project.org/) or Microsoft Office Excel. Data were represented as the mean ± s.e.m. or as box-and-whisker plots in which the centre line indicates the median, the bounds of the box indicate the 25th and 75th percentiles, and the whiskers indicate 1.5 × the interquartile range between the 25th and the 75th percentile. Statistical analyses were performed using R Studio/R or JMP (SAS). Unless otherwise stated, graphs present data from a single experiment. Data were tested for normal distribution with Shapiro–Wilk test and equal variance with Fligner–Killeen (R) or Levene's test (JMP). Data with non-normal distribution were tested for significant differences using two-sided Wilcoxon rank-sum test with continuity correction (for two groups) or Kruskal–Wallis test with a post-hoc two-sided Steel–Dwass test (for more than two groups). For Extended Data Fig. 1a, the Steel–Dwass test revealed no significant differences between genotypes as this test is very stringent with large group sizes and small sample numbers (*n*). We therefore further performed two-sided Wilcoxon rank-sum pairwise tests, which are not affected by group size. Data with normal distribution were analysed with a two-sided Student's *t*-test or, if variances were unequal, a two-sided Welch's *t*-test. A summary of statistical analyses is provided in Supplementary Table 5. Data and statistical analysis for MS analyses are provided in Supplementary Tables 1, 2.

Reporting summary

Further information on research design is available in the Nature Research Reporting Summary linked to this paper.

Data availability

All data are available within this article and its Supplementary Information. Proteomics data are available via the ProteomeXchange Consortium with the identifier PXD026120. MS data were searched against a combined database containing protein sequences from *A. thaliana* TAIR10_pep_20101214 (https://www.arabidopsis.org/download/index-auto.jsp?dir=%2Fdownload_files%2FProteins%2FTAIR10_protein_lists). Genomics data from *A. thaliana* accessions were obtained from the 1001 Genomes project (https://1001genomes.org/data-center.html) and mapped to the TAIR10 assembly of the genome (https://arabidopsis.org). Original gel blots are shown in Supplementary Fig. 1. Statistical analyses for all quantitative data are provided in Supplementary Tables 1, 2 and 5. Source data are provided with this paper.

31. Felix, G., Duran, J. D., Volko, S. & Boller, T. Plants have a sensitive perception system for the most conserved domain of bacterial flagellin. *Plant J.* **18**, 265–276 (1999).
32. Kunze, G. et al. The N terminus of bacterial elongation factor Tu elicits innate immunity in *Arabidopsis* plants. *Plant Cell* **16**, 3496–3507 (2004).
33. Jehle, A. K. et al. The receptor-like protein ReMAX of *Arabidopsis* detects the microbe-associated molecular pattern eMax from *Xanthomonas*. *Plant Cell* **25**, 2330–2340 (2013).
34. Bai, Y. et al. Functional overlap of the *Arabidopsis* leaf and root microbiota. *Nature* **528**, 364–369 (2015).
35. Albert, M. et al. Regulation of cell behaviour by plant receptor kinases: pattern recognition receptors as prototypical models. *Eur. J. Cell Biol.* **89**, 200–207 (2010).
36. Jin, L. & Mackey, D. M. Measuring callose deposition, an indicator of cell wall reinforcement, during bacterial infection in *Arabidopsis*. *Methods Mol. Biol.* **1578**, 195–205 (2017).
37. Willmann, R., Haischer, D. J. & Gust, A. A. Analysis of MAPK activities using MAPK-specific antibodies. *Methods Mol. Biol.* **1171**, 27–37 (2014).
38. Chinchilla, D. et al. A flagellin-induced complex of the receptor FLS2 and BAK1 initiates plant defence. *Nature* **448**, 497–500 (2007).
39. El Kasmi, F. et al. Signaling from the plasma-membrane localized plant immune receptor RPM1 requires self-association of the full-length protein. *Proc. Natl Acad. Sci. USA* **114**, E7385–E7394 (2017).
40. Grefen, C. & Blatt, M. R. A 2in1 cloning system enables ratiometric bimolecular fluorescence complementation (rBiFC). *Biotechniques* **53**, 311–314 (2012).
41. Mehlhorn, D. G., Wallmeroth, N., Berendzen, K. W. & Grefen, C. 2in1 vectors improve in planta BiFC and FRET analyses. *Methods Mol. Biol.* **1691**, 139–158 (2018).
42. Chen, H. et al. Firefly luciferase complementation imaging assay for protein–protein interactions in plants. *Plant Physiol.* **146**, 323–324 (2008).
43. Liebrand, T. W. et al. Receptor-like kinase SOBIR1/EVR interacts with receptor-like proteins in plant immunity against fungal infection. *Proc. Natl Acad. Sci. USA* **110**, 10010–10015 (2013).
44. Nakagawa, T. et al. Development of series of gateway binary vectors, pGWBs, for realizing efficient construction of fusion genes for plant transformation. *J. Biosci. Bioeng.* **104**, 34–41 (2007).
45. Karimi, M., Inzé, D. & Depicker, A. GATEWAY vectors for *Agrobacterium*-mediated plant transformation. *Trends Plant Sci.* **7**, 193–195 (2002).
46. Glöckner, N. et al. Three-fluorophore FRET enables the analysis of ternary protein association in living plant cells. Preprint at https://doi.org/10.1101/722124 (2020).
47. Rappsilber, J., Ishihama, Y. & Mann, M. Stop and go extraction tips for matrix-assisted laser desorption/ionization, nanoelectrospray, and LC/MS sample pretreatment in proteomics. *Anal. Chem.* **75**, 663–670 (2003).
48. Cox, J. & Mann, M. MaxQuant enables high peptide identification rates, individualized p.p.b.-range mass accuracies and proteome-wide protein quantification. *Nat. Biotechnol.* **26**, 1367–1372 (2008).
49. Tyanova, S., Temu, T. & Cox, J. The MaxQuant computational platform for mass spectrometry-based shotgun proteomics. *Nat. Protoc.* **11**, 2301–2319 (2016).
50. Deutsch, E. W. et al. The ProteomeXchange consortium in 2020: enabling 'big data' approaches in proteomics. *Nucleic Acids Res.* **48**, D1145–D1152 (2020).
51. Perez-Riverol, Y. et al. The PRIDE database and related tools and resources in 2019: improving support for quantification data. *Nucleic Acids Res.* **47**, D442–D450 (2019).

52. Li, H. & Durbin, R. Fast and accurate short read alignment with Burrows–Wheeler transform. *Bioinformatics* **25**, 1754–1760 (2009).
53. Li, H. et al. The Sequence Alignment/Map format and SAMtools. *Bioinformatics* **25**, 2078–2079 (2009).
54. Wang, G. et al. A genome-wide functional investigation into the roles of receptor-like proteins in *Arabidopsis*. *Plant Physiol*. **147**, 503–517 (2008).
55. Shiu, S. H. et al. Comparative analysis of the receptor-like kinase family in *Arabidopsis* and rice. *Plant Cell* **16**, 1220–1234 (2004).
56. Kurup, S. et al. Marking cell lineages in living tissues. *Plant J.* **42**, 444–453 (2005).

Acknowledgements This work was supported by Deutsche Forschungsgemeinschaft (DFG) grants Nu 70/15-1 and ERA-CAPS-Grant SICOPID Nu 70/16-1 to T.N.; grant CRC-1101 to K.H., C.O., D.W., F.E.K. and T.N., and grant CRC-1403-414786233 to J.E.P. S. C. Saile was supported by the Reinhard Frank Stiftung (Project 'helperless plant'). F.L., J.E.P., H.N., D.K. and D.W. were supported by the Max Planck Society. We thank S. Harter, M. Fechter, B. Löffelhardt and V. Scholz for assistance with cloning and genotyping; B. Kemmerling for statistical data evaluation; E. Chae for annotation information of NLRs; and P. Schulze-Lefert for the *Lysobacter* strain Root690.

Author contributions R.N.P., M.H.A.J.J., B.P.H.J.T., J.L.D., F.E.K., J.E.P. and T.N. conceived and conceptualized the study. R.N.P., W.-L.W., M.H., S.R. and A.A.G. generated materials used in this study. R.N.P., K.F. and W.-L.W. performed the ethylene assays. R.N.P. and W.-L.W. performed the ROS assays. R.N.P., F.L., L.Z. and S. C. Saile performed co-IPs and western blots. R.N.P. performed the pathoassays. R.N.P., F.L. and C.H. performed the MAPK assays. A.J. performed the callose assays. R.N.P. and F.L. performed the RT–qPCR assays. S. C. Saile and F.E.K. performed the split-YFP assays. M.H. and J.-M.Z. performed the split firefly luciferase assays and analysed the data. F.W., C.O. and K.H. performed the FRET-FLIM assays and confocal microscopy and analysed the data. D.K. and D.W. performed the genetic analysis. Co-IP–MS experiments were designed by F.L., H.N. and J.E.P., executed by F.L. and A.H., and analysed by F.L., S. C. Stolze, H.N. and J.E.P. Statistical analysis was performed by R.N.P., F.L., S. C. Stolze and F.W. T.N. wrote the original draft of the paper. R.N.P., F.L., A.A.G., M.H.A.J.J., B.P.H.J.T., J.L.D., D.W., J.E.P. and T.N. reviewed and edited the paper.

Competing interests The authors declare no competing interests.

Additional information

Supplementary information The online version contains supplementary material available at https://doi.org/10.1038/s41586-021-03829-0.

Correspondence and requests for materials should be addressed to Jane E. Parker or Thorsten Nürnberger.

Peer review information *Nature* thanks Gitta Coaker and the other, anonymous, reviewer(s) for their contribution to the peer review of this work. Peer reviewer reports are available.

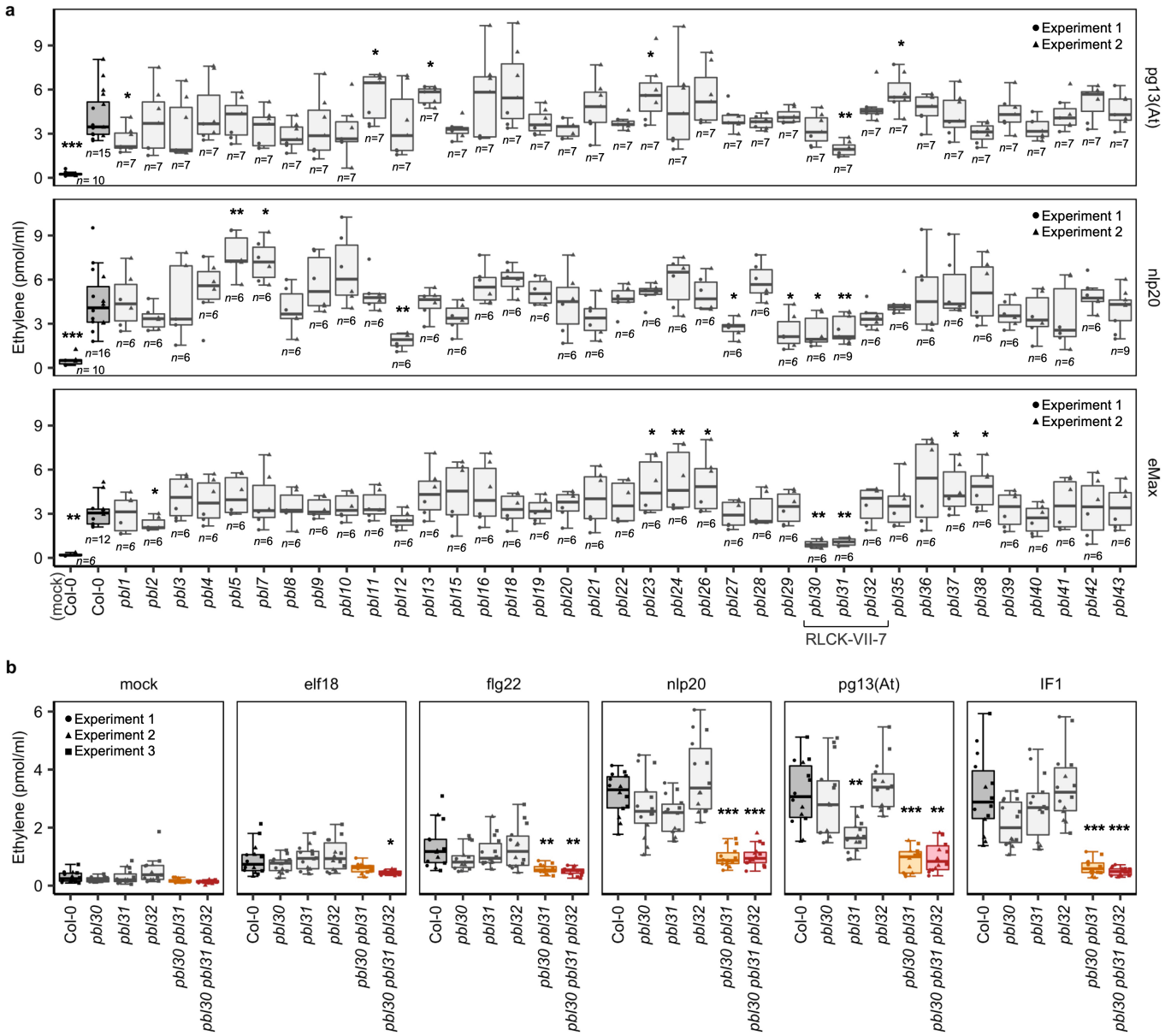

Extended Data Fig. 1 | LRR-RP-mediated ethylene responses are dependent on RLCK-VII-7 kinases PBL30 and PBL31. a, RLCK-VII mutant screen for positive regulators of LRR-RP signalling. $n \geq 6$, each from 3 leaf pieces. Exact n values are shown in the graph. Data are from 2 independent experiments. Two-sided Wilcoxon rank sum pairwise tests with continuity correction were used to analyse significant differences between elicitor-treated Col-0 and the indicated mutant (*$P \leq 0.05$, **$P \leq 0.01$). **b**, Elicitor-induced ethylene production in Col-0 and RLCK-VII-7 mutants. $n = 14$, each from 3 leaf pieces. Data are from 3 independent experiments. Statistical differences between Col-0 and the indicated mutants were analysed using a Kruskal–Wallis test with a post hoc two-sided Steel-Dwass test (*$P \leq 0.05$, **$P \leq 0.01$, ***$P \leq 0.0001$). Centre line: median, bounds of box: 25th and 75th percentiles, whiskers: 1.5 * IQR (IQR: the interquartile range between the 25th and the 75th percentile). Exact P values for all experiments are provided in Supplementary Table 5.

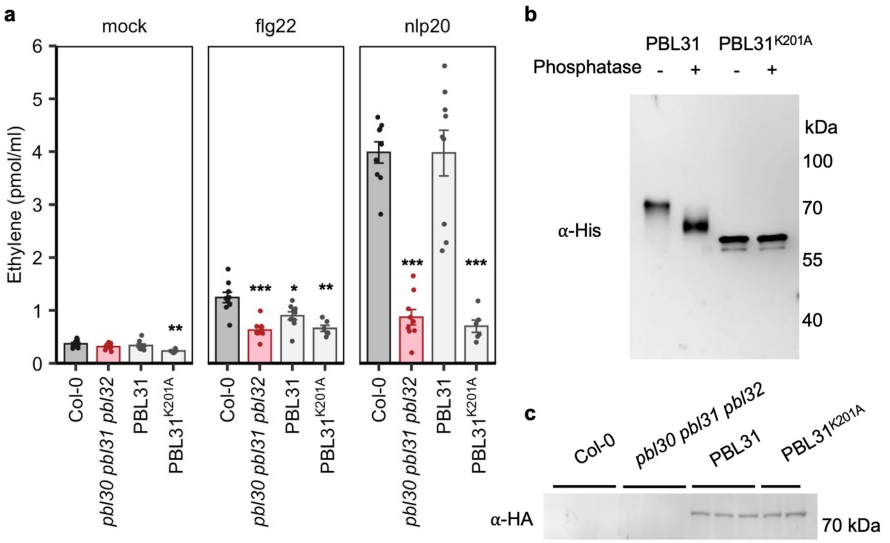

Extended Data Fig. 2 | PBL31 activity in RLP23 signalling requires its kinase activity. a, Ethylene accumulation in *pbl30 pbl31 pbl32* complemented with wild-type PBL31-HA (PBL31) or the kinase-dead variant PBL31^{K201A}-HA (PBL31^{K201A}). Bars indicate mean ethylene response ± s.e.m. For PBL31^{K201A}, $n = 6$; for all others, $n = 9$. A two-sided Welch's *t*-test was used to analyse significant differences between Col-0 and the indicated line for the given elicitor treatment (**$P \leq 0.01$, ***$P \leq 0.0001$). Exact *P* values are provided in Supplementary Table 5. The experiment was repeated 3 times with similar results. **b**, PBL31 has autokinase activity that is abolished in the PBL31^{K201A} mutant. Recombinant PBL31 and PBL31^{K201A} were subjected to SDS–PAGE followed by anti-His protein blot. PBL31^{K201A} runs near the predicted position for the tagged protein (57.4 kDa). The wild-type version migrates more slowly, consistent with it being auto-phosphorylated. Phosphorylation of the wild-type PBL31 was confirmed by treatment with calf intestinal phosphatase, which increased the migration rate of PBL31 but not PBL31^{K201A}. The experiment was repeated 2 times with similar results. **c**, Anti-HA protein blot with material from plants used in **a**. For gel source data, see Supplementary Fig. 1.

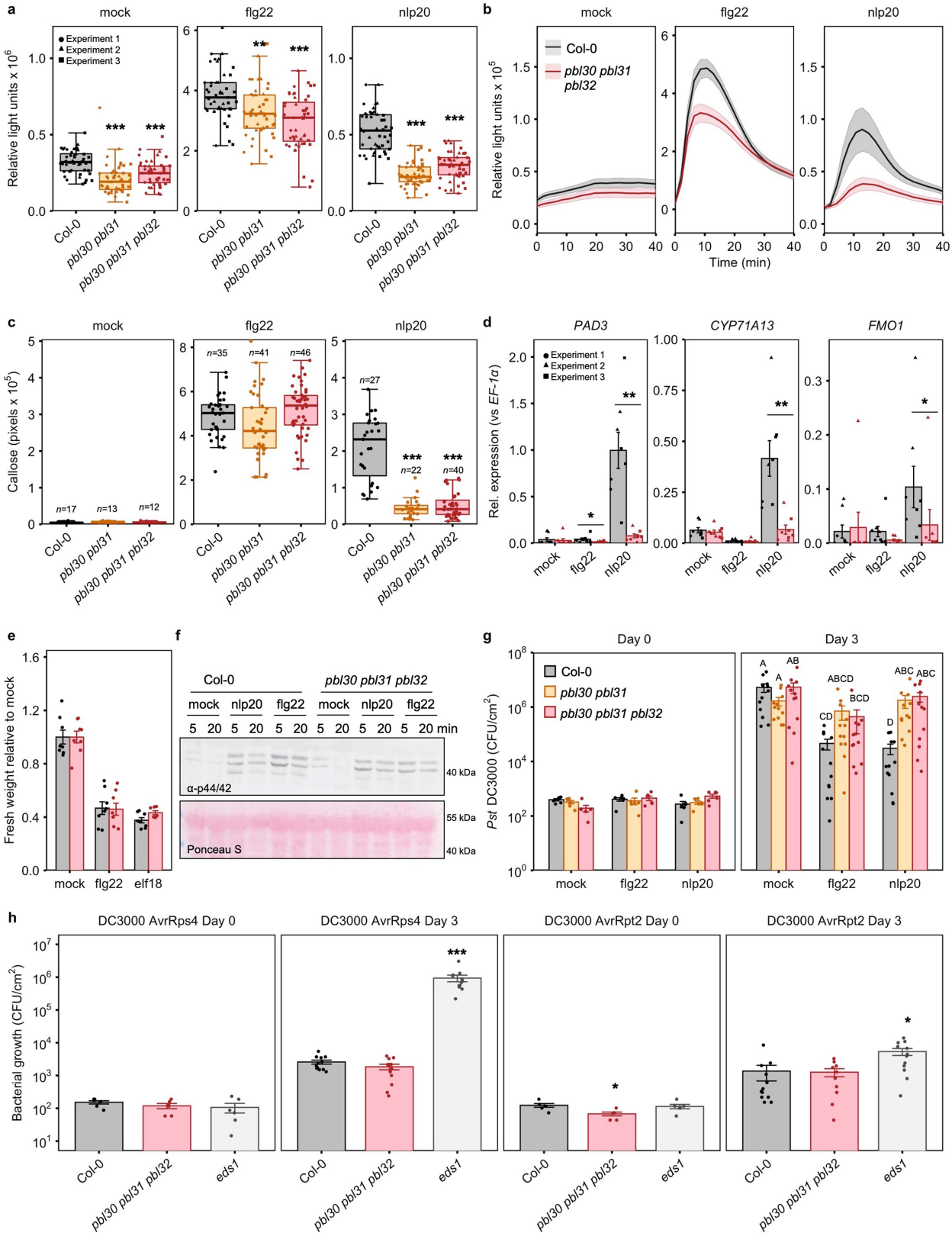

Extended Data Fig. 3 | See next page for caption.

Extended Data Fig. 3 | Immune responses of RLCK-VII-7 mutants treated with LRR-RP-recognized and LRR-RK-recognized elicitors. a, **b**, Elicitor-induced ROS production is impaired in *pbl30 pbl31 pbl32*. **a**, Total elicitor-induced ROS production over 30 min in Col-0, *pbl30 pbl31*, and *pbl30 pbl31 pbl32*. $n = 48$ leaf pieces from 3 independent experiments. For all panels *pbl30 pbl31* is in orange, *pbl30 pbl31 pbl32* is in pink. For **a**, **c**, **h**, statistical differences between Col-0 and the indicated mutants were analysed using a Kruskal–Wallis test with a post hoc two-sided Steel-Dwass test (*$P \leq 0.05$, **$P \leq 0.01$, ***$P \leq 0.0001$). **b**, Mean ROS production over time. Solid line, mean; shaded band, s.e.m.; $n = 16$ leaf pieces. **c**, Nlp20-induced callose deposition in Col-0 is dependent on PBL30 and PBL31. $n \geq 12$ images from at least 3 leaves; exact n values are indicated on the graph. **d**, Nlp20-induced expression of *PAD3*, *CYP71A13*, and *FMO1* is impaired in *pbl30 pbl31 pbl32* plants. Bars indicate mean expression relative to *EF-1α* 6 h after mock or elicitor treatment determined by qRT–PCR. $n = 8$ biological replicates from 3 independent experiments. A two-sided Wilcoxon rank sum test with continuity correction was used to analyse significant differences between Col-0 and *pbl30 pbl31 pbl32* for the given elicitor treatment (*$P \leq 0.05$, **$P \leq 0.01$). **e**, Relative fresh weight of 12 d-old Col-0 and *pbl30 pbl31 pbl32* seedlings grown in the presence of flg22 or elf18. No significant differences were observed between Col-0 and *pbl30 pbl31 pbl32* growth for any treatment ($P > 0.05$, two-sided Wilcoxon rank sum test with continuity correction). $n = 8$ biological replicates comprising 2 seedlings; for *pbl30 pbl31 pbl32* treated with elf18, $n = 7$. **f**, MAP kinase activation in Col-0 and *pbl30 pbl31 pbl32* treated with nlp20 or flg22 was analysed by immunoblot assay. Ponceau S-stained RUBISCO large subunit serves as a loading control. For gel source data, see Supplementary Fig. 1. **g**, Elicitor-induced defence against infection is impaired in *pbl30 pbl31* and *pbl30 pbl31 pbl32*. Leaves were infiltrated with the indicated elicitor and challenged with *Pst* DC3000 infection after 24 h. Bacterial colonization was assessed at Day 0 and Day 3. $n = 6$ (Day 0) or 12 (Day 3) biological replicates comprising 2 leaf discs. Bars with different letters indicate significant differences of $P \leq 0.05$ (Kruskal–Wallis test with post hoc two-sided Steel-Dwass test). No statistical differences were observed for Day 0. CFU, colony forming units. **h**, RLCK-VII-7 kinases are not required for an ETI response to *Pst* DC3000 *AvrRps4* or *Pst* DC3000 *AvrRpt2*. $n = 8$ (Day 0) or 12 (Day 3) biological replicates comprising 2 discs; for *pbl30 pbl31 pbl32* infected with *Pst* DC3000 *AvrRpt2* (Day 3), $n = 10$. Growth on *eds1* plants served as control. For box plots in **a**, **c**, centre line: median, bounds of box: 25th and 75th percentiles, whiskers: 1.5 * IQR. For **d**, **e**, **g**, **h** bars indicate mean ± s.e.m. Experiments in **b**, **c**, **e**–**h** were repeated at least three times with similar results. Exact P values for all quantitative experiments are provided in Supplementary Table 5.

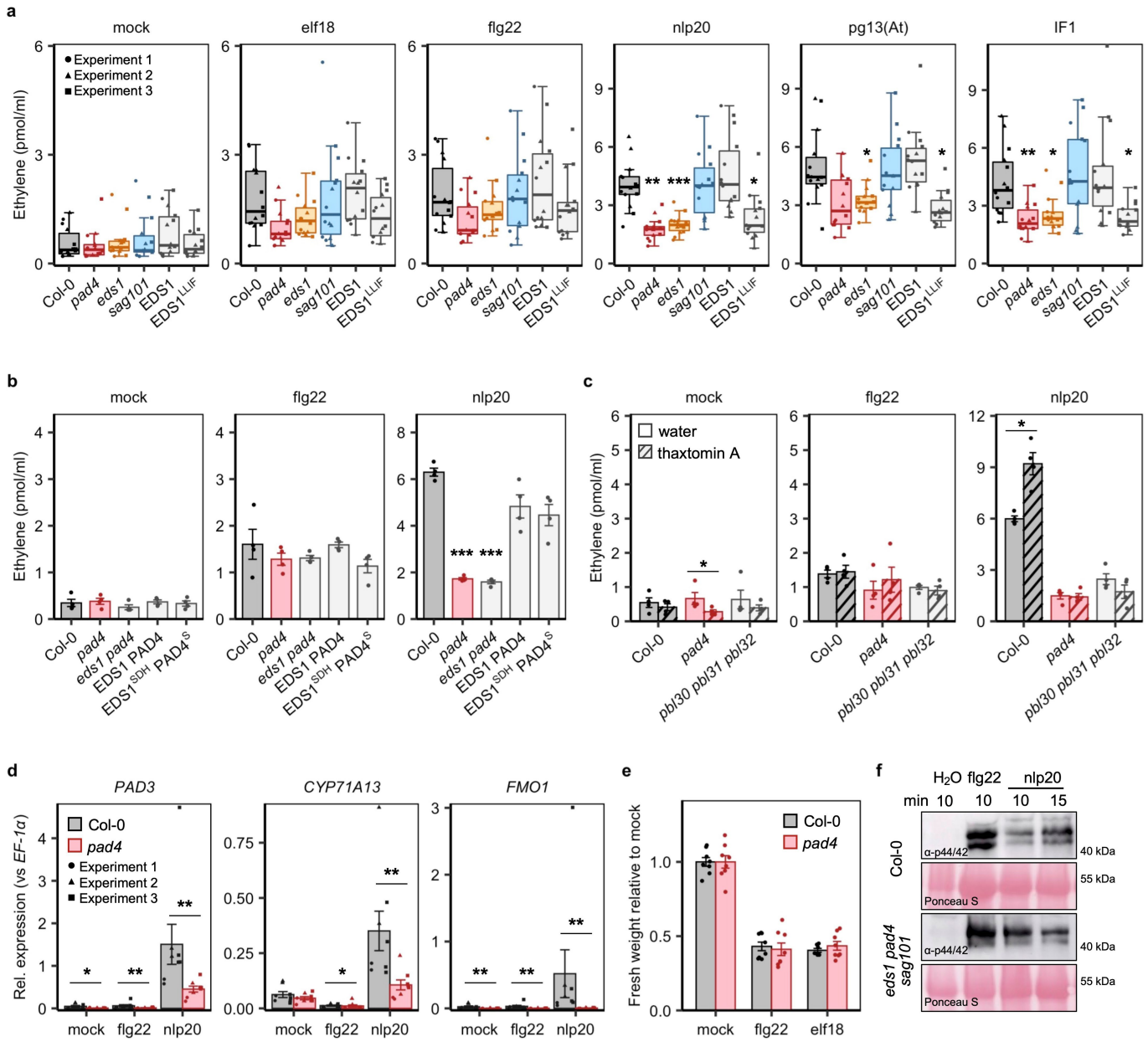

Extended Data Fig. 4 | PTI responses are partially dependent on PAD4 and EDS1. a, Elicitor-induced ethylene production in *pad4*, *eds1*, *sag101*, EDS1 and EDS1^{LLIF} lines. $n = 14$, each from 3 leaf pieces. Data are from 3 independent experiments. Statistical differences between Col-0 and the indicated mutants were analysed using a Kruskal–Wallis test with a post hoc two-sided Steel-Dwass test (*$P \leq 0.05$, **$P \leq 0.01$, ***$P \leq 0.0001$). Centre line: median, bounds of box: 25th and 75th percentiles, whiskers: 1.5 * IQR. **b**, Nlp20-induced ethylene production is not dependent on EDS1 and PAD4 putative lipase activity. The *eds1 pad4* is complemented with wild-type proteins (EDS1 PAD4) or variants harbouring mutations in their putative α/β-hydrolase catalytic residues (EDS1^{SDH} PAD4^{S})[19]. $n = 4$, each from 3 leaf pieces. Statistical differences between Col-0 and the indicated mutants were analysed by two-sided Welch's pairwise tests (**$P \leq 0.01$). For **b**–**e**, bars indicate mean ± s.e.m. **c**, Thaxtomin A pretreatment enhances nlp20-induced ethylene responses in Col-0 but not in *pad4* or *pbl30 pbl31 pbl32* mutants. $n = 4$, each from 3 leaf pieces. Statistical differences between water- and thaxtomin A-treated samples were analysed using a Kruskal–Wallis test with a post hoc two-sided Steel-Dwass test (*$P \leq 0.05$). **d**, Expression of *PAD3*, *CYP71A13* and *FMO1* 6 h after elicitor or mock treatment, determined by qRT–PCR. $n = 8$ biological replicates from 3 independent experiments. A two-sided Wilcoxon rank sum test with continuity correction was used to analyse significant differences between Col-0 and *pad4* for the given elicitor treatment (*$P \leq 0.05$, **$P \leq 0.01$). **e**, Relative fresh weight of 12 d-old Col-0 and *pad4* seedlings grown in the presence of flg22 or elf18. No significant differences were observed between Col-0 and *pad4* growth for any treatment (two-sided Wilcoxon rank sum test with continuity correction). $n = 8$ biological replicates comprising 2 seedlings; for Col-0 treated with elf18, $n = 7$. **f**, MAP kinase activation in Col-0 and *eds1 pad4 sag101* treated with nlp20 or flg22 was analysed by immunoblot assay. Ponceau S-stained RUBISCO large subunit serves as a loading control. For gel source data, see Supplementary Fig. 1. Experiments in **b**–**f** were performed at least three times with similar results. Exact *P* values for all quantitative experiments are provided in Supplementary Table 5.

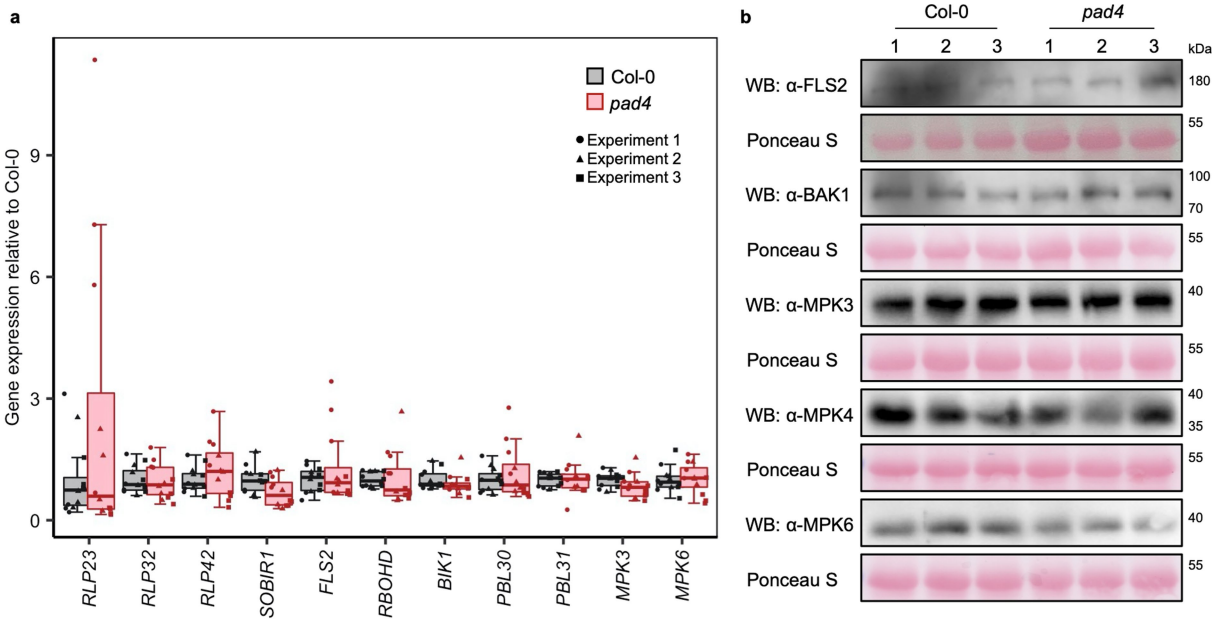

Extended Data Fig. 5 | Transcript and protein levels of immune-related genes in Col-0 and *pad4*. **a**, Background levels of a set of immune-related genes in naive Col-0 and *pad4*. Relative expression was determined by qRT–PCR. Expression was normalized to *EF-1α* transcript and set relative to Col-0. $n = 8$ biological replicates from 3 independent experiments. Centre line: median, bounds of box: 25th and 75th percentiles, whiskers: 1.5 * IQR. No significant differences were identified between Col-0 and *pad4* ($P > 0.05$, two-sided Wilcoxon rank sum test with continuity correction). Exact *P* values are provided in Supplementary Table 5. **b**, Protein levels of FLS2, BAK1, MPK3, MPK4, and MPK6 are similar in Col-0 and *pad4* plants. Leaves were taken from three 6-week-old plants (labelled 1-3) and endogenous protein levels were evaluated by protein blot. Ponceau S-stained RUBISCO large subunit serves as a loading control. For gel source data, see Supplementary Fig. 1. The experiment was repeated at least three times with similar results.

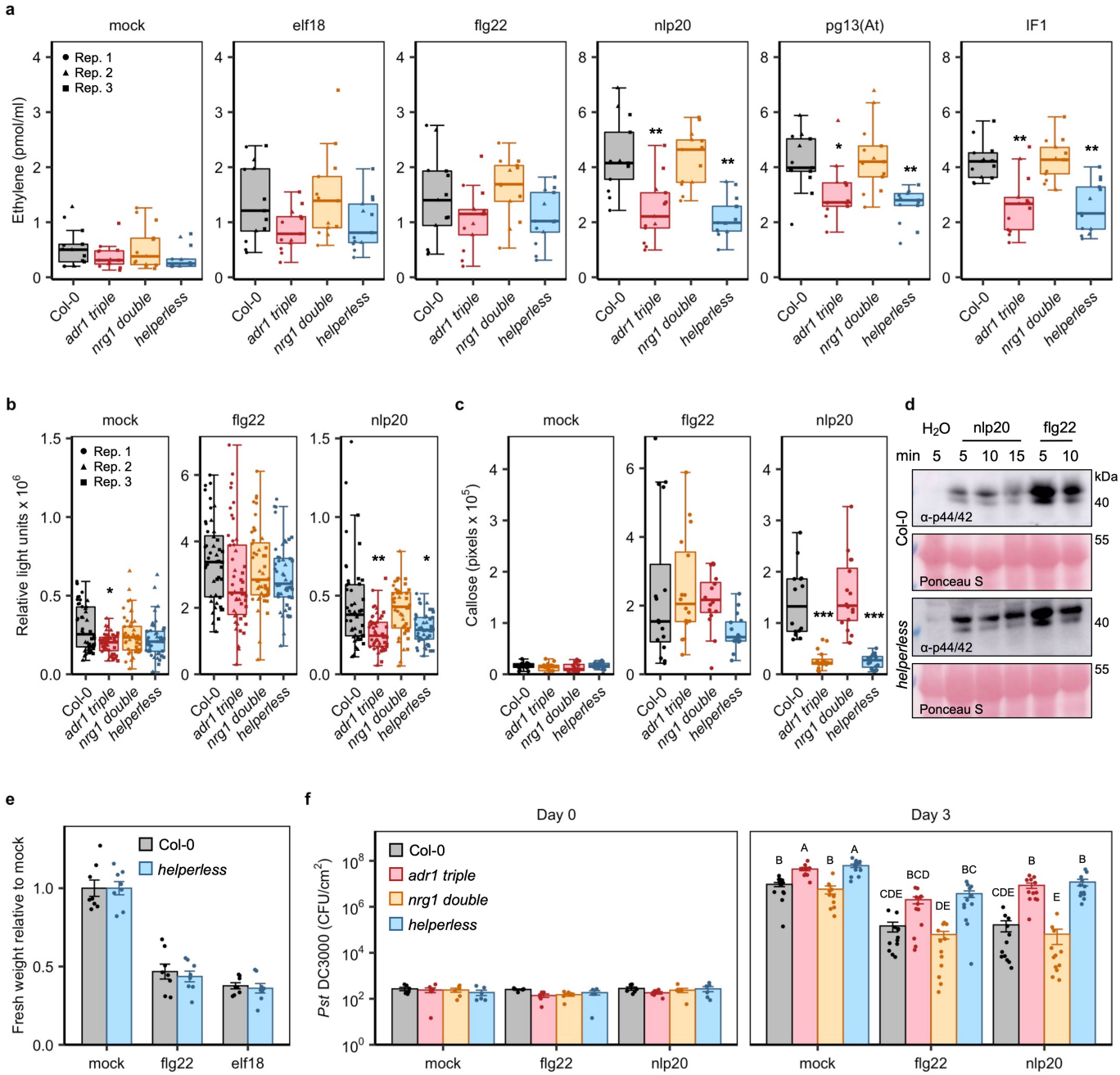

Extended Data Fig. 6 | ADR1 helper NLRs are positive regulators of LRR-RP signalling. a, Elicitor-induced ethylene production in helper NLR mutants. $n = 13$, each from 3 leaf pieces. Data are from 3 independent experiments. Col-0 is grey, *adr1 triple* is pink, *nrg1 double* is orange, and *helperless* is blue for all panels. For **a**–**c**, **f**, statistical differences between Col-0 and the indicated mutant for the given elicitor treatment were analysed using a Kruskal–Wallis test with post hoc two-sided Steel-Dwass test (*$P \leq 0.05$, **$P \leq 0.01$, ***$P \leq 0.0001$). **b**, Total elicitor-induced ROS production over 30 min. $n = 48$ leaf discs from 3 independent experiments. **c**, Nlp20-induced callose deposition is reduced in *adr1 triple* and *helperless* mutants. $n \geq 12$ images from at least 3 leaves. For Col-0 nlp20, $n = 14$ images; for *adr1 triple* mock, $n = 15$; for all others $n = 16$. **d**, Representative immunoblot for MAP kinase activation in Col-0 and *helperless* treated with nlp20 or flg22. Ponceau S-stained RUBISCO large subunit serves as a loading control. For gel source data, see Supplementary Fig. 1. **e**, Relative fresh weight of 12 d-old Col-0 and *helperless* seedlings grown in the presence of flg22 or elf18 ($n = 8$ biological replicates comprising 2 seedlings). No statistical differences between Col-0 and *helperless* were identified for each elicitor treatment ($P > 0.05$, two-sided student's *t*-test). **f**, Elicitor-induced defence against infection is impaired in *adr1 triple* and *helperless* mutants. Leaves were infiltrated with the indicated elicitor and challenged with *Pst* DC3000 24 h after infiltration. Bacterial colonization was assessed at Day 0 and Day 3. $n = 6$ (Day 0) or $n = 12$ (Day 3) biological replicates comprising 2 leaf discs. Bars with different letters indicate significant differences of $P \leq 0.05$ (Kruskal–Wallis test with post hoc two-sided Steel-Dwass test). No statistical differences were observed for Day 0. CFU, colony forming units. For box plots in **a**–**c**, centre line: median, bounds of box: 25th and 75th percentiles, whiskers: 1.5 * IQR. For **e**, **f**, bars indicate mean ± s.e.m. Experiments in **c**–**f** were performed at least three times with similar results. Exact *P* values for all quantitative experiments are provided in Supplementary Table 5.

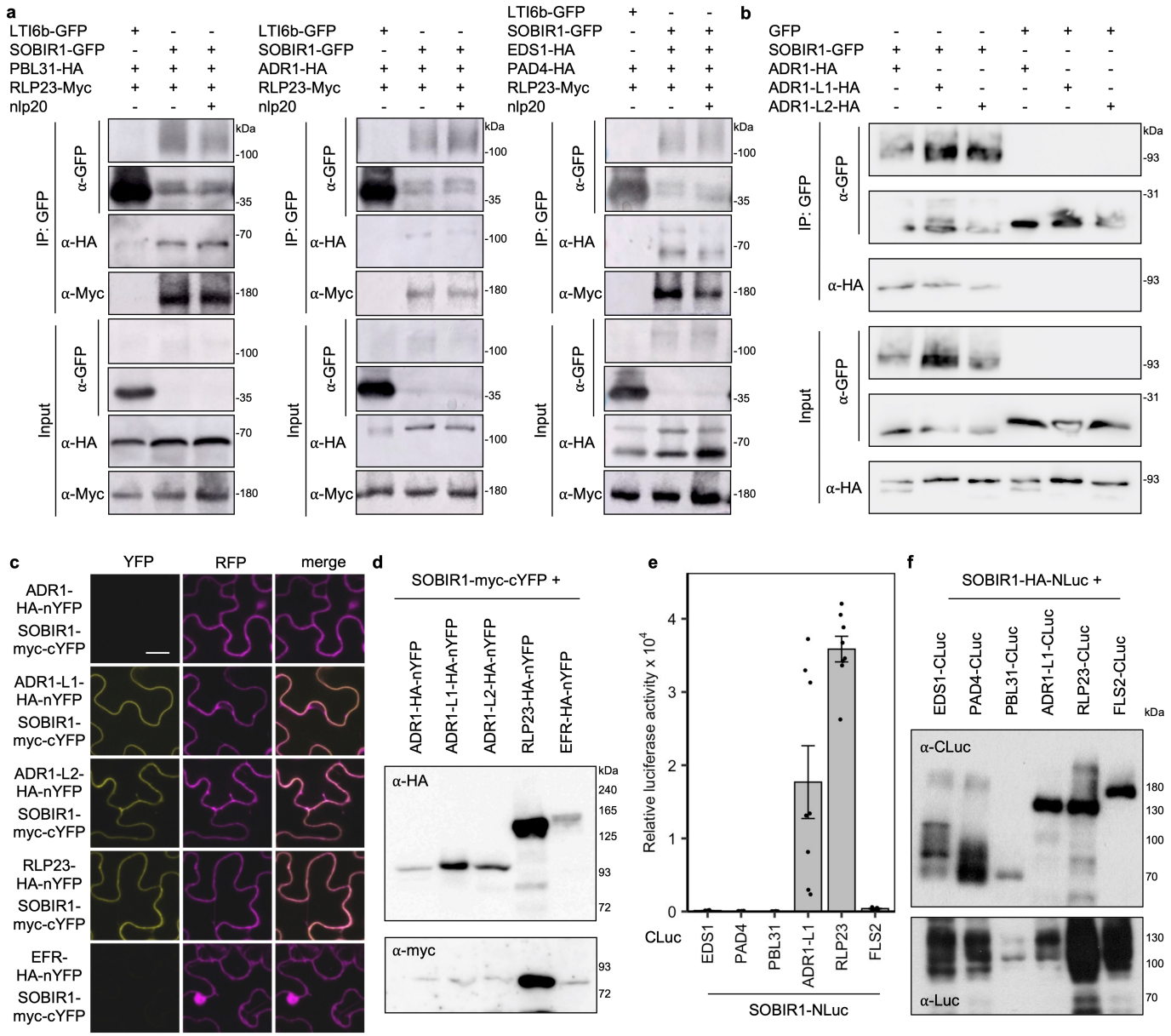

Extended Data Fig. 7 | Co-immunoprecipitation, split-YFP and split-luciferase complementation assays suggest that SOBIR1 is associated with multiple downstream signalling components. a, PBL31, ADR1, EDS1, and PAD4 associate with SOBIR1 in a nlp20-independent manner. The indicated proteins were transiently expressed in *Nicotiana benthamiana*. Leaves treated with nlp20 or water (mock) for 10 min were subjected to co-immunoprecipitation with GFP-trap beads. The proteins were not co-immunoprecipitated with a GFP-fused membrane protein (LTI6b[56]). The experiment was performed twice with similar results. **b**, Pull-down of GFP and SOBIR1-GFP transiently co-expressed with ADR1-HA, ADR1-L1-HA or ADR1-L2-HA. Plants transiently expressing the different proteins were subjected to co-immunoprecipitation using GFP-trap beads and subsequently analysed by protein blot using tag-specific antisera. ADR1-L1-HA and ADR1-L2-HA were co-immunoprecipitated at least three times with similar results; ADR1-HA was tested once. **c**, BiFC between SOBIR1 and the ADR1 isoforms confirms constitutive interaction of SOBIR1 with ADR1-L1 and ADR1-L2 at the plasma membrane. Scale bar indicates 20 µm. The experiment was performed at least three times with similar results. **d**, Protein levels of the transiently expressed proteins in BiFC experiments shown in panel **c**. **e**, Split luciferase complementation assays confirm the interaction of SOBIR1 and ADR1-L1. Bars indicate mean relative luciferase activity ± s.e.m.: $n = 8$ leaf discs from 4 leaves. The experiment was performed three times with similar results. **f**, Protein levels of the transiently expressed proteins in split luciferase experiments shown in panel **e**. Co-expression of the SOBIR1 and PBL31 constructs led to cell death and low protein abundance. The experiment was performed twice with similar results. For gel source data, see Supplementary Fig. 1.

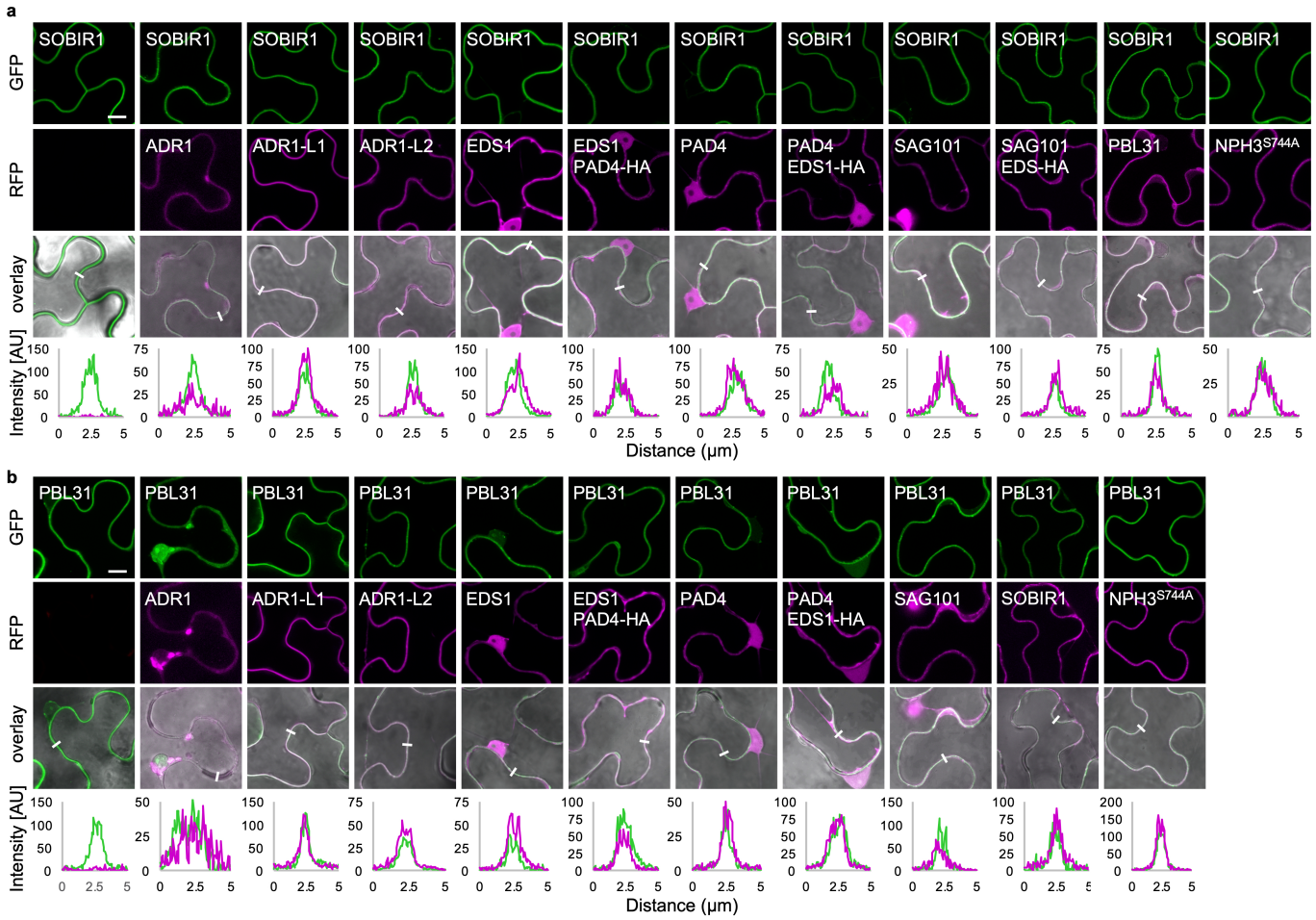

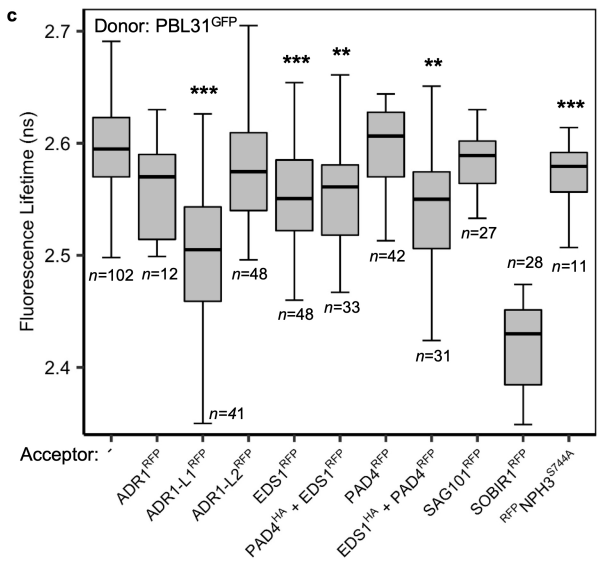

Extended Data Fig. 8 | FRET-FLIM analysis demonstrates association of PBL31-GFP with SOBIR1, ADR1-L1 and EDS1. a, **b**, Representative confocal images show co-localization of (**a**) SOBIR1-GFP or (**b**) PBL31-GFP with RFP fusions of ADR1, ADR1-L1, ADR1-L2, EDS1, PAD4, SAG101, (**a**) PBL31, or (**b**) SOBIR1 at the PM in transiently transformed *N. benthamiana* leaf cells. Plots show the GFP and RFP fluorescence intensity distribution across the PM in the indicated regions (white bars). Scale bars indicate 10 μm. This experiment was repeated three times with similar results. **c**, FRET-FLIM reveals spatial proximity of PBL31-GFP with ADR1-L1-RFP, EDS1-RFP, EDS1-RFP + PAD4-HA, PAD4-RFP + EDS1-HA and SOBIR1-RFP. Membrane-associated protein $NPH3^{S744A}$ serves as control. $n \geq 11$ measurements from at least 3 biological replicates. Exact *n* values are shown below the boxes. Statistical differences in fluorescent lifetime from PBL31-GFP were analysed using a Kruskal–Wallis test with post hoc two-sided Steel-Dwass test (*$P \leq 0.05$, **$P \leq 0.01$, ***$P \leq 0.0001$). Exact *P* values are provided in Supplementary Table 5. Centre line: median, bounds of box: 25th and 75th percentiles, whiskers: 1.5 * IQR.

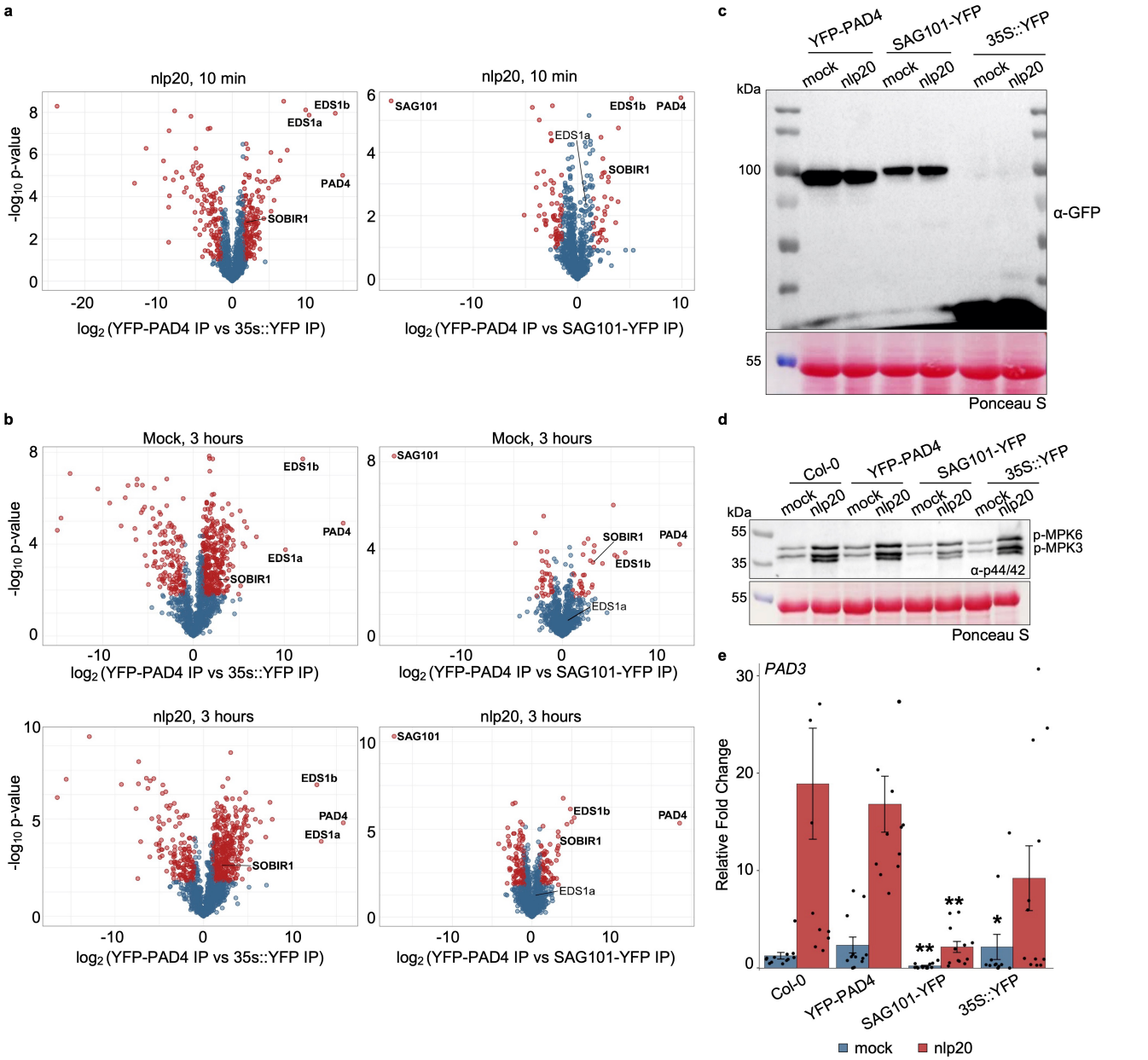

Extended Data Fig. 9 | SOBIR1 specifically co-purifies with YFP-PAD4 in Arabidopsis leaves in mock and nlp20-triggered conditions. **a**, **b**, *Arabidopsis pad4-1/sag101-3* plants complemented with *pPAD4::YFP-gPAD4* (YFP-PAD4) or *pSAG101::gSAG101-YFP* (SAG101-YFP) or *35S::YFP* (YFP) in wild-type Col-0 background were used for immunoprecipitation (IP) assays. Volcano plots show normalized abundances (LFQ, log2 scale) of proteins detected in mass-spectrometry (MS) analyses after IP of total protein extracts from 4.5-week-old *Arabidopsis pad4-1/sag101-3* complementation lines or YFP control line infiltrated with **a**, nlp20 for 10 min, (**b**, upper panels) DMSO (Mock) for 3 h, and (**b**, lower panels) nlp20 for 3 h. Red dots indicate proteins enriched in YFP-PAD4 vs YFP samples (log2(YFP-PAD4 vs YFP) ≥ 1, left) and YFP-PAD4 vs SAG101-YFP samples (log2(YFP-PAD4 vs SAG101-YFP) ≥ 1, right), using permutation-based FDR = 0.05. Graphs represent significantly enriched peptides from four independent experiments ($n = 4$ per genotype per treatment). As shown for 10 min treatments (Fig. 3b), specific enrichment of the two functional Col-0 EDS1 isoforms (EDS1a and EDS1b) was detected in both YFP-PAD4 and SAG101-YFP samples, with EDS1b preferentially enriched following YFP-PAD4 pull-down. **c**, Representative immunoblot analyses to check test protein quality for IP quality in lines used for MS/MS analyses. Total protein extracts (IP inputs) from YFP-PAD4, SAG101-YFP and YFP lines infiltrated with DMSO (mock) or nlp20 for 10 min. Inputs were subsequently immunoprecipitated using GFP-trap agarose beads and analysed by mass spectrometry. The analyses were repeated four times for both 10 min and 3 h treatments with similar results ($n = 8$ per genotype per treatment). **d**, **e**, Nlp20 treatment triggered immune responses at early (10 min) and late (3 h) time points in samples used for IP MS/MS analyses. **d**, Total protein extracts from Col-0, YFP-PAD4, SAG101-YFP and YFP lines infiltrated with DMSO (mock) and nlp20 for 10 min were analysed on immunoblots using an anti-p44/42-ERK antibody. The identity of individual phosphorylated (p)-MAPKs, as determined by their mobility, is indicated by arrows. The analysis was repeated four times with similar results ($n = 4$ samples per genotype per treatment). For gel source data, see Supplementary Fig. 1. **e**, *PAD3* transcript levels were determined by qRT–PCR at 3 h after mock (DMSO) or nlp20 treatment of the indicated genotypes. Relative expression was normalized to *UBQ5* and set to Col-0 mock samples. Bars indicate mean expression ± s.e.m. ($n = 12$ biological replicates from 4 independent experiments). Statistical differences between Col-0 and the indicated genotypes were analysed using Kruskal–Wallis with post hoc two-sided pairwise comparisons using Wilcoxon rank sum test with a Benjamini-Hochberg correction (*$P \leq 0.05$, **$P \leq 0.01$). Exact P values are provided in Supplementary Table 5.

a

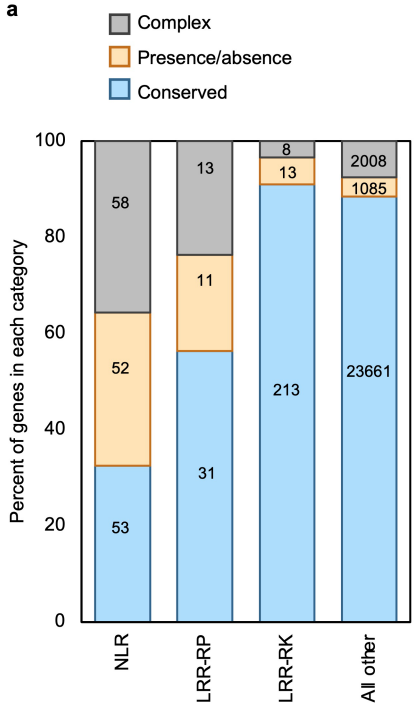

b

COMPLEX		
RLP5 (AT1G34290)	*RLP38 (AT3G23120)*	*RLP43 (AT3G28890)*
RLP7 (AT1G47890)	*RLP39 (AT3G24900)*	*RLP47 (AT4G13810)*
RLP13 (AT1G74170)	*RLP40 (AT3G24982)*	*RLP56 (AT5G49290)*
RLP34 (AT3G11010)	*RLP41 (AT3G25010)*	
RLP37 (AT3G23110)	***RLP42 (AT3G25020)***	

PRESENCE/ABSENCE		
RLP1 (AT1G07390)	*RLP16 (AT1G74200)*	*RLP36 (AT3G23010)*
RLP2 (AT1G17240)	*RLP24 (AT2G33020)*	*RLP48 (AT4G13880)*
RLP3 (AT1G17250)	*RLP25 (AT2G33030)*	*RLP50 (AT4G13920)*
RLP11 (AT1G71390)	*RLP28 (AT2G33080)*	

CONSERVED		
RLP4 (AT1G28340)	*RLP21 (AT2G25470)*	*RLP44 (AT3G49750)*
RLP6 (AT1G45616)	*RLP22 (AT2G32660)*	*RLP45 (AT3G53240)*
RLP8 (AT1G54470)	***RLP23 (AT2G32680)***	*RLP46 (AT4G04220)*
RLP9 (AT1G58190)	*RLP26 (AT2G33050)*	*RLP51 (AT4G18760)*
RLP10 (AT1G65380)	*RLP27 (AT2G33060)*	*RLP52 (AT5G25910)*
RLP12 (AT1G71400)	*RLP29 (AT2G42800)*	*RLP53 (AT5G27060)*
RLP14 (AT1G74180)	***RLP30 (AT3G05360)***	*RLP54 (AT5G40170)*
RLP15 (AT1G74190)	*RLP31 (AT3G05370)*	*RLP55 (AT5G45770)*
RLP17 (AT1G80080)	***RLP32 (AT3G05650)***	*RLP57 (AT5G65830)*
RLP19 (AT2G15080)	*RLP33 (AT3G05660)*	
RLP20 (AT2G25440)	*RLP35 (AT3G11080)*	

Extended Data Fig. 10 | Classification of LRR-RPs, LRR-RKs and NLRs according to genetic conservation in *Arabidopsis* accessions. a, Reads from 80 *Arabidopsis* accessions were mapped to the reference genome of Col-0. Genes were categorised as being conserved, having complex patterns of variation or exhibiting presence/absence polymorphisms according to the distribution of large-scale polymorphisms across all accessions as inferred from stringent read mappings. Criteria for categorization are detailed in the Methods. The numbers of genes falling into each category are provided in the corresponding bars. **b**, LRR-RP genes classified as in **a**. Genes encoding known immune receptors are indicated in bold.

nature portfolio

Corresponding author(s): Thorsten Nürnberger

Last updated by author(s): Jul 5, 2021

Reporting Summary

Nature Portfolio wishes to improve the reproducibility of the work that we publish. This form provides structure for consistency and transparency in reporting. For further information on Nature Portfolio policies, see our Editorial Policies and the Editorial Policy Checklist.

Statistics

For all statistical analyses, confirm that the following items are present in the figure legend, table legend, main text, or Methods section.

n/a	Confirmed	
☐	☒	The exact sample size (*n*) for each experimental group/condition, given as a discrete number and unit of measurement
☐	☒	A statement on whether measurements were taken from distinct samples or whether the same sample was measured repeatedly
☐	☒	The statistical test(s) used AND whether they are one- or two-sided *Only common tests should be described solely by name; describe more complex techniques in the Methods section.*
☒	☐	A description of all covariates tested
☒	☐	A description of any assumptions or corrections, such as tests of normality and adjustment for multiple comparisons
☐	☒	A full description of the statistical parameters including central tendency (e.g. means) or other basic estimates (e.g. regression coefficient) AND variation (e.g. standard deviation) or associated estimates of uncertainty (e.g. confidence intervals)
☐	☒	For null hypothesis testing, the test statistic (e.g. *F*, *t*, *r*) with confidence intervals, effect sizes, degrees of freedom and *P* value noted *Give P values as exact values whenever suitable.*
☒	☐	For Bayesian analysis, information on the choice of priors and Markov chain Monte Carlo settings
☒	☐	For hierarchical and complex designs, identification of the appropriate level for tests and full reporting of outcomes
☒	☐	Estimates of effect sizes (e.g. Cohen's *d*, Pearson's *r*), indicating how they were calculated

Our web collection on statistics for biologists contains articles on many of the points above.

Software and code

Policy information about availability of computer code

Data collection	Leica Microsystems Application Suite X (3.5.7.23225), ZEN Blue (3.1), or ZEN Blue (2.5 lite) for image acquisition.
Data analysis	samtools mpileup version 1.976; parameters: aa; d=10000; Q=0 version 0.7.15-r1140 of the BWA-backtrack algorithm75 with parameters: k=1 in bwa aln command; n=10000; with maximal number of mismatches allowed 1. Paired end information was discarded. ZEN Blue (3.1) and ImageJ (1.53a) software for pixel quantification (callose deposition assay) SymPhoTime 64 software (version 2.3.4724) for Fluorescence Lifetime Imaging and Correlation Software (PICOQUANT) MaxQuant software (version 1.6.3.4, http://www.maxquant.org/) for MS/MS raw data processing Leica Microsystems Application Suite X (3.3.0.16799) for picture editing and intensity plot representation Images processing for ratiometric BiFC with ZEN Blue software (2.5 lite) (Zeiss) Arabidopsis protein identification using Arabidopsis genome information at TAIR10_pep_20101214; ftp://ftp.arabidopsis.org/home/tair/Proteins/TAIR10_protein_lists/ Statistical analysis of MaxLFQ values with Perseus software (version 1.5.8.5, http://www.maxquant.org/) R (4.1.0) (https://www.r-project.org/), R Studio (1.4.1106 and 1.2) JMP (15.2.0 and 16.0.0) (SAS, Cary, NC, US) and MS Office Excel (4.1.0) for statistical data analysis

For manuscripts utilizing custom algorithms or software that are central to the research but not yet described in published literature, software must be made available to editors and reviewers. We strongly encourage code deposition in a community repository (e.g. GitHub). See the Nature Portfolio guidelines for submitting code & software for further information.

Data

Policy information about availability of data

All manuscripts must include a data availability statement. This statement should provide the following information, where applicable:

- Accession codes, unique identifiers, or web links for publicly available datasets
- A description of any restrictions on data availability
- For clinical datasets or third party data, please ensure that the statement adheres to our policy

All data are available within this Article and its Supplementary Information. Proteomics data are available via the ProteomeXchange Consortium with the identifier PXD026120. MS data were searched against a combined database containing protein sequences from A. thaliana TAIR10_pep_20101214; ftp://ftp.arabidopsis.org/home/tair/Proteins/TAIR10_protein_lists/). Genomics data from A. thaliana accessions were obtained from the 1001 Genomes project (https://1001genomes.org/data-center.html) and mapped to the TAIR10 assembly of the genome (https://arabidopsis.org). Original gel blots are shown in Supplementary Fig. 1. Statistical analyses for all quantitative data are provided in Supplementary Tables 1,2, and 5. Source data are provided with this paper.

Field-specific reporting

Please select the one below that is the best fit for your research. If you are not sure, read the appropriate sections before making your selection.

☒ Life sciences ☐ Behavioural & social sciences ☐ Ecological, evolutionary & environmental sciences

For a reference copy of the document with all sections, see nature.com/documents/nr-reporting-summary-flat.pdf

Life sciences study design

All studies must disclose on these points even when the disclosure is negative.

Sample size	Sample size was determined based on experimental trials and previously published studies. No statistical methods were used to predetermine sample size. Previous publications considered to determine sample size include: Ethylene production (Albert, I., et al. An RLP23–SOBIR1–BAK1 complex mediates NLP-triggered immunity. Nature Plants. 1, 15140 (2015)) ROS burst (Wan, W. L. et al. Comparing Arabidopsis receptor kinase and receptor protein-mediated immune signaling reveals BIK1-dependent differences. New Phytol. 221, 2080-2095, (2019)) Callose quantification (Kim M.G., Mackey D. Measuring Cell-Wall-Based Defenses and Their Effect on Bacterial Growth in Arabidopsis. Innate Immunity, 443-452, (2008)) Gene expression analysis (Wan, W. L. et al. Comparing Arabidopsis receptor kinase and receptor protein-mediated immune signaling reveals BIK1-dependent differences. New Phytol. 221, 2080-2095, (2019)) Seedling growth inhibition (Bredow, M. et al. Pattern-Triggered Oxidative Burst and Seedling Growth Inhibition Assays in Arabidopsis thaliana. J. Vis Exp. 147, e59437 (2019)) Induced resistances pathoassays (Böhm, H. et al. A conserved peptide pattern from a widespread microbial virulence factor triggers pattern-induced immunity in Arabidopsis. PLoS Pathog. 10, e1004491, (2014)) FRET/FLIM (Holzwart E., et al. A mutant allele uncouples the brassinosteroid-dependent and independent functions of BRASSINOSTEROID INSENSITIVE 1. Plant Physiol. 182:669–678 (2020)) Split luciferase (Chen, H. et al. Firefly luciferase complementation imaging assay for protein-protein interactions in plants. Plant Physiol. 146, 368-376, (2008)) IP-MS/MS (Sun, X. et al. Pathogen effector recognition-dependent association of NRG1 with EDS1 and SAG101 in TNL receptor immunity. Nat. Comm. 12, 3335, (2021))
Data exclusions	No data were exluded from the analyses provided.
Replication	Reproducibility of data was tested by multiple repetitions of the experiments described. All experiments were conducted at least 3 times on different days using biological materials produced independently (biological replicates). At least 3 technical replicates were included in the individual biological replicate experiments. Statistical evaluation was applied to all data sets obtained and is mentioned in figure legends when applicable. All attempts at replication were successful.
Randomization	Allocation of test plants used in our study was random. There was no targeted selection of individual plants for specific treatments.
Blinding	Blinding was not used in our study as it does not include clinical trials. The nature of the experiments conducted in our study requires that the experimentator knows precisely what plants have received what treatment. In plant, biology blinded/double-blinded studies are uncommon.

Reporting for specific materials, systems and methods

We require information from authors about some types of materials, experimental systems and methods used in many studies. Here, indicate whether each material, system or method listed is relevant to your study. If you are not sure if a list item applies to your research, read the appropriate section before selecting a response.

Materials & experimental systems

n/a	Involved in the study
☐	☒ Antibodies
☒	☐ Eukaryotic cell lines
☒	☐ Palaeontology and archaeology
☒	☐ Animals and other organisms
☒	☐ Human research participants
☒	☐ Clinical data
☒	☐ Dual use research of concern

Methods

n/a	Involved in the study
☒	☐ ChIP-seq
☒	☐ Flow cytometry
☒	☐ MRI-based neuroimaging

Antibodies

Antibodies used

anti-p44/42 (Erk1/2) Thr202/Tyr204 MAPK-Ab, Cell Signaling Technology Europe, Frankfurt, Germany, Cat.-No. 9102, Lot-No. 31
anti-AtMPK3, Sigma-Aldrich, St. Louis, Missouri, US, Cat.-No. M8318, Lot-No. 099M4825V
anti-AtMPK4, Sigma-Aldrich, St. Louis, Missouri, US, Cat.-No. A6979, Lot unknown
anti-AtMPK6, Sigma-Aldrich, St. Louis, Missouri, US, Cat.-No. A7104, Lot unknown
anti-FLS2, Agrisera, Vännäs, Sweden, Cat.-No. AS121857, Lot 1511
anti-BAK1, Agrisera, Vännäs, Sweden, Cat.-No. AS121858, Lot 1506
anti-Luc, Sigma-Aldrich, St. Louis, Missouri, US, Cat.-No. L0159
anti-CLuc, Sigma-Aldrich, St. Louis, Missouri, US, Cat.-No. L2164
anti-Myc, Sigma-Aldrich, St. Louis, Missouri, US, Cat.-No. C3956, Lot 094M4775V
anti-GFP, Torrey Pines Biolabs, Secaucus, New Jersey, US, Cat.-No. TP401, Lot 081211
anti-GFP, Roche, Basel, Switzerland, Cat.-No. 11814460001, Lot unknown
anti-HA, Sigma-Aldrich, St. Louis, Missouri, US, Cat.-No. H3663, Lot 066M4837V3
anti-HA, Roche, Basel, Switzerland, Cat.-No. 11867423001, Lot 42155800

Dilutions used:
p42/44 1:3000
MPK3 1:5000
MPK4 1:1000
MPK6 1:1000
FLS2 1:2000
BAK1 1:10000
Luc 1:5000
CLuc 1:5000
Myc 1:5000
GFP (Torrey Pines) 1:4000
GFP (Roche) 1:1500
HA (Sigma) 1:2000
HA (Roche) 1:2000

Validation

Validation information and experiments can be obtained from the following websites:
p42/44 https://www.cellsignal.de//products/primary-antibodies/p44-42-mapk-erk1-2-antibody/9102
MPK3 https://www.sigmaaldrich.com/catalog/product/sigma/m8318?lang=de&region=DE
MPK4 https://www.sigmaaldrich.com/catalog/product/sigma/a6979?lang=de&region=DE
MPK6 https://www.sigmaaldrich.com/catalog/product/sigma/a7104?lang=de&region=DE
FLS2 https://www.agrisera.com/en/artiklar/fls2-flagellin-sensitive-2-.html
BAK1 https://www.agrisera.com/en/artiklar/bak1-bri1-associated-receptor-kinase.html
Luc https://www.sigmaaldrich.com/deepweb/assets/sigmaaldrich/product/documents/280/065/l2164dat.pdf
CLuc https://www.sigmaaldrich.com/deepweb/assets/sigmaaldrich/product/documents/284/080/l0159dat.pdf
Myc https://www.sigmaaldrich.com/content/dam/sigma-aldrich/docs/Sigma/Datasheet/3/c3956dat.pdf
GFP (Torrey Pines) http://www.chemokine.com/Houston/rat&other/GFP.PDF
GFP (Roche) https://www.sigmaaldrich.com/deepweb/assets/sigmaaldrich/product/documents/294/951/11814460001bul.pdf
HA (Sigma) https://www.sigmaaldrich.com/content/dam/sigma-aldrich/docs/Sigma/Datasheet/2/h3663dat.pdf
HA (Roche) https://www.sigmaaldrich.com/deepweb/assets/sigmaaldrich/product/documents/248/175/roahahabul.pdf

7.4. Saile *et al*., 2021

Arabidopsis ADR1 helper NLR immune receptors localize and function at the plasma membrane in a phospholipid dependent manner

Saile, S. C., Ackermann, F. M., Sunil, S., Keicher, J., Bayless, A., Bonardi, V., Wan, L., Doumane, M., Stöbbe, E., Jaillais, Y., Caillaud, M.-C., Dangl, J. L., Nishimura, M. T., Oecking, C., El Kasmi, F.

New Phytologist.

2021 Dec;232:2440-2456.

doi: 10.1111/nph.17788

Research

New Phytologist

Arabidopsis ADR1 helper NLR immune receptors localize and function at the plasma membrane in a phospholipid dependent manner

Svenja C. Saile[1], Frank M. Ackermann[1], Sruthi Sunil[1], Jutta Keicher[1], Adam Bayless[2], Vera Bonardi[3], Li Wan[3], Mehdi Doumane[4], Eva Stöbbe[1], Yvon Jaillais[4], Marie-Cécile Caillaud[4], Jeffery L. Dangl[3,5], Marc T. Nishimura[2], Claudia Oecking[1] and Farid El Kasmi[1]

[1]Centre for Plant Molecular Biology (ZMBP), University of Tübingen, 72076 Tübingen, Germany; [2]Department of Biology, Colorado State University, Fort Collins, CO 80523-1878, USA; [3]Department of Biology, University of North Carolina, Chapel Hill, NC 27599, USA; [4]Laboratoire Reproduction et Développement des Plantes (RDP), Université de Lyon, ENS de Lyon, UCB Lyon 1, CNRS, INRAE, 69264, Lyon France; [5]Howard Hughes Medical Institute, University of North Carolina, Chapel Hill, NC 27599, USA

Author for correspondence:
Farid El Kasmi
Email: farid.el-kasmi@zmbp.uni-tuebingen.de

Received: *21 December 2020*
Accepted: *15 September 2021*

New Phytologist (2021) **232:** 2440–2456
doi: 10.1111/nph.17788

Key words: *Arabidopsis thaliana*, HeLo-/RPW8-type NLRs, hypersensitive response-like cell death, intracellular localization, nucleotide-binding leucine-rich repeat receptors (NLRs), oligomerization, phospholipids, plant immunity.

Summary

- Activation of nucleotide-binding leucine-rich repeat receptors (NLRs) results in immunity and a localized cell death. NLR cell death activity requires oligomerization and in some cases plasma membrane (PM) localization. The exact mechanisms underlying PM localization of NLRs lacking predicted transmembrane domains or recognizable lipidation motifs remain elusive.
- We used confocal microscopy, genetically encoded molecular tools and protein-lipid overlay assays to determine whether PM localization of members of the Arabidopsis HeLo-/RPW8-like domain 'helper' NLR (RNL) family is mediated by the interaction with negatively charged phospholipids of the PM.
- Our results show that PM localization and stability of some RNLs and one CC-type NLR (CNL) depend on the direct interaction with PM phospholipids. Depletion of phosphatidylinositol-4-phosphate from the PM led to a mis-localization of the analysed NLRs and consequently inhibited their cell death activity. We further demonstrate homo- and hetero-association of members of the RNL family. Our results provide new insights into the molecular mechanism of NLR localization and defines an important role of phospholipids for CNL and RNL PM localization and consequently, for their function.
- We propose that RNLs interact with anionic PM phospholipids and that RNL-mediated cell death and immune responses happen at the PM.

Introduction

Plant intracellular immune receptors of the nucleotide-binding leucine-rich repeat receptor (NLR) family mediate recognition of pathogen-derived effector proteins and the induction of a strong immune response. In many cases, NLR activation leads to the hypersensitive response (HR), a type of programmed cell death of the infected cells (Jones & Dangl, 2006; Monteiro & Nishimura, 2018; Balint-Kurti, 2019). Based on their N-terminal domain architecture, three classes of NLRs have been described in plants: Toll/Interleukin-1 receptor (TIR) NLRs (TNLs), coiled-coil (CC) NLRs (CNLs) and the HeLo/RPW8-like coiled-coil (CC_R) domain NLRs (RNLs) (Monteiro & Nishimura, 2018). In *Arabidopsis thaliana* (Arabidopsis) the RNL subclass consists of two gene families, *ACTIVATED DISEASE RESISTANCE 1* (*ADR1*) and *N REQUIREMENT GENE 1* (*NRG1*), both being required for immune signalling and cell death induction of many other NLRs, particularly TNLs, and thus are also considered as 'helper' NLRs (Bonardi *et al.*, 2011; Qi *et al.*, 2018; Castel *et al.*, 2019; Lapin *et al.*, 2019; Wu *et al.*, 2019; Saile *et al.*, 2020). CNLs, TNLs and most likely RNLs might induce immune signalling and cell death by oligomerization (Wang *et al.*, 2019a; Hu *et al.*, 2020; Li *et al.*, 2020; Ma *et al.*, 2020; Martin *et al.*, 2020; Bi *et al.*, 2021; Jacob *et al.*, 2021; Wu *et al.*, 2021). CNL activation was speculated to result in the formation of a pore-like or membrane disrupting structure of the CC domains (a so-called resistosome) at the plasma membrane (PM) (Collier *et al.*, 2011; Burdett *et al.*, 2019; Wang *et al.*, 2019a; Xiong *et al.*, 2020; Bi *et al.*, 2021). Recently, it was demonstrated that the pentameric resistosome formed by CNL Arabidopsis HOPZ-ACTIVATED RESISTANCE 1 (AtZAR1) forms a cation-selective and calcium-permeable channel at the PM (Bi *et al.*, 2021). Calcium influx is known to trigger defence activation and cell death upon

NLR activation (Yoshioka *et al.*, 2006; Zhao *et al.*, 2021). PM localization is required for cell death and immune function of many CNLs, including Arabidopsis RESISTANCE TO PSEUDOMONAS SYRINGAE 5 (AtRPS5), RESISTANCE TO PSEUDOMONAS SYRINGAE PV MACULICOLA 1 (AtRPM1) and AtZAR1 (Gao *et al.*, 2011; Qi *et al.*, 2012; El Kasmi *et al.*, 2017; Wang *et al.*, 2019a, 2020a). By contrast, the subcellular localization of RNLs has not yet been analysed in detail. So far only the localization of AtNRG1s, but not of AtADR1s, was described. AtNRG1s were found to display a partial endoplasmic reticulum (ER) as well as a PM and cytosolic localization (Lapin *et al.*, 2019; Wu *et al.*, 2019; Jacob *et al.*, 2021). Remarkably, the autoactivated mutant AtNRG1.1^{DV} was observed to display an increased PM localization and additionally localized to puncta on the PM, suggesting that also RNLs function at the PM (Jacob *et al.*, 2021). The expression of activated AtNRG1.1^{DV} and AtADR1 resulted in an increase of the intracellular calcium concentration and further electrophysiological analysis revealed that RNLs can also act as potential PM-localized calcium-permeable channels (Jacob *et al.*, 2021), similar as shown for the CNL AtZAR1 (Bi *et al.*, 2021). Interestingly, many PM-localized CNLs and the RNLs have no predicted transmembrane domain/sequence or N- or C-terminal lipidation motifs and the mechanism that tethers them to the PM is unknown (Gao *et al.*, 2011). Thus, the molecular determinants driving their localization and cell death function at the membrane are not identified.

Homology modelling suggested that the CC_R domains of RNLs share structural similarities with the N-terminal 4-helix bundle (HeLo domain) of mammalian MIXED-LINEAGE KINASE DOMAIN-LIKE (MLKL) proteins and fungal HET-s/HELL proteins (Daskalov *et al.*, 2016; Bentham *et al.*, 2018; Jubic *et al.*, 2019). X-ray crystal structures of two mutant NRG1.1 CC_R domains recently confirmed that AtNRG1.1 CC_R resembles the MLKL 4-helix bundle (Jacob *et al.*, 2021). HeLo domains mediate the cell death function of MLKL and HET-s/HELL proteins and are proposed to oligomerize and disrupt or permeabilize the PM (Hofmann, 2020; Murphy, 2020). PM localization and hence, cell death function of MLKL proteins requires the interaction of their HeLo domain with specific phospholipids at the PM (Dondelinger *et al.*, 2014; Quarato *et al.*, 2016).

Negatively charged phospholipids are low abundant lipids that mediate electrostatic interactions between membranes and proteins that contain polybasic or basic hydrophobic domains or clusters (McLaughlin & Murray, 2005; Heo *et al.*, 2006). Anionic phospholipids, including phosphatidylinositol phosphates (PIPs), phosphatidic acid (PA) and phosphatidylserine (PS), are particularly partitioned in membranes by type and thereby, contribute to organelle identity (Noack & Jaillais, 2017). The PM is the most electronegative compartment across eukaryotes (Yeung *et al.*, 2006; Simon *et al.*, 2016). In plants, phosphatidylinositol-4-phosphate (PI4P), PA and PS are required for the generation of the high electrostatic field of the PM (Simon *et al.*, 2016; Platre *et al.*, 2018). Especially, PI4P was found to be the main driver of the plant PM electronegativity (Simon *et al.*, 2016). While phosphatidylinositol 4,5 bisphosphate ($PI(4,5)P_2$) can also be found at the plant PM, it does not contribute to the PM surface charge (Simon *et al.*, 2016).

Expression of the PM-anchored catalytic domain of the yeast phospholipid-phosphatase Sac1p protein, which specifically dephosphorylates PM PI4P and therefore reduces PI4P levels and the PM electronegativity (Simon *et al.*, 2016; Gronnier *et al.*, 2017), can be used to determine whether a protein requires the presence of PI4P (or a high electronegativity) for localization and/or function at the PM. Depleting PI4P from the PM affects the localization and function of several proteins, including the auxin transport regulator PINOID or the BRASSINOSTEROID INSENSITITVE 1 (BRI1) kinase inhibitor 1 (BKI1) (Simon *et al.*, 2016).

We show that decreasing PI4P abundance at the PM results in the rapid degradation of the CNL AtRPM1 and the RNL family members AtADR1-L1 and AtADR1-L2. We also show that depleting PI4P from the PM causes a mis-localization of AtADR1 and the AtADR1s CC_R domains. Mis-localized AtADR1 and AtADR1s CC_R domains were severely impaired in their cell death activity, demonstrating that AtADR1s function at the PM.

Our results provide new insights into the molecular mechanism of NLR PM localization and defines an important role of the PM PI4P pool for the PM localization of AtRPM1 and AtADR1s. Further, our work indicates that AtADR1s deploy a lipid–protein interaction similar to mammalian MLKL proteins for PM localization, which is likely necessary for cell death execution at the PM. Our data also show that AtADR1s are capable of both homo- and hetero-association, suggesting that they form at least dimers or oligomeric complexes (resistosomes) for cell death induction.

Materials and Methods

Plasmid construction

Plasmid construction was done using standard techniques, including TOPO® cloning, GATEWAY™ cloning and Golden Gate cloning. Details are provided in Supporting Information Methods S1.

Transient expression in *Nicotiana benthamiana*

Agrobacterium tumefaciens overnight cultures were centrifuged and resuspended in induction buffer (10 mM $MgCl_2$, 10 mM MES pH 5.6, 150 µM acetosyringone). The optical density at 600 nm (OD_{600}) of all constructs was adjusted to 0.3 except of *35S::P19* which was adjusted to 0.05. Samples were mixed as indicated. Agrobacteria mixtures were infiltrated into leaves of 4 to 6-wk-old *N. benthamiana* wild-type (WT) plants. SAC1^{dead} and SAC1^{WT} as well as dOCRL^{dead} (*Drosophila melanogaster* orthologue of human oculocerebrorenal syndrome of *Lowe 1*) and dOCRL^{WT} co-infiltrations were always done on the same leaf to avoid expression differences that might arise from leaf-to-leaf variation. *Nicotiana benthamiana* plants were grown on soil under 12 h : 12 h, light : dark cycles (24°C : 22°C, 70% humidity). Induction of

protein expression was done 24 h post-infiltration by spraying using either 30 μM dexamethasone (Sigma-Aldrich, St Louis, MO, USA) and 0.001% (v/v) Silwet L-77 or 20 μM estradiol (Sigma-Aldrich) and 0.001% (v/v) Silwet L-77.

Chemical treatments

For protease inhibitor cocktail (PIC) and bortezomib (BTZ) treatments, *N. benthamiana* leaves were infiltrated with induction buffer only as Mock control or with induction buffer containing 2.5 μM BTZ (Santa Cruz Biotechnology, Dallas, TX, USA) or 1× Halt™ PIC (Thermo Fisher Scientific, Waltham, MA, USA) at 23 h post-Agrobacteria infiltration (hpi), For ADR1, 20 μM estradiol and 0.001% Silwet L-77 was infiltrated together with the Mock solution or the inhibitors to induce ADR1 expression. Leaf samples were collected 4 h (ADR1) or 5 h (ADR1-L1, ADR1-L2, RPM1) post-inhibitor/mock treatment.

Cell death assay

Indicated constructs were transiently expressed in *N. benthamiana* leaves and leaves were imaged for cell death as described in Methods S1.

Confocal imaging

Protein localization was analysed at the indicated time points with an inverse confocal laser scanning microscope LSM880 from Zeiss (Oberkochen, Germany) and an upright confocal laser scanning microscope TCS SP8 from Leica (Wetzlar, Germany) as described in Methods S1.

Western blot analysis of transiently expressed proteins

Frozen *N. benthamiana* leaf tissue was homogenized using a tissue homogenizer (Mill Retsch MM400; Retsch GmbH, Haan, Germany) and resuspended in grinding buffer (20 mM Tris-HCl pH 7, 150 mM NaCl, 1 mM EDTA pH 8, 1% (v/v) Triton X-100, 0.1% (w/v) SDS, 5 mM DTT, 1× Halt™ PIC (Thermo Fisher Scientific)). Samples were incubated on ice for 10 min and then centrifuged for 15 min at 16 000 ***g*** and 4°C. Then, 5× sodium dodecyl sulphate (SDS) loading buffer (250 mM Tris-HCl pH 6.8, 50% (v/v) glycerol, 500 mM DTT, 10% (w/v) SDS, 0.005% (w/v) bromophenol blue) was added to the supernatants, respectively. Proteins were denatured by incubation at 95°C for 5 min. SDS-PAGE (polyacrylamide gel electrophoresis), Western blotting and immunodetection followed standard procedures. Details for primary and secondary antibody dilutions are provided in Methods S1. Chemiluminescence was detected using an Amersham ImageQuant 800 (GE Healthcare, Chalfont St Giles, UK). Images were processed with Adobe Photoshop CS2 (Adobe Inc., San José, CA, USA) for adjustment of brightness and contrast. Protein band intensities were determined by Western blot quantification using ImageJ as described by Hossein Davarinejad (http://www.yorku.ca/yisheng/Internal/Protocols/ImageJ.pdf). The quantification reflects the relative protein amounts as a ratio of the intensity of each protein band relative to the intensity of the lane's loading control (Rubisco band of the Ponceau stained membranes). Relative protein amounts were normalized to corresponding values from relative protein amounts of $SAC1^{dead}$ or $dOCRL^{dead}$ co-infiltrations, respectively.

Co-immunoprecipitation

Frozen *N. benthamiana* leaf tissue (*c.* 200 mg) was ground using liquid nitrogen and resuspended in 2.5 ml of extraction buffer (50 mM HEPES pH 7.5, 50 mM NaCl, 10 mM EDTA pH 8.0, 0.5% (v/v) Triton X-100, 5 mM DTT, 1× Halt™ PIC (Thermo Fisher Scientific)). Samples were kept for 20 min on ice and cleared by centrifugation at 16 000 ***g*** for 5 min and 16 000 ***g*** for 15 min at 4°C. Proteins were immunoprecipitated for 1 h using green fluorescent protein (GFP) Trap Beads (ChromoTek, Planegg-Martinsried, Germany). Further details are provided in Methods S1.

Microsomal fractionation

Microsomal membrane fractions were prepared from transgenic Arabidopsis plants expressing either *pADR1-L2::ADR1-L2-HA* or *pADR1-L2::ADR1-L2^{DV}-HA* (Roberts *et al.*, 2013). Plant tissue was ground in liquid nitrogen and sucrose buffer (20 mM Tris pH 8.0, 0.33 M sucrose, 1 mM EDTA, 5 mM DTT and 1× Halt™ PIC (Thermo Fisher Scientific)) was added in a ratio of 3 : 1. Samples were centrifuged at 2000 ***g*** for 10 min at 4°C to remove debris. Supernatants were transferred to fresh tubes and centrifuged again at 2000 ***g*** for 10 min at 4°C followed by an ultra-centrifugation step at 100 000 ***g*** for 45 min at 4°C. The microsomal pellet was resuspended in 50 μl sucrose buffer. 20 μg or 40 μg protein of each protein fraction (total, soluble, microsomes) was used for SDS-PAGE, respectively.

In vitro transcription and translation and PIP strip assay

ADR1 CC_R-HA (1–146 aa), ADR1-L1 CC_R-HA (1–155 aa), ADR1-L2 CC_R-HA (1–153 aa), RPM1 CC-HA (1–156 aa) and Citrine-HA were expressed *in vitro* using the TnT® SP6 High-Yield Wheat Germ Protein Expression System (Promega, Madison, WI, USA) according to the manufacturer's instructions. A PCR-generated DNA fragment was used as template for the transcription and translation reaction. Primers are listed in Table S1. Protein synthesis was confirmed on Western blot using an haemagglutinin (HA)-specific antibody. Lipid overlay assays using PIP strips were performed according to the manufacturer's instructions (Echelon Biosciences, Salt Lake City, UT, USA) and as described in Reuter *et al.* (2021).

Transmembrane, lipidation and membrane binding sites predictions

Predictions for transmembrane domains, lipidation motifs and membrane binding sites were done using different online tools as described in Methods S1.

Results

AtADR1s localize to the plasma membrane in *N. benthamiana*

The subcellular localization of two Arabidopsis full length RNLs, AtNRG1.1 and AtNRG1.2, was recently described. Both proteins localize to ER membranes, partially to the PM and in the cytosol when transiently expressed in *N. benthamiana* and analysed by confocal microscopy or subcellular fractionation experiments (Lapin *et al.*, 2019; Wu *et al.*, 2019; Jacob *et al.*, 2021). Their intracellular localization was not changed upon effector-triggered and TNL-mediated activation (Qi *et al.*, 2018; Wu *et al.*, 2019). However, the autoactivated mutant of AtNRG1.1 displayed increased PM localization and additionally, localized in puncta on or close to the PM (Jacob *et al.*, 2021). Information on the localization of the other RNL subfamily, the AtADR1s, is missing. To investigate the subcellular localization of the three AtADR1 proteins pre- and post-activation, we transiently expressed C-terminally EYFP- or Citrine-HA-tagged WT AtADR1, AtADR1-L1 and AtADR1-L2 in *N. benthamiana* leaves under the control of an estradiol inducible or 35s promotor (Figs 1a,d,g, S1a,c,e,g) and their native promotors (Fig. S2a–c). We observed no difference in the localization pattern of the AtADR1 proteins, regardless of the promotor used (Figs 1a,d,g, S1a,c,e,g, S2a–c). All three AtADR1 WT proteins co-localized with the PM-localized receptor-like kinase BRI1-mRFP (Figs 1a, d,g, S1a,e,g, S2a–c) (Friedrichsen *et al.*, 2000). In contrast to AtADR1-L1 and AtADR1-L2 the localization of AtADR1 was not restricted to the PM. AtADR1 additionally localized to (1) the ER membrane, since we observed a co-localization with the ER-resident plant V-ATPase assembly factor AtVMA12-RFP (Fig. S1c) (Viotti *et al.*, 2013) and to (2) puncta, some of which might be PM and/or ER associated (Fig. S1a,c).

In order to confirm the membrane association of AtADR1s in Arabidopsis, we performed subcellular fractionation experiments of protein extracts prepared from Arabidopsis seedlings stably expressing AtADR1-L2-HA under control of its native promoter. AtADR1-L2-HA was clearly enriched in the microsomal membrane fraction compared to the soluble fraction, demonstrating that also in Arabidopsis, AtADR1-L2 is mainly associated with membranes (Fig. S2d). These results suggest that AtADR1 proteins might display a similar localization pattern in Arabidopsis as observed in *N. benthamiana* and hence, might also primarily be PM localized.

Since NLR localization might change once the receptor is activated (Wang *et al.*, 2019a; Jacob *et al.*, 2021), we generated autoactive versions of AtADR1s by mutating a conserved aspartic acid in the MHD motif to valine, referred to as DV (QHD to QHV in AtRNLs; cell death phenotype of autoactivated AtRNLs shown in Figs 2a, S3) (Van Ooijen *et al.*, 2008; Williams *et al.*, 2011; Roberts *et al.*, 2013). We also generated AtADR1 P-loop mutants (GKT to AAA), referred to as AAA, to determine whether loss of P-loop function, which was shown to affect the canonical function of at least AtADR1-L2 (Roberts *et al.*, 2013), has an effect on AtADR1s localization. Confocal microscopy analyses revealed that all three AtADR1 P-loop mutant proteins still localized to the PM, but also in the cytosol and/or to the ER (Fig. 1b,e,h), similar as observed previously for AtNRG1.1 loss of cell death function mutants (Jacob *et al.*, 2021). By contrast, autoactivated AtADR1 proteins strongly resembled the localization of AtADR1 WT proteins and thus, were found to be localized to the PM (AtADR1^{DV}, AtADR1-L1^{DV}, AtADR1-L2^{DV}) and ER (ADR1^{DV}) (Figs 1c,f,i, S1b,d,f,h). We also noticed that AtADR1^{DV} and AtADR1-L1^{DV} localized to BRI1-mRFP positive puncta (Figs 1c,f, S1b,f), most likely endosomes and/or PM nanodomains. This however was not observed for AtADR1-L2^{DV} (Figs 1i, S1h).

We performed subcellular fractionation experiments using protein extracts prepared from transgenic Arabidopsis plants expressing the auto-activated mutant AtADR1-L2^{DV}-HA under control of its endogenous promoter to validate the membrane association of activated AtADR1s in Arabidopsis. AtADR1-L2^{DV}-HA was enriched in the microsomal membrane fraction compared to the soluble fraction, confirming that also in Arabidopsis, AtADR1-L2^{DV} primarily is associated with membranes (Fig. S2e).

These results demonstrate that the three members of the AtADR1 subfamily localize to the plant PM pre- and post-activation and further suggest that AtADR1 WT (steady-state) additionally localizes to ER membranes and ER-associated dot-like structures, as observed for AtNRG1.1 (Lapin *et al.*, 2019; Wu *et al.*, 2019; Jacob *et al.*, 2021). Given the high similarity (70–75%) of the protein sequence between the AtADR1 family members, the additional ER localization of AtADR1 was unexpected. We speculate that differences in interaction partners of the three AtADR1s are likely causal for this localization. However, the PM localization of all (auto-)activated AtADR1s suggests that they also execute their immune (cell death) function at the PM.

Homo- and hetero-association of AtADR1s

NLR function in plants and animals is proposed to require oligomerization for proper induction of cell death and immunity (Wang & Chai, 2020). Recently, it has been shown that autoactive AtNRG1.1^{DV} forms high molecular weight complexes, whereas inactive mutant AtNRG1.1 variants did not (Jacob *et al.*, 2021). If the formation of the high molecular weight complexes of AtNRG1.1^{DV} involves homo-oligomerization is not known, but very likely, given that *N. benthamiana* NRG1 self-associates (Qi *et al.*, 2018). Likewise, AtADR1-L1 was found to self-associate and this self-association was enhanced upon immune activation (Wu *et al.*, 2021). On that basis, we tested, whether all three AtADR1 proteins are capable of forming homo- and also hetero-dimers and whether these associations are dependent on their activation status. First, we analysed the capability of AtADR1 WT and the autoactivated QHV mutant (DV) proteins to induce a cell death response after transient over-expression in *N. benthamiana*. We observed that over-expression of AtADR1, AtADR1^{DV} and AtADR1-L1^{DV} induced a HR-like cell death, whereas the over-expression of ADR1-L2^{DV} only resulted in a

New Phytologist

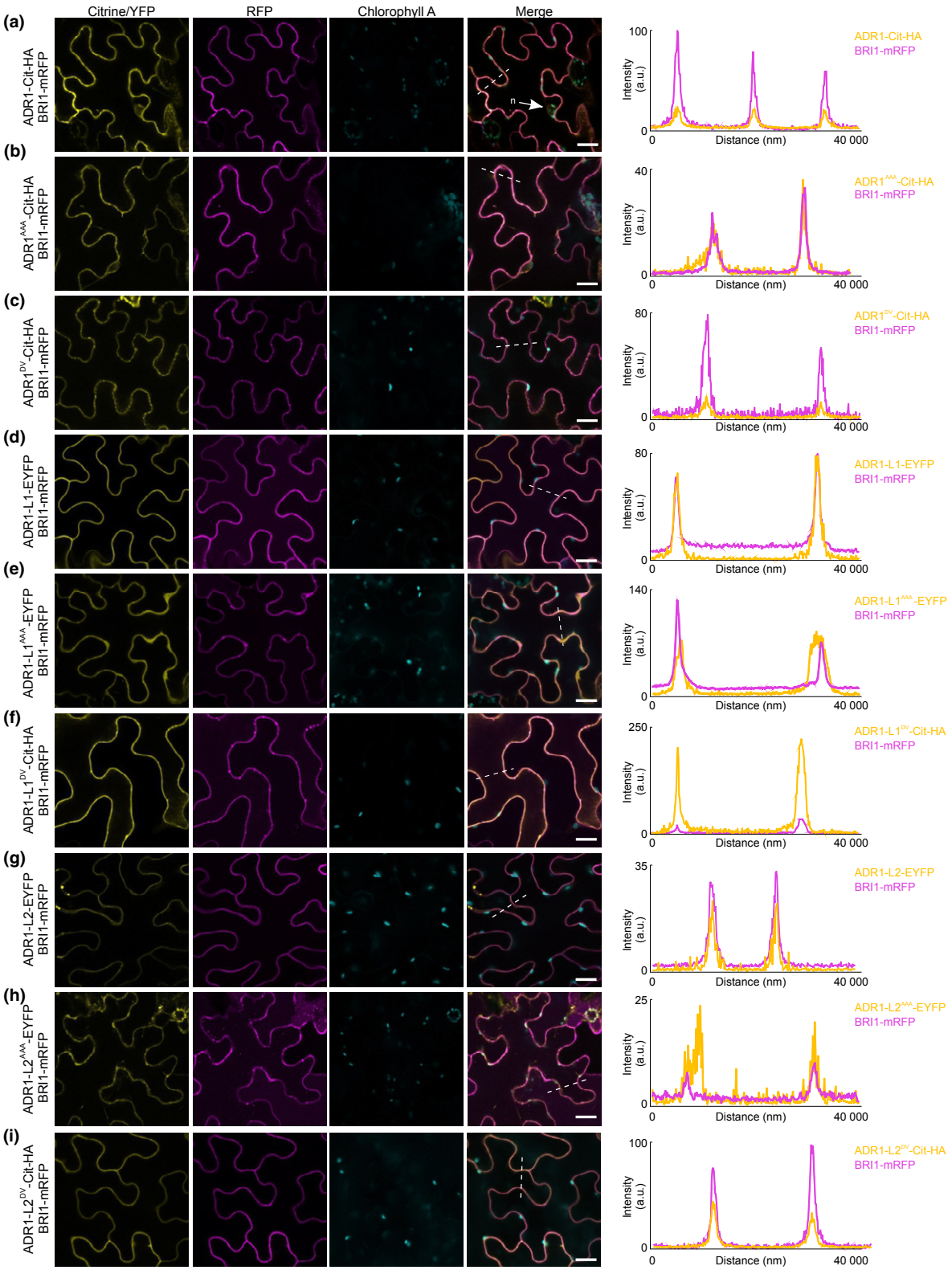

Fig. 1 AtADR1 proteins mainly localize to the plasma membrane (PM). Single plane secant views showing that AtADR1 proteins (ADR1, ADR1-L1, ADR1-L2) and auto-activated QHD (DV) mutants localize mainly to the PM, whereas the AtADR1 P-loop (AAA) mutants additionally display cytosolic and endoplasmic reticulum (ER) localization. The indicated ADR1 proteins fused to Citrine-HA or EYFP were transiently co-expressed with the PM-resident protein BRI1-mRFP in *Nicotiana benthamiana* leaves and confocal imaging was done at 4 h (a, b, c, f) or 5 h (i) post-estradiol induction or 2 d post-infiltration (d, e, g, h). Localization of ADR1s is shown with the first column (Citrine/YFP, in yellow) and the co-localized PM-localized BRI1 is shown in the second column (RFP, in magenta). Chloroplasts are shown in the third column (chlorophyll *A*, in cyan) and the merged images are shown in the fourth column (merge). Fluorescence intensities were measured along the dotted line depicted in the merge images. Bars, 20 μm; n, nucleus.

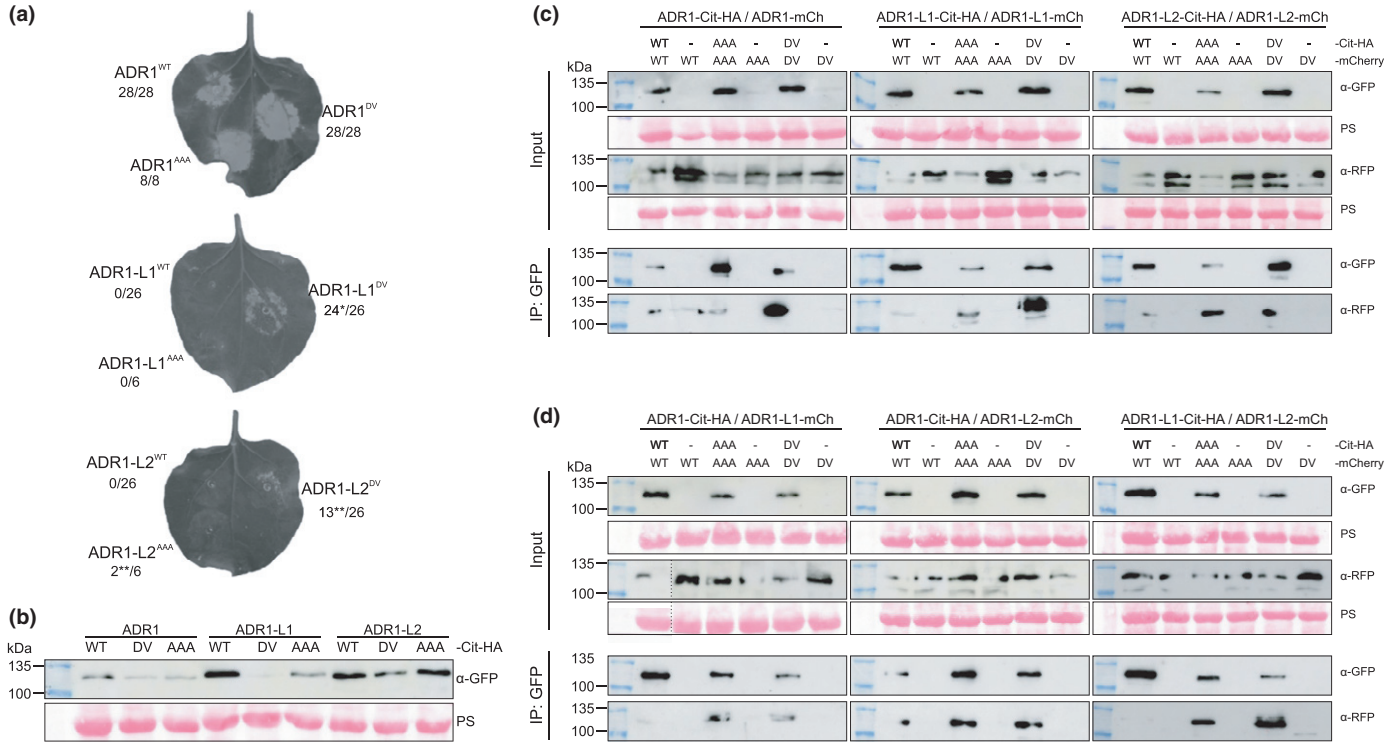

Fig. 2 Homo- hetero-association of AtADR1 proteins. Characterization of the wild-type (WT), P-loop (AAA) and QHD (DV) variants of AtADR1 proteins. (a) Transient expression of steady-state (WT), P-loop mutant (AAA) or auto-activated mutant (DV) AtADR1s-Citrine-HA fusion proteins in *Nicotiana benthamiana*. Photographs were taken under ultraviolet (UV) light at 23 h post-estradiol induction and 47 h post-infiltration. White/light grey areas correspond to dead leaf tissue. Numbers represent the number of leaves showing cell death out of the number of leaves analysed. Asterisk indicates weak cell death. Double-asterisk indicates very weak cell death. Images of the same leaves under normal light are shown in Supporting Information Fig. S3. (b) Immunoblot analysis of the transiently expressed proteins (see (a)) using anti-GFP antibody. Equal loading of the proteins is indicated by the Rubisco band from the Ponceau staining (PS). Proteins were extracted 3 h post-estradiol induction. (c, d) AtADR1 proteins form both homo-dimers (c) and hetero-dimers (d). The indicated proteins were transiently co-expressed in *N. benthamiana* and leaf tissue was harvested 3 h post-estradiol induction. Total proteins were immunoprecipitated with anti-GFP beads and immunoblotted with anti-GFP and anti-RFP antibody, respectively. Immunoblots using total proteins before immunoprecipitation are shown as input (upper panel) and immunoprecipitated proteins are shown as IP (lower panel). Equal loading of the proteins is indicated by the Rubisco band from the PS. Co-immunoprecipitation was repeated two times with similar results. For $ADR1^{WT}$/$ADR1\text{-}L1^{WT}$ interaction, $ADR1^{WT}$-Cit-HA from the flow-through is shown as input since we were not able to detect it in the input fraction. $ADR1^{DV}$, $ADR1^{D461V}$; $ADR1\text{-}L1^{DV}$, $ADR1\text{-}L1^{D489V}$; $ADR1\text{-}L2^{DV}$, $ADR1\text{-}L2^{D484V}$; $ADR1^{AAA}$, $ADR1^{212AAA214}$; $ADR1\text{-}L1^{AAA}$, $ADR1\text{-}L1^{212AAA214}$; $ADR1\text{-}L2^{AAA}$, $ADR1\text{-}L2^{212AAA214}$; IP, immunoprecipitation.

very weak cell death response that was not reliably reproducible (only 13 of 26 leaves showed mild or weak HR-like symptoms; Figs 2a,b, S3). We also found that the AtADR1-induced HR-like cell death occurred earlier in comparison to the cell death response triggered by both $AtADR1\text{-}L1^{DV}$ and $AtADR1\text{-}L2^{DV}$. AtADR1-L1 and AtADR1-L2 WT proteins did not induce a cell death response. The same applies to the catalytic P-loop mutant (AAA) $AtADR1\text{-}L1^{AAA}$, whereas $AtADR1\text{-}L2^{AAA}$ did sometimes, but not strongly and reliably induce a cell death response under our conditions (Figs 2a,b, S3). By contrast, $AtADR1^{AAA}$ consistently induced a strong cell death response in all our experiments, suggesting that P-loop function is not required for at least AtADR1 cell death activity. These observations suggest that some RNLs may not require a functional P-loop for their immune activity.

Our data indicate that WT AtADR1 is already highly active under steady-state conditions, whereas AtADR1-L1 and AtADR1-L2 are kept inactive. However, exchange of D for V in the QHD motif renders $AtADR1\text{-}L1^{DV}$ and $AtADR1\text{-}L2^{DV}$ into active proteins.

We next analysed whether AtADR1s WT and mutant variants are capable of forming homo- and hetero-oligomers by co-immunoprecipitation experiments. Therefore, differently tagged AtADR1s WT and mutant proteins were transiently co-expressed in *N. benthamiana*. Our co-immunoprecipitation experiments revealed that all AtADR1 WT and mutant proteins self-associated (Fig. 2c). While AtADR1 WT proteins strongly self-associated, the capability of AtADR1-L1 and AtADR1-L2 WT proteins to homo-dimerize seems to be reduced. Exchange of D for V in AtADR1 and AtADR1-L1 clearly increased the amount of the co-immunoprecipitated AtADR1 and AtADR1-L1, respectively (Fig. 2c). Interestingly, the P-loop mutations (AAA) did not abolish self-association capability. We even observed enhanced self-association, in particular of $AtADR1\text{-}L1^{AAA}$ and $AtADR1\text{-}L2^{AAA}$ compared to their WT proteins (Fig. 2c). Likewise, we found that AtADR1 proteins are also capable of forming hetero-dimers and that the hetero-association is positively affected by mutations in both the P-loop regions and QHD motifs of all three AtADR1s, respectively (Fig. 2d).

Taken together, AtADR1 proteins associate into homomeric and heteromeric complexes, suggesting that they might exist as dimers/oligomers when inducing cell death. However, homo- and hetero-associations seemed to be stabilized by mutations in both the P-loop region and the QHD motif. Mutations in both regions might interfere with intramolecular interactions, resulting in a conformational change that might favour, promote or stabilize RNL–RNL interactions.

AtADR1s and CNL RPM1 localization and protein stability require PM PI4P

The PM localization of AtADR1, AtADR1-L1 and AtADR1-L2 suggests that they execute their immune function at this cellular compartment as observed for other NLRs, such as AtRPM1 or AtZAR1 and the RNL AtNRG1.1 (Gao *et al.*, 2011; Bi *et al.*, 2021; Jacob *et al.*, 2021). Interestingly, for both RNL families and many PM-localized CNLs, including AtRPM1, no transmembrane region could be identified and thus, they are most likely peripheral membrane proteins (Table S2) (Boyes *et al.*, 1998). Given the structural homology of RNL CC_R domains with the phosphatidyl-inositol phosphate binding HeLo domain of mammalian MLKL (Dondelinger *et al.*, 2014; Jacob *et al.*, 2021), we investigated whether the presence of specific phosphoinositide species might be important for the PM localization of AtADR1s and the CNL AtRPM1. Since PI4P is one of the major phospholipids of the plant PM (Simon *et al.*, 2016), we tested whether AtADR1s and AtRPM1 PM localization require PI4P. Transient expression of the catalytic domain of the PM-localized PI4P-specific yeast phosphatase SAC1p can be used to specifically decrease the PI4P pool at the PM and therefore, to determine the requirement of PI4P for the PM localization and function of proteins of interest (Simon *et al.*, 2016; Gronnier *et al.*, 2017; Doumane & Caillaud, 2020). We co-expressed the three AtADR1s and AtRPM1 with SAC1 and determined their subcellular localization and protein abundance by confocal microscopy and Western blot analysis, respectively. The N-terminally myristoylated and PM localized Arabidopsis CNL AtRPS5 was included as a control NLR as AtRPS5 PM localization (and function) was not expected to be affected by PM PI4P reduction (Qi *et al.*, 2012; Pottinger & Innes, 2020). Co-expression with the WT SAC1 (SAC^{WT}), but not with the catalytically inactive SAC1 ($SAC1^{dead}$), affected the PM localization of all tested NLRs except AtRPS5 (Figs 3a,c,e,g, S4a). Thus, the effect of SAC1 activity on the PM localization of AtADR1s and AtRPM1 is specific and not of general nature. Co-localization of AtADR1 with $SAC1^{WT}$ at the PM was rarely detectable and the majority of AtADR1 was localized inside the cell, likely at the ER and/or cytosol (Fig. 3a). However, no fluorescence was observed for either AtADR1-L1 or AtRPM1, and only a very weak fluorescence was detectable in the cell for AtADR1-L2, after co-expression with $SAC1^{WT}$ (Fig. 3c,e,g). Western blot analysis of AtADR1-L1, AtADR1-L2 and AtRPM1 confirmed a remarkable or even a complete loss of NLR protein accumulation upon co-expression with $SAC1^{WT}$ (Fig. 3d,f,h). By contrast, AtADR1 displayed a slightly reduced accumulation in Western blot analysis when co-expressed with $SAC1^{WT}$ (Fig. 3b). These findings indicate that depleting the PM PI4P pool severely affects the localization and consequently, protein accumulation of AtADR1-L1, AtADR1-L2 and AtRPM1. A similar observation was previously reported for a PS specific binding protein, which is unstable in the Arabidopsis *pss1* mutant that is impaired in PS production (Platre *et al.*, 2018). By contrast, though depletion of PI4P from the PM severely affected the subcellular localization of AtADR1, AtADR1 protein abundance was only marginally reduced. 82% of AtADR1 was still detectable by protein blot analysis upon co-expression with $SAC1^{WT}$.

In order to test whether the reduced or complete loss of NLR protein accumulation upon $SAC1^{WT}$ co-expression was due to degradation of the mis-localized proteins, we analysed protein levels by Western blot in presence of both protease and proteasome inhibitors. The specific inhibition of proteasomal degradation by BTZ had an observable effect on the accumulation of AtADR1 and AtADR1-L2 (Fig. S5a,c) and a weak effect on AtADR1-L1 (Fig. S5b). This indicates that proteasomal degradation is, at least partially, responsible for the degradation of mis-localized AtADR1s. By contrast, mis-localized AtRPM1 could not be stabilized in the presence of BTZ (Fig. S5d), suggesting that the proteasome plays no major role in AtRPM1 degradation. This is consistent with previously published data (Gao *et al.*, 2011).

Together these results clearly demonstrate that all three AtADR1s and AtRPM1 require PI4P or a high

Fig. 3 Phosphatidylinositol-4-phosphate (PI4P) depletion reduces plasma membrane (PM) localization and stability of AtADR1s and AtRPM1. Effects on the localization and stability of AtADR1s (ADR1, ADR1-L1, ADR1-L2) and AtRPM1 after transient co-expression with $SAC1^{dead}$ (upper panel) or $SAC1^{WT}$ (lower panel). (a) MAP-mCherry-$SAC1^{WT}$ co-expression affects ADR1-Citrine-HA PM localization but not its endoplasmic reticulum localization. (c, e, g) ADR1-L1-, ADR1-L2- and RPM1-EYFP fluorescence is not (c, g) or only weakly (e) detectable when co-expressed with MAP-mCherry-$SAC1^{WT}$. Fusion proteins were transiently expressed in *Nicotiana benthamiana* leaves and confocal imaging was done at 4 h after estradiol induction (a), 2 d post-infiltration (c, e) or 24 h post-infiltration (g). Localization of ADR1-Citrine-HA and ADR1-L1-, ADR1-L2- and RPM1-EYFP proteins is shown in the first column (Citrine/YFP, in yellow) and MAP-mCherry-$SAC1^{WT}$ or MAP-mCherry-$SAC1^{dead}$ is shown in the second column (mCherry, in magenta). Chloroplasts are shown in the third column (chlorophyll *A*, in cyan) and the merged images are shown in the fourth column. Images are single plane secant views. Bar, 20 μm. (b) Immunoblot analysis indicates a slightly reduced accumulation of ADR1-Citrine-HA after co-expression with MAP-mCherry-$SAC1^{WT}$ compared to co-expression with MAP-mCherry-$SAC1^{dead}$. (d, f, h) Co-expression of ADR1-L1 (d), ADR1-L2 (f) and RPM1 (h) -EYFP with MAP-mCherry-$SAC1^{WT}$ severely affects their stability. Immunoblot analysis of the transiently expressed proteins (see (a), (c), (e), (g)) using anti-GFP and anti-RFP antibody, respectively, are shown. Equal loading of the proteins is indicated by the Rubisco band from the Ponceau staining (PS). Numbers show quantification of band intensities normalized to the Rubisco band from the PS. Protein samples were collected at 4 h after estradiol induction (b), 2 d post-infiltration (d, f) or 24 h post-infiltration (h).

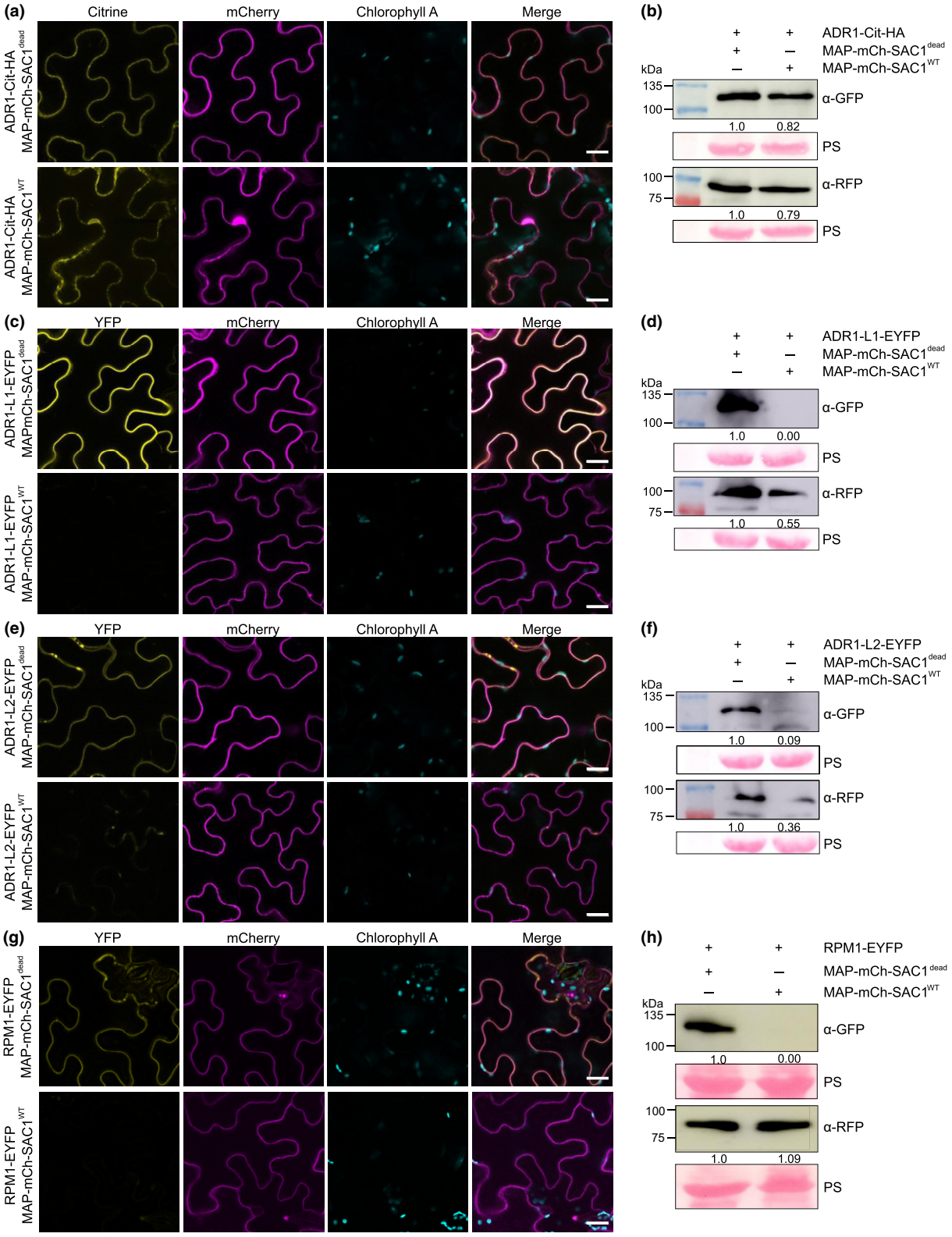

electronegativity driven by PI4P at the PM for their proper localization and that loss of PM localization severely affects their protein stability. Degradation of the mis-localized NLRs is, at least for the AtADR1s, partially mediated by the proteasome.

Cell death function of PM-localized AtADR1s and CNL AtRPM1 is PI4P dependent

Plasma membrane localization of several NLRs, including AtRPM1, was shown to be important for their immune and cell

death function (Gao *et al.*, 2011; Qi *et al.*, 2012; El Kasmi *et al.*, 2017; Wang *et al.*, 2019a, 2020a). The severe effect of PI4P depletion from the PM on the localization and stability of the AtADR1s and AtRPM1, prompted us to analyse whether their cell death function was also affected.

To examine this, we co-expressed $SAC1^{WT}$ or $SAC1^{dead}$ with the cell death-inducing AtADR1 WT and $AtADR1^{DV}$ mutant (Fig. 4a,b). Co-expression with $SAC1^{WT}$, but not with $SAC1^{dead}$, suppressed the cell death response of both AtADR1 WT (Fig. 4a) and $AtADR1^{DV}$ (Fig. 4b). We conclude that PI4P depletion severely affects AtADR1 cell death activity, most likely due to loss or severe reduction of PM localization, as ADR1 protein abundance was not massively affected (Figs 3a,b, 4a).

AtRPM1 guards the immune regulatory protein RIN4 (RPM1 INTERACTING PROTEIN 4) and is activated by an effector-triggered phosphorylation of RIN4 threonine 166 (Chung *et al.*, 2011; Liu *et al.*, 2011). AtRPM1 activation can be reconstituted in *N. benthamiana* by co-expression of AtRPM1 and a phosphomimic mutant of AtRIN4 ($AtRIN4^{T166D}$) (Gao *et al.*, 2011; Chung *et al.*, 2014). The strong cell death response upon AtRPM1 activation by $AtRIN4^{T166D}$ was completely inhibited by $SAC1^{WT}$ co-expression, but not by $SAC1^{dead}$ (Fig. 4c). Cell death activity of effector-activated AtRPM1 was also severely affected by $SAC1^{WT}$ co-expression (Fig. S6b), suggesting that AtRPM1-mediated cell death activity requires PM localization and consequently, depends on the PM PI4P pool.

To demonstrate that the effect of decreasing the PM PI4P pool on the cell death activity of AtADR1s and AtRPM1 is specific and not of general nature, we analysed whether $SAC1^{WT}$ activity affects cell death mediated by the myristoylated and 'constitutively' PM localized AtRPS5. Similar to the AtRPM1-mediated cell death response, the AtRPS5-mediated and effector-triggered cell death can be reconstituted in transient expression assays in *N. benthamiana* (Ade *et al.*, 2007). Neither the expression of $SAC1^{WT}$ nor $SAC1^{dead}$ suppressed effector-triggered and AtRPS5-mediated cell death (Fig. S4e). These results suggest that the effect of SAC1 activity on cell death induction by the AtADR1s and AtRPM1 is specific.

Transient over-expression of the CC_R domains of the AtRNLs AtADR1, AtADR1-L2 and AtNRG1.1 is sufficient to induce a cell death response in *N. benthamiana* (Fig. 4d–f) (Collier *et al.*, 2011). CC_R domain induced cell death activity was dramatically diminished by $SAC1^{WT}$, but not $SAC1^{dead}$ co-expression (Fig. 4d–f), similar as observed for full-length AtADR1. These results suggest that the RNL CC_R domains also induce cell death at the PM and that their activity is affected by PM PI4P depletion. Expression of the AtADR1-L1 CC_R domain did not induce a visible cell death response in transient expression assays under our conditions and hence, could not be tested for PI4P dependency (Fig. S6a). Interestingly, in contrast to the measurable negative effect of $SAC1^{WT}$ activity on the accumulation of the full-length NLR proteins (Fig. 3d,f,h) we did not observe a similar effect on the CC_R domains (Fig. 4d–f). Altogether, PI4P depletion does not affect CC_R domain stability, but substantially affects CC_R domain-induced cell death.

Taken together, our results demonstrate that AtRNL and AtRPM1 cell death activity is significantly affected by PI4P depletion from the PM and further suggest that cell death activity of all AtRNLs, including the partially ER-localized AtNRG1s (Lapin *et al.*, 2019; Wu *et al.*, 2019; Jacob *et al.*, 2021), takes place at the PM.

PI4P depletion affects PM localization of AtADR1, AtADR1-L1 and AtADR1-L2 CC_R domains

Cell death activity of the AtADR1 and AtADR1-L2 CC_R domains was notably diminished by $SAC1^{WT}$ co-expression (Fig. 4d,e). However, unlike the full length AtADR1s, the stability of the AtADR1s CC_R-domains was not affected (Fig. 4d,e). To test whether PI4P depletion affects AtADR1s CC_R localization and hence function, we co-expressed the CC_R domains of all three AtADR1s with $SAC1^{WT}$ or $SAC1^{dead}$ and analysed their localization by confocal microscopy. The AtADR1s CC_R domains showed a similar localization pattern as their 'parental' full-length proteins. All three CC_R domains localized to the PM in the presence of $SAC1^{dead}$ (Figs 5, S7). We also observed that the AtADR1 CC_R domain localized to dot-like structures and to ER membranes (Figs 5a, S7a). However, the PM localization of all three AtADR1s CC_R domains was affected by $SAC1^{WT}$ co-expression. Fluorescence of the CC_R domains was detected at intracellular puncta and also at ER membranes and/or the cytosol (Figs 5, S7).

Taken together, PI4P depletion from the PM leads to a reduced PM localization (and loss of cell death function) of the AtADR1s CC_R domains and potentially a (mis-)localization to endosomal compartments and the ER or cytosol. Proteins that are normally interacting with the PM in a PI4P- or electronegativity-dependent manner have been shown to 'adopt' endosomal localization once the PM PI4P pool is depleted (Simon *et al.*, 2016; Platre *et al.*, 2018).

AtADR1, AtADR1-L1, AtADR1-L2 CC_R and AtRPM1 CC domains specifically interact with anionic lipids *in vitro*

Reducing the abundance of PM PI4P levels negatively influenced the function, localization and stability of the tested AtADR1s and AtRPM1. Thus, it is very likely that a direct interaction of AtADR1s and AtRPM1 with PM PI4P or other anionic lipids is causal for their PM localization. Given the structural homology of the CC_R domains with the N-terminal HeLo domain of MLKL (Jacob *et al.*, 2021) and the importance of the CC domain for cell death function of many CNLs (Bentham *et al.*, 2018) we investigated whether the AtADR1s CC_R and the AtRPM1 CC domains bind to specific phospholipids. We generated C-terminally HA-tagged CC domain proteins *in vitro* and incubated the proteins on a lipid array (PIP strip). As a negative control we included *in vitro* transcribed and translated Citrine-HA. All three AtADR1s CC_R domains and the AtRPM1 CC domain directly interacted with phospholipids carrying polyacidic headgroups and hence, bound to all PIPs and PA (Fig. 6a–d). For the AtADR1s CC_R domains we additionally observed a weak interaction with the anionic and low abundant PS (Fig. 6a–c) (Colin & Jaillais, 2020). We also

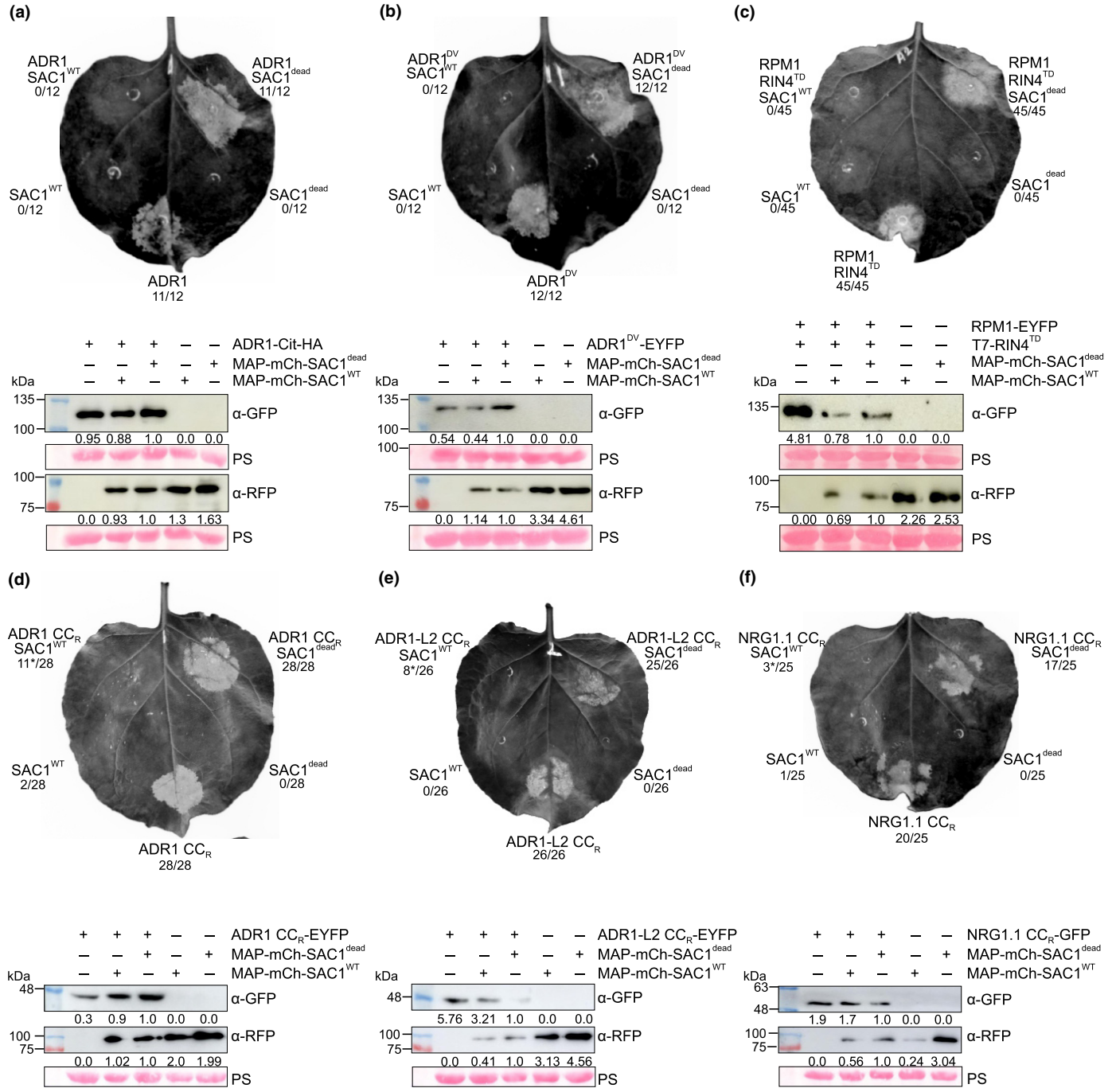

Fig. 4 MAP-mCherry-SAC1 strongly affects AtADR1s and AtRPM1 cell death activity. Cell death activity of full-length AtADR1 and the autoactive AtADR1^{DV} mutant, the phospho-mimic T7-RIN4^{T166D} activated RPM1 as well as the autoactive AtADR1s CC_R domains (ADR1 CC_R and ADR1-L2 CC_R), is suppressed by SAC1^{WT} co-expression. (a–f, upper panels) Transient expression of ADR1 (a), ADR1^{D461V} (b), phospho-mimic T7-RIN4^{T166D} (RIN4^{TD})-activated RPM1 (c), ADR1 CC_R (d), ADR1-L2 CC_R (e) and NRG1.1 CC_R (f) Citrine-HA- or EYFP-fusion proteins in *Nicotiana benthamiana* co-expressed with MAP-mCherry-SAC1^{WT} or MAP-mCherry-SAC1^{dead}. Images of leaves were taken under ultraviolet (UV) light at 8 h post-estradiol induction (a), 30 h post-infiltration (hpi) (b), 24 hpi (c), 23 hpi (d), 26 hpi (e) and 28 hpi (f). Phospho-mimic T7-RIN4^{T116D} was co-expressed to activate RPM1. White/light grey areas on the leaves indicate dead tissue. Numbers represent the number of leaves showing cell death out of the number of leaves analysed. Asterisk indicates weak cell death. (a–f, lower panels), Immunoblot analysis of the transiently expressed proteins (see upper panels) using anti-GFP and anti-RFP antibody, respectively. Membranes were horizontally cut into two pieces and probed with anti-GFP or anti-RFP antibody, respectively (a–c). Equal loading of the proteins is indicated by the Rubisco band from the Ponceau staining (PS). Numbers show quantification of band intensities normalized to the Rubisco band from the Ponceau staining. Protein samples were collected at 24 hpi (a), 4 h post-estradiol induction (b), 22 hpi (c) or 20 hpi (d–f).

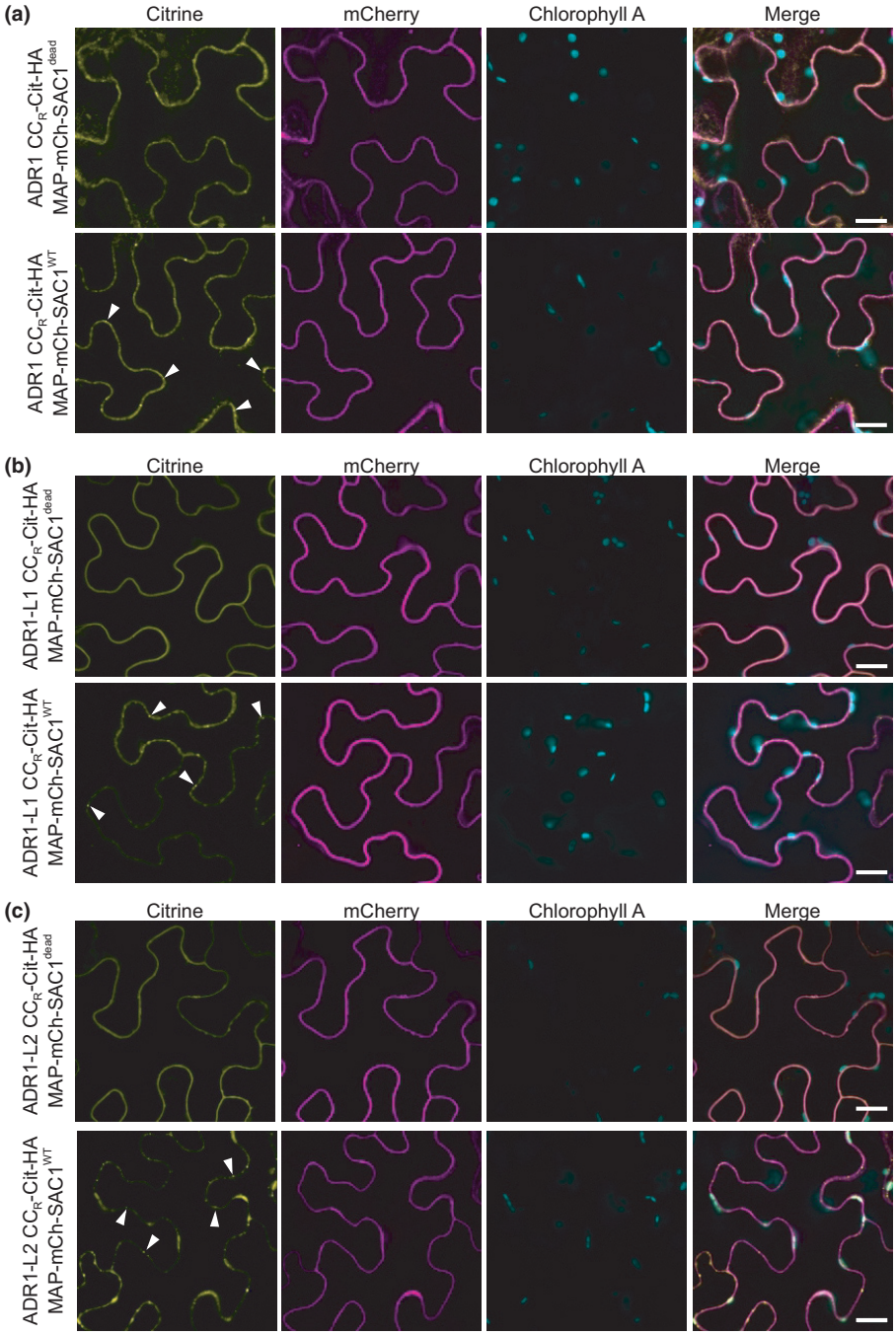

Fig. 5 Phosphatidylinositol-4-phosphate (PI4P) depletion affects plasma membrane (PM) localization of AtADR1 CC_R domains. Co-expression of SAC1^{WT} noticeably affects ADR1 CC_R (a), ADR1-L1 CC_R (b) and ADR1-L2 CC_R (c) localization. (a–c) Citrine-HA tagged AtADR1 (ADR1, ADR1-L1, ADR1-L2) CC_R domains were transiently co-expressed with MAP-mCherry-SAC1^{dead} (upper panels) or MAP-mCherry-SAC1^{WT} (lower panels) in *Nicotiana benthamiana* leaves and confocal imaging was done at 3 h (a) or 4 h (b, c) post-estradiol induction. MAP-mCherry-SAC1^{WT} induces ADR1 CC_R, ADR1-L1 CC_R and ADR1-L2 CC_R re-localization to intracellular puncta, most likely endosomes (white arrowheads in lower panels of a–c). Localization of ADR1 CC_R-Cit-HA domains is shown with the first column (Citrine, in yellow) and MAP-mCherry-SAC1^{dead} or MAP-mCherry-SAC1^{WT} is shown in the second column (mCherry, in magenta). Chloroplasts are shown in the third column (chlorophyll *A*, in cyan) and the merged images are shown in the fourth column (merge). Images are single plane secant views. Bar, 20 μm.

detected a very weak interaction of Citrine-HA to PIPs, but much weaker than observed for the AtADR1s CC_R and AtRPM1 CC domains (Fig. 6e). These results suggest a strong binding of the AtADR1s and AtRPM1 CC_R/CC domains to negatively charged polyacidic phospholipids most likely via an electrostatic interaction.

$PI(4,5)P_2$ depletion has no impact on PM localization and cell death function of AtADR1s and AtRPM1

The strong effect of PI4P depletion at the PM on the function and localization of AtADR1s and AtRPM1 and the specific interaction of their CC_R/CC domains with anionic lipids (including

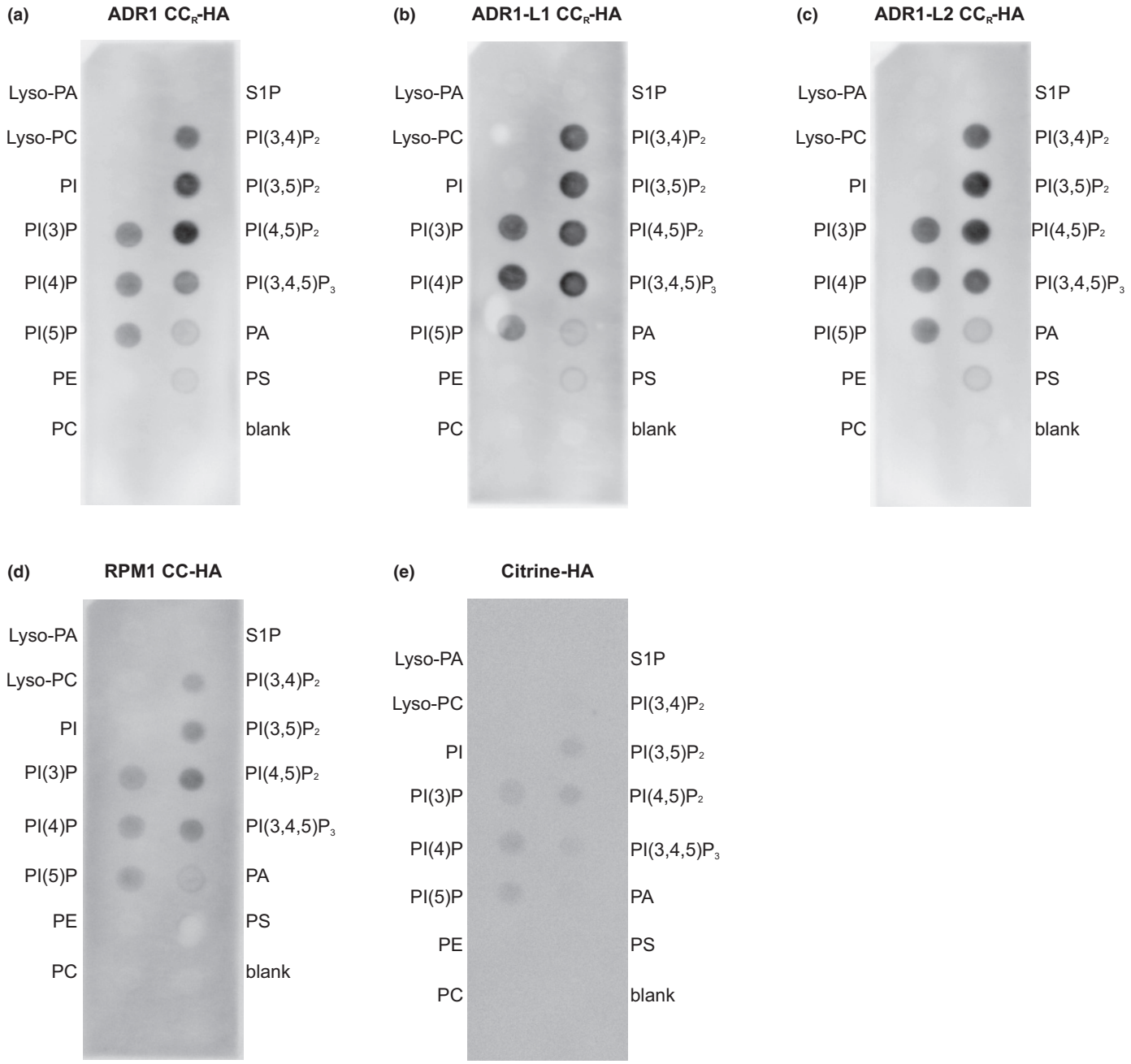

Fig. 6 AtADR1s CC$_R$ and AtRPM1 CC interact *in vitro* with anionic lipids. Arabidopsis ADR1s CC$_R$ and RPM1 CC domains can directly bind to anionic lipids *in vitro*. *In vitro* transcribed and translated AtADR1 CC$_R$ (a), AtADR1-L1 CC$_R$ (b), AtADR1-L2 CC$_R$ (c), AtRPM1 CC (d) domains and Citrine (e) fused with a C-terminal single haemagglutinin (HA) tag were incubated with a commercial phosphatidylinositol phosphate (PIP) strip. Binding was analysed by immunoblotting with anti-HA antibody. The analysed CC$_R$ domains bind strongly and the RPM1 CC domain binds weakly to PI(3)P, PI(4)P, PI(5)P, PI(3,4)P2, PI(3,5)P2, PI(4,5)P2 and PI(3,4,5)P3. A weak interaction of the AtADR1s CC$_R$ domains was also detected with phosphatidic acid (PA) and phosphatidylserine (PS). Citrine (negative control) showed a very weak association with PI(3)P, PI(4)P, PI(5)P, PI(3,5)P2, PI(4,5)P2 and PI(3,4,5)P3.

PI4P) *in vitro*, suggest that PI4P plays a major role for their interaction with and consequently, for their function at the PM. PI(4,5)P_2 fulfils similar important cellular functions, is specifically found at the plant PM, and is also required for the PM association of many proteins (Doumane *et al.*, 2020), like the mammalian MLKL protein (Dondelinger *et al.*, 2014; Quarato *et al.*, 2016). However, PI(4,5)P_2 is not required for plant PM electronegativity (Simon *et al.*, 2016). Our observation of the additional direct binding of the AtADR1s CC$_R$ and AtRPM1 CC domains to PI(4,5)P_2 (Fig. 6), prompted us to test whether PI(4,5)P_2 is also required for AtADR1s and AtRPM1 PM localization and cell death function. We co-expressed the PM-anchored WT PI(4,5)P_2 5-phosphatase domain from the Drosophila OCRL protein (dOCRL^{WT}) that specifically depletes the PI(4,5)P_2 pool at the plant PM (Doumane *et al.*, 2020) with AtADR1, AtADR1-L1, AtADR1-L2, AtRPM1 and AtRPS5. As

a control we co-expressed a phosphatase dead mutant version of dOCRL (dOCRL^{dead}) that is catalytically inactive (Doumane *et al.*, 2020). Co-expression of dOCRL^{WT} or dOCRL^{dead} with AtADR1s, AtRPM1 and AtRPS5 had no visible effect on their (PM-) localization or protein accumulation (Figs S4c,d, S8). Co-expression of dOCRL^{WT}, but not of the catalytically inactive dOCRL^{dead}, with the cell death-inducing CC_R domains of AtADR1, AtADR1-L2 and AtNRG1.1 did not inhibit their activity and a cell death induction was visible for all three CC_R domains (Fig. S9a–c). Similarly, depleting the $PI(4,5)P_2$ pool from the PM did not affect AtADR1 and AtADR1^{DV}-induced cell death responses (Fig. S9d,e). Further, we found no inhibition of the cell death activity of AtRPM1 or AtRPS5 in either the presence of dOCRL^{WT} or dOCRL^{dead} (Figs S4f, S6c, S9f). Consistent with the fact that $PI(4,5)P_2$ depletion does not affect AtRNL and AtRPM1-mediated cell death, we also did not observe a negative effect on protein accumulation by PM $PI(4,5)P_2$ depletion (Figs S8, S9). This suggests that AtRNLs, AtRPM1 and AtRPS5 PM localization and their PM-coupled cell death function is independent of $PI(4,5)P_2$.

Collectively, this demonstrates that $PI(4,5)P_2$ is likely not a major contributor for AtADR1s, AtRPM1 and AtRPS5 localization and function at the PM.

Discussion

Upon effector-induced activation, the CNL AtZAR1 oligomerizes and translocates to the PM where it forms a pore-like structure via the alpha 1 helix of its CC domain that acts as a cation selective channel to induce a cell death and immune response (Wang *et al.*, 2019a,b; Bi *et al.*, 2021). PM or endomembrane localization was shown to be necessary for the cell death and immune function of many CNLs (Gao *et al.*, 2011; Engelhardt *et al.*, 2012). Some CNLs localize to membranes via N-terminal myristoylation and/or palmitoylation, and the residues required for this post-translational modification were demonstrated to be important for the function of these CNLs (Qi *et al.*, 2012; Kawano *et al.*, 2014). However, the molecular mechanism underlying the localization of nonacylated PM/membrane-localized NLRs remains elusive. We present data that suggests a model in which AtADR1s and the CNL AtRPM1 require PI4P at the PM for proper localization that is required for protein stability and cell death function upon (auto-)activation (Fig. 7). The localization is most likely regulated by direct binding of their CC/CC_R domains to anionic lipids (including the very abundant PI4P), possibly via positive charges in a basic hydrophobic stretch that we found in all the CC/CC_R domains (Fig. S10). We, however, cannot rule out the possibility that other mechanisms and/or domains are also required, for example the interaction with other (structural) lipids or integral membrane proteins. In this context, it has recently been shown that AtADR1s interact with a member of the receptor-like kinase family (Pruitt *et al.*, 2021). However, the strong effect of PI4P depletion from the PM on NLR localization and function, suggests that PI4P contributes significantly to AtADR1s and AtRPM1 PM localization. By contrast, PI4P does not or only marginally contribute to the PM localization of

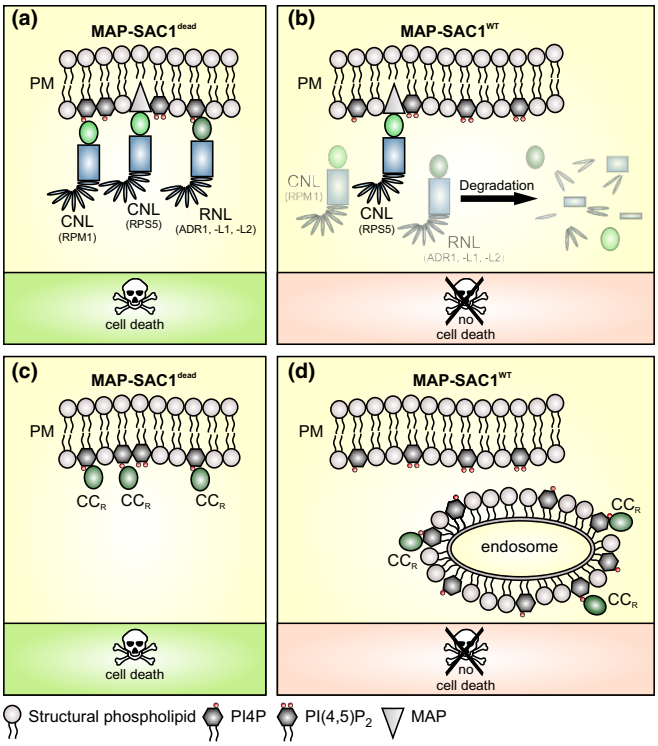

Fig. 7 Proposed model of AtADR1s and the CNL RPM1 localization and cell death/resistance function at the plasma membrane (PM). Localization of the RNLs AtADR1, AtADR1-L1 and AtADR1-L2 and nonacylated CNLs, here shown for AtRPM1, to the PM is mediated by a direct interaction of their CC_R or CC domains with anionic lipids, of which phosphatidylinositol-4-phosphate (PI4P) is the most abundant at the plant PM. (a) Expression of catalytically inactive and forced PM-localized MAP-SAC1^{dead} does not affect AtADR1s, myristoylated (AtRPS5) or nonacylated CNL (AtRPM1) PM localization, and consequently also not their cell death activity upon (auto-)activation. (b) MAP-SAC1^{WT}-mediated PI4P depletion from the PM severely affects AtADR1s and nonacylated CNL AtRPM1, but not myristoylated CNL AtRPS5, localization. The decreased PI4P levels strongly affect PM electronegativity and this leads to a loss of binding to the PM and rapid degradation of AtADR1s and the nonacylated CNL AtRPM1. The reduced accumulation of AtADR1s and AtRPM1 in the cell consequently leads to loss of AtADR1s- and AtRPM1-mediated cell death induction. (c) The localization of AtADR1s CC_R domains (ADR1 CC_R, ADR1-L1 CC_R, ADR1-L2 CC_R) is not affected by MAP-SAC1^{dead} expression, similar to full-length AtADR1s. Thus, there is no observable effect on CC_R domain autoactivity (cell death induction). (d) PI4P depletion by MAP-SAC1^{WT} expression causes a re-localization of the AtADR1s CC_R domains to intracellular puncta, probably endosomal compartments as their membranes might exhibit the highest electronegativity when MAP-SAC1^{WT} is expressed. This mis- or re-localization of AtADR1s CC_R domains does not lead to their degradation. However, AtADR1s CC_R cell death activity is severely reduced.

CNLs with myristoylation or acylation motifs, such as AtRPS5 (Fig. S4), and hence PI4P depletion does not affect their function.

Interestingly, recent studies demonstrated that there is a reduction in the PI4P levels and a specific enrichment of $PI(4,5)P_2$ on interfacial membranes during successful infections, like the extrahaustorial membrane (EHM) in Arabidopsis powdery mildew infections, the extra-invasive hyphal membrane (EIHM) in Arabidopsis *Colletotrichum* infections or at the potato (*Solanum tuberosum*) *Phytophthora infestans* infection sites (Shimada *et al.*,

2019; Qin *et al.*, 2020; Rausche *et al.*, 2020). The PI(4,5)P_2 enrichment at the EHM and EIHM is an essential susceptibility factor, which is most likely pathogen-induced and requires the function of the host phosphatidylinositol 4-phosphate 5-kinases (PIP5K) (Shimada *et al.*, 2019; Qin *et al.*, 2020). It is possible that the depletion of PI4P and the simultaneous enrichment of PI(4,5)P_2 at these host–pathogen interfaces result in a reduced accumulation of immune-regulatory proteins, for example NLRs, by removing possible binding sites and/or enhancing endocytosis of immune signalling components (Qin *et al.*, 2020). Plants however have evolved means to counteract this potentially pathogen/effector-induced enrichment of PI(4,5)P_2 by downregulating the activity of PIP5Ks or upregulating the activity of phosphoinositide 5-phosphatases upon pathogen perception by cell-surface localized immune receptors (Menzel *et al.*, 2019; Rausche *et al.*, 2020). Recently, it was also shown that members of the AtRPW8 protein family specifically localize to the EHM (Berkey *et al.*, 2017), and that the solanaceous helper NLR NRC4 (NLR REQUIRED FOR CELL DEATH 4) dynamically associates with the EHM during *P. infestans* infection (Duggan *et al.*, 2021), indicating that at least the RPW8/HR proteins and NRC4 may not require PI4P for membrane localization. Thus, actively changing or adjusting the lipid and protein composition and homeostasis of the plant PM is part of the evolutionary arms race between the host and the pathogen. This indicates the importance of the regulation/manipulation of lipid homeostasis and the associated changes in protein localization/stability in this battle.

Likewise, a correlation between the lipid composition of the PM and immunity as well as NLR (CNL) function and stability and an important function for phospholipase-dependent signalling in immunity was previously reported (Andersson *et al.*, 2006; Bargmann & Munnik, 2006; Johansson *et al.*, 2014; Yuan *et al.*, 2018; Schloffel *et al.*, 2020). Plant phospholipase families C (PLCs) and D (PLDs) are involved in many aspects of abiotic and biotic stress responses (Hong *et al.*, 2016). However, the exact mechanisms of how these enzymes and their product(s) influence immunity are not well understood (Li & Wang, 2019). Perception of pathogen-derived danger signals by NLRs and cell-surface localized pathogen-recognition receptors (PRRs) lead to the rapid activation and recruitment of PLDs and PLCs to pathogen entry sites at the PM as well as a biphasic transient calcium ion (Ca^{2+}) influx (Johansson *et al.*, 2014; Xing *et al.*, 2019; Schloffel *et al.*, 2020; Bi *et al.*, 2021; Jacob *et al.*, 2021). PLDs and PLCs induce the production of inositol polyphosphates, PA and diacylglycerol (DAG), all of which can function as second messengers during immunity as well as other stress responses (Li & Wang, 2019). The PLC- and PLD-mediated generation of PA is required for NLR-triggered reactive oxygen species (ROS) production and HR-like cell death, and external application of PA is sufficient to induce a cell death response and the transcriptional activation of the pathogen-responsive *PR1* promoter (Andersson *et al.*, 2006). The cation (Ca^{2+})-channel forming capability of some CNLs and RNLs at membranes is required for their cell death activity and downstream immune signalling (Jubic *et al.*, 2019; Wang *et al.*, 2020b; Bi *et al.*, 2021; Jacob *et al.*, 2021). In light of our results it is tempting to hypothesize that (1) AtADR1s interact with PM/membrane anionic lipids, like PI4P, and that activation might lead to oligomerization (or at least stabilization of a higher order complex), and the formation of a cation-permeable channel/pore that (2) results in a transient Ca^{2+} influx and subsequently, in the (3) activation of Ca^{2+}-dependent and probably NLR-interacting phospholipases that (4) in turn produce lipid messengers, such as PA and DAG, which (5) might participate in the activation of downstream signalling components required for (6) NLR-mediated immune responses (Fig. S11) (Andersson *et al.*, 2006; Yuan *et al.*, 2018; Jubic *et al.*, 2019; Wang *et al.*, 2019a; Bi *et al.*, 2021; Jacob *et al.*, 2021).

Acknowledgements

The authors are grateful for technical support from Christel Kulibaba-Mattern and Elke Sauberzweig. The authors would like to thank the ZMBP gardeners and the microscopy facility for their support and advice. The authors thank Karin Schumacher for the VMA12 construct, Klaus Harter for the BRI1 construct and Roger Innes for PBS1-HA and AvrPphB-Myc clones. The authors also thank Andrea Gust for sharing an unpublished GoldenGate level I vector with us. The authors would also like to thank Friederike Wanke and Thomas Stanislas for critical comments on the project. The authors thank the University of Tübingen, the German Research Foundation (DFG) (grant no. DFG-CRC1101 – project D09 to FEK, and grants for scientific equipment -INST 37/965-1 FUGG) and the Reinhard Frank Stiftung (Project 'helperless plant' to FEK) for the financial support to FEK, the DFG (grant no. DFG-CRC1101 – project B09 to CO) for the financial support to CO, the National Science Foundation (grant IOS-1758400 to MTN and JLD) and National Institutes of Health (grants GM107444 to JLD) for the financial support to MTN and JLD. MTN was also supported by start-up funds from Colorado State University, and JLD is a Howard Hughes Medical Institute (HHMI) Investigator. YJ and M-CC were supported by ERC no. 3363360-APPL under FP/2007–2013 and ANR (caLIPSO; ANR-18-CE13-0025-02) to YJ, ANR JC/JC Junior Investigator Grant (INTERPLAY; ANR-16-CE13-0021) and a SEED Fund ENS LYON-2016 to M-CC. Open access funding enabled and organized by ProjektDEAL.

Author contributions

SCS created RNL entry and destination constructs, performed confocal and cell death analysis for all RNLs, the co-immunoprecipitation experiments, the *in vitro* transcription and translation assay, the PIP strip analysis and all Western blot analysis for the RNL experiments and the degradation experiments; FMA performed confocal and cell death analysis for all RPM1 experiments; SS created RPS5 entry and destination constructs, performed cell death and Western blot analysis for RPM1 and RPS5, and confocal analysis for RPS5.; JK created pADR1::ADR1-YFP and assisted in the co-immunoprecipitation experiments; AB performed some cell death analysis for RNLs; ES, VB and LW assisted in creating RNL and CNL entry and destination constructs; MD generated and characterized SAC1 and dOCRL

constructs; YJ and M-CC provided unpublished SAC1 and dOCRL constructs; SCS, FMA, MTN and FEK conceived the study and designed the experiments; FEK wrote the manuscript with help of SCS and FMA; SCS and FEK edited the revised version of the manuscript with help of CO; SS, AB, YJ, M-CC, JLD and MTN reviewed and edited the manuscript.

ORCID

Marie-Cécile Caillaud https://orcid.org/0000-0002-0348-7024
Jeffery L. Dangl https://orcid.org/0000-0003-3199-8654
Farid El Kasmi https://orcid.org/0000-0002-4634-7689
Yvon Jaillais https://orcid.org/0000-0003-4923-883X
Marc T. Nishimura https://orcid.org/0000-0003-4666-6900
Claudia Oecking https://orcid.org/0000-0003-0635-6457
Svenja C. Saile https://orcid.org/0000-0003-2258-3166
Sruthi Sunil https://orcid.org/0000-0002-2142-5935

Data availability

The data that support the findings of this study are available from the corresponding author upon reasonable request.

References

Ade J, DeYoung BJ, Golstein C, Innes RW. 2007. Indirect activation of a plant nucleotide binding site-leucine-rich repeat protein by a bacterial protease. *Proceedings of the National Academy of Sciences, USA* **104**: 2531–2536.

Andersson MX, Kourtchenko O, Dangl JL, Mackey D, Ellerstrom M. 2006. Phospholipase-dependent signalling during the AvrRpm1- and AvrRpt2-induced disease resistance responses in *Arabidopsis thaliana*. *The Plant Journal* **47**: 947–959.

Balint-Kurti P. 2019. The plant hypersensitive response: concepts, control and consequences. *Molecular Plant Pathology* **20**: 1163–1178.

Bargmann BO, Munnik T. 2006. The role of phospholipase D in plant stress responses. *Current Opinion in Plant Biology* **9**: 515–522.

Bentham AR, Zdrzalek R, De la Concepcion JC, Banfield MJ. 2018. Uncoiling CNLs: structure/function approaches to understanding CC domain function in plant NLRs. *Plant and Cell Physiology* **59**: 2398–2408.

Berkey R, Zhang Y, Ma X, King H, Zhang Q, Wang W, Xiao S. 2017. Homologues of the RPW8 resistance protein are localized to the extrahaustorial membrane that is likely synthesized de novo. *Plant Physiology* **173**: 600–613.

Bi G, Su M, Li N, Liang YU, Dang S, Xu J, Hu M, Wang J, Zou M, Deng Y *et al.* 2021. The ZAR1 resistosome is a calcium-permeable channel triggering plant immune signaling. *Cell* **184**: 3528–3541.

Bonardi V, Tang S, Stallmann A, Roberts M, Cherkis K, Dangl JL. 2011. Expanded functions for a family of plant intracellular immune receptors beyond specific recognition of pathogen effectors. *Proceedings of the National Academy of Sciences, USA* **108**: 16463–16468.

Boyes DC, Nam J, Dangl JL. 1998. The *Arabidopsis thaliana RPM1* disease resistance gene product is a peripheral plasma membrane protein that is degraded coincident with the hypersensitive response. *Proceedings of the National Academy of Sciences, USA* **95**: 15849–15854.

Burdett H, Bentham AR, Williams SJ, Dodds PN, Anderson PA, Banfield MJ, Kobe B. 2019. The plant "resistosome": structural insights into immune signaling. *Cell Host & Microbe* **26**: 193–201.

Castel B, Ngou PM, Cevik V, Redkar A, Kim DS, Yang Y, Ding P, Jones JD. 2019. Diverse NLR immune receptors activate defence via the RPW 8-NLR NRG 1. *New Phytologist* **222**: 966–980.

Chung EH, da Cunha L, Wu AJ, Gao Z, Cherkis K, Afzal AJ, Mackey D, Dangl JL. 2011. Specific threonine phosphorylation of a host target by two unrelated type III effectors activates a host innate immune receptor in plants. *Cell Host & Microbe* **9**: 125–136.

Chung EH, El-Kasmi F, He Y, Loehr A, Dangl JL. 2014. A plant phosphoswitch platform repeatedly targeted by type III effector proteins regulates the output of both tiers of plant immune receptors. *Cell Host & Microbe* **16**: 484–494.

Colin LA, Jaillais Y. 2020. Phospholipids across scales: lipid patterns and plant development. *Current Opinion in Plant Biology* **53**: 1–9.

Collier SM, Hamel LP, Moffett P. 2011. Cell death mediated by the N-terminal domains of a unique and highly conserved class of NB-LRR protein. *Molecular Plant–Microbe Interactions* **24**: 918–931.

Daskalov A, Habenstein B, Sabate R, Berbon M, Martinez D, Chaignepain S, Coulary-Salin B, Hofmann K, Loquet A, Saupe SJ. 2016. Identification of a novel cell death-inducing domain reveals that fungal amyloid-controlled programmed cell death is related to necroptosis. *Proceedings of the National Academy of Sciences, USA* **113**: 2720–2725.

Dondelinger Y, Declercq W, Montessuit S, Roelandt R, Goncalves A, Bruggeman I, Hulpiau P, Weber K, Sehon C, Marquis R *et al.* 2014. MLKL compromises plasma membrane integrity by binding to phosphatidylinositol phosphates. *Cell Reports* **7**: 971–981.

Doumane M, Caillaud MC. 2020. Assessing extrinsic membrane protein dependency to PI4P using a plasma membrane to endosome relocalization transient assay in *Nicotiana benthamiana*. *Methods in Molecular Biology* **2177**: 95–108.

Doumane M, Colin L, Lebecq A, Fangain A, Bareille J, Hamant O, Belkhadir Y, Jaillais Y, Caillaud M-C. 2020. iDePP: a genetically encoded system for the inducible depletion of PI(4,5)P_2 in *Arabidopsis thaliana*. *bioRxiv*. doi: 10.1101/2020.05.13.091470.

Duggan C, Moratto E, Savage Z, Hamilton E, Adachi H, Wu C-H, Leary AY, Tumtas Y, Rothery SM, Maqbool A *et al.* 2021. Dynamic localization of a helper NLR at the plant–pathogen interface underpins pathogen recognition. *Proceedings of the National Academy of Sciences, USA* **118**: e2104997118.

El Kasmi F, Chung EH, Anderson RG, Li J, Wan L, Eitas TK, Gao Z, Dangl JL. 2017. Signaling from the plasma-membrane localized plant immune receptor RPM1 requires self-association of the full-length protein. *Proceedings of the National Academy of Sciences, USA* **114**: E7385–E7394.

Engelhardt S, Boevink PC, Armstrong MR, Ramos MB, Hein I, Birch PR. 2012. Relocalization of late blight resistance protein R3a to endosomal compartments is associated with effector recognition and required for the immune response. *Plant Cell* **24**: 5142–5158.

Friedrichsen DM, Joazeiro CA, Li J, Hunter T, Chory J. 2000. Brassinosteroid-insensitive-1 is a ubiquitously expressed leucine-rich repeat receptor serine/threonine kinase. *Plant Physiology* **123**: 1247–1256.

Gao Z, Chung EH, Eitas TK, Dangl JL. 2011. Plant intracellular innate immune receptor resistance to *Pseudomonas syringae* pv. *maculicola* 1 (RPM1) is activated at, and functions on, the plasma membrane. *Proceedings of the National Academy of Sciences, USA* **108**: 7619–7624.

Gronnier J, Crowet J-M, Habenstein B, Nasir MN, Bayle V, Hosy E, Platre MP, Gouguet P, Raffaele S, Martinez D *et al.* 2017. Structural basis for plant plasma membrane protein dynamics and organization into functional nanodomains. *eLife* **6**: e26404.

Heo WD, Inoue T, Park WS, Kim ML, Park BO, Wandless TJ, Meyer T. 2006. PI(3,4,5)P3 and PI(4,5)P2 lipids target proteins with polybasic clusters to the plasma membrane. *Science* **314**: 1458–1461.

Hofmann K. 2020. The evolutionary origins of programmed cell death signaling. *Cold Spring Harbor Perspectives in Biology* **12**: a036442.

Hong Y, Zhao J, Guo L, Kim SC, Deng X, Wang G, Zhang G, Li M, Wang X. 2016. Plant phospholipases D and C and their diverse functions in stress responses. *Progress in Lipid Research* **62**: 55–74.

Hu M, Qi J, Bi G, Zhou JM. 2020. Bacterial effectors induce oligomerization of immune receptor ZAR1 in vivo. *Molecular Plant* **13**: 793–801.

Jacob P, Kim NH, Wu F, El-Kasmi F, Chi Y, Walton WG, Furzer OJ, Lietzan AD, Sunil S, Kempthorn K *et al.* 2021. Plant "helper" immune receptors are Ca(2+)-permeable nonselective cation channels. *Science* **373**: 420–425.

Johansson ON, Fahlberg P, Karimi E, Nilsson AK, Ellerstrom M, Andersson MX. 2014. Redundancy among phospholipase D isoforms in resistance triggered by recognition of the *Pseudomonas syringae* effector AvrRpm1 in *Arabidopsis thaliana*. *Frontiers in Plant Science* **5**: 639.

Jones JD, Dangl JL. 2006. The plant immune system. *Nature* **444**: 323–329.

Jubic LM, Saile S, Furzer OJ, El Kasmi F, Dangl JL. 2019. Help wanted: helper NLRs and plant immune responses. *Current Opinion in Plant Biology* **50**: 82–94.

Kawano Y, Fujiwara T, Yao A, Housen Y, Hayashi K, Shimamoto K. 2014. Palmitoylation-dependent membrane localization of the rice resistance protein pit is critical for the activation of the small GTPase OsRac1. *Journal of Biological Chemistry* **289**: 19079–19088.

Lapin D, Kovacova V, Sun X, Dongus JA, Bhandari D, von Born P, Bautor J, Guarneri N, Rzemieniewski J, Stuttmann J *et al.* 2019. A coevolved EDS1-SAG101-NRG1 module mediates cell death signaling by TIR-domain immune receptors. *Plant Cell* **31**: 2430–2455.

Li J, Wang X. 2019. Phospholipase D and phosphatidic acid in plant immunity. *Plant Science* **279**: 45–50.

Li L, Habring A, Wang K, Weigel D. 2020. Atypical resistance protein RPW8/HR triggers oligomerization of the NLR immune receptor RPP7 and autoimmunity. *Cell Host & Microbe* **27**: 405–417 e406.

Liu J, Elmore JM, Lin ZJ, Coaker G. 2011. A receptor-like cytoplasmic kinase phosphorylates the host target RIN4, leading to the activation of a plant innate immune receptor. *Cell Host & Microbe* **9**: 137–146.

Ma S, Lapin D, Liu LI, Sun Y, Song W, Zhang X, Logemann E, Yu D, Wang J, Jirschitzka J *et al.* 2020. Direct pathogen-induced assembly of an NLR immune receptor complex to form a holoenzyme. *Science* **370**: eabe3069.

Martin R, Qi T, Zhang H, Liu F, King M, Toth C, Nogales E, Staskawicz BJ. 2020. Structure of the activated ROQ1 resistosome directly recognizing the pathogen effector XopQ. *Science* **370**: abd9993.

McLaughlin S, Murray D. 2005. Plasma membrane phosphoinositide organization by protein electrostatics. *Nature* **438**: 605–611.

Menzel W, Stenzel I, Helbig LM, Krishnamoorthy P, Neumann S, Eschen-Lippold L, Heilmann M, Lee J, Heilmann I. 2019. A PAMP-triggered MAPK cascade inhibits phosphatidylinositol 4,5-bisphosphate production by PIP5K6 in *Arabidopsis thaliana*. *New Phytologist* **224**: 833–847.

Monteiro F, Nishimura MT. 2018. Structural, functional, and genomic diversity of plant NLR proteins: an evolved resource for rational engineering of plant immunity. *Annual Review of Phytopathology* **56**: 243–267.

Murphy JM. 2020. The killer pseudokinase mixed lineage kinase domain-like protein (MLKL). *Cold Spring Harbor Perspectives in Biology* **12**: a036376.

Noack LC, Jaillais Y. 2017. Precision targeting by phosphoinositides: how PIs direct endomembrane trafficking in plants. *Current Opinion in Plant Biology* **40**: 22–33.

Platre MP, Noack LC, Doumane M, Bayle V, Simon MLA, Maneta-Peyret L, Fouillen L, Stanislas T, Armengot L, Pejchar P *et al.* 2018. A combinatorial lipid code shapes the electrostatic landscape of plant endomembranes. *Developmental Cell* **45**: 465–480.e11.

Pottinger SE, Innes RW. 2020. RPS5-mediated disease resistance: fundamental insights and translational applications. *Annual Review of Phytopathology* **58**: 139–160.

Pruitt RN, Locci F, Wanke F, Zhang L, Saile SC, Joe A, Karelina D, Hua C, Fröhlich K, Wan W-L *et al.* 2021. The EDS1-PAD4-ADR1 node mediates *Arabidopsis thaliana* pattern-triggered immunity. *Nature*. doi: 10.1038/s41586-021-03829-0.

Qi D, DeYoung BJ, Innes RW. 2012. Structure-function analysis of the coiled-coil and leucine-rich repeat domains of the RPS5 disease resistance protein. *Plant Physiology* **158**: 1819–1832.

Qi T, Seong K, Thomazella DPT, Kim JR, Pham J, Seo E, Cho M-J, Schultink A, Staskawicz BJ. 2018. NRG1 functions downstream of EDS1 to regulate TIR-NLR-mediated plant immunity in *Nicotiana benthamiana*. *Proceedings of the National Academy of Sciences, USA* **115**: E10979–E10987.

Qin LI, Zhou Z, Li Q, Zhai C, Liu L, Quilichini TD, Gao P, Kessler SA, Jaillais Y, Datla R *et al.* 2020. Specific recruitment of phosphoinositide species to the plant-pathogen interfacial membrane underlies Arabidopsis susceptibility to fungal infection. *Plant Cell* **32**: 1665–1688.

Quarato G, Guy CS, Grace CR, Llambi F, Nourse A, Rodriguez DA, Wakefield R, Frase S, Moldoveanu T, Green DR. 2016. Sequential engagement of distinct MLKL phosphatidylinositol-binding sites executes necroptosis. *Molecular Cell* **61**: 589–601.

Rausche J, Stenzel I, Stauder R, Fratini M, Trujillo M, Heilmann I, Rosahl S. 2020. A phosphoinositide 5-phosphatase from *Solanum tuberosum* is activated by PAMP-treatment and may antagonize phosphatidylinositol 4,5-bisphosphate at *Phytophthora infestans* infection sites. *New Phytologist* **229**: 469–487.

Reuter L, Schmidt T, Manishankar P, Throm C, Keicher J, Bock A, Oecking C. 2021. Light-triggered and phosphorylation-dependent 14-3-3 association with NONPHOTOTROPIC HYPOCOTYL 3 is required for hypocotyl phototropism. *bioRxiv*. doi: 10.1101/2021.04.09.439179.

Roberts M, Tang S, Stallmann A, Dangl JL, Bonardi V. 2013. Genetic requirements for signaling from an autoactive plant NB-LRR intracellular innate immune receptor. *PLoS Genetics* **9**: e1003465.

Saile SC, Jacob P, Castel B, Jubic LM, Salas-Gonzalez I, Backer M, Jones JDG, Dangl JL, El Kasmi F. 2020. Two unequally redundant "helper" immune receptor families mediate *Arabidopsis thaliana* intracellular "sensor" immune receptor functions. *PLoS Biology* **18**: e3000783.

Schloffel MA, Salzer A, Wan WL, van Wijk R, Del Corvo R, Semanjski M, Symeonidi E, Slaby P, Kilian J, Macek B *et al.* 2020. The BIR2/BIR3-associated phospholipase Dγ1 negatively regulates plant immunity. *Plant Physiology* **183**: 371–384.

Shimada TL, Betsuyaku S, Inada N, Ebine K, Fujimoto M, Uemura T, Takano Y, Fukuda H, Nakano A, Ueda T. 2019. Enrichment of phosphatidylinositol 4,5-bisphosphate in the extra-invasive hyphal membrane promotes colletotrichum infection of *Arabidopsis thaliana*. *Plant and Cell Physiology* **60**: 1514–1524.

Simon ML, Platre MP, Marques-Bueno MM, Armengot L, Stanislas T, Bayle V, Caillaud MC, Jaillais Y. 2016. A PtdIns(4)P-driven electrostatic field controls cell membrane identity and signalling in plants. *Nature Plants* **2**: 16089.

Van Ooijen G, Mayr G, Kasiem MMA, Albrecht M, Cornelissen BJC, Takken FLW. 2008. Structure-function analysis of the NB-ARC domain of plant disease resistance proteins. *Journal of Experimental Botany* **59**: 1383–1397.

Viotti C, Kruger F, Krebs M, Neubert C, Fink F, Lupanga U, Scheuring D, Boutte Y, Frescatada-Rosa M, Wolfenstetter S *et al.* 2013. The endoplasmic reticulum is the main membrane source for biogenesis of the lytic vacuole in *Arabidopsis*. *Plant Cell* **25**: 3434–3449.

Wang J, Chai J. 2020. Molecular actions of NLR immune receptors in plants and animals. *Science China Life Sciences* **63**: 1–14.

Wang J, Chen T, Han M, Qian L, Li J, Wu M, Han T, Cao J, Nagalakshmi U, Rathjen JP *et al.* 2020a. Plant NLR immune receptor Tm-22 activation requires NB-ARC domain-mediated self-association of CC domain. *PLoS Pathogens* **16**: e1008475.

Wang J, Chern M, Chen X. 2020b. Structural dynamics of a plant NLR resistosome: transition from autoinhibition to activation. *Science China Life Sciences* **63**: 617–619.

Wang J, Hu M, Wang J, Qi J, Han Z, Wang G, Qi Y, Wang HW, Zhou JM, Chai J. 2019a. Reconstitution and structure of a plant NLR resistosome conferring immunity. *Science* **364**: eaav5870.

Wang J, Wang J, Hu M, Wu S, Qi J, Wang G, Han Z, Qi Y, Gao N, Wang HW *et al.* 2019b. Ligand-triggered allosteric ADP release primes a plant NLR complex. *Science* **364**: eaav5868.

Williams SJ, Sornaraj P, deCourcy-Ireland E, Menz RI, Kobe B, Ellis JG, Dodds PN, Anderson PA. 2011. An autoactive mutant of the M flax rust resistance protein has a preference for binding ATP, whereas wild-type M protein binds ADP. *Molecular Plant–Microbe Interactions* **24**: 897–906.

Wu Z, Li M, Dong OX, Xia S, Liang W, Bao Y, Wasteneys G, Li X. 2019. Differential regulation of TNL-mediated immune signaling by redundant helper CNLs. *New Phytologist* **222**: 938–953.

Wu Z, Tian L, Liu X, Zhang Y, Li X. 2021. TIR signal promotes interactions between lipase-like proteins and ADR1-L1 receptor and ADR1-L1 oligomerization. *Plant Physiology* **187**: 681–686.

Xing J, Li X, Wang X, Lv X, Wang L, Zhang L, Zhu Y, Shen Q, Baluska F, Samaj J *et al.* 2019. Secretion of phospholipase Dδ functions as a regulatory mechanism in plant innate immunity. *Plant Cell* **31**: 3015–3032.

Xiong Y, Han Z, Chai J. 2020. Resistosome and inflammasome: platforms mediating innate immunity. *Current Opinion in Plant Biology* **56**: 47–55.

Yeung T, Terebiznik M, Yu L, Silvius J, Abidi WM, Philips M, Levine T, Kapus A, Grinstein S. 2006. Receptor activation alters inner surface potential during phagocytosis. *Science* **313**: 347–351.

Yoshioka K, Moeder W, Kang HG, Kachroo P, Masmoudi K, Berkowitz G, Klessig DF. 2006. The chimeric *Arabidopsis* CYCLIC NUCLEOTIDE-GATED ION CHANNEL11/12 activates multiple pathogen resistance responses. *Plant Cell* **18**: 747–763.

Yuan X, Wang Z, Huang J, Xuan H, Gao Z. 2018. Phospholipidase Dδ negatively regulates the function of resistance to *Pseudomonas syringae* pv. *maculicola* 1 (RPM1). *Frontiers in Plant Science* **9**: 1991.

Zhao C, Tang Y, Wang J, Zeng Y, Sun H, Zheng Z, Su R, Schneeberger K, Parker JE, Cui H. 2021. A mis-regulated cyclic nucleotide-gated channel mediates cytosolic calcium elevation and activates immunity in *Arabidopsis*. *New Phytologist* **230**: 1078–1094.

Supporting Information

Additional Supporting Information may be found online in the Supporting Information section at the end of the article.

Fig. S1 Subcellular localization of AtADR1 proteins after transient over-expression in *Nicotiana benthamiana*.

Fig. S2 Subcellular localization of native promoter-driven AtADR1 proteins.

Fig. S3 Characterization of the cell death activity of wild-type (WT), P-loop and QHD variants of AtADR1s.

Fig. S4 AtRPS5 plasma membrane localization and its cell death activity are not affected by MAP-SAC1 or MAP-dOCRL co-expression.

Fig. S5 Degradation of mis-localized AtRPM1 and AtADR1 proteins is not or only partially blocked by proteasome inhibitors.

Fig. S6 Effector-triggered AtRPM1-mediated cell death activity is diminished by PI4P depletion.

Fig. S7 PI4P depletion affects the PM localization of AtADR1 CC_R domains.

Fig. S8 $PI(4,5)P_2$ is not required for the PM localization and stability of AtADR1s and AtRPM1.

Fig. S9 AtADR1s and AtRPM1 cell death activity is not affected by depletion of $PI(4,5)P_2$ from the plasma membrane via MAP-dOCRL co-expression.

Fig. S10 Basic-hydrophobic (BH) profile analysis of CC/CC_R domains.

Fig. S11 Proposed model of AtADR1 localization, oligomerization and function during immunity.

Methods S1 Protocols for the experiments used in this work.

Table S1 Primer list.

Table S2 Transmembrane domain and lipidation prediction summary for *Arabidopsis thaliana* RNLs and the CNLs RPM1 and RPS5.

Please note: Wiley Blackwell are not responsible for the content or functionality of any Supporting Information supplied by the authors. Any queries (other than missing material) should be directed to the *New Phytologist* Central Office.

Arabidopsis ADR1 helper NLR immune receptors localize and function at the plasma membrane in a phospholipid dependent manner

Svenja C. Saile[1], Frank M. Ackermann[1], Sruthi Sunil[1], Jutta Keicher[1], Adam Bayless[2], Vera Bonardi[3], Li Wan[3], Mehdi Doumane[4], Eva Stöbbe[1], Yvon Jaillais[4], Marie-Cécile Caillaud[4], Jeffery L. Dangl[3,5], Marc T. Nishimura[2], Claudia Oecking[1] and Farid El Kasmi*[,1]

Article acceptance date: 15 September 2021

Supporting Information

includes: -Supplementary Figures S1 – S11 and figure legends
-Supplementary Tables S1 and S2
-Supplementary Methods S1

Supplementary Figure legends

Fig. S1 Subcellular localization of AtADR1 proteins after transient over-expression in *N. benthamiana.*

Maximum projection of Z-stack images clearly demonstrates that AtADR1 proteins localize to the plasma membrane after transient expression in *N. benthamiana* leaves. (**a, b, e, f, g, h**) AtADR1 proteins (ADR1, ADR1-L1, ADR1-L2) localize mainly to the plasma membrane. The indicated ADR1 proteins fused to EYFP or Citrine-HA were transiently co-expressed with the PM-resident BRI1-mRFP fusion-protein and confocal imaging was done at 4 hours (**a, b, f**) or 5 hours (**h**) post Estradiol induction or 2 days post infiltration (**e, g**). (**c, d**) ADR1 also localizes to the endoplasmic reticulum (ER). Wildtype ADR1 or the autoactivated mutant ADR1^{DV} fused to Citrine-HA was transiently co-expressed with the ER-localized AtVMA12-RFP fusion-protein and confocal imaging was done at 3 hours (**c**) and 4 hours (**d**) post Estradiol induction. ADR1, ADR1^{DV} and ADR1-L1^{DV} additionally localize to puncta indicated by white arrowheads in **a, b, c, d, f**). Localization of EYFP and Citrine-HA tagged ADR1 proteins is shown with the first column (Citrine/YFP, in yellow) and the co-localized PM-localized BRI1-mRFP or ER-localized VMA12-RFP is shown in the second column (RFP, in magenta). Chloroplasts are shown in the third column (Chlorophyll A, in cyan) and the merged images are shown in the fourth column. Images shown here are a maximum projection of Z-stack images. Scale bars, 20 μm.

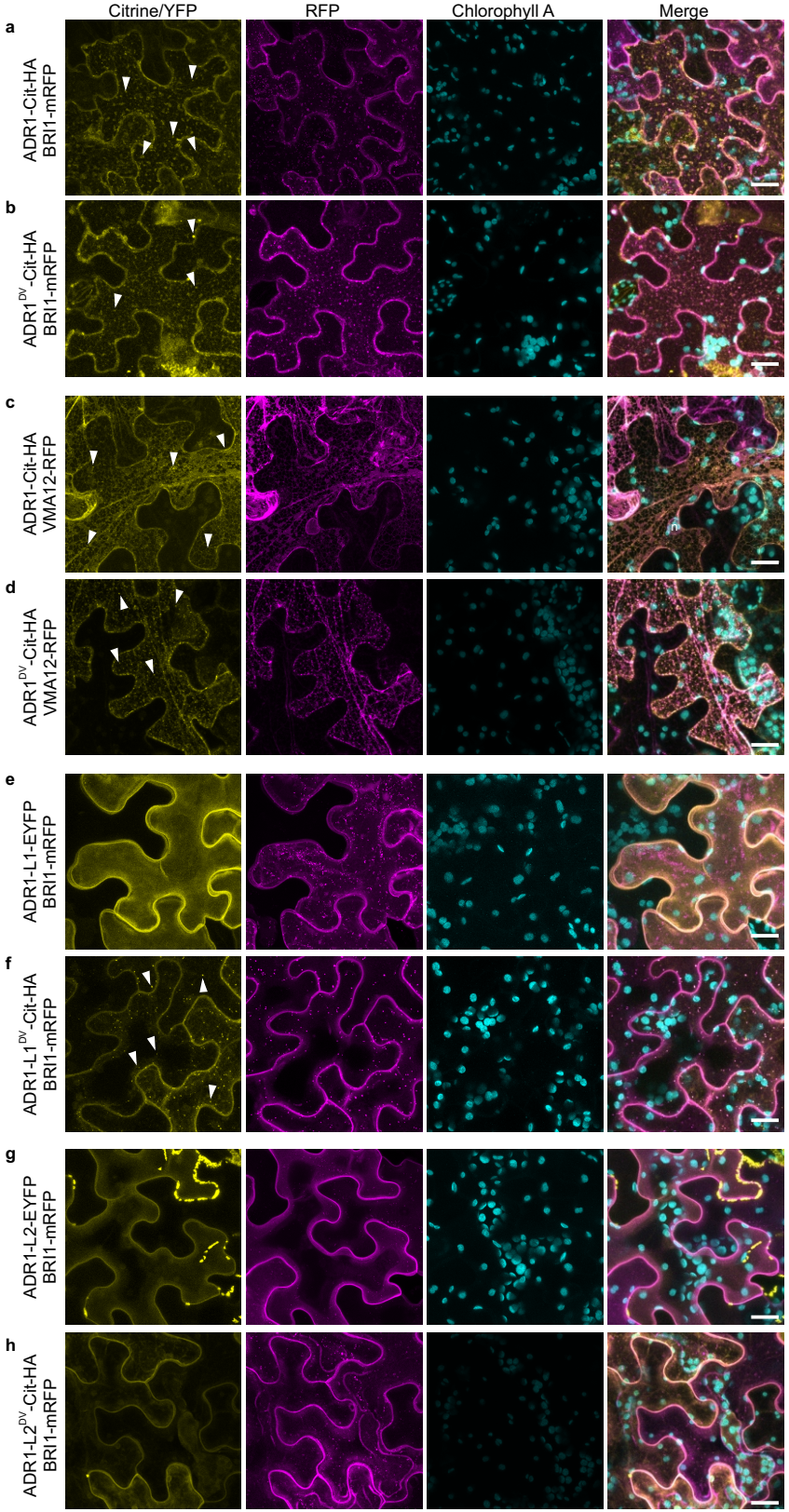
Citrine/YFP
RFP
Chlorophyll A
Merge
a
ADR1-Cit-HA
BRI1-mRFP
b
ADR1DV-Cit-HA
BRI1-mRFP
c
ADR1-Cit-HA
VMA12-RFP
n
d
ADR1DV-Cit-HA
VMA12-RFP
e
ADR1-L1-EYFP
BRI1-mRFP
f
ADR1-L1DV-Cit-HA
BRI1-mRFP
g
ADR1-L2-EYFP
BRI1-mRFP
h
ADR1-L2DV-Cit-HA
BRI1-mRFP

Figure S1

Fig. S2 Subcellular localization of native promoter-driven AtADR1 proteins.

(**a-c**) Single plane secant views show that AtADR1 proteins (ADR1, ADR1-L1, ADR1-L2) localize to the plasma membrane (PM) when expressed under control of their native promoters. The indicated ADR1 proteins fused to YFP/EYFP were transiently co-expressed with the PM-resident protein BRI1-mRFP in *N. benthamiana* leaves and confocal imaging was done 3 days post infiltration (dpi; **a**) or 2 dpi (**b, c**). Localization of ADR1s is shown with the first column (YFP, in yellow) and the co-localized PM-resident BRI1 is shown in the second column (RFP, in magenta). Chloroplasts are shown in the third column (Chlorophyll A, in cyan) and the merged images are shown in the fourth column (merge). Fluorescence intensities were measured along the dotted line depicted in the merge images. Scale bars, 20 μm. (**d, e**) Subcellular fractionation experiments of protein extracts prepared from 7-day old *A. thaliana* seedlings stably expressing AtADR1-L2-HA under control of its native promoter (**d**) or from 6-week-old *A. thaliana* plants stably expressing AtADR1-L2^{DV}-HA under control of its native promoter (**e**) reveal a strong membrane association of AtADR1-L2-HA (**d**) and ADR1-L2^{DV} (**e**). Shown are immunoblots of ADR1-L2-HA (**d**) and ADR1-L2^{DV}-HA (**e**) and the cytosolic marker UDP-glucose pyrophosphorylase (UGPase) using anti-HA or anti-UGPase antibody, respectively. 20 μg (**d**) or 40 μg (**e**) protein of each protein fraction (total, soluble, microsomes) was used for SDS-PAGE. Numbers show quantification of band intensities normalized to the band of the total protein fractions, respectively. T: total extract, S: soluble protein fraction, M: microsomal protein fraction.

Figure S2

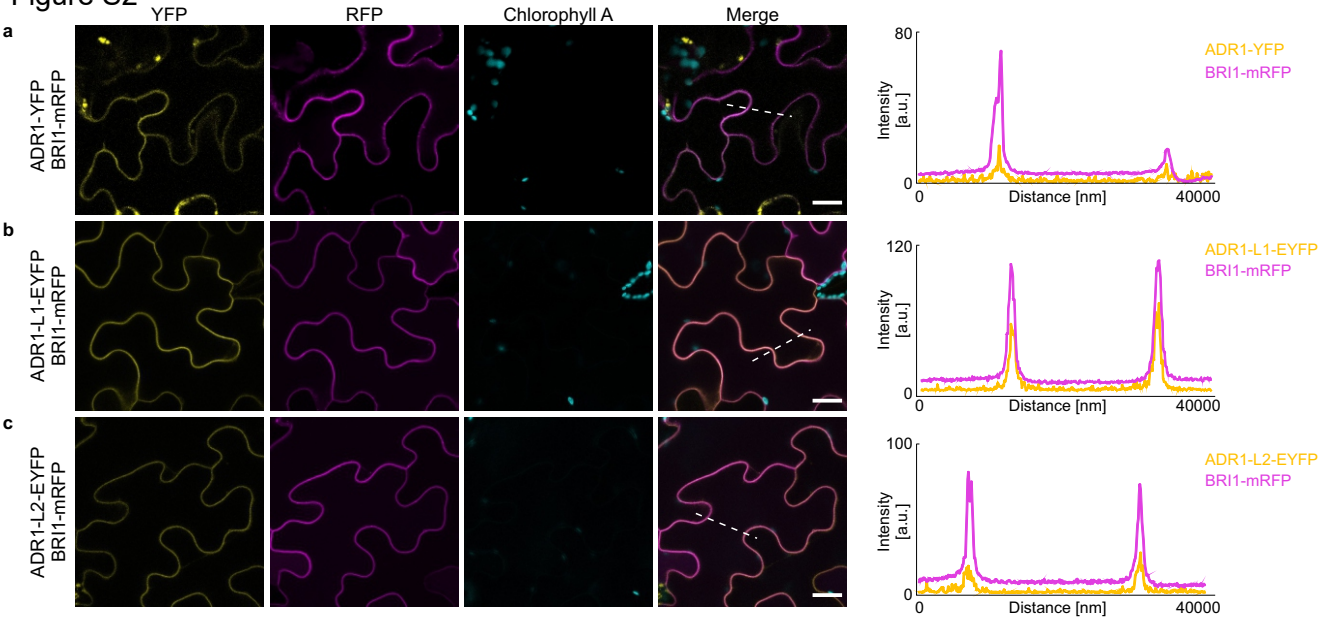
a
b
c
YFP
RFP
Chlorophyll A
Merge
ADR1-YFP
BRI1-mRFP
ADR1-L1-EYFP
BRI1-mRFP
ADR1-L2-EYFP
BRI1-mRFP
Intensity [a.u.]
Distance [nm]
0
40000
80
120
100
ADR1-YFP
BRI1-mRFP
ADR1-L1-EYFP
BRI1-mRFP
ADR1-L2-EYFP
BRI1-mRFP

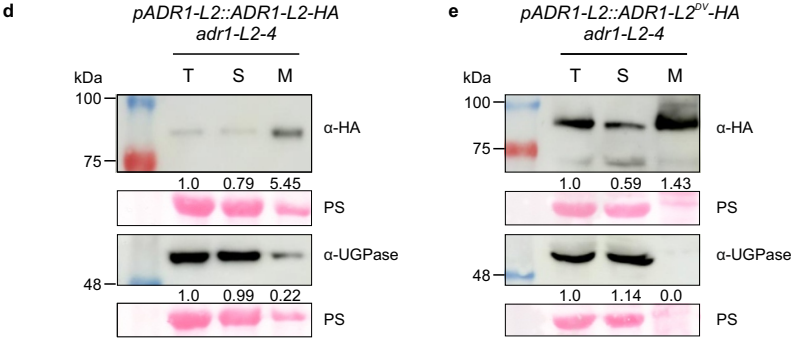
d
pADR1-L2::ADR1-L2-HA
adr1-L2-4
kDa
T
S
M
100
75
48
α-HA
1.0
0.79
5.45
PS
α-UGPase
1.0
0.99
0.22
PS
e
pADR1-L2::ADR1-L2pv-HA
adr1-L2-4
kDa
T
S
M
100
75
48
α-HA
1.0
0.59
1.43
PS
α-UGPase
1.0
1.14
0.0
PS

Fig. S3 Characterization of the cell death activity of WT, P-loop and QHD variants of AtADR1s.

Transient expression of AtADR1s steady-state (WT), P-loop mutant (AAA) or QHD mutant (DV) Citrine-HA fusion proteins in *N. benthamiana*. ADR1, ADR1^{AAA} and ADR1^{DV} induce a strong HR-like cell death, whereas ADR1-L1^{DV} triggers a weak and ADR1-L2^{DV} a very weak HR-like cell death. Photos were taken under normal light at 23 hours post Estradiol induction and 47 hours post infiltration. Numbers represent the number of leaves showing cell death out of the number of leaves analysed. Asterisk indicates weak cell death, double-asterisk indicates very weak cell death.

Figure S3


ADR1WT
28/28
ADR1DV
28/28
ADR1AAA
8/8
ADR1-L1WT
0/26
ADR1-L1DV
24*/26
ADR1-L1AAA
0/6
ADR1-L2WT
0/26
ADR1-L2DV
13**/26
ADR1-L2AAA
2**/6

Fig. S4 AtRPS5 plasma membrane localization and its cell death activity are not affected by MAP-SAC1 or MAP-dOCRL co-expression.

(**a**) Plasma membrane localization of AtRPS5-EYFP is not affected by co-expression of MAP-mCherry-SAC1^{dead} (upper panel) or MAP-mCherry-SAC1^{WT} (lower panel). (**c**) Co-expression of MAP-mCherry-dOCRL^{dead} (upper panel) or MAP-mCherry-dOCRL^{WT} (lower panel) does not affect RPS5-EYFP PM localization. Indicated proteins were transiently expressed in *N. benthamiana* leaves and confocal imaging was done at 24 hours post infiltration. Localization of RPS5-EYFP is shown with the first column (YFP, in yellow) and MAP-mCherry-SAC1^{WT}, MAP-mCherry-SAC1^{dead}, MAP-mCherry-dOCRL^{dead} and MAP-mCherry-dOCRL^{WT} are shown in the second column (mCherry, in magenta). Chloroplasts are shown in the third column (Chlorophyll A, in cyan) and the merged images are shown in the fourth column (merge). Images are single plane secant views. Scale bars, 20 μm. (**b, d**) Immunoblot analysis of the transiently expressed proteins (see (**a**, **c**)) using anti-GFP and anti-RFP antibody, respectively. Equal loading of the proteins is indicated by the Rubisco band from the Ponceau staining (PS). Numbers show quantification of band intensities normalized to the Rubisco band from the Ponceau staining. Samples were collected 24 hours post infiltration. (**e, f**) Effector (AvrPphB)-triggered and RPS5-EYFP mediated cell death is not suppressed by MAP-mCherry-SAC1^{WT} (**e**) or MAP-mCherry-dOCRL^{WT} (**f**) co-expression in *N. benthamiana*. Leaf images showing cell death induction by activated RPS5-EYFP (upper panels). Transient expression of the Dexamethasone-inducible effector AvrPphB-MYC and the guardee protein PBS1-HA with constitutively expressed RPS5-EYFP, MAP-mCherry-SAC1^{WT} or MAP-mCherry-SAC1^{dead} (**e**) or MAP-mCherry-dOCRL^{dead} and MAP-mCherry-dOCRL^{WT} (**f**). Leaf images were taken under UV light at 24 hours post Dexamethasone induction, which corresponds to 2 days post infiltration (**e, f**). AvrPphB-MYC and PBS1-HA expression was induced with 30 μM Dexamethasone to activate RPS5-EYFP. White/light grey areas indicate dead leaf tissue. Numbers represent the number of leaves showing cell death out of the number of leaves analysed. Immunoblot analysis (lower panels) of the transiently expressed proteins (see upper panels) using anti-GFP and anti-RFP antibody, respectively. Equal loading of the proteins is indicated by the Rubisco band from the Ponceau staining (PS). Numbers show quantification of band intensities normalized to the Rubisco band from the Ponceau staining. Protein samples were collected at 6 hours post Dexamethasone induction, which corresponds to 28 hours post infiltration.

Figure S4

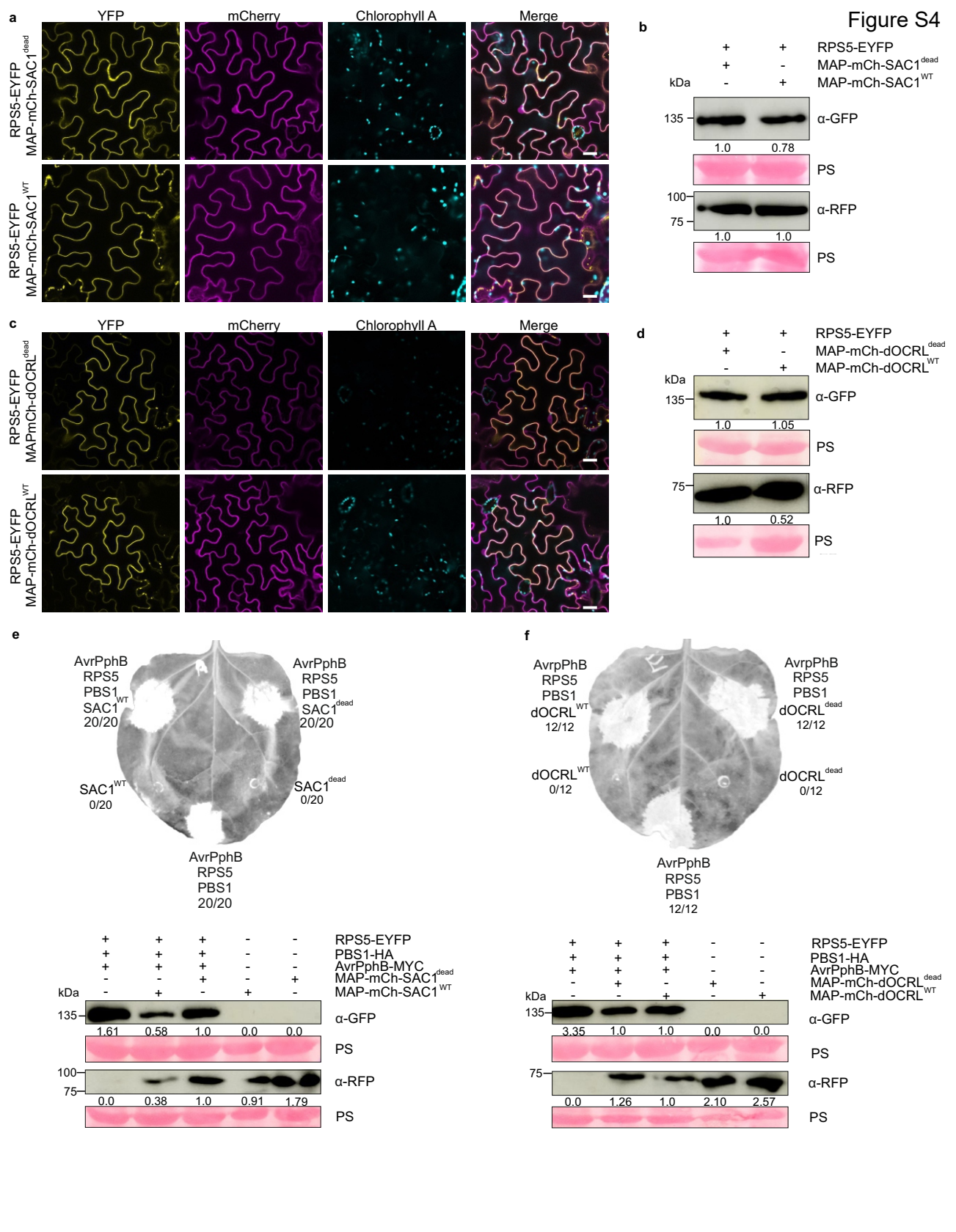
a
YFP
mCherry
Chlorophyll A
Merge
RPS5-EYFP
MAP-mCh-SAC1dead
RPS5-EYFP
MAP-mCh-SAC1WT
b
RPS5-EYFP
MAP-mCh-SAC1dead
MAP-mCh-SAC1WT
kDa
135
α-GFP
1.0 0.78
PS
100
75
α-RFP
1.0 1.0
PS
c
YFP
mCherry
Chlorophyll A
Merge
RPS5-EYFP
MAPmCh-dOCRLdead
RPS5-EYFP
MAP-mCh-dOCRLWT
d
RPS5-EYFP
MAP-mCh-dOCRLdead
MAP-mCh-dOCRLWT
kDa
135
α-GFP
1.0 1.05
PS
75
α-RFP
1.0 0.52
PS
e
AvrPphB
RPS5
PBS1WT
SAC1
20/20
AvrPphB
RPS5
PBS1
SAC1dead
20/20
SAC1WT
0/20
SAC1dead
0/20
AvrPphB
RPS5
PBS1
20/20
RPS5-EYFP
PBS1-HA
AvrPphB-MYC
MAP-mCh-SAC1dead
MAP-mCh-SAC1WT
kDa
135
α-GFP
1.61 0.58 1.0 0.0 0.0
PS
100
75
α-RFP
0.0 0.38 1.0 0.91 1.79
PS
f
AvrpPhB
RPS5
PBS1
dOCRLWT
12/12
AvrpPhB
RPS5
PBS1
dOCRLdead
12/12
dOCRLWT
0/12
dOCRLdead
0/12
AvrPphB
RPS5
PBS1
12/12
RPS5-EYFP
PBS1-HA
AvrPphB-MYC
MAP-mCh-dOCRLdead
MAP-mCh-dOCRLWT
kDa
135
α-GFP
3.35 1.0 1.0 0.0 0.0
PS
75
α-RFP
0.0 1.26 1.0 2.10 2.57
PS

Fig. S5 Degradation of mis-localized AtRPM1 and AtADR1 proteins is not or only partially blocked by proteasome inhibitors.

(**a-c**) Treatment of a 1x Protease Inhibitor Cocktail (PIC) or 2.5 µM Bortezomib (BTZ) fully (**a**) or partially (**b, c**) inhibit the degradation of mis-localized AtADR1 proteins. (**d**) Mis-localized AtRPM1 protein degradation can partially be blocked by a PIC treatment, however not by BTZ. Shown are anti-GFP immunoblots of AtADR1 (**a**), AtADR1-L1 (**b**), AtADR1-L2 (**c**) and AtRPM1 (**d**) Citrine-HA or EYFP fusion proteins that were transiently co-expressed with MAP-mCherry-SAC1^{WT} or MAP-mCherry-SAC1^{dead} in *N. benthamiana*. Equal loading of the proteins is indicated by the Rubisco band from the Ponceau staining (PS). Numbers show quantification of band intensities normalized to the Rubisco band from the Ponceau staining. Samples were collected 4 hours (**a**) or 5 hours (**b-d**) post inhibitor and Estradiol (**a**) treatments, which corresponds to 27 (**a**) and 25 hours (**b-d**) post infiltration.

Figure S5

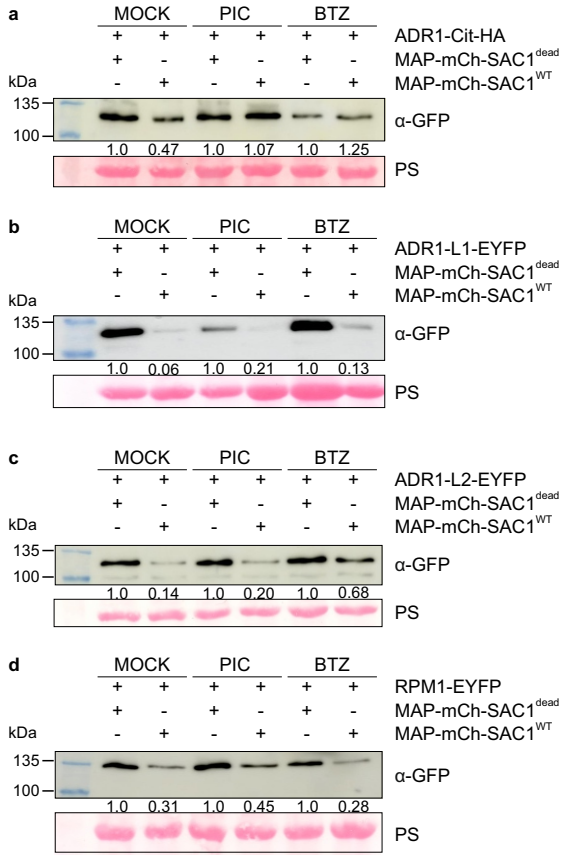
a
MOCK
PIC
BTZ
+ + + + + +
ADR1-Cit-HA
+ - + - + -
MAP-mCh-SAC1dead
- + - + - +
MAP-mCh-SAC1WT
kDa
135
100
1.0 0.47 1.0 1.07 1.0 1.25
α-GFP
PS
b
MOCK
PIC
BTZ
+ + + + + +
ADR1-L1-EYFP
+ - + - + -
MAP-mCh-SAC1dead
- + - + - +
MAP-mCh-SAC1WT
kDa
135
100
1.0 0.06 1.0 0.21 1.0 0.13
α-GFP
PS
c
MOCK
PIC
BTZ
+ + + + + +
ADR1-L2-EYFP
+ - + - + -
MAP-mCh-SAC1dead
- + - + - +
MAP-mCh-SAC1WT
kDa
135
100
1.0 0.14 1.0 0.20 1.0 0.68
α-GFP
PS
d
MOCK
PIC
BTZ
+ + + + + +
RPM1-EYFP
+ - + - + -
MAP-mCh-SAC1dead
- + - + - +
MAP-mCh-SAC1WT
kDa
135
100
1.0 0.31 1.0 0.45 1.0 0.28
α-GFP
PS

Fig. S6 Effector-triggered AtRPM1-mediated cell death response is diminished by PI4P depletion.

(**a**, upper panel) CC_R domain of AtADR1-L1 induces no visible cell death symptoms and thus no effect of MAP-mCherry-SAC1^{WT} co-expression on AtADR1-L1 CC_R activity is observable. Transient co-expression of ADR1-L1 CC_R-EYFP, MAP-mCherry-SAC1^{WT} or MAP-mCherry-SAC1^{dead} in *N. benthamiana* leaves. (**b**, upper panel) mCherry-SAC1^{WT} co-expression noticeably reduced cell death activity of AvrRpm1-HA activated RPM1-EYFP. Transient expression of RPM1-EYFP, AvrRPM1-HA, T7-RIN4 and MAP-mCherry-SAC1^{WT} or MAP-mCherry-SAC1^{dead} in *N. benthamiana* leaves. (**c**, upper panel) Cell death activity of AvrRpm1-HA activated RPM1-EYFP was not blocked by co-expression of MAP-mCherry-dOCRL^{dead} or MAP-mCherry-dOCRL^{WT}. Transient expression of RPM1-EYFP, AvrRPM1-HA, T7-RIN4 and MAP-mCherry-dOCRL^{dead} or MAP-mCherry-dOCRL^{WT} in *N. benthamiana* leaves. AvrRPM1-HA expression was induced with 30 μM Dexamethasone 20 hours post infiltration. Leaf images were taken under UV light at 24 hours post infiltration (**a**) or 24 hours post Dexamethasone induction (**b**, **c**). The effector AvrRpm1 and the guardee protein RIN4 was co-expressed to activate RPM1. White/light grey areas indicate dead leave tissue. Numbers represent the number of leaves showing cell death out of the number of leaves analysed. Asterisk in (**b**) indicates weak cell death. (**a-c**, lower panels) Immunoblot analysis of the proteins transiently expressed in leaves (see upper panels) using anti-GFP and anti-RFP antibody, respectively. Equal loading of the proteins is indicated by the Rubisco band from the Ponceau staining (PS). Numbers show quantification of band intensities normalized to the Rubisco band from the Ponceau staining. Protein samples were collected at 20 hours post infiltration (**a**) and 6 hours post Dexamethasone induction, which corresponds to 26 hours post infiltration (**b, c**).

Figure S6

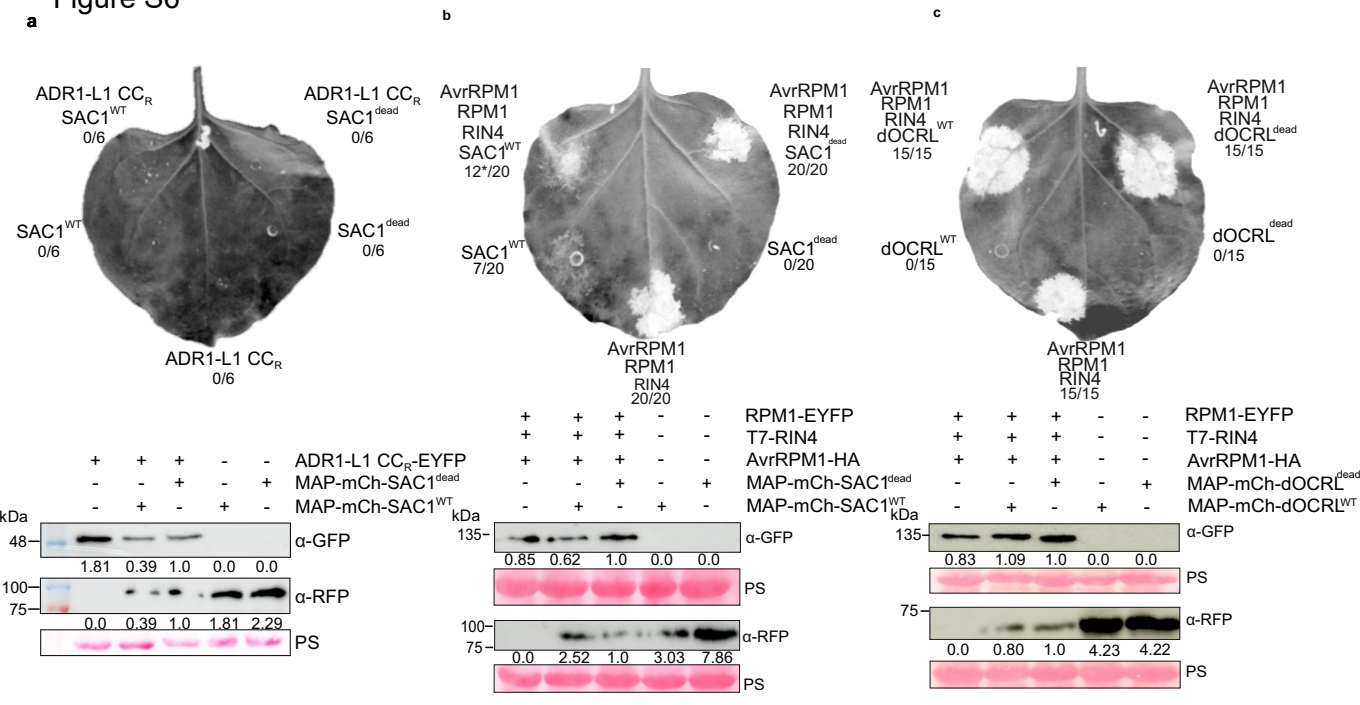
a
ADR1-L1 CC$_R$
SAC1^{WT}
0/6
ADR1-L1 CC$_R$
SAC1^{dead}
0/6
SAC1^{WT}
0/6
SAC1^{dead}
0/6
ADR1-L1 CC$_R$
0/6
ADR1-L1 CC$_R$-EYFP
MAP-mCh-SAC1^{dead}
MAP-mCh-SAC1^{WT}
kDa
48
α-GFP
1.81 0.39 1.0 0.0 0.0
100
75
α-RFP
0.0 0.39 1.0 1.81 2.29
PS
b
AvrRPM1
RPM1
RIN4
SAC1^{WT}
12*/20
AvrRPM1
RPM1
RIN4$_{dead}$
SAC1^{dead}
20/20
SAC1^{WT}
7/20
SAC1^{dead}
0/20
AvrRPM1
RPM1
RIN4
20/20
RPM1-EYFP
T7-RIN4
AvrRPM1-HA
MAP-mCh-SAC1^{dead}
MAP-mCh-SAC1^{WT}
kDa
135
α-GFP
0.85 0.62 1.0 0.0 0.0
PS
100
75
α-RFP
0.0 2.52 1.0 3.03 7.86
PS
c
AvrRPM1
RPM1
RIN4
dOCRL^{WT}
15/15
AvrRPM1
RPM1
RIN4
dOCRL^{dead}
15/15
dOCRL^{WT}
0/15
dOCRL^{dead}
0/15
AvrRPM1
RPM1
RIN4
15/15
RPM1-EYFP
T7-RIN4
AvrRPM1-HA
MAP-mCh-dOCRL^{dead}
MAP-mCh-dOCRL^{WT}
kDa
135
α-GFP
0.83 1.09 1.0 0.0 0.0
PS
75
α-RFP
0.0 0.80 1.0 4.23 4.22
PS

Fig. S7 PI4P depletion affects the PM localization of AtADR1 CC_R domains.

Co-expression with $SAC1^{WT}$ affects AtADR1 CC_R (**a**), AtADR1-L1 CC_R (**b**) and AtADR1-L2 CC_R (**c**) localization. C-terminally Citrine-HA tagged AtADR1 (ADR1, ADR1-L1, ADR1-L2) CC_R domains were transiently co-expressed with MAP-mCherry-$SAC1^{dead}$ (**a-c**, upper panel) or MAP-mCherry-$SAC1^{WT}$ (**a-c**, lower panel) in *N. benthamiana* leaves. Confocal imaging was done at 3 hours (**a**) or 4 hours after Estradiol induction (**b, c**). AtADR1 CC_R, AtADR1-L1 CC_R and AtADR1-L2 CC_R domains re-localize to intracellular puncta (white arrow heads), potentially endosomes. Localization of AtADR1 CC_R-Citrine-HA domains is shown with the first column (Citrine, in yellow) and MAP-mCherry-$SAC1^{WT}$ or MAP-mCherry-$SAC1^{dead}$ is shown in the second column (mCherry, in magenta). Chloroplasts are shown in the third column (Chlorophyll A, in cyan) and the merged images are shown in the fourth column (merge). Images shown here are a maximum projection of Z-stack images. Scale bars, 20 μm.

Figure S7

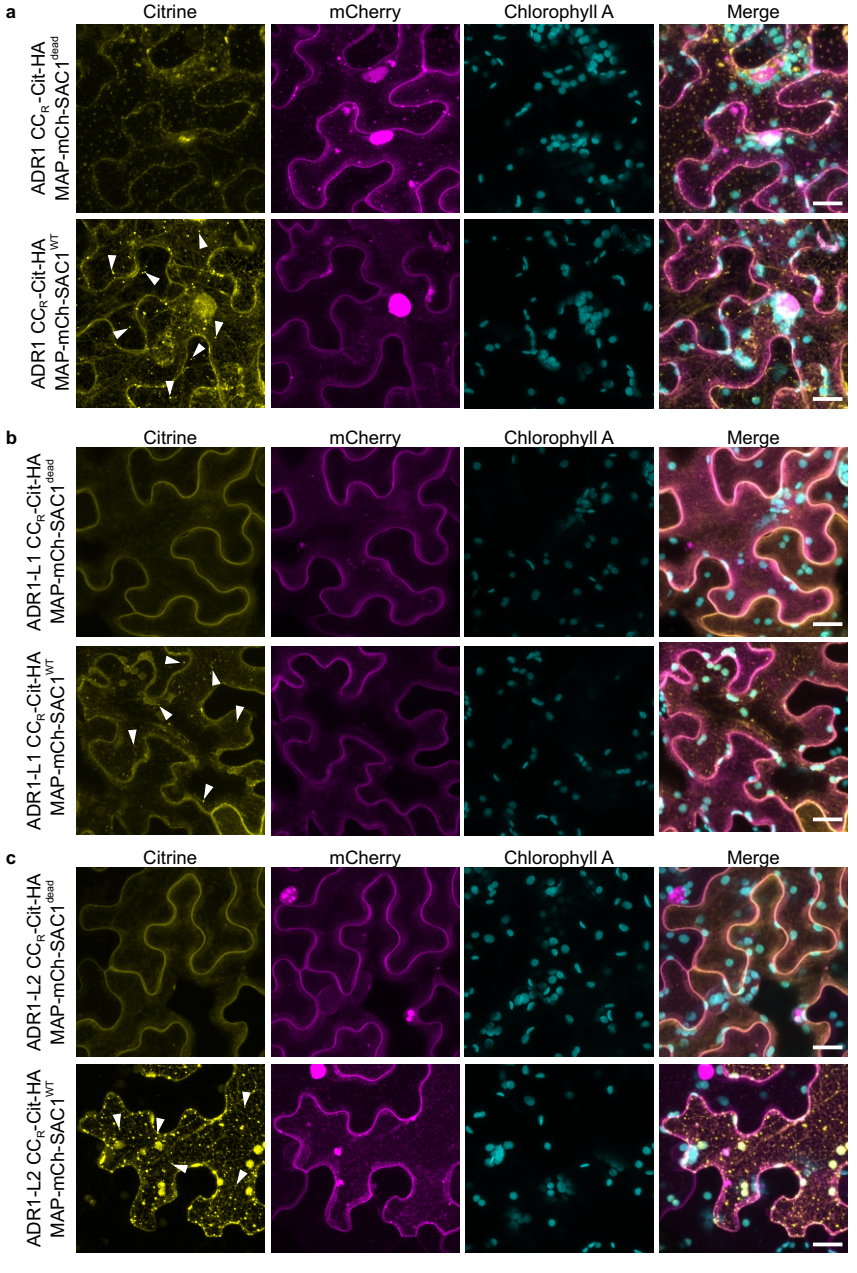
a
Citrine
mCherry
Chlorophyll A
Merge
ADR1 CC$_R$-Cit-HA
MAP-mCh-SAC1^{dead}
ADR1 CC$_R$-Cit-HA
MAP-mCh-SAC1^{WT}
b
Citrine
mCherry
Chlorophyll A
Merge
ADR1-L1 CC$_R$-Cit-HA
MAP-mCh-SAC1^{dead}
ADR1-L1 CC$_R$-Cit-HA
MAP-mCh-SAC1^{WT}
c
Citrine
mCherry
Chlorophyll A
Merge
ADR1-L2 CC$_R$-Cit-HA
MAP-mCh-SAC1^{dead}
ADR1-L2 CC$_R$-Cit-HA
MAP-mCh-SAC1^{WT}

Fig. S8 PI(4,5)P_2 is not required for the PM localization and stability of AtADR1s and AtRPM1.

(**a, c, e, g**) Plasma membrane localization of AtADR1s (ADR1-Citrine-HA, ADR1-L1-EYFP, ADR1-L2-EYFP) and AtRPM1-EYFP is not altered when dOCRL^{dead} (upper panel) or dOCRL^{WT} (lower panel) is co-expressed. Proteins were transiently expressed in *N. benthamiana* leaves and confocal imaging was done 3 hours post Estradiol induction (**a**), 2 days post infiltration (**c, e**) or 24 hours post infiltration (**g**). Localization of Citrine-HA/-EYFP tagged ADR1s and RPM1-EYFP is shown with the first column (Citrine/YFP, in yellow) and MAP-mCherry-dOCRL^{WT} or MAP-mCherry-dOCRL^{dead} is shown in the second column (mCherry, in magenta). Chloroplasts are shown in the third column (Chlorophyll A, in cyan) and the merged images are shown in the fourth column (merge). Images are single plane secant views. Scale bars, 20 μm. (**b, d, f, h**) Immunoblot analysis of transiently expressed proteins (see (**a**), (**c**), (**e**), (**g**)) using anti-GFP and anti-RFP antibody, respectively, show no effect on NLR stability by dOCRL^{WT} or dOCRL^{dead} co-expression. Equal loading of proteins is indicated by the Rubisco band from the Ponceau staining (PS). Numbers show quantification of band intensities normalized to the Rubisco band from the Ponceau staining. Samples were collected at 4 hours post Estradiol induction (**b**), 2 days post infiltration (**d, f**) or 24 hours post infiltration (**h**).

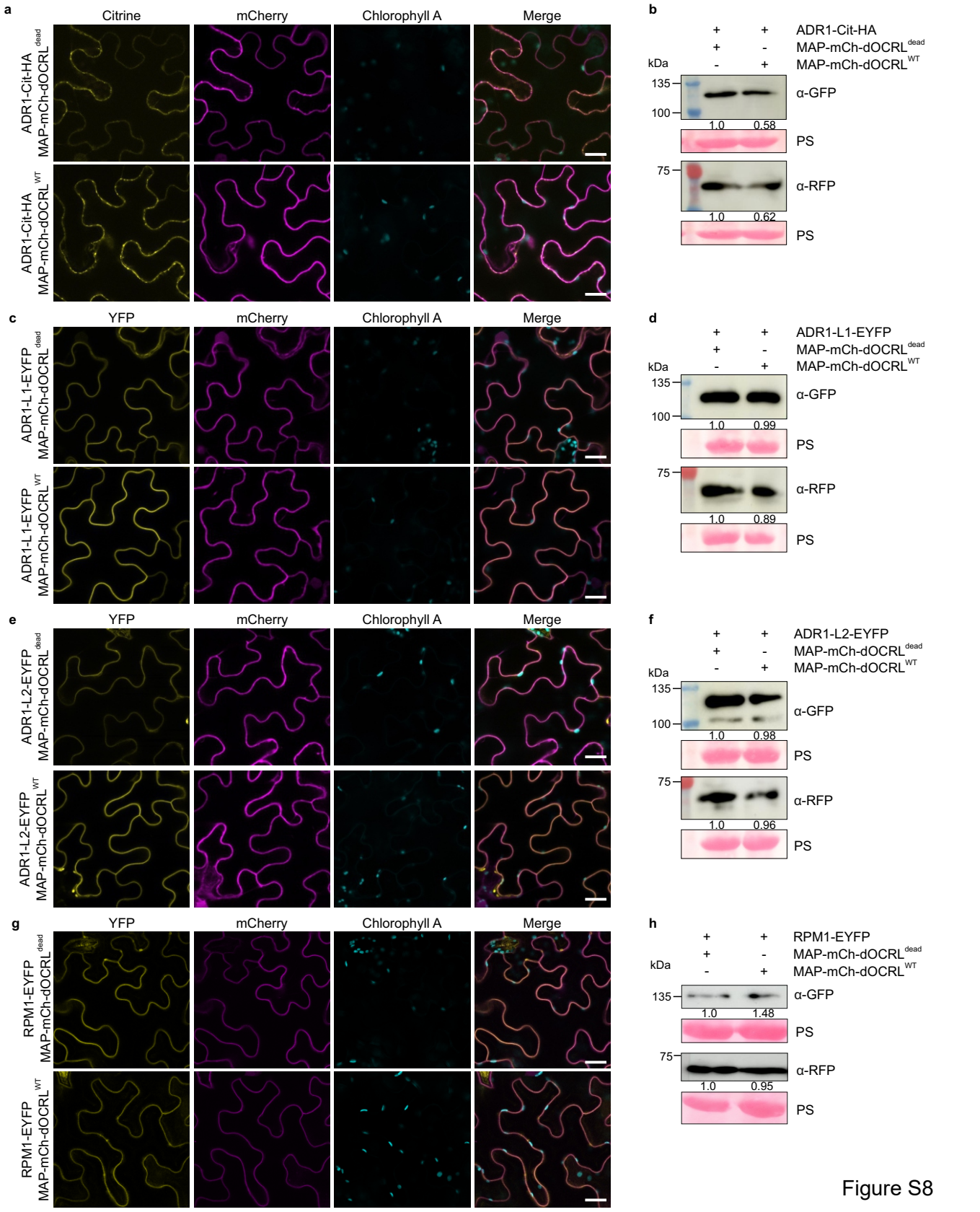
a
Citrine
mCherry
Chlorophyll A
Merge
ADR1-Cit-HA
MAP-mCh-dOCRL dead
ADR1-Cit-HA
MAP-mCh-dOCRL WT
b
ADR1-Cit-HA
MAP-mCh-dOCRL dead
MAP-mCh-dOCRL WT
kDa
135
100
1.0
0.58
α-GFP
PS
75
1.0
0.62
α-RFP
PS
c
YFP
mCherry
Chlorophyll A
Merge
ADR1-L1-EYFP
MAP-mCh-dOCRL dead
ADR1-L1-EYFP
MAP-mCh-dOCRL WT
d
ADR1-L1-EYFP
MAP-mCh-dOCRL dead
MAP-mCh-dOCRL WT
kDa
135
100
1.0
0.99
α-GFP
PS
75
1.0
0.89
α-RFP
PS
e
YFP
mCherry
Chlorophyll A
Merge
ADR1-L2-EYFP
MAP-mCh-dOCRL dead
ADR1-L2-EYFP
MAP-mCh-dOCRL WT
f
ADR1-L2-EYFP
MAP-mCh-dOCRL dead
MAP-mCh-dOCRL WT
kDa
135
100
1.0
0.98
α-GFP
PS
75
1.0
0.96
α-RFP
PS
g
YFP
mCherry
Chlorophyll A
Merge
RPM1-EYFP
MAP-mCh-dOCRL dead
RPM1-EYFP
MAP-mCh-dOCRL WT
h
RPM1-EYFP
MAP-mCh-dOCRL dead
MAP-mCh-dOCRL WT
kDa
135
1.0
1.48
α-GFP
PS
75
1.0
0.95
α-RFP
PS

Figure S8

Fig. S9 AtADR1s and AtRPM1 cell death activity is not affected by depletion of PI(4,5)P_2 from the plasma membrane via MAP-dOCRL co-expression.

dOCRL^{WT} co-expression does not affect the cell death induced by AtADR1 CC_R (**a**), AtADR1-L2 CC_R (**b**), AtNRG1.1 CC_R (**c**) domains, full-length AtADR1 (**d**), autoactive mutant AtADR1^{DV} (**e**) or activated AtRPM1 (**f**). (**a-f**, upper panels) Transient expression of Citrine-HA or EYFP tagged ADR1 (**d**), autoactive ADR1^{D461V} mutant (**e**) and phospho-mimic T7-RIN4^{T166D}-activated RPM1 (**f**) co-expressed with MAP-mCherry-dOCRLWT or MAP-mCherry-dOCRL^{dead} in *N. benthamiana*. Leaf images were taken under UV light at 24 hours post infiltration (hpi) (**a**), 26 hpi (**b**), 28 hpi (**c**), 9 hours post Estradiol induction (**d**), 30 hpi (**e**) and 24 hpi (**f**). Phospho-mimic T7-RIN4^{T166D} (RIN4^{TD}) was co-expressed to activate RPM1. White/light grey areas in leaves indicate dead tissue. Numbers represent the number of leaves showing cell death out of the number of leaves analysed. Asterisk indicates weak HR. (**a-f**, lower panels) Immunoblot analysis of transiently expressed proteins (see upper panels) using anti-GFP and anti-RFP antibody, respectively. Equal loading of proteins is indicated by the Rubisco band from the Ponceau staining (PS). Numbers show quantification of band intensities normalized to the Rubisco band from the Ponceau staining. Samples were collected at 20 hpi (**a-c**), 24 hpi (**d**), 4 hours post Estradiol induction (**e**) or 22 hpi (**f**).

Figure S9

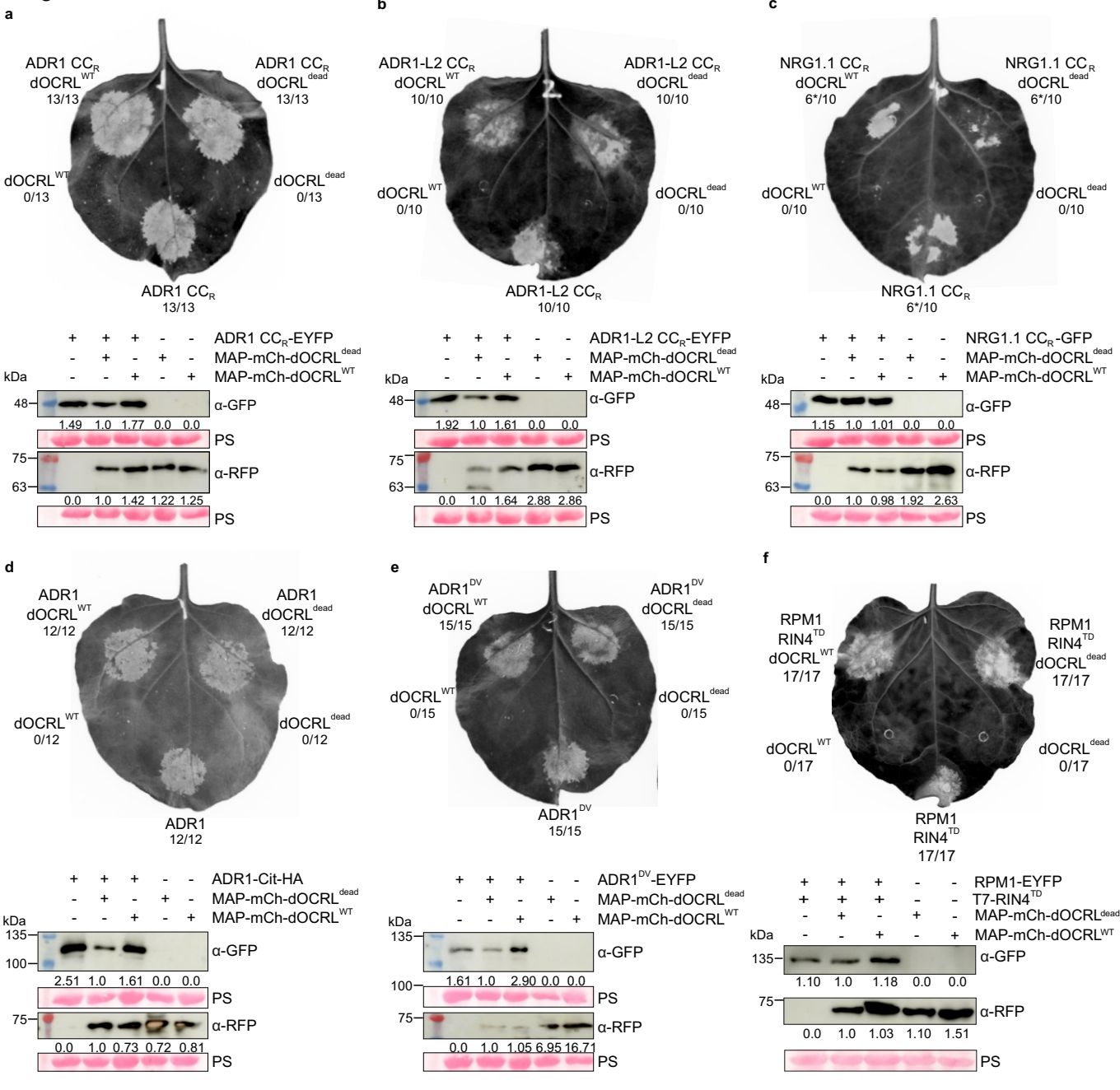
a
ADR1 CC$_R$ dOCRL^{WT} 13/13
ADR1 CC$_R$ dOCRL^{dead} 13/13
dOCRL^{WT} 0/13
dOCRL^{dead} 0/13
ADR1 CC$_R$ 13/13
+ + + - - ADR1 CC$_R$-EYFP
- + - + - MAP-mCh-dOCRL^{dead}
kDa - - + - + MAP-mCh-dOCRL^{WT}
48 α-GFP
1.49 1.0 1.77 0.0 0.0
PS
75 α-RFP
63
0.0 1.0 1.42 1.22 1.25
PS
b
ADR1-L2 CC$_R$ dOCRL^{WT} 10/10
ADR1-L2 CC$_R$ dOCRL^{dead} 10/10
dOCRL^{WT} 0/10
dOCRL^{dead} 0/10
ADR1-L2 CC$_R$ 10/10
+ + + - - ADR1-L2 CC$_R$-EYFP
- + - + - MAP-mCh-dOCRL^{dead}
kDa - - + - + MAP-mCh-dOCRL^{WT}
48 α-GFP
1.92 1.0 1.61 0.0 0.0
PS
75 α-RFP
63
0.0 1.0 1.64 2.88 2.86
PS
c
NRG1.1 CC$_R$ dOCRL^{WT} 6*/10
NRG1.1 CC$_R$ dOCRL^{dead} 6*/10
dOCRL^{WT} 0/10
dOCRL^{dead} 0/10
NRG1.1 CC$_R$ 6*/10
+ + + - - NRG1.1 CC$_R$-GFP
- + - + - MAP-mCh-dOCRL^{dead}
kDa - - + - + MAP-mCh-dOCRL^{WT}
48 α-GFP
1.15 1.0 1.01 0.0 0.0
PS
75 α-RFP
63
0.0 1.0 0.98 1.92 2.63
PS
d
ADR1 dOCRL^{WT} 12/12
ADR1 dOCRL^{dead} 12/12
dOCRL^{WT} 0/12
dOCRL^{dead} 0/12
ADR1 12/12
+ + + - - ADR1-Cit-HA
- + - + - MAP-mCh-dOCRL^{dead}
kDa - - + - + MAP-mCh-dOCRL^{WT}
135 α-GFP
100
2.51 1.0 1.61 0.0 0.0
PS
75 α-RFP
0.0 1.0 0.73 0.72 0.81
PS
e
ADR1^{DV} dOCRL^{WT} 15/15
ADR1^{DV} dOCRL^{dead} 15/15
dOCRL^{WT} 0/15
dOCRL^{dead} 0/15
ADR1^{DV} 15/15
+ + + - - ADR1^{DV}-EYFP
- + - + - MAP-mCh-dOCRL^{dead}
kDa - - + - + MAP-mCh-dOCRL^{WT}
135 α-GFP
100
1.61 1.0 2.90 0.0 0.0
PS
75 α-RFP
0.0 1.0 1.05 6.95 16.71
PS
f
RPM1 RIN4^{TD} dOCRL^{WT} 17/17
RPM1 RIN4^{TD} dOCRL^{dead} 17/17
dOCRL^{WT} 0/17
dOCRL^{dead} 0/17
RPM1 RIN4^{TD} 17/17
+ + + - - RPM1-EYFP
+ + + - - T7-RIN4^{TD}
- + - + - MAP-mCh-dOCRL^{dead}
kDa - - + - + MAP-mCh-dOCRL^{WT}
135 α-GFP
1.10 1.0 1.18 0.0 0.0
75 α-RFP
0.0 1.0 1.03 1.10 1.51
PS

Fig. S10 Basic-hydrophobic (BH) profile analysis of CC/CC$_R$ domains.

In silico analysis to identify potential basic-hydrophobic stretches in the CC/CC$_R$ domains of three Arabidopsis CNLs and the whole RNL family. (**a**) BH score profile (window size 19) of AtADR1, AtADR1-L1, AtADR1-L2, AtRPM1, AtZAR1, AtNRG1.1, AtNRG1.2 and AtRPS5 CC/CC$_R$ domains (amino acids 1-160/170). Potential BH-stretches are represented as peaks above the 0.6 BH score threshold shown as a green line. Isoelectric point (pI) of each CC/CC$_R$ domain is shown in parentheses behind the protein names and indicates that all but two (RPM1 and ZAR1) CC and CC$_R$ domains may have an overall positive charge in the cytosolic environment (pH ~7.2). (**b**) Amino acid sequences of CC and CC$_R$ domains as in (**a**) with the putative BH-stretch indicated by italic, underlined letters and highlighted in yellow. Positively charged lysine (K) and arginine (R) residues in the BH-stretch are shown in bold and red letters.

Figure S10

Figure S10

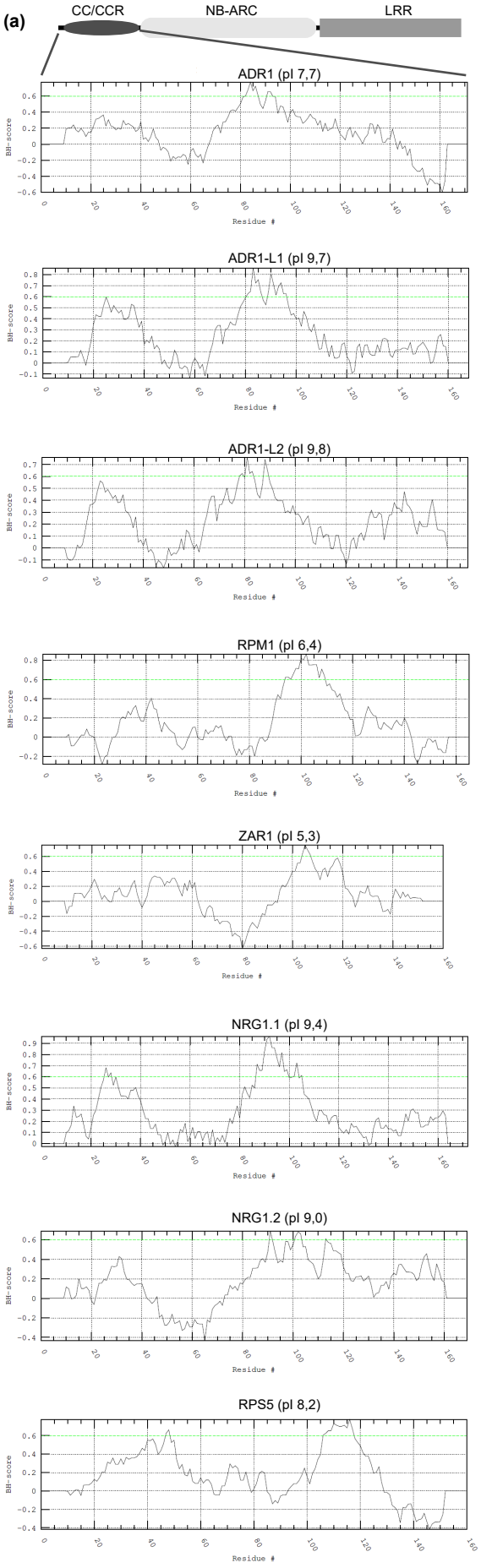

(b)

>AT1g33560_ADR1

MASFIDLFAGDITTQLLKLLALVANTVYSCKGIAERLIT
MIRDVQPTIREIQYSGAELSNHHQTQLGVFYEILEKAR
KLCE*KVLRCNRWNLKHV*YHANKMKDLEKQISRFLNS
QILLFVLAEVCHLRVNGDRIERNMDRLLTERNDSLSFP
ETMMEIETV

>AT4g33300_ADR1-L1

MAITDFFAGEIATELLKQLFTISTTAWRYKNTAKQLLTL
IDSIRPTIKEIQYSGVELPAHRQAQIGMLFDTLEKGKKL
TD*KVLSSKRWNLYRQLTL*ARKMEKLEKTISNFLKNEV
FTHILADVHHLRADTSVRLDRVDMSLDRVIQQVGSMK
IGGGGLIS

>AT5g04720_ADR1-L2

MADIIGGEVVTELVRQLYAVSQKTLRCRGIAKNLATMI
DGLQPTIKEIQYSGVELTPHRQAQLRMFSETLDKCRK
LTE*KVLKSSRWNMVRQ*LLHVRKMENLQSKVSSFLNG
QLLVHVLADVHHVRADSEFRFDRIDRKVDSLNEKLGS
MKLRGSESLREALKTAEATV

>At3g07040_RPM1

MASATVDFGIGRILSVLENETLLLSGVHGEIDKMKKEL
LIMKSFLEDTHKHGGNGSTTTTTQLFQTFVANTRDLA
YQIEDILDEFGYHIHGYR*SCAKIWRAFHFPRYMW*ARH
SIAQKLGMVNVMIQSISDSMKRYYHSENYQAALLPPID
DGDAKWVNNI

>AT3g50950_ZAR1

MVDAVVTVFLEKTLNILEEKGRTVSDYRKQLEDLQSE
LKYMQSFLKDAERQKRTNETLRTLVADLRELVYEAED
ILVDCQLADGDDGNEQRSSNAWLSRLH*PARVPLQYK
KSKRLQEI*NERITKIKSQVEPYFEFITPSNVGRDNGTD
RWSSPVYDHTQV

>AT5g66900_NRG1.1

MNDWASLGIGSIGEAVFSKLLKVVIDEAKKFKAFKPLS
KDLVSTMEILFPLTQKIDSMQKELDFGVKELKELRDTI
ERADVAVRKF*PRVKWYEKSKYTRKIERIN*KDMLKFC
QIDLQLLQHRNQLTLLGLTGNLVNSVDGLSKRMDLLS
VPAPVFRDLCS

>AT5g66910_NRG1.2

MVVVDWLGLGLGSVAGALVSEGLKVLISEAKKVLAFK
SVSNELASTMESLLPVIKEIESMQDGMELQDLKDTIDK
ALLLVEKCSHVEKWN*IILKSKYTRKVEEIN*RKMLKFCQ
VQLQLLLFRNQLKSMPSMEAILNNYFQNINKKLDRLS
GSPAPPLVSK

>AT1g12220_RPS5

MGGCFSVSLPCDQVVSQFSQLLCVRGSYIHNLSKNL
ASLQKAMRMLKARQYDVIRRLETEEFTGRQQRLSQV
QVWLTSVLIIQNQFNDLLRSNEVELQRLCLCGF*CSKD
LKLSYRYGKR*VIMMLKEVESLSSQGFFDVVSEATPFA
DVDEIPFQPTIVGQ

Fig. S11 Proposed model of AtADR1 family members localization, oligomerization and function during immunity.

Arabidopsis ADR1s constitutively localize at the plasma membrane through the interaction of their CC_R domains with anionic lipids, including PI4P. AtADR1 activation, either by pathogen infection or autoactivating mutations, leads to (**1**) conformational changes inducing or strengthening oligomerization andthe formation of a transient Ca^{2+}-permeable cation channel that results in (**2**) Ca^{2+} influx and in the (**3**) subsequent recruitment or activation of calcium dependent and probably NLR-interacting phospholipases that (**4**) in turn produce lipid messengers, such as PA and DAG, which (**5**) might activate downstream signalling components required for NLR-mediated (**6**) immunity. The lipase-like protein AtEDS1 (ENHANCED DISEASE SUSCEPTIBLE 1) and its sequence-related direct partner AtPAD4 (PHYTOALEXIN DEFICIENT 4) are key immune regulators of AtADR1s-mediated immunity, but also of basal resistance, and may be part of an ADR1s immune-signalling complex.

Figure S11

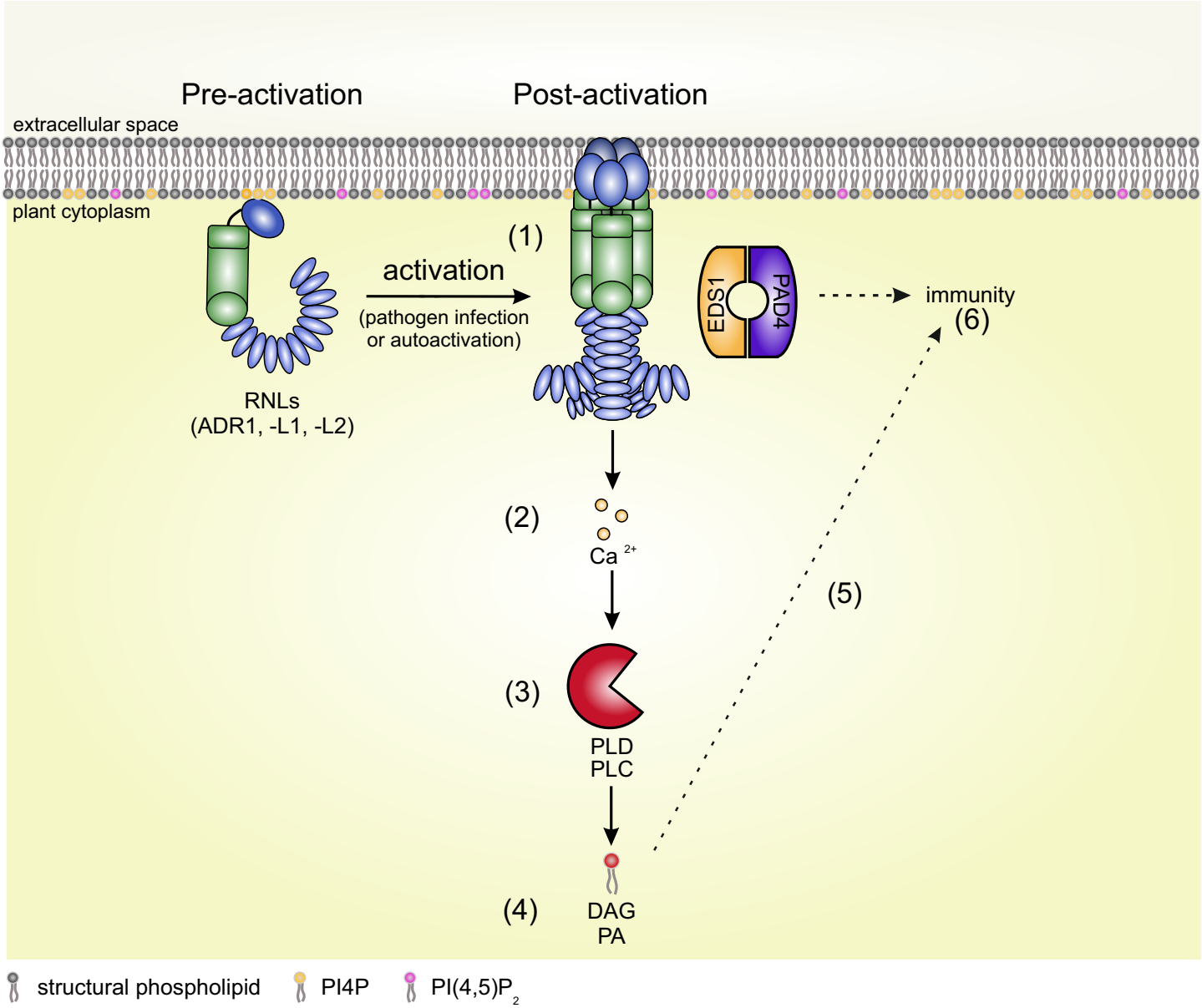
Pre-activation
Post-activation
extracellular space
plant cytoplasm
RNLs
(ADR1, -L1, -L2)
activation
(pathogen infection
or autoactivation)
(1)
EDS1
PAD4
immunity
(6)
(2)
Ca 2+
(5)
(3)
PLD
PLC
(4)
DAG
PA
structural phospholipid
PI4P
PI(4,5)P 2

226 **Table S1.** Primer list.

Primer	sequence	purpose
FEK_1014	GACGCAACACGtTGTTTTGAGAGACCTAG	ADR1 D461V (site-directed mutagenesis)
FEK_1015	CTAGGTCTCTCAAAACAaCGTGTTGCGTC	ADR1 D461V (site-directed mutagenesis)
FEK_1012	GTGACACAGCATGtTGTTCTGCGAGAC	ADR1-L1 D489V (site-directed mutagenesis)
FEK_1013	GTCTCGCAGAACAaCATGCTGTGTCAC	ADR1-L1 D489V (site-directed mutagenesis)
FEK_948	GTCACGCAGCATGtTGTTCTAAGAGATG	ADR1-L2 D484V (site-directed mutagenesis)
FEK_949	CATCTCTTAGAACAaCATGCTGCGTGAC	ADR1-L2 D484V (site-directed mutagenesis)
FEK_1002	GAATGAGCGGTTCAGcGgcAgCCACTCTTG	ADR1 198AAA200 (site-directed mutagenesis)
FEK_1003	CAAGAGTGGcTgcCgCTGAACCGCTCATTC	ADR1 198AAA200 (site-directed mutagenesis)
FEK_1000	GAATGGGCGGTGTTGcTgcAgCCACTCTTGCC	ADR1-L1 212AAA214 (site-directed mutagenesis)
FEK_1001	GGCAAGAGTGGcTgcAgCAACACCGCCCATTC	ADR1-L1 212AAA214 (site-directed mutagenesis)
FEK_973	GGATGAGTGGTTCAGcGgcAgCCACTCTTG	ADR1-L2 212AAA214 (site-directed mutagenesis)
FEK_974	CAAGAGTGGcTgcCgCTGAACCACTCATCC	ADR1-L2 212AAA214 (site-directed mutagenesis)
FEK_1475	gtGGTCTCaGCGGGCTAACTTATGTTGACTTCACGA	ADR1 promoter with *Bsa*I site and GCGG overhang (GG)
FEK_1476	atGGTCTCaCAGACGAGACCGATCTTGGAGTGTAAG	ADR1 promoter with *Bsa*I site and

		GCGG overhang (GG)
FEK_1477	gtGGTCTCaTCTGATGGCTTCGTTCATAGATCTTTTCG	ADR1 CDS with *Bsa*I site and TCTG overhang (GG)
FEK_1478	atGGTCTCaCCTTATCGTCAAGCCAATCCACGGTGAAGC	ADR1 CDS with *Bsa*I site and CCTT overhang and w/o stop (GG)
FEK_1420	GGGGACAAGTTTGTACAAAAAAGCAGGCTTActccactcatggcagcaatact	ADR1-L1 promoter with attB1 site (GW)
FEK_1421	GGTGATGGCCATtggataccaccaagtcaagtc	ADR1-L1 promoter with ADR1-L1 CDS overhang
FEK_1422	gtggtatccaATGGCCATCACCGATTTTTTCG	ADR1-L1 CDS with ADR1-L1 promoter overhang
FEK_1423	GGGGACCACTTTGTACAAGAAAGCTGGGTGTTCGTCAAGCCAGTCTAGG	ADR1-L1 CDS with attB2 site
PMNLR_013	GGGGACAAGTTTGTACAAAAAAGCAGGCTtaATGGGAGGTTGTTTCTCTGTTTCATTGCC	RPS5 forward primer for pDONOR gateway cloning
PMNLR_014	GGGGACCACTTTGTACAAGAAAGCTGGGTtTGTTTCTCTCCACCGCCACCTGGATGAAGG	RPS5 reward primer for pDONOR gateway cloning
FEK_1311	cgtagatctatttaggtgacactatagaacag*accacc*ATGGCTTCGGCTACTGTTGATTTT	SP6 RPM1 CC 1-156 (TnT)
FEK_1312	cgtagatcCTAAGCGTAATCTGGAACGTCATATGGATACTTTGCATCGCCATCATCAAT	1xHA rev for RPM1 CC 1-156 (TnT)
FEK_1329	cgtagatctatttaggtgacactatagaacag*accacc*ATGGCTTCGTTCATAGATC	SP6 ADR1 CC 1-146 (TnT)
FEK_1330	cgtagatcCTAAGCGTAATCTGGAACGTCATATGGATAATCATTCCGCTCAGTCAAC	1xHA rev for ADR1 CC 1-146 (TnT)
FEK_1331	cgtagatctatttaggtgacactatagaacag*accacc*ATGGCCATCACCGATTTTTTCG	SP6 ADR1-L1 CC 1-155 (TnT)
FEK_1332	cgtagatcCTAAGCGTAATCTGGAACGTCATATGGATATCCCCCAATTTTCATGGAAC	1xHA rev for ADR1-L1 CC 1-155 (TnT)
FEK_1313	cgtagatctatttaggtgacactatagaacag*accacc*ATGGCAGATATAATCGGCG	SP6 ADR1-L2 CC 1-153 (TnT)
FEK_1314	cgtagatcCTAAGCGTAATCTGGAACGTCATATGGATATCCCCTGAGTTTCATAGAACC	1xHA rev for ADR1-L2 CC 1-153 (TnT)
FEK_1425	cgtagatctatttaggtgacactatag*aacagaccacc*ATGGTGAGCAAGGGCGAG	SP6 Citrine (TnT)

FEK_1426	cgtagatcTCAGGCATAGTCTGGGACGTCATATGGATACTTG	1xHA rev for Citrine (TnT)
5phos	catcatactcctttgcctgctgccgctgccgctatggtgagcaagggcgaggagg	5' phosphorylated primers for MAP-mCherrynoSTOP/ pDONR207 cloning
5phos_R	TCGACTTCTACTGCAGAGTAAGCCCATGGTAGCCTGCTTTTTTGTACAAACTTGGC	5' phosphorylated primers for MAP-mCherrynoSTOP/ pDONR207 cloning

Table S2. Transmembrane domain and lipidation prediction summary for *Arabidopsis thaliana* RNLs and the CNLs RPM1 and RPS5.

NLR (type)	TMD prediction*		Lipidation prediction*		
	Tool	result	Tool	# of sites	position in protein
AtRPM1 (CNL) At3g07040	TMHMM2.0	no	NBA-Palm		0
	CCTOP	no	GPS-Palm	3	438,567,704
	PredictProtein	no	ExPASy Myristoylator		0
AtRPS5 (CNL) At1g12220	TMHMM2.0	no	NBA-Palm		0
	CCTOP	no	GPS-Palm	4	**4**,103,106,463
	PredictProtein	no	ExPASy Myristoylator	1	N-terminus
AtADR1 (RNL) At1g33560	TMHMM2.0	no	NBA-Palm		0
	CCTOP	no	GPS-Palm	1	661
	PredictProtein	no	ExPASy Myristoylator		0
AtADR1-L1 (RNL) At4g33300	TMHMM2.0	no	NBA-Palm		0
	CCTOP	no	GPS-Palm	4	301,347,638,690
	PredictProtein	no	ExPASy Myristoylator		0
AtADR1-L2 (RNL) At5g04720	TMHMM2.0	no	NBA-Palm		0
	CCTOP	no	GPS-Palm	2	73,685
	PredictProtein	no	ExPASy Myristoylator		0
AtNRG1.1 (RNL) At5g66900	TMHMM2.0	no	NBA-Palm		0
	CCTOP	no	GPS-Palm	5	198,592,683,705,731
	PredictProtein	no	ExPASy Myristoylator		0
AtNRG1.2 (RNL) At5g66910	TMHMM2.0	no	NBA-Palm		0
	CCTOP	no	GPS-Palm	6	200,598,689,711,737,764
	PredictProtein	no	ExPASy Myristoylator		0

*, web-pages of the used prediction tools are listed in the Material and Methods section.

Methods S1. Protocols for the experiments used in this work.

Plasmid construction

The CDS from *ADR1* and *RPM1* were cloned into pENTR/D-TOPO via TOPO® cloning (Thermo Fisher Scientific; Waltham, USA), while the CDS from *ADR1-L1, ADR1-L2, ADR1 CC_R* (1-146 aa)*, ADR1-L1 CC_R* (1-155 aa) *and ADR1-L2 CC_R* (1-153 aa) were cloned into the GATEWAY™ compatible vector pDONR221 by GATEWAY™ cloning (Thermo Fisher Scientific, Waltham, USA) generating pEntry clones. The corresponding point mutations for the QHV mutants $ADR1^{D461V}$, $ADR1\text{-}L1^{D489V}$ and $ADR1\text{-}L2^{D484V}$ as well as the mutations for the P-loop mutants $ADR1^{198AAA200}$, $ADR1\text{-}L1^{212AAA214}$ and $ADR1\text{-}L2^{212AAA214}$ were introduced by site-directed mutagenesis PCR using primers listed in Table S2. The PCR products were digested with *Dpn*I (NEB; Ipswich, USA) overnight and subsequently transformed into *Escherichia coli* DH5α.

For the assembly of *pADR1::ADR1-YFP*, a 1822 bp *ADR1* promoter fragment (Wu *et al.*, 2020) and the *ADR1* CDS were amplified with Golden Gate-compatible *Bsa*I overhangs from either Col-0 genomic DNA or plasmid DNA using the Phusion polymerase (NEB; Ipswich, USA) and the primers listed in Table S2 (Binder *et al.*, 2014). PCR products were gel-purified using the NucleoSpin Gel and PCR Clean-up Kit (Macherey-Nagel; Düren, Germany) and sub-cloned into the pGEM-T Easy vector (Promega; Fitchburg, USA), resulting in the Level I vectors LI A-B *p*ADR1 and LI B-D ADR1, respectively. The obtained LI vectors were assembled into a functional expression vector as described in (Binder *et al.*, 2014) using the *BB10* backbone via *Bsa*I cut-ligation in the following order: LI A-B *p*ADR1, LI B-D ADR1 CDS, LI D-E YFP (Binder *et al.*, 2014), LI E-F nos terminator (Binder *et al.*, 2014), LI F-G pFAST (gift of A. Gust).

For the generation of *pADR1-L1::ADR1-L1-EYFP*, a 2036 bp *ADR1-L1* promoter fragment (Wu *et al.*, 2020) was PCR-amplified from Col-0 genomic DNA and the CDS of *ADR1-L1* was amplified from plasmid DNA using the Phusion polymerase (NEB; Ipswich, USA) and the primers listed in Table S2. *ADR1-L1* promoter and CDS PCR products were gel-purified and equimolar amounts of both products were further used in the overlap extension PCR reaction using the Q5 Polymerase (NEB; Ipswich, USA). Overlap PCR and the following final fusion gene PCR amplification were performed as described in (Hilgarth & Lanigan, 2020). The resulting PCR product was gel-purified and directly used for cloning into the GATEWAY™ compatible vector pDONR207 via the GATEWAY™ cloning technology (Thermo Fisher Scientific, Waltham, USA).

Cloning of *pADR1-L2::ADR1-L2* that contains a 500 bp upstream region of the start codon of *ADR1-L2* was described before (Roberts *et al.*, 2013).

The CDS of *RPS5* was amplified from Col-0 cDNA and introduced into the GATEWAY™ compatible vector pDONR207 via GATEWAY™ cloning technology (Thermo Fisher Scientific, Waltham, USA). The *NRG1.1 CC_R* (1-180 aa) CDS was synthesized with 5' and 3' GATEWAY™ attachment sites into the pUC57Kan vector (Genescript, Piscataway NJ, USA). LR reactions (GATEWAY™ Cloning Technology, Thermo Fisher Scientific, Waltham, USA) were performed to introduce specific CDS or promoter-CDS fusions into a modified Estradiol-inducible destination vector pMDC7-Citrine-HA (Curtis & Grossniklaus, 2003), the Estradiol-inducible destination vector pABindmCherry (Bleckmann *et al.*, 2010), the 35s-driven destination vector pGWB641 (Nakamura *et al.*, 2010) or the promoterless destination vector pGWB640 (Nakamura *et al.*, 2010) as indicated.

The 36 first amino acid of AtGPA1 (i.e. MAP sequence) were added to mCHERRYnoSTOP in pDONR207 (Jaillais *et al.*, 2011) to generate MAP-mCHERRYnoSTOP in pDONR207. 2x35Sprom/pDONRP4-P1R (Marques-Bueno *et al.*, 2016), MAP-mCHERRYnoSTOP in pDONR207 and SAC1in pDONR-P2R-P3 (or SAC1dead in pDONR-P2RP3) (Simon *et al.*, 2016) were recombined using LR reaction into pH7m34GW (Karimi *et al.*, 2007) to generate 2x35Sprom::MAP-mCHERRY-SAC1 in pH7m34GW (or 2x35Sprom::MAP-mCHERRY-SAC1dead in pH7m34GW). 2x35Sprom in pDONRP4-P1R (Marques-Bueno *et al.*, 2016), MAP-mCHERRYnoSTOP in pDONR207 and the PI(4,5)P2 phosphatase dOCRL (*Drosophila melanogaster* ortholog of human oculocerebrorenal syndrome of *Lowe 1*) in pDONR-P2R-P3 (or dOCRLdead in pDONR-P2RP3) (Doumane *et al.*, 2020) were recombined using LR reaction into pH7m34GW (Karimi *et al.*, 2007) to generate 2x35Sprom::MAP-mCHERRY-dOCRL in pH7m34GW (or 2x35Sprom::MAP-mCHERRY-dOCRLdead in pH7m34GW). Constructs were verified by sequencing and transformed into *Agrobacterium tumefaciens* strain GV3101/pMP90 and used for transient expression in *Nicotiana benthamiana.*

Cell Death Assay

Nicotiana benthamiana leaves were imaged for cell death at the indicated time points. Cell death images were taken under normal light using a Canon 80D (Canon; Öta, Japan) or under UV light using the Amersham ImageQuant 800 Western blot imaging system and an integrated Cy5 filter (GE Healthcare; Chalfont St. Giles, UK). Images were processed with Adobe Photoshop CS2 (Adobe Inc.; San José, USA) or Corel PAINT (Corel Corporation; Ottawa, Canada) for adjustment of brightness and contrast. Note, since 35s::MAP-mCh-SAC1^{WT} often

induces tissue collapse at around 52 hours post infiltration, cell death imaging had to be done at earlier timepoints.

Confocal imaging

Confocal imaging was done using a 40x or 63x water-immersion objective and the ZEN black software. EYFP and Citrine were excited using a 514 nm laser with a detected emission between 516-556 nm; RFP and mCherry were excited using a 561 nm laser with a detected emission spectrum of 597-634 nm, Chlorophyll A was excited with a 561 nm laser and the emission spectrum was 661-682 nm. Focal plane images were processed with the ZEN blue software (Zeiss) for adjustment of brightness and contrast. Maximum Z-projection images were processed with ImageJ.

Western blot analysis of transiently expressed proteins

Primary and secondary antibody dilutions were as follows: α-GFP 1:1,500 (Roche Diagnostics; Basel, Switzerland), α-RFP 1:1,000 (ChromoTek; Planegg-Martinsried, Germany), α-Myc 1:1000 (ChromoTek; Planegg-Martinsried, Germany), α-HA 1:2,000 (Roche Diagnostics; Basel, Switzerland), α-UGPase 1:2,000 (Agrisera; Vännäs, Sweden), α-T7 Tag HRP conjugate 1:10,000 (Merck, Darmstadt, Germany), α-mouse HRP-conjugated 1:10,000 (Sigma-Aldrich; St. Louis, USA), α-rat HRP-conjugated 1:10,000 (Thermo Fisher Scientific; Waltham, USA), α-rabbit HRP-conjugated 1:10,000 (Sigma-Aldrich; St. Louis, USA).

Co-immunoprecipitation

After immunoprecipitation, samples were captured by centrifugation at 2,400 g at 4°C and washed two times with 1 ml of wash buffer (50 mM HEPES buffer pH 7.5, 150 mM NaCl, 10 mM EDTA pH 8.0, 0.2% [v/v] Triton X-100, 5 mM DTT, 1x Halt^{TM} Protease Inhibitor Cocktail (Thermo Fisher Scientific; Waltham, USA)) by incubating the extracts for 5 min on a rotating wheel at 4°C and two additional times by inverting the tube six times. Bound proteins were eluted in 120 µl 2x SDS loading buffer (100 mM Tris-HCl pH 6.8, 20% [v/v] glycerol, 200 mM DTT, 4% [w/v] SDS, 0.002% [w/v] bromophenol blue) and denatured by boiling the proteins at 95°C for 5 min.

Transmembrane, lipidation and membrane binding sites predictions

Full length protein sequences of Arabidopsis RPM1, RPS5, ADR1, ADR1-L1, ADR1-L2, NRG1.1 and NRG1.2 were used for prediction of potential transmembrane domains (TMDs)

with three online tools: TMHMM2.0 (http://www.cbs.dtu.dk/services/TMHMM/) (Sonnhammer *et al.*, 1998), CCTOP (http://cctop.enzim.ttk.mta.hu/?_) and PredictProtein (https://predictprotein.org/) (Yachdav *et al.*, 2014), and for lipidation with the online tools: NBA-Palm (http://nbapalm.biocuckoo.org/) (Xue *et al.*, 2006), GPS-Palm (http://gpspalm.biocuckoo.cn/) (Ning *et al.*, 2020) and ExPASy Myristoylator (https://web.expasy.org/myristoylator/). CC domain sequences (amino acid 1-160) of Arabidopsis RPM1, RPS5, ADR1, ADR1-L1, ADR1-L2, NRG1.1 and NRG1.2 were used to identify basic hydrophobic stretches as potential membrane binding sites using the BH-search tool (https://hpcwebapps.cit.nih.gov/bhsearch/) (Brzeska et al., 2010) with a window size of 19 for residue averaging and BH parameters. Analysis of the isoelectric point (pI) for all CC and CC_R domains was done with the ExPASy online tool (https://web.expasy.org/cgi-bin/compute_pi/pi_tool).

References

Binder A, Lambert J, Morbitzer R, Popp C, Ott T, Lahaye T, Parniske M. 2014. A modular plasmid assembly kit for multigene expression, gene silencing and silencing rescue in plants. *PLoS One* **9**(2): e88218.

Bleckmann A, Weidtkamp-Peters S, Seidel CA, Simon R. 2010. Stem cell signaling in Arabidopsis requires CRN to localize CLV2 to the plasma membrane. *Plant Physiol* **152**(1): 166-176.

Curtis MD, Grossniklaus U. 2003. A gateway cloning vector set for high-throughput functional analysis of genes in planta. *Plant Physiol* **133**(2): 462-469.

Doumane, M., Colin L, Lebecq A, Fangain A, Bareille J, Hamant O, Belkhadir Y, Jaillais Y, Caillaud M-C. 2020. iDePP: a genetically encoded system for the inducible depletion of PI(4,5)P_2 in *Arabidopsis thaliana*. *bioRxiv* **doi: 10.1101/2020.05.13.091470**.

Hilgarth RS, Lanigan TM. 2020. Optimization of overlap extension PCR for efficient transgene construction. *MethodsX* **7**: 100759.

Jaillais Y, Belkhadir Y, Balsemao-Pires E, Dangl JL, Chory J. 2011. Extracellular leucine-rich repeats as a platform for receptor/coreceptor complex formation. *Proc Natl Acad Sci U S A* **108**(20): 8503-8507.

Karimi M, Bleys A, Vanderhaeghen R, Hilson P. 2007. Building blocks for plant gene assembly. *Plant Physiol* **145**(4): 1183-1191.

Marques-Bueno MDM, Morao AK, Cayrel A, Platre MP, Barberon M, Caillieux E, Colot V, Jaillais Y, Roudier F, Vert G. 2016. A versatile Multisite Gateway-compatible promoter and transgenic line collection for cell type-specific functional genomics in Arabidopsis. *Plant J* **85**(2): 320-333.

Nakamura S, Mano S, Tanaka Y, Ohnishi M, Nakamori C, Araki M, Niwa T, Nishimura M, Kaminaka H, Nakagawa T, et al. 2010. Gateway binary vectors with the bialaphos resistance gene, bar, as a selection marker for plant transformation. *Biosci Biotechnol Biochem* **74**(6): 1315-1319.

Ning W, Jiang P, Guo Y, Wang C, Tan X, Zhang W, Peng D, Xue Y. 2020. GPS-Palm: a deep learning-based graphic presentation system for the prediction of S-palmitoylation sites in proteins. *Brief Bioinform*.

Roberts M, Tang S, Stallmann A, Dangl JL, Bonardi V. 2013. Genetic requirements for signaling from an autoactive plant NB-LRR intracellular innate immune receptor. *PLoS Genet* **9**(4): e1003465.

Simon ML, Platre MP, Marques-Bueno MM, Armengot L, Stanislas T, Bayle V, Caillaud MC, Jaillais Y. 2016. A PtdIns(4)P-driven electrostatic field controls cell membrane identity and signalling in plants. *Nat Plants* **2**: 16089.

Sonnhammer EL, von Heijne G, Krogh A. 1998. A hidden Markov model for predicting transmembrane helices in protein sequences. *Proc Int Conf Intell Syst Mol Biol* **6**: 175-182.

Wu Y, Gao Y, Zhan Y, Kui H, Liu H, Yan L, Kemmerling B, Zhou JM, He K, Li J. 2020. Loss of the common immune coreceptor BAK1 leads to NLR-dependent cell death. *Proc Natl Acad Sci U S A* **117**(43): 27044-27053.

Xue Y, Chen H, Jin C, Sun Z, Yao X. 2006. NBA-Palm: prediction of palmitoylation site implemented in Naive Bayes algorithm. *BMC Bioinformatics* **7**: 458.

Yachdav G, Kloppmann E, Kajan L, Hecht M, Goldberg T, Hamp T, Honigschmid P, Schafferhans A, Roos M, Bernhofer M, et al. 2014. PredictProtein--an open resource for online prediction of protein structural and functional features. *Nucleic Acids Res* **42**(Web Server issue): W337-343.

7.5. Saile *et al*., in preparation

Autoimmunity induced by the Arabidopsis helper NLR ADR1-L2 requires the receptor-like kinase BKK1

Saile, S. C., Bonardi, V., Keicher, J., Wünsch, L. K., Jacob, P., Teixeira P. J. P. L., Dangl, J. L., El Kasmi, F.

Autoimmunity induced by the Arabidopsis helper NLR ADR1-L2 requires the receptor-like kinase BKK1

Svenja C. Saile[1], Vera Bonardi[2&], Jutta Keicher[1], Lisa K. Wünsch[2], Pierre Jacob[2,3], Paulo JPL Teixeira[2#], Jeffery L. Dangl[2,3] and Farid El Kasmi[1]

[1] Centre for Plant Molecular Biology (ZMBP), University of Tübingen, Tübingen, Germany

[2] Department of Biology, University of North Carolina, Chapel Hill, NC, United States of America

[3] Howard Hughes Medical Institute, University of North Carolina, Chapel Hill, NC, United States of America

[&] Current address: Novozymes North America Inc, 108 T W Alexander Driver Bldg 1 A, Raleigh, NC, United States of America

[#] Current address: Department of Biology, "Luiz de Queiroz" College of Agriculture – ESALQ, University of São Paulo, Piracicaba, SP, Brazil

Abstract

Nucleotide-binding leucine-rich repeat (NLR) proteins serve as intracellular immune receptors that sense pathogen-derived effector molecules and consequently, induce effector-triggered immunity (ETI). Members of the ACTIVATED DISEASE RESISTANCE 1 (ADR1) family have been shown to act as helper NLRs and are required for ETI mediated by multiple sensor NLRs. Despite their important role in plant innate immunity, the molecular mechanisms by which ADR1s are controlled remain poorly defined. In *Arabidopsis thaliana*, the expression of the autoactivated mutant allele ADR1-LIKE 2^{D484V} (ADR1-L2^{D484V}) leads to an autoimmune phenotype characterized by stunted plant growth, constitutively high SA levels and increased disease resistance. A forward genetic screen identified the mutant *suppressor of ADR1-L2^{D484V} 2* (*sadr2*) based on the suppression of the reduced plant size normally caused by the expression of *ADR1-L2^{D484V}*. We could reveal that *sadr2* carries a point-mutation in the leucine-rich repeat (LRR) receptor-like kinase (RLK) *BAK1-LIKE 1* (*BKK1*). Our genetic data demonstrate that BKK1 is likely a specific regulator of ADR1-L2^{D484V}. As BKK1 does not control ADR1-L2^{D484V} homeostasis, BKK1 might regulate ADR1-L2^{D484V} activity or downstream signaling. Here, we show that BKK1 constitutively associates with ADR1-L2 in *N. benthamiana*, suggesting that both proteins exist in a pre-formed complex. We further demonstrate that ADR1-L2^{D484V} autoactivity induces many typical PTI responses, however, BKK1-independently. Thus, the exact molecular mechanism by which BKK1 regulates ADR1-L2^{D484V} autoactivity remains to be fully clarified.

Introduction

In order to defend themselves against invading pathogens, plants employ two major types of immune receptors, plasma-membrane (PM)-localized pattern recognition receptors (PRRs) and intracellular nucleotide-binding leucine-rich repeat receptors (NLRs) (Albert et al. 2020; El Kasmi 2021). Recognition of conserved pathogen-associated molecular patterns (PAMPs) or host released damage-associated molecular patterns (DAMPs) by PRRs results in pattern-triggered immunity (PTI) (Gomez-Gomez & Boller 2000; Huffaker et al. 2006; Zipfel et al. 2006; Miya et al. 2007; Boller & Felix 2009). The activation of PTI is accompanied by a plethora of reactions, including the production of reactive oxygen species (ROS), calcium influxes, phosphorylation of mitogen-activated protein kinases (MAPKs) and induction of defense gene expression (Doke 1983; Blume et al. 2000; Tao et al. 2003; Zipfel et al. 2004; Boudsocq et al. 2010; Jeworutzki et al. 2010; Ranf et al. 2011; Nomura et al. 2012). In summary, activation of PTI results in broad-spectrum resistance. PRRs include receptor-like kinases (RLKs) and receptor-like proteins (RLPs) (Macho & Zipfel 2014). Unlike RLKs, RLPs lack a cytoplasmic kinase domain and thus, transduce defense activation through adaptor kinases, like the leucine-rich repeat (LRR)-RLK SUPPRESSOR OF BIR1 (SOBIR1) (Gust & Felix 2014; Liebrand et al. 2014). However, upon ligand binding, both RLKs and RLPs interact with a co-receptor to initiate defense activation. The LRR-RLK BRI1-ASSOCIATED RECEPTOR KINASE 1 (BAK1) and BAK1-LIKE 1 (BKK1) serve as common co-receptors of PRRs (Chinchilla et al. 2007; Roux et al. 2011; Gust & Felix 2014; Albert et al. 2015; Postma et al. 2016). BAK1 and BKK1 belong to the small SOMATIC EMBRYOGENESIS RECEPTOR-LIKE KINASE (SERK) family that comprises 5 members in Arabidopsis (Albrecht et al. 2008). Apart from their roles in PTI, BAK1 and BKK1 also act in an unequally redundant manner in brassinosteroid (BR) and cell death signaling (He et al. 2007; Heese et al. 2007; Roux et al. 2011), suggesting that they might function as integration points of multiple RLK-induced signaling pathways.

Adapted pathogens, however, can overcome PTI by secreting or delivering virulence factors (effector molecules) into plant cells that target PTI key components and consequently, suppress PTI (Boller & Felix 2009). For example, BAK1 and BKK1 are targeted by multiple effector molecules to dampen PTI signaling (Shan et al. 2008; Cheng et al. 2011a; Zhou et al. 2014; Li et al. 2016). To combat adapted pathogens, plants employ NLRs that induce effector-triggered immunity (ETI) following the perception of pathogen-derived effector molecules (Dangl & Jones 2001; El Kasmi 2021). The induction of ETI leads to similar immune responses as elicited by PRRs, though the duration and amplitude of ETI responses are often larger than those of PTI responses (Peng et al. 2018). Interestingly, however, full ETI requires the activation of PTI (Ngou et al. 2021; Yuan et al. 2021). In contrast to PTI, ETI is typically

associated with a programmed cell death at the infection site, termed hypersensitive response (HR) (Coll et al. 2011; Balint-Kurti 2019).

NLRs are classified into three groups depending on their N-terminal domains: Toll-like/Interleukin 1 receptor (TIR)-type NLRs (TNLs), coiled-coil (CC)-type NLRs (CNLs) and RESISTANCE TO POWDERY MILDEW 8 (RPW8)-like coiled-coil (CC_R)-type NLRs (RNLs) (El Kasmi 2021). In *Arabidopsis thaliana* (hereafter Arabidopsis) the RNL subclass consists of two gene families, *ACTIVATED DISEASE RESISTANCE 1* (*ADR1*) and *N REQUIREMENT GENE 1* (*NRG1*), both acting as helper NLRs in immune signaling and cell death induction of several NLRs, mainly TNLs (Bonardi et al. 2011; Castel et al. 2019; Wu et al. 2019; Saile et al. 2020; Schulze et al. 2021). Interestingly, the ADR1 subfamily has recently been linked to RLP- and to a lesser extent to LRR-RLK-mediated PTI (Pruitt et al. 2021; Tian et al. 2021), suggesting that ADR1s might represent a node of convergence of PRR- and NLR-mediated immune signaling pathways. Despite their important functions in plant innate immunity, the molecular mechanisms underlying the strict regulation of ADR1s remain largely unknown.

The autoactivated mutant allele *ADR1-LIKE 2^{D484V}* (*ADR1-L2^{D484V}*) carries a gain-of-function mutation caused by the substitution of the aspartic acid (D) by valine (V) in the conserved QHD motif of ADR1-L2. Expression of *ADR1-L2^{D484V}-HA* under the control of the *ADR1-L2* promoter in the *adr1-L2-4* mutant background leads to an autoimmune phenotype coupled with constitutively activated immune responses, stunted growth and curled leaves (Roberts et al. 2013). This conspicuous phenotype makes plants expressing *ADR1-L2^{D484V}* a practical tool for forward genetic screens. To obtain insights into the signaling events of ADR1-L2^{D484V}-mediated autoimmunity and thus, to learn more about the regulatory mechanisms of RNL helper NLRs, we performed an EMS suppressor screen targeted to identify positive regulators of ADR1-L2^{D484V}. In this screen, we identified the LRR-RLK *BKK1* as being required for ADR1-L2^{D484V}-induced autoimmunity. Our genetic data suggest that BKK1 is specifically required for the autoactivity of ADR1-L2^{D484V}. Further, our biochemical analyses indicate that BKK1 and ADR1-L2 exist in a pre-formed complex. However, the molecular mechanism by which BKK1 regulates the autoactivity of ADR1-L2^{D484V} has yet to be determined.

Results

Identification of genes regulating ADR1-L2^{D484V} autoactivity

In order to identify positive regulators of ADR1-L2^{D484V} autoactivity in Arabidopsis, we performed an EMS mutagenesis screen aimed at identifying suppressors of the *ADR1-L2^{D484V}* (*sadr*) phenotype (Jacob et al., unpublished). *Sadr2* was one of the isolated mutants that strongly suppressed the *ADR1-L2^{D484V}* phenotype. Genetic mapping by whole-genome sequencing revealed that the *sadr2* mutant carried a point mutation in the first exon of *AT2G13790* which encodes the LRR-RLK BKK1, also known as SERK4 (Fig. 1 e). The

mutation in *sadr2* leads to exchange of arginine (R) 9 to lysine (K) and is located in the signal peptide of BKK1. To confirm that loss-of-function of *BKK1* suppresses the autoimmune phenotype of *ADR1-L2^{D484V}*, we crossed the *bkk1-1* T-DNA insertion mutant (Fig. 1 e) with *ADR1-L2^{D484V} adr1-L2-4*. While *bkk1-1* fully suppressed the dwarfism of ADR1-L2^{D484V} *adr1-L2-4* (Fig. 1 a, b), trypan blue and DAB staining showed that ADR1-L2^{D484V}-triggered cell death and H_2O_2 accumulation were not suppressed (Fig. 1 a). Further, *bkk1-1* suppressed, although not fully, the expression of the defense-related gene *PATHOGENESIS-RELATED 1* (*PR1)* which is strongly induced in *ADR1-L2^{D484V} adr1-L2-4* (Fig. 1 c). Despite still having elevated *PR1* expression in *ADR1-L2^{D484V} adr1-L2-4 bkk1-1*, enhanced disease resistance against the virulent bacterial pathogen *Pseudomonas syringae* (*Pst*) DC3000 in *ADR1-L2^{D484V} adr1-L2-4* plants was completely suppressed by *bkk1-1* (Fig. 1 d). This demonstrates that some, but not all, of the ADR1-L2^{D484V}-induced autoimmune responses require the presence of BKK1.

Remarkably, when expressed under control of its native promoter, the ADR1-L2^{D484V}-HA protein level was not altered in *adr1-L2-4 bkk1-1* compared to *adr1-L2-4* (Fig. 1 c). These data clearly show that ADR1-L2^{D484V} stability is not regulated by BKK1 and suggest that BKK1 regulates ADR1-L2^{D484V} autoactivity or the downstream signaling, and not its homeostasis.

The kinase activity of the BKK1 paralog BAK1 is required for its function during PTI (Schwessinger et al. 2011). To determine whether BKK1 requires kinase activity for ADR1-L2^{D484V}-induced autoimmunity and to confirm that loss of BKK1 is the cause of the suppression of the ADR1-L2^{D484V} autoimmune phenotype, we introduced WT *BKK1-Myc* and a kinase dead version of *BKK1* (*BKK1^{K322E}*)-*Myc* under control of its native promoter into *ADR1-L2^{D484V}-HA adr1-L2-4 bkk1-1* plants, respectively. However, expression of BKK1-Myc did not restore the morphology of ADR1-L2^{D484V} plants, similar to the expression of BKK1^{K322E}-Myc (Fig. S1, S2). As C-terminal tags have been shown to strongly impair the immune function of BAK1 (Ntoukakis et al. 2011), we assume that the C-terminal Myc tag might similarly affect BKK1 function. Collectively, our genetic data suggest that *BKK1* is required for some of the ADR1-L2^{D484V}-induced autoimmune responses.

BKK1 is not a general regulator of NLR-mediated (auto-) immunity

To test whether *BKK1* is required for the autoimmune phenotypes mediated by other autoactivated NLRs, we crossed the *bkk1-1* T-DNA mutant with additional autoimmune mutants, including the mutant *suppressor of npr1-1 constitutive 1* (*snc1)* (Li et al. 2001; Zhang et al. 2003*)* and *nrg1.1-1* mutant plants expressing the autoactivated *NRG1.1^{D485V}*-HA that is under control of its endogenous promoter (*NRG1.1^{D485V} nrg1.1-1) (*Wu et al. 2019). Although the *ADR1* subfamily has been linked previously to *snc1*-caused autoimmunity (Dong et al. 2016), *bkk1-1* did not suppress the *snc1* autoimmune phenotype (Fig. S3). Accordingly, homozygous *bkk1-1 snc1* double mutants remained dwarf in morphology (Fig. S3 a, b),

displayed increased *PR1* expression (Fig. S3 c) and enhanced resistance against the virulent pathogen *Pst* DC3000 (Fig. S3 d). Apart from the *ADR1s*, *NRG1s* constitute the other RNL subfamily that is involved in NLR-mediated immune signaling (Castel et al. 2019; Wu et al. 2019; Saile et al. 2020; Schulze et al. 2021). Interestingly, *bkk1-1* did not suppress the NRG1.1^{D485V}-mediated autoimmune phenotype (Fig. S4). Taken together, *bkk1-1* does not suppress the autoimmune phenotypes caused by *snc1* and NRG1.1^{D485V}, suggesting that *BKK1* might be specifically required for the activity of ADR1-L2^{D484V} or the ADR1 subfamily.

ADR1-L2 has two close homologs, ADR1 and ADR1-L1 that share 76% and 75% amino acid sequence similarity with ADR1-L2. Since mutations in *BKK1* suppressed the autoactivity of ADR1-L2^{D484V}, we tested whether *BKK1* also regulates the function of the other two ADR1 family members. As ADR1s act redundantly downstream of several NLRs during ETI (Bonardi et al. 2011; Saile et al. 2020), we analysed whether *bkk1-1* is impaired in ADR1s-mediated ETI responses. We therefore challenged Col-0, *adr1 triple*, *bkk1-1* and *adr1 triple bkk1-1* mutants with *Pst* DC3000 carrying either the effector *AvrRpt2* or *AvrRps4*, that induce ETI via the CNL RPS2 or the TNL pair RPS4/RRS1, respectively (Kunkel et al. 1993; Hinsch & Staskawicz 1996; Gassmann et al. 1999). RPS2 and RPS4/RRS1 signal through the *ADR1* subfamily to trigger resistance against *Pst* DC3000 (Saile et al. 2020). The *bkk1-1* mutant showed similar bacterial growth compared to Col-0 after infection with either *Pst* DC3000 *AvrRpt2* or *Pst* DC3000 *AvrRps4*, whereas *adr1 triple bkk1-1* was as susceptible as *adr1 triple* (Fig. S5). These data suggest that *BKK1* might be specifically required for ADR1-L2 functions, though further experiments are needed to prove this conclusion (see conclusion and perspectives section).

ADR1-L2 might constitutively associate with BKK1

We have recently shown that ADR1-L2 is localized at the PM (Saile et al. 2021) where it interacts with the LRR-RLK SOBIR1 and the receptor-like cytoplasmic kinase PBL31 (Pruitt et al. 2021). As BKK1 is an LRR-RLK with predicted PM localization that acts as a co-receptor of the PM-localized PRRs FLAGELLIN-SENSITIVE 2 (FLS2), EF-Tu Receptor (EFR) and Perception of the Arabidopsis Danger Signal Peptide 1 or 2 (PEPR1/2) (Roux et al. 2011), we tested whether ADR1-L2 associates with BKK1. Physical interaction was examined by co-immunoprecipitation (Co-IP) experiments using the transient expression system in *Nicotiana benthamiana* (hereafter *N. benthamiana*). Both ADR1-L2-HA and ADR1-L2^{D484V}-HA co-immunoprecipitated with BKK1-Myc (Fig. 2 a), suggesting that ADR1-L2 forms a constitutive complex with BKK1, independent of the ADR1-L2 activation state. Interestingly, we noted an upward shifted band of ADR1-L2-HA and ADR1-L2^{D484V}-HA that co-immunoprecipitated with BKK1-Myc. These results suggest that BKK1 might phosphorylate wildtype and autoactivated ADR1-L2^{D484V}. To prove this hypothesis, we co-expressed ADR1-L2-HA and ADR1-L2^{D484V}-HA

with the kinase inactive allele of BKK1, BKK1^{K322E}-Myc, in *N. benthamiana* and performed Co-IP experiments. Again, wildtype and autoactivated ADR1-L2-HA co-immunoprecipitated with BKK1^{K322E}-Myc (Fig. 2 a). However, we still observed an upward shifted band of ADR1-L2-HA and ADR1-L2^{D484V}-HA co-immunoprecipitating with the kinase inactive BKK1^{K322E}-Myc. This indicates that either BKK1 might not phosphorylate ADR1-L2 or that the upper band might represent another post-translational modification of ADR1-L2. The latter hypothesis is further supported by the fact that treatment with λ-protein phosphatase did not abolish the appearance of the higher migrating band (Fig. S6). Although wildtype and autoactivated ADR1-L2 clearly associated with BKK1 in Co-IP experiments in *N. benthamiana*, we were not able to validate this interaction by bimolecular fluorescence complementation (BiFC) (Fig. 2 b, c). As we observed that BKK1-EYFP was strongly localized at the ER after transient expression in *N. benthamiana* (Fig. S7), we propose that the fused fluorophore might cause the retention of BKK1 at the ER. Consequently, BKK1-nYFP might be in insufficient proximity with the PM-localized ADR1-L2-cYFP and ADR1-L2^{D484V}-cYFP and hence, this might explain the negative BiFC results. Taken together, our results suggest that BKK1 constitutively interacts with ADR1-L2 irrespective of the activation state of ADR1-L2, and that this interaction does not require the kinase activity of BKK1.

The Arabidopsis genome encodes 5 SERKs that mediate plant immunity and developmental processes (Albrecht et al. 2008). The interaction between BKK1 (SERK4) and ADR1-L2/ADR1-L2^{D484V} prompted us to test whether ADR1-L2 can also interact with other members of the SERK family. Indeed, our Co-IP experiments revealed that wildtype and autoactivated ADR1-L2 interact with all SERK proteins after transient overexpression in *N. benthamiana* (Fig. S8). Collectively, although BAK1 and BKK1 have been shown to be recruited to the LRR-RLKs FLS2, EFR and BRI1 following ligand binding (Chinchilla et al. 2007; Schulze et al. 2010; Roux et al. 2011), our data suggest that ADR1-L2 and the SERKs exist in a pre-formed complex. However, it remains to be investigated whether ADR1-L2 constitutively interacts with SERK proteins in Arabidopsis when expressed at native levels.

BKK1 is not required for the membrane association of ADR1-L2^{D484V}

Arabidopsis ADR1s function at the plasma membrane to initiate cell death (Jacob et al. 2021; Saile et al. 2021). Although ADR1s have been demonstrated to localize to the PM by the interaction of their CC_R domains with negatively charged phospholipids (Saile et al. 2021), it is likely that there are additional mechanisms contributing to the PM localization of ADR1s. Many peripheral membrane proteins for example require protein-protein interactions to localize to the PM (Marmagne et al. 2004; Tang et al. 2008). To test whether BKK1 is required for tethering ADR1-L2^{D484V} to the PM, we performed subcellular fractionation experiments with protein extracts from transgenic Arabidopsis plants expressing ADR1-L2^{D484V}-HA in either the

adr1-L2-4 or *adr1-L2-4 bkk1-1* background. ADR1-L2^{D484V}-HA was enriched in the microsomal membrane fraction prepared from both *adr1-L2-4* and *adr1-L2-4 bkk1-1* transgenic plants (Fig. S9), demonstrating that *bkk1-1* does not *per se* affect the membrane association of ADR1-L2^{D484V}-HA. These results suggest that BKK1 might not be required for the general membrane localization of ADR1-L2^{D484V}, albeit the used method does not allow for distinguishing PM from organelle membranes.

ADR1-L2^{D484V}-induced activation of PTI does not depend on BKK1

BKK1 and other PRR co-receptors, including BAK1 and CHITIN ELICITOR RECEPTOR KINASE 1 (CERK1), have been shown to be required for NLR-mediated ETI responses during bacterial infections (Yuan *et al.* 2021). Activation of NLR-mediated ETI was revealed to potentiate the output of PTI key components that is needed to provide resistance against avirulent pathogens (Ngou *et al.* 2021; Yuan *et al.* 2021). Based on these recent findings we hypothesized that PTI might also be activated in NLR autoimmune mutants in the absence of pathogens and that BKK1 might be involved in ADR1-L2^{D484V}-triggered PTI potentiation that could be required for the observed autoimmune phenotype. The lack of HR- or severe cell death symptoms in ADR1-L2^{D484V} *adr1-L2-4* (Fig. 1 a) is reminiscent of PRR-induced immune responses and hence, would support such an idea. To prove this hypothesis, we first analysed the protein levels of the PTI key components BOTRYTIS-INDUCED KINASE 1 (BIK1) and SOBIR1 in NLR autoimmune mutants, including *ADR1-L2^{D484V}-HA adr1-L2-4 (*Roberts et al*.* 2013*)*, *NRG1.1^{D485V}-HA nrg1.1-1* (Wu et al*.* 2019), *RPM1^{D505V} rpm1 rps2 (Gao* et al. *2011)* and *snc1 (Li* et al. *2001; Zhang* et al. *2003)*. BIK1 and SOBIR1 were induced in all analysed autoimmune mutants*,* but not in Col-0 or the *ADR1-L2-HA adr1-L2-4* line (Fig. S10 a). This suggests that the expression of autoactivated NLRs might induce the activation of PTI in the absence of pathogen attacks. Indeed, we found a strong phosphorylation and activation of MAPKs (Fig. S10 c) as well as the upregulation of several PTI-associated genes, including *FLG22-INDUCED RECEPTOR-LIKE 1* (*FRK1)* and *NDR1/HIN1-LIKE 10* (*NHL10*) in the autoimmune mutant *ADR1-L2^{D484V} adr1-L2-4* (Fig. S10 d). These data demonstrate that PTI is indeed activated in *ADR1-L2^{D484V} adr1-L2-4*. However, BKK1 was not required for the ADR1-L2^{D484V}-induced activation of PTI, as induced expression of PTI key components, MAPKs activation and upregulation of PTI-associated genes were similarly induced or activated in *ADR1-L2^{D484V} adr1-L2-4 bkk1-1* compared to *ADR1-L2^{D484V} adr1-L2-4* (Fig. S10 b, c, d). In summary, the expression of ADR1-L2^{D484V} and other autoactivated NLRs results in the activation of PTI. BKK1*,* however, is not required for the ADR1-L2^{D484V}-induced PTI potentiation.

Overexpression of *SOBIR1* in Arabidopsis triggers the constitutive activation of immune responses (Gao et al. 2009). Since SOBIR1 was specifically up-regulated in ADR1-L2^{D484V} *adr1-L2-4*, we hypothesized that overactivated SOBIR1 might boost autoimmunity in ADR1-L2^{D484V} *adr1-L2-4*. To prove this hypothesis, we crossed the *sobir1-12* T-DNA mutant with ADR1-L2^{D484V} *adr1-L2-4*. Homozygous *ADR1-L2^{D484V} adr1-L2-4 sobir1-12* plants resembled the morphology of *ADR1-L2^{D484V} adr1-L2-4* (Fig. S11 a, b) and retained increased *PR1* expression (Fig. S11 c). These results suggest that ADR1-L2^{D484V} functions independently or downstream of *SOBIR1*. The latter hypothesis is supported by the recent findings demonstrating that ADR1s are required for RLP23-mediated PTI responses (Pruitt et al. 2021).

Conclusion and Perspectives

NLRs constitute crucial surveillance components that induce a robust immune response following the detection of pathogen-derived effector molecules (El Kasmi 2021). Helper NLRs of the ADR1 subfamily have been shown to be required for several NLRs to mediate a proper ETI response (Bonardi et al. 2011; Saile et al. 2020). While plants that lack the ADR1 subfamily are susceptible against certain pathogens (Bonardi et al. 2011; Saile et al. 2020), the overexpression of *ADR1s* results in the constitutive activation of immune responses (Grant et al. 2003; Wu et al. 2020). Likewise, the expression of the autoactivated mutant *ADR1-L2^{D484V}* causes autoimmunity in Arabidopsis (Roberts et al. 2013). As the induction of immune responses is an energetically demanding process that negatively impacts plant fitness (Tian et al. 2003), NLRs are tightly regulated on transcriptional, post-transcriptional and protein level (Richard et al. 2018). Apart from epigenetic modifications such as DNA methylation and histone modifications (Palma et al. 2010; Xia et al. 2013), NLR transcription can also be modulated by an SA-dependent feedback regulation (Yang & Hua 2004; Venugopal et al. 2009). On post-transcriptional level, NLR expression is regulated by small RNAs and by the mRNA control machinery nonsense mediated mRNA decay (NMD) (Li et al. 2012; Shivaprasad et al. 2012; Gloggnitzer et al. 2014). In contrast, NLR stability and/or activity can be modulated by post-translational modifications (PTMs) and/or interactions with proteins, including chaperones or effectors/effector host targets (Kadota et al. 2010; Cheng et al. 2011b; Kadota & Shirasu 2012; He et al. 2017). PTMs as well as protein-protein interactions can affect protein activity by modulating protein conformation, subcellular localization, stability or other protein-protein-interactions. Together, NLR homeostasis and activity are tightly controlled at multiple levels in order to avoid the ectopic activation of defense responses associated with severe fitness costs. Although ADR1s represent important players involved plant immunity (Bonardi et al. 2011; Saile et al. 2020; Pruitt et al. 2021; Tian et al. 2021) it is poorly understood how they are regulated. Genetic analyses showed that *ADR1-L2* can be regulated on a transcriptional level partially by an SA-dependent feedback loop (Roberts et al. 2013) and on

the post-transcriptional level by NMD (Nasim et al. 2020). How exactly ADR1s are regulated on the protein level is however largely unknown, as the autoactivity of ADR1 CC_R and ADR1-L2^{D484V} was shown to be (largely) independent of the co-chaperones SUPPRESSOR OF G2 ALLELE OF SKP 1 (SGT1) or REQUIRED FOR MLA12 RESISTANCE 1 (RAR1), respectively (Collier et al. 2011; Roberts et al. 2013).

Our work revealed that the LRR-RLK BKK1 is a positive regulator of ADR1-L2^{D484V}-mediated autoimmunity (Fig. 1). Interestingly, SERKs have been linked before to NLR-mediated autoimmune signaling, as resistance mediated by the autoactivated CNL Mi-1.2 was found to require *SlSERK1* in tomato (Mantelin et al. 2011). However, since *bkk1-1* did not suppress the autoimmune phenotypes caused by *snc1* and *NRG1.1^{D485V}* (Fig. S3, S4), we propose that BKK1 is likely a specific regulator of ADR1-L2^{D484V} activity. As *bkk1-1* was not impaired in ADR1s-dependend ETI responses (Fig. S5), it could be possible (i) that *BKK1* is not required for the activity of ADR1 and/or ADR1-L1, as they act redundantly during ETI (Bonardi et al. 2011) or (ii) that *BKK1* is not needed for the non-canonical "helper" function of ADR1-L2 and hence, might constitute a specific regulator of ADR1-L2s' canonical functions. To prove these hypotheses, one could analyse RPS2- and RPS4/RRS1-mediated bacterial growth restriction in *adr1-1 adr1-L1-1 bkk1-1.* If *BKK1* is needed in general for the activity and/or function of ADR1-L2, one would expect the *adr1-1 adr1-L1-1 bkk1-1* mutant to phenocopy *adr1 triple*. In contrast, if *BKK1* is specifically required for the autoactivity/canonical functions of ADR1-L2, *adr1-1 adr1-L1-1 bkk1-1* would show WT-like growth of *Pst* DC3000 *AvrRpt2* and *Pst* DC3000 *AvrRps4*. In case BKK1 acts as a general regulator of ADR1-L2 activity, the generation of additional combinatorial triple mutants, including *adr1-1 adr1-L2-4 bkk1-1* and *adr1-L1-1 adr1-L2-4 bkk1-1* would help to reveal whether *BKK1* regulates apart from ADR1-L2 also the other ADR1 family members. Additionally, one could cross the ADR1 overexpression line (Grant et al. 2003) that shows an autoimmune phenotype with *bkk1-1*. Suppression of the ADR1 autoimmune phenotype would demonstrate that BKK1 is also required for the activity of ADR1. In summary, these experiments would help to clarify whether BKK1 is required for the activity of ADR1-L2 in general or rather acts as a specific regulator of its autoactivity. In the latter case, BKK1 would bridge a gap between how the different activation modes/functions of ADR1-L2 are achieved. Further, the proposed experiments would provide insights into the specificity underlying the regulation of the ADR1 family members and might help to explain differences in their biochemical properties.

As the ADR1-L2^{D484V} protein abundance was not affected in *bkk1-1* (Fig. 1 c), BKK1 does not regulate ADR1-L2^{D484V} autoactivity by modulating ADR1-L2 abundance, but rather by regulating its activity/signaling function. NLR activity can be regulated for example by affecting NLR conformation or localization most likely by protein-protein interactions. Indeed, using Co-IP experiments we found that BKK1 interacts with both wildtype and autoactivated ADR1-

L2^{D484V} (Fig. 2 a), suggesting that ADR1-L2 and BKK1 exist in a pre-formed complex which might be required to induce immune signaling upon (auto-) activation of ADR1-L2. In addition, we observed that ADR1-L2 constitutively interacts with all SERK family members after transient overexpression in *N. benthamiana* (Fig. S8). Yet, the constitutive interactions remain to be confirmed in Arabidopsis. Further, it needs to be determined whether other SERK proteins are also required for ADR1-L2^{D484V} autoactivity. Interestingly, SlSERK1, which is required for CNL Mi-1.2 autoactivity (Mantelin et al. 2011), was also shown to constitutively associate with Mi-1.2 in Co-IP experiments, irrespective of the activation state of Mi-1.2 (Peng et al. 2016). Effector-triggered activation of Mi-1.2 was proposed to result in conformational changes of the pre-formed complex, as SlSERK1-Mi-1.2 interaction in BiFC experiments was only observed in presence of effector molecules (Peng et al. 2016). It is possible that the (auto-) activation of ADR1-L2 might also cause structural rearrangements within the pre-formed complex. How ADR1-L2^{D484V}-induced signaling is regulated by BKK1 is, however, still unclear. In order to uncover the molecular mechanisms underlying the BKK1-dependent regulation of ADR1-L2^{D484V} autoactivity, it would be important to test whether BKK1 requires its kinase activity or whether it rather plays a structural role. BKK1 has an intracellular, catalytically active kinase domain that regulates BR signaling (He et al. 2007). As BAK1 requires its kinase activity for its function in BR- and PTI-signaling (Wang et al. 2008; Schwessinger et al. 2011) as well as in cell death control (Wu et al. 2020), it is likely that BKK1 might also induce diverse signaling pathways via phosphorylation of downstream clients. Thus, it is possible that BKK1 might require kinase activity to regulate ADR1-L2^{D484V} autoactivity. Expression of the kinase-dead mutant allele *BKK1^{K322E}* in *ADR1-L2^{D484V}-HA adr1-L2-4 bkk1-1* could provide insights into whether the kinase activity of BKK1 is required for ADR1-L2^{D484V} autoactivity. If the expression of *BKK1^{K322E}* in *ADR1-L2^{D484V}-HA adr1-L2-4 bkk1-1* plants does not result in the reversion of the ADR1-L2^{D484V} autoimmune phenotype (and plants still show the suppressor phenotype), BKK1 kinase activity would be required for ADR1-L2^{D484V} autoactivity. *Vice versa*, if complementation of *ADR1-L2^{D484V} adr1-L2-4 bkk1-1* with *BKK1^{K322E}* results in the reversion of the *ADR1-L2^{D484V}* autoimmune phenotype, BKK1 kinase activity would be dispensable for ADR1-L2^{D484V} autoactivity.

If the kinase activity of BKK1 is indispensable for the autoimmune phenotype induced by the expression of ADR1-L2^{D484V}, one could test whether ADR1-L2/ADR1-L2^{D484V} is a substrate of BKK1 and hence, is phosphorylated by BKK1 *in vitro* and *in vivo*. In mice, the helper NLR NLR family CARD domain-containing protein 4 (NLRC4) was found be phosphorylated in a stimulus-dependent manner and NLRC4 phosphorylation was shown to promote pyroptosis, a form of programmed cell death, by assembling an inflammasome complex (Qu et al. 2012). As ADR1s also likely signal though oligomerization (Jacob et al. 2021; Wu et al. 2021), it could be possible that activation-dependent phosphorylation of ADR1-L2 might induce structural

rearrangements within the pre-formed complex into a signaling-competent state. In agreement with this idea, we have previously shown that ADR1-L2 self-associates irrespectively of its activation state (Saile et al. 2021) and thus, induced structural changes within the pre-formed complex are likely needed to activate immune signaling.

In contrast, if the kinase activity of BKK1 is not required for the ADR1-L2^{D484V}-induced autoimmune phenotype, BKK1 might likely play a structural role in regulating ADR1-L2^{D484V} autoactivity, yet the underlying mechanism remains again a matter of speculation. One idea is that BKK1 might act as scaffold to recruit ADR1-L2^{D484V} to specific sites within the PM. ADR1s require PM localization for their cell death (signaling) function in *N. benthamiana* (Saile et al. 2021). Using subcellular fractionation experiments we found that BKK1 does not regulate *per se* the membrane-association of ADR1-L2^{D484V} (Fig. S9). As immune and growth receptors have been shown to localize to distinct PM nanodomains, which is essential for signal transduction (Bucherl et al. 2017), it might be tempting to speculate that activated ADR1-L2^{D484V} localizes to PM nanodomains and that BKK1 might regulate ADR1-L2^{D484V} PM nanodomain organization. If BKK1 itself is organized in PM nanodomains is not established yet, but very likely, given the distribution of BAK1, its close paralog, in PM nanoclusters (Hutten et al. 2017). Thus, by using high-resolution microscopy techniques, one could analyse the dynamics of ADR1-L2 and ADR1-L2^{D484V} within the PM in both *adr1-L2-4* and *adr1-L2-4 bkk1-1* in future.

Together, the proposed experiments could shed light on how BKK1 regulates the (auto-) activity of ADR1-L2 and might lead to a better understanding of plant innate immunity. Nonetheless, the presented data provide evidence for a novel function of the LRR-RLK BKK1 in plant innate immunity. While BKK1 has a well-established role as a negative regulator of plant cell death (He et al. 2007), we could clearly show that BKK1 does also have a positive function in promoting NLR-induced autoimmunity (Fig. 1). Thus far however, BKK1 functions were only observed in the absence of its close paralog *BAK1*, as they act in an unequally redundant manner in cell death control and PTI signaling (He et al. 2007; Kemmerling et al. 2007; Roux et al. 2011). While PRRs seem to favour the co-receptor BAK1 over BKK1 to initiate immune signaling, activated ADR1-L2 might favour BKK1 over BAK1 to induce autoimmunity. We observed that ADR1-L2 also constitutively associates with BAK1 after transient overexpression in *N. benthamiana* (Fig. S8). However, whether this interaction is of biological relevance for the (auto-) activity ADR1-L2^{D484V} has yet to be determined. Based on the finding that loss-of-function of *BKK1* suppresses the ADR1-L2^{D484V} autoimmune phenotype (Fig. 1), BAK1 and BKK1 do not have redundant but rather might have additive functions in regulating ADR1-L2^{D484V} autoactivity. Thus, the generation of transgenic plants expressing *ADR1-L2^{D484V}-HA* in either *adr1-L2-4 bak1* or *adr1-L2-4 bkk1-1 bak1* mutant backgrounds is eagerly awaited. Interestingly, just recently the *ADR1s* have been identified for being required

for the *bak1 bkk1*-induced cell death phenotype, with ADR1-L2 being the most important player (Wu et al. 2020). Hence, there is an important mutual relationship between ADR1-L2-dependent *bak1 bkk1*-induced autoimmunity and BKK1-dependent ADR1-L2^{D484V}-induced autoimmunity, suggesting a cross-regulation between ADR1-L2 and BKK1.

In conclusion, our work shows that BKK1 is a positive regulator of ADR1-L2^{D484V}-mediated autoimmunity in Arabidopsis. It will be interesting to uncover the molecular mechanism underlying this regulation in future.

Material and Methods

Plant material, growth conditions and generation of transgenic lines

ADR1-L2^{D484V} adr1-L2-4 (Roberts et al. 2013), *adr1 triple* (*adr1-1 adr1-L1-1 adr1-L2-4*) (Bonardi et al. 2011), *bkk1-1* (He et al. 2007), *sobir1-12* (Gao et al. 2009), *NRG1.1^{D485V} nrg1.1-1 (*Wu et al. 2019*), rrs1a/b* (Saucet et al. 2015), *rps2-101C* (Venugopal et al. 2009), *RPM1^{D505V} rpm1 rps2 rin4* (Gao et al. 2011) and *snc1* (Li et al. 2001) have been described previously. Plants were grown under short day conditions (8-hour light/16-hour dark cycle) at 21°/18°C and 45% humidity.

In this study, transgenic plants expressing *ADR1-L2^{D484V}-HA* in *adr1-L2-4 bkk1-1* and *adr1-L2-4 sobir1-12* mutant background were generated by crossing *ADR1-L2^{D484V}-HA adr1-L2-4* with the corresponding T-DNA mutant, respectively. Transgenic plants expressing *NRG1.1^{D485V}-HA* in the *nrg1.1-1 bkk1-1* mutant background were generated by crossing *NRG1.1^{D485V}-HA nrg1.1-1* with the *bkk1-1* T-DNA mutant. The double mutant *bkk1-1 snc1* was generated by crossing both T-DNA insertion lines and the quadruple mutant *adr1-1 adr1-L1-1 adr1-L2-4 bkk1-1 was* generated by crossing *adr1 triple* with *bkk1-1*.

Transgenic plants expressing *pBKK1::BKK1_CDS-4xMyc* (pGWB16) and *pBKK1::BKK1^{K322E}_CDS-4xMyc* (pGWB16) were generated using Agrobacterium (GV3101)-mediated floral dip transformation (Clough & Bent 1998). Transformants were selected on ½ MS agar medium containing 20 µg/ml hygromycin.

Plasmid construction

The generation of *ADR1-L2* (CDS) and *ADR1-L2^{D484V}* (CDS) *pDONR221* (Thermo Fisher Scientific, Waltham, USA) entry constructs was described previously (Saile et al. 2021). *ADR1-L2* constructs were cloned into *pGWB614* or *pGWB660* (Nakamura et al. 2010) by GATEWAY™ cloning (Thermo Fisher Scientific, Waltham, USA).

For complementation studies, the CDS of *BKK1 and BKK1^{K322E}* (without stop codon) including its native promoter (2065 bp) was synthesized with 5' *attL1* and 3' *attL2* sites into the standard vector pUC57 (Baseclear, Netherlands). Subsequently, *BKK1* and *BKK1^{K322E}* were cloned into

the GATEWAY™-compatible *pGWB16* (hygromycin resistant) vector (Nakamura et al. 2010) by GATEWAY LR CLONASE II mix reaction (Thermo Fisher Scientific; Waltham, USA).
The CDS of *BKK1* in *pENTR/D-TOPO* was provided by Cyril Zipfel (Roux et al. 2011). The corresponding point mutation in *BKK1*^{K322E} pENTR/D-TOPO was introduced by site-directed mutagenesis PCR using primers listed in Table S1. The PCR products were digested with *Dpn*I (NEB, Massachusetts, USA) overnight, purified and transformed into *Escherichia coli* strain DH10B. The introduction of the mutations was confirmed by sequencing. Verified constructs were cloned into *pGWB641* and *pGWB17* (Nakamura et al. 2010) using GATEWAY LR CLONASE II enzyme mix reaction (Thermo Fisher Scientific; Waltham, USA).
For *BiFC 2in1* vector cloning, *BKK1* CDS and *ADR1-L2* or *ADR1-L2*^{D484V} CDS were amplified with *attB3 attB2* and *attB1 attB4* sites from existing entry plasmids *(*Roux et al. 2011; Saile et al. 2021) using primers listed in Table S1. PCR products were cloned into *pDONR221_P3P2* and *pDONR221_P1P4*, respectively and combined into the *2in1 BiFC CC* destination vector by gateway cloning (Grefen & Blatt 2012; Mehlhorn et al. 2018). The resulting constructs were verified by restriction analyses.
All confirmed plasmids were transformed into *Agrobacterium tumefaciens* strain GV3101.

Transient expression in *N. benthamiana*

Agrobacterium tumefaciens containing the indicated constructs were grown overnight at 28°C in LB media containing the appropriate antibiotics. Overnight cultures were spun down (4,000 g for 8 min) and pellets were resuspended in 2 mL induction buffer (10 mM $MgCl_2$, 10 mM MES pH 5.6, 150 µM acetosyringone). OD_{600} was adjusted to 0.05 (35s::P19) and 0.3 (SERKs/ADR1-L2). Agrobacteria mixtures were infiltrated into 4-5-week-old *N. benthamiana* leaves using a needleless syringe. Leaves were harvested for protein extraction, co-immunoprecipitation or confocal imaging at the indicated timepoints. *N. benthamiana* plants were grown on soil under 12-hour light / 12-hour dark cycles (24°C/22°C) at 70% humidity.

Protein extraction and western blot analyses

For protein extraction 4 leaf discs of 5 mm diameter (from *N. benthamiana*) or 2 leaves (from Arabidopsis) were frozen in liquid nitrogen and ground using a tissue homogenizer (Retsch GmbH; Haan, Germany). Plant material was solubilised in 190 µl grinding buffer (20 mM Tris-HCl pH 7, 150 mM NaCl, 1 mM EDTA pH 8, 1% [v/v] Triton X-100, 0.1% [w/v] SDS, 5 mM DTT, 1x Halt™ Protease Inhibitor Cocktail (Thermo Fisher Scientific; Waltham, USA). For protein extraction used for the detection of PTI-involved key components, plant material was resuspended in 190 µl extraction buffer (50mM HEPES pH 7.5, 50 mM NaCl, 10 mM EDTA pH 8.0, 0.5% [v/v] Triton X-100, 5 mM DTT, 1x Halt™ Protease Inhibitor Cocktail (Thermo Fisher Scientific; Waltham, USA)). Protein extracts were spun down for 15 min at 16,000 g and

4°C, and 5x SDS loading buffer (250 mM Tris-HCl pH 6.8, 50% [v/v] glycerol, 500 mM DTT, 10% [w/v] SDS, 0.005% [w/v] bromophenol blue) was added to the supernatants. Proteins were denatured at 95°C for 5 min. Proteins were resolved by electrophoresis on 8-10% SDS-PAGE gels and blotted onto nitrocellulose membranes (GE Healthcare; Chalfont St. Giles, UK). Membranes were blocked in 5% [w/v] milk in TBS-Tween (0.1% [v/v]) for 1 h. Primary antibody incubations were done for 1 h 30 min at RT (α-Myc, α-HA) or overnight at 4°C (α-SOBIR1, α-BIK1, α-PR1). Primary and secondary antibody dilutions were as follows: α-Myc 1:1000 (ChromoTek; Planegg-Martinsried, Germany), α-HA 1:2000 (Roche Diagnostics; Basel, Switzerland), α-SOBIR1 1:1000 (Agrisera; Vännäs, Sweden), α-BIK1 (1:3000) (Agrisera; Vännäs, Sweden), α-PR1 1:2500 (Agrisera; Vännäs, Sweden), α-UGPase 1:2,000 (Agrisera; Vännäs, Sweden), α-Histone H3 1:5,000 (Agrisera; Vännäs, Sweden), α-rat HRP-conjugated 1:10.000 (Thermo Fisher Scientific, Waltham, USA), α-mouse HRP-conjugated 1:10.000 (Sigma-Aldrich; St. Louis, USA) and α-rabbit HRP-conjugated 1:10.000 (Sigma-Aldrich; St. Louis, USA). Chemiluminescence was detected using an ImageQuant 800 (GE Healthcare; Chalfont St Giles, UK).

Co-immunoprecipitation

N. benthamiana leaf tissue was homogenized with a mortar and pestle using liquid nitrogen. The fine plant powder was resuspended in 2.5 mL of extraction buffer (50mM HEPES pH 7.5, 50 mM NaCl, 10 mM EDTA pH 8.0, 0.5% [v/v] Triton X-100, 5 mM DTT, 1x Halt™ Protease Inhibitor Cocktail (Thermo Fisher Scientific; Waltham, USA)). Samples were incubated on ice for 10-30 min and then cleared by centrifugation at 16,000 g for 5 min and 16,000 g for 15 min at 4°C. IP was performed in the cold room for 1h with 1.5 mL of protein extracts and 20 µl Myc trap (ChromoTek; Planegg-Martinsried, Germany). Samples were centrifuged at 2,400 g at 4°C and washed two times with 1 mL and two times with 500 µl of wash buffer (50 mM HEPES pH 7.5, 150 mM NaCl, 10 mM EDTA pH 8.0, 0.2% [v/v] Triton X-100) by inverting the tubes six times, respectively. Bound proteins were eluted in 120 µl 2x SDS loading buffer (100 mM Tris-HCl pH 6.8, 20% [v/v] glycerol, 200 mM DTT, 4% [w/v] SDS, 0.002% [w/v] bromophenol blue) and denatured by incubating the samples at 95°C for 5 min.

Phosphatase treatment

Phosphatase treatment was performed on immunoprecipitated proteins. After the washing steps (see co-immunoprecipitation), beads were washed twice with wash buffer 2 (50mM HEPES pH 7.5, 50 mM NaCl). Treatment with protein Lambda Protein Phosphatase (NEB, Massachusetts, USA) was done according to the manufacturers' instructions. In short, 40 µl protein sample (beads resuspended in wash buffer 2) was added to 5 µl 10x NEBuffer for Protein MetalloPhosphatases and 5 µl of 10 mM $MnCl_2$. 1 µl Lambda Protein Phosphatase or

1 µl wash buffer 2 was added and mixtures were incubated on ice (4°C) or at 30°C for 30 min. Beads were centrifuged at 2,300 g for 2 min. Supernatant was removed and bound proteins were eluted in 70 µl 2x SDS loading buffer (100 mM Tris-HCl pH 6.8, 20% [v/v] glycerol, 200 mM DTT, 4% [w/v] SDS, 0.002% [w/v] bromophenol blue) and denatured by boiling the samples at 95°C for 5 min.

MAP Kinase Assay

Proteins were extracted from 6-week-old plants. Plant material was frozen in liquid nitrogen, homogenized using a tissue homogenizer (Retsch GmbH; Haan, Germany) and resuspended in extraction buffer (50 mM Tris pH 7.5, 200 mM NaCl, 1mM EDTA pH 8.0, 10% [v/v] glycerol, 0.1% [v/v] Tween20, 1mM DTT, 1x Halt™ Protease Inhibitor Cocktail (Thermo Fisher Scientific; Waltham, USA), 1x Phosphatase-Inhibitor-Mix II (SERVA electrophoresis GmbH; Heidelberg, Germany)). Samples were solubilized for 10 min on ice and spun down by centrifugation at 16,000 g for 30 min at 4°C. 30 µg total protein was diluted with 5x SDS loading buffer (250 mM Tris-HCl pH 6.8, 50% [v/v] glycerol, 500 mM DTT, 10% [w/v] SDS, 0.005% [w/v] bromophenol blue) boiled at 95°C for 5 min and subsequently subjected to SDS-PAGE. Membranes were blocked by incubation in 2% [w/v] BSA in 1x TBS-Tween (0.01%) for 1h. Activated MAP kinases were detected by overnight incubation with anti-p42/p44 MAPK primary antibody diluted in 2% [w/v] BSA in 1x TBS-T (1:2500; Cell Signaling Technology; Cambridge, UK), followed by incubation with anti-rabbit-HRP secondary antibody also diluted in 2% [w/v] BSA in 1x TBS-T (1:10.000; Sigma-Aldrich; St. Louis, USA).

Subcellular fractionation

Subcellular fractionation experiments were done from 1g of 6-week old Arabidopsis plants expressing *pADR1-L2::ADR1-L2*^{D484V}*-HA* in either *adr1-L2-4* or *adr1-L2-4 bkk1-1*. Plants were grown on soil under short day conditions. Plant tissue was homogenized using mortar, pestle and liquid nitrogen, and 3 mL of sucrose buffer (20 mM Tris pH 8.0, 0.33 M sucrose, 1 mM EDTA, 5 mM DTT and 1x Halt™ Protease Inhibitor Cocktail (Thermo Fisher Scientific; Waltham, USA)) was added. Samples were spun down at 2,000 g for 10 min at 4°C to remove debris. After transferring the supernatants to new tubes, samples were spun down again at 2,000 g for 10 min at 4°C, followed by an ultra-centrifugation step at 100,000 g for 45 min at 4°C. The microsomal pellet was resuspended in 150 µl sucrose buffer and subjected to another ultra-centrifugation step at 100,000 g for 15 min. Pellets were resuspended in 100 µl sucrose buffer, respectively and 40 µg protein of each protein fraction (total, soluble, microsomes) was loaded onto SDS-gel, respectively.

Confocal imaging

For subcellular localization and BiFC studies, constructs were transiently expressed in *N. benthamiana*. 45-48 hours post infiltration, samples were imaged with the confocal laser scanning microscope LSM880 (Zeiss; Oberkochen, Germany) by using the 63x water-immersion objective. YFP was excited using a 514 nm laser, collecting emission between 516-556 nm; RFP was excited using a 561 nm laser with an emission spectrum of 597-634 nm. Images were processed with the ZEN blue software (Zeiss; Oberkochen, Germany) for adjustment of brightness and contrast.

RNA isolation, cDNA synthesis and RT-PCR

Total RNA was isolated from leaves of 6-week-old plants that were grown on soil under short day conditions. RNA was extracted from ~100 mg ground plant material using the RNeasy® Plant Mini Kit (QIAGEN; Hilden, Germany) according to the manufacturers' protocol. RNA samples were treated with DNase (Thermo Fisher Scientific, Waltham, USA) in a total volume of 50 µl, following the manufacturers' instructions. 1 µg total RNA was reverse transcribed with oligo-dT primer using the components of the RevertAid RT Kit (Thermo Fisher Scientific, Waltham, USA). cDNA was amplified by standard PCR using primers listed in Table S1.

Trypan blue staining

Arabidopsis leaves of 6-week-old plants were transferred into a 6-well plate containing 3 mL trypan blue staining solution (8% [v/v] lactic acid, 8% [v/v] glycerol, 8% [v/v] phenol, 67% [v/v] ethanol absolute, 0.27% [w/v] trypan blue) and boiled in a 100°C water bath for 5 min. Leaves were transferred into fresh wells containing 1 mg/ml chloralhydrate dissolved in distilled water and incubated overnight under mild shaking. The chloralhydrate solution was replaced by a fresh chloralhydrate solution and incubated for at least 4 h. Destained leaves were immersed in 20% [v/v] glycerol and imaged using the Axiocam stereomicroscope (Zeiss; Oberkochen, Germany).

DAB staining

Arabidopsis leaves of 6-week-old plants were transferred into a 6-well plate containing 3 mL freshly prepared DAB staining solution (1 mg/ml 3,3-diaminobenzidine-HCl pH 3.8) and wrapped completely with aluminium foil. Leaves were incubated in the dark overnight at room temperature with mild agitation. The DAB staining solution was removed and leaves were rinsed with distilled H_2O to remove excess staining solution. Water was replaced by absolute ethanol and incubated in a water bath at 65°C for 2 h to clear the chlorophyll. Absolute ethanol was replaced by 75% ethanol and incubated for 1 h at RT with mild agitation. 75% ethanol was replaced by 50% ethanol and incubated at RT with mild agitation until the leaves had lost their

green coloration. Destained leaves were immersed in 20% [v/v] glycerol and imaged using the Axiocam stereomicroscope (Zeiss; Oberkochen, Germany).

Bacterial growth curves

Pst DC3000 (*AvrRpt2* or *AvrRps4*) were grown on KB plates supplemented with the appropriate antibiotics and resuspended in 10 mM $MgCl_2$ to a final concentration of 5 x 10^5 colony-forming units (cfu)/mL (OD_{600} 0.001). Bacterial suspensions were syringe-infiltrated into leaves of 5-week-old plants. At 0 and 3 dpi, leaf discs were taken and homogenized using a tissue lyser (Retsch GmbH; Haan, Germany). Dilution series were prepared and dropped on KB plates containing the appropriate antibiotics. Cfu were counted after 2 days of growth. Statistical analysis from 4 technical replicates was done by one-way ANOVA Tukey's test using GraphPad Prism 8.0.2. Experiments were repeated 2 times with similar results.

Pst DC3000 (EV) was grown on KB plates containing appropriate antibiotics and resuspended in 10 mM $MgCl_2$ to a final concentration of 2.5 x 10^5 cfu/mL (OD_{600} 0.0005). Silwet L-77 was added at a final concentration of 200 µl/L. 21-day old seedlings were dip-inoculated by submerging the pot in the bacterial solution for 10 sec as described in (Tornero & Dangl 2001). After the inoculation, plants were covered with a lid for 1 h. 1 h after the dip inoculation (0 dpi) as well as at 3 dpi, three seedlings were taken and homogenized using a tissue lyser (Retsch GmbH; Haan, Germany). Dilution series were prepared and plated on KB plates with appropriate antibiotics and cfu were counted 2 dpi. Statistical analysis from 4 technical replicates was done by one-way ANOVA Tukey's test using GraphPad Prism 8.0.2. Experiments were repeated 2-3 times with similar results.

Acknowledgements

We are grateful for technical support from Sonja Harter, Christel Kulibaba-Mattern and Elke Sauberzweig, the ZMBP plant cultivation team for excellent assistance, Andrea Gust and Klaus Harter for critical and helpful discussions and Andrea Gust additionally for providing *sobir1-12* seeds, Cyril Zipfel for providing *SERK1 to 5* entry plasmids, Isabell Albert for *SERK1* to *5* Myc destination plasmids, Karin Schumacher for the *VMA12-RFP* construct, Birgit Kemmerling for *bkk1-1* seeds; Xin Li for *NRG1.1*^{D485V} *nrg1.1-1* and *snc1* mutant seeds and Thorsten Nürnberger for sharing anti-p42/p44 MAPK primary antibody. We thank the University of Tübingen, the German Research Foundation (DFG; grand no. DFG-CRC1101 – project D09 to F.E.K, and grants for scientific equipment -INST 37/965-1 FUGG) and the Reinhard Frank Stiftung (Project 'helperless plant' to F.E.K) for the financial support to F.E.K.

References

1. Albert I., Bohm H., Albert M., Feiler C.E., Imkampe J., Wallmeroth N., Brancato C., Raaymakers T.M., Oome S., Zhang H., Krol E., Grefen C., Gust A.A., Chai J., Hedrich R., Van den Ackerveken G. & Nurnberger T. (2015) An RLP23-SOBIR1-BAK1 complex mediates NLP-triggered immunity. Nat Plants 1, 15140.
2. Albert I., Hua C., Nurnberger T., Pruitt R.N. & Zhang L. (2020) Surface Sensor Systems in Plant Immunity. Plant Physiol 182, 1582-96.
3. Albrecht C., Russinova E., Kemmerling B., Kwaaitaal M. & de Vries S.C. (2008) Arabidopsis SOMATIC EMBRYOGENESIS RECEPTOR KINASE proteins serve brassinosteroid-dependent and -independent signaling pathways. Plant Physiol 148, 611-9.
4. Balint-Kurti P. (2019) The plant hypersensitive response: concepts, control and consequences. Mol Plant Pathol 20, 1163-78.
5. Blume B., Nurnberger T., Nass N. & Scheel D. (2000) Receptor-mediated increase in cytoplasmic free calcium required for activation of pathogen defense in parsley. Plant Cell 12, 1425-40.
6. Boller T. & Felix G. (2009) A renaissance of elicitors: perception of microbe-associated molecular patterns and danger signals by pattern-recognition receptors. Annu Rev Plant Biol 60, 379-406.
7. Bonardi V., Tang S., Stallmann A., Roberts M., Cherkis K. & Dangl J.L. (2011) Expanded functions for a family of plant intracellular immune receptors beyond specific recognition of pathogen effectors. Proc Natl Acad Sci U S A 108, 16463-8.
8. Boudsocq M., Willmann M.R., McCormack M., Lee H., Shan L., He P., Bush J., Cheng S.H. & Sheen J. (2010) Differential innate immune signalling via Ca(2+) sensor protein kinases. Nature 464, 418-22.
9. Bucherl C.A., Jarsch I.K., Schudoma C., Segonzac C., Mbengue M., Robatzek S., MacLean D., Ott T. & Zipfel C. (2017) Plant immune and growth receptors share common signalling components but localise to distinct plasma membrane nanodomains. Elife 6.
10. Castel B., Ngou P.M., Cevik V., Redkar A., Kim D.S., Yang Y., Ding P. & Jones J.D.G. (2019) Diverse NLR immune receptors activate defence via the RPW8-NLR NRG1. New Phytol 222, 966-80.
11. Cheng W., Munkvold K.R., Gao H., Mathieu J., Schwizer S., Wang S., Yan Y.B., Wang J., Martin G.B. & Chai J. (2011a) Structural analysis of Pseudomonas syringae AvrPtoB bound to host BAK1 reveals two similar kinase-interacting domains in a type III Effector. Cell Host Microbe 10, 616-26.
12. Cheng Y.T., Li Y., Huang S., Huang Y., Dong X., Zhang Y. & Li X. (2011b) Stability of plant immune-receptor resistance proteins is controlled by SKP1-CULLIN1-F-box (SCF)-mediated protein degradation. Proc Natl Acad Sci U S A 108, 14694-9.
13. Chinchilla D., Zipfel C., Robatzek S., Kemmerling B., Nurnberger T., Jones J.D., Felix G. & Boller T. (2007) A flagellin-induced complex of the receptor FLS2 and BAK1 initiates plant defence. Nature 448, 497-500.
14. Clough S.J. & Bent A.F. (1998) Floral dip: a simplified method for Agrobacterium-mediated transformation of Arabidopsis thaliana. Plant J 16, 735-43.
15. Coll N.S., Epple P. & Dangl J.L. (2011) Programmed cell death in the plant immune system. Cell Death Differ 18, 1247-56.

16. Collier S.M., Hamel L.P. & Moffett P. (2011) Cell death mediated by the N-terminal domains of a unique and highly conserved class of NB-LRR protein. Mol Plant Microbe Interact 24, 918-31.

17. Dangl J.L. & Jones J.D. (2001) Plant pathogens and integrated defence responses to infection. Nature 411, 826-33.

18. Doke N. (1983) Generation of superoxide anion by potato tuber protoplasts during hypersensitive response to hyphal wall components of Phytophtora infestans and specific inhibition of the reaction with supressors of hypersensitivity. Physiol. Plant Pathol. 23, 359-67.

19. Dong O.X., Tong M., Bonardi V., El Kasmi F., Woloshen V., Wunsch L.K., Dangl J.L. & Li X. (2016) TNL-mediated immunity in Arabidopsis requires complex regulation of the redundant ADR1 gene family. New Phytol 210, 960-73.

20. El Kasmi F. (2021) How activated NLRs induce anti-microbial defenses in plants. Biochemical Society Transactions.

21. Gao M., Wang X., Wang D., Xu F., Ding X., Zhang Z., Bi D., Cheng Y.T., Chen S., Li X. & Zhang Y. (2009) Regulation of cell death and innate immunity by two receptor-like kinases in Arabidopsis. Cell Host Microbe 6, 34-44.

22. Gao Z., Chung E.H., Eitas T.K. & Dangl J.L. (2011) Plant intracellular innate immune receptor Resistance to Pseudomonas syringae pv. maculicola 1 (RPM1) is activated at, and functions on, the plasma membrane. Proc Natl Acad Sci U S A 108, 7619-24.

23. Gassmann W., Hinsch M.E. & Staskawicz B.J. (1999) The Arabidopsis RPS4 bacterial-resistance gene is a member of the TIR-NBS-LRR family of disease-resistance genes. Plant J 20, 265-77.

24. Gloggnitzer J., Akimcheva S., Srinivasan A., Kusenda B., Riehs N., Stampfl H., Bautor J., Dekrout B., Jonak C., Jimenez-Gomez J.M., Parker J.E. & Riha K. (2014) Nonsense-mediated mRNA decay modulates immune receptor levels to regulate plant antibacterial defense. Cell Host Microbe 16, 376-90.

25. Gomez-Gomez L. & Boller T. (2000) FLS2: an LRR receptor-like kinase involved in the perception of the bacterial elicitor flagellin in Arabidopsis. Mol Cell 5, 1003-11.

26. Grant J.J., Chini A., Basu D. & Loake G.J. (2003) Targeted activation tagging of the Arabidopsis NBS-LRR gene, ADR1, conveys resistance to virulent pathogens. Mol Plant Microbe Interact 16, 669-80.

27. Grefen C. & Blatt M.R. (2012) A 2in1 cloning system enables ratiometric bimolecular fluorescence complementation (rBiFC). Biotechniques 53, 311-14.

28. Gust A.A. & Felix G. (2014) Receptor like proteins associate with SOBIR1-type of adaptors to form bimolecular receptor kinases. Current Opinion in Plant Biology 21, 104-11.

29. He K., Gou X., Yuan T., Lin H., Asami T., Yoshida S., Russell S.D. & Li J. (2007) BAK1 and BKK1 regulate brassinosteroid-dependent growth and brassinosteroid-independent cell-death pathways. Curr Biol 17, 1109-15.

30. He Z., Huang T., Ao K., Yan X. & Huang Y. (2017) Sumoylation, Phosphorylation, and Acetylation Fine-Tune the Turnover of Plant Immunity Components Mediated by Ubiquitination. Front Plant Sci 8, 1682.

31. Heese A., Hann D.R., Gimenez-Ibanez S., Jones A.M., He K., Li J., Schroeder J.I., Peck S.C. & Rathjen J.P. (2007) The receptor-like kinase SERK3/BAK1 is a central regulator of innate immunity in plants. Proc Natl Acad Sci U S A 104, 12217-22.

32. Hinsch M. & Staskawicz B. (1996) Identification of a new Arabidopsis disease resistance locus, RPs4, and cloning of the corresponding avirulence gene, avrRps4, from Pseudomonas syringae pv. pisi. Mol Plant Microbe Interact 9, 55-61.

33. Huffaker A., Pearce G. & Ryan C.A. (2006) An endogenous peptide signal in Arabidopsis activates components of the innate immune response. Proc Natl Acad Sci U S A 103, 10098-103.

34. Hutten S.J., Hamers D.S., Aan den Toorn M., van Esse W., Nolles A., Bucherl C.A., de Vries S.C., Hohlbein J. & Borst J.W. (2017) Visualization of BRI1 and SERK3/BAK1 Nanoclusters in Arabidopsis Roots. PLoS One 12, e0169905.

35. Jacob P., Kim N.H., Wu F., El-Kasmi F., Chi Y., Walton W.G., Furzer O.J., Lietzan A.D., Sunil S., Kempthorn K., Redinbo M.R., Pei Z.M., Wan L. & Dangl J.L. (2021) Plant "helper" immune receptors are Ca(2+)-permeable nonselective cation channels. Science.

36. Jeworutzki E., Roelfsema M.R., Anschutz U., Krol E., Elzenga J.T., Felix G., Boller T., Hedrich R. & Becker D. (2010) Early signaling through the Arabidopsis pattern recognition receptors FLS2 and EFR involves Ca-associated opening of plasma membrane anion channels. Plant J 62, 367-78.

37. Kadota Y. & Shirasu K. (2012) The HSP90 complex of plants. Biochim Biophys Acta 1823, 689-97.

38. Kadota Y., Shirasu K. & Guerois R. (2010) NLR sensors meet at the SGT1-HSP90 crossroad. Trends Biochem Sci 35, 199-207.

39. Kemmerling B., Schwedt A., Rodriguez P., Mazzotta S., Frank M., Qamar S.A., Mengiste T., Betsuyaku S., Parker J.E., Mussig C., Thomma B.P., Albrecht C., de Vries S.C., Hirt H. & Nurnberger T. (2007) The BRI1-associated kinase 1, BAK1, has a brassinolide-independent role in plant cell-death control. Curr Biol 17, 1116-22.

40. Kunkel B.N., Bent A.F., Dahlbeck D., Innes R.W. & Staskawicz B.J. (1993) RPS2, an Arabidopsis disease resistance locus specifying recognition of Pseudomonas syringae strains expressing the avirulence gene avrRpt2. Plant Cell 5, 865-75.

41. Li F., Pignatta D., Bendix C., Brunkard J.O., Cohn M.M., Tung J., Sun H., Kumar P. & Baker B. (2012) MicroRNA regulation of plant innate immune receptors. Proc Natl Acad Sci U S A 109, 1790-5.

42. Li L., Kim P., Yu L., Cai G., Chen S., Alfano J.R. & Zhou J.M. (2016) Activation-Dependent Destruction of a Co-receptor by a Pseudomonas syringae Effector Dampens Plant Immunity. Cell Host Microbe 20, 504-14.

43. Li X., Clarke J.D., Zhang Y. & Dong X. (2001) Activation of an EDS1-mediated R-gene pathway in the snc1 mutant leads to constitutive, NPR1-independent pathogen resistance. Mol Plant Microbe Interact 14, 1131-9.

44. Liebrand T.W.H., van den Burg H.A. & Joosten M.H.A.J. (2014) Two for all: receptor-associated kinases SOBIR1 and BAK1. Trends in Plant Science 19, 123-32.

45. Macho A.P. & Zipfel C. (2014) Plant PRRs and the activation of innate immune signaling. Mol Cell 54, 263-72.

46. Mantelin S., Peng H.C., Li B., Atamian H.S., Takken F.L. & Kaloshian I. (2011) The receptor-like kinase SlSERK1 is required for Mi-1-mediated resistance to potato aphids in tomato. Plant J 67, 459-71.

47. Marmagne A., Rouet M.A., Ferro M., Rolland N., Alcon C., Joyard J., Garin J., Barbier-Brygoo H. & Ephritikhine G. (2004) Identification of new intrinsic proteins in Arabidopsis plasma membrane proteome. Mol Cell Proteomics 3, 675-91.

48. Mehlhorn D.G., Wallmeroth N., Berendzen K.W. & Grefen C. (2018) 2in1 Vectors Improve In Planta BiFC and FRET Analyses. Methods Mol Biol 1691, 139-58.

49. Miya A., Albert P., Shinya T., Desaki Y., Ichimura K., Shirasu K., Narusaka Y., Kawakami N., Kaku H. & Shibuya N. (2007) CERK1, a LysM receptor kinase, is essential for chitin elicitor signaling in Arabidopsis. Proc Natl Acad Sci U S A 104, 19613-8.

50. Nakamura S., Mano S., Tanaka Y., Ohnishi M., Nakamori C., Araki M., Niwa T., Nishimura M., Kaminaka H., Nakagawa T., Sato Y. & Ishiguro S. (2010) Gateway binary vectors with the bialaphos resistance gene, bar, as a selection marker for plant transformation. Biosci Biotechnol Biochem 74, 1315-9.

51. Nasim Z., Fahim M., Gawarecka K., Susila H., Jin S., Youn G. & Ahn J.H. (2020) Role of AT1G72910, AT1G72940, and ADR1-LIKE 2 in Plant Immunity under Nonsense-Mediated mRNA Decay-Compromised Conditions at Low Temperatures. Int J Mol Sci 21.

52. Ngou B.P.M., Ahn H.K., Ding P. & Jones J.D.G. (2021) Mutual potentiation of plant immunity by cell-surface and intracellular receptors. Nature 592, 110-5.

53. Nomura H., Komori T., Uemura S., Kanda Y., Shimotani K., Nakai K., Furuichi T., Takebayashi K., Sugimoto T., Sano S., Suwastika I.N., Fukusaki E., Yoshioka H., Nakahira Y. & Shiina T. (2012) Chloroplast-mediated activation of plant immune signalling in Arabidopsis. Nat Commun 3, 926.

54. Ntoukakis V., Schwessinger B., Segonzac C. & Zipfel C. (2011) Cautionary notes on the use of C-terminal BAK1 fusion proteins for functional studies. Plant Cell 23, 3871-8.

55. Palma K., Thorgrimsen S., Malinovsky F.G., Fiil B.K., Nielsen H.B., Brodersen P., Hofius D., Petersen M. & Mundy J. (2010) Autoimmunity in Arabidopsis acd11 is mediated by epigenetic regulation of an immune receptor. PLoS Pathog 6, e1001137.

56. Peng H.C., Mantelin S., Hicks G.R., Takken F.L. & Kaloshian I. (2016) The Conformation of a Plasma Membrane-Localized Somatic Embryogenesis Receptor Kinase Complex Is Altered by a Potato Aphid-Derived Effector. Plant Physiol 171, 2211-22.

57. Peng Y., van Wersch R. & Zhang Y. (2018) Convergent and Divergent Signaling in PAMP-Triggered Immunity and Effector-Triggered Immunity. Mol Plant Microbe Interact 31, 403-9.

58. Postma J., Liebrand T.W., Bi G., Evrard A., Bye R.R., Mbengue M., Kuhn H., Joosten M.H. & Robatzek S. (2016) Avr4 promotes Cf-4 receptor-like protein association with the BAK1/SERK3 receptor-like kinase to initiate receptor endocytosis and plant immunity. New Phytol 210, 627-42.

59. Pruitt R.N., Locci F., Wanke F., Zhang L., Saile S.C., Joe A., Karelina D., Hua C., Frohlich K., Wan W.L., Hu M., Rao S., Stolze S.C., Harzen A., Gust A.A., Harter K., Joosten M., Thomma B., Zhou J.M., Dangl J.L., Weigel D., Nakagami H., Oecking C., Kasmi F.E., Parker J.E. & Nurnberger T. (2021) The EDS1-PAD4-ADR1 node mediates Arabidopsis pattern-triggered immunity. Nature 598, 495-9.

60. Qu Y., Misaghi S., Izrael-Tomasevic A., Newton K., Gilmour L.L., Lamkanfi M., Louie S., Kayagaki N., Liu J., Komuves L., Cupp J.E., Arnott D., Monack D. & Dixit V.M. (2012) Phosphorylation of NLRC4 is critical for inflammasome activation. Nature 490, 539-42.

61. Ranf S., Eschen-Lippold L., Pecher P., Lee J. & Scheel D. (2011) Interplay between calcium signalling and early signalling elements during defence responses to microbe- or damage-associated molecular patterns. Plant J 68, 100-13.

62. Richard M.M.S., Gratias A., Meyers B.C. & Geffroy V. (2018) Molecular mechanisms that limit the costs of NLR-mediated resistance in plants. Mol Plant Pathol 19, 2516-23.

63. Roberts M., Tang S., Stallmann A., Dangl J.L. & Bonardi V. (2013) Genetic requirements for signaling from an autoactive plant NB-LRR intracellular innate immune receptor. PLoS Genet 9, e1003465.

64. Roux M., Schwessinger B., Albrecht C., Chinchilla D., Jones A., Holton N., Malinovsky F.G., Tor M., de Vries S. & Zipfel C. (2011) The Arabidopsis leucine-rich repeat receptor-like kinases BAK1/SERK3 and BKK1/SERK4 are required for innate immunity to hemibiotrophic and biotrophic pathogens. Plant Cell 23, 2440-55.

65. Saile S.C., Ackermann F.M., Sunil S., Keicher J., Bayless A., Bonardi V., Wan L., Doumane M., Stobbe E., Jaillais Y., Caillaud M.C., Dangl J.L., Nishimura M.T., Oecking C. & El Kasmi F. (2021) Arabidopsis ADR1 helper NLR immune receptors localize and function at the plasma membrane in a phospholipid dependent manner. New Phytol 232, 2440-56.

66. Saile S.C., Jacob P., Castel B., Jubic L.M., Salas-Gonzales I., Backer M., Jones J.D.G., Dangl J.L. & El Kasmi F. (2020) Two unequally redundant "helper" immune receptor families mediate Arabidopsis thaliana intracellular "sensor" immune receptor functions. PLoS Biol 18, e3000783.

67. Saucet S.B., Ma Y., Sarris P.F., Furzer O.J., Sohn K.H. & Jones J.D. (2015) Two linked pairs of Arabidopsis TNL resistance genes independently confer recognition of bacterial effector AvrRps4. Nat Commun 6, 6338.

68. Schulze B., Mentzel T., Jehle A.K., Mueller K., Beeler S., Boller T., Felix G. & Chinchilla D. (2010) Rapid heteromerization and phosphorylation of ligand-activated plant transmembrane receptors and their associated kinase BAK1. J Biol Chem 285, 9444-51.

69. Schulze S., Yu L., Ehinger A., Kolb D., Saile S.C., Stahl M., Franz-Wachtel M., Li L., Kasmi F.E., Cevik V. & Kemmerling B. (2021) The TIR-NBS-LRR protein CSA1 is required for autoimmune cell death in Arabidopsis pattern recognition co-receptor bak1 and bir3 mutants. bioRxiv, 2021.04.11.438637.

70. Schwessinger B., Roux M., Kadota Y., Ntoukakis V., Sklenar J., Jones A. & Zipfel C. (2011) Phosphorylation-dependent differential regulation of plant growth, cell death, and innate immunity by the regulatory receptor-like kinase BAK1. PLoS Genet 7, e1002046.

71. Shan L., He P., Li J., Heese A., Peck S.C., Nurnberger T., Martin G.B. & Sheen J. (2008) Bacterial effectors target the common signaling partner BAK1 to disrupt multiple MAMP receptor-signaling complexes and impede plant immunity. Cell Host Microbe 4, 17-27.

72. Shivaprasad P.V., Chen H.M., Patel K., Bond D.M., Santos B.A. & Baulcombe D.C. (2012) A microRNA superfamily regulates nucleotide binding site-leucine-rich repeats and other mRNAs. Plant Cell 24, 859-74.

73. Tang W., Deng Z., Oses-Prieto J.A., Suzuki N., Zhu S., Zhang X., Burlingame A.L. & Wang Z.Y. (2008) Proteomics studies of brassinosteroid signal transduction using prefractionation and two-dimensional DIGE. Mol Cell Proteomics 7, 728-38.

74. Tao Y., Xie Z., Chen W., Glazebrook J., Chang H.S., Han B., Zhu T., Zou G. & Katagiri F. (2003) Quantitative nature of Arabidopsis responses during compatible and incompatible interactions with the bacterial pathogen Pseudomonas syringae. Plant Cell 15, 317-30.

75. Tian D., Traw M.B., Chen J.Q., Kreitman M. & Bergelson J. (2003) Fitness costs of R-gene-mediated resistance in Arabidopsis thaliana. Nature 423, 74-7.

76. Tian H., Wu Z., Chen S., Ao K., Huang W., Yaghmaiean H., Sun T., Xu F., Zhang Y., Wang S., Li X. & Zhang Y. (2021) Activation of TIR signalling boosts pattern-triggered immunity. Nature.

77. Tornero P. & Dangl J.L. (2001) A high-throughput method for quantifying growth of phytopathogenic bacteria in Arabidopsis thaliana. Plant J 28, 475-81.

78. Venugopal S.C., Jeong R.D., Mandal M.K., Zhu S., Chandra-Shekara A.C., Xia Y., Hersh M., Stromberg A.J., Navarre D., Kachroo A. & Kachroo P. (2009) Enhanced disease susceptibility 1 and salicylic acid act redundantly to regulate resistance gene-mediated signaling. PLoS Genet 5, e1000545.

79. Wang X., Kota U., He K., Blackburn K., Li J., Goshe M.B., Huber S.C. & Clouse S.D. (2008) Sequential transphosphorylation of the BRI1/BAK1 receptor kinase complex impacts early events in brassinosteroid signaling. Dev Cell 15, 220-35.

80. Wu Y., Gao Y., Zhan Y., Kui H., Liu H., Yan L., Kemmerling B., Zhou J.M., He K. & Li J. (2020) Loss of the common immune coreceptor BAK1 leads to NLR-dependent cell death. Proc Natl Acad Sci U S A 117, 27044-53.

81. Wu Z., Li M., Dong O.X., Xia S., Liang W., Bao Y., Wasteneys G. & Li X. (2019) Differential regulation of TNL-mediated immune signaling by redundant helper CNLs. New Phytol 222, 938-53.

82. Wu Z., Tian L., Liu X., Zhang Y. & Li X. (2021) TIR signal promotes interactions between lipase-like proteins and ADR1-L1 receptor and ADR1-L1 oligomerization. Plant Physiology.

83. Xia S., Cheng Y.T., Huang S., Win J., Soards A., Jinn T.L., Jones J.D., Kamoun S., Chen S., Zhang Y. & Li X. (2013) Regulation of transcription of nucleotide-binding leucine-rich repeat-encoding genes SNC1 and RPP4 via H3K4 trimethylation. Plant Physiol 162, 1694-705.

84. Yang S. & Hua J. (2004) A haplotype-specific Resistance gene regulated by BONZAI1 mediates temperature-dependent growth control in Arabidopsis. Plant Cell 16, 1060-71.

85. Yuan M., Jiang Z., Bi G., Nomura K., Liu M., Wang Y., Cai B., Zhou J.M., He S.Y. & Xin X.F. (2021) Pattern-recognition receptors are required for NLR-mediated plant immunity. Nature 592, 105-9.

86. Zhang Y., Goritschnig S., Dong X. & Li X. (2003) A gain-of-function mutation in a plant disease resistance gene leads to constitutive activation of downstream signal transduction pathways in suppressor of npr1-1, constitutive 1. Plant Cell 15, 2636-46.

87. Zhou J., Wu S., Chen X., Liu C., Sheen J., Shan L. & He P. (2014) The Pseudomonas syringae effector HopF2 suppresses Arabidopsis immunity by targeting BAK1. Plant J 77, 235-45.

88. Zipfel C., Kunze G., Chinchilla D., Caniard A., Jones J.D., Boller T. & Felix G. (2006) Perception of the bacterial PAMP EF-Tu by the receptor EFR restricts Agrobacterium-mediated transformation. Cell 125, 749-60.

89. Zipfel C., Robatzek S., Navarro L., Oakeley E.J., Jones J.D., Felix G. & Boller T. (2004) Bacterial disease resistance in Arabidopsis through flagellin perception. Nature 428, 764-7.

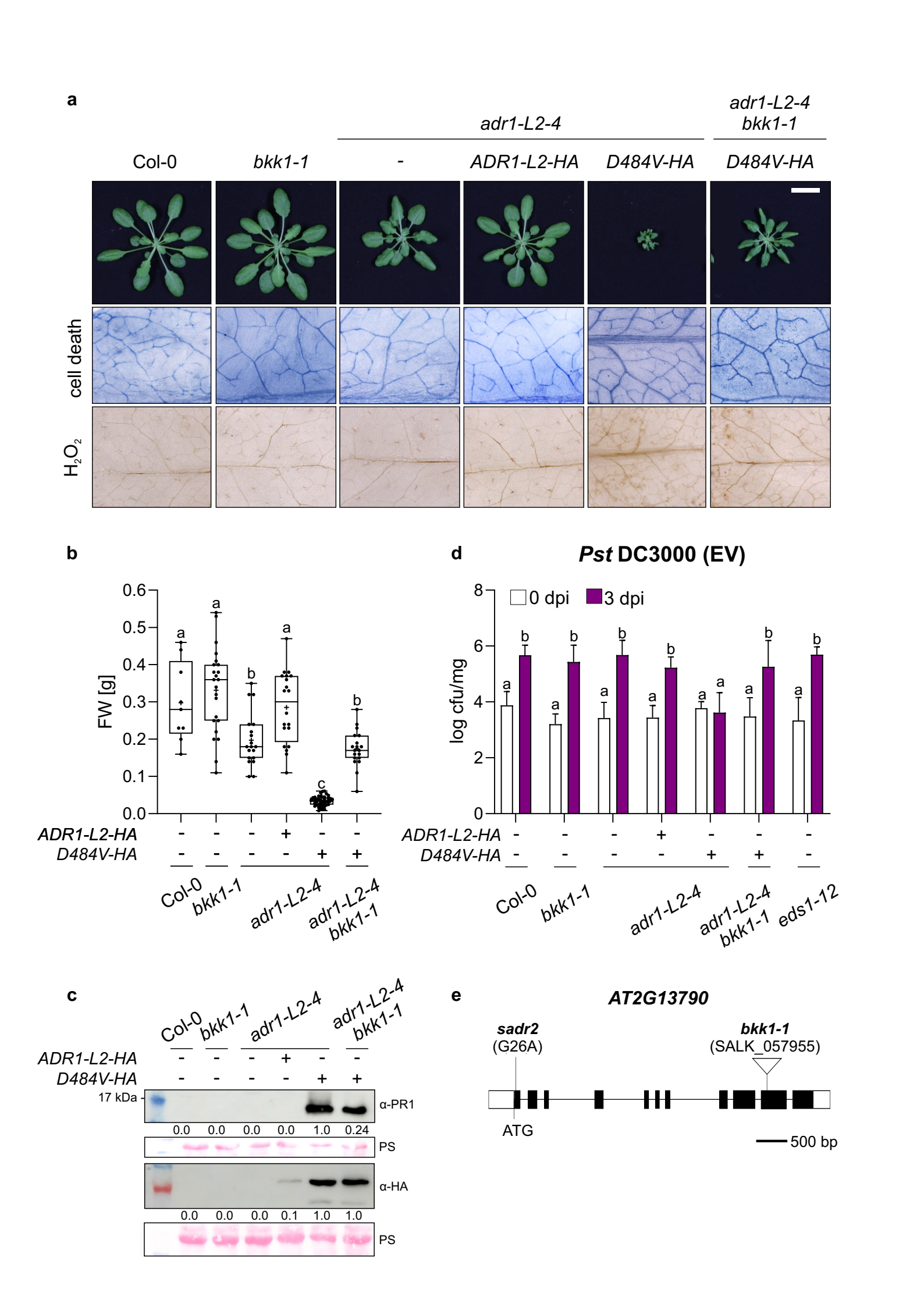
a
adr1-L2-4
adr1-L2-4 bkk1-1
Col-0
bkk1-1
-
ADR1-L2-HA
D484V-HA
D484V-HA
cell death
H2O2
b
FW [g]
ADR1-L2-HA
D484V-HA
Col-0
bkk1-1
adr1-L2-4
adr1-L2-4 bkk1-1
d
Pst DC3000 (EV)
0 dpi
3 dpi
log cfu/mg
ADR1-L2-HA
D484V-HA
Col-0
bkk1-1
adr1-L2-4
adr1-L2-4 bkk1-1
eds1-12
c
Col-0
bkk1-1
adr1-L2-4
adr1-L2-4 bkk1-1
ADR1-L2-HA
D484V-HA
17 kDa
α-PR1
PS
α-HA
PS
e
AT2G13790
sadr2
(G26A)
bkk1-1
(SALK_057955)
ATG
500 bp

Figure 1: *bkk1-1* partially suppresses the autoimmune phenotypes of *ADR1-L2^{D484V} adr1-L2-4*. a, Upper panel: Morphology of 6.5-week-old Col-0, *bkk1-1*, *adr1-L2-4*, *ADR1-L2-HA adr1-L2-4*, *ADR1-L2^{D484V}-HA adr1-L2-4* and *ADR1-L2^{D484V}-HA adr1-L2-4 bkk1-1* plants. Expression of ADR1-L2-HA and ADR1-L2^{D484V}-HA is driven by its native promoter. Plants were grown on soil under short-day conditions. Scale, 2 cm. Middle/lower panels: Leaves from plants in (upper panel) were stained with trypan blue (middle panel) or with DAB (lower panel) to visualize cell death or H_2O_2 accumulation, respectively. **b,** Quantification of fresh weights of plants in (a). Statistical significance is indicated by different letters following ANOVA with Tukey's test ($p < 0.05$). Box limit represents upper and lower quartile, maximum and minimum values are displayed in whiskers. The middle line shows the median, the cross indicates the mean FW. Dots represent biological replicates (plants) in one experiment. **c,** Expression of PR1 and ADR1-L2-HA/ADR1-L2^{D484V}-HA in plants shown in (a). Numbers show quantification of band intensities normalized to the Rubisco band from the Ponceau staining, respectively. **d,** 21-day old seedlings were dip-inoculated with *Pst* DC3000 EV (OD_{600} = 0.0005) and bacterial growth was assessed on the day of inoculation (0 dpi) and 3 days after inoculation (3 dpi). Experiment was done 3 times with similar results. Bars represent means of four technical replicates + SD. Letters indicate statistically significant differences following ANOVA with Tukey's test ($p < 0.05$). **e,** Gene structure of *BKK1*. Black boxes indicate exons, white boxes represent untranslated regions (UTRs). Introns are marked with lines, the T-DNA insertion site is labelled with a triangle.

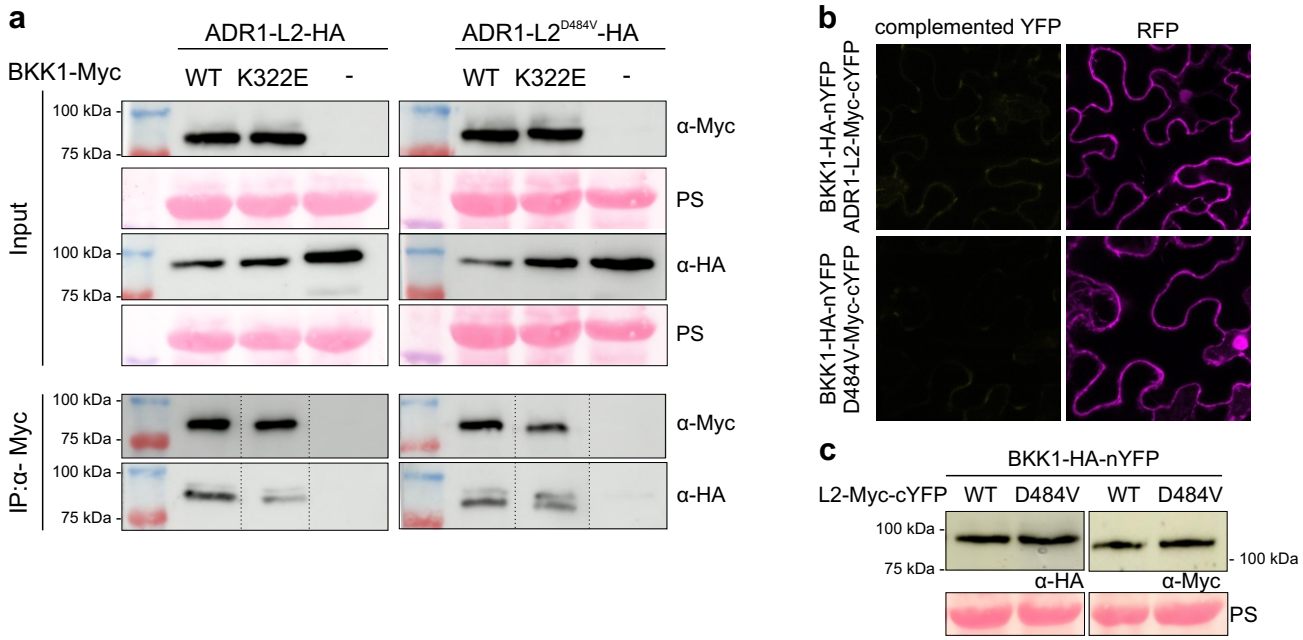

Figure 2: Analyses of BKK1-ADR1-L2 interactions. a, BKK1-Myc wildtype (WT) or the kinase inactive allele (K322E) were transiently co-expressed in *N. benthamiana* with either ADR1-L2-HA or ADR1-L2^{D484V}-HA, respectively. Expression of transgenes was under control of the 35S promoter. Leaf tissue was harvested 2 days post infiltration. Total proteins were subjected to immunoprecipitation (IP) with anti-Myc beads and immunoblotted with anti-Myc and anti-HA antibody, respectively. Immunoblots using total proteins prior to immunoprecipitation are shown as input (upper panel) and immunoprecipitated proteins are shown as IP (lower panel). Equal loading of the proteins is indicated by the Rubisco band from the Ponceau staining (PS). Co-immunoprecipitation was repeated three times with similar results. **b,** BiFC analysis of BKK1 with ADR1-L2 and ADR1-L2^{D484V}, respectively. Displayed are representative images of transiently transfected *N. benthamiana* leaves. The experiment was performed two times with similar results. **c,** Immunoblot analysis of the transiently expressed proteins in (b) using anti-HA and anti-Myc antibody, respectively. Equal loading of the proteins is indicated by the Rubsico band from the Ponceau staining (PS).

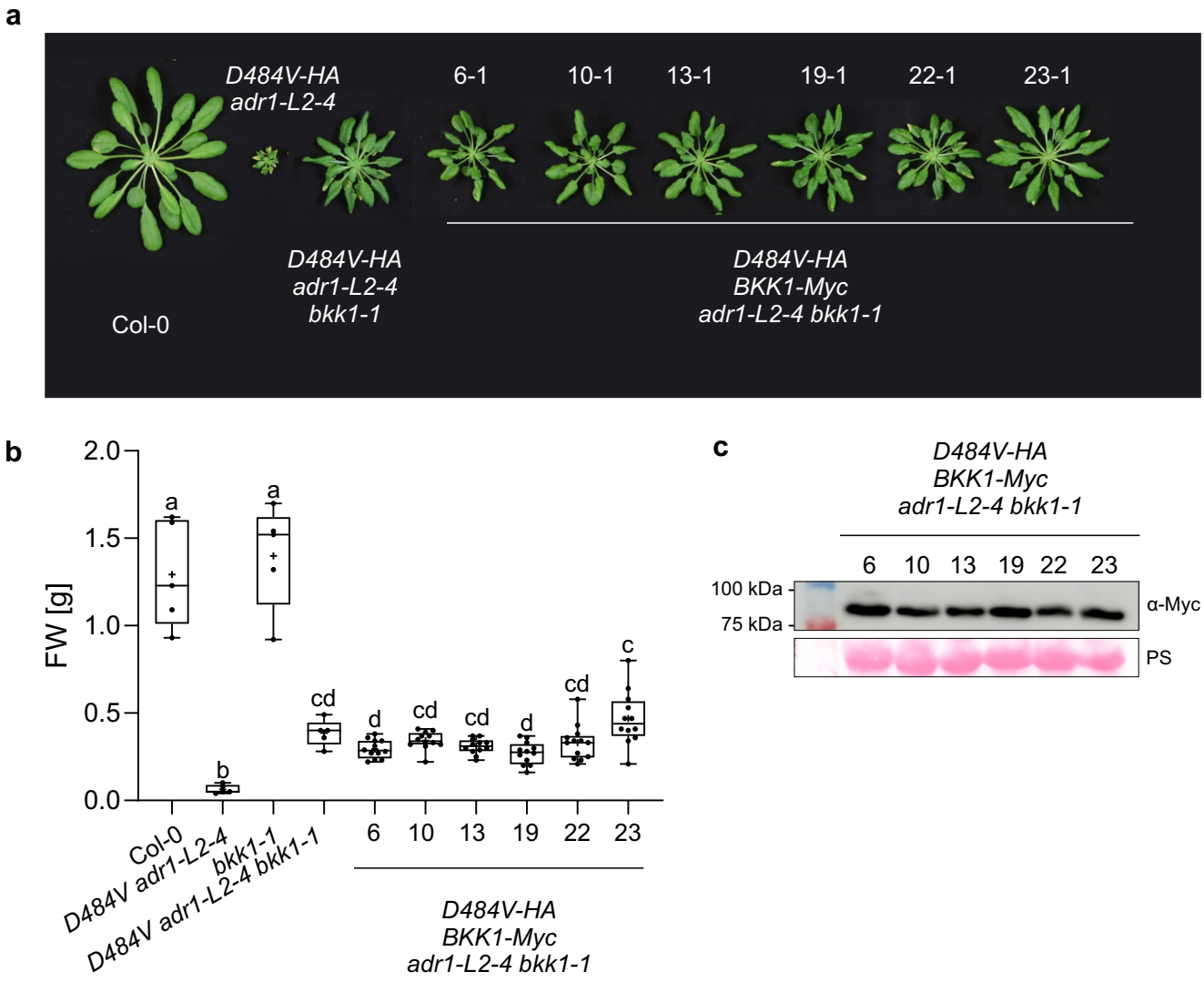

Figure S1: Complementation of *ADR1-L2^{D484V}-HA adr1-L2-4 bkk1-1* by BKK1-Myc. a, Morphology of 7-week-old Col-0, *ADR1-L2^{D484V}-HA adr1-L2-4*, *ADR1-L2^{D484V}-HA adr1-L2-4 bkk1-1* and six independent T2 plants (*ADR1-L2^{D484V}-HA BKK1-Myc adr1-L2-4 bkk1-1*) grown under short day conditions for 2 weeks on ½ MS plates supplemented with 20 µg/ml hygromycin and afterwards transferred to soil (short day conditions). Expression of ADR1-L2^{D484V}-HA and BKK1-Myc is under control of their native promoters, respectively. **b,** Quantification of fresh weights of plants in (a). Statistical significance is indicated by different letters following ANOVA with Tukey's test ($p < 0.05$). Box limit represents upper and lower quartile, maximum and minimum values are displayed in whiskers. The middle line shows the median, the cross indicates the mean FW. Dots represent biological replicates (plants) in one experiment. **c,** Immunoblot analysis of BKK1-Myc of plants shown in (a) using anti-Myc antibody. Equal loading is indicated by the Rubsico band from the Ponceau staining (PS).

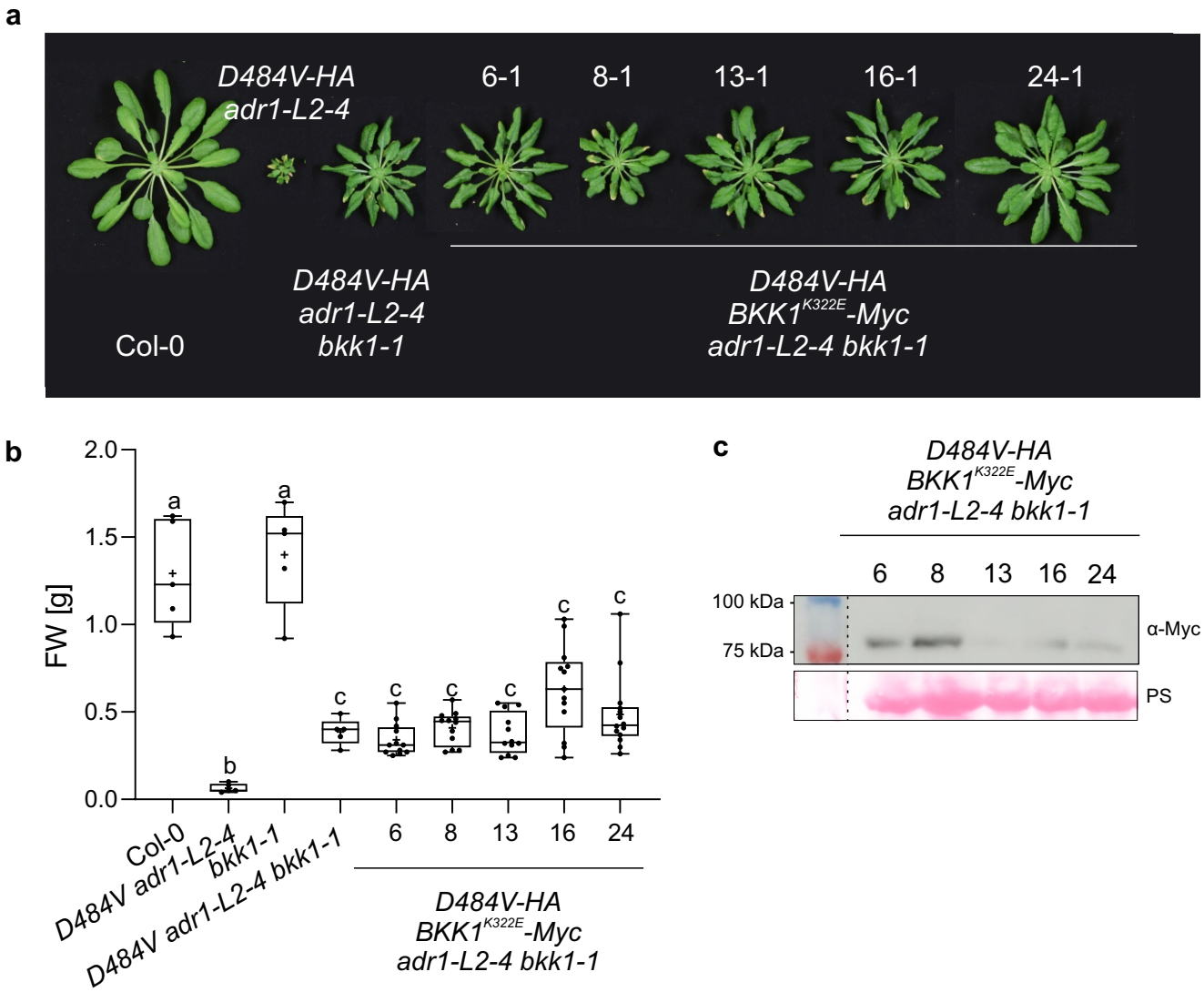

Figure S2: Complementation of *ADR1-L2^{D484V}-HA adr1-L2-4 bkk1-1* by BKK1^{K322E}-Myc. a, Morphology of 7-week-old Col-0, *ADR1-L2^{D484V}-HA adr1-L2-4*, *ADR1-L2^{D484V}-HA adr1-L2-4 bkk1-1* and five independent T2 plants (*ADR1-L2^{D484V}-HA BKK1^{K322E}-Myc adr1-L2-4 bkk1-1*) under short day conditions for 2 weeks on ½ MS plates supplemented with 20 µg/ml hygromycin and afterwards transferred to soil (short day conditions). Expression of ADR1-L2^{D484V}-HA and BKK1^{K322E}-Myc is under control of their native promoters, respectively. **b,** Quantification of fresh weights of plants in (a). Statistical significance is indicated by different letters following ANOVA with Tukey's test ($p < 0.05$). Box limit represents upper and lower quartile, maximum and minimum values are displayed in whiskers. The middle line shows the median, the cross indicates the mean FW. Dots represent biological replicates (plants) in one experiment. **c,** Immunoblot analysis of BKK1^{K322E}-Myc of plants shown in (a) using anti-Myc antibody. Equal loading is indicated by the Rubsico band from the Ponceau staining (PS).

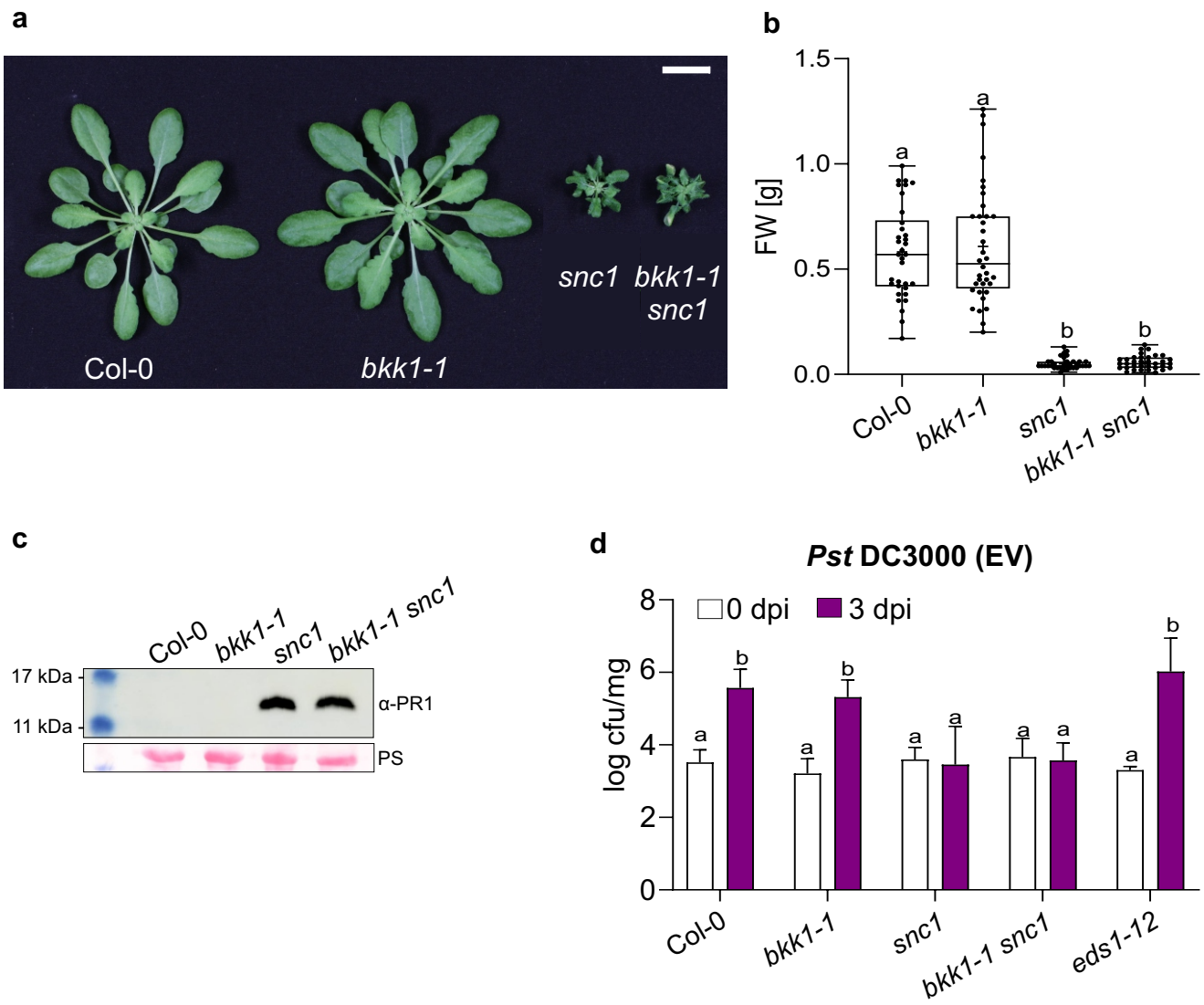

Figure S3: *bkk1-1* does not suppress the autoimmune phenotype of *snc1*. a, Morphology of 6-week-old Col-0, *bkk1-1*, *snc1 and bkk1-1 snc1* plants. Plants were grown on soil under short-day conditions. Scale, 2 cm. **b,** Quantification of fresh weights of plants in (a). Statistical significance is indicated by different letters following ANOVA with Tukey's test ($p < 0.05$). Box limit represents upper and lower quartile, maximum and minimum values are displayed in whiskers. The middle line shows the median, the cross indicates the mean FW. Dots represent biological replicates (plants) in one experiment. **c,** Expression of PR1 in plants shown in (a). **d,** 21-day old seedlings were dip-inoculated with *Pst* DC3000 EV (OD_{600} = 0.0005) and bacterial growth was assessed on the day of inoculation (0 dpi) and 3 days after inoculation (3 dpi). Letters indicate statistically significant differences following ANOVA with Tukey's test ($p < 0.05$). Experiment was done twice with similar results. Bars represent means of four technical replicates + SD.

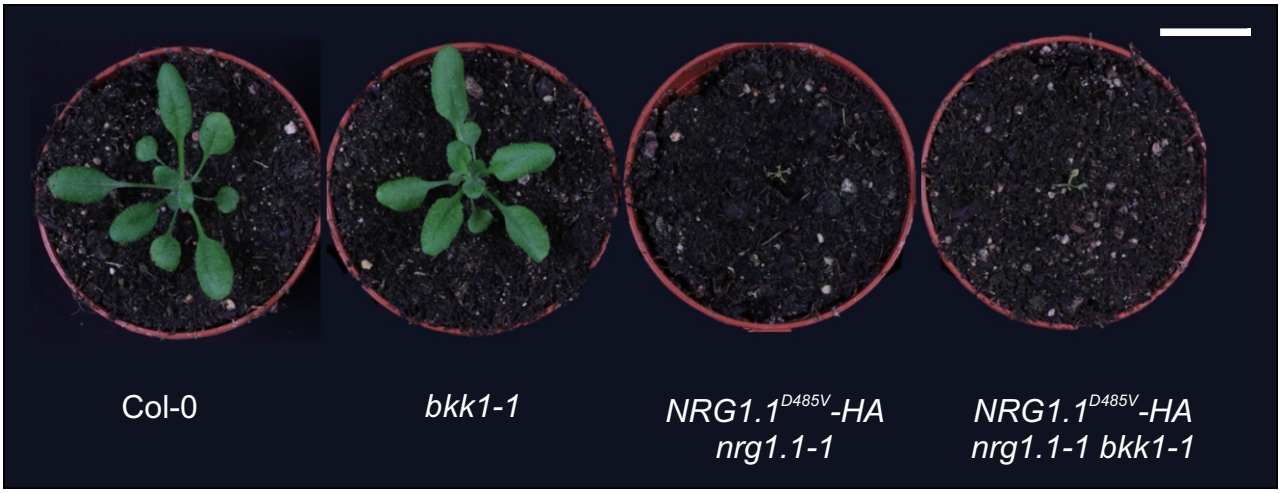

Figure S4: *bkk1-1* does not suppress the autoimmune phenotype of NRG1.1^{D485V}. Morphology of 4-week-old Col-0, *bkk1-1*, *NRG1.1^{D485V}-HA nrg1.1-1 and NRG1.1^{D485V}*-HA *nrg1.1-1* plants. Plants were grown on soil under long-day conditions. Expression of *NRG1.1^{D485V}-HA* is driven by its endogenous promoter. Scale, 2 cm.

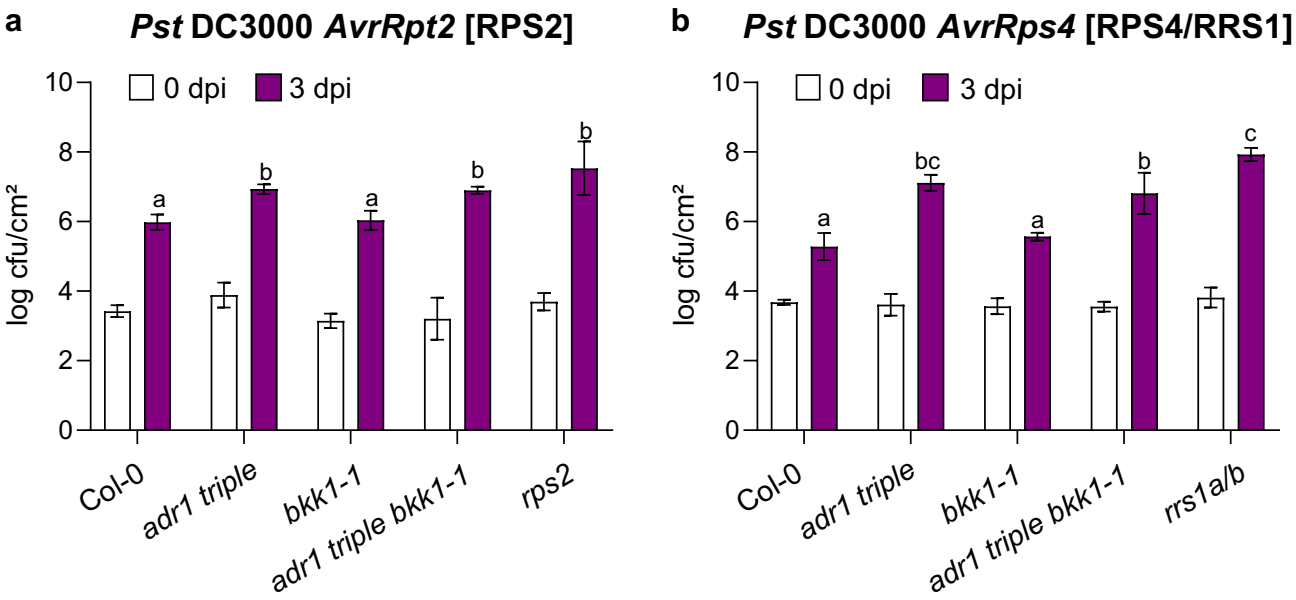

Figure S5: Resistance against adapted Pseudomonas strains is not affected in *bkk1-1*. a, b, 5-week-old plants of indicated genotypes were hand-infiltrated with either *Pst* DC3000 *AvrRpt2* (a) or *Pst* DC3000 *AvrRps4* (b). Bacterial growth was assessed at 0 and 3 dpi. Bars represent means of four technical replicates ± SD. Letters indicate statistically significant differences following ANOVA with Tukey's test ($p < 0.05$). Experiment was done twice with similar results.

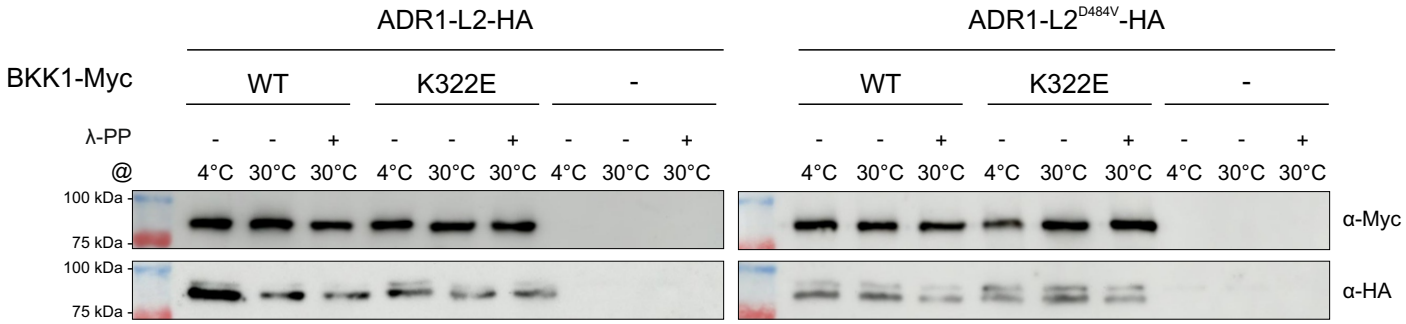

Figure S6: ADR1-L2-HA and ADR1-L2^{D484V}-HA might not be phosphorylated. Wildtype (WT) BKK1-Myc or the kinase inactive allele (K322E) were transiently co-expressed in *N. benthamiana* with either ADR1-L2-HA or ADR1-L2^{D484V}-HA, respectively. Expression of transgenes was under control of the 35S promoter, respectively. Leaf tissue was harvested 2 days post infiltration. BKK1-Myc proteins were immunoprecipitated (IP) with anti-Myc beads. Immunoprecipitated proteins were treated with lambda protein phosphatase (λ-PP) or with λ-PP buffer only at 4°C or 30°C. Proteins were processed for immunoblot using anti-Myc and anti-HA antibody, respectively.

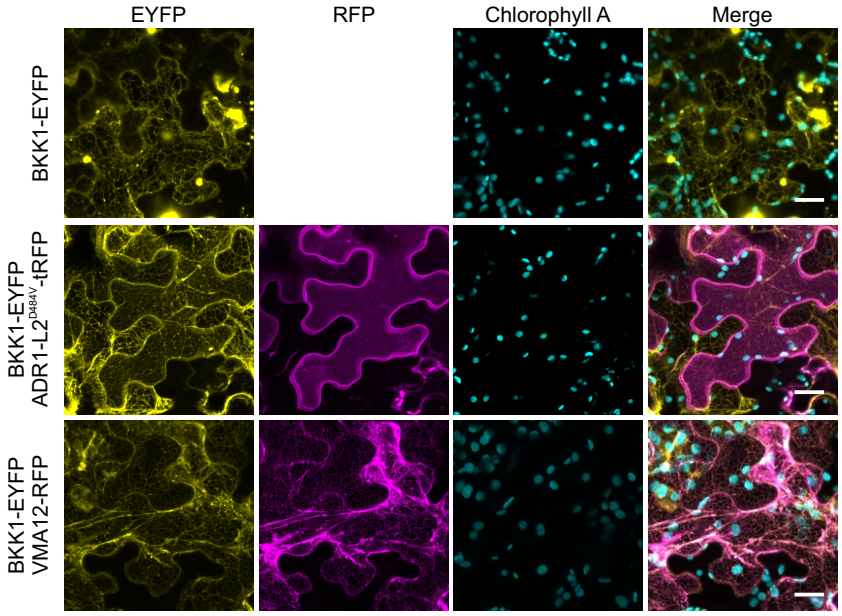

Figure S7: Subcellular localization of BKK1 after transient in *N. benthamiana.* BKK1-EYFP was transiently expressed or co-expressed with either the PM-localized ADR1-L2^{D484V}-tRFP or the ER-localized VMA12-RFP. Expression of all transgenes was driven by the 35S promoter. Confocal imaging was done 45-48 hours post infiltration. Displayed are representative maximum projections of Z-stack images. Scale, 20 µm.

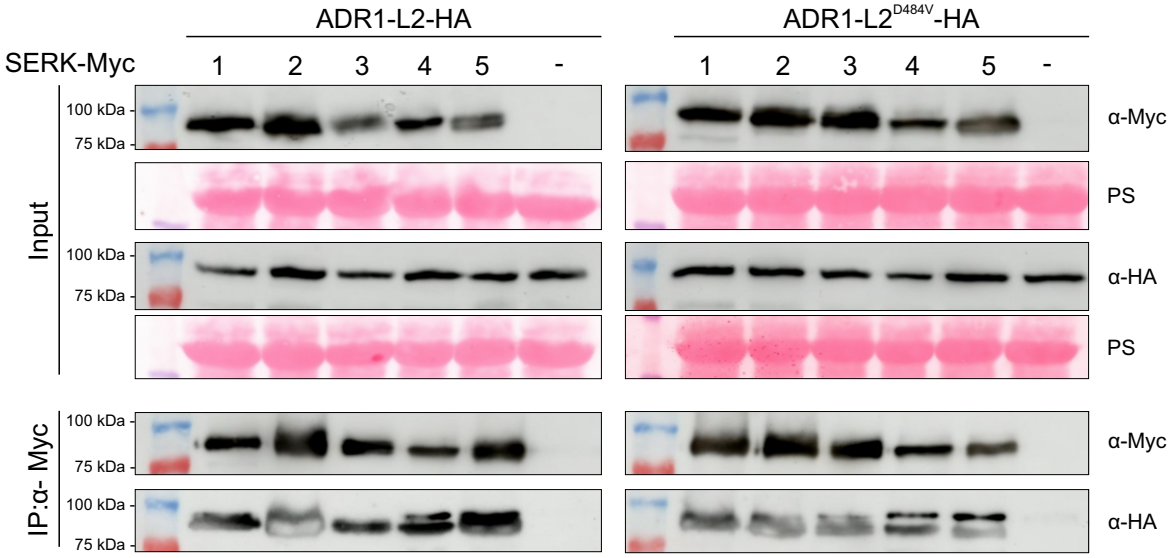

Figure S8: Analyses of SERKs-ADR1-L2 interactions. C-terminal Myc-tagged SERK1 to 5 were transiently co-expressed in *N. benthamiana* with either ADR1-L2-HA or ADR1-L2^{D484V}-HA, respectively. Expression of transgenes was under control of the 35S promoter. Leaf tissue was harvested 2 days post infiltration. SERK-Myc proteins in total protein extracts were immunoprecipitated (IP) with anti-Myc beads and precipitates were immunoblotted with anti-Myc and anti-HA antibody, respectively. Immunoblots using total proteins prior to immunoprecipitation are shown as input (upper panel) and immunoprecipitated proteins are shown as IP (lower panel). Equal loading of the proteins is indicated by the Rubisco band from the Ponceau staining (PS). Co-immunoprecipitation was repeated twice with similar results.

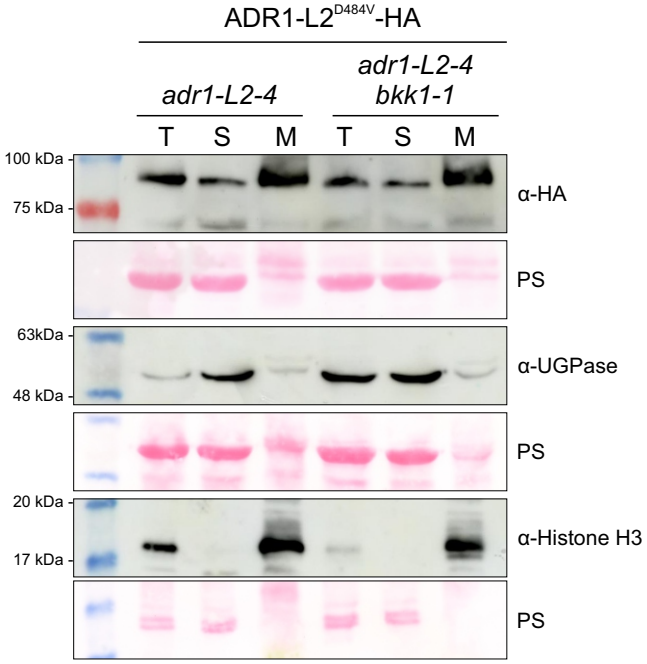

Figure S9: *bkk1-1* does not affect the membrane-association of ADR1-L2^{D484V}. Subcellular fractionation experiments of protein extracts prepared from 6-week-old Arabidopsis plants stably expressing ADR1-L2^{D484V}-HA under control of its native promoter. Shown are immunoblots of ADR1-L2^{D484V}-HA, the cytosolic marker UDP-glucose pyrophosphorylase (UGPase) and the nuclear marker histone H3 using anti-HA, anti-UGPase or anti-Histone H3 antibody, respectively. 40 µg protein of each fraction (total, soluble, microsomes) was used for SDS-PAGE. T: total extract, S: soluble protein fraction, M: microsomal protein fraction. Note: The left part of the blot showing the fractionation of ADR1-L2^{D484V} *adr1-L2-4* is identical to Figure S2 e from (Saile et al. 2021).

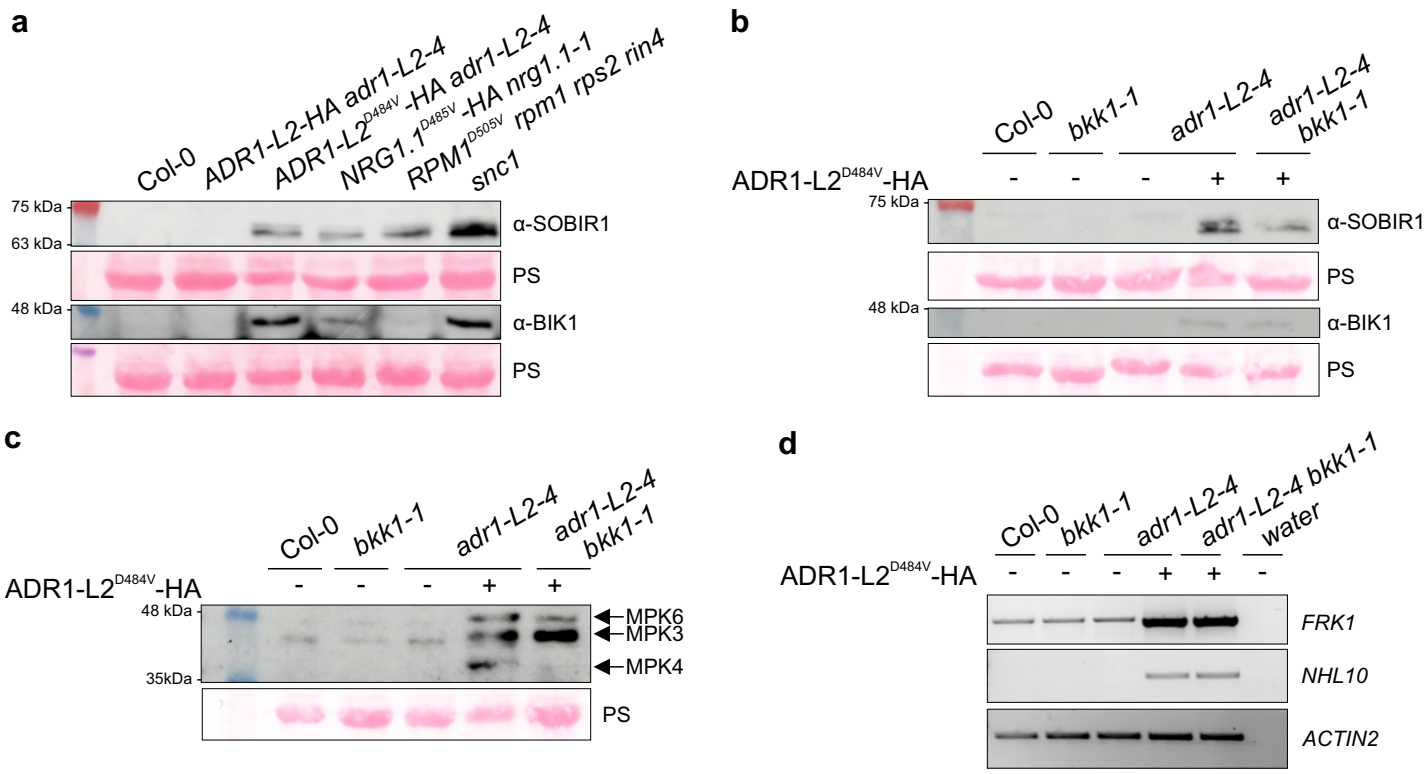

Figure S10: ADR1-L2^{D484V}-induced activation of PTI is *BKK1* independent. a, Immunoblot analysis of the PTI key components SOBIR1 and BIK1 using anti-SOBIR1 and anti-BIK1 antibody on total protein extracts of Col-0, *ADR1-L2-HA adr1-L2-4* and the autoimmune mutants *ADR1-L2^{D484V}-HA adr1-L2-4*, *NRG1.1^{D485V}-HA nrg1.1-1*, *RPM1^{D505V} rpm1 rps2 rin4* and *snc1*. Expression of all transgenes was under control of their endogenous promoters. Total protein extracts were prepared from 4-week-old Arabidopsis plants that were grown under short day conditions. Equal loading of the proteins is indicated by the Rubisco band from the Ponceau staining (PS). **b,** Immunoblot analysis of the PTI key components SOBIR1 an BIK1 using anti-SOBIR1 and anti-BIK1 antibody, respectively on total protein extracts of Col-0, *bkk1-1*, *adr1-L2-4*, *ADR1-L2^{D484V}-HA adr1-L2-4* and *ADR1-L2^{D484V}-HA adr1-L2-4 bkk1-1*. Expression of *ADR1-L2^{D484V}-HA* was driven by its native promoter. Total protein extracts were prepared from 6-week-old Arabidopsis plants that were grown under short day conditions. Equal loading of the proteins is indicated by the Rubisco band from the Ponceau staining (PS). **c,** MAPK activation/phosphorylation in Col-0, *bkk1-1*, *adr1-L2-4*, *ADR1-L2^{D484V}-HA adr1-L2-4*, *ADR1-L2^{D484V}-HA adr1-L2-4 bkk1-1* as shown by immunoblot analysis using anti-p44/p42 antibody. Bands of the individual MAPKs are indicated by arrows. Total protein extracts were prepared from 6-week-old Arabidopsis plants that were grown under short day conditions. Equal loading of the proteins is indicated by the Rubisco band from the Ponceau staining (PS). **d**, Expression of the PTI-induced marker genes *FRK1* and *NHL10* in the indicated genotypes was analysed by RT-PCR. RNA was isolated from 6-week-old plants that were grown under short day conditions. *ACTIN2* was used as a loading/reference control. The following number of PCR cycles were used: *ACTIN2*, 25 cycles, *NHL10*, 30 cycles, *FRK1*, 40 cycles.

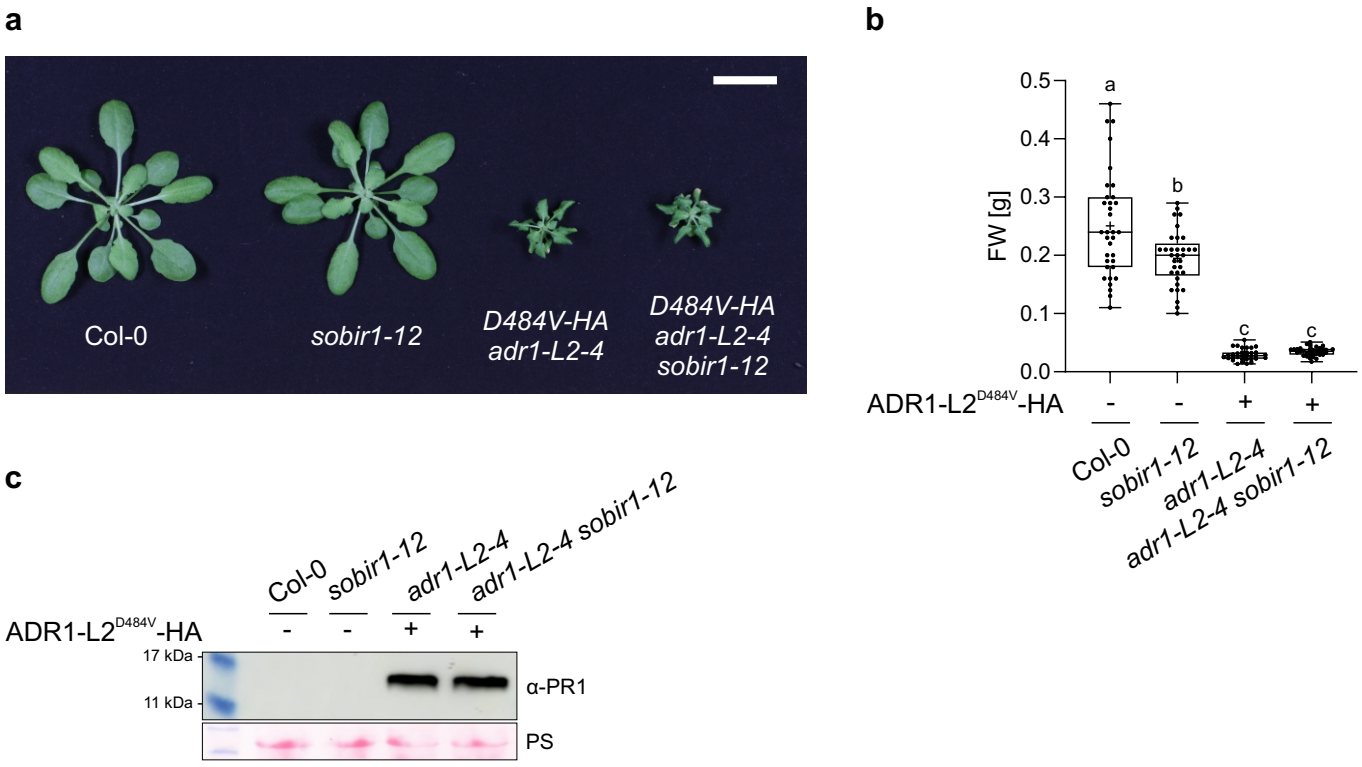

Figure S11: *sobir1-12* does not suppress the autoimmune phenotypes of ADR1-L2^{D484V}. a, Morphology of 7-week-old Col-0, *sobir1-12*, ADR1-L2^{D484V}-HA *adr1-L2-4 and* ADR1-L2^{D484V}-HA *adr1-L2-4 sobir1-12* plants. Plants were grown on soil under short-day conditions. Scale, 2 cm. **b,** Quantification of fresh weights of plants in (a). Statistical significance is indicated by different letters following ANOVA with Tukey's test ($p < 0.05$). Box limit represents upper and lower quartile, maximum and minimum values are displayed in whiskers. The middle line shows the median, the cross indicates the mean FW. Dots represent biological replicates (plants) in one experiment. **c,** Expression of PR1 of plants shown in (a).

Table S1: Primer list.

Sequence (5'-3')	orientation	usage
CTAGTGGCTGTCgAAAGGCTAAAAGAAG	fwd	SDM BKK1 K322E
CTTCTTTTAGCCTTTcGACAGCCACTAG	rev	SDM BKK1 K322E
GGGGACAAGTTTGTACAAAAAAGCAGGCTtaATGGCAGATATAATCGGCGG	fwd	BiFC ADR1-L2 attB1
GGGGACAACTTTGTATAGAAAAGTTGGGTgATCGTCGAGCCAATCCCTGC	rev	BiFC ADR1-L2 attB4
GGGGACAACTTTGTATAATAAAGTTGGAATGACAAGTTCAAAAATGGA	fwd	BiFC BKK1 attB3
GGGGACCACTTTGTACAAGAAAGCTGGGTGTCTTGGACCCGAGGGGTAAT	rev	BiFC BKK1 attB2
GCTCTTCTGTTCTTTCTTGTTCATG	fwd	RT-PCR_FRK1
GAAATTGATCGACAGTGAGAGATG	rev	RT-PCR_FRK1
CTGAACAACCTCTCAATGGC	fwd	RT-PCR_NHL10
CCCTCGTAGTAGGCATGAGC	rev	RT-PCR_NHL10
TCCAAGCTGTTCTCTCCTTG	fwd	RT-PCR_ACTIN2
GAGGGCTGGAACAAGACTTC	rev	RT-PCR_ACTIN2